

FINAL REPORT

Developing Quantum Chemical and Polyparameter Models for Predicting Environmentally Significant Parameters for New Munition Compounds

SERDP Project ER-1734

MAY 2017

Dominic M. Di Toro
Herbert E. Allen
Stanley I. Sandler
Dave Ta Fu Kuo
Tiffany L. Torralba-Sanchez
Yuzhen Liang
University of Delaware Newark, DE

Ronald T. Checkai
Roman G. Kuperman
Michael Simini
U.S. Army Edgewood Chemical Biological Center

Geoffrey I. Sunahara
Jalal Hawari
Sabine G. Dodard
National Research Council Canada, Biotechnology Research Institute

Distribution Statement A

This document has been cleared for public release



Page Intentionally Left Blank

This report was prepared under contract to the Department of Defense Strategic Environmental Research and Development Program (SERDP). The publication of this report does not indicate endorsement by the Department of Defense, nor should the contents be construed as reflecting the official policy or position of the Department of Defense. Reference herein to any specific commercial product, process, or service by trade name, trademark, manufacturer, or otherwise, does not necessarily constitute or imply its endorsement, recommendation, or favoring by the Department of Defense.

Page Intentionally Left Blank

REPORT DOCUMENTATION PAGE					Form Approved OMB No. 0704-0188	
<p>The public reporting burden for this collection of information is estimated to average 1 hour per response, including the time for reviewing instructions, searching existing data sources, gathering and maintaining the data needed, and completing and reviewing the collection of information. Send comments regarding this burden estimate or any other aspect of this collection of information, including suggestions for reducing the burden, to Department of Defense, Washington Headquarters Services, Directorate for Information Operations and Reports (0704-0188), 1215 Jefferson Davis Highway, Suite 1204, Arlington, VA 22202-4302. Respondents should be aware that notwithstanding any other provision of law, no person shall be subject to any penalty for failing to comply with a collection of information if it does not display a currently valid OMB control number.</p> <p>PLEASE DO NOT RETURN YOUR FORM TO THE ABOVE ADDRESS.</p>						
1. REPORT DATE (DD-MM-YYYY) 05/31/2017		2. REPORT TYPE Final Report			3. DATES COVERED (From - To) 8/19/2010 - 8/18/2013	
4. TITLE AND SUBTITLE Developing Quantum Chemical and Polyparameter Models for Predicting Environmentally Significant Parameters for New Munition Compounds				5a. CONTRACT NUMBER W912HQ-10-C-0057		
				5b. GRANT NUMBER		
				5c. PROGRAM ELEMENT NUMBER		
6. AUTHOR(S) Dominic M. Di Toro Herbert E. Allen Stanley I. Sandler				5d. PROJECT NUMBER ER-1734		
				5e. TASK NUMBER		
				5f. WORK UNIT NUMBER		
7. PERFORMING ORGANIZATION NAME(S) AND ADDRESS(ES) University of Delaware Department of Civil and Environmental Engineering Pierre S. Du Pont Hall, 127 The Green Newark, DE 19716					8. PERFORMING ORGANIZATION REPORT NUMBER ER-1734	
9. SPONSORING/MONITORING AGENCY NAME(S) AND ADDRESS(ES) Strategic Environmental Research and Development Program 4800 Mark Center Drive, Suite 17D03 Alexandria, VA 22350-3605					10. SPONSOR/MONITOR'S ACRONYM(S) SERDP	
					11. SPONSOR/MONITOR'S REPORT NUMBER(S) ER-1734	
12. DISTRIBUTION/AVAILABILITY STATEMENT Public distribution; unlimited						
13. SUPPLEMENTARY NOTES						
14. ABSTRACT The project objectives as stated in the statement of need (SON) are to (1) Improve methods for the prediction of physical properties relevant for assessing environmental fate and transport, and (2) Develop predictive models to assess the bioaccumulation of the chemical in relevant environmental receptors (plants, and soil invertebrates). The models will be used to assess the environmental impact of new munitions compounds. Models that fulfill these objectives have been developed in this project as described below.						
15. SUBJECT TERMS Quantum Chemical, Polyparameter Models, Munition Compounds, cuticular membranes, Equilibrium Partitioning, Interstitial Water, Munitions Component, Quantum Mechanics,						
16. SECURITY CLASSIFICATION OF:			17. LIMITATION OF ABSTRACT	18. NUMBER OF PAGES	19a. NAME OF RESPONSIBLE PERSON	
a. REPORT	b. ABSTRACT	c. THIS PAGE			Dominic Di Toro	
UNCLASS	UNCLASS	UNCLASS	UNCLASS	378	19b. TELEPHONE NUMBER (Include area code) 302-831-4092	

Page Intentionally Left Blank

TABLE OF CONTENTS

LIST OF TABLES	viii
LIST OF FIGURES	xiv
LIST OF ACRONYMS	xxix
KEYWORDS	xxxii
ACKNOWLEDGEMENTS	xxxiii
ABSTRACT	xxxiv

1 OBJECTIVES AND BACKGROUND	1
1.1 Overall Objective	1
1.2 Abraham Polyparameter Model	2
1.2.1 Estimating Abraham Solute Parameters	4
1.2.2 ABSOLV Estimates of Abraham Solute Parameters for Munitions Compounds	5
1.2.3 Quantum Chemical Estimates of Abraham Solute Parameters for Munitions Compounds	6
1.3 Bioconcentration Model for Plants	9
1.3.1 Plant-Water Partitioning	9
1.3.2 Plant-Cuticle Partitioning Model	10
1.3.3 Plant Concentration Model	12
1.4 Bioconcentration Model for Oligochaetes	13
1.4.1 Lipid-Water and Protein-Water Partitioning	14
1.4.2 Lipid-Water and Protein-Water pp-LFERs and Prediction of Oligochaete BCFs	14
1.5 Bioconcentration Model for Fish	17
1.6 Model Performance and Applicability to Munitions Compounds	20
REFERENCES	24

2 EXPERIMENTAL DETERMINATION OF SOLVENT-WATER PARTITION COEFFICIENTS AND ABRAHAM PARAMETERS FOR MUNITION CONSTITUENTS	25
2.1 Introduction	25
2.1.1 Polyparameter Linear Free Energy Relationships (pp-LFERs) ...	28

2.1.2	Octanol-Water Partition Coefficient	29
2.2	Materials and Methods.....	29
2.2.1	Materials	29
2.2.2	Selection of Solvent-Water Partitioning Systems.....	30
2.2.3	Experimental Methods.....	30
2.2.4	Determination of Abraham Solute Parameters	31
2.2.4.1	McGowan Characteristic Volume (<i>V</i>)	31
2.2.4.2	Excess Molar Refraction (<i>E</i>).....	31
2.2.4.3	Dipolarity/Polarizability (<i>S</i>), Hydrogen-Bond Acidity (<i>A</i>), and Hydrogen-Bond Basicity (<i>B</i>)	32
2.3	Results and Discussion	32
2.3.1	Validation of Experiment Results.....	32
2.3.2	Analysis of Experiment Results.....	33
2.3.3	Correlation of Partition Coefficients.....	36
2.3.4	Analysis of the Experimentally Derived Abraham Parameters ...	36
2.3.5	Comparison of Solvent-Water Partition Coefficients between Experimental Measurements and Model Predictions	38
2.3.6	Comparison of Physico-Chemical Properties between Experimental Measurements and Model Predictions	40
2.4	Summary and Conclusions	42
A	SUPPLEMENTARY INFORMATION FOR: EXPERIMENTAL DETERMINATION OF SOLVENT-WATER PARTITION COEFFICIENTS AND ABRAHAM PARAMETERS FOR MUNITION CONSTITUENTS	48
3	QUANTUM CHEMICALLY ESTIMATED ABRAHAM SOLUTE PARAMETERS USING MULTIPLE SOLVENT-WATER PARTITION COEFFICIENTS AND MOLECULAR POLARIZABILITY	61
3.1	Introduction.....	61
3.2	Materials and Methods.....	64
3.2.1	Data Compilation	64
3.2.2	Estimating <i>E</i>	65
3.2.3	Determining <i>S</i> , <i>A</i> , and <i>B</i>	66
3.3	Results and Discussion	67
3.3.1	Determining <i>E</i> Independently	67
3.3.2	Comparisons between ABSOLV and QCAP for Various Solvent-Water Systems	68

3.3.3	Comparisons between ABSOLV and QCAP for Munition Constituents and Munition-like Compounds	69
3.3.4	Adjusted Quantum Chemically Estimated Abraham Parameters (Adjusted QCAP).....	70
3.3.5	Comparison of QCAP and Adjusted QCAP	73
3.3.6	Comparisons between ABSOLV, QCAP, and Adjusted QCAP for Various Solvent-Water Systems	73
3.3.7	Comparisons between ABSOLV, QCAP, and Adjusted QCAP for Munition Constituents and Munition-like Compounds	74
3.3.8	Comparison of Adjusted QCAP and COSMOments	75
3.4	Conclusions.....	77
REFERENCES		78
B	SUPPLEMENTARY INFORMATION FOR: QUANTUM CHEMICAL ESTIMATED ABRAHAM SOLUTE PARAMETERS USING MULTIPLE SOLVENT-WATER PARTITION COEFFICIENTS AND MOLECULAR POLARIZABILITY	85
C	QUANTUM CHEMICAL ESTIMATED ABRAHAM SOLUTE PARAMETERS USING MULTIPLE SOLVENT-WATER PARTITION COEFFICIENTS AND MOLECULAR POLARIZABILITY: SUPPLEMENTARY INFORMATION.....	87
REFERENCES		108
4	QUANTUM CHEMICALLY ESTIMATED ABRAHAM SOLUTE AND SYSTEM PARAMETERS FOR SOLVENT-WATER AND PLANT CUTICLE-WATER PARTITION COEFFICIENTS.....	109
4.1	Introduction.....	109
4.2	Materials and Methods.....	111
4.2.1	Partition Coefficient Data	111
4.2.2	Determination of System Parameters using Estimated Solute Parameters	111
4.3	Results and Discussion	112
4.3.1	Analysis of the Refitted Models for Solvent-Water Systems	112
4.3.2	Comparison of the Original and Refitted Models for Solvent-Water Systems	114
4.3.3	Comparison of QCAP and ABSOLV for Solvent-Water Systems.....	116
4.3.4	Comparison of QCAP and ABSOLV for Solvent-Water Partitioning for Munition Constituents.....	117
4.3.5	Comparison of QCAP and ABSOLV for Plant Cuticle-Water Partitioning	118
4.4	Conclusions.....	120

REFERENCES	121
------------------	-----

D	SUPPLEMENTARY INFORMATION FOR: QUANTUM CHEMICALLY ESTIMATED ABRAHAM SOLUTE AND SYSTEM PARAMETERS FOR SOLVENT-WATER AND PLANT CUTICLE-WATER PARTITION COEFFICIENTS.....	125
---	--	-----

E	SUPPLEMENTARY INFORMATION FOR: QUANTUM CHEMICALLY ESTIMATED ABRAHAM SOLUTE AND SYSTEM PARAMETERS FOR SOLVENT-WATER AND PLANT CUTICLE-WATER PARTITION COEFFICIENTS.....	126
---	--	-----

5	BIOCONCENTRATION FACTORS AND PLANT–WATER PARTITION COEFFICIENTS OF MUNITIONS COMPOUNDS IN BARLEY	133
---	--	-----

5.1	Introduction.....	133
-----	-------------------	-----

5.2	Materials and Methods.....	137
-----	----------------------------	-----

5.2.1	Chemical and Reagents.....	137
-------	----------------------------	-----

5.2.2	Plant Growth Conditions.....	137
-------	------------------------------	-----

5.2.3	Preliminary Tests	138
-------	-------------------------	-----

5.2.3.1	Plant Growth in Sand	138
---------	----------------------------	-----

5.2.3.2	Toxicity Screening	138
---------	--------------------------	-----

5.2.4	Bioconcentration Uptake Assays	138
-------	--------------------------------------	-----

5.2.5	Plant–Water Partitioning.....	139
-------	-------------------------------	-----

5.2.6	Analytical Methods	140
-------	--------------------------	-----

5.2.7	Data Analyses	140
-------	---------------------	-----

5.3	Results and Discussion	140
-----	------------------------------	-----

5.3.1	Preliminary Tests	140
-------	-------------------------	-----

5.3.1.1	Plant Growth in Sand	140
---------	----------------------------	-----

5.3.1.2	Toxicity Screening	140
---------	--------------------------	-----

5.3.2	Bioconcentration Uptake Assays	141
-------	--------------------------------------	-----

5.3.3	Plant–Water Partitioning vs. Uptake.....	144
-------	--	-----

5.4	Conclusions.....	148
-----	------------------	-----

REFERENCES	149
------------------	-----

F	SUPPLEMENTARY INFORMATION FOR: BIOCONCENTRATION FACTORS AND PLANT–WATER PARTITION COEFFICIENTS OF MUNITIONS COMPOUNDS IN BARLEY	155
---	---	-----

	Literature Data for Plant Uptake of Munitions Compounds (MCs).	157
--	--	-----

MCs and MLCs Studied.....	165
Plant Growth Conditions.....	167
Plant Growth in Sand.....	167
High Performance Liquid Chromatography (HPLC) Analytical Method	168
Toxicity Screening.....	169
Bioconcentration Uptake Assays	203
Procedure for Extraction of MCs and MLCs from Plant Biomass	203
Plant–Water Partitioning vs. BCF.....	211
REFERENCES	221
6 ESTIMATING GRASS–SOIL BIOCONCENTRATION OF MUNITIONS COMPOUNDS FROM MOLECULAR STRUCTURE.....	223
6.1 Introduction.....	223
6.2 Methodology	224
6.2.1 Basis for Modeling Approach.....	224
6.2.2 Polyparameter Linear Free Energy Relationship (pp–LFER) Models	226
6.2.2.1 Plant Cuticle–Water pp–LFER	226
6.2.2.2 Soil Organic Carbon–Water pp–LFER.....	227
6.2.3 Experimental Data	227
6.2.3.1 Plant Cuticle–Water Partition Coefficients (K_{Cut}) Data.....	229
6.2.3.2 Data from Plant Uptake Assays	230
6.2.4 Estimation of Concentrations in Plants Observed in Independent Uptake Assays	230
6.3 Results and Discussion	231
6.3.1 Plant Cuticle–Water pp–LFER	231
6.3.1.1 Plant Cuticle–Water pp–LFER Including MCs and MLCs	233
6.3.2 Estimation of Concentrations in Plants Observed in Independent Uptake Assays	235
6.4 Conclusions.....	239
REFERENCES	240

G	SUPPLEMENTARY INFORMATION FOR: ESTIMATING GRASS–SOIL BIOCONCENTRATION OF MUNITIONS COMPOUNDS FROM MOLECULAR STRUCTURE	247
	MCs and Munitions–Like Compounds (MLCs)	249
	Transport of Munitions Compounds (MCs) between Soil and Plant.....	251
	Comparison of pp-LFERs for Soil Organic Carbon–Water Partition Coefficients (K_{oc})	254
	Polyparameter Linear Free Energy Relationship (pp-LFER) Models	257
	Estimation of Concentrations in Plants Observed in Independent Uptake Assays	262
	Estimation of Concentrations in Plants Observed in Independent Uptake Assays Including the Contribution from Carbohydrates.....	266
	REFERENCES	269
7	PREDICTING OLIGOCHAETE WORMS–SOIL BIOCONCENTRATION OF MUNITIONS COMPOUNDS FROM MOLECULAR STRUCTURE	273
	7.1 Introduction.....	273
	7.2 Methodology	275
	7.2.1 Estimation of Oligochaete Worms Bioconcentration Factors (BCFs)	275
	7.2.2 Polyparameter Linear Free Energy Relationship (pp-LFER) Models	276
	7.2.2.1 Lipid–Water and Protein–Water pp-LFERs.....	276
	7.2.2.2 Soil Organic Carbon–Water pp-LFER.....	278
	7.2.3 Experimental Data	279
	7.2.3.1 Oligochaete Worms Bioconcentration Factors	279
	7.2.3.2 Concentrations in Oligochaete Worms	280
	7.2.4 Prediction of Concentrations in Oligochaete Worms Observed in Independent Uptake Assays.....	280
	7.3 Results and Discussion	281
	7.3.1 Lipid–Water and Protein–Water pp-LFERs and Estimation of Oligochaete Worms BCFs	281
	7.3.2 Prediction of Concentrations in Oligochaete Worms Observed in Independent Uptake Assays.....	289
	7.4 Conclusions.....	293
	REFERENCES	294

H	SUPPLEMENTARY INFORMATION FOR: PREDICTING OLIGOCHAETE WORMS–SOIL BIOCONCENTRATION OF MUNITIONS COMPOUNDS FROM MOLECULAR STRUCTURE	300
	Munitions Compounds (MCs) and Munitions-Like Compounds (MLCs)	302
	Oligochaete Worms Bioconcentration Factors (BCFs)	304
	Prediction of Concentrations in Oligochaete Worms Observed in Independent Uptake Assays	321
8	CONCLUSIONS AND IMPLICATIONS FOR FUTURE RESEARCH/IMPLEMENTATION	332
	Future Research	332
	REFERENCES	334
I	PRESENTATIONS AT CONFERENCES AND PUBLICATIONS GENERATED FROM THIS PROJECT	335
I.1	Presentations at Conferences	335
I.2	Peer-reviewed Publications.....	337

LIST OF TABLES

Table 1-1	Abraham pp-LFER models.....	3
Table 1-2	Equations for the prediction of concentrations in plants exposed to MCs, or MLCs, in soil and sand or water culture.....	12
Table 1-3	A partitioning–based oligochaete bioconcentration model ^a	17
Table 1-4	Equations for fish BCF model.	21
Table 2-1	Physical and chemical properties of munition constituents.	27
Table 2-2	Validation of partition coefficients measured in this study by comparison with literature reported values.	34
Table 2-3	Summary of the measured solvent-water partition coefficients.	35
Table 2-4	List of ABSOLV estimated (ABSOLV-AP), literature reported, and experimentally derived (Exp-AP) Abraham parameters.	37
Table A-1	List of system parameters.	49
Table A-2	Solute descriptors collected from literature.	50
Table A-3	The statistics of the experimentally derived Abraham parameters.....	51
Table A-4	Solvent-water partition coefficients from literature compilations, experimental measurements, and model predictions.	53
Table A-5	List of pp-LFERs used for model validation.	54
Table A-6	Physical-chemical properties of experimental measurements and model predictions.....	55
Table 3-1	Linear equations ^a for Adjusted QCAP solute parameters <i>E</i> , <i>S</i> , <i>A</i> , <i>B</i> , and <i>V</i> .73	
Table B-1	Residuals of COSMO-SAC predicted solvent-water partition coefficients and summary statistics. Located in Chapter_3_Appendix B_Tables.xlsx file.	85
Table B-2	System parameters used for computing Abraham solute parameters. Located in Chapter_3_Appendix B_Tables.xlsx file.....	85
Table B-3	COSMO-SAC predicted solvent-water partition coefficients (as well as the corresponding solute and system parameters) used for computing QCAP solute parameters. Located in Chapter_3_Appendix B_Tables.xlsx file.	85
Table B-4	Polarizability and solute parameters (QCAP, ABSOLV, and UFZ-LSER). Located in Chapter_3_Appendix B_Tables.xlsx file.....	85

Table B-5	Experimental and predicted (ABSOLV, QCAP, and Adjusted QCAP) solvent-water partition coefficients. Located in Chapter_3_Appendix B_Tables.xlsx file.	85
Table B-6	RMSEs of prediction (ABSOLV, QCAP, and Adjusted QCAP) of solvent-water partition coefficients. Located in Chapter_3_Appendix B_Tables.xlsx file.	85
Table B-7	Solute parameters (ABSOLV and QCAP) and partition coefficients (observed, ABSOLV, QCAP, and Adjusted QCAP) for munition constituents and munition-like compounds. Located in Chapter_3_Appendix B_Tables.xlsx file.	85
Table B-8	Comparison of the estimated (QCAP, Adjusted QCAP, and COSMOments) and experimentally-based solute parameters. Located in Chapter_3_Appendix B_Tables.xlsx file.	86
Table 4-1	The literature (original), QCAP, and ABSOLV system parameters ^a for selected systems.	113
Table D-1	Experimental and predicted solvent-water partition coefficients as well as ABSOLV and QCAP solute parameters. Located in Chapter_4_Appendix D_Tables.xlsx file.	125
Table D-2	Refitted system parameters determined using QCAP solute parameters. Located in Chapter_4_Appendix D_Tables.xlsx file.	125
Table D-3	Refitted system parameters determined using ABSOLV solute parameters. Located in Chapter_4_Appendix D_Tables.xlsx file.	125
Table D-4	Summary of the RMSEs of prediction of partition coefficients. Located in Chapter_4_Appendix D_Tables.xlsx file.	125
Table D-5	Experimental and predicted solvent-water partition coefficients, together with ABSOLV and QCAP solute parameters, for munition constituents. Located in Chapter_4_Appendix D_Tables.xlsx file.	125
Table F-1	Literature data for concentrations of MCs in plants grown in soil during uptake assays.	157
Table F-2	Literature data for MCs bioconcentration factors (BCFs) in plants grown in soil during uptake assays.	163
Table F-3	Selected characteristics and physicochemical properties of the MCs and MLCs studied.	165
Table F-4	Composition of aqueous solution used to supply nutrients for plant growth in sand.	167

Table F-5	Barley shoot height and root elongation for each measured exposure concentration in toxicity screening with MCs and MLCs.	171
Table F-6	NOAEC, LOAEC, and EC ₅₀ for MCs and MLCs in toxicity screening test with barley.	197
Table F-7	Summary statistics for the fluctuation in measured exposure concentrations for MCs and MLCs during toxicity screening with barley ^a	201
Table F-8	Summary statistics for the fluctuation in measured exposure concentrations for MCs and MLCs during bioconcentration uptake assays with barley ^a ...	203
Table F-9	Summary statistics for the significance of sorption of MCs and MLCs onto the solid growth medium (sand) during bioconcentration uptake assays with barley ^a	204
Table F-10	Summary statistics for the significance of exposure time in the ratios of CiPlantCiIW for MCs and MLCs during bioconcentration uptake assays with barley ^a	205
Table F-11	Ratios of CiPlantCiIW ^b for the compounds evaluated in bioconcentration uptake assays with barley.	206
Table F-12	Plant–water partition coefficients (K _{PW}) for 4-NAN with barley and the summary statistics for the significance of contact time (kinetics) on log K _{PW} values ^a	211
Table F-13	Summary statistics for the significance of the concentration of the initial solution added on log K _{PW} values ^a	212
Table F-14	Plant–water partition coefficients (K _{PW}) for the compounds evaluated.	213
Table F-15	Time course data obtained from Sunahara ³ and Dodard et al. ⁹ , and estimated degradation rates for MCs ^a	217
Table 6-1	Munitions Compounds (MCs), Munitions–Like Compounds (MLCs), and plant species included in the datasets.	228
Table 6-2	Equations for the prediction of concentrations in plants exposed to MCs, or MLCs, in soil and sand or water culture.....	236
Table G-1	Selected characteristics and physicochemical properties of the MCs and MLCs.	249
Table G-2	Literature measured average volumetric flows in xylem and phloem for four plant species ^a	253

Table G-3	Observed and predicted Soil Organic Carbon–Water Partition Coefficients (K_{OC}) for comparison of log K_{OC} pp–LFERs performance. Located in Chapter_6_Appendix G_Tables.xlsx file.	255
Table G-4	Comparison of solute descriptor space coverage for three log K_{OC} pp–LFERs.	257
Table G-5	Plant cuticle–water partition coefficients (K_{Cut}) data. Located in Chapter_6_Appendix G_Tables.xlsx file.	257
Table G-6	Plant cuticle membrane–water partition coefficients (K_{CM}) and plant cuticle matrix–water partition coefficients (K_{MX}) for undissociated organic compounds from Sabljic et al. ¹⁵ and the summary statistics for the significance of the cuticular component on the resulting plant cuticle–water partition coefficient (K_{Cut}).	258
Table G-7	Absolv estimated Abraham Parameters (Absolv–AP) ²² and K_{Cut} calculated using pp–LFERs with Absolv–AP. Located in Chapter_6_Appendix G_Tables.xlsx file.	259
Table G-8	Experimentally derived Abraham Parameters (Exp–AP) ^{5, 23} and K_{Cut} calculated using pp–LFERs with Exp–AP ^a . Located in Chapter_6_Appendix G_Tables.xlsx file.	259
Table G-9	Adjusted Quantum Chemically estimated Abraham Parameters (Adjusted QCAP) ¹² and K_{Cut} calculated using pp–LFER with QCAP. Located in Chapter_6_Appendix G_Tables.xlsx file.	259
Table G-10	Quantum Chemically estimated Abraham Parameters (QCAP) ¹² and K_{Cut} calculated using pp–LFER with QCAP. Located in Chapter_6_Appendix G_Tables.xlsx file.	259
Table G-11	Results of the K_{Cut} pp–LFER multiple linear regression analyses fitting the general Abraham polyparameter model (Eq. (6-1)) to K_{Cut} data using three different sources of solute descriptors ^a	260
Table G-12	Range of solute descriptor space for the plant cuticle–water pp–LFERs by Platts and Abraham ¹ and this work.	261
Table G-13	Data from published uptake assays with plants exposed to MCs, or MLCs, in the growth medium. Located in Chapter_6_Appendix G_Tables.xlsx file.	262
Table G-14	Solute descriptors used in the partitioning-based bioconcentration model, Eq. (6-9), for the prediction of MCs and MLCs concentrations in plant biomass. Located in Chapter_6_Appendix G_Tables.xlsx file.	262
Table G-15	Fraction of cuticle, f_{Cut} , for plant species in the uptake assays dataset.	263

Table G-16	Example for prediction of a MC (HMX) concentration in grass (<i>Perennial ryegrass</i>).	264
Table G-17	Predicted values for MCs and MLCs concentrations in interstitial water and plant biomass using the partitioning–based bioconcentration model (Eq. (6-9)) ^a . Located in Chapter_6_Appendix G_Tables.xlsx file.	266
Table G-18	Examples of MCs plant uptake data surveyed but excluded from the validation dataset. Located in Chapter_6_Appendix G_Tables.xlsx file.	266
Table G-19	Observed K_{Ch} and fitted K_{Ch} with pp–LFER using QCAP. Located in Chapter_6_Appendix G_Tables.xlsx file.	266
Table G-20	K_{Ch} pp–LFER from the multiple linear regression analysis fitting the general Abraham polyparameter model (Eq. (6-1)) to K_{Ch} data using QCAP solute descriptors ^a	267
Table G-21	Predicted values for MCs and MLCs concentrations in plant biomass using the partitioning–based bioconcentration model that includes contributions from carbohydrates (Eq. (G-6)) ^a . Located in Chapter_6_Appendix G_Tables.xlsx file.	268
Table 7-1	Comparison of the competitiveness for solutes between lipid and protein, calculated as the difference between the solvent parameters in the K_{Lipid} and $K_{Protein}$ pp–LFERs obtained by Kuo and Di Toro ^{30,33} , Eq. (7-5) and Eq. (7-6), respectively.	278
Table 7-2	Comparison of the competitiveness for solutes between lipid and organic carbon, calculated as the difference between the solvent parameters in the K_{Lipid} pp–LFER by Kuo and Di Toro ^{30,33} , Eq. (7-5), and K_{OC} pp–LFER by Kipka and Di Toro ³⁴ , Eq. (7-7).....	279
Table 7-3	Comparison of the competitiveness for solutes between lipid and protein, calculated as the difference between the solvent parameters in the K_{Lipid} obtained in this work and $K_{Protein}$ pp–LFER obtained by Kuo and Di Toro ^{30,33} , Eq. (7-11) and Eq. (7-6), respectively.	287
Table 7-4	Sequence of equations for the prediction of concentrations in oligochaetes exposed to MCs, or MLCs, in soil.	290
Table H-1	Selected characteristics and physicochemical properties of the MCs and MLCs included in the oligochaete worms lipid–water pp–LFER and the model validation.	302
Table H-2	Oligochaete worms bioconcentration factors (BCFs) dataset.....	304
Table H-3	Worm mass fraction of dry weight f_{dwt} , fraction of lipid f_{Lipid} , and fraction of protein $f_{Protein}$ obtained from the literature.	308

Table H-4	Worm mass fractions of lipid (<i>fLipid</i>), protein (<i>fProtein</i>), dry weight (<i>fdwt</i>), and water (<i>fWater</i>) used for the estimation of oligochaete BCFs ^a	310
Table H-5	Quantum Chemically estimated Abraham Parameters (QCAP) and Adjusted QCAP ^a from Liang ³¹ used for the prediction of the oligochaete BCFs dataset ^b	313
Table H-6	Estimated oligochaete BCFs using the partition-based model (Eq. (7-3)) with K_{Lipid} pp-LFER either from Kuo and Di Toro ^{30,33} (Eq. (7-5)) or from this work (Eq. (7-11)), and $K_{Protein}$ pp-LFER from Kuo and Di Toro ^{30,33} (Eq. (7-6)) ^a .	316
Table H-7	Statistics for the comparison of the lipid phase descriptors between the K_{Lipid} pp-LFERs from Kuo and Di Toro ^{30,33} (Eq. (7-5)) and the K_{Lipid} pp-LFERs from this work (Eq. (7-11)) ^a	320
Table H-8	Data from independent uptake assays with oligochaetes exposed to MCs in soil.	321
Table H-9	Values for <i>fLipid</i> , <i>fProtein</i> , <i>fdwt</i> , and <i>fWater</i> , QCAP, and adjusted QCAP ³¹ used for the prediction of the concentrations in oligochaetes from the independent uptake assays dataset ^a	323
Table H-10	Worked example for the prediction of a MC (2,4-DNAN) concentration in an oligochaete worm (<i>Eisenia andrei</i>).	325
Table H-11	Predicted values for soil organic carbon-water partition coefficient KOC , concentration in interstitial water, and concentration in worm for MCs data from independent uptake studies using the partition-based model (Eq. (7-12)) with K_{Lipid} pp-LFER from this work (Eq. (7-11)).	328
Table H-12	Predicted values for soil organic carbon-water partition coefficient KOC , concentration in interstitial water, and concentration in worm for MCs data from independent uptake studies using the partition-based model (Eq. (7-9)) with K_{Lipid} pp-LFER obtained by Kuo and Di Toro ^{30,33} (Eq. (7-5)).....	330

LIST OF FIGURES

Figure 1-1	Problem framework. Estimating the physical-chemical and environmental partition coefficients between water and the interacting phases.....	1
Figure 1-2	Modeling framework for the predictive model of bioaccumulation between soil and soil exposed organisms. The soil-water and organism components are assumed to be at steady state equilibrium. The arrows represent the partition coefficients illustrated in Figure 1-1.....	2
Figure 1-3	Comparison of experimental and model predicted solvent-water partition coefficients: grey symbols are experimental measurements, red symbols are model predictions. Upper row are for model predictions using ABSOLV estimated AP (ABSOLV-AP), lower row are for model predictions using experimentally derived AP (Exp-AP) from this work. The solvents in the solvent-water systems are hexane, toluene, octanol, trichloromethane (TCM), and dichloromethane (DCM). Experimental measurements and model predictions for solvent-water partition coefficients are summarized in Chapter 2 Table A-4.	4
Figure 1-4	Comparisons between experimental measurements and model predictions with ABSOLV estimated (ABSOLV-AP) or experimentally derived (Exp-AP) AP from this work for water-air partition coefficient ($\log K_{wa}$, L_{air}/L_{water}), organic carbon-water partition coefficient ($\log K_{oc}$, L_{kg-1}), and water solubility ($\log S$, $mol\ L^{-1}$). $\log K_{wa}$ y-axis on left, $\log K_{oc}$ and $\log S$ y-axis on right. Experimental values from different sources are plotted. Two grey dots per property denote the reported ranges. Experimental measurements and model predictions are summarized in Chapter 2 Table A-6.	5
Figure 1-5	(A). RMSEs of the residuals (predicted $\log K_{sw}$ - observed $\log K_{sw}$) for solvent-water partition coefficients. Predictions by three models ABSOLV, QCAP, and Adjusted QCAP. Solvents (left axis) ordered from the smallest to the largest QCAP RMSE. Right axis N = number of solutes in each system. (B) Prediction errors (predicted $\log K_{sw}$ - observed $\log K_{sw}$) for predictions of ABSOLV, QCAP, and Adjusted QCAP for munition constituents and munition-like compounds (Right axis). Left axis: partitioning systems: wet octanol-water, toluene-water, hexane-water, trichloromethane (TCM)-water, and dichloromethane (DCM)-water.....	7

- Figure 1-6 Results for pp-LFERs constructed using the indicated solute parameters. (A) RMSEs of residuals (log predicted - log observed partition coefficients) for solvent-water partition coefficients. Predictions by four models (1) ABSOLV, (2) original model with QCAP, (3) refitted model with ABSOLV, and (4) refitted model with QCAP. Solvents (left axis). Right axis N = number of solutes in each system (B) Prediction errors (predicted log K_{sw} – observed log K_{sw}) for solvent-water partition coefficients for munition constituents and munition-like compounds (Right axis). Left axis list of the corresponding partitioning systems: wet octanol-water, toluene-water, hexane-water, and chloroform-water. .8
- Figure 1-7 Schematic diagram of the Equilibrium Partitioning (EqP) modeling approach: Left–right arrows indicate partitioning of MC (or MLC) *i* between two phases. *KiOC* = soil organic carbon–water partition coefficient ($L_{\text{water}} \text{ kgoc}^{-1}$), *Kiroot* = root–water partition coefficient ($L_{\text{water}} \text{ kgroot}^{-1}$), and *KiCut* = plant cuticle–water partition coefficient ($L_{\text{water}} \text{ kgcuticle}^{-1}$).9
- Figure 1-8 Plant (barley)-water partition coefficients (*K_{PW}*) and octanol-water partition coefficients (*K_{OW}*) for MCs and MLCs. See Chapter 5, Figure 5-4 for details. Boxes’ widths proportional to the square-root of the number of observations in the groups.....9
- Figure 1-9 Comparison between BCF (labeled Uptake) and plant-water partition coefficient *K_{PW}* (labeled Partitioning) for MCs and MLCs. Compounds ordered from small to large difference between log *K_{PW}* and log BCF. Box width proportional to the square-root of the number of observations in the group.....10
- Figure 1-10 Predicted concentrations in the plant versus observed values from published uptake studies (Chapter 6 Table 6-2, Table H-13, and Table H-17). Color coding assigned based on: (A) MCs and MLCs (Chapter 6 Table 6-1), (B) growth medium, and (C) plant species. Unfilled symbols indicate that the predicted concentration in the interstitial water exceeded solubility. The border color for the unfilled symbols corresponds to the color identification in each panel legend. Root mean square error of prediction (log predicted - log observed) RMSE = 0.429 excluding the unfilled symbols. The solid line indicates the best agreement (unity), dashed lines are spaced at 1 log unit from unity.....11
- Figure 1-11 pp-LFER, Eq. (1-1) fitted to the full *K_{Cut}* dataset collected from the literature. Abraham solute parameters from (A) Absolv–AP, (B) Exp–AP, (C) QCAP. RMSE: root mean square error of prediction (log fitted - log observed) for all compounds included in the full *K_{Cut}* dataset (Chapter 6, Table H-5). The RMSEs for only MCs and MLCs are (A) 1.261; (B) 0.478; and (C) 0.421. The solid line indicates the best agreement (unity), dashed lines are spaced at 1 log unit from unity line.11

- Figure 1-12 Schematic diagram of the Equilibrium Partitioning (EqP) modeling approach: Left–right arrows indicate partitioning of MC (or MLC) i between two phases. $KiOC$ = soil organic carbon–water partition coefficient ($L_{water} \text{ kgoc}^{-1}$), $Kiroot$ = root–water partition coefficient ($L_{water} \text{ kgroot}^{-1}$), and $KiCut$ = plant cuticle–water partition coefficient ($L_{water} \text{ kgcuticle}^{-1}$).13
- Figure 1-13 Predicted vs observed (a) lipid–water and (b) protein–water partitioning using Abraham solvation parameters. For lipid–water partition LFER, $n=248$, $RMSE=0.57$. For protein–water partition LFER, $n=69$, $RMSE=0.38$14
- Figure 1-14 Estimated versus observed oligochaete BCFs for organic compounds (Chapter 7 Table I-6). Predictions made using a partition–based BCF model (Chapter 7 Eq. (7-3)) with the K_{Lipid} pp–LFER (A) fitted to the oligochaete BCF data and ((Eq. (7-11)) or (B) fitted to an independent data set (Eq. (7-5)). Legend: Chemical class with corresponding count; PAH: polycyclic aromatic hydrocarbon. RMSE: Root mean square error of prediction (log predicted - log observed BCF). The solid line indicates the best agreement (unity), dashed lines are spaced at 1 log unit from unity.16
- Figure 1-15 Fitted versus observed oligochaete BCFs for organic compounds partitioning to three components, lipid, protein, and internal water (Chapter 7 Eq. (7-10), Eq. (7-11), and Eq. (7-6)). Color coding assigned based on: (A) organic compound, (B) exposure medium, and (C) oligochaete species. Root mean square error of prediction (log predicted - log observed BCF), $RMSE = 0.499$. Abbreviations defined in Table I-2. The solid line indicates the best agreement (unity), dashed lines are spaced at 1 log unit from unity.16
- Figure 1-16 Schematic diagram of the Equilibrium Partitioning (EqP) modeling approach: Left–right arrows indicate partitioning of MC (or MLC) i between two phases. The arrows in the fish denote partitioning equilibria between lipid–water and protein–water. The arrows in the water column denote partitioning equilibria between dissolved organic carbon–water and particulate organic carbon –water.18
- Figure 1-17 Prediction of fish BCF using the model in Table 1-4. The $RMSE = 0.56$. Kuo and Di Toro ¹.19
- Figure 1-18 Predicted versus observed log half-life. Compound biotransformation half-life = $\ln(2)/k_M$. $RMSE = 0.71$, $N = 424$. Kuo and Di Toro ¹. **Error! Bookmark not defined.**
- Figure 1-19 (A) Percent of the residuals that exceed the indicated limits, e.g. for $RMSE = 0.5$, 34% of the residuals exceed the limits 3 and 1/3; 16% exceed the limits 5 and 1/5; and 5% exceed the limits 10 and 1/10. (B, C) Statistics of the model fit: mean, standard deviation, and $RMSE$ **Error! Bookmark not defined.**

- Figure 1-20 Model performance for munitions components. Estimates from models not calibrated to munitions components. (A) Soil partition coefficient (K_{oc}) (L/kg OC) Eq. (1-3). (B) Plant cuticle partition coefficient (L/kg cuticle) Eq.(1-5). (C) Plant shoot concentration (mg/kg dry wt.) from soil exposure Table 1-2. (D) Oligochaete BCF (L/kg lipid) Table 1-3.. **Error! Bookmark not defined.**
- Figure 2-1 Comparisons between experimentally derived Abraham parameters (Exp-AP) from this work and ABSOLV estimated Abraham parameters (ABSOLV-AP). The dots are for nitroaromatics compounds and the squares are for cyclic nitramines and nitrosamines.38
- Figure 2-2 Solvent-water partition coefficients: grey symbols are experimental measurements, red symbols are estimates. Upper row are model predictions using ABSOLV estimated Abraham parameters (ABSOLV-AP), lower row are experimentally derived Abraham parameters (Exp-AP) from this work. The solvents in the solvent-water systems are hexane, toluene, octanol, trichloromethane (TCM), and dichloromethane (DCM). Values of experimental measurements and model predictions for solvent-water partition coefficients are summarized in Table A-4 (Solvent-water partition coefficients from literature compilations, experimental measurements, and model predictions).40
- Figure 2-3 Comparisons between experimental measurements and model predictions with ABSOLV estimated (ABSOLV-AP) or experimentally derived (Exp-AP) Abraham parameters from this work for water-air partition coefficient ($\log K_{wa}$, L_{air}/L_{water}), organic carbon-water partition coefficient ($\log K_{oc}$, $L \cdot kg^{-1}$), and water solubility ($\log S$, $mol \cdot L^{-1}$). The y-axis on the left is for $\log K_{wa}$ and y-axis on the right is for $\log K_{oc}$ and $\log S$. Experimental values from different sources were plotted individually, against model predictions. Those with two grey dots per property denote the reported ranges. Experimental measurements were compiled from several sources for K_{wa} ²⁷, K_{oc} ^{12, 30, 47-49}, and S ^{27, 30, 50}. Literature system parameters^{44, 51, 52} are listed in Table A-5. Values of experimental measurements and model predictions are summarized in Table A-6 (Physical-chemical properties of experimental measurements and model predictions). 41
- Figure A-1 Comparisons of E between estimations using ABSOLV algorithm and those from experimental refractive index. The solid line shows perfect agreement. Experimental refractive index was taken from Katritzky et al.¹⁷.56
- Figure A-2 Pairs plot¹⁸ of solvent-water partition coefficients ordered by solvent. The blue dots are cyclic nitramines and nitrosamines, and the green dots are nitroaromatics. For each data plot, x axis label is the solvent above the plot, y axis label is to the right of the plot. The upper triangular panels display the coefficient of determination (R^2) of the respective pair. For each R^2 panel, x axis label is the solvent below the plot, y axis label is to the left of the plot. .57

- Figure A-3 Pairs plot of solvent-water partition coefficients ordered by MCs. For each data plot, x axis label is the MC above the plot, y axis label is the MC to the right of the plot. The upper triangular panels display the coefficient of determination (R^2) of the respective pair. For each R^2 panel, x axis label is the MC below the plot, y axis label is the MC to the left of the plot.....58
- Figure 3-1 (1) Comparison of experimentally derived Abraham parameters (Exp-AP)¹⁹ and ABSOLV estimated Abraham parameter (ABSOLV) for hexahydro-1,3,5-trinitro-1,3,5-triazacyclohexane (RDX), octahydro-1,3,5,7-tetranitro-1,3,5,7-tetraazacyclooctane (HMX), hexahydro-1-nitroso-3,5-dinitro-1,3,5-triazine (MNX), hexahydro-1,3,5-trinitroso-1,3,5-triazine (TNX), and hexahydro-1,3-dinitroso-5-nitro-1,3,5-triazine (DNX). (2) Comparison of experimental¹⁹ and ABSOLV predicted solvent-water partition coefficients for RDX, HMX, DNX, MNX, and TNX. The solvents are hexane, toluene, octanol, trichloromethane (TCM), and dichloromethane (DCM).....63
- Figure 3-2 Hexbin two dimensional histogram plots⁶⁸ comparing the predicted versus experimental solute parameters from the UFZ-LSER database (labeled UFZ) for E and S determined by the two methods listed at the top of each column. See text in Section 3.3.1 for an explanation of the hexbin plot. Panels (1) and (2) estimate E , S , A , and B jointly with an MLR, and an independently estimated V , labeled ESAB; panels (3) and (4) estimate E from molecular polarizability, V from molecular volume and S , A , and B from an MLR, which is the QCAP method.68
- Figure 3-3 Dot plot presenting RMSEs of the residuals (predicted $\log K_{sw}$ - observed $\log K_{sw}$) for the predictions of solvent-water partition coefficients. Predictions by two models are compared: (1) ABSOLV and (2) QCAP. The solvents listed on the left axis are ordered from the smallest to the largest QCAP RMSE. The right axis presents N , the number of solutes in each system. Summary of the RMSEs of prediction of solvent-water partition coefficients is in Table B-6.....69
- Figure 3-4 Dot plot presenting prediction errors (predicted $\log K_{sw}$ - observed $\log K_{sw}$) for predictions of ABSOLV and QCAP for munition constituents and munition-like compounds listed on the right axis and for solvents listed on the left axis: wet octanol-water, toluene-water, hexane-water, trichloromethane (TCM)-water, and dichloromethane (DCM)-water. See the legend in Figure 3-1 for the solutes' chemical names.....70
- Figure 3-5 Hexbin two dimensional histogram plots⁶⁸ comparing the solute parameters (S , A , B , E , V) between QCAP and UFZ, and between Adjusted QCAP and UFZ. See text in Section 3.3.1 for an explanation of the hexbin plot.72

- Figure 3-6 Dot plot presenting RMSEs of the residuals (predicted $\log K_{sw}$ - observed $\log K_{sw}$) for the predictions of solvent-water partition coefficients. Predictions by three models are compared: (1) ABSOLV, (2) QCAP, and (3) Adjusted QCAP. The solvents listed on the left axis are ordered from the smallest to the largest QCAP RMSE. The right axis presents N, the number of solutes in each system. Summary of the RMSEs of prediction of solvent-water partition coefficients is in Table B-6.74
- Figure 3-7 Dot plot presenting prediction errors (predicted $\log K_{sw}$ - observed $\log K_{sw}$) for predictions of ABSOLV, QCAP, and Adjusted QCAP for munition constituents and munition-like compounds listed on the right axis. Left axis: list of the corresponding partitioning systems: wet octanol-water, toluene-water, hexane-water, trichloromethane (TCM)-water, and dichloromethane (DCM)-water. See the legend in Figure 3-1 for the solutes' chemical names.75
- Figure 3-8 Bar chart comparing the prediction root mean square errors (RMSEs) for Adjusted QCAP and COSMOments estimates of the solute parameters. See Table B-8 for the complete statistical comparison.76
- Figure C-1 Plots showing the decrease of the interquartile range (IQR) of COSMO-SAC predicted solvent-water partition coefficient errors as the number of data points increases. N = minimum number of data points used to compute the IQR. Data are from Table B-1. Chemicals are plotted in the solvent sequence in the table. Note that a solvent with greater than 20 observations appears in all four plots, e.g. the first IQR on the left hand side.88
- Figure C-2 A histogram plot of COSMO-SAC predicted solvent-water partition coefficient (K_{sw}) errors. 24 solvent-water systems and 3095 data points are included.89
- Figure C-3 The solvent-water system parameters e , s , a , b , and v for the 65 solvent-water systems used for computing QCAP. Parameters are grouped by solvent chemical classes. Within each group, the solvents are ordered from the smallest to the largest magnitude of v90
- Figure C-4 Comparing molecular polarizability computed using M062X¹ with aug-cc-pVDZ and with aug-cc-pVTZ basis set.91
- Figure C-5 Hexbin two dimensional histogram plots² comparing the predicted versus experimental values from the UFZ-LSER database (labeled UFZ) for the solute parameters A , B , and V determined by two methods listed at the top of each column: (1) estimates E , S , A , and B jointly with an MLR, and an independently estimated V , labeled ESAB; (2) estimate of E from molecular polarizability, V from molecular volume and S , A , and B from an MLR, which is the QCAP method.92
- Figure C-6 Hexbin two dimensional histogram plot² of E versus S solute parameters compiled from the UFZ-LSER database.93

Figure C-7	A histogram plot of COSMO-SAC predicted solvent-water partition coefficient (K_{sw}) errors. 24 solvent-water systems and 3095 data points are included.	94
Figure C-8	Hexbin two dimensional histogram plot ² of predicted versus observed log wet octanol-water partition coefficients. Solid lines show perfect agreement. Dashed lines represent ± 1 order of magnitude.	95
Figure C-9	Hexbin two dimensional histogram plot ² of predicted versus observed log tetrachloromethane-water partition coefficients. Solid lines show perfect agreement. Dashed lines represent ± 1 order of magnitude.	95
Figure C-10	Hexbin two dimensional histogram plot ² of predicted versus observed log tetrahydrofuran-water partition coefficients. Solid lines show perfect agreement. Dashed lines represent ± 1 order of magnitude.	96
Figure C-11	Hexbin two dimensional histogram plot ² of predicted versus observed log toluene-water partition coefficients. Solid lines show perfect agreement. Dashed lines represent ± 1 order of magnitude.	96
Figure C-12	Hexbin two dimensional histogram plot ² of predicted versus observed log 1-butanol-water partition coefficients. Solid lines show perfect agreement. Dashed lines represent ± 1 order of magnitude.	97
Figure C-13	Hexbin two dimensional histogram plot ² of predicted versus observed log 1-pentanol-water partition coefficients. Solid lines show perfect agreement. Dashed lines represent ± 1 order of magnitude.	97
Figure C-14	Hexbin two dimensional histogram plot ² of predicted versus observed log 1-propanol-water partition coefficients. Solid lines show perfect agreement. Dashed lines represent ± 1 order of magnitude.	98
Figure C-15	Hexbin two dimensional histogram plot ² of predicted versus observed log bromobenzene-water partition coefficients. Solid lines show perfect agreement. Dashed lines represent ± 1 order of magnitude.	98
Figure C-16	Hexbin two dimensional histogram plot ² of predicted versus observed log chlorobenzene-water partition coefficients. Solid lines show perfect agreement. Dashed lines represent ± 1 order of magnitude.	99
Figure C-17	Hexbin two dimensional histogram plot ² of predicted versus observed log chlorobutane-water partition coefficients. Solid lines show perfect agreement. Dashed lines represent ± 1 order of magnitude.	99
Figure C-18	Hexbin two dimensional histogram plot ² of predicted versus observed log chloroform-water partition coefficients. Solid lines show perfect agreement. Dashed lines represent ± 1 order of magnitude.	100

Figure C-19	Hexbin two dimensional histogram plot ² of predicted versus observed log cyclohexane-water partition coefficients. Solid lines show perfect agreement. Dashed lines represent ± 1 order of magnitude.	100
Figure C-20	Hexbin two dimensional histogram plot ² of predicted versus observed log decane-water partition coefficients. Solid lines show perfect agreement. Dashed lines represent ± 1 order of magnitude.	101
Figure C-21	Hexbin two dimensional histogram plot ² of predicted versus observed log dimethylacetamide-water partition coefficients. Solid lines show perfect agreement. Dashed lines represent ± 1 order of magnitude.....	101
Figure C-22	Hexbin two dimensional histogram plot ² of predicted versus observed log dimethylformamide-water partition coefficients. Solid lines show perfect agreement. Dashed lines represent ± 1 order of magnitude.....	102
Figure C-23	Hexbin two dimensional histogram plot ² of predicted versus observed log dioxane-water partition coefficients. Solid lines show perfect agreement. Dashed lines represent ± 1 order of magnitude.	102
Figure C-24	Hexbin two dimensional histogram plot ² of predicted versus observed log ethanol-water partition coefficients. Solid lines show perfect agreement. Dashed lines represent ± 1 order of magnitude.	103
Figure C-25	Hexbin two dimensional histogram plot ² of predicted versus observed log ethyl acetate-water partition coefficients. Solid lines show perfect agreement. Dashed lines represent ± 1 order of magnitude.	103
Figure C-26	Hexbin two dimensional histogram plot ² of predicted versus observed log heptane-water partition coefficients. Solid lines show perfect agreement. Dashed lines represent ± 1 order of magnitude.	104
Figure C-27	Hexbin two dimensional histogram plot ² of predicted versus observed log hexadecane-water partition coefficients. Solid lines show perfect agreement. Dashed lines represent ± 1 order of magnitude.	104
Figure C-28	Hexbin two dimensional histogram plot ² of predicted versus observed log hexane-water partition coefficients. Solid lines show perfect agreement. Dashed lines represent ± 1 order of magnitude.	105
Figure C-29	Hexbin two dimensional histogram plot ² of predicted versus observed log methanol-water partition coefficients. Solid lines show perfect agreement. Dashed lines represent ± 1 order of magnitude.	105
Figure C-30	Hexbin two dimensional histogram plot ² of predicted versus observed log octane-water partition coefficients. Solid lines show perfect agreement. Dashed lines represent ± 1 order of magnitude.	106

- Figure C-31 Hexbin two dimensional histogram plot² of predicted versus observed log propanone-water partition coefficients. Solid lines show perfect agreement. Dashed lines represent ± 1 order of magnitude.106
- Figure C-32 Hexbin two dimensional histogram plots² presenting residuals (= predicted log K_{ow} – observed log K_{ow}) of wet octanol-water partition coefficients versus E , S , A , B , V of QCAP parameters.107
- Figure 4-1 Dot plot presenting the root mean square errors (RMSEs) of the residuals (log predicted - log observed partition coefficients) for solvent-water systems. Panel (1) compares predictions of original model and refitted model with QCAP. Panel (2) compares predictions of original model and refitted model with ABSOLV. For each panel, the solvents listed on the left axis are ordered from the smallest to the largest RMSE of the refitted model, and the right axis presents N = number of solutes in each system. RMSE values are available in Table D-4 in Appendix D.115
- Figure 4-2 Dot plot presenting the root mean square errors (RMSEs) of the residuals (log predicted - log observed partition coefficients) for predictions of solvent-water partition coefficients. Predictions by four models are compared: original model with ABSOLV, original model with QCAP, refitted model with ABSOLV, and refitted model with QCAP. The solvents listed on the left axis are ordered from the smallest to the largest RMSE of refitted model with QCAP. The right axis presents N = number of solutes in each system. RMSE values are available in Table D-4 in Appendix D.116
- Figure 4-3 Dot plot presenting prediction errors (predicted log K_{sw} – observed log K_{sw}) for prediction of solvent-water partition coefficients for munition constituents and munition-like compounds listed on the right axis. On the left axis is listed the the corresponding partitioning systems: wet octanol-water, toluene-water, hexane-water, and chloroform water. Predictions by four models are compared: original model with ABSOLV, original model with QCAP, refitted model with ABSOLV, and refitted model with QCAP. Experimental and predicted log K_{sw} as well as ABSOLV and QCAP solute parameters are available in Table D-5 in Appendix D.117
- Figure 4-4 Crossplot comparing the predicted versus experimental log K_{cw} . Predictions by four models are compared: (1) original model with ABSOLV, (2) original model with QCAP, (3) refitted model with ABSOLV, and (4) refitted model with QCAP. Solid lines show perfect agreement. Dashed lines represent ± 1 order of magnitude.119

- Figure E-1 Pairs plot³ of QCAP solute parameters. The lower triangular panels are hexbin two dimensional histogram plots². For each data plot, x axis label is the parameter above the plot, y axis label is to the right of the plot. Solid lines show perfect agreement. The upper triangular panels display the coefficient of determination (R^2) and the scaling of the respective pair. For each R^2 panel, x axis label is the parameter below the plot, y axis label is to the left of the plot. 127
- Figure E-2 Pairs plot³ of Adjusted QCAP solute parameters. The lower triangular panels are hexbin two dimensional histogram plots². For each data plot, x axis label is the parameter above the plot, y axis label is to the right of the plot. Solid lines show perfect agreement. The upper triangular panels display the coefficient of determination (R^2) and the scaling of the respective pair. For each R^2 panel, x axis label is the parameter below the plot, y axis label is to the left of the plot. 128
- Figure E-3 Comparison of standard errors of regression coefficients for fitting using QCAP and Adjusted QCAP..... 129
- Figure E-4 Regression coefficients for fitting using QCAP and Adjusted QCAP. . 130
- Figure 5-1 Results from published uptake studies (Tables F-1 and F-2): (A) MCs concentrations in plants on the last day of exposure (C_{Plant}), and (B) bioconcentration factors expressed relative to concentrations in soil solids ($\text{BCF}_{\text{Solids}}$) as $\text{kg}_{\text{dwt soil}} (\text{kg}_{\text{dwt plant}})^{-1}$. C_{Soil} : Concentration in soil at the beginning of exposure. Circles' size proportional to the exposure duration. Data presented for the whole plant or only for the aboveground plant parts when available. TNT* = TNT or TNT degradation products; TNT is reported as not detected in plant tissues in some sources..... 135
- Figure 5-2 Exposure concentrations over time for MCs and MLCs in bioconcentration uptake assays with barley. Legend: Solution added is the aqueous solution sampled just before being loaded into plant pots; Treatment are samples from displaced solutions of pots exposed to MCs or MLCs; first and last fraction of displaced solution refer to the first and last pore volume replenished daily; Control are samples from displaced solutions of untreated plant pots (not exposed to MCs or MLCs). Displaying 2nd trial for 2,4-DNAN and 1st trial for 4-NAN. Data presented as means and error bars represent the range. Sample size ≥ 2 pots (Table F-11). If not visible, error bars are smaller than the symbol. 142

Figure 5-3	Logarithmic ratios of concentration in the plant to concentration in the interstitial water $\log C_i \text{Plant} / C_i \text{IW}$ versus time of exposure for MCs and MLCs in bioconcentration uptake assays with barley. <i>CiPlant</i> : concentration of compound <i>i</i> in barley ($\text{mg kg}_{\text{dwt}}^{-1}$), <i>CiIW</i> : concentration of compound <i>i</i> in the interstitial water – displaced solution (mg L^{-1}). BCF: steady state bioconcentration factor ($\text{L kg}_{\text{dwt}}^{-1}$). Trials refer to repetitions of a particular uptake assay. Data presented as means \pm standard error of the mean (SEM). Sample size ≥ 2 pots (Table F-11). If not visible, error bars smaller than the symbol.....	144
Figure 5-4	Plant–water partition coefficients (K_{PW}) for MCs and MLCs with barley and their respective octanol–water partition coefficients (K_{OW}). Data ordered by K_{PW} . K_{OW} values are experimental data obtained from EPI Suite database ⁵³ for all compounds except 2,4-DNAN that is reported by Hawari et al. ⁵⁴ and 2,5-DM-4-NANE that is an estimate from EPI Suite ⁵³ in absence of an experimental value. Box width proportional to the square–root of the number of observations in the group (Table F-14).....	146
Figure 5-5	Comparison between uptake (as measured by BCF, Figure 5-3) and plant–water partition coefficient (K_{PW} , Figure 5-4) for MCs and MLCs. Compounds ordered from small to larger discrepancy between $\log K_{\text{PW}}$ and $\log \text{BCF}$. Box width proportional to the square–root of the number of observations in the group.	147
Figure F-1	Growth of barley (unexposed to MCs or MLCs) in three different solid media over a period of 21 days. Data presented as the ratios of the average shoot height of plants grown in either sand or sand–Matapeake soil relative to that of those growing in only Matapeake soil. Horizontal dotted line is a visual reference at ratio = 1.....	168
Figure F-2	Barley shoot and root lengths versus measured exposure concentrations of MCs and MLCs. Vertical dotted line shows nominal concentration chosen to perform bioconcentration uptake assays (10 mg L^{-1}). Data presented as means \pm standard error of the mean (SEM). Sample size ≥ 2 pots (Table F-5). Dashed colored lines are visual guides for data trends. If not visible, error bars are smaller than the symbol.....	196
Figure F-3	Biomass profiles (shoot height) for barley exposed to individual munitions compounds (MCs) or munitions-like compounds (MLCs) at increasing concentration of solution added (nominal: Control, 1, 10, 50, and 100 mg L^{-1}) during toxicity screening. Data presented as means \pm standard error of the mean (SEM). If not visible, error bars are smaller than the symbol.	199

- Figure F-4 Exposure concentrations over time for MCs and MLCs in toxicity screening with barley at five concentrations of solution added (nominal: Control, 1, 10, 50, and 100 mg L⁻¹). Legend: Solution added is the solution sampled just before being loaded into plant pots; Treatment are samples from displaced solutions of pots exposed to MCs or MLCs; first and last fraction of displaced solution refer to the first and last pore volume replenished daily; Control are samples from displaced solutions of untreated plant pots (not exposed to MCs or MLCs). Data presented as means and error bars represent the range.200
- Figure F-5 Concentrations in displaced solutions collected at the end of each consecutive pore volume (pv, 100 mL per pv) on the first day of exposure to MCs and MLCs for selected chemicals during toxicity screening with barley. Solution added: Aqueous solution containing TNT or 4-NAN and being loaded to plant pots. Replicates: Plant pots subjected to the same solution added. Difference in TNT concentration between solution added and displaced solution collected from 4th pore volume were not statistically significant (p-value = 0.80).202
- Figure F-6 Biomass profiles (shoot height) for barley exposed to individual MCs, or MLCs, during bioconcentration uptake assays. Legend: Treatment are plant pots exposed to MCs or MLCs at a nominal concentration of 10 mg L⁻¹; Control are untreated plant pots (not exposed to MCs or MLCs). Displaying 2nd trial for 2,4-DNAN and 1st trial for 4-NAN. Data presented as means \pm standard error of the mean (SEM). Sample size \geq 2 pots (Table F-11).210
- Figure F-7 Concentration in the plant (*CiPlantt*) over time and estimated degradation rates ($k_{\text{degradation}}$) for MCs. An exponential decay model fitted to time course data obtained from Sunahara ³ and Dodard et al. ⁹ (Table F-15).219
- Figure F-8 Comparison between the ratios of plant–water partitioning to uptake $KPWBC$ and estimated degradation/transformation rates ($k_{\text{degradation}}$) for MCs....220
- Figure 6-1 Schematic diagram of the basis for the modeling approach: Equilibrium partitioning. Left–right arrows indicate partitioning of MC (or MLC) i between two phases. $KiOC$ = soil organic carbon–water partition coefficient of MC i (L_{water} kg_{OC}⁻¹), $Kiroot$ = root–water partition coefficient of MC i (L_{water} kg_{root}⁻¹), and $KiCut$ = plant cuticle–water partition coefficient of MC i (L_{water} kg_{cuticle}⁻¹).225

- Figure 6-2 pp-LFER-predicted K_{Cut} versus observed K_{Cut} for organic compounds (Table G-5 and Table G-7 to Table G-9). Predictions made using the pp-LFER model from Platts and Abraham ⁹, Eq. (6-2), for the full K_{Cut} dataset collected from the literature. Solute descriptors, uppercase letters for Eq. (6-2), are: (A) Absolv-AP ⁵⁷; (B) Exp-AP from either Liang et al. ⁵⁸ or the UFZ-LSER database ⁵⁹, and Absolv-AP when Exp-AP were not available; and (C) Adjusted QCAP ⁶⁰. RMSE: root mean square error of prediction (log predicted - log observed) for all compounds included in the full K_{Cut} dataset (Table G-5). The RMSEs for only MCs and MLCs were = (A) 3.154; (B) 0.544; and (C) 0.507. The solid line indicates the best agreement (unity), dashed lines are spaced at 1 log unit from unity.232
- Figure 6-3 pp-LFER-fitted K_{Cut} versus observed K_{Cut} for organic compounds (Table G-5, Table G-7, Table G-8, and Table G-10). Calculations made using the general pp-LFER, Eq. (6-1), fitted to the full K_{Cut} dataset collected from the literature. Solute descriptors, uppercase letters for Eq. (6-1), are: (A) Absolv-AP ⁵⁷; (B) Exp-AP from either Liang et al. ⁵⁸ or the UFZ-LSER database ⁵⁹, and Absolv-AP when Exp-AP were not available; and (C) QCAP ⁶⁰. RMSE: root mean square error of prediction (log fitted - log observed) for all compounds included in the full K_{Cut} dataset (Table G-5). The RMSEs for only MCs and MLCs were = (A) 1.261; (B) 0.478; and (C) 0.421. The solid line indicates the best agreement (unity), dashed lines are spaced at 1 log unit from unity.234
- Figure 6-4 Predicted concentrations in the plant versus observed values from published uptake studies (Table 6-2, Table G-13, and Table G-17). Color coding assigned based on: (A) MCs and MLCs (Table 6-1), (B) growth medium, and (C) plant species. Unfilled symbols indicate that the predicted concentration in the interstitial water (using Eq. (6-6)) was replaced by the corresponding MC aqueous solubility as the predicted concentration in the interstitial water exceeded solubility limits. The border color for the unfilled symbols corresponds to the color identification in each panel legend. Root mean square error of prediction (log predicted - log observed), excluding predictions bounded at aqueous solubility, RMSE = 0.429. The solid line indicates the best agreement (unity), dashed lines are spaced at 1 log unit from unity.237
- Figure G-1 Schematic diagram for the advective and diffusive transport of MCs and MLCs between soil and water. Q_{in} = inward flow moving along the plant xylem; Q_{out} = outward flow moving along the plant phloem; ϵ_{diff} = diffusive exchange.252
- Figure G-2 Predicted soil organic carbon-water partition coefficients (K_{oc}) versus observed K_{oc} from published partitioning studies (Table G-3). Predicted K_{oc} were calculated with pp-LFER from: (A) Kipka and Di Toro ⁸ (Eq. (6-3)), (B) Nguyen et al. ⁶ (Eq. (G-3)), and (C) Poole and Poole ⁷ (Eq. (G-4)). RMSE: Root mean square error of prediction (log predicted - log observed). The solid line indicates the best agreement (unity), dashed lines are spaced at 1 log unit from unity.255

- Figure G-3 Predicted soil organic carbon–water partition coefficients (K_{oc}) versus MC–averaged observed K_{oc} from published partitioning studies (Table G-3). Predicted K_{oc} were calculated with pp–LFER from: (A) Kipka and Di Toro ⁸ (Eq. (6-3)), (B) Nguyen et al. ⁶ (Eq. (G-3)), and (C) Poole and Poole ⁷ (Eq. (G-4)). RMSE: Root mean square error of prediction (log predicted - log observed). Error bars represent the standard error of the mean (SEM). The solid line indicates the best agreement (unity), dashed lines are spaced at 1 log unit from unity.256
- Figure G-4 Predicted concentrations in the plant versus observed values from published uptake studies including the contribution from carbohydrates and cuticle (Eq. (G-6)) (Table G-21). Color coding assigned based on: (A) MCs and MLCs (Table G-1), (B) growth medium, and (C) plant species. Unfilled symbols indicate that the predicted concentration in the interstitial water (using Eq. (6-6)) is substituted for the corresponding MC aqueous solubility since the predicted concentration in the interstitial water exceeds solubility. See main text for further details. The border color for the unfilled symbols corresponds to the color identification in each panel legend. Root mean square error of prediction (log predicted - log observed), excluding predictions bounded at aqueous solubility, RMSE = 0.431. The solid line indicates the best agreement (unity), dashed lines are spaced at 1 log unit from unity.268
- Figure 7-1 Fitted versus observed BCFs for organic compounds (Table H-6). Regression made using a BCF model (Eq. (7-10)) with partitioning to three worm components, lipid (Eq. (7-11)), protein (Eq. (7-6)), and internal water. Color coding assigned based on: (A) organic compound, (B) exposure medium, and (C) oligochaete species. Root mean square error of estimation (log estimated - log observed BCF), RMSE = 0.499. Abbreviations defined in Table H-2. The solid line indicates the best agreement (unity), dashed lines are spaced at 1 log unit from unity.282
- Figure 7-2 Estimated versus observed BCFs for organic compounds (Table H-6). Estimations made using a partitioning–based BCF model (Eq. (7-3)) with the K_{Lipid} pp–LFER from: (A) this work (Eq. (7-11)), and (B) Kuo and Di Toro ^{30,33} (Eq. (7-5)). Legend: Chemical class with corresponding count; PAH: polycyclic aromatic hydrocarbon. RMSE: Root mean square error of estimation (log estimated - log observed BCF). The solid line indicates the best agreement (unity), dashed lines are spaced at 1 log unit from unity.284
- Figure 7-3 Contribution of worm components (lipid, protein and internal water) to the fitted BCF (Eq. (7-3)) for MCs, MLCs, and other chemical classes in the oligochaete dataset presented in Figure 7-1. Estimation of partitioning to lipid component made using K_{Lipid} pp–LFER from this work (Eq. (7-11)), and to protein component using $K_{Protein}$ pp–LFER from Kuo and Di Toro ^{30,33} (Eq. (7-6)). Numbers in parenthesis are the corresponding count. Abbreviations are defined in Table H-2.286

- Figure 7-4 Contribution from solute–solvent products (χX , Eq. (7-4)) to the estimated $\log K_{\text{Lipid}}$ (Eq. (7-11)) and $\log K_{\text{Protein}}$ (Eq. (7-6)) for MCs, MLCs, and other chemical classes in the oligochaete BCF dataset presented in Figure 7-1.289
- Figure 7-5 Predicted versus observed concentrations of MCs in oligochaetes from independent studies. Predictions made using a partitioning–based model (Eq. (7-12)) with the K_{Lipid} pp–LFER from (A) this work (Eq. (7-11)) or (B) Kuo and Di Toro ^{30,33} (Eq. (7-5)). Unfilled symbols represent predictions made with concentrations in the interstitial water at aqueous solubility. RMSE: Root mean square error ($\log \text{predicted} - \log \text{observed concentration in worm}$), excluding predictions at aqueous solubility. The solid line indicates the best agreement (unity), dashed lines are spaced at 1 log unit from unity.292

LIST OF ACRONYMS

1,2,3,4-TCB	1,2,3,4-tetrachlorobenzene
1,2,3,4-TCN	1,2,3,4-tetrachloronaphthalene
1,2,3-TCB	1,2,3-trichlorobenzene
1,3,5-TCB	1,3,5-trichlorobenzene
2,3,4,5,6-PCT	2,3,4,5,6-pentachlorotoluene
2,4-DNAN	1-Methoxy-2,4-dinitrobenzene
2-A-4-NAN	2-Amino-4-Nitroanisole
2-M-5-NPYNE	2-Methoxy-5-nitropyridine
3,5-DN-o-TAME	3,5-Dinitro-o-toluamide
4-NAN	4-Nitroanisole
B[a]A	benzo[a]anthracene
HCB	hexachlorobenzene
HCBT	hexachlorobutadiene
PChB	pentachlorobenzene
α -HCH	α -hexachlorocyclohexane
γ -HCH	γ -hexachlorocyclohexane
2,4-DNAN	2,4-dinitroanisole
2,4-DNT	2,4-dinitrotoluene
2,5-DM-4-NANE	2,5-dimethoxy-4-nitroaniline
2-M-5-NPYNE	2-methoxy-5-nitropyridine
ABSOLV	http://www.acdlabs.com/products/percepta/predictors/absolv/
ADF	Amsterdam Density Functional quantum mechanics package
AdjustedQCAP	Abraham parameters for use in existing Abraham models.
AP	Abraham Parameter
BAA	Broad Agency Announcement
BAF	Bioaccumulation Factor
BCF	Bioconcentration Factor
BSAF	Biota Sediment Accumulation Factor
CM	cuticular membranes
COSMOments	Moments of the sigma profile of a molecule
COSMO-RS	COnductor like Screening MOdel for Real Solvents
COSMO-SAC	COnductor-like Screening Model for Segment Activity Coefficient
DCM	dichloromethane
DFT	Density Functional Theory
DNX	hexahydro-1,3-dinitroso-5-nitro-1,3,5-triazine
DOC	Dissolved Organic Carbon
EqP	Equilibrium Partitioning
f_{Clay}	fraction clay

f_{Lipid}	fraction lipid
$f_{Protein}$	fraction protein
f_{Water}	fraction water
HL	Half Life
HMX	octahydro-1,3,5,7-tetranitro-1,3,5,7-tetrazocine
HPLC	high-performance liquid chromatography
IW	Interstitial Water
K_{Cut}	Plant-cuticle water partition coefficient
K_{cw}	trichloromethane-water partition coefficient
K_{dw}	dichloromethane-water partition coefficient
K_{hw}	hexane-water partition coefficient
K_{lipidw}	Lipid-water partition coefficient
K_{OC}	Soil Organic Carbon - Water Partition coefficient (L/kg Organic Carbon)
K_P	Partition Coefficient
K_{protw}	Protein water partition coefficient
K_{PW}	Plant water partition coefficient
K_{sw}	Solvent-water partition coefficient
K_{wa}	Water air partition coefficient
LFER	Linear Free Energy Relationship
MC	Munitions Component
MLC	Munitions Like Component
MLR	Multiple Linear Regression
MLRA	Multiple Linear Regression Analysis
MNX	hexahydro-1-nitroso-3,5-dinitro-1,3,5-triazine
MW	Molecular Weight
MX	Cuticle matrices
NQ	Nitroguanidine
OC	Organic Carbon
PAH	Polycyclic Aromatic Hydrocarbons
PGDP	propylene glycol dipelagronate
POC	Particulate Organic Carbon
pp-LFER	Polyparameter Linear Free Energy Relationship
PSD	Predicted standard deviation
QCAP	Quantum Chemical Abraham Parameter
QM	Quantum Mechanics
QSAR	Quantitative Structure-Activity Relationships
RDX	hexahydro-1,3,5-trinitro-1,3,5-triazine
RMSE	Root Mean Square Error

SERDP	Strategic Environmental Research and Development Program
SI	Supplemental Information
SON	Statement of Need
Std.Dev	Standard Deviation
TCM	Trichloromethane
TNB	1,3,5-trinitrobenzene
TNT	2,4,6-trinitrotoluene
TNX	hexahydro-1,3,5-trinitroso-1,3,5-triazine
TSCA	EPA's Toxic Substances Control Act
UFZ-LSER	Helmholtz Centre for Environmental Research-UFZ: Leipzig, Germany

KEYWORDS

Quantum Chemistry Solvation Model; COSMO-SAC; Abraham Polyparameter Linear Free Energy Relationship; pp-LFER; Fish Bioconcentration Model; Bioaccumulation Model; Grass Barley *Hordeum*; BCF; Organic Carbon; Cuticle; Oligochaete; *Eisenia*; Quantum Chemical Abraham Parameters; QCAP; ABSOLV; Solvent Water Partition Coefficient; Clausius Mossotti Equation; Molecular Polarization; Hydrogen Bonding.

ACKNOWLEDGEMENTS

The Principal Investigator would particularly like to thank Dave Ta Fu Kuo, Tiffany L. Torralba-Sanchez and Yuzhen Liang for their assistance in preparation of this report. Substantial portions were based on the PhD dissertations of Tiffany L. Torralba-Sanchez and Yuzhen Liang. Several undergraduate and graduate students and technicians at the University of Delaware contributed to the projects. We would particularly like to acknowledge Olga Dmytrenko, Craig Warren Davis, and PhD candidates; Kathleen Boone and Kevin Hickey for their contributions to this project.

ABSTRACT

Objectives

The project objectives as stated in the statement of need (SON) are to (1) Improve methods for the prediction of physical properties relevant for assessing environmental fate and transport, and (2) Develop predictive models to assess the bioaccumulation of the chemical in relevant environmental receptors (plants, and soil invertebrates). The models will be used to assess the environmental impact of new munitions compounds. Models that fulfill these objectives have been developed in this project as described below.

Technical Approach

The models are designed to predict the equilibrium steady state concentration of munitions compounds in terrestrial plants and soil invertebrates exposed via the soil. The models assume that the phases in the soil are in equilibrium with the phases in the organism which contain the accumulated munitions compound.

The schematic to the right illustrates the

framework. The arrows represent partitioning equilibrium between the phases and the partition coefficients associated with each arrow are the parameters that are required to estimate the contaminant concentration in the organism that results from exposure to the contaminated soil.

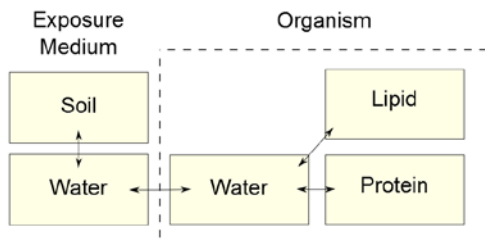
The Abraham polyparameter model is used to estimate the partition coefficients between the phases and water. The partition coefficient, K_P , is the ratio of concentrations of a solute in the system phases, for example, the ratio of a munitions component concentration in soil organic carbon to the concentration in water. The model specifies the dependence of K_P on the chemical properties of the solute and the system phases. The equation is

$$\text{Log } K_P = c + eE + sS + aA + bB + vV$$

The upper case variables are the Abraham solute parameters and the lower case variables are the system phase Abraham parameters. Each pair quantifies the chemical interaction between the solute and the system phases. For example aA quantifies the strength of the hydrogen bond between the solute hydrogen bond donation, A , and system pair hydrogen bond acceptance, a . Both sets of upper case and lower case parameters are required to make the estimate.

Quantum chemical methods have been developed to estimate the upper case Abraham solute parameters. They rely solely on the molecular structure of the solute. The lower case Abraham system parameters are estimated by fitting the above equation to data sets of experimentally determined partition coefficients for many solutes. This also requires the Abraham solute parameters.

The available databases for the bioconcentration factor (BCF = concentration of chemical in organism / concentration of chemical in water) in fish, plants, and soil invertebrates have been used to build the models. In addition the BCFs for a soil invertebrate (oligochaete *Eisenia Andrei*) and a plant (barley *Hordeum vulgare* L) for munitions components and analog chemicals have been measured and added to the databases. This was necessary in order to expand the chemical space to include munitions compounds that are not represented in the extent data bases.



Results

A methodology has been developed using quantum chemical computations to estimate Abraham solute parameters for two types of applications: for use with presently existing Abraham models, or for use in building new Abraham models. In both cases the solute parameters have a smaller error than all other available estimation methods. This is the case for non-munitions component and for munition components for which parameters were experimentally determined for the comparisons.

Bioaccumulation models for plants (grasses) and soil invertebrates (oligochaetes) that are exposed from compounds in soils have been developed as well as a bioconcentration model for fish exposed from compounds in water. The three models require partition coefficients for which models have also been developed: partitioning between water and organism lipid, organism protein, and plant cuticle, and a previously developed model for water-soil organic carbon. The number of observations in the data sets are: oligochaetes (57), protein (69) grasses (191), lipids (248), soil organic carbon (444) and fish (601).

The performance of the models is gauged using the root mean square error of the residuals: the difference between \log_{10} modeled and \log_{10} observed of either partition coefficients or concentration, which is equal to \log_{10} of the ratio: model/observed. It is approximately equal to 0.40 for all the models, corresponding to approximately 80% of the residuals between 1/3 and 3 and approximately 90% of the residuals between 1/5 and 5.

Benefits

The models can be used in a number of ways, in particular for the stated objective of the SON: to assess the environmental impact of new munitions compounds. All that is required to make estimates of the extent of bioaccumulation for grasses, oligochaetes and fish is the molecular structure of the compound. In addition the physical chemical parameters: octanol-water and air-water (Henry's Law constant) partition coefficients and aqueous solubility can also be estimated. Both the physical chemical and environmental partition coefficients are not as accurate as experimental determinations. However they are sufficiently quantitative for a number of tasks, for example to rank a sequence of proposed new munitions compounds to bioaccumulate in organisms, or to establish that the risk is either low enough so that no further experimental information is necessary, or, conversely that the risk is estimated to be high enough so that further investigation is required if the compound is to move forward. This ability to determine the potential extent of environmental risk for new munitions compounds is the most immediate benefit from using the models developed in this project.

Chapter 1

OBJECTIVES AND BACKGROUND

1.1 Overall Objective

The Strategic Environmental Research and Development Program (SERDP) identified a research need under the 2008 Broad Agency Announcement (BAA) ERSON-10-01 entitled "Predictive Techniques For Assessment of the Environmental Impact of New Munition Compounds." Our project addressed the following objectives of this statement of need (SON)

- Improve methods for the prediction of physical properties relevant for assessing environmental fate and transport.
- Develop predictive models to assess the bioaccumulation of the chemical in relevant environmental receptors (fish, plants, and soil invertebrate).

"Proposers should clearly show how the proposed research effort builds on past and ongoing efforts to assess the environmental impact of new munitions compounds."

The overall project objective is the development of models for predicting the physical chemical properties and the partition coefficients to assess the bioaccumulation of new munitions compounds into soil organisms and plants. Figure 1-1 illustrates the problem addressed: Estimating the partitioning between water and pure phases on the left, and between water and environmental phases on the right. Environmental partition coefficients are required as they form the basis of the models that have been constructed. Figure 1-2 illustrates the general modeling framework that has been applied to predict the concentration of a chemical in the organisms that results from exposure to the chemical in soil.

The soil soil-water system is assumed to be at steady state equilibrium. The organism components that accumulate the chemical are also assumed to be at steady state equilibrium.

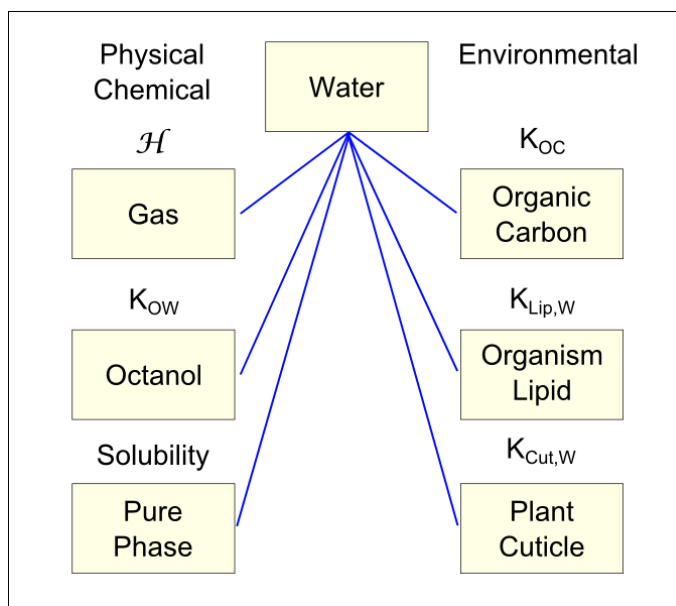


Figure 1-1 Problem framework. Estimating the physical-chemical and environmental partition coefficients between water and the interacting phases.

Finally the organism system and soil soil-water system are also assumed to be at steady state equilibrium. That is, the entire system is at an equilibrium state. The arrows in the schematic represent partition coefficients that quantify the concentration ratio between the concentration in each phase and water. For example, the partition coefficient between soil organic carbon and water is K_{OC} . These are the partition coefficients illustrated in Figure 1-1.

To obtain the partition coefficients, a methodology is required that can deal with the two requirements in the SON: (i) Estimating the partition coefficients between both types of phases. The essential difference is that the molecular structures are known for the pure phases (e.g. octanol) and are unknown for the environmental phases, e.g. soil organic carbon. Soil organic carbon, organism lipid, and plant cuticle are complex mixtures of chemicals for which only general properties are known. (ii) The SON requires that the models be applicable for “new munitions compounds.” Therefore the parameters in the bioaccumulation modeling framework can be estimated using only the chemical’s molecular structure.

Quantum chemical methods have been chosen to estimate the necessary model parameters. The large extent databases for bioconcentration factor ($BCF = \text{concentration of chemical in organism} / \text{concentration of chemical in water}$) in fish, plants, and soil invertebrates have been used to build the models. In addition the BCFs for a soil invertebrate (oligochaete *Eisenia Andrei*) and a plant (barley *Hordeum vulgare* L) for munitions components and analog chemicals have been measured and added to the databases.

Initially it was proposed to use the currently available quantum chemical solvation models to make the estimates for the physical-chemical partition coefficients and to develop Abraham polyparameter models for the environmental partition coefficients. Since the environmental partition coefficients are the more difficult problem, a quantum chemically based method was used to estimate the required Abraham Parameter (AP) solute descriptors. The result is a new method – QCAP (Quantum Chemical Abraham Parameters) – that provides the most accurate AP estimates available to date. In addition, these solute parameters can be used to estimate the physical-chemical partition coefficients to an accuracy that exceeds that using the quantum chemical solvation models. Therefore, both aims of the project are met using QCAP for the chemical parameters and either existing models for the physical-chemical parameters or the newly developed BCF models for plants and soil invertebrates.

1.2 Abraham Polyparameter Model

The Abraham polyparameter model has been the basis for models of many environmentally important parameters. Table 1-1 presents a list of available models. The model relates a partition coefficient, K_P , typically the ratio of concentrations of a solute, e.g. a

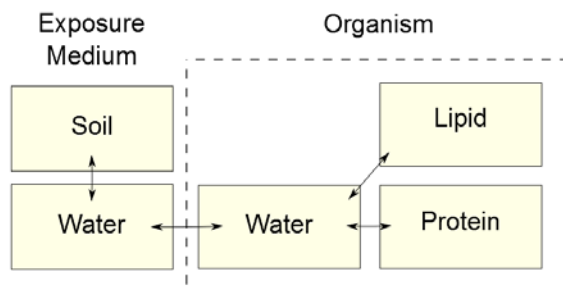


Figure 1-2 Modeling framework for the predictive model of bioaccumulation between soil and soil exposed organisms. The soil-water and organism components are assumed to be at steady state equilibrium. The arrows represent the partition coefficients illustrated in Figure 1-1.

munitions component, in two phases, e.g. soil organic carbon and water, to the chemical properties of the solute. The equation is

$$\text{Log } K_P = c + eE + sS + aA + bB + vV \quad (1-1)$$

where $K_P = C_{\text{Phase}} / C_{\text{Water}}$. The upper case variables are the solute parameters, and the lower case variables are the solvent-water system parameters. The product terms represent the following chemical interactions between the solute and solvent pair: eE = molecular polarizability resulting in van der Waals attraction; sS = dipole/induced dipole attraction due to electrostatic interactions; aA and bB quantify hydrogen bond donation and acceptance interactions; and vV = quantifies the energy difference required to form cavities in the solvent pair for the solute. c is the regression constant that carries the units. The lower case parameters are specific to the partition coefficient K_P being modeled, e.g. the soil organic carbon-water partition coefficient, $K_P = K_{OC}$. The upper case parameters are solute specific, e.g. a munitions component such as RDX.

To use an existing model, the solute parameters in Eq. (1-1): E, S, A, B, V are required. To develop a new model for a specific partition coefficient, e.g. the ratio of an oligochaete body burden to soil water concentrations, a data set of measured partition coefficients K_P is required as well as the solute parameters E, S, A, B, V for the compounds in the data set. The solvent pair parameters: c, e, a, b, v are estimated using by fitting Eq. (1-1) to the K_P data using multiple linear regression. Therefore in order to develop and/or apply a model for a specific compound, the solute parameters E, S, A, B, V for that compound need to be estimated.

Table 1-1 Abraham pp-LFER models.

Partitioning	
Environmental Phase/Water	Biological Phases/Blood
Particulate Organic Carbon	Lung
Dissolved Organic Carbon	Fat
Coal Tar	Kidney
Environmental Phase/Air	Heart
Aerosol	Brain
Diesel Soot	Toxicity/Aquatic Species
Mineral Surfaces	Baseline Narcosis
Water	Polar Narcosis
Water Surface	Toxicity/Mammals
Snow Surface	Water-Skin Permeation
Biological Phases/Water	Eye Irritation
Storage Lipid	Nasal Pungency
Phospholipid Membrane	Resp. Irritation Mice
Serum Albumin	Odor Thresholds
Muscle Protein	

1.2.1 Estimating Abraham Solute Parameters

Estimating solute parameters E , S , A , B , V from experimental data makes use of Eq. (1-1) and relies on the availability of pure solvent-water system parameters c , e , a , b , v . These were estimated initially to quantify the influence of various solvents on the changes in absorbance spectra for various organic compounds. The application of these ideas to estimating solute-solvent interactions came later and was pioneered by Abraham.

Estimating solute parameters for a new compound, for which no experimental partitioning data are available, must rely on only the molecular structure. At the start of this project the only available estimation method that relied on only molecular structure was the commercially available computer program ABSOLV. It relies on a fragment decomposition of the molecular structure and makes estimates of $\log K_P$ by adding or subtracting increments appropriate to each fragment. The range of applicability of this method depends on the chemical space spanned by the compounds used to estimate the fragment constants. Unfortunately the chemicals and data used to estimate the fragment constants are not available for ABSOLV. Therefore there is no way of determining whether the estimates of E , S , A , B , V for a new compound can be relied on.

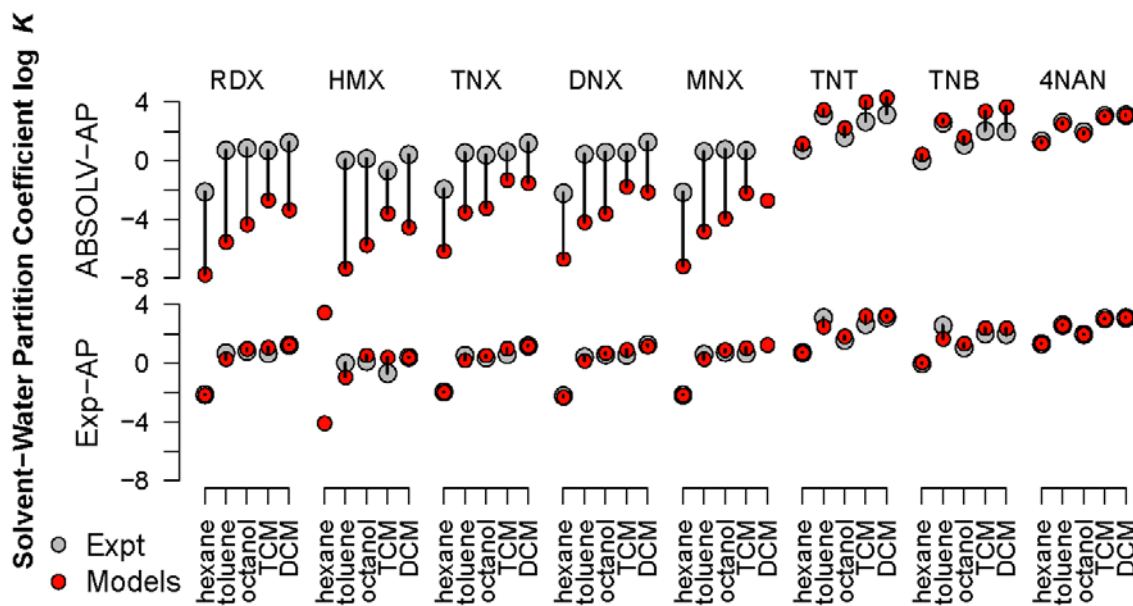


Figure 1-3 Comparison of experimental and model predicted solvent-water partition coefficients: grey symbols are experimental measurements, red symbols are model predictions. Upper row are for model predictions using ABSOLV estimated AP (ABSOLV-AP), lower row are for model predictions using experimentally derived AP (Exp-AP) from this work. The solvents in the solvent-water systems are hexane, toluene, octanol, trichloromethane (TCM), and dichloromethane (DCM). Experimental measurements and model predictions for solvent-water partition coefficients are summarized in Chapter 2 Table A-4.

1.2.2 ABSOLV Estimates of Abraham Solute Parameters for Munitions Compounds

Reliable Abraham solute parameters for the munitions compounds were required in order to build the models being developed for plant and soil invertebrate BCFs. Solvent-water partition coefficients were measured for four munitions and four munition-like compounds and these were used to estimate their Abraham Parameters (AP). The results are shown in Figure 1-3 and compared to the ABSOLV estimates. The experimental details and a more complete presentation are contained in Chapter 2.

The predictions are made using ABSOLV-AP (Figure 1-3 upper row) and experimentally based AP (Exp-AP, Figure 1-3 lower row). Since the experimental measurements are used to estimate Exp-AP, it is not a surprise that the predictions using Exp-AP compare favorably to the measurements. It is the ABSOLV-AP results that are noteworthy. The ABSOLV-AP predictions for nitroaromatics TNT, TNB, and 4NAN are generally in good agreement with experimental measurements. Larger discrepancies are observed for $\log K_{cw}$ and $\log K_{dw}$ of TNT (errors = 1.33 and 1.14 log units respectively), and also for TNB (errors = 1.32 and 1.68 log units respectively). However, errors are much larger for the cyclic nitramines and nitrosamines (RDX, HMX, TNX, DNX, and MNX). The overall RMSE of ABSOLV-AP predictions is up to 3.56 log units. The large discrepancy is probably due to missing -R2N-NO and -R2N-NO₂ functional groups in the ABSOLV fragment database. The accuracy of a fragment model depends on the availability of experimental data for molecules containing the fragment of interest. If the fragment is not in the database, the method fails.

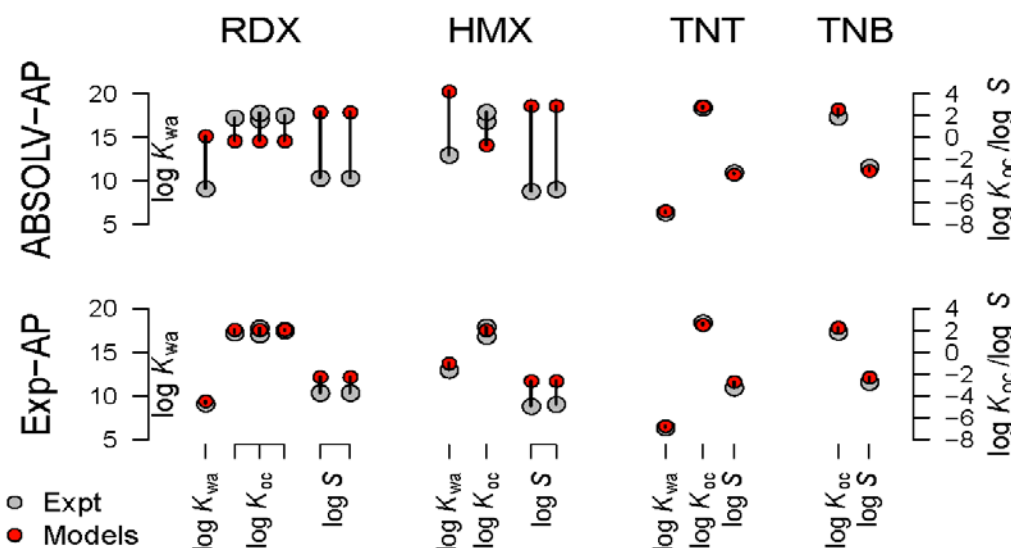


Figure 1-4 Comparisons between experimental measurements and model predictions with ABSOLV estimated (ABSOLV-AP) or experimentally derived (Exp-AP) AP from this work for water-air partition coefficient ($\log K_{wa}$, L air /L water), organic carbon-water partition coefficient ($\log K_{oc}$, L kg⁻¹), and water solubility ($\log S$, mol L⁻¹). $\log K_{wa}$ y-axis on left, $\log K_{oc}$ and $\log S$ y-axis on right. Experimental values from different sources are plotted. Two grey dots per property denote the reported ranges. Experimental measurements and model predictions are summarized in Chapter 2 Table A-6.

Comparisons are made in Figure 1-4 for predicting K_{WA} = Water-Air partition coefficient (the Henry's constant), K_{OC} = Organic Carbon-Water partition coefficient, and S = aqueous solubility. Results are similar to Figure 1-3 with large errors RDX and HMXABSOLV estimates.

1.2.3 Quantum Chemical Estimates of Abraham Solute Parameters for Munitions Compounds

The recommended experimental method for estimating Abraham solute parameters uses measured solvent-water partition coefficients for five solvents: hexane, dichloromethane, trichloromethane, octanol and toluene. E is derived from an estimate of the molar refractivity using a fragment bases estimate. V is the McGowan molecular volume estimate. S , A , and B are estimated using Eq. (1-1) and a multiple linear regression to estimate the three unknowns with E and V as known quantities.

The Quantum Chemical based Abraham Parameter method (QCAP) mirrors the classical experimental method with two important differences. (i) E is estimated from the molecular polarizability of the solute computed using a standard quantum chemical program (Gaussian 09). The Clausius–Mossotti equation relates molecular polarizability to molar refractivity from which E is computed. V is obtained from the same quantum chemical computation. (ii) The measured five solvent-water partition coefficients used in the classical method are replaced by sixty-five estimated solvent-water partition coefficients using the quantum chemical solvation model COSMO-SAC, an open source program developed by a Co-PI on this project. It requires a standard quantum chemical structural optimization, computation of the electron density, which is processed by the COSMO-SAC code to estimate the solvent-water partition coefficient. The use of a large number (65) of solvents compensates for the relatively large prediction error in each individual estimated solvent-water partition coefficient that is characteristic of any quantum chemical solvation model. It is demonstrated (Chapter 2) that the errors produced by COSMO-SAC are not biased so that the error cancelation does in fact take place.

Figure 1-5A compares the root mean square errors for the prediction of experimental solvent-water partition coefficients and the estimates using ABSOLV, QCAP, and Adjusted QCAP solute parameters. The Adjusted QCAP, which are linear combinations of the QCAP, are fit to the experimental AP. They are designed to be used for pp-LFERs that were constructed using experimentally derived solute parameters. The reason that QCAP perform less well is that E is computed using a different method – quantum chemically computed molecular polarizability and the Clausius–Mossotti equation – then the method used for the experimental or ABSOLV estimated parameters. Therefore for pp-LFERs constructed using experimental or ABSOLV estimated parameters the Adjusted QCAP are the appropriate choice. In all cases examined, using the Adjusted QCAP provides the best performance for both predicting solvent-water partition coefficients for conventional (Figure 1-5A) and munitions components (Figure 1-5B).

The situation is reversed when a new pp-LFER is being developed. For this case, the QCAP parameters are the best choice. Figure 1-6 presents the results for (A) refitting the solvent-water partition coefficients for conventional compounds and (B) for munitions compounds. In almost all cases the pp-LFER developed using the QCAP solute parameter performs the best.

In summary, Adjusted QCAP should be used for pp-LFERs for which the system parameters (the lower case parameters in Eq. (1-1)) have been estimated using experimental and/or ABSOLV solute parameters. QCAP should be used for new pp-LFERs for which the system parameters (the lower case parameters in Eq. (1-1)) are estimated using experimental partition coefficients K_P .

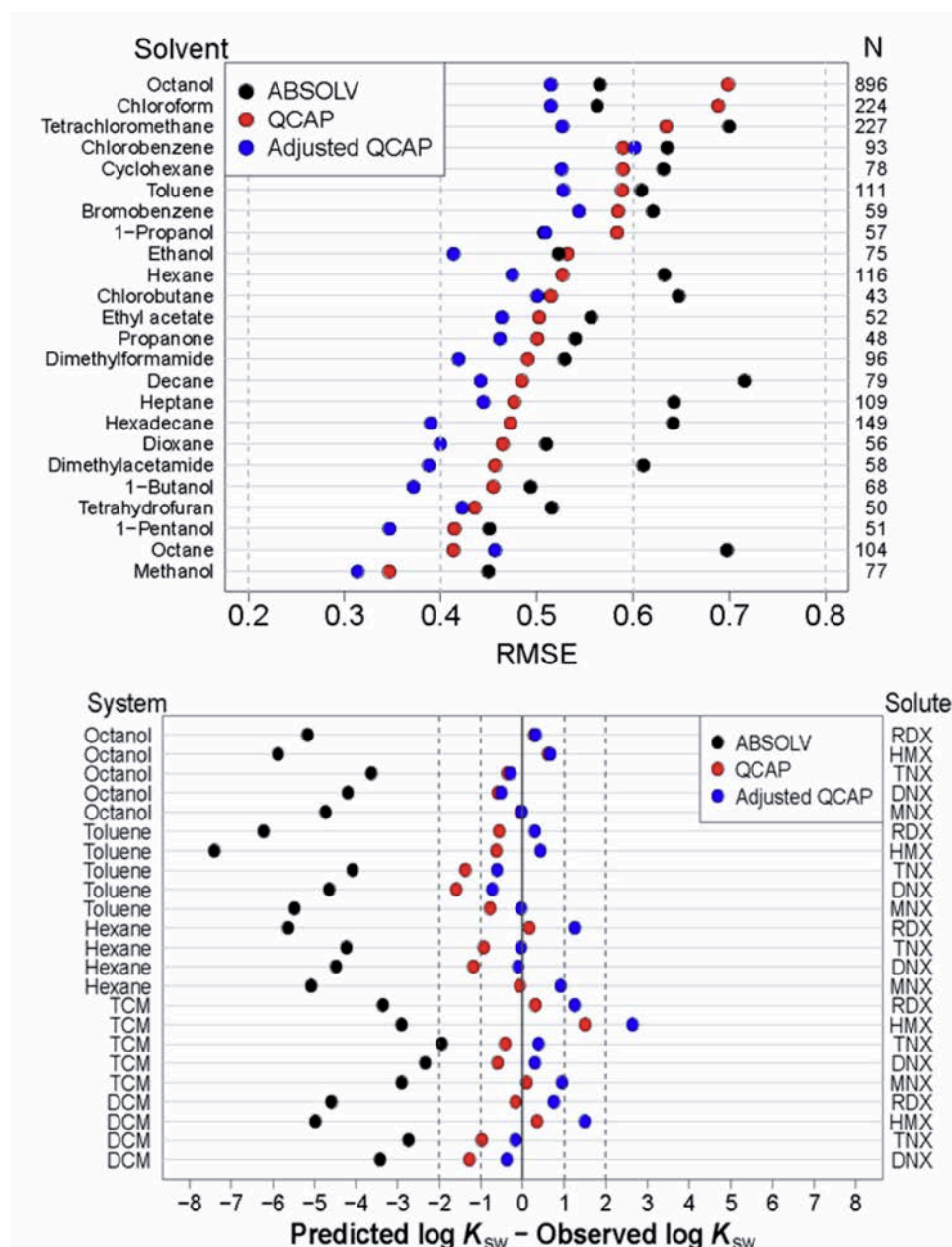


Figure 1-5 (A). RMSEs of the residuals (predicted $\log K_{sw}$ - observed $\log K_{sw}$) for solvent-water partition coefficients. Predictions by three models ABSOLV, QCAP, and Adjusted QCAP. Solvents (left axis) ordered from the smallest to the largest QCAP RMSE. Right axis N = number of solutes in each system. (B) Prediction errors (predicted $\log K_{sw}$ - observed $\log K_{sw}$) for predictions of ABSOLV, QCAP, and Adjusted QCAP for munition constituents and munition-like compounds (Right axis). Left axis: partitioning systems: wet octanol-water, toluene-water, hexane-water, trichloromethane (TCM)-water, and dichloromethane (DCM)-water.

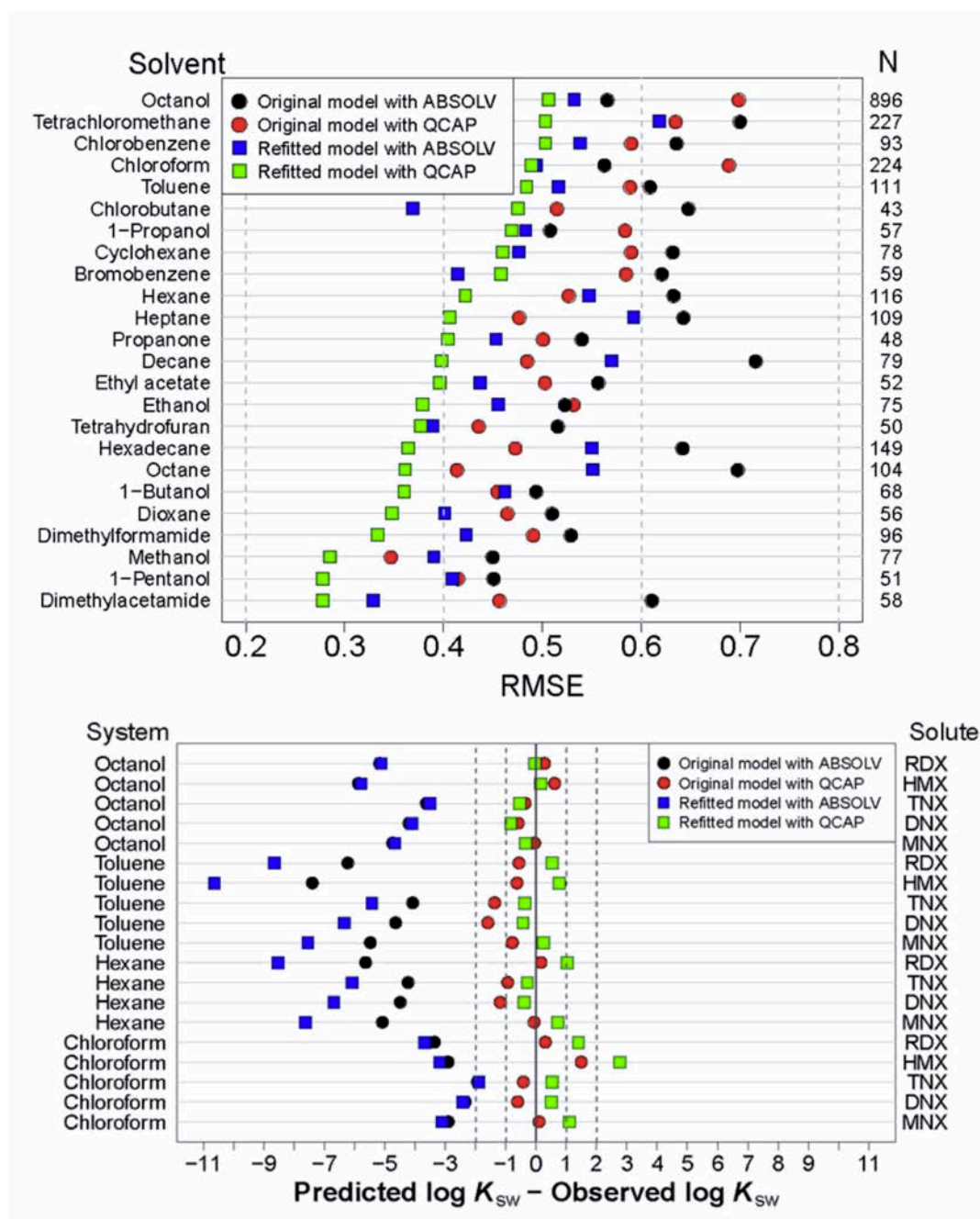


Figure 1-6 Results for pp-LFERs constructed using the indicated solute parameters. (A) RMSEs of residuals (log predicted - log observed partition coefficients) for solvent-water partition coefficients. Predictions by four models (1) ABSOLV, (2) original model with QCAP, (3) refitted model with ABSOLV, and (4) refitted model with QCAP. Solvents (left axis). Right axis N = number of solutes in each system (B) Prediction errors (predicted log K_{sw} - observed log K_{sw}) for solvent-water partition coefficients for munition constituents and munition-like compounds (Right axis). Left axis list of the corresponding partitioning systems: wet octanol-water, toluene-water, hexane-water, and chloroform-water.

1.3 Bioconcentration Model for Plants

All the models built in this project are based on the assumption that the receptors: plants, soil invertebrates, and fish, are in partitioning equilibrium with the source of the compound being

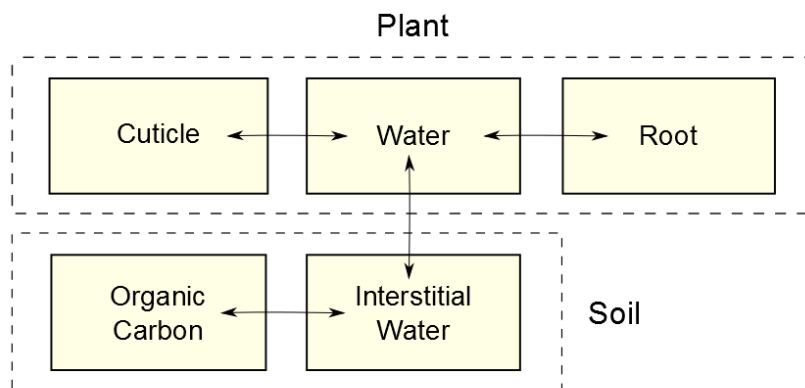


Figure 1-7 Schematic diagram of the Equilibrium Partitioning (EqP) modeling approach: Left-right arrows indicate partitioning of MC (or MLC) i between two phases. $K_{i_{OC}}$ = soil organic carbon–water partition coefficient ($L_{water} \text{ kg}_{OC}^{-1}$), $K_{i_{root}}$ = root–water partition coefficient ($L_{water} \text{ kg}_{root}^{-1}$), and $K_{i_{Cut}}$ = plant cuticle–water partition coefficient ($L_{water} \text{ kg}_{cuticle}^{-1}$).

considered (Figure 1-2). The schematic for the plant BCF model (Figure 1-7) includes only plant cuticle as the plant leaf component being considered as the quantities of compound in the other phases were estimated to be negligible as discussed in Chapter 6.

1.3.1 Plant-Water Partitioning

The bioconcentration factor (BCF) is the steady state concentration of the compound in living plants grown in various media (water, sand, or soil) contaminated with the compound. It is of interest to examine the concentration in plant biomass achieved by simply equilibrating it with dissolved compound. This was tested using whole barley plants (*Hordeum vulgare* L.) sectioned into approximately 0.5 cm sections and equilibrated with

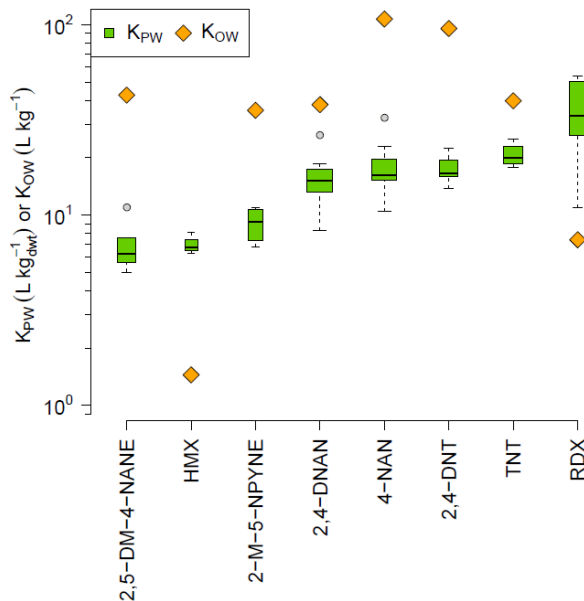


Figure 1-8 Plant (barley)-water partition coefficients (K_{pw}) and octanol-water partition coefficients (K_{ow}) for MCs and MLCs. See Chapter 5, Figure 5-4 for details. Boxes' widths proportional to the square-root of the number of observations in the groups.

solutions containing MCs and MLCs (see Chapter 5 for the experimental details.) The resulting plant-water partition coefficients K_{PW} are shown in Figure 1-8 together with the octanol-water partition coefficients K_{OW} . K_{PW} 's vary by almost an order of magnitude. However they show no relationship to K_{OW} which indicates that a pp-LFER using only log K_{OW} would not be a successful predictor of K_{PW} for munitions and munitions like compounds.

Experiments were performed to obtain BCFs for MCs and MLCs. Barley was grown in a water-sand media at non-toxic concentrations. Daily renewals kept the water concentrations from excessively varying (Chapter 5, Figure 5-2). BCFs are the plant-water concentration ratio at steady state (Chapter 5, Figure 5-3). Comparison of K_{PW} and BCF are presented in Figure 1-9. K_{PW} is either equal to the BCF (2,4-DNAN) or greater than the BCF for the remainder of the MC/MLCs. A likely explanation is that there is metabolism in the plant that is reducing the concentration (Chapter 5, Figure F-8).

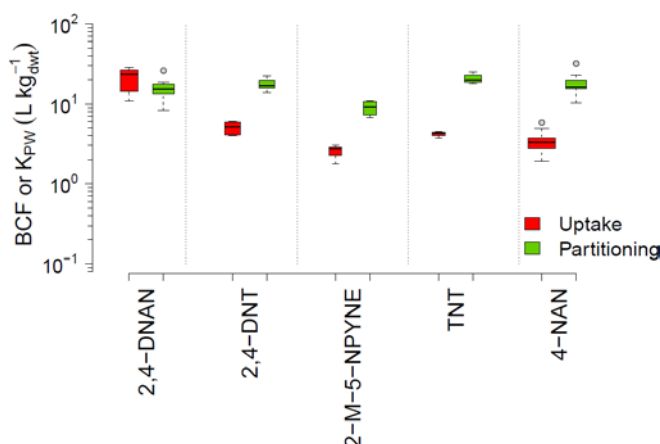


Figure 1-9 Comparison between BCF (labeled Uptake) and plant-water partition coefficient K_{PW} (labeled Partitioning) for MCs and MLCs. Compounds ordered from small to large difference between log K_{PW} and log BCF. Box width proportional to the square-root of the number of observations in the group.

1.3.2 Plant-Cuticle Partitioning Model

A plant-cuticle partitioning model was built using a large dataset collected from the literature. Two types of experimental data were collected: (i) reported K_{Cut} values, which are used to develop the K_{Cut} model. This dataset, to which was added the training set used by Platts and Abraham, comprises 8 MC/MLC compounds and 69 non MC/MLC compounds in 16 plant species for a total of 143 observations (Chapter 6, Table G-5). Figure 1-11 presents the results using three sets of AP (A) ABSOLV-AP, (B) Exp-AP: Experimental + ABSOLV if experimental were not available, and (C) QCAP. The fit using ABSOLV-AP is distorted due to the highly inaccurate estimates for cyclic nitramines and nitrosamines (RDX, HMX, TNX, DNX, and MNX) as seen in Figure 1-3. Comparable RMSEs are obtained using either Exp-AP or QCAP estimates. The pp-LFERs are able to fit both MC/MLC and non MC/MLC compounds. Note that the Exp-AP are experimentally derived whereas the QCAP are estimated from quantum chemical computations only.

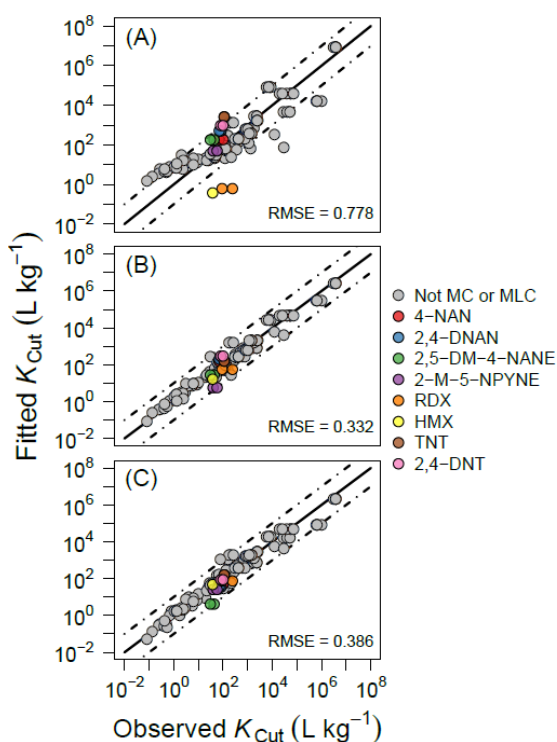


Figure 1-11 pp-LFER, Eq. (1-1) fitted to the full K_{Cut} dataset collected from the literature. Abraham solute parameters from (A) Absolv-AP, (B) Exp-AP, (C) QCAP. RMSE: root mean square error of prediction (log fitted - log observed) for all compounds included in the full K_{Cut} dataset (Chapter 6, Table H-5). The RMSEs for only MCs and MLCs are (A) 1.261; (B) 0.478; and (C) 0.421. The solid line indicates the best agreement (unity), dashed lines are spaced at 1 log unit from unity line.

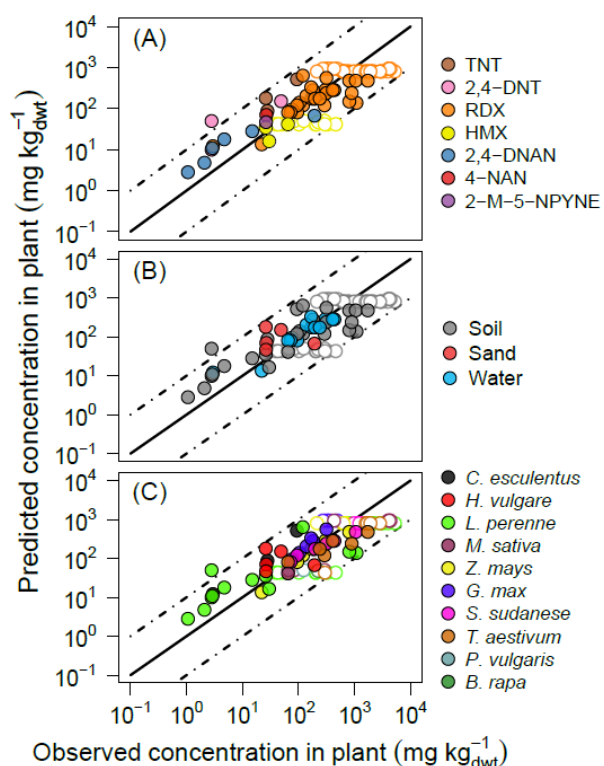


Figure 1-10 Predicted concentrations in the plant versus observed values from published uptake studies (Chapter 6 Table 6-2, Table H-13, and Table H-17). Color coding assigned based on: (A) MCs and MLCs (Chapter 6 Table 6-1), (B) growth medium, and (C) plant species. Unfilled symbols indicate that the predicted concentration in the interstitial water exceeded solubility. The border color for the unfilled symbols corresponds to the color identification in each panel legend. Root mean square error of prediction (log predicted - log observed) RMSE = 0.429 excluding the unfilled symbols. The solid line indicates the best agreement (unity), dashed lines are spaced at 1 log unit from unity.

1.3.3 Plant Concentration Model

The validation dataset for the plant BCF model is compiled from measurements of concentrations in plant biomass made during uptake assays where plants were exposed to MCs, or MLCs, in the growth medium. Since the growth medium is soil, predicting the BCF requires the K_{OC} to predict the soil-water concentrations. The model for the plant concentration C_{iPlant} from an exposure concentration in soil $C_{iSoil Solids}$ for compound i is

$$C_{iPlant} = \frac{K_{iCut} f_{Cut} C_{iSoil Solids}}{K_{iOC} f_{OC}} \quad (1-2)$$

where the parameters are defined in Table 1-2. The results are shown in Figure 1-10. The three panels contain the same predicted and observed concentrations in the plant but with different coding by (A) compound, (B) growth medium, and (C) plant species. Unfilled symbols indicate that the predicted concentration in the interstitial water C_{iIW} was replaced by the corresponding MC aqueous solubility as the predicted concentration in the interstitial water exceeded the aqueous solubility of the compound. These are experiments for which very large soil concentrations were used. The points that are horizontal in Figure 1-10 are data from different experimental observations for the same compound. The model predictions are made using the QCAP parameters. This result demonstrates that the BCF model can be applied to MC/MLC with a RMSE = 0.429. A more detailed statistical evaluation of the goodness of fit is given below.

Table 1-2 Equations for the prediction of concentrations in plants exposed to MCs, or MLCs, in soil and sand or water culture.

$C_{iPlant} = \frac{K_{iCut} f_{Cut} C_{iSoil Solids}}{K_{iOC} f_{OC}}$		Eq. (1-2)
Var.	Equation	#
K_{iOC} :	$\log K_{OC} = 0.670 + 1.075E - 0.277S - 0.363A - 1.697B + 1.468V$	(1-3)
C_{iIW} :	$C_{iIW} = \frac{C_{iSoil Solids}}{K_{iOC} f_{OC}}$	(1-4)
K_{iCut} :	$\log K_{Cut} = -0.593 + 0.433E + 0.900S - 0.587A - 5.409B + 3.442V$	(1-5)
C_{iPlant} :	$C_{iPlant} = K_{iCut} f_{Cut} C_{iIW}$	(1-6)

^a Var.: Variables; i : MC, or MLC, of interest; C_{iPlant} : concentration of compound i in the plant biomass ($\text{mg kg}_{\text{dwt}}^{-1}$); K_{iCut} : plant cuticle–water partition coefficient of i ($\text{L}_{\text{water}} \text{kg}_{\text{cuticle}}^{-1}$); f_{Cut} : dry weight fraction of cuticle in the plant ($\text{kg}_{\text{cuticle}} \text{kg}_{\text{dwt plant}}^{-1}$); $C_{iSoil Solids}$: concentration of i in the soil solids ($\text{mg kg}_{\text{dwt}}^{-1}$); K_{iOC} : soil organic carbon–water partition coefficient of i ($\text{L}_{\text{water}} \text{kg}_{\text{OC}}^{-1}$); f_{OC} : dry weight fraction of organic carbon in the soil ($\text{kg}_{\text{OC}} \text{kg}_{\text{dwt soil}}^{-1}$); E , S , A , B , and V : solute descriptors for i (Chapter 6 Table G-14); C_{iIW} : concentration of i in the growth medium interstitial water (IW) (mg L^{-1})

1.4 Bioconcentration Model for Oligochaetes

The BCF model for oligochaetes is built following the same procedure applied to plants. Figure 1-12 is a schematic of the model. Soil water is in equilibrium with the three organism compartments that accumulate significant quantities of compound: lipid, protein, and water. Two datasets were compiled from published uptake assays: oligochaete BCFs from studies with measured concentrations in the interstitial water, and concentrations in oligochaetes from studies performed in soil for which measured concentrations in the interstitial water were unavailable. Data exclusion criteria are discussed in Chapter 7. The data are listed in Chapter 7 Tables H-2 and H-8. The dataset is chemically diverse and includes seven oligochaete species. The compounds include MCs, MLCs, polycyclic aromatic hydrocarbons (PAHs), and organochlorines (Chapter 7 Table H-2). The exposure media include coarse quartz sand (0.5–1.0 mm effective diameter particles, hereafter referred to as "sand"), spiked or contaminated soil more complex than simple sand (hereafter referred to as "soil"), spiked or contaminated sediment, and water. A total of 60 observed oligochaete BCFs values for undissociated organic compounds were compiled (Chapter 7 Table H-8).

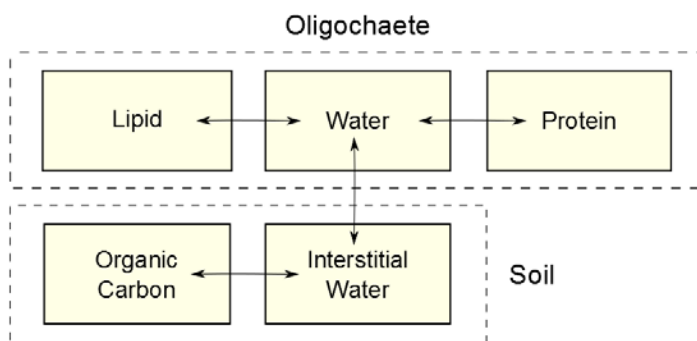


Figure 1-12 Schematic diagram of the Equilibrium Partitioning (EqP) modeling approach: Left–right arrows indicate partitioning of MC (or MLC) i between two phases. K_{iOC} = soil organic carbon–water partition coefficient ($\text{L}_{\text{water}} \text{kg}_{\text{OC}}^{-1}$), K_{iroot} = root–water partition coefficient ($\text{L}_{\text{water}} \text{kg}_{\text{root}}^{-1}$), and K_{iCut} = plant cuticle–water partition coefficient ($\text{L}_{\text{water}} \text{kg}_{\text{cuticle}}^{-1}$).

1.4.1 Lipid-Water and Protein-Water Partitioning

Lipid–water partition coefficient (K_{lipidw}) and protein–water partition coefficient (K_{protw}) are required for the oligochaete BCF model (Figure 1-12). Lipid-water partitioning data were collected from studies that have examined various types of lipids as well as lipid-surrogates: real animal body fats such as cod liver oil, fish and rat fat; surrogates for storage lipids include triglycerides such as tricaprylin and triolein; and phospholipid or liposome. (See Kuo and Di Toro ¹ for details).

For protein-water partition coefficient (K_{protw}), a data set has been utilized which comprises 120 pharmaceuticals binding to human serum albumin as protein surrogate (Kuo and Di Toro (2013) ¹). This data set was chosen because the studied chemicals had low log K_{ow} 's. Since lipids are the dominant phase for partitioning of organic compounds with moderate to high log K_{ow} , it is more important to model protein-water partitioning accurately for low log K_{ow} chemicals. Finally, only the chemicals that were predominantly neutral at typical biota pH (pH~7 to 7.4) were used. See Kuo and Di Toro ¹ for more details.

A comparison of predicted versus observed log K_{lipidw} and log K_{protw} is presented in Figure 1-13A and B. The final model parameters are presented in Table 1-3. For lipid–water partition LFER, RMSE=0.57 and for protein–water partition LFER, RMSE=0.38.

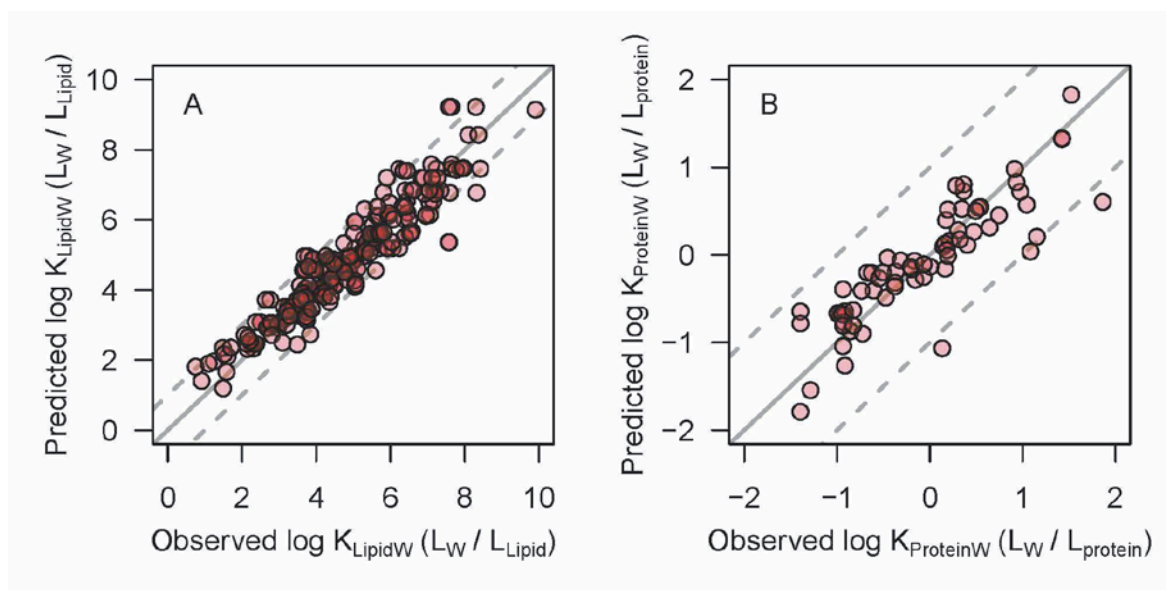


Figure 1-13 Predicted vs observed (a) lipid–water and (b) protein–water partitioning using Abraham solvation parameters. For lipid–water partition LFER, n=248, RMSE=0.57. For protein–water partition LFER, n=69, RMSE=0.38.

1.4.2 Lipid–Water and Protein–Water pp-LFERs and Prediction of Oligochaete BCFs

The pp-LFER for oligochaete BCFs is

$$BCF_i = \left(f_{Lipid} K_{i_{Lipid}} + f_{Protein} K_{i_{Protein}} + \frac{f_{Water}}{\rho_{Water}} \right) \frac{1}{f_{dwt}} \quad (1-7)$$

where values for f_{Lipid} , $f_{Protein}$, f_{Water} , and f_{dwt} were obtained from the literature (Chapter 7, Table H-4). $K_{iProtein}$ is estimated using the model developed from the data in Figure 1-13B. The solute descriptors are estimated using QCAP (Chapter 7 Table H-5), for the same reasons as discussed in the plant BCF.

Two versions of the model have been constructed. The first was constructed by fitting the solvent parameters for lipid and using the protein model presented above (Figure 1-13 and Eq. (1-12)). The pp-LFER for the oligochaete lipid phase partition coefficient (Eq. (1-10)) was estimated by fitting to the BCF data with

$$BCF_i = \left[f_{Lipid} 10^{(c+eE+sS+aA+bB+vV)} + f_{Protein} K_{iProtein} + \frac{f_{Water}}{\rho_{Water}} \right] \frac{1}{f_{dwt}} \quad (1-8)$$

The second is a model developed using the independently determined lipid (Eq. (1-10)) and protein (Eq. (1-12)) partition coefficients.

The results of the first model are shown in Figure 1-15. The color coding identifies each data point by compound (Figure 1-15A), exposure medium (Figure 1-15B), and oligochaete species (Figure 1-15C). The BCFs covered a range of approximately five orders of magnitude ($0.664 < \log BCF < 5.39$) for which MCs and MLCs constitute the lower end of the range (Figure 1-15A). No bias was observed for the prediction of any compound.

The resulting RMSE of the predictions depended on the exposure media (Figure 1-15B) with RMSEs for each group increasing in the order of sand < water < soil < sediment (0.177, 0.365, 0.467, and 0.768, respectively). This was expected as the concentrations measured in oligochaetes and exposure phases: sediments or soils are, less reliable than those in assays with sand or water. This is due to the analytical and experimental challenges in collecting oligochaetes or interstitial water (i.e., exposure phase) from sediment or soil without also disturbing the sample and changing it in some way, for example by oxidation.

No trend was observed in the prediction as a function of the oligochaetes being terrestrial or aquatic (Figure 1-15C), suggesting that the model could be applied to a variety of oligochaete species.

The second model was evaluated using the independent pp-LFER for organism lipid (Eq. (1-7)) was that was developed by fitting to a set of lipid-water partitioning data (Figure 1-13A). The results are shown in Figure 1-14B, and can be compared to the results using the fitted pp-LFER (Figure 1-14A). The RMSE increases from RMSE = 0.499 to 0.677. The lipid pp-LFER itself has a RMSE = 0.57 so it is expected that the RMSE = 0.677 for the BCF employing it should be larger, as it is, but not excessively so. In fact it is reassuring that the BCF model using completely independent pp-LFERs produces reasonable results.

The procedure for the estimation of concentrations in oligochaetes from soil is validated by predicting concentrations in an independent dataset (23 observations) compiled from published uptake assays. The estimations are performed using a partitioning-based oligochaete bioconcentration model (Table 1-3).

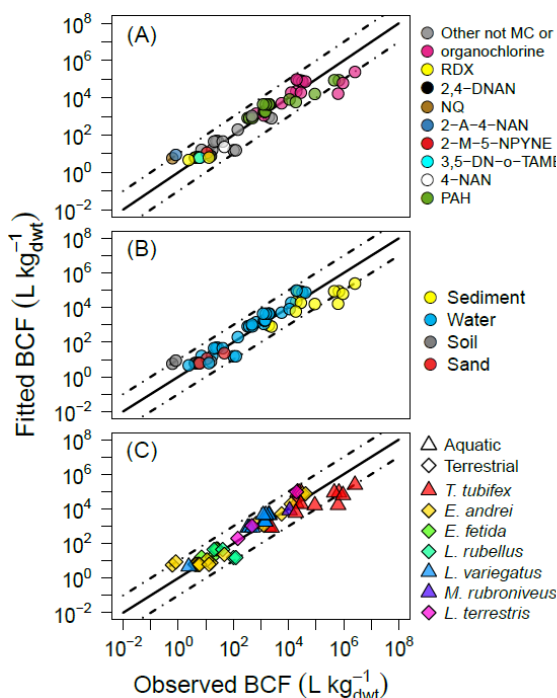


Figure 1-15 Fitted versus observed oligochaete BCFs for organic compounds partitioning to three components, lipid, protein, and internal water (Chapter 7 Eq. (7-10), Eq. (7-11), and Eq. (7-6)). Color coding assigned based on: (A) organic compound, (B) exposure medium, and (C) oligochaete species. Root mean square error of prediction (log predicted - log observed BCF), RMSE = 0.499. Abbreviations defined in Table I-2. The solid line indicates the best agreement (unity), dashed lines are spaced at 1 log unit from unity.

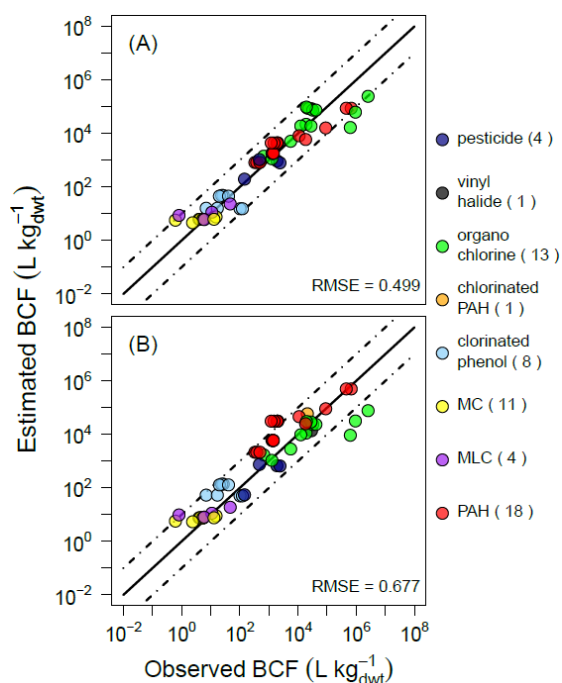


Figure 1-14 Estimated versus observed oligochaete BCFs for organic compounds (Chapter 7 Table I-6). Predictions made using a partition-based BCF model (Chapter 7 Eq. (7-3)) with the $K_{Lipid\ pp}$ -LFER (A) fitted to the oligochaete BCF data and ((Eq. (7-11)) or (B) fitted to an independent data set (Eq. (7-5)). Legend: Chemical class with corresponding count; PAH: polycyclic aromatic hydrocarbon. RMSE: Root mean square error of prediction (log predicted - log observed BCF). The solid line indicates the best agreement (unity), dashed lines are spaced at 1 log unit from unity.

Table 1-3 A partitioning-based oligochaete bioconcentration model^a

$C_{i_{Worm}} = \left(f_{Lipid} K_{i_{Lipid}} + f_{Protein} K_{i_{Protein}} + \frac{f_{Water}}{\rho_{Water}} \right) \frac{C_{i_{Soil Solids}}}{f_{dwt} f_{OC} K_{i_{OC}}} \quad (1-9)$		
Var.	Equation	#
$K_{i_{OC}}$:	$\log K_{OC} = 0.670 + 1.075E - 0.277S - 0.363A - 1.697B + 1.468V$	(1-3)
$C_{i_{IW}}$:	$C_{i_{IW}} = \frac{C_{i_{Soil Solids}}}{K_{i_{OC}} f_{OC}}$	(1-4)
$K_{i_{Lipid}}$ ^b :	$\log K_{Lipid} = 0.84 + 0.77E - 1.10S - 0.47A - 3.52B + 3.37V$	(1-10)
$K_{i_{Lipid}}$ ^c :	$\log K_{Lipid} = 0.751 + 0.431E - 2.409S - 0.787A - 2.106B + 4.553V$	(1-11)
$K_{i_{Protein}}$:	$\log K_{Protein} = -0.88 + 0.74E - 0.37S - 0.13A - 1.37B + 1.06V$	(1-12)
$C_{i_{Worm}}$	$C_{i_{Worm}} = \left(f_{Lipid} K_{i_{Lipid}} + f_{Protein} K_{i_{Protein}} + \frac{f_{Water}}{\rho_{Water}} \right) \frac{C_{i_{IW}}}{f_{dwt}}$	(1-13)

^a Var.: Variables; *i*: MC, or MLC, of interest; $C_{i_{Worm}}$: concentration of *i* in the worm (mg kg_{dwt}⁻¹); f_{Lipid} and $f_{Protein}$: wet weight worm fraction of lipid and protein, respectively (kg_{lipid} kg_{wwt} worm⁻¹ and kg_{protein} kg_{wwt} worm⁻¹, wwt: wet weight); $K_{i_{Lipid}}$ and $K_{i_{Protein}}$: lipid–water and protein–water partition coefficients of *i*, respectively (L_{water} kg_{lipid}⁻¹ and L_{water} kg_{protein}⁻¹); f_{Water} and f_{dwt} : worm mass fraction of water and dry weight, respectively (kg_{water} kg_{wwt} worm⁻¹ and kg_{dwt} kg_{wwt} worm⁻¹); ρ_{Water} : density of water (kg_{water} L_{water}⁻¹); $C_{i_{Soil Solids}}$: concentration of compound *i* in the soil solids (mg kg_{dwt} soil⁻¹); f_{OC} : dry weight fraction of organic carbon in the soil (kg_{OC} kg_{dwt} soil⁻¹); $K_{i_{OC}}$: organic carbon–water partition coefficient of *i* (L_{water} kg_{OC}⁻¹); *E*, *S*, *A*, *B*, and *V*: QCAP for *i* (Chapter 7 Table H-9); $C_{i_{IW}}$: dissolved concentration of *i* in the interstitial water (IW) (mg L⁻¹)

^b Estimated from an independent data set

^c Estimated using the oligochaete BCF data

1.5 Bioconcentration Model for Fish

The development of pp-LFER models depends critically on the availability of large and well understood data sets. The data for fish BCF is the largest and most detailed available. Therefore it was chosen for developing the first BCF pp-LFER using Abraham parameters. All previous fish BCF models used the octanol–water partition coefficients in the pp-LFER for the fish lipid–water partition coefficient.

The BCF model for fish is illustrated in Figure 1-16. The fish compartments are lipid, water, and protein. The exposure is from the water column. The freely dissolved concentration in the water column is in equilibrium with the internal water phase of the fish. Therefore, partitioning in the water column is considered as well as partitioning in the fish.

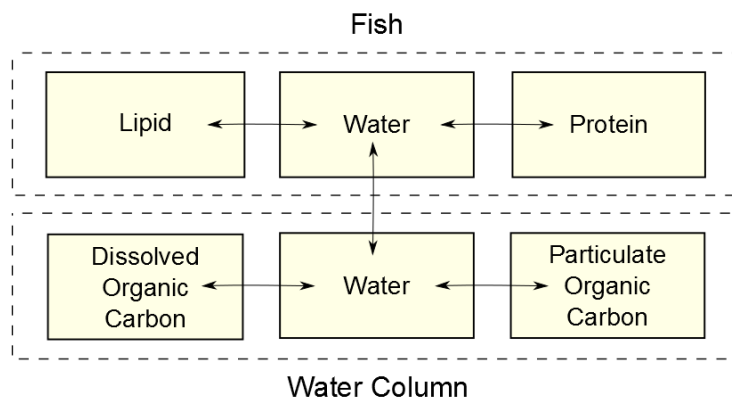


Figure 1-16 Schematic diagram of the Equilibrium Partitioning (EqP) modeling approach: Left–right arrows indicate partitioning of MC (or MLC) i between two phases. The arrows in the fish denote partitioning equilibria between lipid–water and protein–water. The arrows in the water column denote partitioning equilibria between dissolved organic carbon–water and particulate organic carbon – water.

The model formulation, the data used to estimate the model parameters and a detailed analysis of the results are available in two published papers and the supplementary information (Kuo and Di Toro (2013) ¹). The BCF model (Table 1-4, Eq. (1-15)) requires two kinetic constants, the respiratory elimination rate constant k_2 , and the metabolism/biotransformation rate constant k_M , as well as the partition coefficients. The pp-LFERs and estimation equations are listed in Table 1-4. These estimation equations have been developed using data from various sources (Kuo and Di Toro ¹).

The BCF model is validated using an independent data set containing 18 chemicals (N = 601) each with at least 20 or more measurements. The comparison of predicted versus observed BCFs is presented in Figure 1-17. The prediction RMSE = 0.56.

The fish BCF model incorporates the biotransformation rate of compound. The parameters in Eqs.(1-18) to (1-20) are estimated by fitting to the data presented in Figure 1-18. The residuals RMSE = 0.71, which is the largest RMSE of all the models developed in this project. It is presented since this is a new model of an important process – biodegradation – that considers internal chemical partitioning and uses Abraham solvation parameters as reactivity descriptors. It assumes that only chemicals freely dissolved in the body fluid may bind with enzymes and subsequently undergo biotransformation reactions. Consequently, the whole-body biotransformation rate of a chemical is retarded by the extent of its distribution in different biological compartments (Kuo and Di Toro ¹).

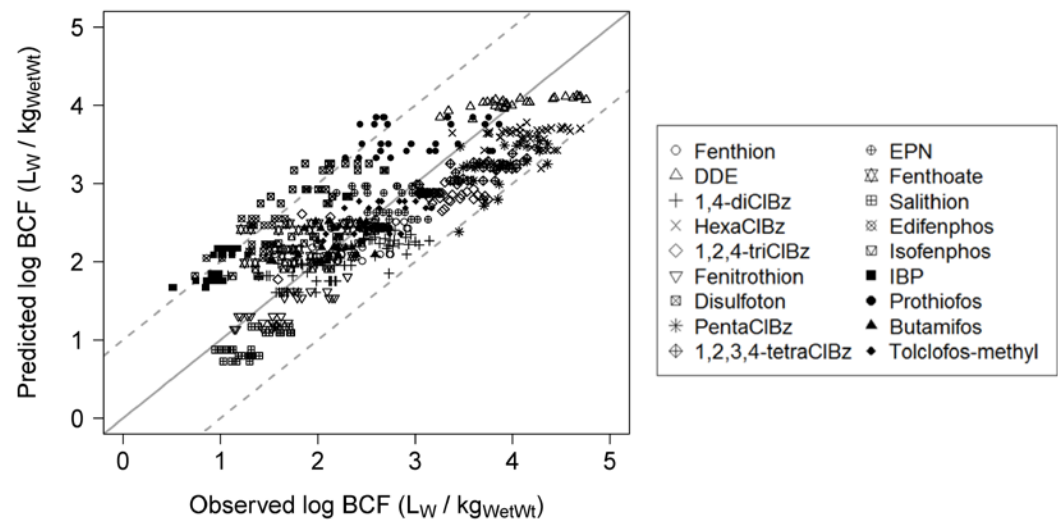


Figure 1-17 Prediction of fish *BCF* using the model in Table 1-4. The RMSE = 0.56. Kuo and Di Toro ¹.

1.6 Model Performance and Applicability to Munitions Compounds

The quality of the models developed in this project has been assessed using the RMSE of the residuals = $\log(\text{Predicted}) - \log(\text{Observed}) = \log(\text{Predicted}/\text{Observed})$ which is a unitless ratio. Therefore the RMSE of the different models can be compared.

It is useful to relate the RMSE to the fraction of the residuals that exceed certain limits. For example, what percentage of the residuals exceed the limits 3 and 1/3 if $\text{RMSE} = 0.5$. This can be estimated if the probability distribution of the residuals is assumed to be normal. Figure 1-19A presents the results. The dashed line indicates a 10% exceedance of the limits. For $\text{RMSE} = 0.3, 0.4$, and 0.6 the corresponding limits are 1/3 and 3, 1/5 and 5, and 1/10 and 10. Thus a model with $\text{RMSE} = 0.3, 0.4$, or 0.6 can be thought of as a model having a predictive capability of a factor of 3, 5, or 10, respectively.

Figure 1-19B presents the statistics of the residuals for the models developed or used in this project. The mean, standard deviation, and RMSE and their standard errors are presented for both classes of data: the MC and MLC (yellow) and the Non MC/MLC data (grey). The number of data points are indicated in the x axis legend.

For all the models, the $\text{RMSE} \approx 0.4$ so that the models have approximately 90% of the residuals within the limits of 1/5 and 5. The RMSE is a function of the residual mean and standard deviation

$$\text{RMSE} = \sqrt{\text{Mean}^2 + \text{Standard Deviation}^2} \quad (1-14)$$

All the Non MC models have small residual means indicating a lack of bias. The model performance is approximately the same for munitions components and non-munition components as the RMSEs are all approximately the same. For K_{OC} and the Plant concentrations the results are predictions as the MC and MLC data were not used in the model fitting. The RMSE for K_{OC} is surprising small and the Plant concentrations are in line with the other RMSEs.

Plots of model prediction or model fitted results versus observed data are presented in Figure 1-20. The MC and MLCs are indicated. Note the multiple orders of magnitude spanned by the data sets and the relation of the MC/MLC data to the rest of the data. For oligochaete BCFs the MC/MLC data is at the low end of the data. For soil organic carbon partition coefficient MC/MLC data is in the lower third of the range. For plant cuticle, however, MC/MLC is in the middle of the range. As noted in Chapter 6, plant cuticle has a quite different pp-LFER (Eq. (1-5)) than does either soil organic carbon (Eq. (1-3)) or organism lipid (Eqs.(1-10) and (1-11)). It is this difference that necessitates the use of Abraham pp-LFERs that can accommodate the properties of quite different solutes (MC/MLC versus the Non MC/MLC) and different environmental phases (soil organic carbon, organism lipid, and plant cuticle) with markedly different partitioning properties.

Table 1-4 Equations for fish BCF model.

$CF = \frac{\phi_{sys} K_{FW}}{1 + k_M/k_2}$ (1-15)		
Var.	Equation	#
ϕ_{sys}	$\phi_{sys} = \frac{1}{1 + [DOC]K_{DOCw} + [POC]K_{POCw}}$	(1-16)
K_{FW}	$K_{FW} = f_{lipid}K_{lipidw} + f_{prot}K_{protw} + f_{wat}/\rho_{wat}$	(1-17)
k_M	$\phi_{fish} = \frac{1}{1 + K_{lipidw}f_{lipid}\rho_{wat}/f_{wat} + K_{protw}f_{prot}\rho_{wat}/f_{wat}}$	(1-18)
	$\log HL = 2.2(\pm 0.3)B - 2.1(\pm 0.2)V - 0.6(\pm 0.3) - \log \phi_{fish}$	(1-19)
	$k_M = \ln(2) / HL$	(1-20)
K_{lipidw}	$\log K_{lipidw} = 0.84 + 0.77E - 1.10S - 0.47A - 3.52B + 3.37V$	(1-10)
K_{protw}	$\log K_{protw} = -0.88 + 0.74E - 0.37S - 0.13A - 1.37B + 1.06V$	(1-12)
K_{DOCw}	$\log K_{DOCw} = 3.10 + 0.87E - 1.03S - 3.81A + 0.14B + 0.67V$	(1-21)
	$\log K_{DOCw} = 0.97\log K_{OW} - 1.27$	(1-22)
k_2	$k_1 = \frac{1}{5.46 \times 10^{-6} MW + \frac{0.261}{K_{OW}}}$	(1-23)
	$k_2 = k_1 / K_{FW}$	(1-24)

ϕ_{sys} = freely dissolved fraction of chemical in the aqueous phase; K_{FW} = wet-weight fish–water partition coefficient; f_{lipid} = fish lipid content; f_{prot} = fish protein content; f_{wat} = fish water content; K_{lipidw} = lipid–water partition coefficient; K_{protw} = protein–water partition coefficient; k_M = whole body biotransformation rate constant; ϕ_{fish} = fraction of freely dissolved chemical within the fish; K_{DOCw} = dissolved organic carbon–water partition coefficient; k_1 = respiratory uptake rate constant; k_2 = respiratory elimination rate constant; K_{lipidw} and K_{protw} in units [L_{wat}/kg_{lipid}] and [L_{wat}/kg_{prot}], respectively. Dissolved organic carbon (DOC) and particulate organic carbon (POC) concentrations were assumed to be 1 mgDOC/L and 0 mgPOC/L respectively.

REFERENCES

1. Kuo, D.T.F.; Di Toro, DM. A reductionist mechanistic model for bioconcentration of neutral and weakly polar organic compounds in fish. *Environmental Toxicology and Chemistry*. 2013;32(9):2089-2099.

Chapter 2

EXPERIMENTAL DETERMINATION OF SOLVENT–WATER PARTITION COEFFICIENTS AND ABRAHAM PARAMETERS FOR MUNITION CONSTITUENTS

Abstract

There is increasing concern about the environmental fate and effects of munition constituents (MCs). Polyparameter linear free energy relationships (pp-LFERs) that employ Abraham solute parameters are available for a variety of parameters that can aid in evaluating the risk of MCs to the environment. However, poor predictions using pp-LFERs and ABSOLV estimated Abraham solute parameters are found for some key physico-chemical properties, particularly for novel MCs. In this work, the Abraham solute parameters of eight MCs and munition-like compounds are determined using experimentally determined partition coefficients in various solvent-water systems. The compounds investigated include hexahydro-1,3,5-trinitro-1,3,5-triazacyclohexane (RDX), octahydro-1,3,5,7-tetranitro-1,3,5,7-tetraazacyclooctane (HMX), Hexahydro-1-nitroso-3,5-dinitro-1,3,5-triazine (MNX), hexahydro-1,3,5-trinitroso-1,3,5-triazine (TNX), hexahydro-1,3-dinitroso-5-nitro-1,3,5-triazine (DNX), 2,4,6-trinitrotoluene (TNT), 1,3,5-trinitrobenzene (TNB), and 4-nitroanisole (4NAN). The solvents in the solvent-water systems are hexane, dichloromethane, trichloromethane, octanol, and toluene. The measured partition coefficients span a range from -2.19 to 3.17 log units. The only available reported partition coefficients are for octanol-water for some of the investigated compounds and they are in good agreement with the experimental measurements from this study. Correlations of the measured solvent-water partition coefficients for some solute pairs or solvent system pairs indicate the consistency and reliability of the experimental data, and also serve to estimate missing values. The predictions of solvent-water partition coefficients ($\log K_p$) using experimentally derived solute parameters have much lower root mean square error of prediction of $\log K_p$ (RMSE = 0.38) than those using ABSOLV estimated parameters (RMSE = 3.56) for the investigated compounds. Additionally, the predictions for various physico-chemical properties using the solute parameters derived in this study agree with available literature reported values with prediction errors within 0.79 log units except for water solubility of RDX and HMX with errors of 1.48 and 2.16 log units respectively. However, predictions using ABSOLV estimated solute parameters have larger prediction errors of up to 7.68 log units. This large discrepancy is probably due to the missing $-R_2N-NO_2$ and $-R_2N-NO_2$ functional groups in the ABSOLV fragment database.

2.1 Introduction

The US Department of Defense reported that 12,000 sites throughout the United States were contaminated by munition constituents (MCs).¹ For example, the concentration of hexahydro-1,3,5-trinitro-1,3,5-triazacyclohexane (RDX), 2,4,6-trinitrotoluene (TNT), and octahydro-1,3,5,7-tetranitro-1,3,5,7-tetraazacyclooctane (HMX) in some sites exceeded 3000 mg·kg⁻¹, 87000 mg·kg⁻¹, and 3000 mg·kg⁻¹, respectively.² Because of improper handling and disposal techniques, these MCs and their degradation products may enter into the environment, posing risks to a variety of organisms including microorganisms³⁻⁶, algae⁵, plants⁷, fish⁵, and humans⁸.

In addition to MCs, metabolites, degradation products, or industrial by-products of MCs can also pose environmental concern. Hexahydro-1-nitroso-3,5-dinitro-1,3,5-triazine (MNX), hexahydro-1,3,5-trinitroso-1,3,5-triazine (TNX), and hexahydro-1,3-dinitroso-5-nitro-1,3,5-triazine (DNX), the degradation products of RDX, have been detected in soil and groundwater^{9, 10}. It has been found that these degradation products are toxic to organisms.¹¹ 1,3,5-trinitrobenzene (TNB) is a high explosive used for mining and military application and is a degradation product of TNT or a by-product of TNT manufacturing.¹² With a structure similar to TNT, TNB is suggested to pose similar health problems and environmental risks.¹² The compound 4-nitroaniline (4NAN) was selected in this study because it is structurally similar to the investigated MCs. The compounds studied are listed in Table 2-1, together with their physico-chemical properties and chemical structures. Among them, RDX and HMX are cyclic nitramines with -R₂N-NO₂ structure¹³; MNX, DNX, and TNX have R₂N-NO and/or R₂N-NO₂ and will be referred to as cyclic nitrosamines; TNT, TNB, and 4NAN are nitroaromatics with Ar-NO₂ structure¹³.

In order to assess the fate of MCs and their degradation products in the environment, physico-chemical properties are required, such as vapor pressure, water solubility, and particularly partition coefficients. The partition coefficient is defined as the ratio of the concentrations of a compound in a two-immiscible-phase system at equilibrium¹⁴:

$$K_{12} = \frac{C_{i1}}{C_{i2}} \quad (2-1)$$

where K_{12} denotes the partition coefficient, C_{i1} and C_{i2} denote the equilibrium concentrations of substance i in phase 1 and in phase 2, respectively.

Table 2-1 Physical and chemical properties of munition constituents.

Property	RDX	HMX	MNX	DNX	TNX	TNT	TNB	4NAN
CAS number	121-82-4	2691-41-0	5755-27-1	80251-29-2	13980-04-6	118-96-7	99-35-4	100-17-4
Formula	$C_3H_6N_6O_6$	$C_4H_8N_8O_8$	$C_3H_6N_6O_5$	$C_3H_6N_6O_4$	$C_3H_6N_6O_3$	$C_7H_5N_3O_6$	$C_6H_3N_3O_6$	$C_7H_7NO_3$
Molar mass ($g \cdot mol^{-1}$)	222.12	296.16	206.12	190.12	174.12	227.13	213.11	153.14
Density ($g \cdot mL^{-1}$)	1.82	1.78 to 1.903	a	a	a	1.65	1.688	1.23
Melting point ($^{\circ}C$)	205.5	281	a	a	a	80.1	121.5	51 to 53
Physical state ($25^{\circ}C$)	white solid	White Solid	white solid	white solid	white solid	yellow solid	yellow solid	green to brown solid
Structure								

^a Not found.

2.1.1 Polyparameter Linear Free Energy Relationships (pp-LFERs)

Experimentally measured physico-chemical properties are available for only 1% of the approximately 70,000 industrial compounds compiled in EPA's Toxic Substances Control Act (TSCA) inventory¹⁵. Many attempts have been made to develop predictive models since it is not practical to measure all the required physico-chemical properties for all existing and newly emerging environmental contaminants. Among the available models, the Polyparameter Linear Free Energy Relationships (pp-LFERs), such as the Abraham solvation model, have been proposed to predict partitioning in a broad variety of environmental systems and chemicals.^{16, 17} This model evaluates the logarithm of the partition coefficient (K) between two phases using the equation:

$$\log K = c + eE + sS + aA + bB + vV \quad (2-2)$$

where the lower case parameters pertain to the two phases, e.g. the solvent-water system, and the upper case parameters pertain to the solute. The model assumes that the interaction Gibbs free energy contributions to the partitioning process are separable and additive¹⁸: eE describes the dispersion van der Waals interaction, sS describes the dipole-dipole and dipole-induced dipole interactions, aA and bB measure the hydrogen-bond interactions, and vV describes the energy required for cavity formations. The pp-LFER model assumes that the effects of the solute are independent from those of the solvent.¹⁶ That is, a set of solute parameters for a given substance is considered constant, regardless of the solvent, and vice versa. The upper case letters E , S , A , B , V denote solute's excess molar refraction, dipolarity/polarizability, effective hydrogen-bond acidity (i.e. the ability of the solute to donate a hydrogen bond), effective hydrogen-bond basicity (i.e. the ability of the solute to accept a hydrogen bond), and molar volume, respectively. The lowercase letters c , e , s , a , b , v are solvent/system parameters, which represent the complimentary effects of the solvent phase, relative to the water phase.

Over the years, Abraham and co-workers have successfully correlated the solute parameters to more than 400 properties or processes.¹⁹ The properties include partitioning between solvent-solvent, solvent-water, gas-solvent, and aqueous solubility; partitioning to biomaterials of plant, protein, lipid, and blood; sorption to organic carbon, mineral surfaces, and coal tar; narcotic toxicity, skin permeation, eye irritation, nasal pungency, and odor thresholds. Once the solute parameters are obtained, the properties or processes of the substance can be predicted.

A common method to estimate Abraham solute parameters is the ABSOLV prediction module, which is a fragment based method.²⁰ The estimations of each solute parameter are based on the Platts-type fragment descriptors²¹. A set of 81 atom and functional group fragments is used to estimate the E , S , and B parameters and a separate set of 51 fragments for the A parameter.²¹ The coefficients of the atom/fragments have been further optimized by performing statistical analysis on available experimental partitioning data or experimentally-based solute parameters.²⁰ The V parameter is calculated as McGowan characteristic volume.²² The reported root mean square errors (RMSE) of the ABSOLV parameters are 0.12, 0.22, 0.07, 0.15, and 0.01 for E , S , A , B , and V respectively.²⁰ Stenzel et al.²³ performed a rigorous validation of ABSOLV for a diverse set of complex multifunctional compounds in various partition systems. They concluded that the overall performance of ABSOLV was reasonably good. However, large errors

were found for certain functional groups or chemical classes (e.g., bridged ring structures, highly halogenated compounds, triazoles, steroids, etc.).

2.1.2 Octanol-Water Partition Coefficient

The octanol-water partition coefficient (K_{ow}) is used to predict distribution among various environmental components in predictive models.^{14, 24, 25} For example, good correlations have been found between K_{ow} and the partition coefficient between aqueous solution and soils, sediments, and suspended particles.¹⁴ A relationship was also found between K_{ow} and the bioaccumulation in animals and plants.²⁴ The Target Lipid Model that predicts the toxicity of narcotic chemicals to organisms uses K_{ow} as the chemical parameter.²⁵

Nevertheless, the availability of K_{ow} is still a problem for certain compounds. Literature reported K_{ow} are available for only five of the compounds of interest: RDX²⁶⁻³⁰, HMX^{27, 28, 30}, TNT^{27-29, 31}, TNB^{28, 32, 33}, and 4NAN³² (Table 2-2). Moreover, model predictions of K_{ow} with ABSOLV estimated solute descriptors are inaccurate for some of the investigated compounds as shown below. For TNT, TNB, and 4NAN, the predictions of K_{ow} using ABSOLV estimated solute parameters are in reasonable agreement with the literature reported values. However, poor predictions are observed for both RDX and HMX. The literature reported values of $\log K_{ow}$ for RDX range from 0.81 to 0.9, but the prediction using ABSOLV estimates is -4.32, a discrepancy is more than 5 orders of magnitude. The discrepancy of up to 6 orders of magnitude is found for HMX. The large prediction errors indicate that the ABSOLV estimated solute parameters of RDX and HMX are problematic and should be revised. ABSOLV fails to predict other physico-chemical properties for these compounds as well as shown below (Section 2.3.5(2-5) and 2.3.6). Therefore, a direct determination of Abraham solute parameters based on experimental measurements is necessary.

An experimental method to determine the solute Abraham parameters is to use measured solvent-water partition coefficients.³⁴ The purpose of this paper is to experimentally determine solvent-water partition coefficients in a set of chemically diverse systems and to estimate the Abraham solute parameters for the MCs: RDX, HMX, TNT, and TNB, and munition-like compounds: MNX, DNX, MNX, and 4NAN.

2.2 Materials and Methods

2.2.1 Materials

All the chemicals were used as received without further purification. The RDX, HMX, TNT, and TNB aqueous solutions were prepared by the U.S. Army Edgewood Chemical Biological Center (Aberdeen Proving Ground, MD, USA). MNX (solid, $\geq 99\%$), TNX (solid, $\geq 99\%$), and DNX (solid, 81% pure with 13% MNX and 5% TNX) were purchased from SRI International (Menlo Park, CA, USA). 4NAN (solid, 97%) and acetone (liquid, $\geq 99.9\%$) were received from Sigma-Aldrich (St. Louis, MO, USA). All the solvents (liquid, $\geq 97.0\%$) used in this study were obtained from Sigma-Aldrich (St. Louis, MO, USA). Deionized water (18 m Ω resistance) was used in all experiments.

2.2.2 Selection of Solvent-Water Partitioning Systems

To compute the solute parameters using a set of solvent-water partition coefficients, it is necessary to choose solvents that are sufficiently different so that the multiple linear regression used to estimate the solute parameters has a unique solution. For example, choosing octanol, hexanol, butanol, and decanol is not appropriate since they are within a homologous series and the solvent parameters of one solvent are almost proportional to the other. Also, a diverse set of solvent-water systems covers different types of relevant intermolecular interactions with a given solute, thus better characterizing the chemical properties of that solute.

As a guide to selecting solvents, Leahy et al.³⁵⁻³⁷ proposed the term “critical quartet”, arguing that only four carefully selected water-solvent systems: octanol, an alkane, chloroform, and propylene glycol dipelargonate (PGDP), were adequate to characterize the chemical information of all solvent-water systems. Zissimos et al. selected a slightly different combination: octanol, chloroform, cyclohexane, and toluene, given the commercial unavailability of PGDP.³⁴

There are solvent-water systems that are preferred for other reasons. According to the OECD guideline, $\log K = -2$ to 4 can be experimentally determined by the shake-flask method.³⁸ Also, practical considerations, including availability, toxicity, volatility, and viscosity, should be taken into account.³⁴ As a result of these considerations, four solvents were selected: hexane, toluene, trichloromethane (chloroform), and octanol. They are similar to those of Zissimos et al.³⁴. One more solvent, dichloromethane, was added to provide some redundancy.

2.2.3 Experimental Methods

Partition coefficients were determined using the shake-flask method at room temperature (20 ± 1 °C). The systems investigated were octanol-water, toluene-water, chloroform-water, dichloromethane-water, and hexane-water. At least three replicates of different volume ratios of solvent and water were used for each test substance and for each solvent-water system. All the glassware was cleaned with laboratory detergent, oven dried, and then tripled-rinsed with dichloromethane before use. Solvents used in the partitioning experiment were pre-saturated with deionized water.

Aqueous RDX, HMX, TNT, and TNB solutions were received in the concentrations of $40 \text{ mg}\cdot\text{L}^{-1}$, $4.5 \text{ mg}\cdot\text{L}^{-1}$, $130 \text{ mg}\cdot\text{L}^{-1}$, and $130 \text{ mg}\cdot\text{L}^{-1}$, respectively. The solutes TNX, DNX, MNX, and acetone (as a reference compound) were dissolved in deionized water with corresponding initial concentrations of $5.84 \text{ mg}\cdot\text{L}^{-1}$, $4.36 \text{ mg}\cdot\text{L}^{-1}$, $5.36 \text{ mg}\cdot\text{L}^{-1}$, and $500 \text{ g}\cdot\text{L}^{-1}$, respectively. As 4NAN dissolved very slowly in water, it was dissolved in each of the following solvents: octanol, toluene, chloroform, dichloromethane, and hexane, with initial concentrations of $10 \text{ g}\cdot\text{L}^{-1}$. The above solutions were then used as the stock solutions of the test substances.

The aqueous stock solutions of these compounds: RDX, HMX, TNT, TNB, TNX, DNX, and MNX, were used as calibration standards without further dilution for HPLC analysis because of the high HPLC detection limits and the low aqueous solubility of most of the compounds. Even though there is only one concentration per solute for calibration, accurate measurements were obtained as shown in Section 2.3.1 (Validation of experimental results). For the solute acetone, its stock solution was diluted to yield the calibration standards with five concentrations ranging from 100 to $500 \text{ g}\cdot\text{L}^{-1}$. To prepare the 4NAN calibration standards, the 4NAN solid was first dissolved in ethanol, diluted with deionized water to yield the aqueous standards with five concentrations ranging from 1 to $10 \text{ g}\cdot\text{L}^{-1}$.

The solvent-water partitioning experiment was based on the methodology in the OECD guideline³⁸ using volumetric flasks. The volumes of solvent and water were based on the preliminary tests. If the estimate of $\log K$ was greater than zero, a total volume of 100 mL was used; otherwise, a total volume of 250 mL was used because a larger volume of aqueous phase would be used. The solvent phase and the aqueous phase were added carefully and sequentially into one volumetric flask, and the masses of each phase added were determined using a balance with an accuracy of 0.01 g. The volume of each phase was determined by the ratio of the corresponding mass and phase density. After being closed with the stopper and sealed with Parafilm sealing film, the flask was shaken by rotation of 180° about its transverse axis at approximately 100 times per minute for 20 minutes. Based on preliminary tests, equilibrium was reached before 20 minutes using this method. The flask was then wrapped in aluminum foil to avoid photodegradation. The resultant solution was rested until complete separation of phases was obtained. If the solvent density is greater than the water density, the aqueous phase was sampled by a glass pipette; otherwise, the resultant solution was transferred to a glass separatory funnel, and the aqueous phase was withdrawn from the bottom of the separatory funnel. The sample was then analyzed by Agilent 1200 Series high-performance liquid chromatography (HPLC) from Agilent Technologies (Santa Clara, CA, USA). For details of the HPLC analytical method, refer to Gonzalez et al.³⁹. In this way, the concentration of a compound in the aqueous phase was obtained and the equilibrium concentration in the solvent phase was determined by mass balance. The partition coefficient of a given substance was then calculated using Eq. (2-1).

2.2.4 Determination of Abraham Solute Parameters

2.2.4.1 McGowan Characteristic Volume (V)

The volume V refers to the solute molar volume, the volume of one mole of a substance when the molecules are stationary. It can be calculated as the McGowan characteristic volume from the atom fragment constants and number of bonds in a molecule as follows^{22, 40, 41}:

$$V = (\sum C_a - 6.56B_n)/100 \quad (2-3)$$

where V has units of $\text{cm}^3 \cdot \text{mol}^{-1}/100$; $\sum C_a$ is the summation of all the atom fragment contributions; B_n is the number of bonds in a molecule, where all the bonds (single, double or triple) are counted as one. To simplify the counting of the number of bonds, Abraham developed the following algorithm⁴⁰:

$$B_n = N_a - 1 + R_g \quad (2-4)$$

where N_a is the total number of atoms, R_g is the total number of rings regardless of their types. This algorithm is implemented in the ABSOLV prediction module for V estimation.

2.2.4.2 Excess Molar Refraction (E)

The excess molar refraction, E , is defined as the molar refraction of a solute, less the molar refraction for a normal alkane of the same characteristic volume.⁴¹ It can be calculated as a function of the index refraction (η) and the McGowan characteristic volume (V)⁴¹:

$$E = 10 \left[\frac{(\eta^2 - 1)}{(\eta^2 + 2)} \right] V - 2.832V + 0.526 \quad (2-5)$$

where E has the units $\text{cm}^3 \cdot \text{mol}^{-1}/10$.

As proposed by Abraham et al.⁴¹, E is nearly an additive property and can be calculated by summing up fragment contributions²¹, which is the method ABSOLV uses to estimate E . A comparison of the ABSOLV estimates of E , and E computed from the experimental refractive index using Eq. (2-5) for a diverse set of organic compounds⁴², are in close agreement with $\text{RMSE} = 0.064$ and $R^2 = 0.96$ (see Fig. A-1 in Appendix A for a graphical comparison).

The ABSOLV estimate of E is used in this work for the following reasons. It has been found that E and S are strongly correlated⁴³. Therefore they cannot both be reliably estimated simultaneously using multiple linear regression. As a guide to their reliability, it is noted that E estimated by ABSOLV for the MCs and munition-like compounds have a range from 0.89 to 1.77 as shown below (Table 2-4) and this range is within the range of the dataset in Fig. A-1. Finally there are no experimental refractive indices available.

2.2.4.3 Dipolarity/Polarizability (S), Hydrogen-Bond Acidity (A), and Hydrogen-Bond Basicity (B)

The remaining Abraham solute parameters S , A , and B are estimated from the experimental solvent-water partition coefficients. For the Abraham solvation model, $\log K$ in Eq. (2-2) refers to the solvent-water partition coefficients determined in this study. This is the equation that is used to estimate S , A , and B . In this study, five solvent-water systems were employed. The solvent-water system parameters c , e , s , a , b , and v for each solvent-water system are collected from literature⁴⁴ (Table A-1). V and E parameters are calculated by the ABSOLV prediction module as explained above (Sections 2.2.4.1 and 2.2.4.2). Since E and V are known, the Abraham solvation model can be rearranged with the known variables (E and V) on the left and the unknown variables (S , A , and B) on the right, as follows:

$$\log K_i - c_i - v_i V - e_i E = s_i S + a_i A + b_i B \quad (2-6)$$

where $i = 1, \dots, 5$ denotes the solvent-water system. Estimates of S , A , and B were determined by performing a multiple linear regression using Eq. (2-6) and the experimentally measured $\log K_i$ using the package `lm` in the R programming language⁴⁵.

2.3 Results and Discussion

2.3.1 Validation of Experiment Results

In order to validate the experimental results obtained in this study, a comparison between the experimental partition coefficients and the literature reported values are presented in Table 2-2. The differences among the replicates (with different solvent: water volume ratios) are quite small with observed standard deviations within 0.01 log units for RDX, HMX, TNT, TNB, 4NAN and acetone, which indicates that the experimental method used in this study produces reproducible results.

Close agreement is seen between the experimental and literature reported partition coefficients. For RDX, the literature reported values of $\log K_{\text{ow}}$ are quite consistent with a small

range from 0.81 to 0.90 and the measured values (0.86, 0.87, 0.87, and 0.87) are in good agreement. Some differences among the reported values (0.06, 0.16, and 0.26) are found for $\log K_{ow}$ of HMX. The measurements in this study (0.16 ± 0.00) match one reported value. For TNT, disparate literature values (1.60, 1.86, and 2) are reported for $\log K_{ow}$, and the experiment results (1.62 ± 0.01) are in good agreement with one reported value. For $\log K_{ow}$ of TNB, there is close agreement between the experiment measurements (1.11 ± 0.01) and the literature values (1.18). The $\log K_{ow}$ measurements (2.01 ± 0.00) of 4NAN are nearly identical to the literature value (2.03).

In addition, the hexane-water partition coefficient (K_{hw}) of acetone was tested to see if the experimental method could determine $\log K$ for a hydrophilic compound. For $\log K < 0$ (i.e. $K < 1$), the substance partitions preferably to water and the concentration of the substance in the solvent phase may be too low to be accurately determined. No problem is found since the experimental $\log K_{hw}$ values of acetone are basically identical (-0.90 ± 0.01) to the literature value (-0.90) as shown in Table 2-2.

2.3.2 Analysis of Experiment Results

The measured partition coefficients for the eight compounds in the five solvent-water systems are summarized in Table 2-3. The partition coefficient of HMX in hexane-water system was not reported because reliable measurements could not be obtained using the shake flask method. Based on the preliminary measurements, the $\log K_{hw}$ of HMX was smaller than -2. The shake-flask method can only measure $\log K$ within -2 and 4 (occasionally up to 5) according to the OECD guideline.³⁸ The dichloromethane-water partition coefficient (K_{dw}) of MNX could not be determined due to the interference of the dissolved dichloromethane in the aqueous phase.

According to the OECD guideline, the standard deviation of $\log K$ should be within 0.3 units.³⁸ The partition coefficients obtained in this study were highly reproducible with standard deviations typically less than 0.05 log units and never exceeded 0.1.

As shown in Table 2-3, $\log K$ values of RDX (-2.10 to 1.27) and its metabolites MNX (-2.13 to 0.80, without $\log K_{dw}$), DNX (-2.19 to 1.31), and TNX (-1.92 to 1.23), do not vary much among different solvent-water systems. However, the $\log K$ values of TNT (0.77 to 3.17) are larger than those of TNB (0.01 to 2.61) for all the investigated systems. The $\log K$ values of HMX (-0.66 to 0.45, without $\log K_{hw}$) are smaller than those of RDX (-2.10 to 1.27) over the considered solvent-water systems.

Table 2-2 Validation of partition coefficients measured in this study by comparison with literature reported values.

Compound	Systems	log K	
		Measured in this study ^a	Literature
RDX	octanol-water	0.87 ± 0.01 (N = 4)	0.8127, 0.8628, 0.8726, 29, 0.930
HMX	octanol-water	0.16 ± 0.00 (N = 4)	0.0628, 0.1630, 0.2627
TNT	octanol-water	1.62 ± 0.01 (N = 5)	1.6031, 1.8628, 29, 227
TNB	octanol-water	1.11 ± 0.01 (N = 3)	1.1828, 32, 33
4NAN	octanol-water	2.01 ± 0.00 (N = 4)	2.0332
Acetone	hexane-water	-0.90 ± 0.01 (N = 3)	-0.946

^a Values after \pm are standard deviations, and values in the parenthesis denote the number of replicates.

Table 2-3 Summary of the measured solvent-water partition coefficients.

Solvent	RDX	HMX	TNX	DNX	MNX	TNT	TNB	4NAN
hexane	-2.10 ± 0.01 ^a	ND ^b	-1.92 ± 0.04	-2.19 ± 0.02	-2.13 ± 0.07	0.77 ± 0.00	0.01 ± 0.10	1.37 ± 0.00
DCMc	1.27 ± 0.01	0.45 ± 0.01	1.23 ± 0.01	1.31 ± 0.01	ND ^b	3.17 ± 0.05	2.01 ± 0.02	3.13 ± 0.09
TCMd	0.71 ± 0.00	-0.66 ± 0.01	0.63 ± 0.01	0.59 ± 0.01	0.70 ± 0.01	2.69 ± 0.01	2.06 ± 0.01	3.09 ± 0.01
octanol	0.87 ± 0.01	0.16 ± 0.00	0.41 ± 0.01	0.62 ± 0.01	0.80 ± 0.00	1.62 ± 0.01	1.11 ± 0.01	2.01 ± 0.00
toluene	0.74 ± 0.01	0.06 ± 0.00	0.57 ± 0.01	0.47 ± 0.01	0.65 ± 0.01	3.13 ± 0.00	2.61 ± 0.00	2.64 ± 0.04

^a Reported in log units and values after \pm are standard deviations.

^b ND are values that were not determined.

^c Dichloromethane.

^d Trichloromethane.

2.3.3 Correlation of Partition Coefficients

The correlation of solvent-water partition coefficients may be used to check the consistency of the experimental data.¹⁴ If two polar solvents are chemically similar, the contributions to the solvation free energies in both solvents are due to similar solvent-solvent and solute-solvent interactions. A linear relationship can be expected between the free energies or, equivalently, log partition coefficients of solutes in these two solvent-water systems.¹⁴ Among the investigated solvents, trichloromethane and dichloromethane are likely to have similar contributions to the solvation free energies because both are chloroalkanes. The linear fit ($R^2 = 0.96$) between $\log K_{cw}$ (trichloromethane-water partition coefficient) and $\log K_{dw}$ for all the considered compounds supports this expectation (Fig. A-2).

It was not surprising to find high correlations for structurally similar compounds¹⁴. This is illustrated by the good linear fits among pairs of RDX, MNX, DNX, and TNX with values of $R^2 > 0.98$ (Fig. A-3). For structurally closely related compounds TNT and TNB, a relatively high correlation is expected as well and found to be $R^2 = 0.93$. The above findings indicate the consistency of the experimental data. There is not a strong correlation between RDX and HMX probably because the additional $-R_2N-NO_2$ functional group influences not only the vdW interactions but also the polar interactions in each solvent-water system.

The correlation of partition coefficients can also serve as a predictive tool.¹⁴ For example, with the measured value of K_{cw} of HMX, the linear regression equation (Eq. (2-7), $R^2 = 1$)

$$\log K_{hw} = 1.42 \log K_{cw} - 3.01 \quad (2-7)$$

returns the K_{hw} prediction of -3.95 for HMX. Since K_{hw} of HMX was not determined, the estimation can be used below for the calculation of HMX Abraham parameters.

2.3.4 Analysis of the Experimentally Derived Abraham Parameters

The experimentally derived Abraham parameters (Exp-AP) from this study are listed in Table 2-4 (with additional statistical results in Table A-3), together with the ABSOLV estimated Abraham parameters (ABSOLV-AP) and literature reported solute parameters. The literature reported values, which are only available for TNT and 4NAN, vary from different sources but not dramatically. For TNT, $E = 1.39$ is slightly smaller than the reported values of 1.43 and 1.57; Exp-AP $S = 1.81$ is close to the reported values of 1.71 and 1.78, but smaller than that of 2.23; Exp-AP $A = 0.012$ is close to the reported values of 0.00, 0.11, and 0.11; Exp-AP $B = 0.68$ is larger than the reported values of 0.48, but close to 0.61 and 0.62; $V = 1.38$ is identical.

For 4NAN, the $E = 0.89$ and $V = 1.09$ match the literature values of 0.87 and 1.09 respectively. The Exp-AP S , A , and B parameters (1.29, 0.03, and 0.4) are within the ranges of literature values from 1.21 to 1.47, from 0 to 0.20, and from 0.24 to 0.46, respectively.

Table 2-4 List of ABSOLV estimated (ABSOLV-AP), literature reported, and experimentally derived (Exp-AP) Abraham parameters.

Compound	ABSOLV-AP					Literature reported Abraham parameter ^a					Exp-AP ^b		
	<i>E</i>	<i>V</i>	<i>S</i>	<i>A</i>	<i>B</i>	<i>E</i>	<i>V</i>	<i>S</i>	<i>A</i>	<i>B</i>	<i>S</i>	<i>A</i>	<i>B</i>
RDX	1.38	1.24	2.41	0	2.13	--	--	--	--	--	2.25	0.49	0.64
HMX	1.77	1.66	3.13	0	2.84	--	--	--	--	--	2.77	0.68	1.14
DNX	1.26	1.13	2.66	0	1.7	--	--	--	--	--	2.29	0.45	0.57
MNX	1.32	1.19	2.54	0	1.91	--	--	--	--	--	2.27	0.48	0.59
TNX	1.19	1.07	2.78	0	1.48	--	--	--	--	--	2.09	0.33	0.60
TNB	1.37	1.24	2.4	0	0.41	--	--	--	--	--	1.66	0.061	0.71
TNT	1.39	1.38	2.34	0	0.41	1.43, 1.57	1.38, 1.38, 1.38, 1.38	1.71, 1.78, 2.23	0, 0.11, 0.11	0.48, 0.61, 0.62	1.81	0.012	0.68
4NAN	0.89	1.09	1.36	0	0.43	0.87	1.09, 1.09, 1.09	1.21, 1.32, 1.43, 1.47	0, 0, 0.14, 0.20	0.24, 0.25, 0.46	1.29	0.030	0.40

^a Only available for TNT and 4NAN. Details are available in Table A-2.

^b From this work. Solute parameters of HMX were derived with the estimated $\log K_{hw}$ (-3.95); solute parameters of MNX were derived without $\log K_{dw}$. The statistics of the multiple linear regression analysis for the resulted solute parameters are available in Table 2-3.

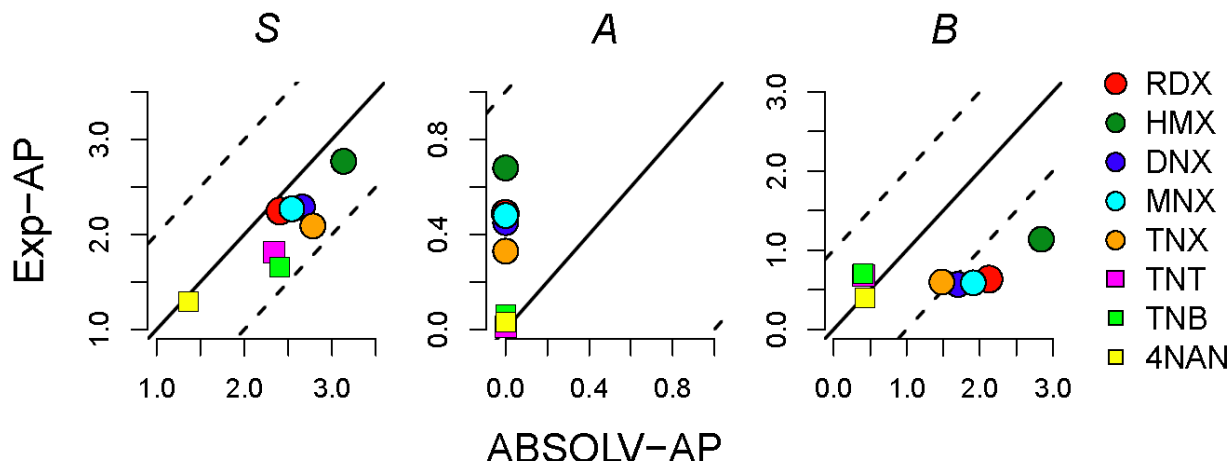


Figure 2-1 Comparisons between experimentally derived Abraham parameters (Exp-AP) from this work and ABSOLV estimated Abraham parameters (ABSOLV-AP). The dots are for nitroaromatics compounds and the squares are for cyclic nitramines and nitrosamines.

Fig. 2-1 shows the comparisons between Exp-AP and ABSOLV-AP for the compounds in this study. The *S* parameters (Fig. 2-1 left panel) of Exp-AP are slightly smaller than ABSOLV-AP but have a similar trend. The Exp-AP and ABSOLV-AP are in agreement that the cyclic nitramines and nitrosamines have stronger dipolarity/polarizability (larger *S* parameters) than the nitroaromatics.

For *A* (Fig. 2-1 middle panel), ABSOLV-AP are all zero. However, Exp-AP distinguish the compounds structurally: $A \approx 0$ for nitroaromatics, while $A > 0$ for cyclic nitramines and nitrosamines. This indicates that there is no, or very weak, hydrogen-bond donating ability of TNT, TNB, and 4NAN but increasing hydrogen-bond donating ability for TNX, DNX, MNX, RDX, and HMX, ordered from low to high.

The *B* parameters (Fig. 2-1 right panel) of Exp-AP (0.68 for TNT, 0.71 for TNB, and 0.40 for 4NAN) are not very different from ABSOLV-AP (0.41 for TNT, 0.41 for TNB, and 0.43 for 4NAN) for nitroaromatics. For cyclic nitramines and nitrosamines, ABSOLV-AP are substantially larger (1.48 to 2.84) than Exp-AP (0.57 to 1.14).

2.3.5 Comparison of Solvent-Water Partition Coefficients between Experimental Measurements and Model Predictions

Graphical comparisons of solvent-water partition coefficients between the experimental measurements from this study and model predictions are shown in Fig. 2-2. The predictions are made using ABSOLV-AP (Fig. 2-2 upper row) and Exp-AP (Fig. 2-2 lower row). Since the experimental measurements are used to estimate Exp-AP, it is not a surprise that the predictions using Exp-AP compare favorably to the measurements. It is the ABSOLV-AP results that are

noteworthy. The ABSOLV-AP predictions for nitroaromatics TNT, TNB, and 4NAN are generally in good agreement with experimental measurements. The large discrepancies are observed for $\log K_{cw}$ and $\log K_{dw}$ of TNT (errors = 1.33 and 1.14 log units respectively), and also for $\log K_{cw}$ and $\log K_{dw}$ of TNB (errors = 1.32 and 1.68 log units respectively). However, errors are significantly larger for the cyclic nitramines and nitrosamines (RDX, HMX, TNX, DNX, and MNX). An error of up to 7 log units is observed for the $\log K_{tw}$ (toluene-water partition coefficient) of HMX. The overall RMSE of ABSOLV-AP predictions is up to 3.56 log units. The large discrepancy is probably due to the missing -R₂N-NO and -R₂N-NO₂ functional groups in the ABSOLV fragment database²¹. The accuracy of a fragment model depends on the availability of experimental data for molecules containing the fragment of interest. If the fragment is not in the database, the method fails.

Using S , A , and B parameters of Exp-AP in the pp-LFER equations, the prediction accuracy increases significantly with RMSE reduced to 0.38 log units. All the errors are within one order of magnitude except for the $\log K_{cw}$ of HMX of 1.09 log units. For 4NAN, the predictions using Exp-AP are in very good agreement with experimental measurements with errors less than 0.03 log units.

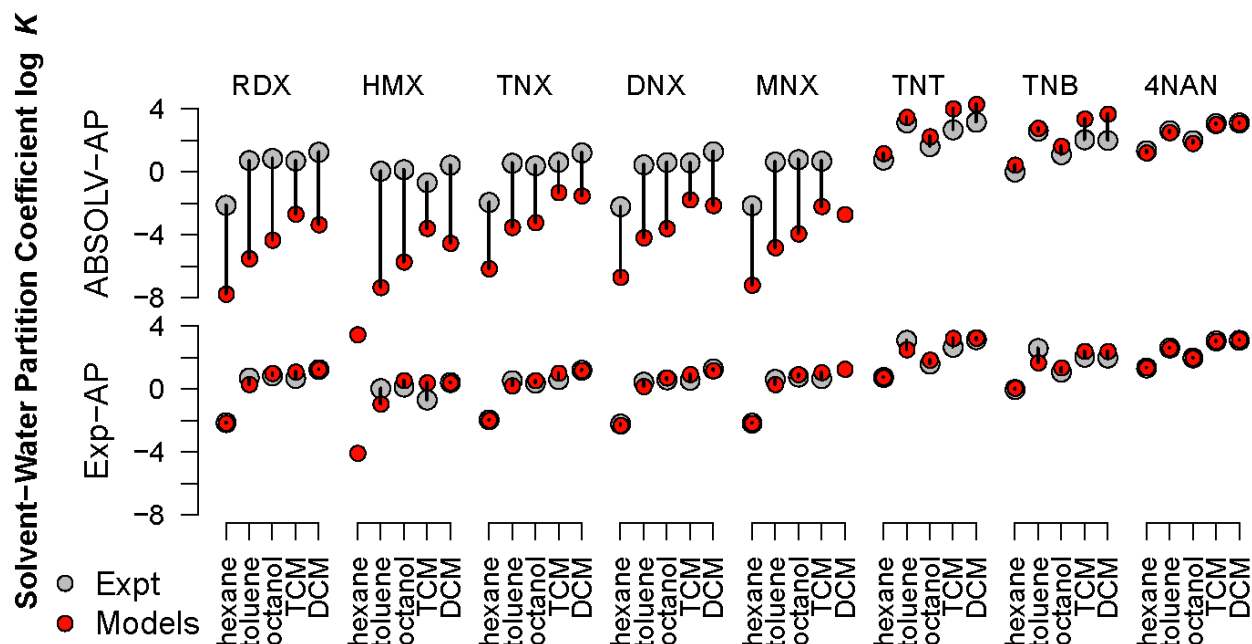


Figure 2-2 Solvent-water partition coefficients: grey symbols are experimental measurements, red symbols are estimates. Upper row are model predictions using ABSOLV estimated Abraham parameters (ABSOLV-AP), lower row are experimentally derived Abraham parameters (Exp-AP) from this work. The solvents in the solvent-water systems are hexane, toluene, octanol, trichloromethane (TCM), and dichloromethane (DCM). Values of experimental measurements and model predictions for solvent-water partition coefficients are summarized in Table A-4 (Solvent-water partition coefficients from literature compilations, experimental measurements, and model predictions).

2.3.6 Comparison of Physico-Chemical Properties between Experimental Measurements and Model Predictions

Because Exp-AP derived in this study were obtained from the solvent-water partitioning data, it is useful to compare their predictions relative to ABSOLV-AP for other physico-chemical properties not used in their estimation. Fig. 2-3 presents comparisons for water-air, organic carbon-water, and for water solubility. For water-air partition coefficient (K_{wa}), predictions using Exp-AP agree well with the experimental data for RDX, HMX, and TNT with prediction errors within 0.79 log units whereas predictions with ABSOLV-AP have errors up to 7.34 log units. For organic carbon-water partition coefficient (K_{oc}), predictions using Exp-AP fit experimental measurements within 0.40 log units for RDX, HMX, TNT, and TNB. Errors using ABSOLV-AP for TNT and TNB are comparable, but much larger for RDX and HMX with errors up to 2 log units. For water solubility (S) of TNT and TNB, using both sets of parameters (Exp-AP and ABSOLV-AP) have prediction errors within 0.57 and 0.32 log units respectively. Surprisingly,

both have problems with RDX and HMX. However, the prediction errors of ABSOLV are much larger. In summary, predictions using Exp-AP are more accurate than those using ABSOLV-AP.

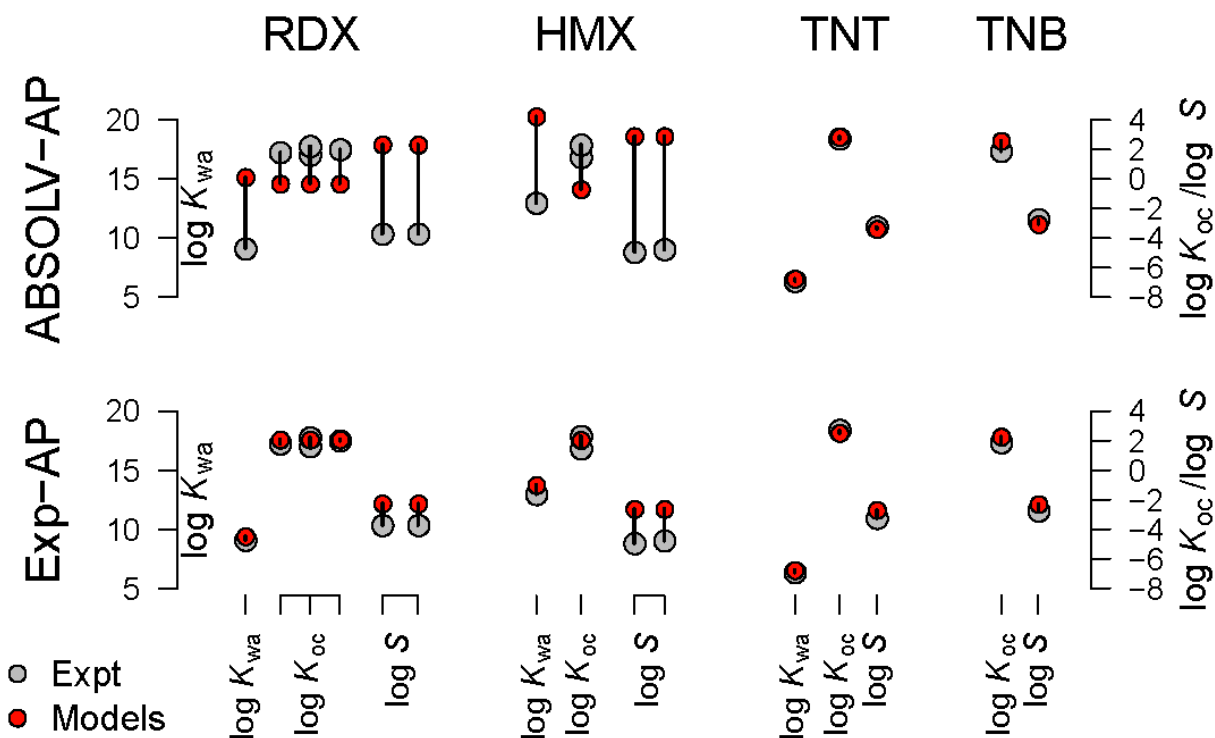


Figure 2-3 Comparisons between experimental measurements and model predictions with ABSOLV estimated (ABSOLV-AP) or experimentally derived (Exp-AP) Abraham parameters from this work for water-air partition coefficient ($\log K_{wa}$, L_{air}/L_{water}), organic carbon-water partition coefficient ($\log K_{oc}$, $L \cdot kg^{-1}$), and water solubility ($\log S$, $mol \cdot L^{-1}$). The y-axis on the left is for $\log K_{wa}$ and y-axis on the right is for $\log K_{oc}$ and $\log S$. Experimental values from different sources were plotted individually, against model predictions. Those with two grey dots per property denote the reported ranges. Experimental measurements were compiled from several sources for K_{wa} ²⁷, K_{oc} ^{12, 30, 47-49}, and S ^{27, 30, 50}. Literature system parameters^{44, 51, 52} are listed in Table A-5. Values of experimental measurements and model predictions are summarized in Table A-6 (Physical-chemical properties of experimental measurements and model predictions).

2.4 Summary and Conclusions

The Exp-AP of the eight MCs (RDX, HMX, TNT, and TNB) and munition-like compounds (MNX, DNX, TNX, and 4NAN) were determined using the experimental solvent-water partition coefficients measured in this study. The solvents in the solvent-water systems included octanol, hexane, toluene, trichloromethane and dichloromethane. The only available literature reported partition coefficients were for octanol-water for some investigated compounds and they were in good agreement with the experimental measurements from this study. The correlations of experimental partition coefficients for some solute pairs or solvent system pairs indicated the consistency of the experimental data, and therefore could be used as predictive tools.

The predictions using Exp-AP were in good agreement with the experimental values, and had higher accuracy than those using ABSOLV-AP for partitioning in solvent-water, water-air, and organic carbon-water systems, as well as water solubility. The failure of ABSOLV based predictions particularly for cyclic nitramines and nitrosamines is probably due to the missing $-R_2N-NO_2$ and $-R_2N-NO_2$ functional groups in its fragment database. Special attention should be paid when using ABSOLV-AP for novel and complex compounds.

References

1. Halasz, A.; Groom, C.; Zhou, E.; Paquet, L.; Beaulieu, C.; Deschamps, S.; Corriveau, A.; Thiboutot, S.; Ampleman, G.; Dubois, C.; Hawari, J. Detection of explosives and their degradation products in soil environments. *J. Chromatogr. A* **2002**, *963* (1–2), 411-418.
2. Simini, M.; Wentsel, R. S.; Checkai, R. T.; Phillips, C. T.; Chester, N. A.; Major, M. A. Evaluation of soil toxicity at Joliet army ammunition plant. *Environ. Toxicol. Chem.* **1995**, *14* (4), 623-630.
3. Klausmeier, R.; Osmon, J.; Walls, D. The effect of trinitrotoluene on microorganisms. *Dev. Ind. Microbiol.* **1973**, (15), 309-317.
4. Spanggord, R. J., Mabey, W. R., Chou, T. W., Haynes, D. L., Alferness, P. L., Tse, D. S., Mill, T. *Environmental fate studies of HMX screening studies*; Final Report, Phase I, LSU-4412; SRI International: Menlo Park, CA. 1982.
5. Smock, L. A.; Stoneburner, D. L.; Clark, J. R. The toxic effects of trinitrotoluene (TNT) and its primary degradation products on two species of algae and the fathead minnow. *Water Res.* **1976**, *10* (6), 537-543.
6. Won, W. D.; DiSalvo, L. H.; Ng, J. Toxicity and mutagenicity of 2,4,6-trinitrotoluene and its microbial metabolites. *Appl. Environ. Microbiol.* **1976**, *31* (4), 576-80.
7. Palazzo, A. J.; Leggett, D. C. Effect and disposition of TNT in a terrestrial plant. *J. Environ. Qual.* **1986**, *15* (1).
8. Yinon, J. *Toxicity and Metabolism of Explosives*; CRC Press: Boca Raton, FL, 1990.
9. Beller, H. R.; Tiemeier, K. Use of liquid chromatography/tandem mass spectrometry to detect distinctive indicators of in situ RDX transformation in contaminated groundwater. *Environ. Sci. Technol.* **2002**, *36* (9), 2060-2066.
10. Moshe, S. S. B.; Ronen, Z.; Dahan, O.; Bernstein, A.; Weisbrod, N.; Gelman, F.; Adar, E. Isotopic evidence and quantification assessment of in situ RDX biodegradation in the deep unsaturated zone. *Soil Biol. Biochem.* **2010**, *42* (8), 1253-1262; <http://dx.doi.org/10.1016/j.soilbio.2010.04.011>.
11. Zhang, B.; Kendall, R. J.; Anderson, T. A. Toxicity of the explosive metabolites hexahydro-1,3,5-trinitroso-1,3,5-triazine (TNX) and hexahydro-1-nitroso-3,5-dinitro-1,3,5-triazine (MNX) to the earthworm *Eisenia fetida*. *Chemosphere* **2006**, *64* (1), 86-95.

12. Reddy, G.; Williams, M. A. Wildlife toxicity assessment for 1,3,5-Trinitrobenzene (TNB). In *Wildlife Toxicity Assessments for Chemicals of Military Concern*; Williams, M. A., Reddy, G., Quinn, M. J., Johnson, M. S., Eds.; Elsevier: Amsterdam, 2015; pp 183-204.
13. Sunahara, G. I., Lotufo, G., Kuperman, R. G., Hawari, J., Eds. *Ecotoxicology of Explosives*; CRC Press: Boca Raton, FL, 2009.
14. Schwarzenbach, R. P.; Gschwend, P. M.; Imboden, D. M. *Environmental Organic Chemistry*; Wiley: Hoboken, NJ, 2003.
15. Karickhoff, S. W., Carreira, L. A., Melton, C., McDaniel, V. K., Vellino, A. N., Nate, D. E. *Computer prediction of chemical reactivity-The ultimate SAR*; US EPA 600. M-89-017; US Environmental Protection Agency: Athens, GA, 1989.
16. Endo, S.; Goss, K. U. Applications of polyparameter linear free energy relationships in environmental chemistry. *Environ. Sci. Technol.* **2014**, *48* (21), 12477-12491.
17. Abraham, M. H. Application of solvation equations to chemical and biochemical processes. *Pure Appl. Chem.* **1993**, *65* (12), 2503.
18. Abraham, M. H.; Grellier, P. L.; Hamerton, I.; McGill, R. A.; Prior, D. V.; Whiting, G. S. Solvation of gaseous non-electrolytes. *Faraday Discuss. Chem. Soc.* **1988**, *85*, 107-115.
19. UFZ-LSER database, v 2.1. Helmholtz Centre for Environmental Research-UFZ: Leipzig, Germany, 2015. [https://www.ufz.de/index.php?en=31698&contentonly=1&m=0&lserd_data\[mvc\]=Public/start](https://www.ufz.de/index.php?en=31698&contentonly=1&m=0&lserd_data[mvc]=Public/start) (accessed Feb 2, 2016).
20. ACD/Percepta, v 2012. ACD/Labs: Toronto, Canada, 2015. <https://www.acdlabs.com> (accessed Feb 20, 2016).
21. Platts, J. A.; Butina, D.; Abraham, M. H.; Hersey, A. Estimation of molecular linear free energy relation descriptors using a group contribution approach. *J. Chem. Inf. Comput. Sci.* **1999**, *39* (5), 835-845.
22. Abraham, M. H.; McGowan, J. C. The use of characteristic volumes to measure cavity terms in reversed phase liquid chromatography. *Chromatographia* **1987**, *23* (4), 243-246.
23. Stenzel, A.; Goss, K. U.; Endo, S. Prediction of partition coefficients for complex environmental contaminants: Validation of COSMOtherm, ABSOLV, and SPARC. *Environ. Toxicol. Chem.* **2014**, *33* (7), 1537-1543.
24. Briggs, G. G. Theoretical and experimental relationships between soil adsorption, octanol-water partition coefficients, water solubilities, bioconcentration factors, and the parachor. *J. Agric. Food Chem.* **1981**, *29* (5), 1050-1059.

25. Di Toro, D. M.; McGrath, J. A.; Hansen, D. J. Technical basis for narcotic chemicals and polycyclic aromatic hydrocarbon criteria. I. Water and tissue. *Environ. Toxicol. Chem.* **2000**, *19* (8), 1951-1970.
26. LOGKOW Databank, a databank of evaluated octanol-water partition coefficients. Sangster Research Laboratories: Montreal, Quebec, Canada, **1993**.
27. Burrows, E. P., Rosenblatt, D. H., Mitchell, W. R., Parmer, D. L. *Organic explosives and related compounds. Environmental and health considerations*; No. USABRDL-TR-8901; US Army Biomedical Research and Development Lab: Frederick, MD, 1989.
28. Walsh, M. E.; Jenkins, T. F.; Thorne, P. G. Laboratory and analytical methods for explosives residues in soil. *J. Energ. Mater.* **1995**, *13* (3-4), 357.
29. Banerjee, S.; Yalkowsky, S. H.; Valvani, C. Water solubility and octanol/water partition coefficients of organics. Limitations of the solubility-partition coefficient correlation. *Environ. Sci. Technol.* **1980**, *14* (10), 1227-1229.
30. Monteil-Rivera, F.; Groom, C.; Hawari, J. Sorption and degradation of octahydro-1,3,5,7-tetranitro-1,3,5,7-tetrazocine in soil. *Environ. Sci. Technol.* **2003**, *37* (17), 3878-3884.
31. Technical Fact Sheet-2,4,6-Trinitrotoluene(TNT). https://www.epa.gov/sites/production/files/2014-03/documents/ffrrofactsheet_contaminant_tnt_january2014_final.pdf.
32. Hansch, C.; Leo, A.; Hoekman, D. H. *Exploring QSAR - Hydrophobic, Electronic, and Steric Constants*; American Chemical Society: Washington, DC, 1995, p 27.
33. Hansch, C.; Leo, A. *Substituent Constants for Correlation Analysis in Chemistry and Biology*; Wiley: New York, 1979.
34. Zissimos, A. M.; Abraham, M. H.; Barker, M. C.; Box, K. J.; Tam, K. Y. Calculation of Abraham descriptors from solvent-water partition coefficients in four different systems; evaluation of different methods of calculation. *J. Chem. Soc., Perkin Trans. 2* **2002**, 2001–2010.
35. Leahy, D. E.; Taylor, P. J.; Wait, A. R. Model solvent systems for QSAR Part 1. propylene glycol dipelargonate (PGDP). A new standard solvent for use in partition coefficient determination. *Quant. Struct.-Act. Relat.* **1989**, *8* (1), 17-31.
36. Leahy, D. E.; Morris, J. J.; Taylor, P. J.; Wait, A. R. Model solvent systems for QSAR. Part 2. Fragment values ('f-values') for the 'critical quartet'. *J. Chem. Soc., Perkin Trans. 2* **1992**, (4), 723-731.

37. Leahy, D. E.; Morris, J. J.; Taylor, P. J.; Wait, A. R. Model Solvent Systems for QSAR. Part 3. An LSER analysis of the "Critical Quartet". New light on hydrogen bond strength and directionality. *J. Chem. Soc., Perkin Trans. 2* **1992**, (4), 705-722.
38. Organization for Economic Co-operation and Development. Test No. 107: Partition coefficient (n-octanol/water): Shake flask method. OECD Publishing, 1995.
39. Gonzalez, R.; Michelson, K.; Di Toro, D. M.; Allen, H. E. Modeling the reversible and resistant components of munition constituent adsorption and desorption on soils. *Water, Air, Soil Pollut.* **2015**, 226 (7), 1-11.
40. Abraham, M. H. Scales of solute hydrogen-bonding: Their construction and application to physicochemical and biochemical processes. *Chem. Soc. Rev.* **1993**, 22 (2), 73.
41. Abraham, M. H.; Ibrahim, A.; Zissimos, A. M. Determination of sets of solute descriptors from chromatographic measurements. *J. Chromatogr. A* **2004**, 1037 (1-2), 29-47.
42. Katritzky, A. R.; Sild, S.; Karelson, M. General quantitative structure-property relationship treatment of the refractive index of organic compounds. *J. Chem. Inf. Model.* **1998**, 38 (5), 840-844.
43. Arey, J. S.; Green, W. H.; Gschwend, P. M. The electrostatic origin of Abraham's solute polarity parameter. *J. Phys. Chem. B.* **2005**, 109 (15), 7564-7573.
44. Abraham, M. H.; Smith, R. E.; Luchtefeld, R.; Boorem, A. J.; Luo, R.; Acree, W. E. Prediction of solubility of drugs and other compounds in organic solvents. *J. Pharm. Sci.* **2010**, 99 (3), 1500-1515.
45. The R Stats Package, v 3.0.2. R Foundation for Statistical Computing: Vienna, Austria, 2013. <http://www.R-project.org/>.
46. Seiler, P. Interconversion of lipophilicities from hydrocarbon-water systems into octanol-water system. *Eur. J. Med. Chem.* **1974**, 9 (5), 473-479.
47. Technical Fact Sheet-Hexahydro-1,3,5-trinitro-1,3,5-triazine (RDX). https://www.epa.gov/sites/production/files/2014-03/documents/ffrrofactsheet_contaminant_rdx_january2014_final.pdf.
48. Spanggord, R. J., Mill, T., Chou, T. W., Mabey, W. R., Smith, J. H. *Environmental fate studies on certain munitions wastewater constituents*; SRI International: Menlo Park, CA, 1980.
49. Rosenblatt, D. H. *Contaminated soil cleanup objectives for Cornhusker army ammunition plant*; No. USAMBRDL-TR-8603; US Army Biomedical Research and Development Lab: Frederick, MD, 1986.

50. Thiboutot, S., Ampleman, G., Hewitt, A. *Guide for characterization of sites contaminated with energetic materials*; No. ERDC/CRREL-TR-02-1; US Army Engineer Research and Development Center Cold Regions Research and Engineering Laboratory: Hanover, NH, 2002.
51. Kipka, U.; Di Toro, D. M. A linear solvation energy relationship model of organic chemical partitioning to particulate organic carbon in soils and sediments. *Environ. Toxicol. Chem.* **2011**, *30* (9), 2013-2022.
52. Le, J. Ph.D. Dissertation, University of London, London, UK, 2001.

Appendix A

SUPPLEMENTARY INFORMATION FOR: EXPERIMENTAL DETERMINATION OF SOLVENT–WATER PARTITION COEFFICIENTS AND ABRAHAM PARAMETERS FOR MUNITION CONSTITUENTS

CONTENTS:

Table A-1	List of system parameters.
Table A-2	Solute descriptors collected from literature.
Table A-3	The statistics of the experimentally derived Abraham parameters.
Table A-4	Solvent-water partition coefficients from literature compilations, experimental measurements, and model predictions.
Table A-5	List of pp-LFERs used for model validation.
Table A-6	Physical-chemical properties of experimental measurements and model predictions.
Figure A-1	Comparisons of E between estimations using ABSOLV algorithm and those from experimental refractive index.
Figure A-2	Pairs plot ¹⁸ of solvent-water partition coefficients ordered by solvent.
Figure A-3	Pairs plot of solvent-water partition coefficients ordered by MCs.

Table A-1 List of system parameters.

Solvent	c	e	s	a	b	ν	Reference
hexane	0.361	0.579	-1.723	-3.599	-4.764	4.344	¹
octanol	0.088	0.562	-1.054	0.034	-3.460	3.814	¹
toluene	0.143	0.527	-0.720	-3.010	-4.824	4.545	¹
dichloromethane	0.319	0.102	-0.187	-3.058	-4.090	4.324	¹
trichloromethane	0.191	0.105	-0.403	-3.112	-3.514	4.395	¹

Table A-2 Solute descriptors collected from literature.

Name	Literature reported Abraham parameters					
	E	S	A	B	V	Reference
TNT	-	1.78	0.11	0.48	1.38	2
TNT	1.43	2.23	0.00	0.61	1.38	3
TNT	-	-	-	-	1.38	4
TNT	1.57	1.71	0.11	0.62	1.38	5
4NAN	-	1.43	0.14	0.25	1.09	2
4NAN	-	-	-	-	1.09	4
4NAN	0.87	1.32	0.20	0.24	1.09	5
4NAN	-	1.21	0.00	-	1.09	6
4NAN	-	1.47	0.00	0.46	1.09	7

Table A-3 The statistics of the experimentally derived Abraham parameters.

Compound	Parameter	Estimate	Standard error	N	SD	Adjusted R ²	p-value
RDX	<i>S</i>	2.249	0.394	5	0.421	0.995	0.003
	<i>A</i>	0.491	0.177				
	<i>B</i>	0.637	0.163				
HMX	<i>S</i>	2.774	1.013	5	1.082	0.986	0.009
	<i>A</i>	0.684	0.455				
	<i>B</i>	1.136	0.419				
DNX	<i>S</i>	2.287	0.330	5	0.353	0.996	0.002
	<i>A</i>	0.447	0.148				
	<i>B</i>	0.567	0.137				
MNX	<i>S</i>	2.266	0.615	4	0.523	0.993	0.055
	<i>A</i>	0.480	0.220				
	<i>B</i>	0.593	0.230				
TNX	<i>S</i>	2.093	0.365	5	0.390	0.995	0.003
	<i>A</i>	0.330	0.164				
	<i>B</i>	0.602	0.151				
TNT	<i>S</i>	1.809	0.571	5	0.610	0.982	0.011
	<i>A</i>	0.0119	0.257				
	<i>B</i>	0.683	0.236				

TNB	<i>S</i>	1.664	0.730	5	0.780	0.971	0.017
	<i>A</i>	0.0606	0.328				
	<i>B</i>	0.708	0.302				
4NAN	<i>S</i>	1.292	0.0304	5	0.0325	1.000	0.000
	<i>A</i>	0.0304	0.0137				
	<i>B</i>	0.398	0.0126				

Table A-4 Solvent-water partition coefficients from literature compilations, experimental measurements, and model predictions.

Solvent	Dataa	RDX	HMX	TNX	DNX	MNX	TNT	TNB	4NAN
hexane	observed	-2.10	ND ^b	-1.92	-2.19	-2.13	0.77	0.01	1.37
hexane	ABSOLV-AP	-7.75	-10.33	-6.14	-6.68	-7.18	1.18	0.45	1.22
hexane	Exp-AP	-2.14	-4.05	-1.95	-2.28	-2.15	0.76	0.08	1.38
toluene	observed	0.74	0.06	0.57	0.47	0.65	3.13	2.61	2.64
toluene	ABSOLV-AP	-5.50	-7.33	-3.51	-4.17	-4.80	3.48	2.79	2.51
toluene	Exp-AP	0.32	-0.92	0.24	0.19	0.32	2.53	1.70	2.62
TCMc	observed	0.71	-0.66	0.63	0.59	0.70	2.69	2.06	3.09
TCM	ABSOLV-AP	-2.67	-3.57	-1.30	-1.76	-2.18	4.02	3.38	3.02
TCM	Exp-AP	1.11	0.43	1.04	0.96	1.08	3.25	2.43	3.06
DCMd	observed	1.27	0.45	1.23	1.31	ND	3.17	2.01	3.13
DCM	ABSOLV-AP	-3.34	-4.52	-1.51	-2.12	-2.69	4.31	3.69	3.11
DCM	Exp-AP	1.28	0.42	1.21	1.20	1.29	3.27	2.42	3.15
octanol	observed	0.87	0.16	0.41	0.62	0.80	1.62	1.11	2.01
octanol	ABSOLV-AP	-4.32	-5.71	-3.21	-3.58	-3.92	2.25	1.64	1.82
octanol	Exp-AP	1.02	0.57	0.57	0.74	0.95	1.87	1.38	2.00
octanol	Literature reported values	0.81, 0.86, 0.87, 0.9	0.06, 0.16, 0.26	--	--	--	1.60, 1.86, 2	1.18	2.03

^a Observed denotes experimental measurements from this work; ABSOLV-AP denotes predictions using ABSOLV estimated Abraham parameters; Exp-AP denotes predictions using experimentally derived Abraham parameters from this work; the literature reported values are the same as Table 2-2.

^b Not determined; ^c Trichloromethane; ^d Dichloromethane.

Table A-5 List of pp-LFERs used for model validation.

System	pp-LFER equations	Reference
air-water	$\log K = -0.994 + 0.577E + 2.549S + 3.813A + 4.841B - 0.869V$	1
organic carbon-water	$\log K = 0.67 + 1.075E - 0.277S - 0.363A - 1.697B + 1.468V$	8
water solubility	$\log K = 0.368 - 0.711E + 0.407S + 1.73A + 3.383B - 3.493V - 1.036AB - 0.005(mp - 25)$ where mp = melting point (°C)	9

Table A-6 Physical-chemical properties of experimental measurements and model predictions.

Property	Compounds	Exp-AP ^a	ABSOLV-AP ^b	Observed		
organic carbon-water (log <i>K</i> _{oc} , L·kg ⁻¹)	RDX	2.09	-0.31	1.80 ¹⁰	1.62-2.22 ¹¹	2.00 ¹²
	HMX	2.06	-0.68	1.47-2.32 ¹³		
	TNT	2.53	2.85	2.72 ¹²		
	TNB	2.28	2.60	1.88 ¹⁴		
water-air (log <i>K</i> _{wa} , L _{air} /L _{water})	RDX	9.43	15.18	9.10 ¹⁵		
	HMX	13.76	20.31	12.97 ¹⁵		
	TNT	6.56	6.56	6.35 ¹⁵		
water solubility (log <i>S</i> , mol·L ⁻¹)	RDX	-2.24	2.34	-3.72 ¹⁶	-3.72 ¹³	
	HMX	-2.61	2.91	-4.77 ¹⁶	-4.95 ¹³	
	TNT	-2.67	-3.38	-3.24 ¹⁶		
	TNB	-2.28	-3.06	-2.74 ¹⁵		

^a Predictions using experimentally derived Abraham parameters from this work.

^b Predictions using ABSOLV estimated Abraham parameters.

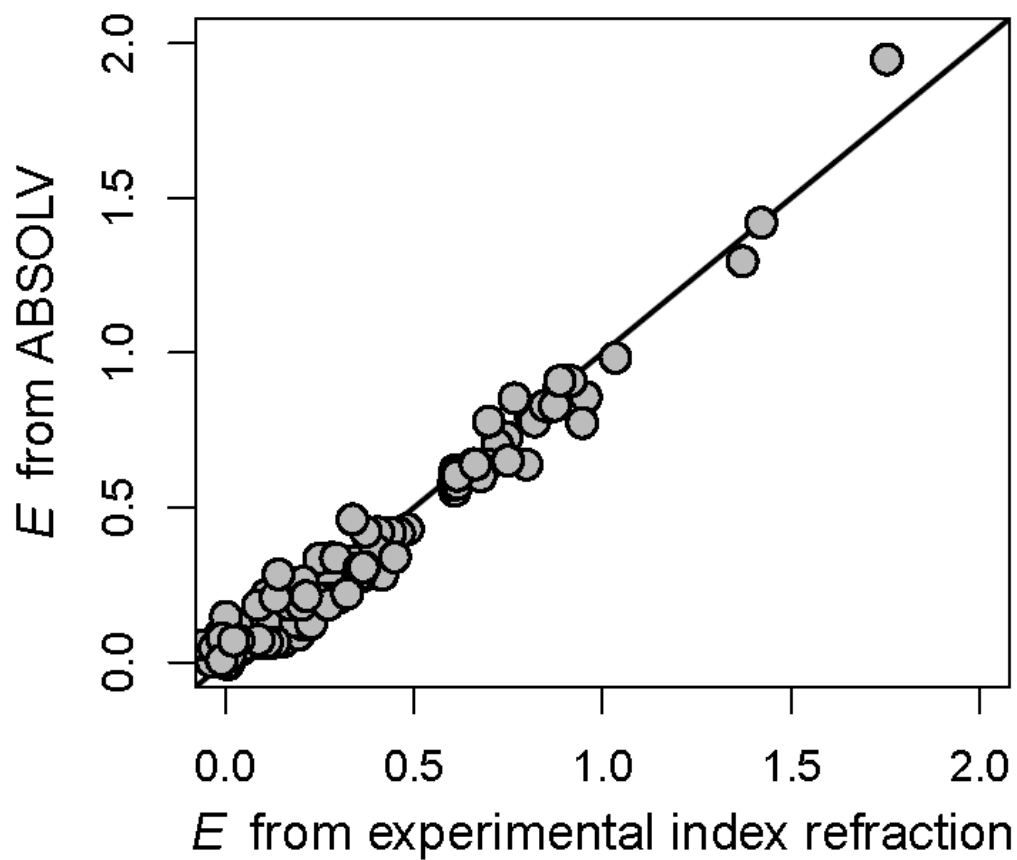


Figure A-1 Comparisons of E between estimations using ABSOLV algorithm and those from experimental refractive index. The solid line shows perfect agreement. Experimental refractive index was taken from Katritzky et al.¹⁷.

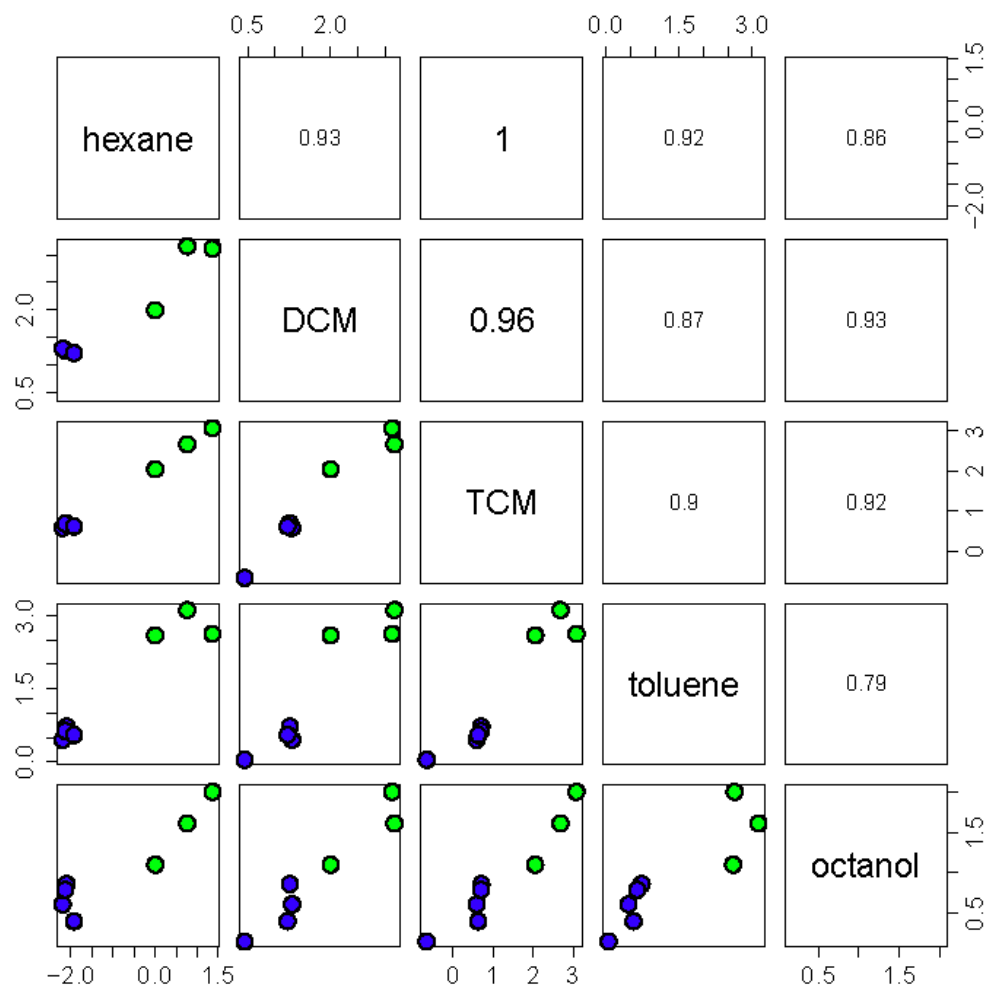


Figure A-2 Pairs plot¹⁸ of solvent-water partition coefficients ordered by solvent. The blue dots are cyclic nitramines and nitrosamines, and the green dots are nitroaromatics. For each data plot, x axis label is the solvent above the plot, y axis label is to the right of the plot. The upper triangular panels display the coefficient of determination (R^2) of the respective pair. For each R^2 panel, x axis label is the solvent below the plot, y axis label is to the left of the plot.

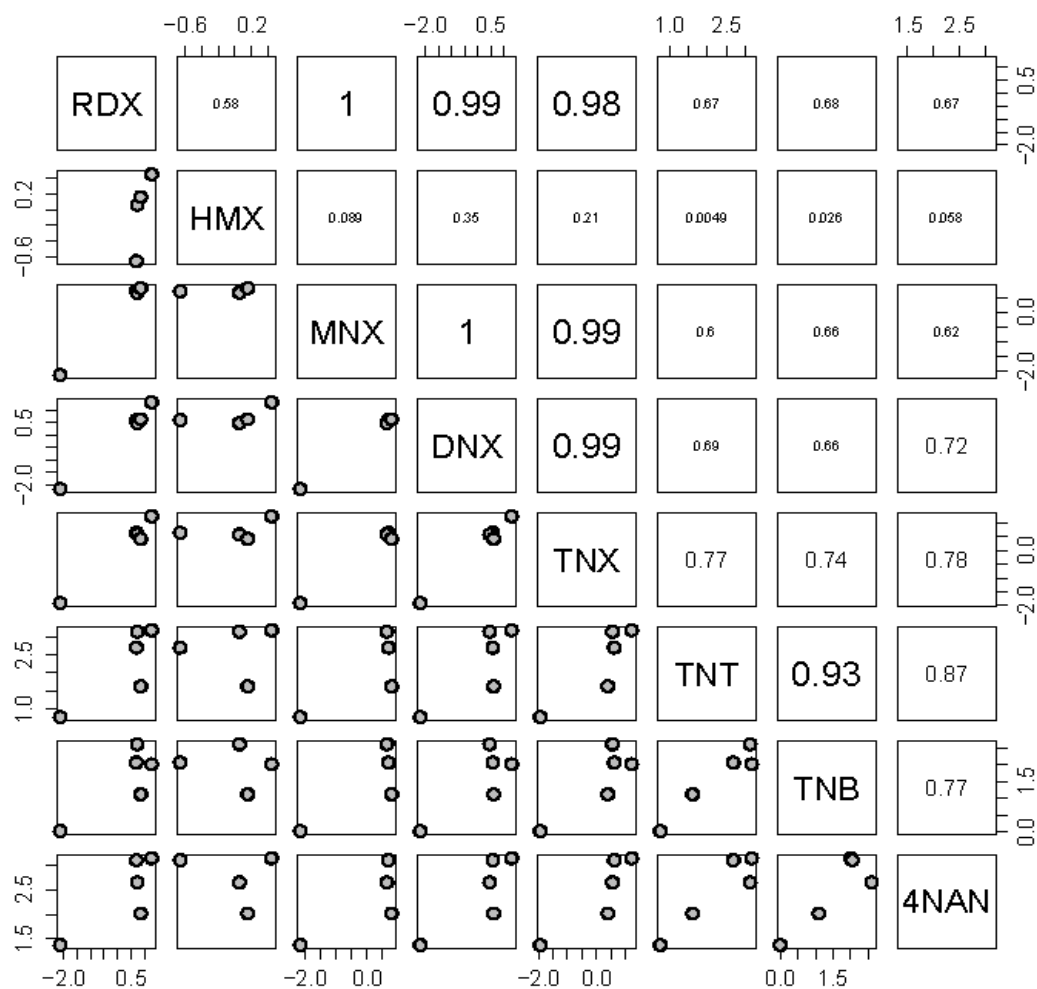


Figure A-3 Pairs plot of solvent-water partition coefficients ordered by MCs. For each data plot, x axis label is the MC above the plot, y axis label is the MC to the right of the plot. The upper triangular panels display the coefficient of determination (R^2) of the respective pair. For each R^2 panel, x axis label is the MC below the plot, y axis label is the MC to the left of the plot.

References

1. Abraham, M. H.; Smith, R. E.; Luchtefeld, R.; Boorem, A. J.; Luo, R.; Acree, W. E. Prediction of solubility of drugs and other compounds in organic solvents. *J. Pharm. Sci.* **2010**, *99* (3), 1500-1515.
2. Bronner, G.; Goss K. U.; Fenner, K. Hexadecane/air partitioning coefficients of multifunctional compounds: Experimental data and modeling. *Fluid Phase Equilib.* **2010**, *299* (2), 207-215.
3. Houser, E. J.; Mlsna, T. E.; Nguyen, V. K.; Chung, R.; Mowery, R. L.; McGill, R. A. Rational materials design of sorbent coatings for explosives: applications with chemical sensors. *Talanta* **2001**, *54* (3), 469-485.
4. Stenzel, A.; Endo, S.; Goss, K. U. Measurements and predictions of hexadecane/air partition coefficients for 387 environmentally relevant compounds. *J. Chromatogr. A* **2012**, *1220*, 132-142.
5. Tulp, H. C.; Goss, K. U.; Schwarzenbach, R. P.; Fenner, K. Experimental determination of LSER parameters for a set of 76 diverse pesticides and pharmaceuticals. *Environ. Sci. Technol.* **2008**, *42* (6), 2034-2040.
6. Abraham, M. H. Hydrogen bonding: XXVII. Solvation parameters for functionally substituted aromatic compounds and heterocyclic compounds, from gas-liquid chromatographic data. *J. Chromatogr. A* **1993**, *644* (1), 95-139.
7. Stenzel, A.; Goss, K. U.; Endo, S. Experimental determination of polyparameter linear free energy relationship (pp-LFER) substance descriptors for pesticides and other contaminants: new measurements and recommendations. *Environ. Sci. Technol.* **2013**, *47* (24), 14204-14.
8. Kipka, U.; Di Toro, D. M. A linear solvation energy relationship model of organic chemical partitioning to particulate organic carbon in soils and sediments. *Environ. Toxicol. Chem.* **2011**, *30* (9), 2013-2022.
9. Le, J. Ph.D. Dissertation, University of London, London, UK, 2001.
10. Technical Fact Sheet-Hexahydro-1,3,5-trinitro-1,3,5-triazine (RDX). https://www.epa.gov/sites/production/files/2014-03/documents/ffirfactsheet_contaminant_rdx_january2014_final.pdf.
11. Spanggord, R. J., Mill, T., Chou, T. W., Mabey, W. R., Smith, J. H. *Environmental fate studies on certain munitions wastewater constituents*; SRI International: Menlo Park, CA, 1980.
12. Rosenblatt, D. H. *Contaminated soil cleanup objectives for Cornhusker army ammunition plant*; No. USAMBRDL-TR-8603; US Army Biomedical Research and Development Lab: Frederick, MD, 1986.

13. Monteil-Rivera, F.; Groom, C.; Hawari, J. Sorption and degradation of octahydro-1,3,5,7-tetranitro-1,3,5,7-tetrazocine in soil. *Environ. Sci. Technol.* **2003**, *37* (17), 3878-3884.
14. Reddy, G.; Williams, M. A. Wildlife toxicity assessment for 1,3,5-Trinitrobenzene (TNB). In *Wildlife Toxicity Assessments for Chemicals of Military Concern*; Williams, M. A., Reddy, G., Quinn, M. J., Johnson, M. S., Eds.; Elsevier: Amsterdam, 2015; pp 183-204.
15. Burrows, E. P., Rosenblatt, D. H., Mitchell, W. R., Parmer, D. L. *Organic explosives and related compounds. Environmental and health considerations*; No. USABRDL-TR-8901; US Army Biomedical Research and Development Lab: Frederick, MD, 1989.
16. Thiboutot, S., Ampleman, G., Hewitt, A. *Guide for characterization of sites contaminated with energetic materials*; No. ERDC/CRREL-TR-02-1; US Army Engineer Research and Development Center Cold Regions Research and Engineering Laboratory: Hanover, NH, 2002.
17. Katritzky, A. R.; Sild, S.; Karelson, M. General quantitative structure-property relationship treatment of the refractive index of organic compounds. *J. Chem. Inf. Model.* **1998**, *38* (5), 840-844.
18. R: A Language and Environment for Statistical Computing. <https://cran.r-project.org/doc/manuals/r-release/fullrefman.pdf> (accessed May 15, 2016, p 849).

Chapter 3

QUANTUM CHEMICALLY ESTIMATED ABRAHAM SOLUTE PARAMETERS USING MULTIPLE SOLVENT-WATER PARTITION COEFFICIENTS AND MOLECULAR POLARIZABILITY

Abstract

Polyparameter Linear Free Energy Relationships (pp-LFERs) predict many environmentally significant properties. However, Abraham solute Parameters (AP) are required. A method is presented for computing the AP based on molecular structure only using quantum chemical calculations. The AP for 1827 neutral solutes are included. Two innovations are (1) using partition coefficients for sixty-five solvent-water systems computed using the quantum mechanical COSMO-SAC solvation model, and (2) computing E using DFT computed molecular polarizability and the Clausius–Mossotti equation. Computing E directly is critical for reliable estimation of the remaining solute parameters S , A , and B using the solvent-water partition coefficients. These solute parameters, referred to as Quantum Chemically estimated Abraham Parameters (QCAP), are further adjusted by fitting to experimentally-based solute parameters using the QCAP parameters as the independent variables. These Adjusted QCAP are compatible with existing Abraham pp-LFERs. Predicted logarithmic solvent-water partition coefficients using Adjusted QCAP for 24 solvent-water systems have the smallest root mean square errors (RMSEs) compared to predictions made using the molecular fragment based method ABSOLV. For munition constituents and munition-like compounds, Adjusted QCAP have much lower RMSE than does ABSOLV which essentially fails for these compounds.

3.1 Introduction

Polyparameter linear free energy relationships (pp-LFERs), such as the Abraham solvation model, have been widely used to predict environmentally significant properties.¹⁻⁴ pp-LFERs predict the solute partition coefficient between two phases, K , for the changes in molecular interaction energies involved in transferring a chemical between the two phases:

$$\log K = c + eE + sS + aA + bB + vV \quad (3-1)$$

where K = ratio of the solute concentrations in the two phases. The capital letters represent solute parameters that describe the following solute properties: E , excess molar refraction; S , dipolarity/polarizability; A , ability to donate hydrogen-bonds; B , ability to accept hydrogen-bonds; and V , molar volume. The lowercase letters are the complementary solvent parameters. The terms in Eq. (3-1) reflect the complementary abilities of one phase (e.g. octanol) relative to the other phase (e.g. water) to undergo the corresponding molecular interactions. Thus, the parameter pairs quantify the following interactions: eE , the polarization induced dispersion interactions; sS , the dipole-dipole and dipole-induced dipole interactions; aA and bB , the H-bond interactions; and vV , the energy of cavity formation. The constant c accounts for the remaining energy difference and has the units of the solute concentrations. Abraham and co-workers have successfully applied Eq. (3-1) to more than 400 properties or processes.⁵ However, the applicability of these pp-LFERs depends on the availability of the Abraham solute Parameters (AP).

Many methods⁶⁻¹⁷ have been proposed to predict the solute AP for neutral organic compounds. A commonly-used method is the ABSOLV prediction module¹⁷ that utilizes a molecular fragment based method with Platts-type fragment descriptors.¹⁶ A set of 81 atom and functional group fragments are used to estimate E , S , and B and a separate set of 51 fragments are used for A .¹⁶ V is the McGowan characteristic volume.¹⁸ The coefficients of the fragment descriptors are estimated using existing experimental partitioning data or experimentally derived solute AP of more than 5000 compounds.¹⁷ The optimization procedures reduced the root mean square errors (RMSEs) comparing predicted to observed solute AP to 0.12, 0.22, 0.07, 0.15, and 0.01 for E , S , A , B , and V , respectively.¹⁷ However, the data used and the details of the optimization procedures used to obtain the fragment constants were not reported. Therefore it is difficult to reproduce an estimate or to diagnose a failure.

Problems can arise when ABSOLV is used to estimate AP for a new substance or substance class that is not within the training scope of the solutes used to obtain the fragment constants. A dramatic failure of ABSOLV was observed for munition constituents (MCs) and munition-like compounds.¹⁹ As shown in Figure 3-1, large discrepancies were found between experimentally derived and ABSOLV estimated AP (Figure 3-1(1)) and between experimental and ABSOLV predicted solvent-water partition coefficients (K_{sw} , Figure 3-1(2)). It was suggested that the failure for these cyclic nitramines and cyclic nitrosamines was due to the missing $-R_2N-NO_2$ and $-R_2N-NO_2$ functional groups in the ABSOLV fragment database.¹⁹

Additionally, ABSOLV assumes that the contribution of a functional group is fixed and not influenced by the chemical environment adjacent to the fragment within the molecule.^{20, 21} Changes due to charge, dipole, and higher multiple moments on adjacent functional groups, electronic push-pull effects, intramolecular hydrogen bond formation, and steric effects are not considered.²⁰ These problems could be addressed by including more correction factors. However, this would require more fitted parameters. Also, positional isomers are not distinguished using a group contribution method²² whereas the quantum chemical method used in this study can distinguish between positional isomers.^{23, 24}

For a proposed method to determine solute AP using measured solvent-water partition coefficients, Leahy et al.^{25, 26} proposed using four carefully selected solvent-water systems that incorporate the necessary interactions between a solvent-water system and a given solute. Zissimos et al.²⁷ proposed using octanol, chloroform, cyclohexane, and toluene. With E obtained from an experimental refractive index or by the summation of fragments,¹⁶ and V , the McGowan characteristic volume, from bond and atom contributions,^{2, 18} the three remaining unknowns (S , A , and B) were obtained by fitting Eq. (3-1) to the four experimental solvent-water partition coefficients using a multiple linear regression (MLR). Estimates can also be made if experimental partitioning data for other systems are used, such as solvent-solvent or solvent-air partition coefficients, solubility, and chromatographic data.²⁸⁻³¹

However, the above methods require experimental data that are either not available, or are not feasible to be measured in various systems for every substance of interest. Therefore, a method that overcomes the shortcomings of ABSOLV and does not rely on experimental data would be a useful addition to the methods available to estimate solute AP.

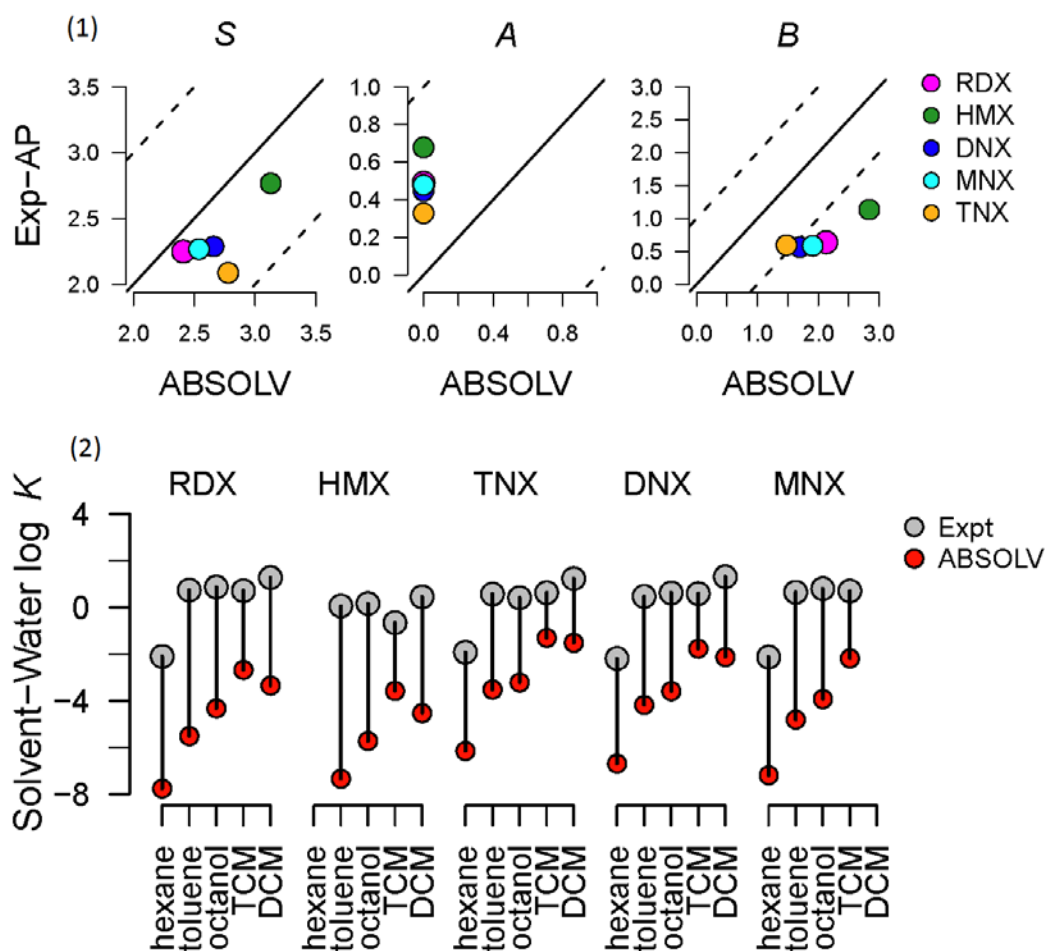


Figure 3-1 (1) Comparison of experimentally derived Abraham parameters (Exp-AP)¹⁹ and ABSOLV estimated Abraham parameter (ABSOLV) for hexahydro-1,3,5-trinitro-1,3,5-triazacyclohexane (RDX), octahydro-1,3,5,7-tetranitro-1,3,5,7-tetraazacyclooctane (HMX), hexahydro-1-nitroso-3,5-dinitro-1,3,5-triazine (MNX), hexahydro-1,3,5-trinitroso-1,3,5-triazine (TNX), and hexahydro-1,3-dinitroso-5-nitro-1,3,5-triazine (DNX). (2) Comparison of experimental¹⁹ and ABSOLV predicted solvent-water partition coefficients for RDX, HMX, DNX, MNX, and TNX. The solvents are hexane, toluene, octanol, trichloromethane (TCM), and dichloromethane (DCM).

The method presented below uses quantum mechanically estimated solvent-water partition coefficients as suggested by Stenzel et al.³² to estimate *S*, *A*, and *B*. The Conductor-like Screening Model for Segment Activity Coefficient (COSMO-SAC)³³⁻³⁶ version 2013³⁶ is used to compute the required solvent-water partition coefficients. The COSMO-SAC predictions are based on molecular structure and account for different molecular conformations and configurations.^{20, 23} The COSMO-SAC (2013) solvation model contains 9 universal parameters and 17 atom bonding specific parameters, many of which are initially calculated from quantum mechanics and further optimized using experimental data.

The method proposed below incorporates a new procedure for estimating AP from quantum chemical computations. There is a real difficulty in estimating E from only solvent-water partition coefficients using Eq. (3-1) and an MLR as demonstrated below. The methods that rely on experimentally determined solvent-water partition coefficients estimate E independently from the measured refractive index or by the summation of fragments.¹⁶ The proposed method also estimates E independently. However, E is estimated using the Clausius–Mossotti equation and the computed molecular polarizability using Gaussian 09 D.01³⁷ with the DFT hybrid functional M062X³⁸ and the aug-cc-pVDZ^{39, 40} basis set. The molecular volume, which is available from the COSMO model⁴¹ output that is the necessary input to COSMO-SAC, is used to estimate the molar volume V . The quantum mechanically estimated E and V are treated as known quantities in the MLR that estimates S , A , and B .

The second modification is to use many (65, see below) estimated solvent-water partition coefficients in the MLR. To solve for three (S , A , and B) unknowns, three independent equations, i.e. partition coefficients in three solvent-water systems, are needed. However, individual partition coefficients computed using COSMO-SAC or any other quantum chemical solvation model are not accurate enough to produce reliable estimates of S , A , and B . Typical errors associated with COSMO-SAC predicted solvent-water partition coefficients are 0.5 to 1 log units.³⁶ Using a large number of chemically diverse solvent-water systems reduces the variation of COSMO-SAC errors as demonstrated by the reduction in the interquartile range of prediction errors as the number of solvent-water systems increases (Figure C-1 in Appendix C). This is expected if the errors in the predicted solvent-water partition coefficients are randomly distributed with zero mean. A histogram of the errors illustrates that the distribution of COSMO-SAC errors is symmetric with mean = 0.05 (Table B-1 in Appendix B and Figure C-2 in Appendix C).

The solute parameter computed using the proposed method are referred to as Quantum Chemically estimated Abraham Parameter (QCAP). QCAP are compared below to the experimentally-based AP from the UFZ-LSER database⁵ that compiles experimentally-based AP from the literature. QCAP are also validated by comparing to the experimental partition coefficients for 24 solvent-water systems. Comparisons to predictions using ABSOLV estimated solute parameters are also made. Since QCAP and experimentally-based AP are not estimated in the same way, it is possible that some of the existing literature system parameters, which were obtained using the experimentally-based solute descriptors, are not compatible with QCAP. To rectify this inconsistency, the QCAP parameters are adjusted using a procedure similar to that used to compute the ABSOLV fragment parameters. The adjusted Quantum Chemically Abraham Parameter (Adjusted QCAP) are compared to the experimentally-based solute parameters and are validated by comparing to the experimental solvent-water partition coefficients.

3.2 Materials and Methods

3.2.1 Data Compilation

The solvent-water system parameters, the lower case constants in Eq. (3-1), were compiled from Abraham et al.⁴² and used without adjustment. To compute solute AP, only systems for which solvents are dry (d) or immiscible with water (w/d) are used. Sixty-five solvent-water systems were selected, which are chemically diverse (Table B-2 and Figure C-3).

COSMO-SAC predicted solvent-water partition coefficients are listed in Table B-3. Solute parameters from ABSOLV¹⁷ as well as from the UFZ-LSER database “Preselected Value”⁵ were compiled and are listed in Table B-4.

The experimental solvent-water partition coefficient data that incorporate chemically diverse solutes and various partitioning systems were collected from Abraham et al.,⁴³⁻⁴⁶ Grubbs et al.,⁴⁷ Saifullah et al.,⁴⁸ Sprunger et al.,⁴⁹ Stephens et al.,⁵⁰ Acree et al.,⁵¹ an EPA Database,⁵² and the cited references therein (Table B-5).

3.2.2 Estimating E

The excess molar refraction, E , is intended to account for the dispersion interaction due to an induced dipole (polarization) on the solute.⁷ Abraham et al.⁵³ define E as the molar refraction of a solute (MR_A), less the molar refraction for an alkane of the same characteristic volume (MR_A^*):

$$E = MR_A - MR_A^* \quad (3-2)$$

with units $\text{cm}^3\text{mol}^{-1}/10$. MR_A can be calculated using the index refraction (η) and McGowan characteristic volume ($V_x, \text{cm}^3\text{mol}^{-1}/100$):²⁸

$$MR_A = 10 \left[\frac{(\eta^2 - 1)}{(\eta^2 + 2)} \right] V_x \quad (3-3)$$

The division by 10 and 100 is to scale E and V to the other solute parameters. MR_A^* can be estimated from the linear regression proposed by Abraham et al.:⁵³

$$MR_A^* = 2.832V_x - 0.526 \quad (3-4)$$

Combining Eqs. (3-2) to (3-4) yields

$$E = 10 \left[\frac{(\eta^2 - 1)}{(\eta^2 + 2)} \right] V_x - 2.832V_x + 0.526 \quad (3-5)$$

Therefore, estimating E requires an estimate of the index of refraction η .

The Lorentz–Lorenz equation,⁵⁴ also known as the Clausius–Mossotti equation, relates the index refraction (η) to the molecular polarizability (α):

$$\left[\frac{(\eta^2 - 1)}{(\eta^2 + 2)} \right] = \frac{4}{3} \pi N_A \frac{\alpha}{\bar{V}} \quad (3-6)$$

where α = molecular linear polarizability of the molecule ($\text{cm}^3\text{molecule}^{-1}/100$), \bar{V} = molar volume ($\text{cm}^3\text{mol}^{-1}/100$), and N_A = Avogadro’s number. The Clausius–Mossotti equation is discussed in detail in the Feynman Lectures on Physics (Vol. 2, Chapter 32).⁵⁵ Therefore, E can be estimated using the molecular polarizability, α :

$$E = 10 \left(\frac{4}{3} \pi N_A \alpha \right) - 2.832V + 0.526 \quad (3-7)$$

The molecular volume (V) is used in Eq. (3-7) instead of the McGowan volume so that only quantum chemically computed quantities, α and V , are used.

A recent study comprehensively evaluated the accuracy of estimating the molecular polarizability (α) using a wide set of quantum chemical methods and basis sets for a diverse set of 46 molecules.⁵⁶ The study reported that using Density Functional Theory (DFT) with the hybrid functionals (e.g. M06³⁸ and B3LYP⁵⁷) resulted in higher accuracy than pure functionals, and yielded comparable accuracy to using CCSD⁵⁸ and MP2⁵⁹ levels of theory. They concluded that aug-cc-pVDZ,^{39, 40} Sadlej cc-pVTZ,⁶⁰ and aug-cc-pVTZ^{39, 40} basis sets were superior to others, and that the aug-cc-pVTZ performed the best.

However, the computational cost increases dramatically (roughly a factor of 7 in computation time) using aug-cc-pVTZ relative to using aug-cc-pVDZ. A comparison using a subset of molecules computed using M062X³⁸ with either aug-cc-pVDZ or aug-cc-pVTZ showed that the molecular polarizabilities were nearly equal ($N = 183$, $R^2 = 0.999$, Figure C-4).

Therefore, the aug-cc-pVDZ basis set is used here for calculating molecular polarizability.

Gaussian 09 D.01³⁷ with the hybrid functional M062X³⁸ is used for all the steps. The geometry is optimized using a smaller basis set 6-31G(d),^{61, 62} followed by a second optimization using the cc-pVDZ^{39, 40} basis set, and a final optimization and frequency calculation using the aug-cc-pVDZ^{39, 40} basis set. The geometry is checked for no imaginary frequencies, thereby ensuring that the energy is at a local minimum. The molecular polarizability (Table B-4) is available in the frequency calculation (isotropic polarizability).

3.2.3 Determining S , A , and B

The solvent-water partition coefficients, $\log K$ in Eq. (3-1), are estimated using the quantum chemical COSMO-SAC model, which is available on request.³⁶ The COSMO⁴¹ solvation model implemented in the Amsterdam Density Functional (ADF) quantum mechanics (QM) package⁶³⁻⁶⁵ produces the molecular volume, and the surface charge distribution, called the sigma profile, that are used by COSMO-SAC (details in Xiong et al.³⁶). The molecular volume that is estimated as part of the COSMO-SAC computation is used as the estimate of V , rather than the McGowan characteristic volume since they are essentially the same ($R^2 = 0.992$, RMSE = 0.074). Using the partition coefficients ($\log K_{sw}$) estimated using COSMO-SAC for the sixty-five solvent-water systems and the literature system AP (c , e , s , a , b , v),⁴² a set of sixty-five equations are constructed using Eq. (3-1).

Since E is computed from the molecular polarizability and V is estimated from the molecular volume, they are known parameters and the equations for the unknown parameters (S , A , and B) are:

$$\log K_i - c_i - v_i V - e_i E = s_i S + a_i A + b_i B \quad (3-8)$$

where the subscript i denotes the solvent of the solvent-water pair. The three unknowns (S , A , and B) are estimated using the MLR function (lm function) in the R programming language⁶⁶ applied to Eq. (3-8). The resulting solute parameters S , A , and B together with E and V are denoted as QCAP (Quantum Chemically estimated Abraham Parameters). The QCAPs for 1827 solutes are available in Table B-4.

The key idea in the proposed method, in addition to making an independent estimate of E , is to use the estimated partition coefficients from a large number of solvent-water systems. This is necessary because the prediction error associated with each COSMO-SAC estimate is large for its direct use. Also, the large number of solvent-water partition coefficients (65) provides a large sample size for the linear regression estimate of the three parameters S , A , and B .

In addition, partitioning into a large and diverse set of solvent-water systems gives an expanded system descriptor space⁶⁷ for characterizing the properties of a given solute. We prefer this approach that employs computed partition coefficients in a fashion that is analogous to the experimental method (Leahy et al.^{25, 26}) rather than approaches that rely on molecular characteristics, e.g. topological properties that have no apparent relationship to partitioning.

3.3 Results and Discussion

3.3.1 Determining E Independently

Direct estimation of E from molecular polarizability is essential in order to obtain reliable results. A comparison is made in Figure 3-2 for the solute parameters E and S determined by (I) estimating E , S , A , and B jointly with an MLR using the COSMO-SAC estimated solvent-water partition coefficients, and an independently estimated V , and (II) the QCAP method described above employing independent estimates of E and V and estimating S , A , and B from an MLR (Eq. (3-8)). They are compared to the experimentally-based solute parameters from the UFZ-LSER database (denoted as UFZ) using a hexbin two dimensional histogram plots.⁶⁸ The color of the circle listed on the legend indicates the number of observations that fall within the square bin containing the circle. The scaling increases by factors of two. For example in Figure 3-2 (1), the rose filled circles contain between 1 and 2 observations whereas the black filled circles contain between 64 and 128 observations. Hexbin is used because there are more than 800 data points and plots using discrete points would not provide a useful comparison due to over plotting of the symbols.

The estimated E parameters from the first method, Figure 3-2 (1), are mostly between 0 and 1, and appear as almost horizontal lines relative to the experimental values with an $R^2 < 0.2$. The S parameters estimated from the first method, Figure 3-2 (2), have a large RMSE = 0.42 and small $R^2 = 0.53$.

In contrast, E parameters estimated from molecular polarizability, Figure 3-2 (3), have a much stronger linear correlation with experimentally-based solute parameters from the UFZ-LSER database with an $R^2 = 0.86$ and RMSE = 0.81. The S parameters of QCAP estimates are also in better agreement with the experimentally-based solute parameters with an RMSE = 0.24 and $R^2 = 0.84$, Figure 3-2 (4). For A and B parameters, there are no large differences between the two methods (Figure C-5).

The failure in estimating E and S using the first method is likely due to the strong correlation between E and S (Figure C-6), which has been pointed out by Arey et al.⁷ Also, there is a moderately strong linear correlation between the system parameters e and s ($r = 0.65$, Figure C-7). The multi-collinearity increases the inaccuracy (standard errors) in estimating regression coefficients and increases the number of solvent-water partition coefficients required.⁶⁹ However in the QCAP method, E is computed independently, which resolves the multicollinearity problem between E and S .

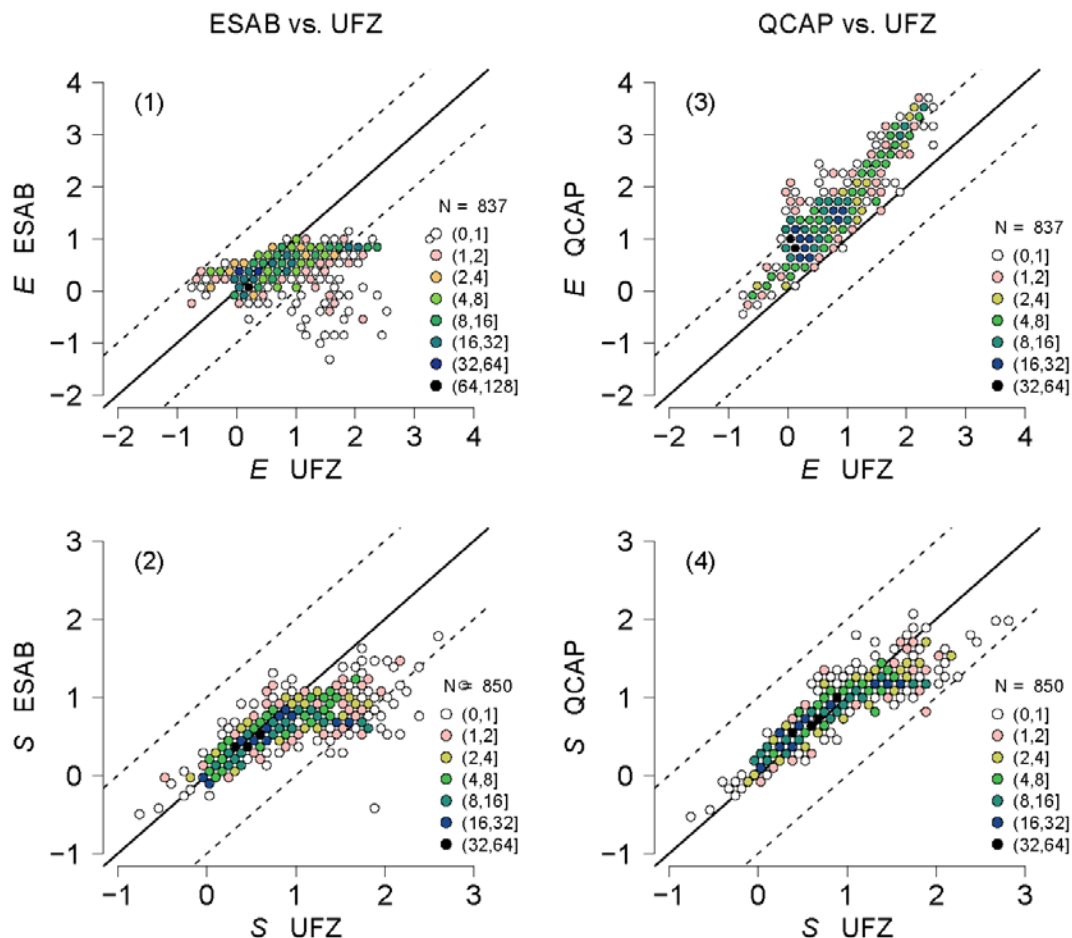


Figure 3-2 Hexbin two dimensional histogram plots⁶⁸ comparing the predicted versus experimental solute parameters from the UFZ-LSER database (labeled UFZ) for E and S determined by the two methods listed at the top of each column. See text in Section 3.3.1 for an explanation of the hexbin plot. Panels (1) and (2) estimate E , S , A , and B jointly with an MLR, and an independently estimated V , labeled ESAB; panels (3) and (4) estimate E from molecular polarizability, V from molecular volume and S , A , and B from an MLR, which is the QCAP method.

3.3.2 Comparisons between ABSOLV and QCAP for Various Solvent-Water Systems

Figure 3-3 compares the RMSEs of the residuals (predicted $\log K_{sw}$ – observed $\log K_{sw}$) for the predictions using ABSOLV and QCAP with solvent-water system parameters from Abraham et al.⁴² The predictions of K_{sw} are comprehensively evaluated for a total of 963 chemically diverse solutes and 24 solvent-water systems. The three largest system sets contain 896 solutes for (wet) octanol-water, 227 for (dry/wet) tetrachloromethane-water, and 224 for (dry/wet) chloroform-water. The solvents are from various chemical classes: alkanes, alcohols, amides, ketones, and aromatics. The K_{sw} values span over 14 orders of magnitude from 10^{-6} to 10^8 . The solvents are ordered from the smallest to the largest QCAP RMSE. QCAP generally performs better: RMSEs range from 0.347 to 0.699 log units for QCAP and from 0.450 to 0.716

log units for ABSOLV. For comparisons between experimental and model predicted K_{sw} for each system, refer to Figure C-8 to Figure C-31.

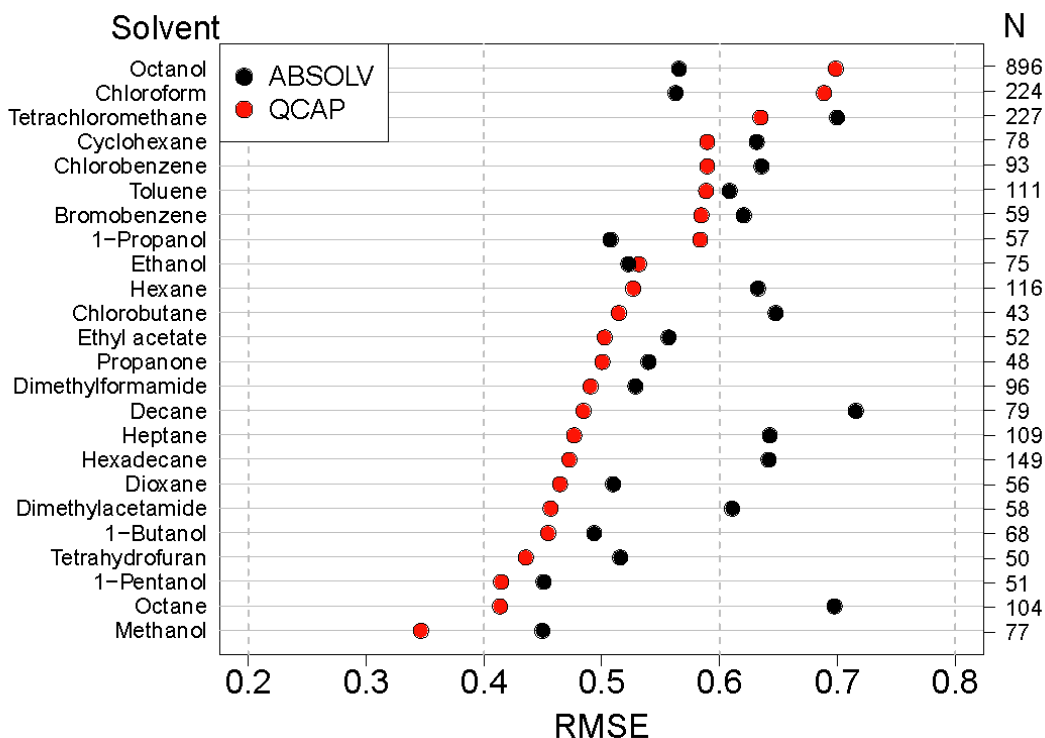


Figure 3-3 Dot plot presenting RMSEs of the residuals (predicted $\log K_{sw}$ - observed $\log K_{sw}$) for the predictions of solvent-water partition coefficients. Predictions by two models are compared: (1) ABSOLV and (2) QCAP. The solvents listed on the left axis are ordered from the smallest to the largest QCAP RMSE. The right axis presents N, the number of solutes in each system. Summary of the RMSEs of prediction of solvent-water partition coefficients is in Table B-6.

3.3.3 Comparisons between ABSOLV and QCAP for Munition Constituents and Munition-like Compounds

The QCAP and ABSOLV solute parameters are compared for five cyclic nitramines and cyclic nitrosamines: HMX, RDX, MNX, TNX, and DNX in Figure 3-4. As discussed previously, the ABSOLV method fails, i.e. it has very large residuals for the five cyclic nitramines and cyclic nitrosamines (RMSE = 4.54 log units), indicating that for these compounds the ABSOLV solute parameters are unreliable. However, QCAP predictions are reasonable with most prediction residuals within 1 log units (RMSE = 0.799 log units). The significant improvement suggests that the quantum mechanically-based QCAP model is a better choice for novel compounds.

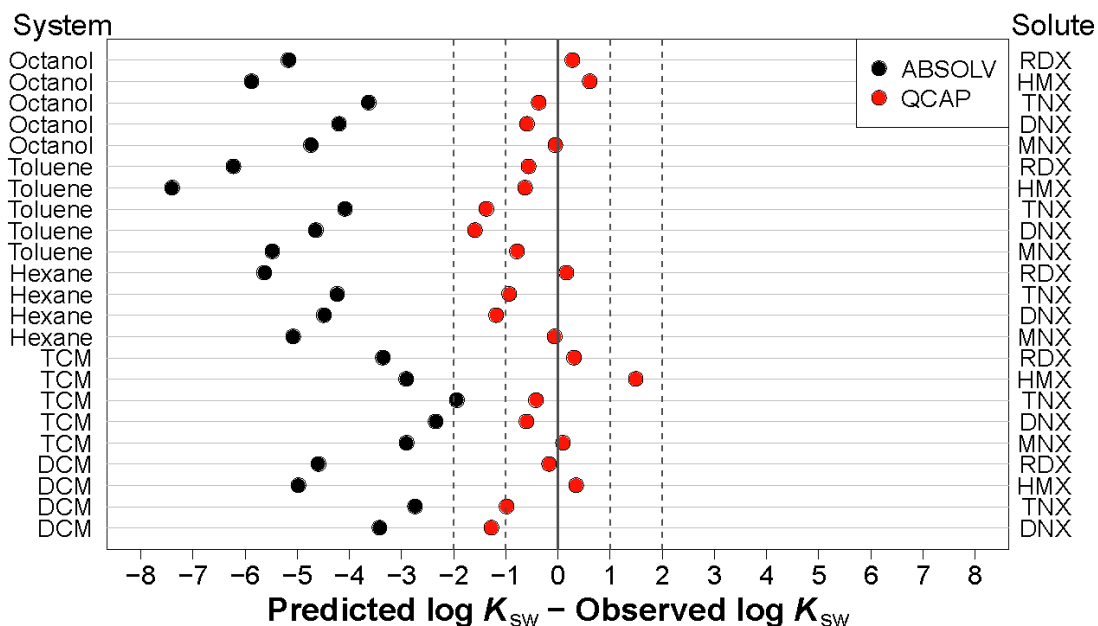


Figure 3-4 Dot plot presenting prediction errors (predicted log K_{sw} - observed log K_{sw}) for predictions of ABSOLV and QCAP for munition constituents and munition-like compounds listed on the right axis and for solvents listed on the left axis: wet octanol-water, toluene-water, hexane-water, trichloromethane (TCM)-water, and dichloromethane (DCM)-water. See the legend in Figure 3-1 for the solutes' chemical names.

The reason that the QCAP prediction error is larger for these munition compounds (compare Figure 3-4 to Figure 3-3) may be that these large, flexible molecules present difficulties when the estimating procedure requires a specific molecular structure. There are different conformers for cyclic nitramines and nitrosamines.^{24, 70-73} For example, 12 major gas-phase conformers have been found for HMX.²⁴ Here, the conformer with the lowest energy in the gas phase was selected to generate the QCAP solute parameters of the investigated solute. This is consistent with methodology used in developing COSMO-SAC.^{20, 23} The QCAP solute parameters for munition constituents and munition-like compounds are listed in Table B-7, as well as the experimental¹⁹ and predicted solvent-water partition coefficients.

3.3.4 Adjusted Quantum Chemically Estimated Abraham Parameters (Adjusted QCAP)

For a diversity of systems, predicted partition coefficients using QCAP were in reasonably good agreement with the experimental K_{sw} . However, overestimation was found for predictions using the QCAP solute parameters and literature system parameters for wet octanol-water for some solutes (Figure C-8), with no indication that the overestimation is associated with a specific solute descriptor of QCAP (Figure C-32). A possible reason is that the system parameters were obtained using the experimental partition coefficients as the dependent variable and the experimentally-based Abraham solute descriptors as the independent variables. However, the QCAP solute parameters are not derived from the experimentally-based solute parameters

used to estimate the system parameters. QCAP solute parameters are based on the quantum chemical estimates of solvent-water partition coefficients and molecular polarizability. The overestimation is a difference between QCAP and experimentally-based solute parameters, particularly for E , as shown in Figure 3-5 (1). It is likely that the existing wet octanol-water system parameters, which were obtained using the experimentally-based solute descriptors, are not compatible with the QCAP solute parameters.

To rectify this inconsistency, the Adjusted Quantum Chemical Abraham Parameters (Adjusted QCAP) that are compatible with presently available conjugate system parameters are derived. The procedure used is analogous to that used to develop the ABSOLV prediction module,¹⁷ where experimental data, either experimental partition coefficients or experimentally-based solute parameters, are fitted to determine fragment/atom descriptors.¹⁷ Adjusted solute QCAP are estimated by fitting the experimentally-based solute parameters from the UFZ-LSER database⁵ using the QCAP parameters (E_{QCAP} , S_{QCAP} , A_{QCAP} , B_{QCAP} , and V_{QCAP}) as the independent variables. The regressions utilize a set of more than 800 experimentally-based solute parameters (data in Table B-4). The regressions were initially performed with all 5 QCAP parameters. Those with large p-values > 0.05 were removed sequentially until all the coefficients were significant at the 0.05 level. The results are Eq. (3-9) to Eq. (3-13) for each Abraham parameter (Table 3-1).

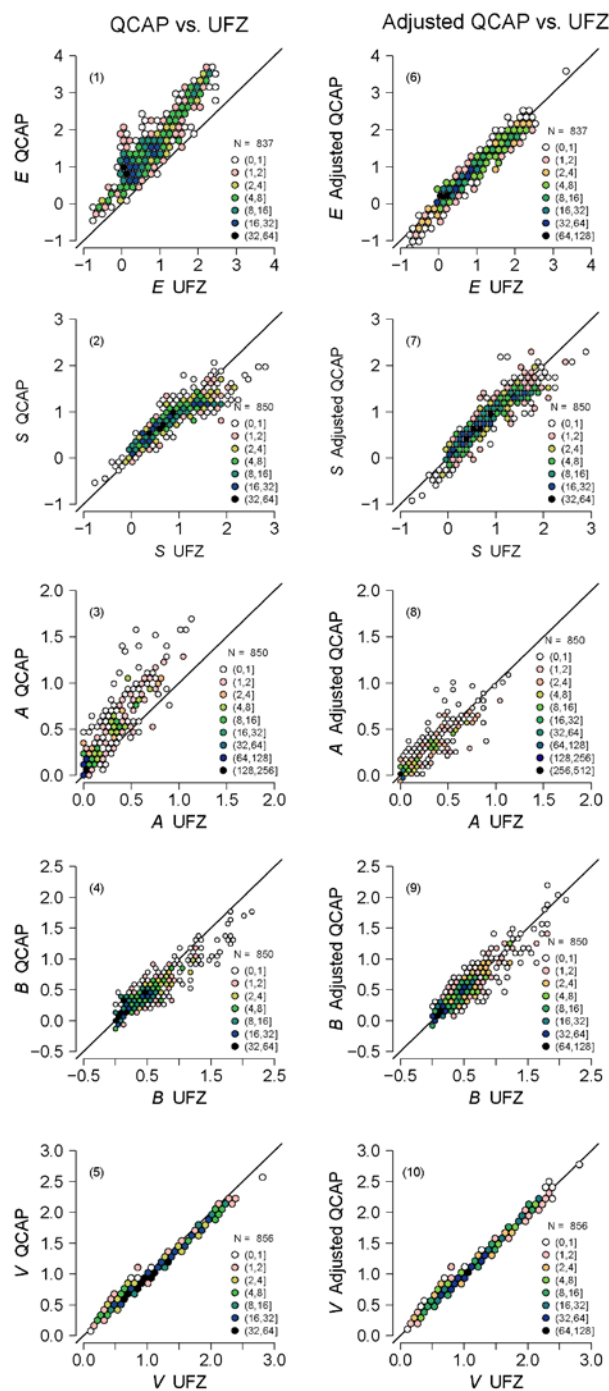


Figure 3-5 Hexbin two dimensional histogram plots⁶⁸ comparing the solute parameters (S , A , B , E , V) between QCAP and UFZ, and between Adjusted QCAP and UFZ. See text in Section 3.3.1 for an explanation of the hexbin plot.

Table 3-1 Linear equations^a for Adjusted QCAP solute parameters E , S , A , B , and V .

Equation	N	Adjusted R^2	SD	Equation number
$E = -0.3554 + 0.8827E_{\text{QCAP}} + 0.4046S_{\text{QCAP}} + 0.1807A_{\text{QCAP}} - 0.5517V_{\text{QCAP}}$	836	0.941	0.165	(3-9)
$S = -0.1948 + 0.2022E_{\text{QCAP}} + 0.9480S_{\text{QCAP}} + 0.1973B_{\text{QCAP}} - 0.1150V_{\text{QCAP}}$	849	0.862	0.204	(3-10)
$A = 0.0185 - 0.0398S_{\text{QCAP}} + 0.6747A_{\text{QCAP}} + 0.0317B_{\text{QCAP}} - 0.0417V_{\text{QCAP}}$	849	0.880	0.075	(3-11)
$B = 0.1036 - 0.0361E_{\text{QCAP}} - 0.1956S_{\text{QCAP}} + 0.1436A_{\text{QCAP}} + 1.2826B_{\text{QCAP}}$	849	0.888	0.117	(3-12)
$V = 0.0408E_{\text{QCAP}} - 0.0582S_{\text{QCAP}} + 0.0862B_{\text{QCAP}} + 1.0096V_{\text{QCAP}}$	855	0.999	0.039	(3-13)

^a N = number of unique solutes used in the multiple linear regression

R^2 = adjusted coefficient of determination adjusted for the number of independent variables in the regression equation ⁶⁹

SD = regression standard deviation

3.3.5 Comparison of QCAP and Adjusted QCAP

Figure 3-5 panels are hexbin two dimensional histogram plots⁶⁸ that compare solute parameters (E , S , A , B , V) from the UFZ-LSER database to QCAP and Adjusted QCAP. As shown in Figure 3-5 left, there are strong linear correlations between QCAP and UFZ solute parameters. However, the slopes are not equal to one and the intercepts are not zero. Reasonably small RMSEs are found for S , A , B , and V , but a large RMSE for E . This indicates that E computed from molecular polarizability is quite different from E in the UFZ-LSER database that are estimated in various ways. Detailed statistics are summarized in Table B-8.

The Adjusted QCAP are designed to predict UFZ solute parameters and they perform very well with slopes close to one and intercepts nearly zero (Figure 3-5 right). Small RMSEs are observed for all E , S , A , B , and V in Table B-8. Estimating each Abraham parameter using more than one QCAP parameter improves the result since the descriptors of pp-LFERs are inherently cross-correlated because the descriptors were chosen based on the molecular interaction mechanisms and are not necessarily orthogonal.¹

3.3.6 Comparisons between ABSOLV, QCAP, and Adjusted QCAP for Various Solvent-Water Systems

Figure 3-6 presents the RMSE of predictions of solvent-water partition coefficients using ABSOLV, QCAP, and Adjusted QCAP. Adjusted QCAP lead to the smallest RMSEs, followed by QCAP, and ABSOLV. There is no obvious bias found for Adjusted QCAP for each individual system (Figure C-8 to Figure C-31). For wet octanol-water system, using the Adjusted QCAP effectively eliminates the bias and reduces the prediction errors (RMSE = 0.515, Figure C-8). Thus, Adjusted QCAP gives the best predictions for the investigated solvent-water systems.

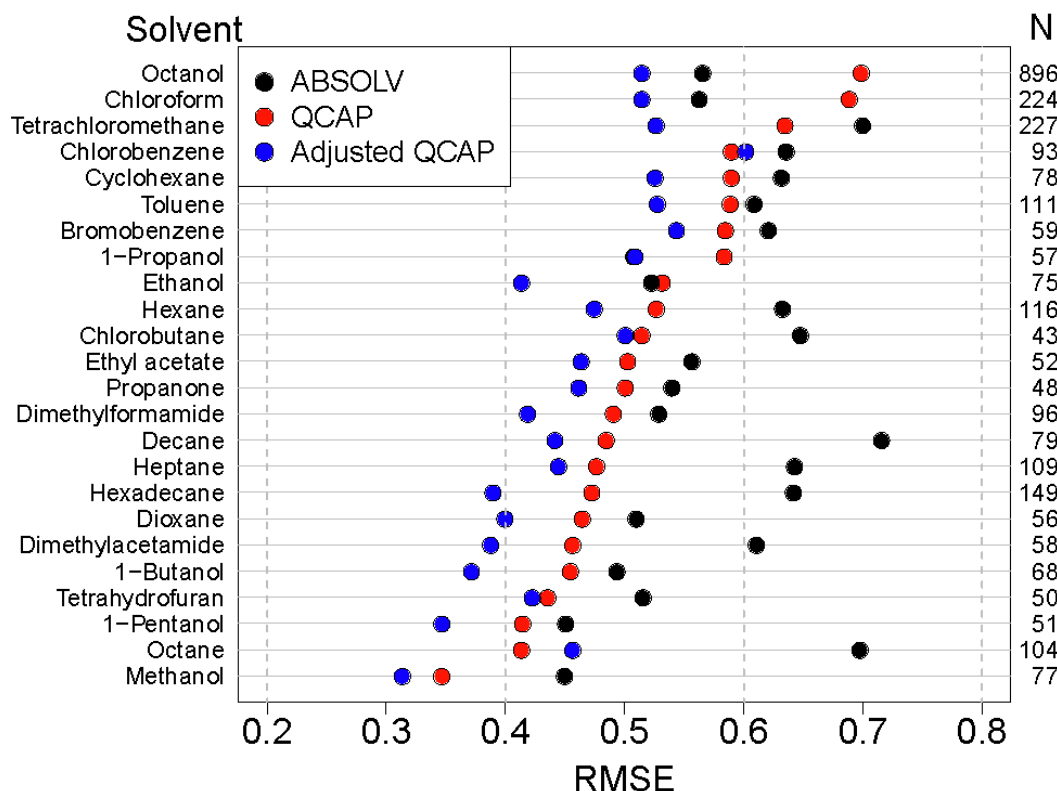


Figure 3-6 Dot plot presenting RMSEs of the residuals (predicted $\log K_{sw}$ - observed $\log K_{sw}$) for the predictions of solvent-water partition coefficients. Predictions by three models are compared: (1) ABSOLV, (2) QCAP, and (3) Adjusted QCAP. The solvents listed on the left axis are ordered from the smallest to the largest QCAP RMSE. The right axis presents N, the number of solutes in each system. Summary of the RMSEs of prediction of solvent-water partition coefficients is in Table B-6.

3.3.7 Comparisons between ABSOLV, QCAP, and Adjusted QCAP for Munition Constituents and Munition-like Compounds

Predictions of solvent-water partition coefficients using Adjusted QCAP for munition constituents and munition-like compounds are compared to predictions using QCAP and ABSOLV in Figure 3-7. Adjusted QCAP gives good predictions (RMSE = 0.860) with all the prediction errors within a reasonable range except for HMX in chloroform-water. There are a number of possible reasons for this discrepancy: (1) The minimum gas-phase free energy HMX configuration that is used to determine the QCAP solute parameters may not be the correct configuration in the chloroform-water system; (2) These munition constituents and munition-like compounds were not included in the data used to obtain linear equations for Adjusted QCAP parameters and HMX may be out of the applicability domain of the regression equations, which depends on the range covered by the solute descriptors^{74, 75} used to determine the Adjusted QCAP parameters. If the prediction of HMX in chloroform-water is removed, the RMSE reduces to 0.676 for Adjusted QCAP. The results illustrate the predictive ability of Adjusted QCAP for novel and complex compounds.

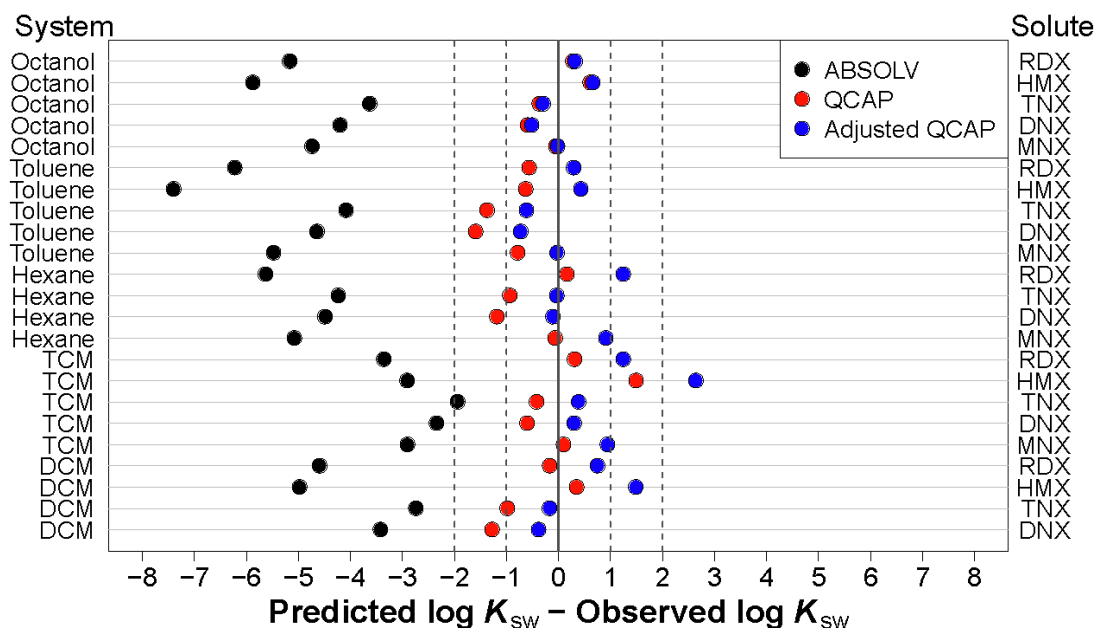


Figure 3-7 Dot plot presenting prediction errors (predicted log K_{sw} - observed log K_{sw}) for predictions of ABSOLV, QCAP, and Adjusted QCAP for munition constituents and munition-like compounds listed on the right axis. Left axis: list of the corresponding partitioning systems: wet octanol-water, toluene-water, hexane-water, trichloromethane (TCM)-water, and dichloromethane (DCM)-water. See the legend in Figure 3-1 for the solutes' chemical names.

3.3.8 Comparison of Adjusted QCAP and COSMOments

Quantum chemically based estimates of E , S , A , B , and V have also been made using COSMOments by Zissimos et al.¹⁵ They calculated five COSMOments that are moments of the σ profile, a histogram of the surface charge density of the molecule. The σ profile is computed by the quantum chemical solvation model COSMO-RS.^{20, 41, 76} Regression equations using the five COSMOments as predictor variables were constructed to predict the experimental solute AP for 470 compounds. The results are compared in Figure 3-8. Detailed statistics are summarized in Table B-8. The results for COSMOments for A , B , and V are similar to the Adjusted QCAP. However, larger RMSEs and lower R^2 values are observed for the COSMOment estimates of E and S . The most substantial difference is for E : RMSE = 0.368 and R^2 = 0.504 for COSMOment, compared to RMSE = 0.165 and R^2 = 0.942 for Adjusted QCAP.

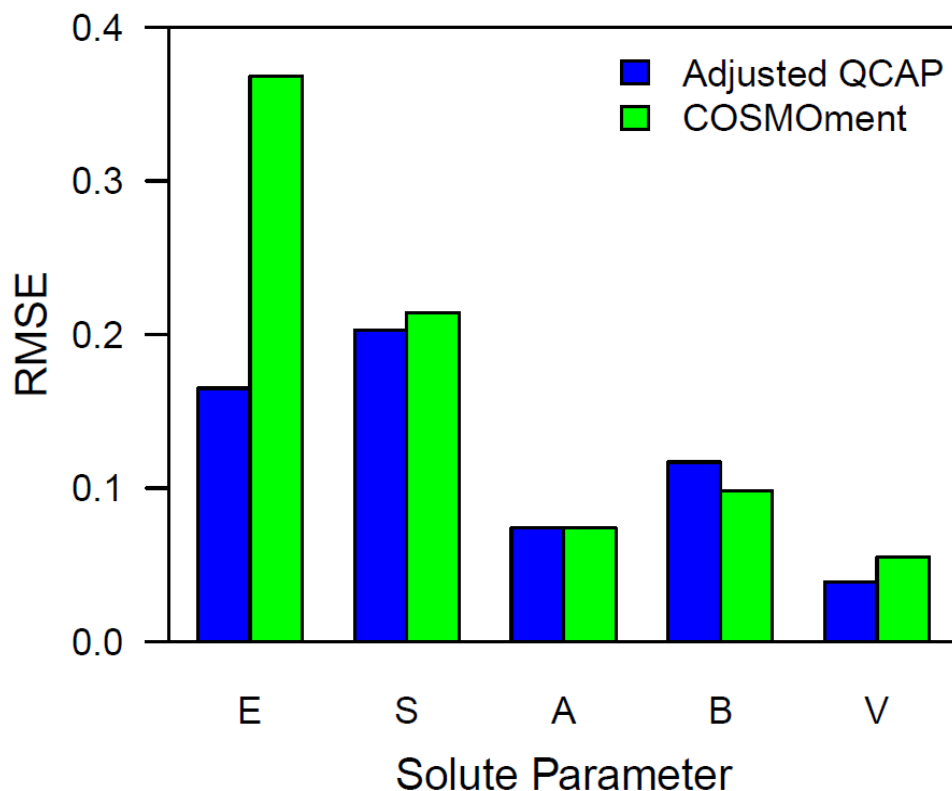


Figure 3-8 Bar chart comparing the prediction root mean square errors (RMSEs) for Adjusted QCAP and COSMOments estimates of the solute parameters. See Table B-8 for the complete statistical comparison.

As mentioned by Zissimos et al.,¹⁵ poor performance of the COSMOment method for *E* may be due to the different chemical information in the two sets of LFER descriptors of Abraham and Klamt (COSMOments). The Abraham set contains additional information that is incorporated in the Abraham descriptor *E*. Because of that, the experimental Abraham descriptor *E* does not correlate well with the five COSMOments ($R^2 = 0.504$) and it is predicted less accurately using the COSMOment method (RMSE = 0.368).

By contrast, Adjusted QCAP *E* is based on the procedure proposed by Abraham et al.⁵³ (Eq. (3-5)) and an independently computed molecular polarizability (Eq. (3-7)), and optimized using the five QCAP parameters (Eq. (3-9)). It is likely that Adjusted QCAP *E* contains similar chemical information as the Abraham descriptor *E*.

Since COSMO-SAC also uses the surface charge density histogram (the σ profile) to compute the solvent-water partition coefficients, it is not surprising that using characteristics of the σ profile – the σ profile moments – can be used to estimate Abraham solute parameters. However, the connection is not direct, whereas using the estimated solvent-water partition coefficients is based directly on Eq. (3-1). This can be useful when problems arise. Failures of the QCAP method can be traced either to problems with the estimated solvent-water partition coefficients – COSMO-SAC estimates are in error -- or to problems with the solvent-water system parameters. In either case, a detailed investigation is possible. For example, subsets of the

solvent-water systems can be used to estimate the QCAP and Adjusted QCAP to detect which solvents are causing the problem. This is not the case, however, with regressions using molecular properties that are not directly related to the parameters being estimated. If the method fails, there is no path available for a diagnostic investigation. It is for this reason that we recommend using Adjusted QCAP.

3.4 Conclusions

In this study, the importance of having an independent estimate of E using the Clausius-Mossotti equation, Eq. (3-6), has been demonstrated. It can then be treated as a known parameter and the MLR can reliably estimate the remaining Abraham solute parameters using quantum chemical estimates of the 65 solvent-water partition coefficients. Since QCAP and Adjusted QCAP are derived from COSMO-SAC partitioning, chemicals for which COSMO-SAC is applicable can be analyzed. However, chemicals with completely new functionalities for which COSMO-SAC has not been evaluated need to be checked. It has been shown⁷⁷ that if a new pp-LFER is developed using a new set of solvent-water partition coefficients, the QCAP and not the Adjusted QCAP parameter produce the best fit. This is the reason that both QCAP and Adjusted QCAP parameters are reported: Adjusted QCAP should be used for existing solvent-water pp-LFERs, and QCAP should be used for developing new pp-LFER.

REFERENCES

1. Endo S, G.K., Applications of polyparameter linear free energy relationships in environmental chemistry. *Environ. Sci. Technol.* **2014**, 48 (21), 12477-91.
2. Abraham, M.H., Application of solvation equations to chemical and biochemical processes. *PURE AND APPLIED CHEMISTRY* **1993**, 65 (12), 2503.
3. Poole, C.F.; Ariyasena, T.C.; Lenca, N. Estimation of the environmental properties of compounds from chromatographic measurements and the solvation parameter model. *Journal of Chromatography A* **2013**, 1317, 85-104; <http://dx.doi.org/10.1016/j.chroma.2013.05.045>.
4. Goss KU, S.R., Linear free energy relationships used to evaluate equilibrium partitioning of organic compounds. *Environ. Sci. Technol.* **2001**, 35 (1), 1-9.
5. UFZ-LSER database.
6. Svozil, Daniel, Sevcik, Jiri G K, Kvasnicka, Vladimir, Neural Network Prediction of the Solvatochromic Polarity/Polarizability Parameter $\pi^H/2$. *Journal of chemical information and computer sciences.* **1997**, 37 (2), 338.
7. Arey, J. S., Green, W. H., Gschwend, P.M., The Electrostatic Origin of Abraham's Solute Polarity Parameter. *The journal of physical chemistry.B, Condensed matter, materials, surfaces, interfaces & biophysical.* **2005**, 109 (15), 7564-7573.
8. Dearden, J. C., Ghafourian, T., Hydrogen Bonding Parameters for QSAR: Comparison of Indicator Variables, Hydrogen Bond Counts, Molecular Orbital and Other Parameters. *J. Chem. Inf. Comput. Sci.* **1999**, 39 (2), 231-235.
9. Ghafourian T, D.J., The use of atomic charges and orbital energies as hydrogen-bonding-donor parameters for QSAR studies: comparison of MNDO, AM1 and PM3 methods. *J. Pharm. Pharmacol.* **2000**, 52 (6), 603-10.
10. Rahaman, Obaidur, Doren, Douglas J., Di Toro, Dominic M., Quantum mechanical estimation of Abraham hydrogen bond parameters using 1:1 donor-acceptor complexes. *POC Journal of Physical Organic Chemistry* **2014**, 27 (10), 783-793.
11. Platts, J.A., Theoretical prediction of hydrogen bond donor capacity. *Physical Chemistry Chemical Physics (Incorporating Faraday Transactions)* **2000**, 2 (5).
12. Platts, J.A., Theoretical prediction of hydrogen bond basicity. *Physical Chemistry Chemical Physics (Incorporating Faraday Transactions)* **2000**, 2 (14), 3115-3120.
13. Lamarche, Olivier, Platts, James A., Hersey, Anne, Theoretical prediction of the polarity/polarizability parameter π^H . *Physical Chemistry Chemical Physics (Incorporating Faraday Transactions)* **2001**, 3 (14), 2747-2753.

14. Schwöbel, Johannes A. H., Ebert, Ralf-Uwe, Kühne, Ralph, Schüürmann, Gerrit, Prediction models for the Abraham hydrogen bond donor strength: comparison of semi-empirical, *ab initio*, and DFT methods. *POC Journal of Physical Organic Chemistry* **2011**, 24 (11), 1072-1080.
15. Zissimos AM, Abraham MH, Klamt A, Eckert F, Wood J, A comparison between the two general sets of linear free energy descriptors of Abraham and Klamt. *J. Chem. Inf. Comput. Sci.* **2002**, 42 (6).
16. Platts, J. A., Butina, D., Abraham, M. H., Hersey, A., Estimation of Molecular Linear Free Energy Relation Descriptors Using a Group Contribution Approach. *J. Chem. Inf. Comput. Sci.* **1999**, 39 (5), 835-845.
17. Advanced Chemistry Development, I. **ACD/Absolv.**
18. Abraham, M. H., McGowan, J. C., The use of characteristic volumes to measure cavity terms in reversed phase liquid chromatography. (Author abstract). *Chromatographia* **1987**, 23 (4).
19. Yuzhen Liang; Dave T.F. Kuo, Herbert E Allen, Dominic M Di Toro Experimental determination of solvent-water partition coefficients and Abraham parameters for munition constituent. ; 10.1016/j.chemosphere.2016.07.028.
20. COSMO-RS from quantum chemistry to fluid phase thermodynamics and drug design.
21. Lin, Shiang-Tai, Sandler, Stanley I., Multipole corrections to account for structure and proximity effects in-group contribution methods: octanol-water partition coefficients. *Journal of Physical Chemistry A* **2000**, 104 (30).
22. Goss, Kai-Uwe, Arp, Hans Peter H., Bronner, Guido, Niederer, Christian, NONADDITIVE EFFECTS IN THE PARTITIONING BEHAVIOR OF VARIOUS ALIPHATIC AND AROMATIC MOLECULES. *Environmental Toxicology and Chemistry* **2008**, 28 (1), 52-60.
23. Shu Wang, Stubbs, John M., Siepmann, J. Ilja, Sandler, Stanley I., Effects of conformational distributions on sigma profiles in COSMO theories. *Journal of Physical Chemistry A* **2005**, 109 (49).
24. Molt RW Jr, Watson T Jr, Bazanté AP, Bartlett RJ, The great diversity of HMX conformers: probing the potential energy surface using CCSD(T). *The journal of physical chemistry.A* **2013**, 117 (16), 3467-74.
25. Leahy, David E., Morris, Jeffrey J., Taylor, Peter J., Wait, Alan R., Model solvent systems for QSAR. Part 2. Fragment values ('f-values') for the 'critical quartet'. *Journal of the Chemical Society, Perkin Transactions 2* **1992**, (4), 723-731.
26. Leahy, David E., Taylor, Peter J., Wait, Alan R., Model Solvent Systems for QSAR Part I. Propylene Glycol Dipelargonate (PGDP). A new Standard Solvent for use in Partition

Coefficient Determination. *QSAR Quantitative Structure-Activity Relationships* **1989**, 8 (1), 17-31.

27. Zissimos, Andreas M., Abraham, Michael H., Barker, Matthew C., Box, Karl J., Tam, Kin Y., Calculation of Abraham descriptors from solvent-water partition coefficients in four different systems; evaluation of different methods of calculation. *Perkin Transactions 2* **2002**, 2002 (3), 470-477.

28. Abraham, M. H., Ibrahim, A., Zissimos, A.M., Determination of sets of solute descriptors from chromatographic measurements. *JOURNAL OF CHROMATOGRAPHY A* **2004**, 1037 (1-2), 29-47.

29. Poole, C.F., Atapattu, S.N., Poole, S.K., Bell, A.K., Fundamental and Applied Analytical Science. A Special Issue In Honour of Alan Townshend., Determination of solute descriptors by chromatographic methods. *Anal. Chim. Acta* **2009**, 652 (1-2), 32-53.

30. Abraham, M. H., Green, C. E., Acree, W. E., Hernandez, C.E., Descriptors for solutes from the solubility of solids: trans-stilbene as an example. *Journal of the Chemical Society. Perkin transactions II*. **1998**, (12), 2677.

31. Ahmed, H., Poole, C.F., Kozerski, G.E., Determination of descriptors for organosilicon compounds by gas chromatography and non-aqueous liquid-liquid partitioning. *Journal of Chromatography A* **2007**, 1169 (1-2), 179-192.

32. Stenzel, Angelika, Goss, Kai-Uwe, Endo, Satoshi, Prediction of partition coefficients for complex environmental contaminants: Validation of COSMOtherm, ABSOLV, and SPARC. *ETC Environmental Toxicology and Chemistry* **2014**, 33 (7), 1537-1543.

33. Lin, Shiang-Tai, Sandler, Stanley I., A Priori Phase Equilibrium Prediction from a Segment Contribution Solvation Model. *Ind. Eng. Chem. Res. Industrial & Engineering Chemistry Research* **2002**, 41 (5), 899-913.

34. Wang, S., Thermodynamic properties predictions using the COSMO-SAC solvation method. , UMI, Ann Arbor, 2007.

35. Hsieh, Chieh-Ming, Sandler, Stanley I., Lin, Shiang-Tai, Improvements of COSMO-SAC for vapor-liquid and liquid-liquid equilibrium predictions. *FLUID Fluid Phase Equilibria* **2010**, 297 (1), 90-97.

36. Xiong R., Sandler S.I., Burnett R.I., An improvement to COSMO-SAC for predicting thermodynamic properties. *Ind. Eng. Chem. Res. Industrial and Engineering Chemistry Research* **2014**, 53 (19), 8265-8278.

37. Frisch, M.; Trucks, G.; Schlegel, H.B.; Scuseria, G.; Robb, M.; Cheeseman, J.; Scalmani, G.; Barone, V.; Mennucci, B.; Petersson, G. Gaussian 09. **2009**, .

38. Zhao, Yan, Truhlar, Donald G., The M06 suite of density functionals for main group thermochemistry, thermochemical kinetics, noncovalent interactions, excited states, and transition elements: two new functionals and systematic testing of four M06-class functionals and 12 other functionals. *Theor Chem Account Theoretical Chemistry Accounts : Theory, Computation, and Modeling* **2008**, 120 (1-3), 215-241.
39. Dunning, T.H., Gaussian basis sets for use in correlated molecular calculations. I. The atoms boron through neon and hydrogen. *J.Chem.Phys.The Journal of Chemical Physics* **1989**, 90 (2), 1007.
40. Woon, David E., Dunning, Thom H., Gaussian basis sets for use in correlated molecular calculations. III. The atoms aluminum through argon. *J.Chem.Phys.The Journal of Chemical Physics* **1993**, 98 (2), 1358.
41. Klamt, A., Schüürmann, G., COSMO: a new approach to dielectric screening in solvents with explicit expressions for the screening energy and its gradient. *Journal of the Chemical Society, Perkin Transactions 2* **1993**, (5), 799-805.
42. Abraham MH, Smith RE, Luchtefeld R, Boorem AJ, Luo R, Acree WE Jr, Prediction of solubility of drugs and other compounds in organic solvents. *J. Pharm. Sci.* **2010**, 99 (3), 1500-15.
43. Abraham, Michael H., Chadha, Harpreet S., Whiting, Gary S., Mitchell, Robert C., Hydrogen bonding. 32. An analysis of water-octanol and water-alkane partitioning and the $\Delta \log p$ parameter of seiler. *JPS Journal of Pharmaceutical Sciences* **1994**, 83 (8), 1085-1100.
44. Abraham, Michael H., Acree, Jr., William E., Leo, Albert J., Hoekman, David, Partition of compounds from water and from air into the wet and dry monohalobenzenes. *New Journal of Chemistry* **2009**, 33 (8), 1685-1692.
45. Abraham, Michael H., Acree Jr, William E., Cometto-Muñiz, J. Enrique, Partition of compounds from water and from air into amides. *New Journal of Chemistry* **2009**, 33 (10), 2034-2043.
46. Abraham, Michael H., Acree, William E., Leo, Albert J., Hoekman, David, The partition of compounds from water and from air into wet and dry ketones. *New Journal of Chemistry* **2009**, 33 (3), 568-573.
47. Grubbs, Laura M., Saifullah, Mariam, De La Rosa, Nohelli E., Ye, Shulin, Achi, Sai S., Acree, William E., Abraham, Michael H., Mathematical correlations for describing solute transfer into functionalized alkane solvents containing hydroxyl, ether, ester or ketone solvents. *FLUID Fluid Phase Equilibria* **2010**, 298 (1), 48-53.
48. Saifullah, Mariam, Ye, Shulin, Grubbs, Laura M., De La Rosa, Nohelli E., Acree, William E., Abraham, Michael H., Abraham Model Correlations for Transfer of Neutral Molecules to

Tetrahydrofuran and to 1,4-Dioxane, and for Transfer of Ions to Tetrahydrofuran. *J Solution Chem Journal of Solution Chemistry* **2011**, 40 (12), 2082-2094.

49. Sprunger, Laura M., Achi, Sai S., Acree, William E., Abraham, Michael H., Leo, Albert J., Hoekman, David, Correlation and prediction of solute transfer to chloroalkanes from both water and the gas phase. *FLUID Fluid Phase Equilibria* **2009**, 281 (2), 144-162.

50. W. Stephens, T., Correlation of Solute Transfer Into Toluene and Ethylbenzene from Water and from the Gas Phase Based on the Abraham Model. *TOTHERJ The Open Thermodynamics Journal* **2011**, 5 (1), 104-121.

51. Correlation of solute transfer into alkane solvents from water and from the gas phase with updated Abraham model equations.

52. EPI Suite™-Estimation Program Interface.

53. Abraham, Michael H., Whiting, Garry S., Doherty, Ruth M., Shuely, Wendel J., Hydrogen bonding. Part 13. A new method for the characterisation of GLC stationary phases—the laffort data set. *Journal of the Chemical Society, Perkin Transactions 2* **1990**, (8), 1451-1460.

54. Todeschini, Roberto, Consonni, Viviana, *Molecular descriptors for chemoinformatics*. Wiley-VCH-Verl.: Weinheim, .

55. Feynman, Richard P., Leighton, Robert B., Sands, Matthew L., *The Feynman lectures on physics*. Addison-Wesley Pub. Co.: Reading, Mass., 1963.

56. Hickey AL, R.C., Benchmarking quantum chemical methods for the calculation of molecular dipole moments and polarizabilities. *The journal of physical chemistry.A* **2014**, 118 (20), 3678-87.

57. Becke, A.D., Density-functional thermochemistry. III. The role of exact exchange. *J.Chem.Phys.The Journal of Chemical Physics* **1993**, 98 (7), 5648.

58. Scuseria, Gustavo E., Janssen, Curtis L., Schaefer, Henry F., An efficient reformulation of the closed-shell coupled cluster single and double excitation (CCSD) equations. *J.Chem.Phys.The Journal of Chemical Physics* **1988**, 89 (12), 7382.

59. Head-Gordon, Martin, Pople, John A., Frisch, Michael J., MP2 energy evaluation by direct methods. *CPLETT</cja:jid> Chemical Physics Letters* **1988**, 153 (6), 503-506.

60. Sadlej, A.J., Medium-size polarized basis sets for high-level-correlated calculations of molecular electric properties : V. Fourth-row atoms: Sn through I. *Theoret.Chim.Acta Theoretica chimica acta* **1992**, 81 (4-5), 339-354.

61. Petersson, G. A., Bennett, Andrew, Tensfeldt, Thomas G., Al-Laham, Mohammad A., Shirley, William A., Mantzaris, John, A complete basis set model chemistry. I. The total energies

of closed-shell atoms and hydrides of the first-row elements. *J.Chem.Phys.The Journal of Chemical Physics* **1988**, 89 (4), 2193.

62. Petersson, G. A., Al-Laham, Mohammad A., A complete basis set model chemistry. II. Open-shell systems and the total energies of the first-row atoms. *J.Chem.Phys.The Journal of Chemical Physics* **1991**, 94 (9), 6081.

63. Amsterdam Density Functional.

64. te Velde, G., Bickelhaupt, F. M., Baerends, E. J., Fonseca Guerra, C., van Gisbergen, S. J. A., Snijders, J. G., Ziegler, T., Chemistry with ADF. *JCC Journal of Computational Chemistry* **2001**, 22 (9), 931-967.

65. Fonseca Guerra, C., Snijders, J. G., te Velde, G., Baerends, E. J., Towards an order-N DFT method. *Theor Chem Acc Theoretical Chemistry Accounts : Theory, Computation and Modeling* **1998**, 99 (6), 391-403.

66. The R Stats Package.

67. Karunasekara, Thushara, Poole, Colin F., Compounds for expanding the descriptor space for characterizing separation systems. *CHROMA Journal of Chromatography A* **2012**, 1266, 124-130.

68. Hexagonal Binning Routines.

69. Draper, Norman Richard., Smith, Harry., *Applied regression analysis*. Wiley: New York, 1998.

70. Smith, Grant D, Bharadwaj, Rishikesh K, ARTICLES - PHYSICAL CHEMISTRY OF MATERIALS: FROM NANOPARTICLES TO MACROMOLECULES - Quantum Chemistry Based Force Field for Simulations of HMX. *The journal of physical chemistry.B, Condensed matter, materials, surfaces, interfaces & biophysical*. **1999**, 103 (18), 3570.

71. Brand, Holmann V., Rabie, Ronald L., Funk, David J., Diaz-Acosta, Irina, Pulay, Peter, Lippert, Thomas K., Theoretical and experimental study of the vibrational spectra of the alpha, beta, and delta phases of octahydro-1,3,5,7-tetrazocine (HMX). *J Phys Chem B* **2002**, 106 (41), 10594-10604.

72. Rice, B. M., Chabalowski, C. F., Ab Initio and Nonlocal Density Functional Study of 1,3,5-Trinitro-s-triazine (RDX) Conformers. *JOURNAL OF PHYSICAL CHEMISTRY A* **1997**, 101 (46), 8720-8726.

73. Molt RW Jr, Watson T Jr, Lotrich VF, Bartlett RJ, RDX geometries, excited states, and revised energy ordering of conformers via MP2 and CCSD(T) methodologies: insights into decomposition mechanism. *The journal of physical chemistry.A* **2011**, 115 (5), 884-90.

74. Dragos H, Gilles M, Alexandre V, Predicting the predictability: a unified approach to the applicability domain problem of QSAR models. *Journal of chemical information and modeling* **2009**, 49 (7), 1762-76.
75. Sprunger L.M., Achi S.S., Pointer R., Acree Jr. W.E., Abraham M.H., Development of Abraham model correlations for solvation characteristics of secondary and branched alcohols. *Fluid Phase Equilib. Fluid Phase Equilibria* **2010**, 288 (1-2), 121-127.
76. Klamt, A., Conductor-like Screening Model for Real Solvents: A New Approach to the Quantitative Calculation of Solvation Phenomena. *The journal of physical chemistry*. **1995**, 99 (7), 2224.

Appendix B

SUPPLEMENTARY INFORMATION FOR: QUANTUM CHEMICAL ESTIMATED ABRAHAM SOLUTE PARAMETERS USING MULTIPLE SOLVENT-WATER PARTITION COEFFICIENTS AND MOLECULAR POLARIZABILITY

CONTENTS: Located in an accompanying Microsoft Excel file.

- Table B-1 Residuals of COSMO-SAC predicted solvent-water partition coefficients and summary statistics. Located in Chapter_3_Appendix B_Tables.xlsx file.
- Table B-2 System parameters used for computing Abraham solute parameters. Located in Chapter_3_Appendix B_Tables.xlsx file.
- Table B-3 COSMO-SAC predicted solvent-water partition coefficients (as well as the corresponding solute and system parameters) used for computing QCAP solute parameters. Located in Chapter_3_Appendix B_Tables.xlsx file.
- Table B-4 Polarizability and solute parameters (QCAP, ABSOLV, and UFZ-LSER). Located in Chapter_3_Appendix B_Tables.xlsx file.
- Table B-5 Experimental and predicted (ABSOLV, QCAP, and Adjusted QCAP) solvent-water partition coefficients. Located in Chapter_3_Appendix B_Tables.xlsx file.
- Table B-6 RMSEs of prediction (ABSOLV, QCAP, and Adjusted QCAP) of solvent-water partition coefficients. Located in Chapter_3_Appendix B_Tables.xlsx file.
- Table B-7 Solute parameters (ABSOLV and QCAP) and partition coefficients (observed, ABSOLV, QCAP, and Adjusted QCAP) for munition constituents and munition-like compounds. Located in Chapter_3_Appendix B_Tables.xlsx file.

Table B-8 Comparison of the estimated (QCAP, Adjusted QCAP, and COSMOments) and experimentally-based solute parameters. Located in Chapter_3_Appendix B_Tables.xlsx file.

Appendix C

QUANTUM CHEMICAL ESTIMATED ABRAHAM SOLUTE PARAMETERS USING MULTIPLE SOLVENT-WATER PARTITION COEFFICIENTS AND MOLECULAR POLARIZABILITY: SUPPLEMENTARY INFORMATION

CONTENTS:

- Figure C-1 The interquartile range of COSMO-SAC predicted solvent-water partition coefficient errors.
- Figure C-2 Histogram of COSMO-SAC predicted solvent-water partition coefficient errors.
- Figure C-3 Solvent-water system parameters e , s , a , b , and v for the 65 solvent-water systems used for computing QCAP.
- Figure C-4 Molecular polarizability computed using M062X with the aug-cc-pVDZ versus aug-cc-pVTZ basis set.
- Figure C-5 Predicted versus experimental solute parameters for A and B determined by ESAB and QCAP methods.
- Figure C-6 Correlation of E and S solute parameters compiled from the UFZ-LSER database.
- Figure C-7 Pairs plot of solvent parameters used to compute QCAP parameters.
- Figure C-8 Predicted versus observed partition coefficients for wet octanol-water.
- Figure C-9
to Figure C-31 Predicted versus observed partition coefficients for other solvent-water systems.
- Figure C-32 Residuals of wet octanol-water partition coefficients versus QCAP parameters.

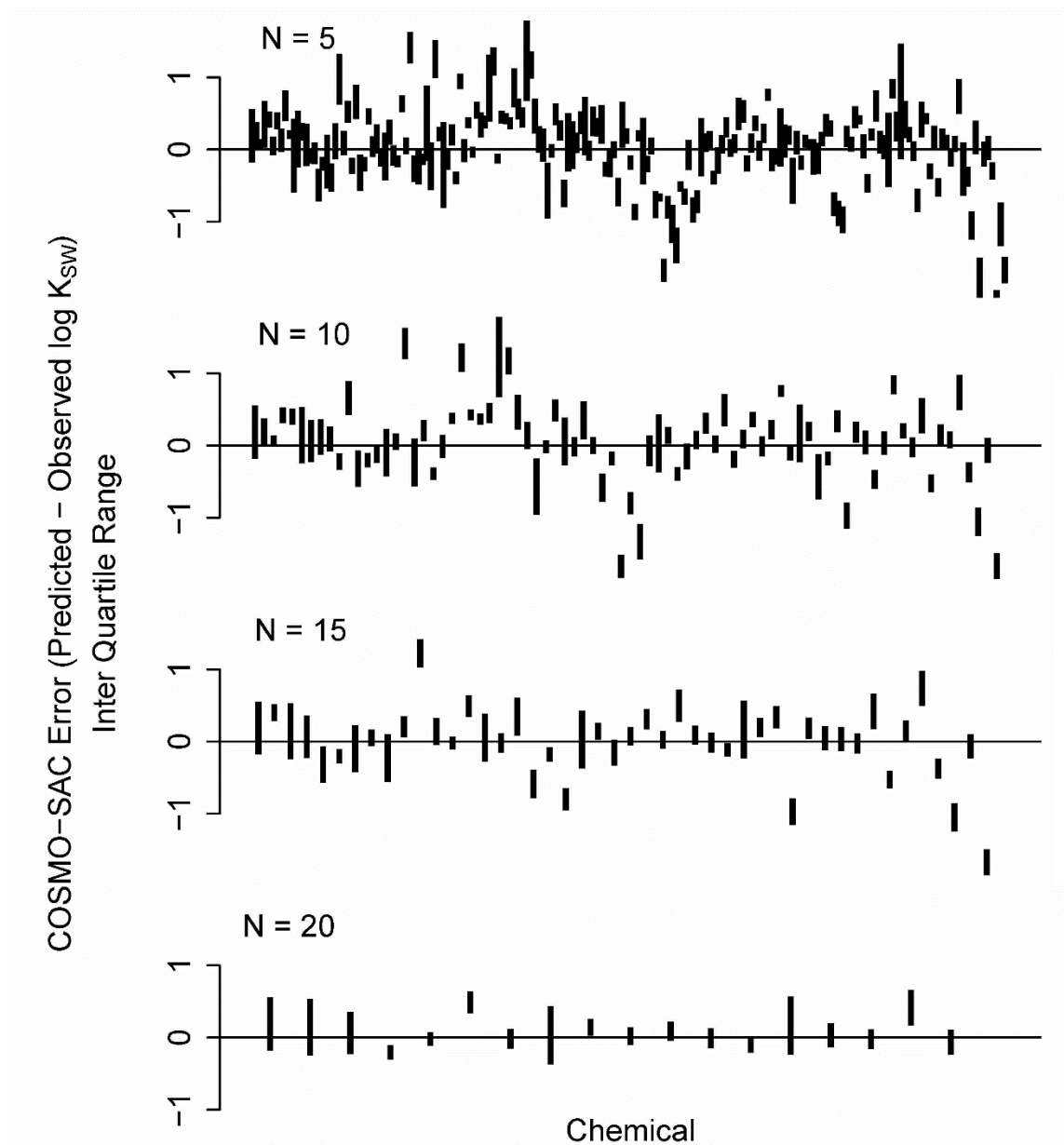


Figure C-1 Plots showing the decrease of the interquartile range (IQR) of COSMO-SAC predicted solvent-water partition coefficient errors as the number of data points increases. N = minimum number of data points used to compute the IQR. Data are from Table B-1. Chemicals are plotted in the solvent sequence in the table. Note that a solvent with greater than 20 observations appears in all four plots, e.g. the first IQR on the left hand side.

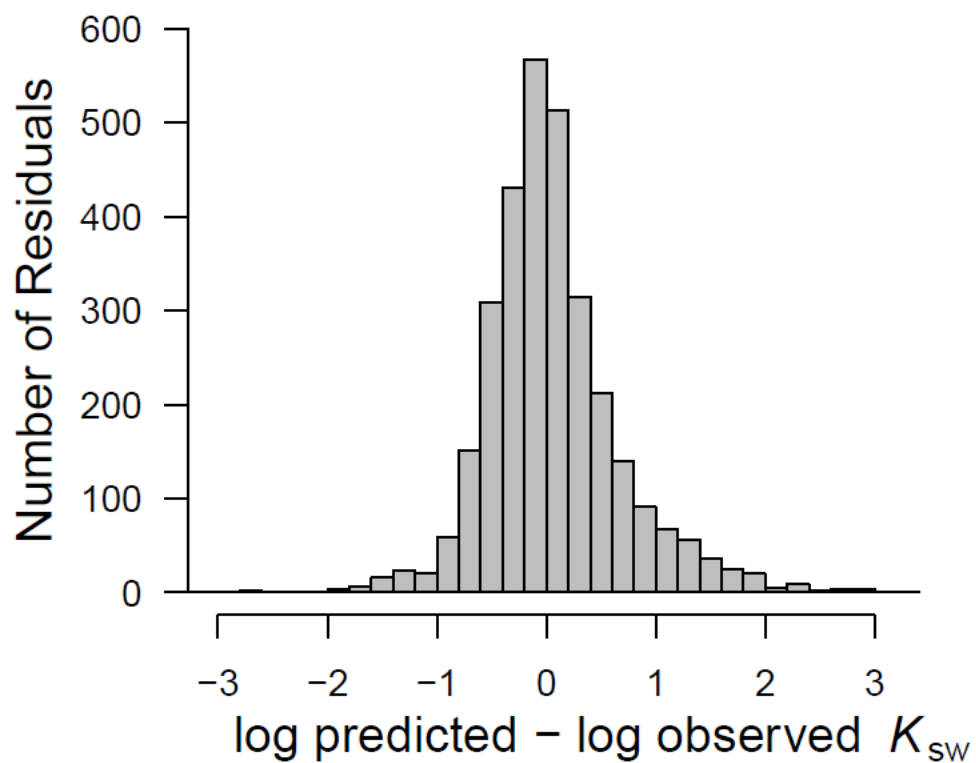


Figure C-2 A histogram plot of COSMO-SAC predicted solvent-water partition coefficient (K_{sw}) errors. 24 solvent-water systems and 3095 data points are included.

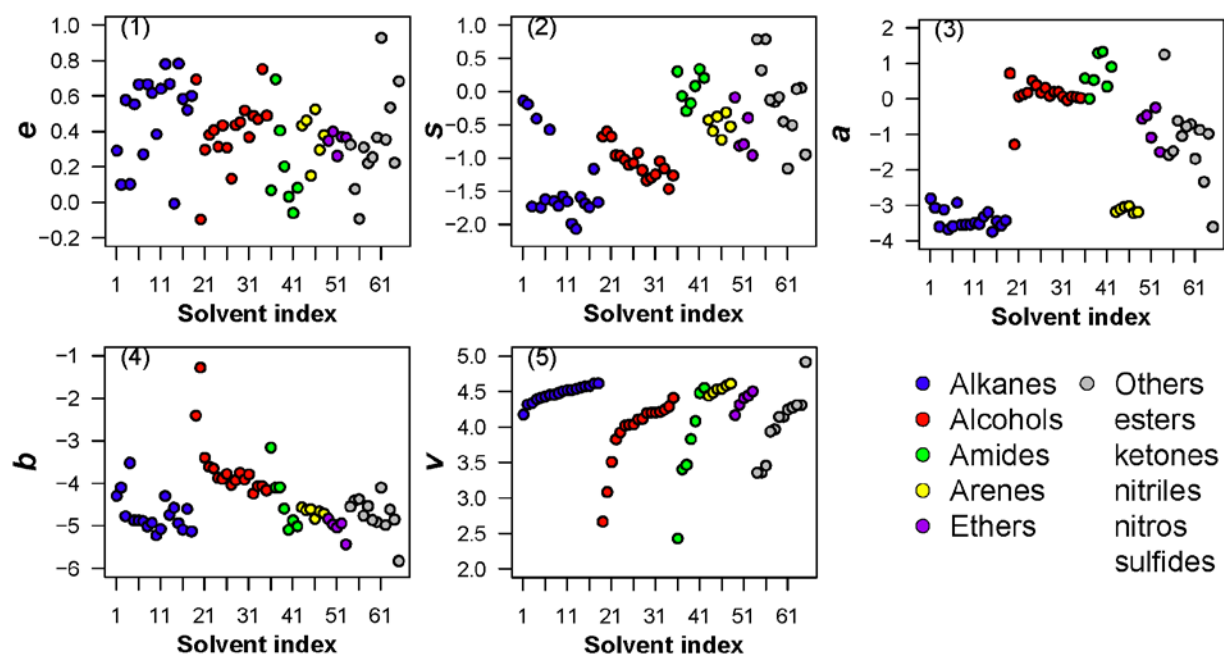


Figure C-3 The solvent-water system parameters e , s , a , b , and v for the 65 solvent-water systems used for computing QCAP. Parameters are grouped by solvent chemical classes. Within each group, the solvents are ordered from the smallest to the largest magnitude of v .

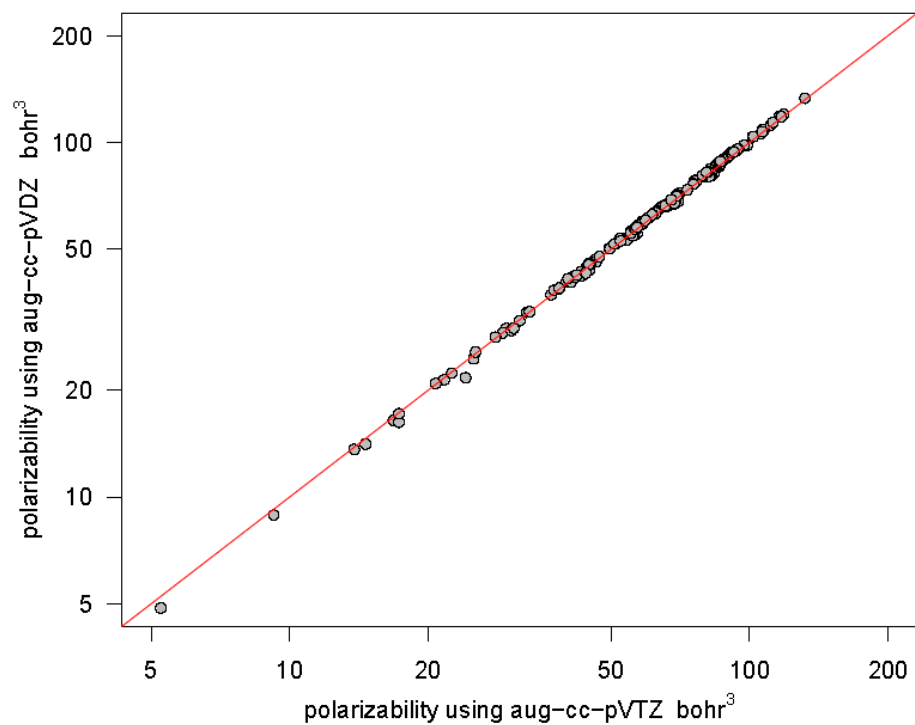


Figure C-4 Comparing molecular polarizability computed using M062X¹ with aug-cc-pVDZ and with aug-cc-pVTZ basis set.

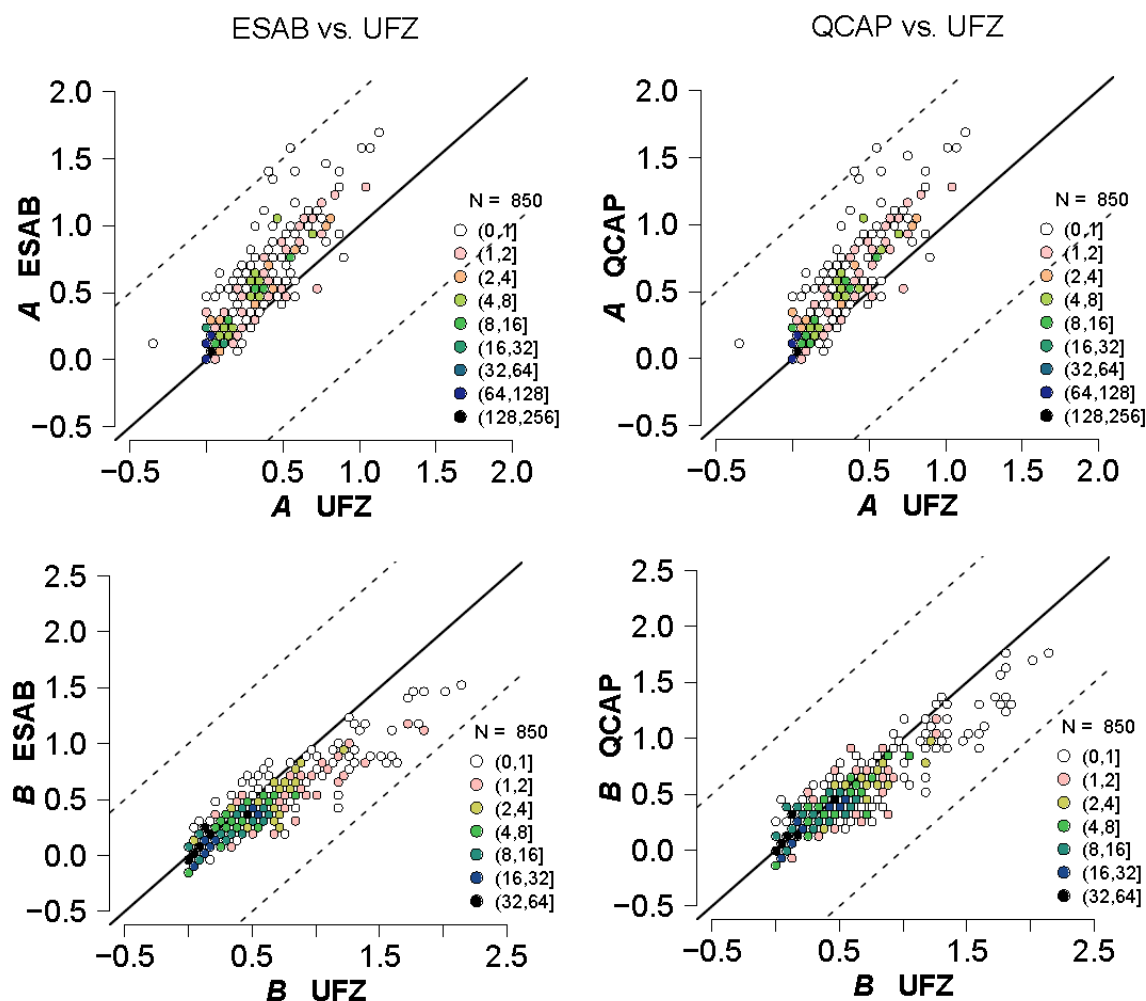


Figure C-5 Hexbin two dimensional histogram plots² comparing the predicted versus experimental values from the UFZ-LSER database (labeled UFZ) for the solute parameters A , B , and V determined by two methods listed at the top of each column: (1) estimates E , S , A , and B jointly with an MLR, and an independently estimated V , labeled ESAB; (2) estimate of E from molecular polarizability, V from molecular volume and S , A , and B from an MLR, which is the QCAP method.

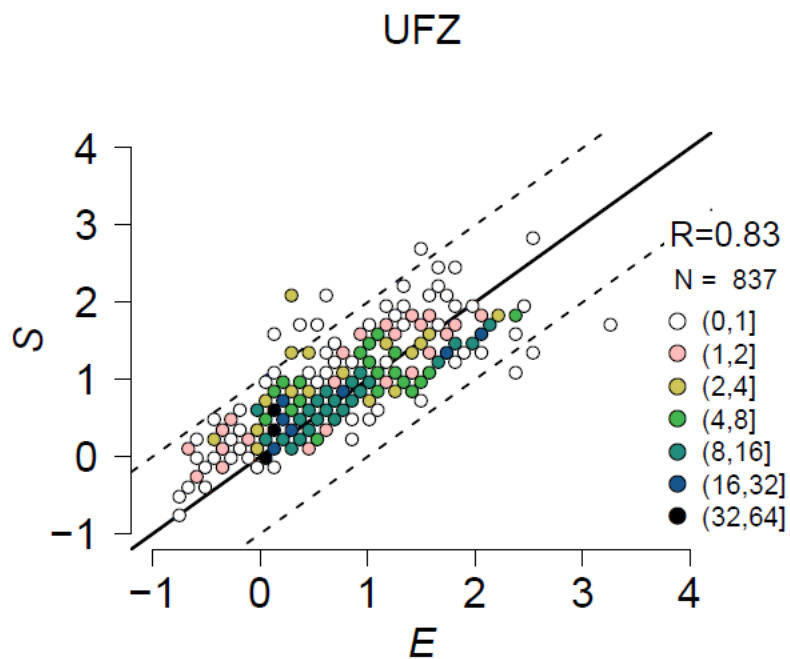


Figure C-6 Hexbin two dimensional histogram plot² of E versus S solute parameters compiled from the UFZ-LSER database.

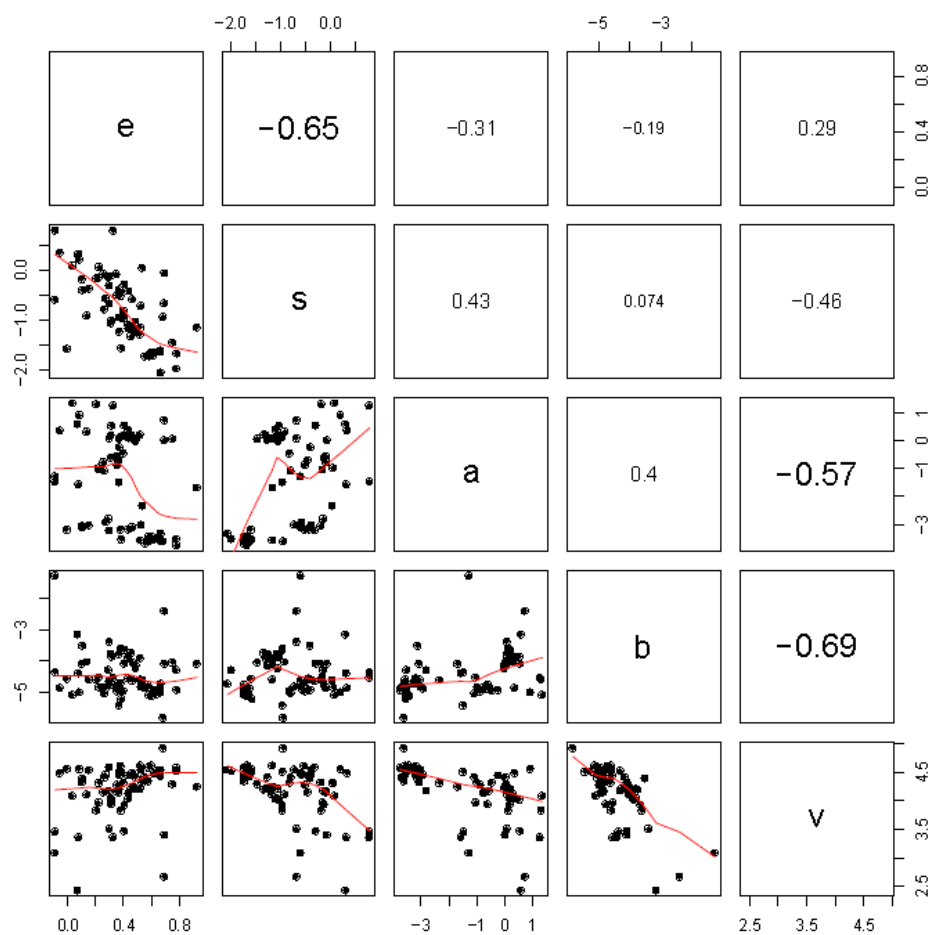


Figure C-7 A histogram plot of COSMO-SAC predicted solvent-water partition coefficient (K_{sw}) errors. 24 solvent-water systems and 3095 data points are included.

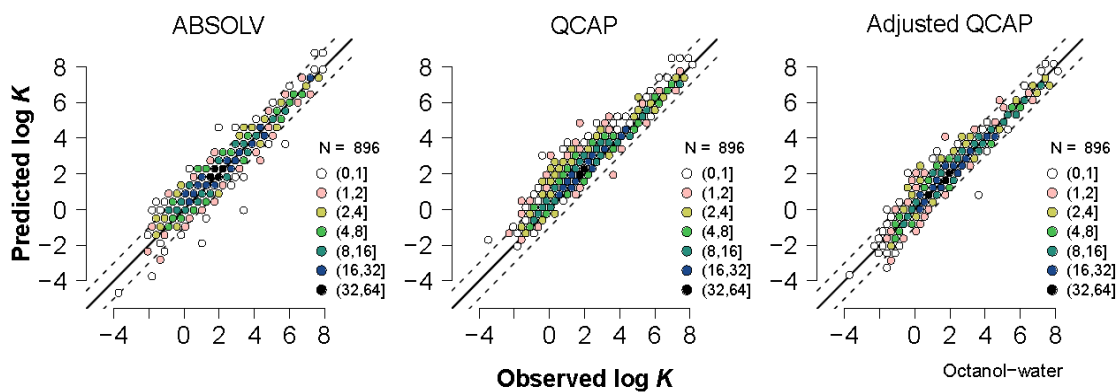


Figure C-8 Hexbin two dimensional histogram plot² of predicted versus observed log wet octanol-water partition coefficients. Solid lines show perfect agreement. Dashed lines represent ± 1 order of magnitude.

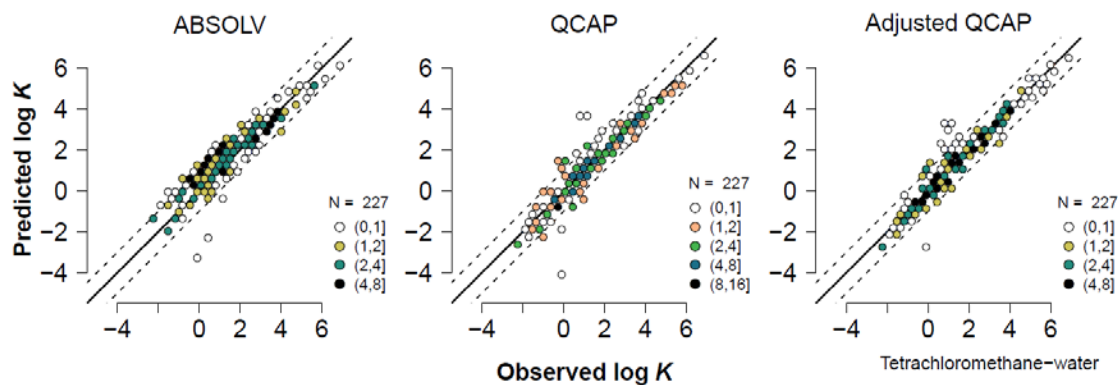


Figure C-9 Hexbin two dimensional histogram plot² of predicted versus observed log tetrachloromethane-water partition coefficients. Solid lines show perfect agreement. Dashed lines represent ± 1 order of magnitude.

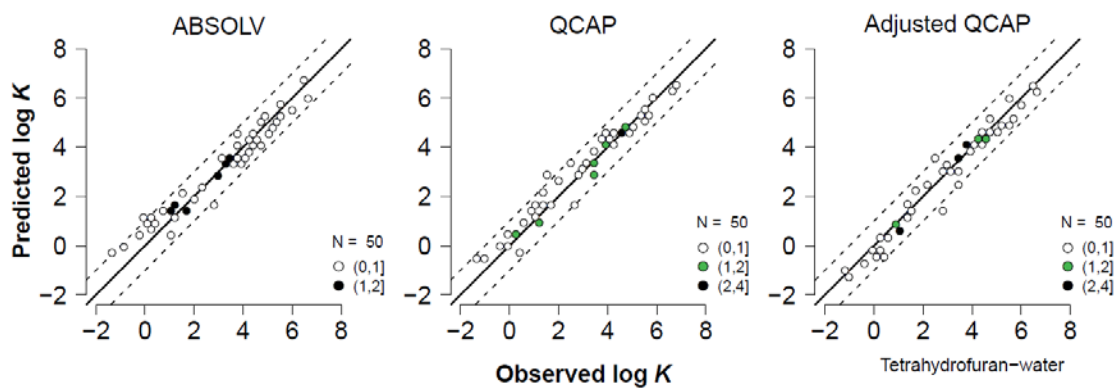


Figure C-10 Hexbin two dimensional histogram plot² of predicted versus observed log tetrahydrofuran-water partition coefficients. Solid lines show perfect agreement. Dashed lines represent ± 1 order of magnitude.

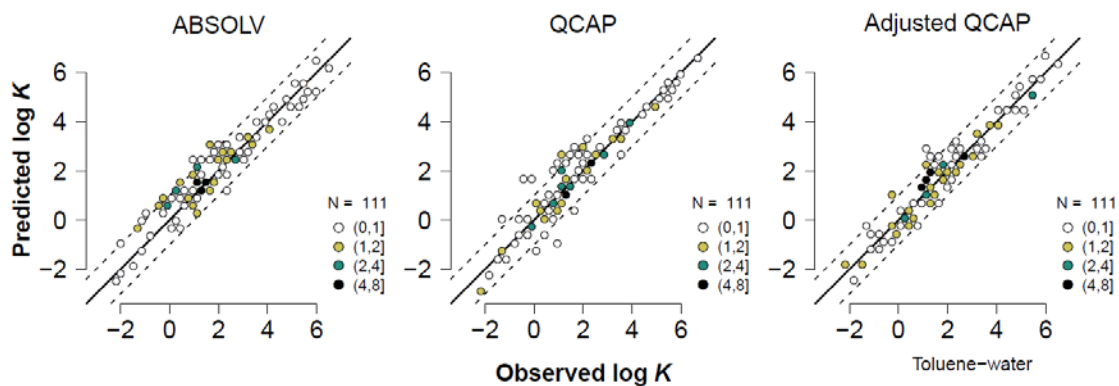


Figure C-11 Hexbin two dimensional histogram plot² of predicted versus observed log toluene-water partition coefficients. Solid lines show perfect agreement. Dashed lines represent ± 1 order of magnitude.

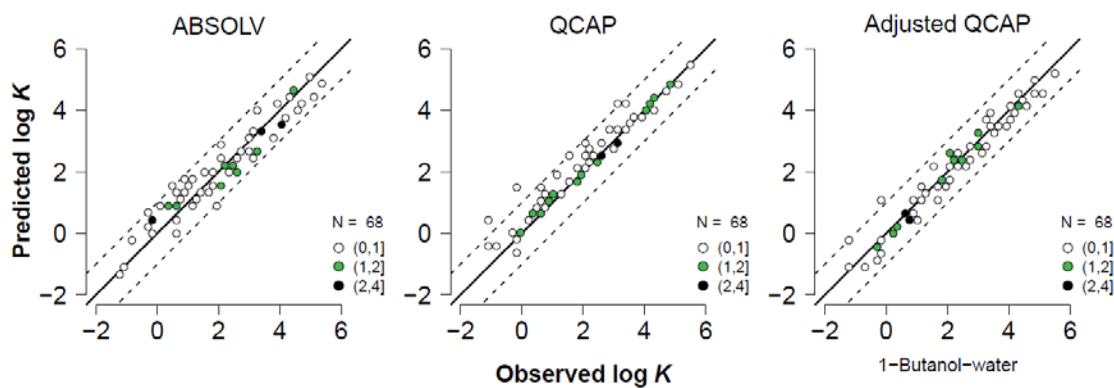


Figure C-12 Hexbin two dimensional histogram plot² of predicted versus observed log 1-Butanol-water partition coefficients. Solid lines show perfect agreement. Dashed lines represent ± 1 order of magnitude.

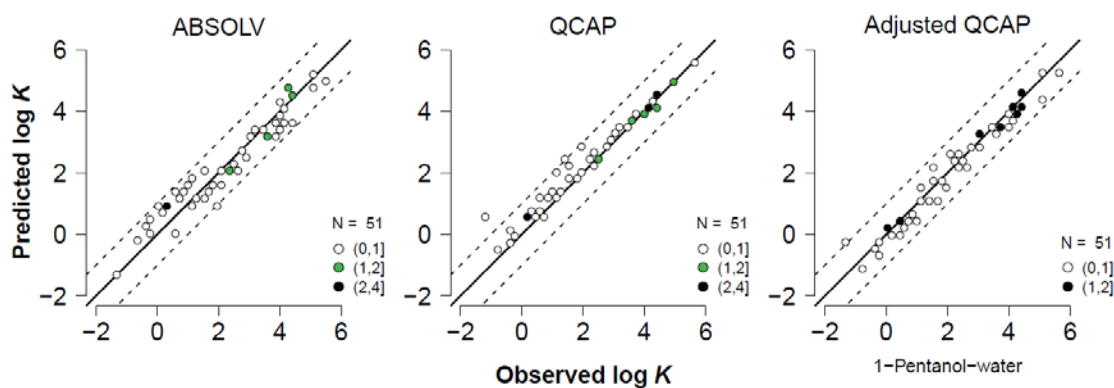


Figure C-13 Hexbin two dimensional histogram plot² of predicted versus observed log 1-Pentanol-water partition coefficients. Solid lines show perfect agreement. Dashed lines represent ± 1 order of magnitude.

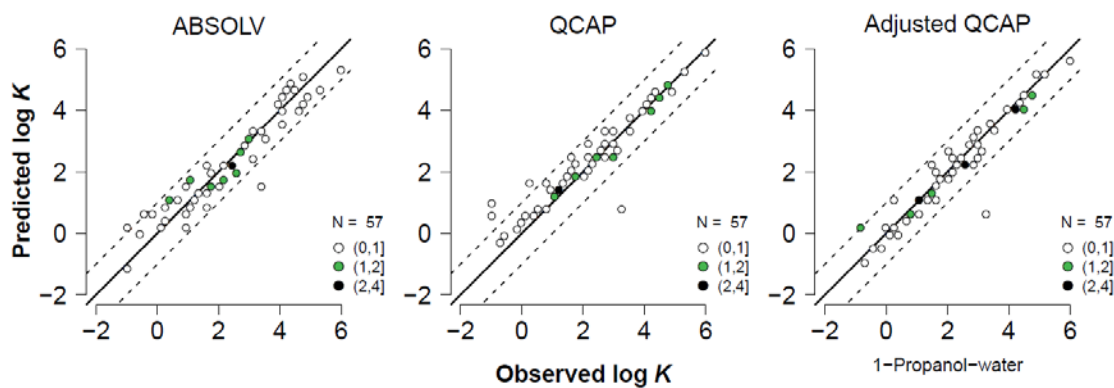


Figure C-14 Hexbin two dimensional histogram plot² of predicted versus observed log 1-Propanol-water partition coefficients. Solid lines show perfect agreement. Dashed lines represent ± 1 order of magnitude.

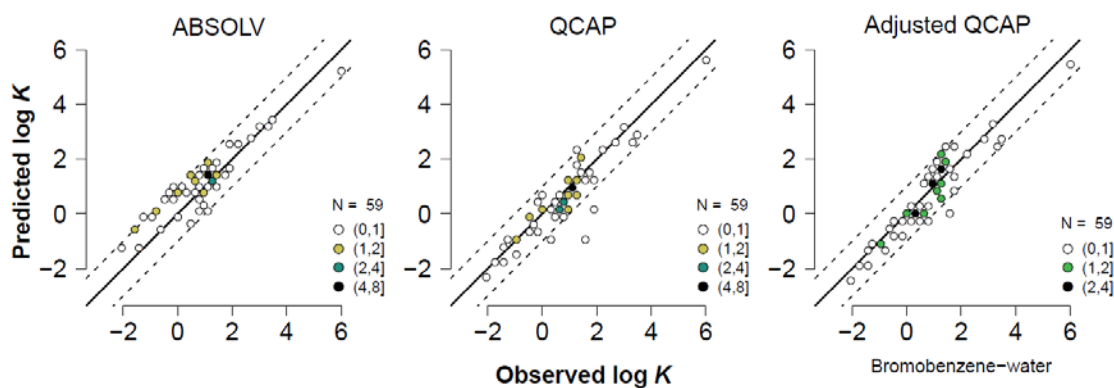


Figure C-15 Hexbin two dimensional histogram plot² of predicted versus observed log Bromobenzene-water partition coefficients. Solid lines show perfect agreement. Dashed lines represent ± 1 order of magnitude.

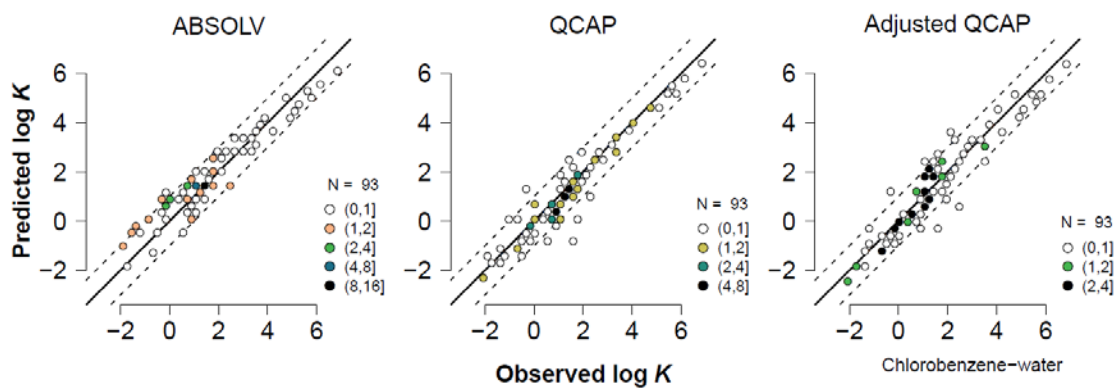


Figure C-16 Hexbin two dimensional histogram plot² of predicted versus observed log chlorobenzene-water partition coefficients. Solid lines show perfect agreement. Dashed lines represent ± 1 order of magnitude.

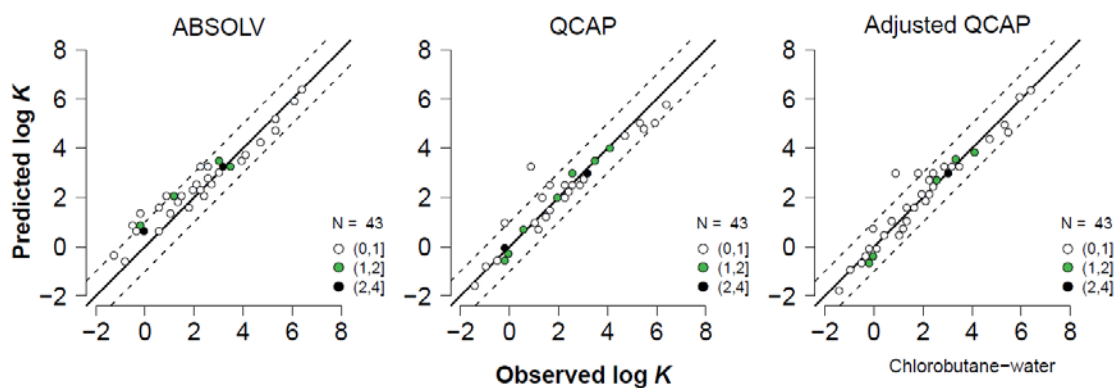


Figure C-17 Hexbin two dimensional histogram plot² of predicted versus observed log chlorobutane-water partition coefficients. Solid lines show perfect agreement. Dashed lines represent ± 1 order of magnitude.

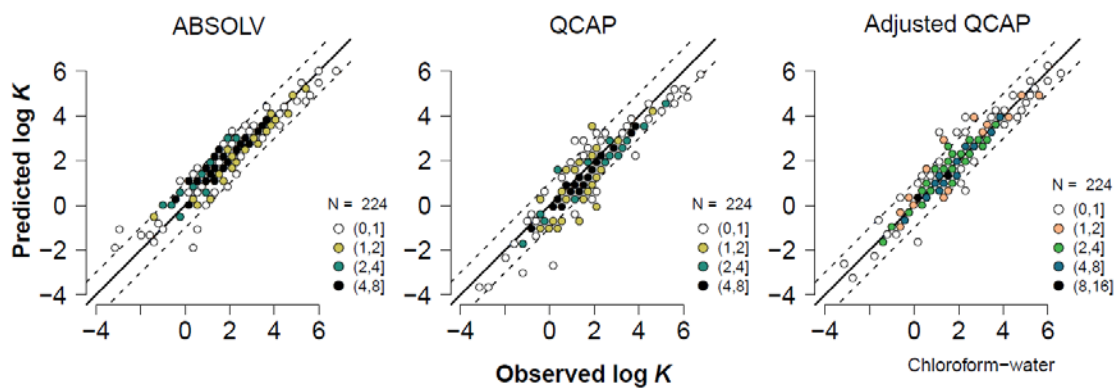


Figure C-18 Hexbin two dimensional histogram plot² of predicted versus observed log chloroform-water partition coefficients. Solid lines show perfect agreement. Dashed lines represent ± 1 order of magnitude.

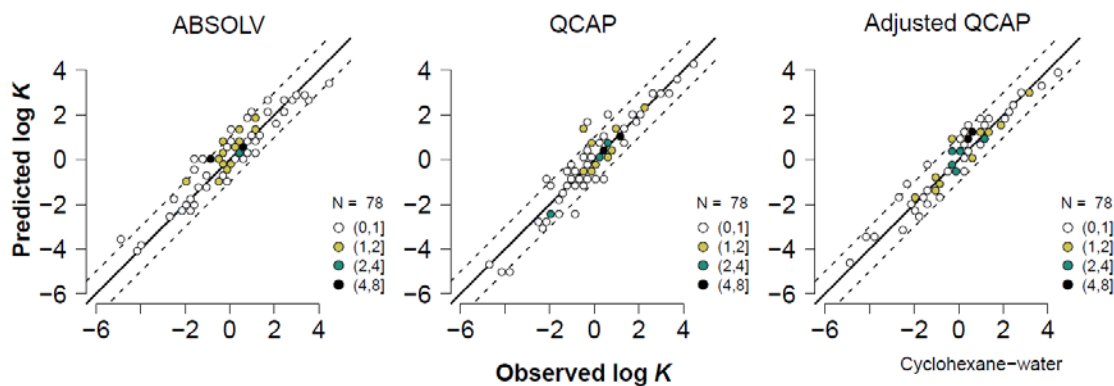


Figure C-19 Hexbin two dimensional histogram plot² of predicted versus observed log cyclohexane-water partition coefficients. Solid lines show perfect agreement. Dashed lines represent ± 1 order of magnitude.

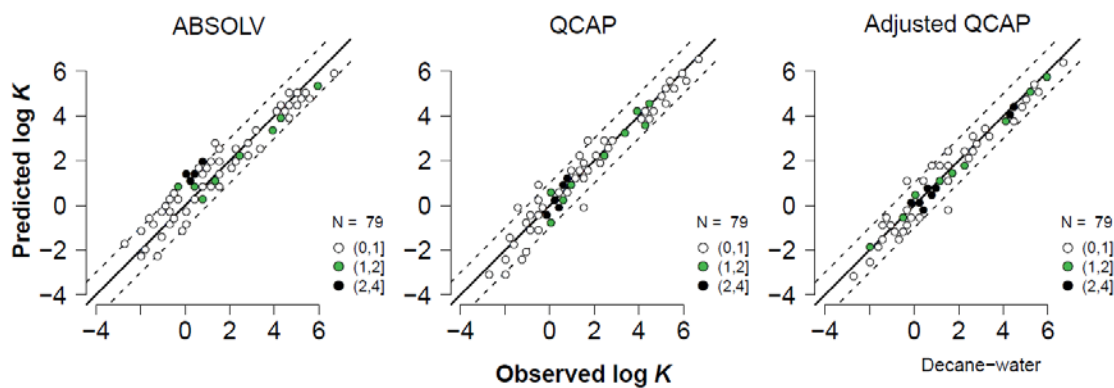


Figure C-20 Hexbin two dimensional histogram plot² of predicted versus observed log decane-water partition coefficients. Solid lines show perfect agreement. Dashed lines represent ± 1 order of magnitude.

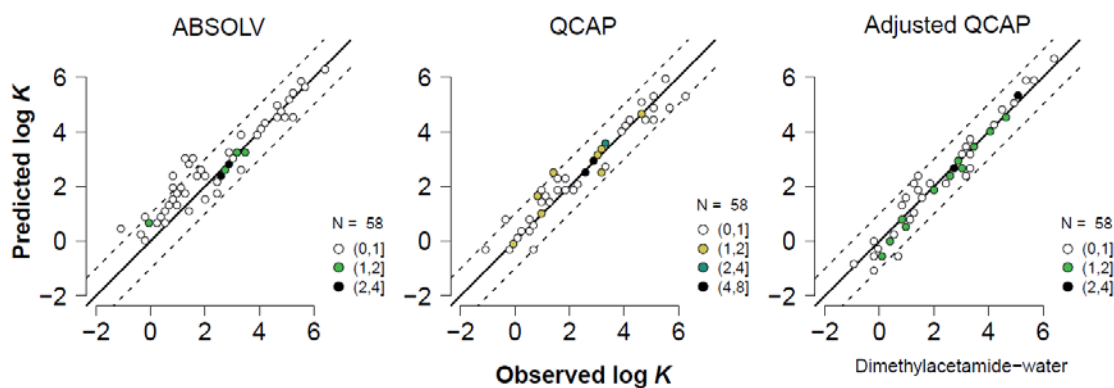


Figure C-21 Hexbin two dimensional histogram plot² of predicted versus observed log dimethylacetamide-water partition coefficients. Solid lines show perfect agreement. Dashed lines represent ± 1 order of magnitude.

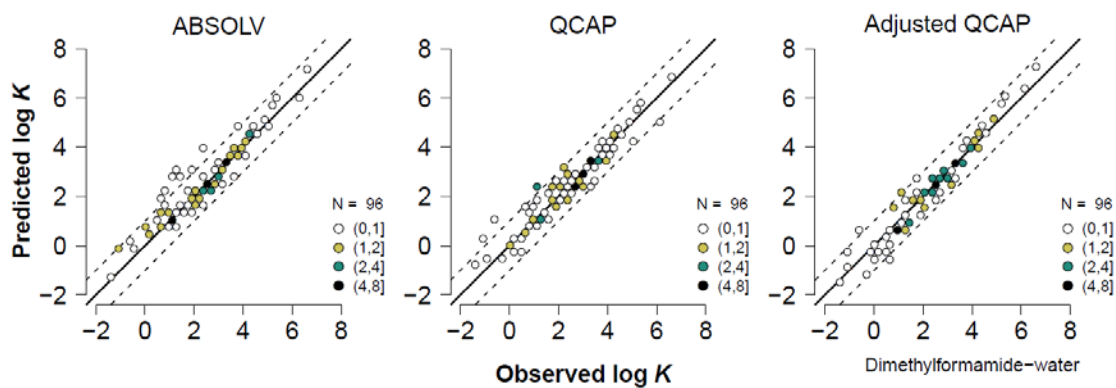


Figure C-22 Hexbin two dimensional histogram plot² of predicted versus observed log dimethylformamide-water partition coefficients. Solid lines show perfect agreement. Dashed lines represent ± 1 order of magnitude.

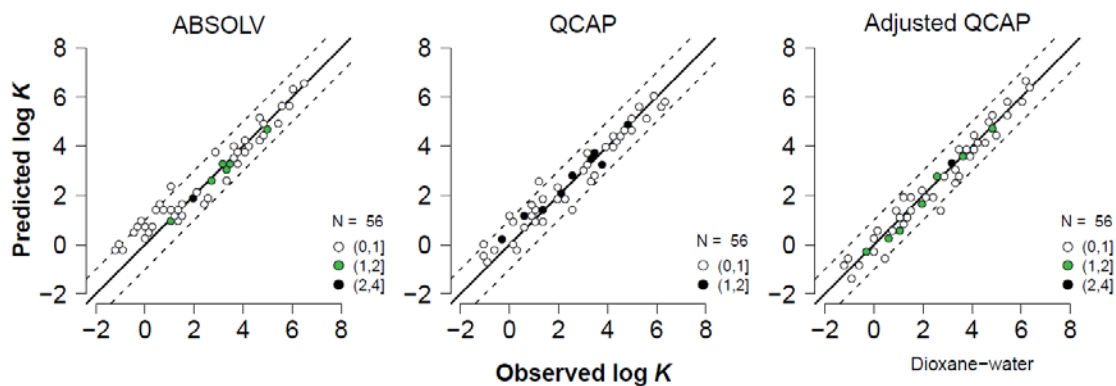


Figure C-23 Hexbin two dimensional histogram plot² of predicted versus observed log dioxane-water partition coefficients. Solid lines show perfect agreement. Dashed lines represent ± 1 order of magnitude.

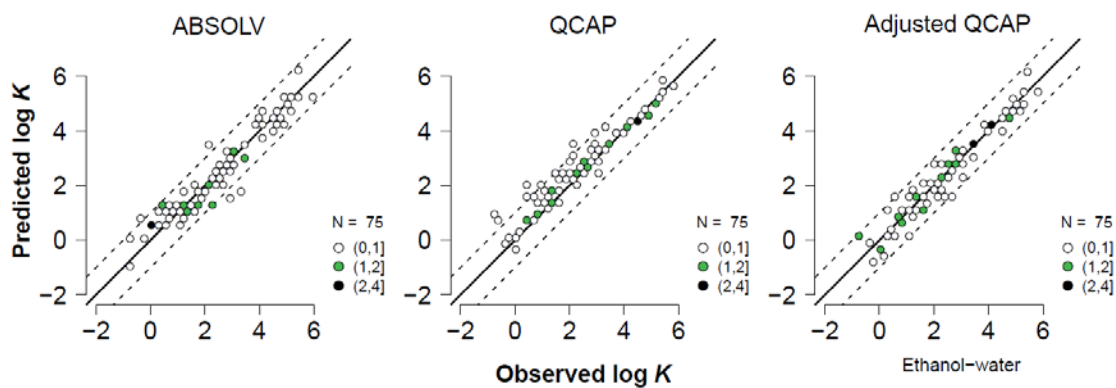


Figure C-24 Hexbin two dimensional histogram plot² of predicted versus observed log ethanol-water partition coefficients. Solid lines show perfect agreement. Dashed lines represent ± 1 order of magnitude.

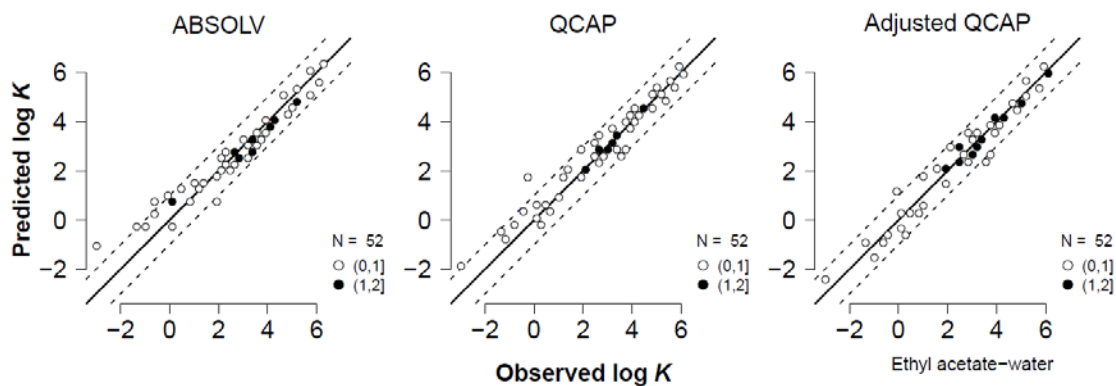


Figure C-25 Hexbin two dimensional histogram plot² of predicted versus observed log ethyl acetate-water partition coefficients. Solid lines show perfect agreement. Dashed lines represent ± 1 order of magnitude.

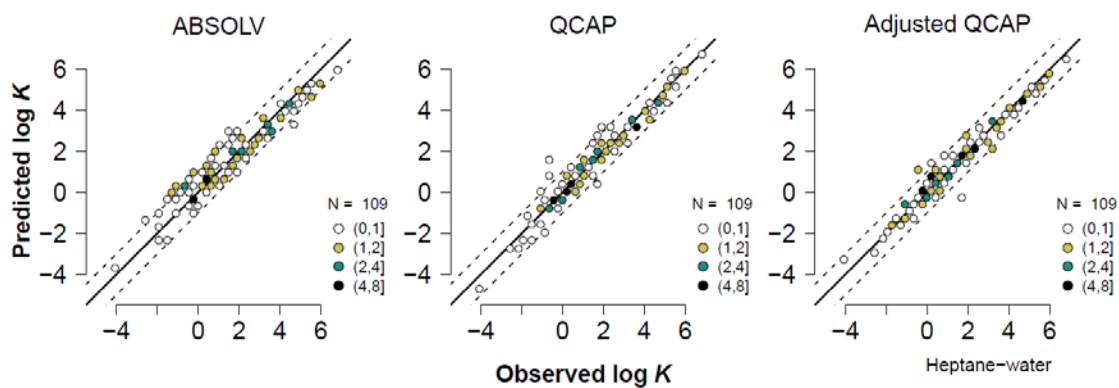


Figure C-26 Hexbin two dimensional histogram plot² of predicted versus observed log heptane-water partition coefficients. Solid lines show perfect agreement. Dashed lines represent ± 1 order of magnitude.

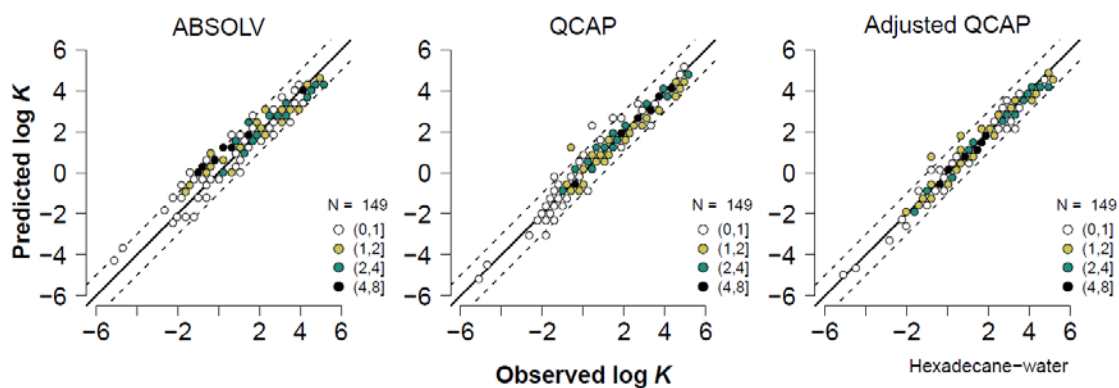


Figure C-27 Hexbin two dimensional histogram plot² of predicted versus observed log hexadecane-water partition coefficients. Solid lines show perfect agreement. Dashed lines represent ± 1 order of magnitude.

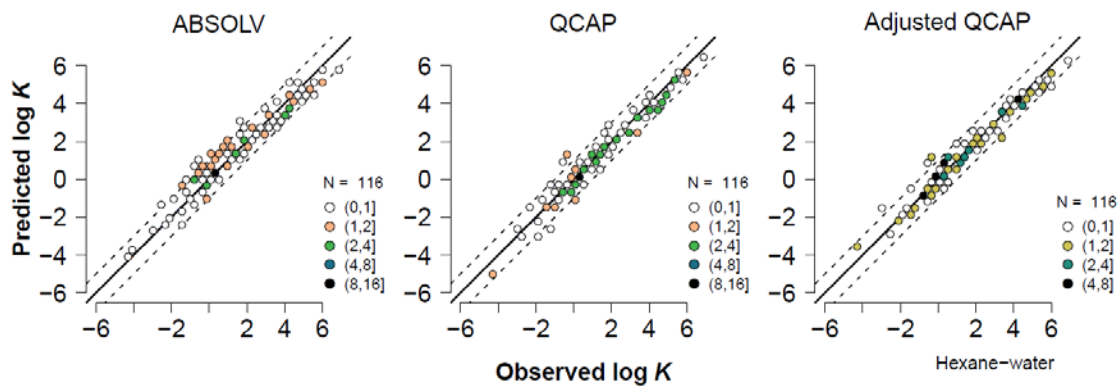


Figure C-28 Hexbin two dimensional histogram plot² of predicted versus observed log hexane-water partition coefficients. Solid lines show perfect agreement. Dashed lines represent ± 1 order of magnitude.

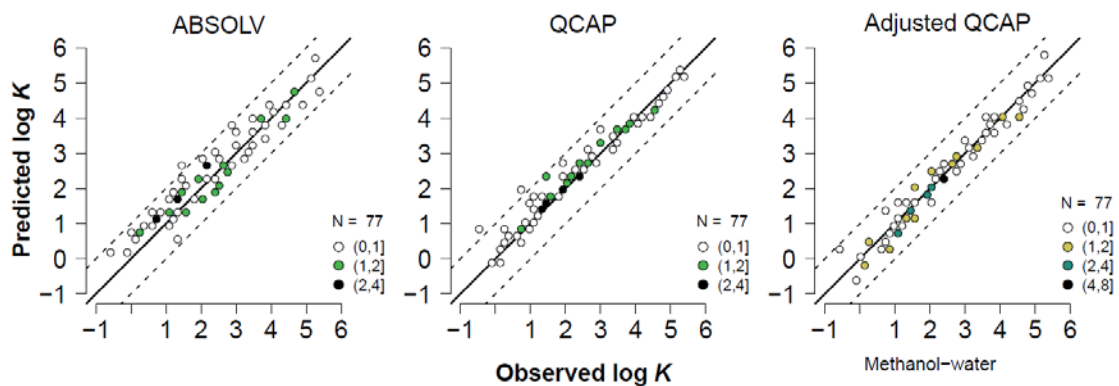


Figure C-29 Hexbin two dimensional histogram plot² of predicted versus observed log methanol-water partition coefficients. Solid lines show perfect agreement. Dashed lines represent ± 1 order of magnitude.

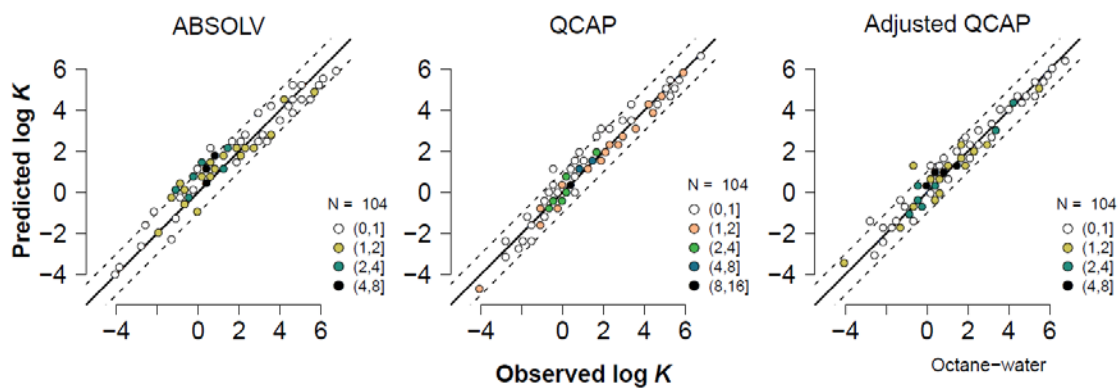


Figure C-30 Hexbin two dimensional histogram plot² of predicted versus observed log octane-water partition coefficients. Solid lines show perfect agreement. Dashed lines represent ± 1 order of magnitude.

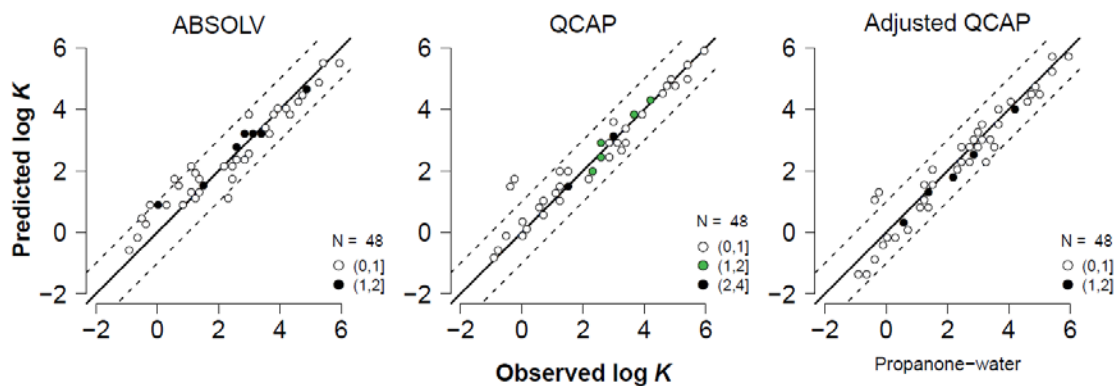


Figure C-31 Hexbin two dimensional histogram plot² of predicted versus observed log propanone-water partition coefficients. Solid lines show perfect agreement. Dashed lines represent ± 1 order of magnitude.

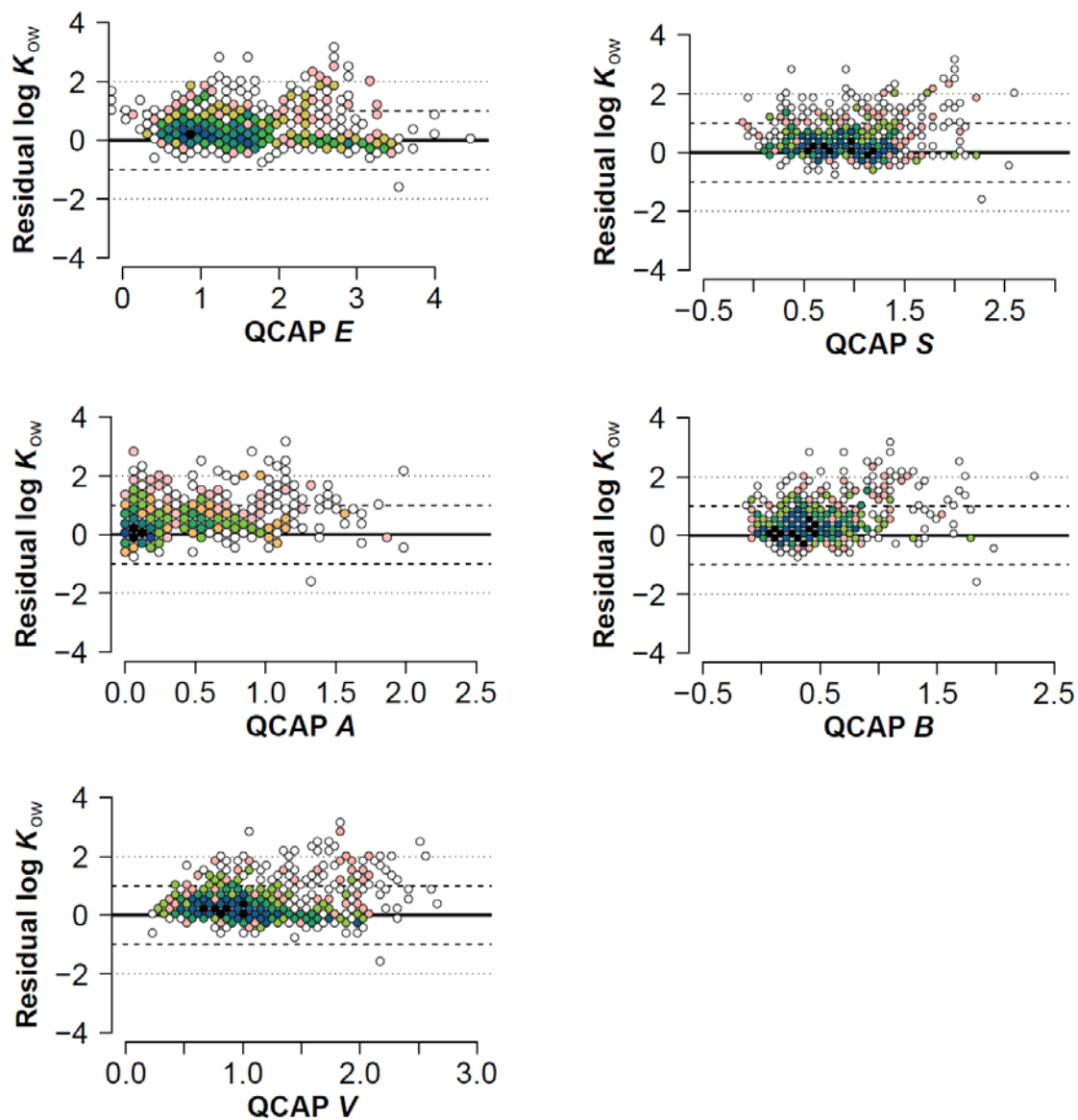


Figure C-32 Hexbin two dimensional histogram plots² presenting residuals (= predicted $\log K_{ow}$ – observed $\log K_{ow}$) of wet octanol-water partition coefficients versus E , S , A , B , V of QCAP parameters.

REFERENCES

1. Zhao, Y.; Truhlar, D. G. The M06 suite of density functionals for main group thermochemistry, thermochemical kinetics, noncovalent interactions, excited states, and transition elements: two new functionals and systematic testing of four M06-class functionals and 12 other functionals. *Theor. Chem. Acc.* **2008**, *120* (1-3), 215-241.
2. Hexagonal Binning Routines, v 1.27.1. Carr, D.; Lewin-Koh, N.; Mächler, M. <http://github.com/edzer/hexbin> (accessed May 22, 2016).

Chapter 4

QUANTUM CHEMICALLY ESTIMATED ABRAHAM SOLUTE AND SYSTEM PARAMETERS FOR SOLVENT-WATER AND PLANT CUTICLE-WATER PARTITION COEFFICIENTS

Abstract

Polyparameter Linear Free Energy Relationships (pp-LFERs) using Abraham system parameters have many useful applications. However, developing the Abraham system parameters depends on the availability and quality of the Abraham solute parameters. Quantum Chemically estimated Abraham solute Parameters (QCAP) have been proposed and shown to have lower root mean square errors of prediction (RMSEs) for certain classes of partition coefficients than do parameters that are presently available. System parameters are estimated using QCAP solute parameters and experimental partition coefficients for solvent-water and plant cuticle-water partition coefficients. Generally, refitted model with QCAP gives the best predictions with the smallest prediction root mean square errors ranging from 0.278 to 0.506 log units, followed by original model with QCAP or refitted model with ABSOLV for solvent-water partition coefficients for 24 systems. For munition constituents and munition-like compounds, QCAP with either original model or refitted model give much better estimates of solvent-water partition coefficients than does ABSOLV. For plant cuticle-water partitioning, predictions with QCAP fit the experimental K_{cut} values (RMSE = 0.513 and 0.395 for original and refitted model, respectively) than those with ABSOLV solute parameters. Therefore, fitting a model with QCAP is the quantum chemical method of choice in situations for which experimental data exist and system parameters can be re-estimated, or for systems whose system parameters do not exist and need to be developed, or need to be refined when more experimental data become available.

4.1 Introduction

Many attempts have been made to develop predictive models to understand the fate and effects of substances in the environment. Among the available models, the Abraham polyparameter linear free energy relationships (pp-LFERs)¹⁻⁴ are widely used. The Abraham model accounts for the molecular interaction involved in the partitioning process between two phases as a linear sum of terms proportional to the interaction energies:

$$\log K = c + eE + sS + aA + bB + vV \quad (4-1)$$

The dependent variable K denotes the partitioning property under consideration, e.g. solvent-water (K_{sw}) or plant cuticle-water (K_{cw}) partition coefficient. The upper case letters are solute parameters that quantify the following solute properties: excess molar refraction (E), electrostatic polarity/polarizability (S), hydrogen-bond acidity (A), hydrogen-bond basicity (B), and molar volume (V). The conjugate system coefficients, the lower case parameters in Eq. (4-1), quantify the complimentary effects of one phase (e.g. octanol) relative to the other phase (e.g. water): excess molar refraction (e), electrostatic polarity and polarizability (s), hydrogen-bond basicity (a), hydrogen-bond acidity (b), the energy required for cavity formation and part of dispersion interaction (v), and the remaining energy difference (c).

Abraham and other researchers have developed pp-LFERs for more than 400 environmentally significant processes and properties: partitioning to organic solvents; partitioning to bio-materials of protein, lipid, and fat; sorption to soil and mineral surfaces; blood-brain distribution, narcotic toxicity, and skin permeation.⁵

These pp-LFERs are constructed by fitting experimental partition coefficient data with known solute descriptors for a set of chemically diverse chemicals using a multiple linear regression (MLR).⁶⁻⁹ However, the origin of the solute descriptors is not clear—strictly experimentally determined or model estimated-- since the methods used to generate their values are usually not reported. Even experimentally-based solute parameters can vary significantly depending on the literature sources. Failures of the pp-LFER models cannot be distinguished between problems with the experimental partitioning data, or problems with the solute descriptors data, or problems with the selected list of chemicals that do not cover enough chemical space.¹⁰ Furthermore, experimentally-based solute parameters are usually not available for all the chemicals whose experimental partitioning data are available, especially for novel chemicals with special functionalities that should be included in the training data set to obtain reliable system coefficients. Therefore, a method that is consistent and is not restricted by the availability of experimental solute parameters would be a useful addition to the methods available to estimate Abraham system parameters.

Kipka and Di Toro¹² developed a pp-LFER model of organic chemical partitioning to particulate organic carbon in soils and sediments by performing an MLR with observed particulate organic carbon-water partition coefficients and estimated solute descriptors (from ABSOLV prediction module¹¹). Davis and Di Toro¹³ also applied estimated solute descriptors (from ABSOLV prediction module¹¹) in a MLR to construct pp-LFERs for nonlinear adsorption to various sorbents. The method presented below uses estimated instead of experimental solute parameters. The use of the estimated solute descriptor enables the use of a more chemically diverse training data set and ensures consistency.

Many estimation methods^{11, 14-24} have been proposed to obtain some or all of the solute parameters from the molecular structure, among which the ABSOLV prediction module¹¹ is widely used. The ABSOLV prediction module utilizes a molecular fragment based method: estimating each solute parameter by summing up the contributions of the Platts-type fragments.²⁴ The coefficients of the fragment descriptors are calibrated by performing statistical analysis on experimental partitioning data or experimentally derived solute parameters of more than 5000 compounds.¹¹ The ABSOLV self-reported root mean square errors (RMSEs) comparing predicted to experimentally-based solute parameters are 0.12, 0.22, 0.07, 0.15, and 0.01 for *E*, *S*, *A*, *B*, and *V*, respectively.¹¹ However, as a molecular fragment based method, ABSOLV has limitations, especially for novel and complex compounds that are not within the scope of the compounds used to estimate the fragment parameters or for which the necessary fragment parameters do not exist.²⁹

Recently, a quantum chemical method was proposed to compute Abraham solute parameters.²⁹ For each compound, the method employs the solvent-water partition coefficients for 65 solvents estimated using the quantum chemical solvation model (COSMO-SAC),²⁵⁻²⁸ and the molecular polarizability computed using M062X/aug-cc-pVDZ. The method used to compute the Quantum Chemically estimated Abraham Parameters (QCAP) is quantum chemically based on molecular structure only. Also, it is straightforward and reproducible. The predictions of QCAP are generally in better agreement with experimental values than those of ABSOLV for solvent-water partition coefficients for 24 systems (RMSE = 0.347 to 0.699 for QCAP, 0.45 to

0.566 for ABSOLV).²⁹ QCAP can be applied to novel and complex compounds, such as munitions constituents and munition-like compounds, for which QCAP give much better estimates of their solvent-water partition coefficients (RMSE = 0.752) than does ABSOLV (RMSE = 4.60).²⁹

A method was further proposed to compute Adjusted Quantum Chemically estimated Abraham Parameters (Adjusted QCAP): Each Adjusted QCAP parameter is estimated with an MLR using the five QCAP solute parameters E , S , A , B , and V as the independent variables and experimentally-based solute parameters as the dependent variables.²⁹ The Adjusted QCAP parameters are in better agreement with experimentally-based solute parameters with RMSE of 0.165, 0.203, 0.074, 0.117, and 0.039 for E , S , A , B , and V respectively. Since the Adjusted QCAP parameters are linear combinations of the QCAP parameters, they would produce the same prediction accuracy. However, QCAP parameters are more preferable than Adjusted QCAP for fitting existing data. The detailed explanation is available in Appendix E.

The objective of this chapter is to find the best set of solute parameters to predict environmentally significant partition coefficients for new systems whose system parameters need to be developed from experimental data. The solute parameters investigated are ABSOLV and QCAP. Abraham system parameters are computed using experimental partition coefficients for solvent-water systems and plant cuticle-water system. The RMSEs yielded using each of the three sets of solute parameters are compared.

4.2 Materials and Methods

4.2.1 Partition Coefficient Data

The experimental solvent-water partition coefficients are compiled from literature references^{6-9, 30-32, 32-34} and the cited references therein. The experimental and predicted partition coefficients for the solvent-water systems and the plant cuticle-water system are available in Table D-1 Appendix D.

The solute parameters (QCAP and ABSOLV) are taken from Liang.²⁹ The literature (original) system parameters are compiled from Abraham et al.³⁵ and from Platts and Abraham³⁶ for solvent-water systems and plant cuticle-water system, respectively.

4.2.2 Determination of System Parameters using Estimated Solute Parameters

The system parameters based on QCAP solute parameters are estimated using the linear regression (lm) function in the R programming language³⁷ applied to Eq. (4-2) with the experimental partition coefficients ($K_{\text{exp},i}$) and QCAP solute parameters (E_i , S_i , A_i , B_i , V_i):

$$\log K_{\text{exp},i} = c + eE_i + sS_i + aA_i + bB_i + vV_i \quad (4-2)$$

where i is the index of the compounds for which the experimental partition coefficients are available. The six system parameters (c , e , s , a , b , v) are estimated using MLR.

Analogously, the fitted system parameters based on ABSOLV solute parameters are obtained using Eq. (4-2) with ABSOLV solute parameters and experimental partition coefficients.

The fitted pp-LFERs used below retain all the terms (full models) in Eq. (4-2). For cases where certain estimated system coefficients are not statistically significant at the 0.05 level,

MLRs are performed with those estimated system coefficients set to zero (reduced models). Summaries of the fitted system parameters for both full and reduced regression equations can be found in Tables D-2 and D-3 for QCAP and ABSOLV, respectively.

4.3 Results and Discussion

4.3.1 Analysis of the Refitted Models for Solvent-Water Systems

The refitted models with either QCAP or ABSOLV solute parameters are listed in Table 4-1, using octanol-water as an example. The octanol-water partition coefficient (K_{ow}) is an important parameter that is used in models³⁸⁻⁴⁰ to predict distribution among environmental components, such as soils and sediments, animals, and plants. The system parameters are computed using experimental K_{ow} of 896 solutes with values of K_{ow} spanning a wider range of approximately 12 log units (-3.70 to 8.16). The system coefficients (c , e , s , a , b , and v) of the refitted octanol-water model with either QCAP or ABSOLV are statistically robust as indicated by the small standard errors (Tables D-2 and D-3). Fitting with QCAP has more favorable statistics ($R^2 = 0.939$, $SE = 0.508$, $PSD = 0.513$) than ABSOLV-SP ($R^2 = 0.933$, $SE = 0.534$, $PSD = 0.539$) as listed in Table 4-1. The PSD (predicted standard deviation) statistics are calculated based on the leave-one-out procedure where the regression equation is fitted with the i^{th} data omitted and the resulting equation is then used to predict the i^{th} data. The PSD statistics are suggested to be useful to assess the predictive ability of the resulting regression equations.⁴¹

Table 4-1 The literature (original), QCAP, and ABSOLV system parameters^a for selected systems.

System	pp-LFER	c	e	s	a	b	v	N	Adjusted R ²	SE	PSD
Wet octanol - water	Original	0.088	0.562	-1.054	0.034	-3.460	3.814	--	--	--	--
	QCAP	-0.115	0.771	-0.557	-0.424	-3.979	3.279	897	0.939	0.508	0.513
	ABSOLV	-0.058	0.819	-0.956	0.013	-3.521	3.605	897	0.933	0.534	0.539
Plant cuticle- water	Original	-0.415	0.596	-0.413	-0.508	-4.096	3.908	62	--	--	--
	QCAP	-0.167	0.417	0.919	-0.546	-5.450	3.478	143	0.936	0.403	0.421
	ABSOLV	0.144	1.200	0.039	-0.453	-1.984	1.700	143	0.747	0.803	0.880

^a N = number of unique solutes used for the calibration

R² = adjusted coefficient of determination adjusted for the number of independent variables in the regression equation ⁴⁷

SE = residual standard error

PSD = predicted standard deviation

4.3.2 Comparison of the Original and Refitted Models for Solvent-Water Systems

Figure 4-1 (1) compares RMSEs of the residuals (\log predicted - \log observed solvent-water partition coefficients K_{sw}) for the predictions of original and refitted models with QCAP solute parameters. Twenty-four solvent-water systems are presented consisting of a variety of solvent chemical classes: alkanes, alcohols, amides, ketones, and aromatics. The solvents are ordered from the smallest to the largest RMSE of refitted model with QCAP. The number of observations for each system is listed on the right axis.

The results in Figure 4-1 (1) demonstrate that the refitted model significantly improves the predictions for QCAP: RMSE from 0.347 to 0.699 for the original model, and from 0.278 to 0.506 for the refitted model. As previously found,²⁹ predictions using the original model tend to overestimate the observed octanol-water partition coefficients. However, refitting with QCAP parameters significantly eliminates the bias for the octanol-water system (Figure E-1, RMSE reduced from 0.699 to 0.506). The reason is that the refitted models are more compatible with QCAP parameters since the QCAP solute parameters are not identical to the experimentally-based solute descriptors (especially the molecular polarizability determined QCAP E parameter) while the original models are based on experimentally-based solute descriptors.

The results in Figure 4-1 (2) reveal the same trend for ABSOLV: predictions with refitted models are better than original models. This improvement relative to original models is again likely due to the improved compatibility of the system parameters with the ABSOLV estimated solute parameters.

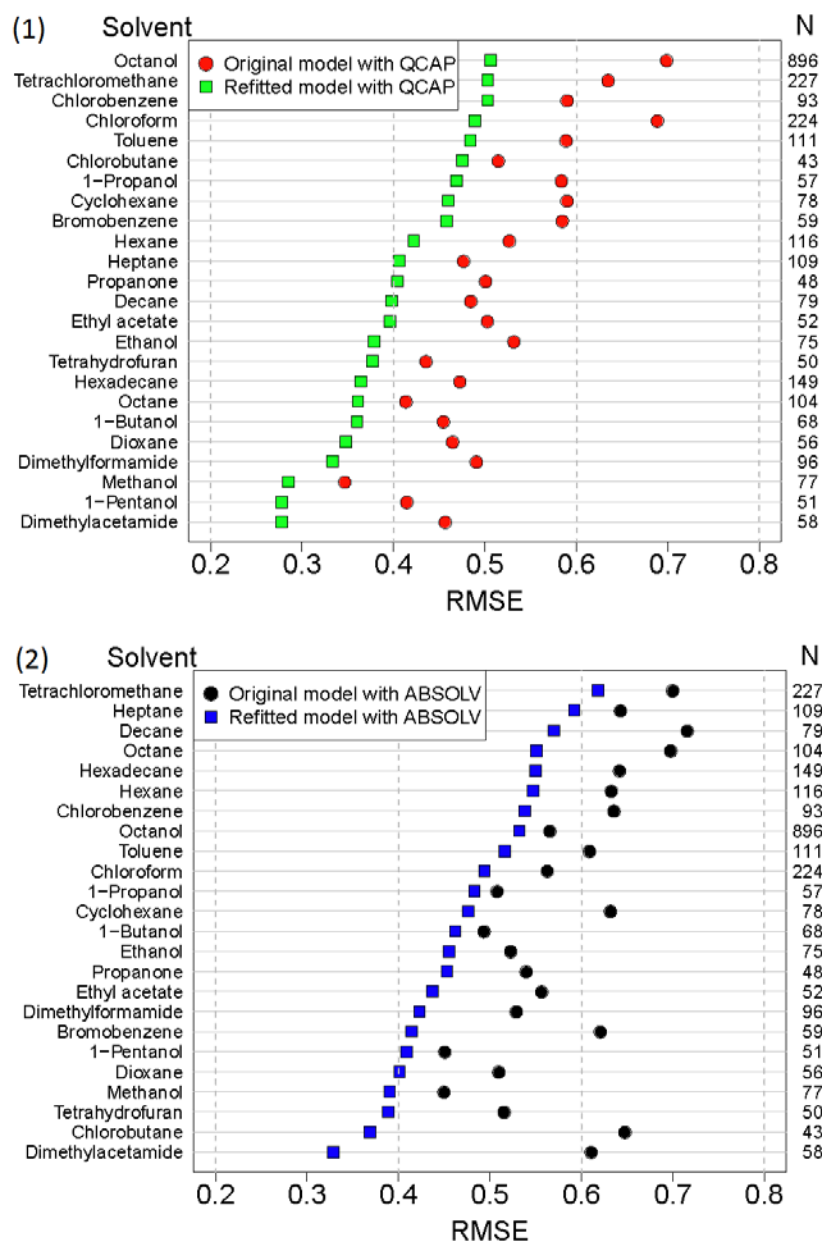


Figure 4-1 Dot plot presenting the root mean square errors (RMSEs) of the residuals (log predicted - log observed partition coefficients) for solvent-water systems. Panel (1) compares predictions of original model and refitted model with QCAP. Panel (2) compares predictions of original model and refitted model with ABSOLV. For each panel, the solvents listed on the left axis are ordered from the smallest to the largest RMSE of the refitted model, and the right axis presents N = number of solutes in each system. RMSE values are available in Table D-4 in Appendix D.

4.3.3 Comparison of QCAP and ABSOLV for Solvent-Water Systems

Figure 4-2 compares RMSEs of the residuals (log predicted – log observed K_{sw}) for the predictions of the four models: original model with QCAP, original model with ABSOLV, refitted model with QCAP, refitted model with ABSOLV. Among the four models, refitted model with QCAP gives the best predictions with the smallest prediction RMSEs ranging from 0.278 to 0.506 log units, followed by original model with QCAP or fitted model with ABSOLV. This comparison suggests that refitted model with QCAP is the best choice for predicting solvent-water partitioning. This comparison also suggests that QCAP should be the parameter set of choice for new systems whose system parameters need to be developed from experimental data.

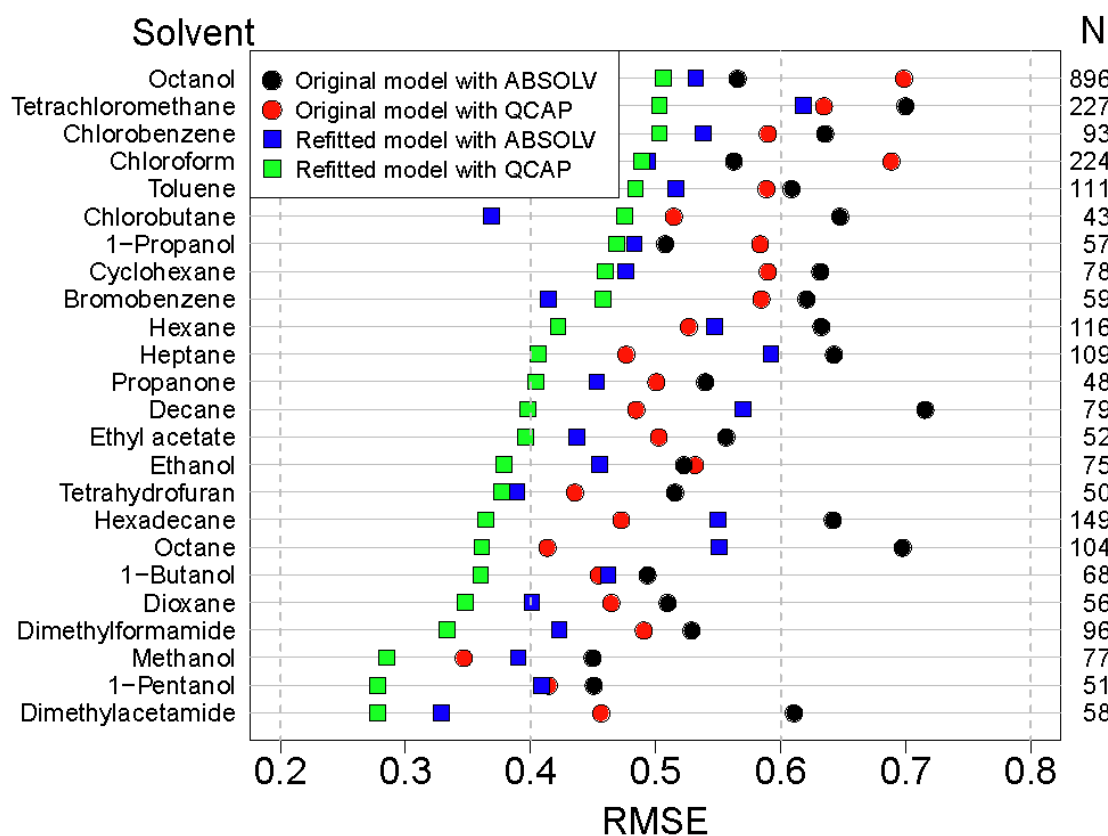


Figure 4-2 Dot plot presenting the root mean square errors (RMSEs) of the residuals (log predicted - log observed partition coefficients) for predictions of solvent-water partition coefficients. Predictions by four models are compared: original model with ABSOLV, original model with QCAP, refitted model with ABSOLV, and refitted model with QCAP. The solvents listed on the left axis are ordered from the smallest to the largest RMSE of refitted model with QCAP. The right axis presents N = number of solutes in each system. RMSE values are available in Table D-4 in Appendix D.

This improvement of QCAP relative to ABSOLV is likely the result of making an independent estimate of E in the QCAP method of estimating solute parameters.²⁹ It might also be due to the diverse set of sixty-five solvents that are employed to estimate S , A , and B .

4.3.4 Comparison of QCAP and ABSOLV for Solvent-Water Partitioning for Munition Constituents

The refitted models are further validated by applying to munitions constituents and munition-like compounds. The results are presented in Figure 4-3. These munition constituents and munition-like compounds were not included in the data used to refit the pp-LFER equations using either ABSOLV or QCAP parameters. Therefore this comparison is a validation of the model for these classes of compounds.

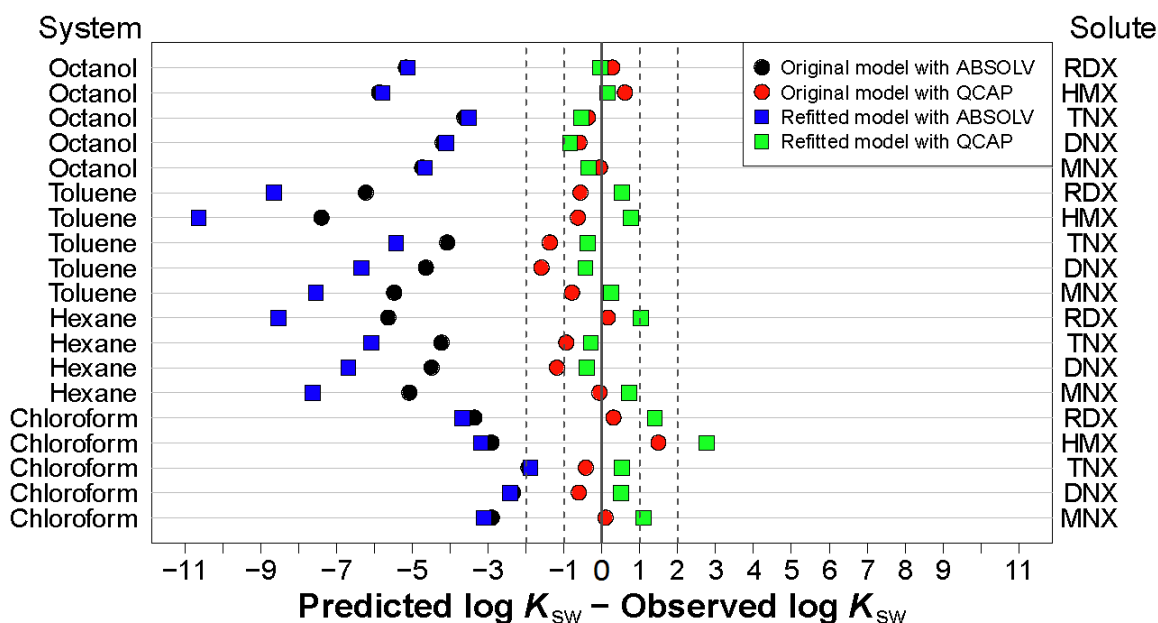


Figure 4-3 Dot plot presenting prediction errors (predicted $\log K_{sw}$ – observed $\log K_{sw}$) for prediction of solvent-water partition coefficients for munition constituents and munition-like compounds listed on the right axis. On the left axis is listed the the corresponding partitioning systems: wet octanol-water, toluene-water, hexane-water, and chloroform water. Predictions by four models are compared: original model with ABSOLV, original model with QCAP, refitted model with ABSOLV, and refitted model with QCAP. Experimental and predicted $\log K_{sw}$ as well as ABSOLV and QCAP solute parameters are available in Table D-5 in Appendix D.

ABSOLV predictions with original and refitted models have very large residuals for RDX, HMX, TNX, DNX, and MNX (RMSE = 4.64 and 5.98 for original and refitted model with ABSOLV, respectively). This indicates that for the compounds the ABSOLV solute parameters are completely unreliable. The possible reasons for this result are discussed in Liang et al.⁴²

Refitting the model does not improve the accuracy of ABSOLV if ABSOLV solute descriptors are incorrect.

QCAP predictions with original and refitted models are reasonable with most prediction residuals within 1 log units (RMSE = 0.792 and 0.904 for original and model respectively). However, large discrepancy is observed for HMX in chloroform-water, especially for prediction of refitted model with QCAP. There are a number of possible reasons for this discrepancy: The minimum gas-phase free energy HMX configuration is used to determine the QCAP solute parameters is not the correct configuration in the chloroform-water system; HMX is out of the applicability domain of the refitted equation, which depends on the range covered by the solute descriptors^{43,44} used to determine the chloroform-water system parameters used by the refitted model. If the prediction of HMX in chloroform-water is removed, the RMSEs reduce to 0.734 for original model and to 0.664 for refitted model with QCAP.

This comparison again suggests that refitted model with QCAP should be the correct path to follow. The results also demonstrate the predictive ability of refitted model with QCAP for novel and complex compounds.

4.3.5 Comparison of QCAP and ABSOLV for Plant Cuticle-Water Partitioning

Understanding the plant uptake is of importance in environmental risk assessment of chemical substances. It was found that the plant uptake process can be equivalently quantified as partitioning-dominated process.⁴⁵ Platts and Abraham³⁶ have proposed a pp-LFER model for predicting partitioning of volatile organic compounds from water into plant cuticular matrix, a lipophilic polymer membrane, which largely determines the uptake of organic chemicals into vegetation.⁴⁶ Their pp-LFER was developed using one plant species and 62 volatile organic compounds.³⁶ However, more experimental plant cuticle-water partition coefficients (K_{cw}) have been compiled which incorporate more diverse plant species (16 in total) and undissociated organic compounds (77 unique solutes and 143 data points in total). Details of the data are available in Table D-1. Thus, an updated pp-LFER is useful to improve its predictive ability.

The refitted models (Table 4-1) are obtained using an MLR with experimental K_{cw} as the dependent variable and the QCAP or ABSOLV solute parameters as independent variables.

Predictions of original model with ABSOLV agree reasonably well with experimental K_{cw} values except for RDX and HMX for which errors up to 6 orders of magnitude are observed, Figure 4-4 (1). The RMSE = 1.173 for all data points and RMSE = 0.622 without the three outliers. It is reasonable to believe that the large errors for RDX and HMX is not due to the system parameters, but is due to the incorrect solute descriptor estimated by ABSOLV. The same as for the solvent-water partitioning, the incorrect solute descriptors is likely due to the missing –R₂N-NO₂ fragment in the ABSOLV fragment database. Refitting the system parameters reduces the overall RMSE to 0.786 log units by reducing the errors for RDX and HMX to around 2 log units. However, this result of compensating the incorrect solute descriptors leads to the misfit for many other compounds, Figure 4-4 (3). Therefore, the quality of the solute parameters used in the calibration dataset is of importance.

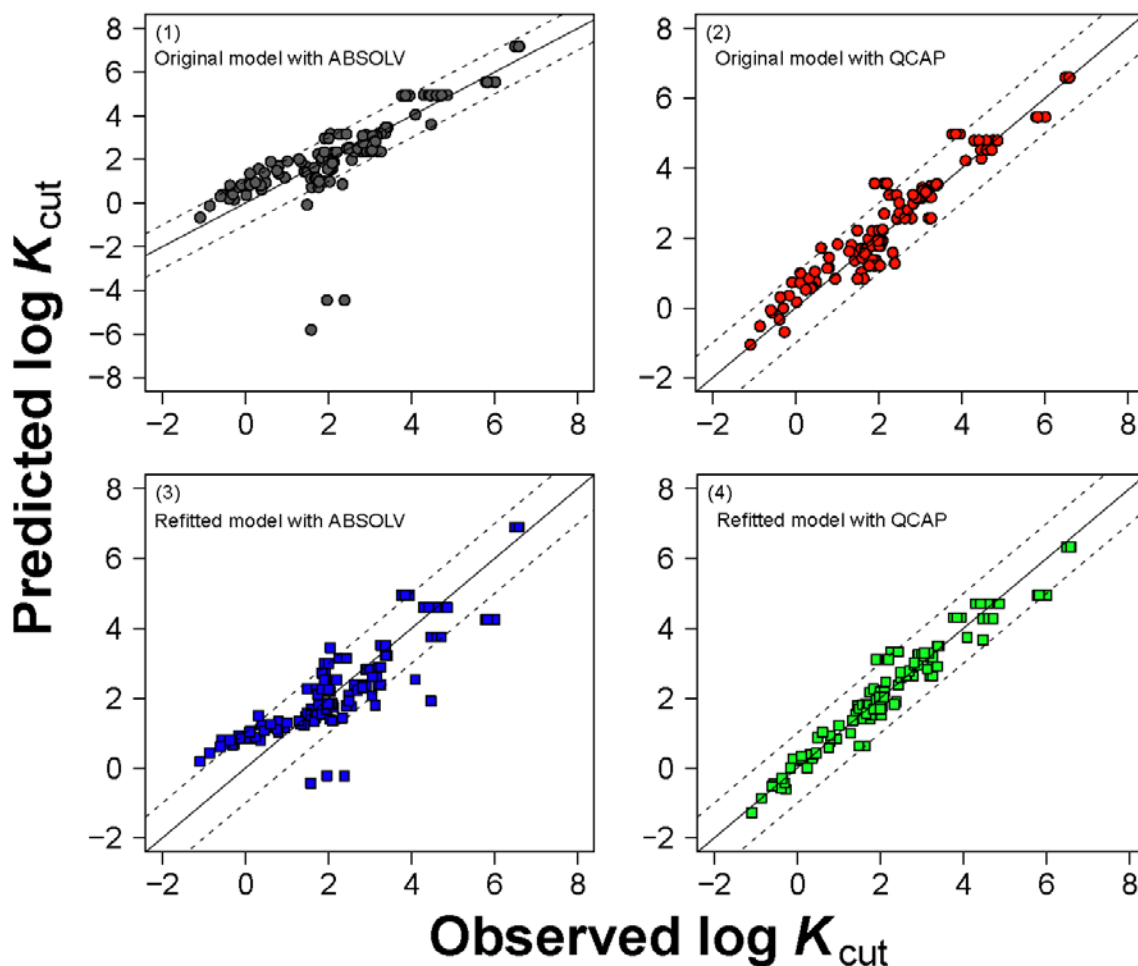


Figure 4-4 Crossplot comparing the predicted versus experimental $\log K_{\text{cw}}$. Predictions by four models are compared: (1) original model with ABSOLV, (2) original model with QCAP, (3) refitted model with ABSOLV, and (4) refitted model with QCAP. Solid lines show perfect agreement. Dashed lines represent ± 1 order of magnitude.

Among the models evaluated, predictions with QCAP fit the experimental K_{cw} values better than those with ABSOLV with most of the prediction errors within one order of magnitude. Refitting the model further improves the predictions for QCAP (RMSE = 0.513 for original model and RMSE = 0.395 for refitted model) as shown in Figure 4-4, panels (2) and (4). The refitted system coefficients (c , e , s , a , b , and v) are statistically robust: $R^2 = 0.936$, SE = 0.403, and PSD = 0.421 log units reflect the quality of the resulting regression equation (Table 4-1). The improvement of the refitted plant cuticle-water model with QCAP is due to not only the improved consistency of the system parameters as for the solvent-water systems, but also the expanded plant species and solute descriptor space.

4.4 Conclusions

Refitted system parameters significantly improves the prediction accuracy and eliminates the bias when using estimated solute parameters in the pp-LFER method. Refitted model with QCAP has the smallest RMSEs for available experimental solvent-water and plant cuticle-water partition coefficients, as well as for novel compounds. Thus, refitting the existing partitioning data with QCAP is the method of choice for predicting environmentally significant partition coefficients, e.g. organic carbon-water, protein-water, and lipid-water partition coefficients, especially for new systems for which system parameters need to be developed from experimental data.

REFERENCES

1. Endo S, G.K., Applications of polyparameter linear free energy relationships in environmental chemistry. *Environ. Sci. Technol.* **2014**, 48 (21), 12477-91.
2. Abraham, M.H., Application of solvation equations to chemical and biochemical processes. *PURE AND APPLIED CHEMISTRY* **1993**, 65 (12), 2503.
3. Poole, C.F.; Ariyasena, T.C.; Lenca, N. Estimation of the environmental properties of compounds from chromatographic measurements and the solvation parameter model. *Journal of Chromatography A* **2013**, 1317, 85-104; <http://dx.doi.org/10.1016/j.chroma.2013.05.045>.
4. Goss KU, S.R., Linear free energy relationships used to evaluate equilibrium partitioning of organic compounds. *Environ. Sci. Technol.* **2001**, 35 (1), 1-9.
5. UFZ-LSER database.
6. Abraham, Michael H., Chadha, Harpreet S., Whiting, Gary S., Mitchell, Robert C., Hydrogen bonding. 32. An analysis of water-octanol and water-alkane partitioning and the $\Delta \log p$ parameter of seiler. *JPS Journal of Pharmaceutical Sciences* **1994**, 83 (8), 1085-1100.
7. Abraham, Michael H., Acree, Jr., William E., Leo, Albert J., Hoekman, David, Partition of compounds from water and from air into the wet and dry monohalobenzenes. *New Journal of Chemistry* **2009**, 33 (8), 1685-1692.
8. Abraham, Michael H., Acree Jr, William E., Cometto-Muñiz, J. Enrique, Partition of compounds from water and from air into amides. *New Journal of Chemistry* **2009**, 33 (10), 2034-2043.
9. Abraham, Michael H., Acree, William E., Leo, Albert J., Hoekman, David, The partition of compounds from water and from air into wet and dry ketones. *New Journal of Chemistry* **2009**, 33 (3), 568-573.
10. Karunasekara, Thushara, Poole, Colin F., Compounds for expanding the descriptor space for characterizing separation systems. *CHROMA Journal of Chromatography A* **2012**, 1266, 124-130.
11. Advanced Chemistry Development, I. **ACD/Absolv**.
12. Kipka, Undine, Di Toro, Dominic M., A linear solvation energy relationship model of organic chemical partitioning to particulate organic carbon in soils and sediments. *ETC Environmental Toxicology and Chemistry* **2011**, 30 (9), 2013-2022.
13. Davis, Craig Warren, Di Toro, Dominic M., Modeling Nonlinear Adsorption with a Single Chemical Parameter: Predicting Chemical Median Langmuir Binding Constants. *Environ. Sci. Technol.* **2015**, 49 (13), 7818-7824.

14. Svozil, Daniel, Sevcik, Jiri G K, Kvasnicka, Vladimir, Neural Network Prediction of the Solvatochromic Polarity/Polarizability Parameter π^*_2 . *Journal of chemical information and computer sciences*. **1997**, 37 (2), 338.
15. Arey, J. S., Green, W. H., Gschwend, P.M., The Electrostatic Origin of Abraham's Solute Polarity Parameter. *The journal of physical chemistry.B, Condensed matter, materials, surfaces, interfaces & biophysical*. **2005**, 109 (15), 7564-7573.
16. Dearden, J. C., Ghafourian, T., Hydrogen Bonding Parameters for QSAR: Comparison of Indicator Variables, Hydrogen Bond Counts, Molecular Orbital and Other Parameters. *J. Chem. Inf. Comput. Sci.* **1999**, 39 (2), 231-235.
17. Ghafourian T, D.J., The use of atomic charges and orbital energies as hydrogen-bonding-donor parameters for QSAR studies: comparison of MNDO, AM1 and PM3 methods. *J. Pharm. Pharmacol.* **2000**, 52 (6), 603-10.
18. Rahaman, Obaidur, Doren, Douglas J., Di Toro, Dominic M., Quantum mechanical estimation of Abraham hydrogen bond parameters using 1:1 donor-acceptor complexes. *POC Journal of Physical Organic Chemistry* **2014**, 27 (10), 783-793.
19. Platts, J.A., Theoretical prediction of hydrogen bond donor capacity. *Physical Chemistry Chemical Physics (Incorporating Faraday Transactions)* **2000**, 2 (5).
20. Platts, J.A., Theoretical prediction of hydrogen bond basicity. *Physical Chemistry Chemical Physics (Incorporating Faraday Transactions)* **2000**, 2 (14), 3115-3120.
21. Lamarche, Olivier, Platts, James A., Hersey, Anne, Theoretical prediction of the polarity/polarizability parameter π^*_2 . *Physical Chemistry Chemical Physics (Incorporating Faraday Transactions)* **2001**, 3 (14), 2747-2753.
22. Schwöbel, Johannes A. H., Ebert, Ralf-Uwe, Kühne, Ralph, Schüürmann, Gerrit, Prediction models for the Abraham hydrogen bond donor strength: comparison of semi-empirical, *ab initio*, and DFT methods. *POC Journal of Physical Organic Chemistry* **2011**, 24 (11), 1072-1080.
23. Zissimos AM, Abraham MH, Klamt A, Eckert F, Wood J, A comparison between the two general sets of linear free energy descriptors of Abraham and Klamt. *J. Chem. Inf. Comput. Sci.* **2002**, 42 (6).
24. Platts, J. A., Butina, D., Abraham, M. H., Hersey, A., Estimation of Molecular Linear Free Energy Relation Descriptors Using a Group Contribution Approach. *J. Chem. Inf. Comput. Sci.* **1999**, 39 (5), 835-845.
25. Lin, Shiang-Tai, Sandler, Stanley I., A Priori Phase Equilibrium Prediction from a Segment Contribution Solvation Model. *Ind. Eng. Chem. Res. Industrial & Engineering Chemistry Research* **2002**, 41 (5), 899-913.

26. Wang, S., Thermodynamic properties predictions using the COSMO-SAC solvation method. , UMI, Ann Arbor, 2007.
27. Hsieh, Chieh-Ming, Sandler, Stanley I., Lin, Shiang-Tai, Improvements of COSMO-SAC for vapor-liquid and liquid-liquid equilibrium predictions. *FLUID Fluid Phase Equilibria* **2010**, 297 (1), 90-97.
28. Xiong R., Sandler S.I., Burnett R.I., An improvement to COSMO-SAC for predicting thermodynamic properties. *Ind.Eng.Chem.Res.Industrial and Engineering Chemistry Research* **2014**, 53 (19), 8265-8278.
29. Yuzhen Liang Determining Abraham Solute and System Parameters for Neutral Organic Compounds Using Quantum Chemical Methods. PhD, University of Delaware, 2016.
30. Saifullah, Mariam, Ye, Shulin, Grubbs, Laura M., De La Rosa, Nohelli E., Acree, William E., Abraham, Michael H., Abraham Model Correlations for Transfer of Neutral Molecules to Tetrahydrofuran and to 1,4-Dioxane, and for Transfer of Ions to Tetrahydrofuran. *J Solution Chem Journal of Solution Chemistry* **2011**, 40 (12), 2082-2094.
31. Grubbs, Laura M., Saifullah, Mariam, De La Rosa, Nohelli E., Ye, Shulin, Achi, Sai S., Acree, William E., Abraham, Michael H., Mathematical correlations for describing solute transfer into functionalized alkane solvents containing hydroxyl, ether, ester or ketone solvents. *FLUID Fluid Phase Equilibria* **2010**, 298 (1), 48-53.
32. Sprunger, Laura M., Achi, Sai S., Acree, William E., Abraham, Michael H., Leo, Albert J., Hoekman, David, Correlation and prediction of solute transfer to chloroalkanes from both water and the gas phase. *FLUID Fluid Phase Equilibria* **2009**, 281 (2), 144-162.
33. W. Stephens, T., Correlation of Solute Transfer Into Toluene and Ethylbenzene from Water and from the Gas Phase Based on the Abraham Model. *TOTHERJ The Open Thermodynamics Journal* **2011**, 5 (1), 104-121.
34. Correlation of solute transfer into alkane solvents from water and from the gas phase with updated Abraham model equations.
35. Abraham MH, Smith RE, Luchtefeld R, Boorem AJ, Luo R, Acree WE Jr, Prediction of solubility of drugs and other compounds in organic solvents. *J. Pharm. Sci.* **2010**, 99 (3), 1500-15.
36. Platts, J. A., Abraham, M.H., Partition of Volatile Organic Compounds from Air and from Water into Plant Cuticular Matrix: An LFER Analysis. *ENVIRONMENTAL SCIENCE AND TECHNOLOGY -WASHINGTON DC-* **2000**, 34, 318-323.
37. The R Stats Package.

38. Schwarzenbach, René P., Gschwend, P. M., Imboden, Dieter M., *Environmental organic chemistry*. John Wiley & Sons: Hoboken, N.J., 2003.
39. Briggs, G.G., Theoretical and experimental relationships between soil adsorption, octanol-water partition coefficients, water solubilities, bioconcentration factors, and the parachor. *J.Agric.Food Chem.Journal of Agricultural and Food Chemistry* **1981**, 29 (5), 1050-1059.
40. Di Toro, Dominic M., McGrath, Joy A., Hansen, David J., Technical basis for narcotic chemicals and polycyclic aromatic hydrocarbon criteria. I. Water and tissue. *ETC Environmental Toxicology and Chemistry* **2000**, 19 (8), 1951-1970.
41. Hawkins, D.M., The Problem of Overfitting. *ChemInform ChemInform* **2004**, 35 (19).
42. Yuzhen Liang; Dave T.F. Kuo, Herbert E Allen, Dominic M Di Toro Experimental determination of solvent-water partition coefficients and Abraham parameters for munition constituent. ; 10.1016/j.chemosphere.2016.07.028.
43. Dragos H, Gilles M, Alexandre V, Predicting the predictability: a unified approach to the applicability domain problem of QSAR models. *Journal of chemical information and modeling* **2009**, 49 (7), 1762-76.
44. Sprunger L.M., Achi S.S., Pointer R., Acree Jr. W.E., Abraham M.H., Development of Abraham model correlations for solvation characteristics of secondary and branched alcohols. *Fluid Phase Equilib. Fluid Phase Equilibria* **2010**, 288 (1-2), 121-127.
45. Tiffany Torralba Sanchez **2016**, .
46. Riederer M, S.J., Accumulation and transport of (2,4-dichlorophenoxy)acetic acid in plant cuticles: I. Sorption in the cuticular membrane and its components. *Ecotoxicol. Environ. Saf.* **1984**, 8 (3), 236-47.
47. Draper, Norman Richard., Smith, Harry., *Applied regression analysis*. Wiley: New York, 1998.

Appendix D

SUPPLEMENTARY INFORMATION FOR: QUANTUM CHEMICALLY ESTIMATED ABRAHAM SOLUTE AND SYSTEM PARAMETERS FOR SOLVENT-WATER AND PLANT CUTICLE-WATER PARTITION COEFFICIENTS

CONTENTS: Located in an accompanying Microsoft Excel file

- Table D-1 Experimental and predicted solvent-water partition coefficients as well as ABSOLV and QCAP solute parameters. Located in Chapter_4_Appendix D_Tables.xlsx file.
- Table D-2 Refitted system parameters determined using QCAP solute parameters. Located in Chapter_4_Appendix D_Tables.xlsx file.
- Table D-3 Refitted system parameters determined using ABSOLV solute parameters. Located in Chapter_4_Appendix D_Tables.xlsx file.
- Table D-4 Summary of the RMSEs of prediction of partition coefficients. Located in Chapter_4_Appendix D_Tables.xlsx file.
- Table D-5 Experimental and predicted solvent-water partition coefficients, together with ABSOLV and QCAP solute parameters, for munition constituents. Located in Chapter_4_Appendix D_Tables.xlsx file.

Appendix E

SUPPLEMENTARY INFORMATION FOR: QUANTUM CHEMICALLY ESTIMATED ABRAHAM SOLUTE AND SYSTEM PARAMETERS FOR SOLVENT-WATER AND PLANT CUTICLE-WATER PARTITION COEFFICIENTS

CONTENTS:

- Figure E-1 Pairs plot of QCAP solute parameters.
- Figure E-2 Pairs plot of Adjusted QCAP solute parameters.
- Figure E-3 Comparison of standard errors of regression coefficients for fitting using QCAP and Adjusted QCAP.
- Figure E-4 Regression coefficients for fitting using QCAP and Adjusted QCAP.

Refitted Model with QCAP and Adjusted QCAP

Comparison of QCAP and Adjusted QCAP System Parameters.

- (1) Since the Adjusted QCAP parameters are linear combinations of the QCAP parameters, they would produce the same result.
- (2) QCAP have not been fitted to experimental data. QCAP is recommended because it does not rely on any experimental data.

There are strong correlations between Adjusted E and S (Figure E-1). The correlations are stronger than those of QCAP (Figure E-2). However, it is found that SE of QCAP are not always larger than those of Adjusted QCAP (Figure E-3). There are linear relationships between system parameters for solvent-water systems (Figure E-4).

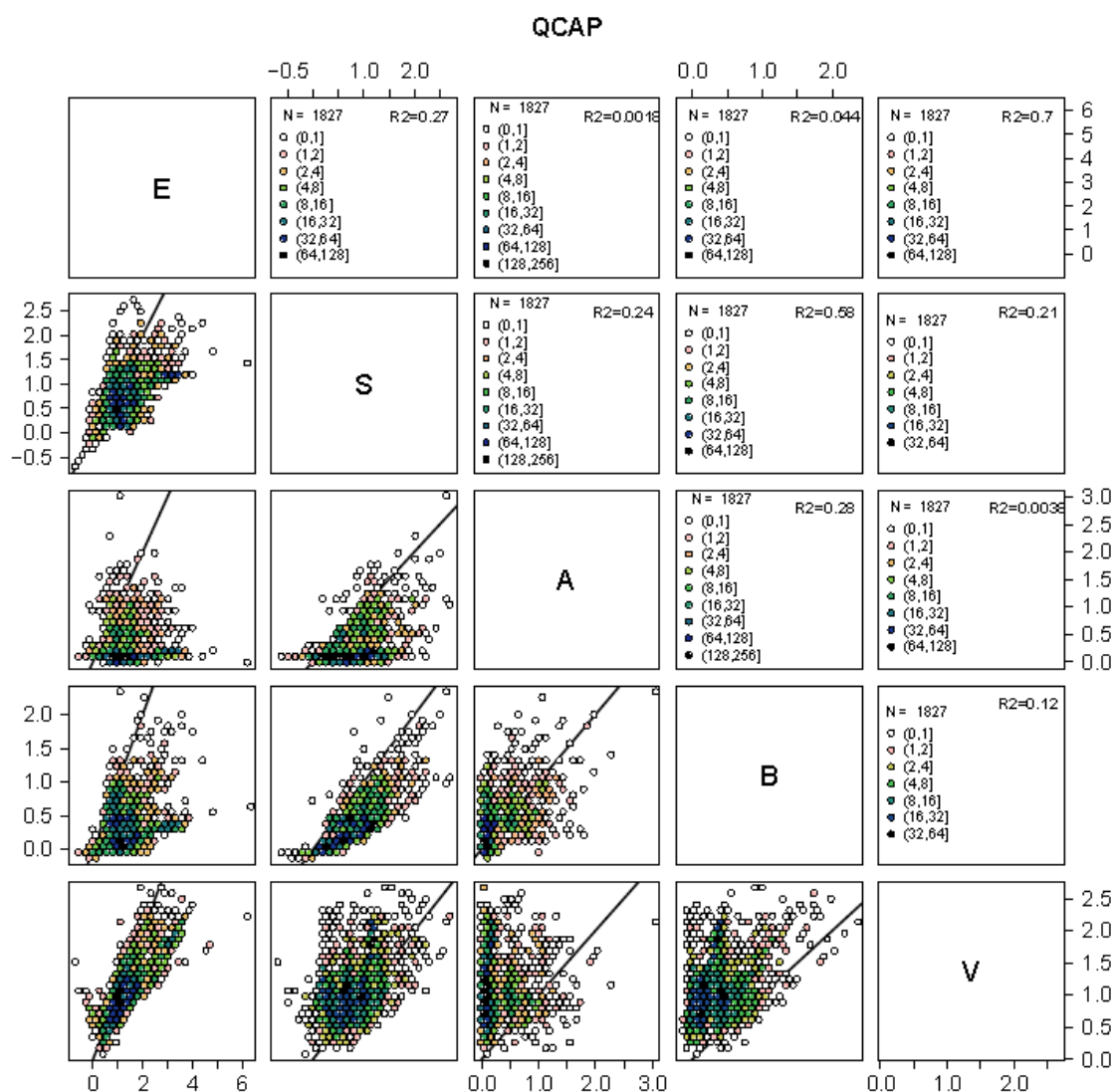


Figure E-1 Pairs plot³ of QCAP solute parameters. The lower triangular panels are hexbin two dimensional histogram plots². For each data plot, x axis label is the parameter above the plot, y axis label is to the right of the plot. Solid lines show perfect agreement. The upper triangular panels display the coefficient of determination (R^2) and the scaling of the respective pair. For each R^2 panel, x axis label is the parameter below the plot, y axis label is to the left of the plot.

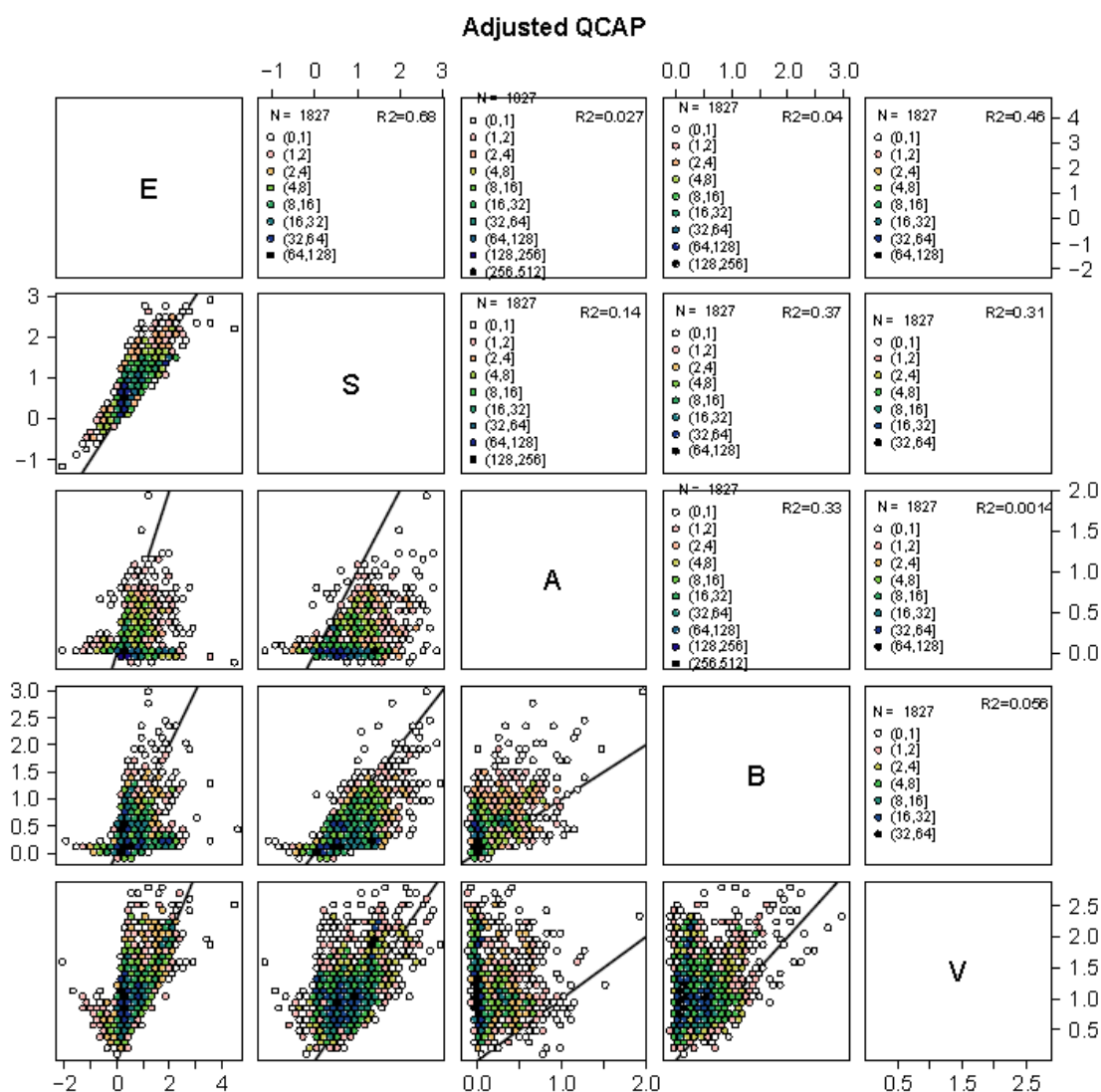


Figure E-2 Pairs plot³ of Adjusted QCAP solute parameters. The lower triangular panels are hexbin two dimensional histogram plots². For each data plot, x axis label is the parameter above the plot, y axis label is to the right of the plot. Solid lines show perfect agreement. The upper triangular panels display the coefficient of determination (R^2) and the scaling of the respective pair. For each R^2 panel, x axis label is the parameter below the plot, y axis label is to the left of the plot.

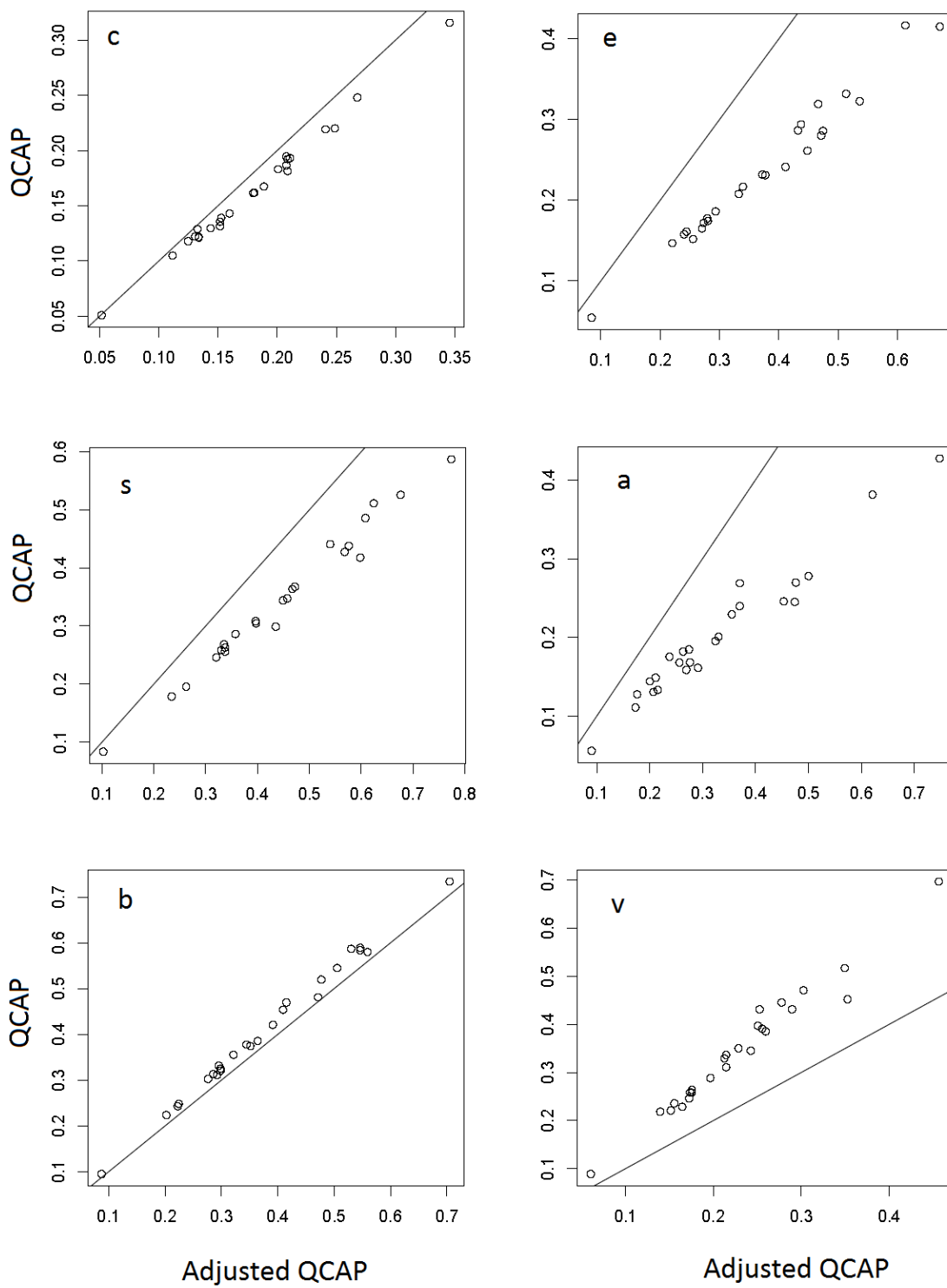


Figure E-3 Comparison of standard errors of regression coefficients for fitting using QCAP and Adjusted QCAP.

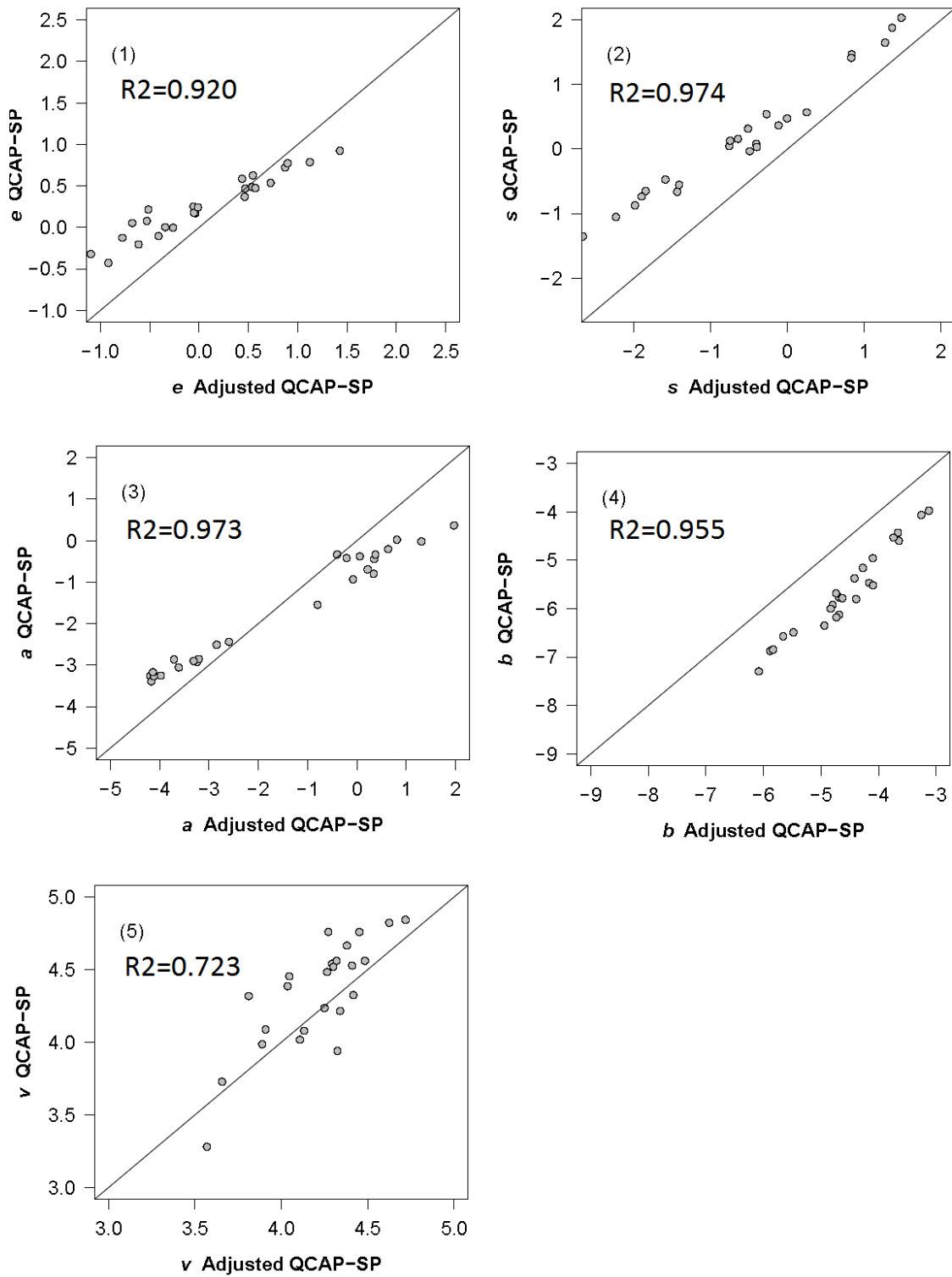


Figure E-4 Regression coefficients for fitting using QCAP and Adjusted QCAP.

The plant cuticle data fitting can be found in the screenshot below:

```
> dd<- read.csv(paste('Plant_cuticle_v20161107.csv',sep=''),header=TRUE, st
> fit=lm(dd$logKobs~dd$Ep+dd$Sq+dd$Aq+dd$Bq+dd$Vcs);
> summary(fit)

Call:
lm(formula = dd$logKobs ~ dd$Ep + dd$Sq + dd$Aq + dd$Bq + dd$Vcs)

Residuals:
    Min       1Q   Median       3Q      Max
-1.20915 -0.17346 -0.02166  0.22896  1.05558

Coefficients:
              Estimate Std. Error t value Pr(>|t|)
(Intercept)  -0.61653    0.10074   -6.120 9.26e-09 ***
dd$Ep         0.41690    0.08769    4.754 4.98e-06 ***
dd$Sq         0.91932    0.16745    5.490 1.89e-07 ***
dd$Aq        -0.54607    0.10193   -5.357 3.48e-07 ***
dd$Bq        -5.44961    0.25928  -21.018 < 2e-16 ***
dd$Vcs        3.47841    0.20816   16.710 < 2e-16 ***
---
Signif. codes:  0 '***' 0.001 '**' 0.01 '*' 0.05 '.' 0.1 ' ' 1

Residual standard error: 0.4033 on 137 degrees of freedom
Multiple R-squared:  0.9386,    Adjusted R-squared:  0.9363
F-statistic: 418.7 on 5 and 137 DF,  p-value: < 2.2e-16
```



```

> E=-0.355 +0.883*dd$Ep +0.405*dd$Sq +0.181*dd$Aq +0*dd$Bq -0.552*dd$Vcs
> S=-0.195 +0.202*dd$Ep +0.948*dd$Sq +0*dd$Aq + 0.197*dd$Bq -0.115*dd$Vcs
> A= 0.019 +0*dd$Ep-0.040*dd$Sq + 0.675*dd$Aq + 0.032*dd$Bq -0.042*dd$Vcs
> B= 0.104 -0.036*dd$Ep -0.196*dd$Sq +0.144*dd$Aq + 1.283*dd$Bq +0*dd$Vcs
> V= 0.041*dd$Ep -0.058*dd$Sq +0.086*dd$Bq + 1.010*dd$Vcs
> L=-1.064 +1.341*dd$Ep +1.039*dd$Sq +0.572*dd$Aq +0.493*dd$Bq +2.371*dd$Vcs
> fit=lm(dd$logKobs~E+S+A+B+V);
> summary(fit)

Call:
lm(formula = dd$logKobs ~ E + S + A + B + V)

Residuals:
    Min       1Q   Median       3Q      Max
-1.20915 -0.17346 -0.02166  0.22896  1.05558

Coefficients:
              Estimate Std. Error t value Pr(>|t|)
(Intercept) -0.07915    0.10343  -0.765   0.445
E             0.07324    0.13871   0.528   0.598
S             0.22452    0.18258   1.230   0.221
A             0.13585    0.14250   0.953   0.342
B            -4.52104    0.22703 -19.914 <2e-16 ***
V             3.51521    0.16225  21.665 <2e-16 ***
---
Signif. codes:  0 '***' 0.001 '**' 0.01 '*' 0.05 '.' 0.1 ' ' 1

Residual standard error: 0.4033 on 137 degrees of freedom
Multiple R-squared:  0.9386,    Adjusted R-squared:  0.9363
F-statistic: 418.7 on 5 and 137 DF,  p-value: < 2.2e-16

```

Chapter 5

BIOCONCENTRATION FACTORS AND PLANT–WATER PARTITION COEFFICIENTS OF MUNITIONS COMPOUNDS IN BARLEY

Abstract

Plants growing in the soils at military ranges and surrounding locations are exposed, and potentially able to uptake, munitions compounds (MCs). Bioconcentration in plants is conventionally measured through uptake experiments with field or synthetic soils. These soils, however, contain multiple components/phases that vary among their different types and affect the bioavailability of the MC. Therefore, using various soils as the exposure medium hinders the ability to separate the effects of soil characteristics from the chemical properties on the resulting plant bioconcentration. To circumvent the problem, this work presents a protocol to measure steady state bioconcentration factors (BCFs) for MCs in barley (*Hordeum vulgare* L.) using inert laboratory sand rather than field or synthetic soils. Three MCs: 2,4,6-trinitrotoluene (TNT); 2,4-dinitrotoluene (2,4-DNT); and 2,4-dinitroanisole (2,4-DNAN); and two munition-like compounds (MLCs): 4-nitroanisole (4-NAN) and 2-methoxy-5-nitropyridine (2-M-5-NPYNE) were evaluated. Approximately constant plant biomass and exposure concentrations were achieved within a one-month period that produced steady state log BCF values: 0.62 ± 0.02 , 0.70 ± 0.03 , 1.30 ± 0.06 , 0.52 ± 0.03 , and 0.40 ± 0.05 L kg_{plant dwt}⁻¹ for TNT; 2,4-DNT; 2,4-DNAN; 4-NAN; and 2-M-5-NPYNE, respectively. Furthermore, results suggest that the upper-bounds of the BCFs can be estimated within an order of magnitude by measuring the partitioning of the compounds between barley biomass and water. This highlights the importance of partition equilibrium as a mechanism for the uptake of MCs and MLCs by barley from interstitial water. The results from this work provide chemically meaningful data for prediction models able to estimate the bioconcentration of these contaminants in plants.

5.1 Introduction

Elevated concentrations of munitions compounds (MCs) – which include explosives and propellants – have been found in soils at military installations¹⁻⁵ as well as in underlying groundwater⁶⁻¹² and surrounding surface water bodies^{13,14}. MCs dissolve into the soil solution and can be taken up by plants. Such mobility makes MCs an environmental concern for organisms growing in the soils at military ranges and surrounding locations. Therefore, risk assessments of these MCs should include an evaluation of their uptake by plants.

The uptake of a chemical substance by plant tissues (e.g., roots, stem, leaves) from the environment (e.g., soil, water, air) has been typically measured by bioconcentration factors (BCFs). BCFs are generally determined through laboratory experiments where plants are grown in spiked or contaminated field soils¹⁵⁻¹⁹ or hydroponically in nutrient solutions containing dissolved contaminants^{20,21}. In the case of solid growth media, various types of BCFs have been used depending on whether expressed relative to the concentration in the medium solids (dry mass) or relative to that in the medium water solution (interstitial/pore water)²². The latter BCF is chemically more meaningful since the concentration available for plant root uptake is only that dissolved in the interstitial water^{23,24}. Therefore, BCFs should be calculated as

$$BCF_i = \left(\frac{C_{i_{Organism}}}{C_{i_{Available\ in\ growth\ medium.}}} \right)_{SS} = \left(\frac{C_{i_{plant}}}{C_{i_{IW}}} \right)_{SS} \quad (5-1)$$

where i = compound of interest (e.g., a MC), BCF_i = bioconcentration factor of i ($L_{water} \text{ kg}_{plant} \text{ dwt}^{-1}$; dwt = dry weight), SS = steady state, $C_{i_{plant}}$ = concentration of i in the plant (mg kg_{dwt}^{-1}), and $C_{i_{IW}}$ = dissolved concentration of i in the interstitial water (IW; mg L^{-1}).

Studies have measured uptake by plants from soils at the laboratory scale for some of the most common MCs: 2,4,6-trinitrotoluene (TNT); 2,4-dinitrotoluene (2,4-DNT); 2,4-dinitroanisole (2,4-DNAN); hexahydro-1,3,5-trinitro-1,3,5-triazine (RDX); and octahydro-1,3,5,7-tetranitro-1,3,5,7-tetrazocine (HMX) ^{15,16,18,19,25-30}. The set of plant concentrations observed in these soil studies is graphically summarized in Figure 5-1A and the data are in Table F-1 in Appendix F. The BCFs are presented in Figure 5-1B (Table F-2) when available. They are BCFs as ratio of the MC concentration in the plant to that in the soil solids (this ratio is hereafter referred to as “ BCF_{Solids} ”). Figure 5-1 reveals large variations among both plant concentrations and BCF_{Solids} for a single MC. The variations in plant concentrations are expected since the corresponding exposure concentration is not considered. The variations found in BCF_{Solids} (up to three orders of magnitude for the same MC) are likely due to three main factors: plant type, exposure time, and available concentration for plant root uptake. These elements are examined below in order to identify their individual role in the lack of consistency among literature plant uptake results (Figure 5-1), especially for BCF_{Solids} (Figure 5-1B).

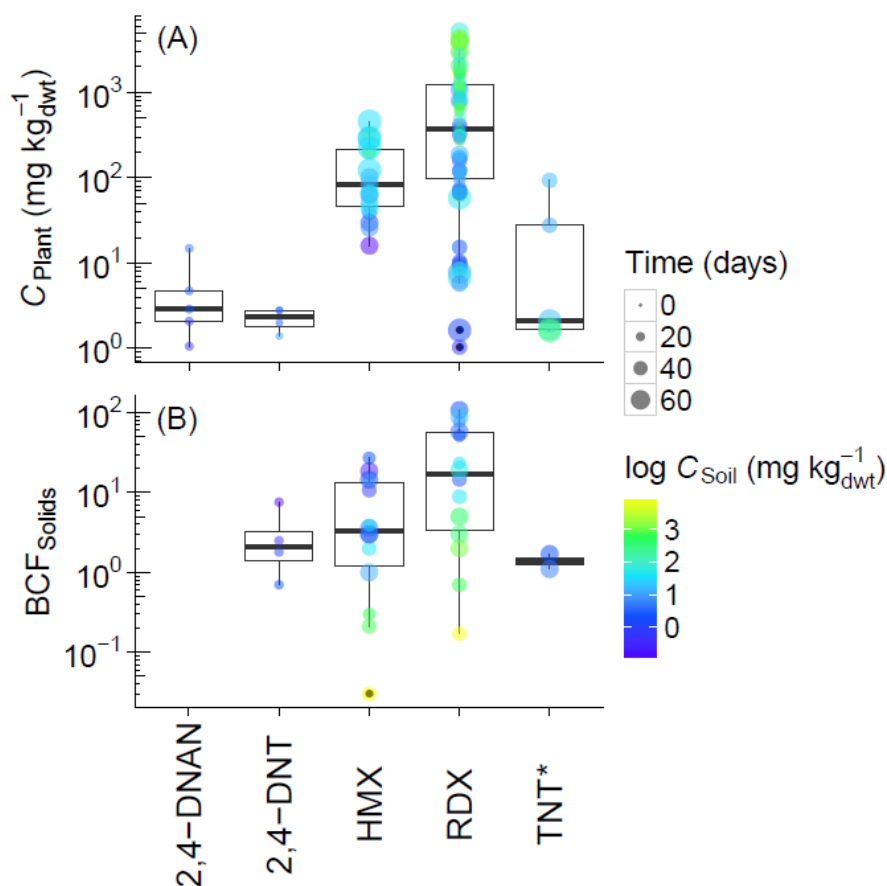


Figure 5-1 Results from published uptake studies (Tables F-1 and F-2): (A) MCs concentrations in plants on the last day of exposure (C_{Plant}), and (B) bioconcentration factors expressed relative to concentrations in soil solids (BCF_{Solids}) as kg_{dwt} soil (kg_{dwt} plant)⁻¹. C_{Soil} : Concentration in soil at the beginning of exposure. Circles' size proportional to the exposure duration. Data presented for the whole plant or only for the aboveground plant parts when available. TNT* = TNT or TNT degradation products; TNT is reported as not detected in plant tissues in some sources.

Plant type: Some plant species have markedly higher potential to bioconcentrate MCs than others, as it has been shown for aquatic plants relative to terrestrial plants^{31,32}. These differences in uptake potential have not been observed, however, between more similar plant types, such as terrestrial monocotyledons and dicotyledons³³. This likely reduces the significance of plant type as a factor for the large variations shown in Figure 5-1 given that the species included are all terrestrial herbaceous plants belonging to closely related families: graminoids (grasses), legumes, and amaryllis.

Exposure time: In contrast to the similarity in plant types, the exposure times in Figure 5-1 vary widely from 19 to 77 days. Plant concentrations obtained at longer exposure times (i.e.,

> 40 days) are generally higher than those measured in short-exposure experiments (Figure 5-1A). However, these comparisons should only be made once growth dilution effects²⁴ (increasing biomass during the growing period dilutes chemical concentrations in the plant tissues) have been taken into account, concentration in the plant is at steady state (i.e., no significant variations with longer exposure time), and BCFs are reported relative to the bioavailable MC concentration (i.e., BCF defined in Eq. (5-1) instead of BCF_{Solids}).

Available concentration for plant root uptake: The bioavailable MC concentration in soil for plant uptake is determined by factors including soil properties such as organic carbon content through sorption-desorption processes³⁴⁻³⁸, transformation/degradation of the parent compound, and aqueous solubility of the MC as it controls the maximum concentration that will dissolve in the soil interstitial water. Therefore, contrary to what might be expected, increments in soil concentration treatments do not necessarily lead to higher BCF_{Solids} in plants. Figure 5-1B, for example, shows decreasing BCF_{Solids} with increasing soil concentrations^{15,16,18} for exposures up to 1×10^4 mg kg_{dwt}⁻¹ for RDX and HMX¹⁸, which have considerably lower solubilities than other MCs (Table F-3). This decrease in BCF_{Solids} wrongly points to conclude that large exposure concentrations do not result in higher plant bioconcentration. Nonetheless, what is actually happening is that the concentration available for plant root uptake is overestimated when: (i) the MC aqueous solubility is exceeded, and (ii) the rate of MC degradation in the soil plus plant uptake outpaces the rate of MC dissolution decreasing the exposure concentration.

In order to establish what the MC concentration available for plant root uptake is, hydroponic systems with water only have been used as an alternative to complex field or synthetic soil (referred to as “soil”) growth media. These type of experiments, however, have shown plants with delayed and less frequent root branching^{39,40}. Root morphology and architecture determine the accessibility of plants to both nutrients and contaminants, thus a solid growth medium represents field conditions more closely. Normal plant root development and minimal influence of the growth medium in the MC bioavailability dictate the choice of using essentially inert solids such as coarse quartz sand (0.85–1.27 mm effective diameter particles, referred to as “sand”) as growth media.

The use of sand for the bioconcentration uptake assays presented in this work had two main purposes: (i) generate BCFs that are not conditioned to any particular soil property so that they can be applicable to estimate bioconcentration across diverse soil types, and (ii) provide data for the development of a model to predict the steady state BCFs of MCs and compounds with similar chemical structure functionalities referred to as munition-like compounds (MLCs). These require the concentrations in the plant and available for plant root uptake to be at steady state. Therefore, using sand as the solid growth medium was convenient because it allowed to: (i) easily conduct fluids thereby providing a more uniform exposure concentration, and thus (ii) make interstitial water sampling, measured in the displaced solution, more representative compared to that obtained in soil studies.

Separating the contributions of the growth medium characteristics from the MCs properties to the BCFs can also advance the understanding of the uptake process from a mechanistic perspective. The uptake of nonionic organic contaminants through plant roots has already been shown to be a passive (i.e., no input of metabolic energy) diffusive process²⁴. This suggests that the uptake of nonionic organic MCs, and MLCs, is largely governed by their aqueous concentration and tendency to sorb onto plant tissues. Partition-dominated steady state

sorption of contaminants by plant materials has been tested and shown to serve as an estimate for the upper-bound of the bioconcentration resulting from the overall uptake process ⁴¹⁻⁴³.

In this work, five nonionic organic compounds were studied for both plant uptake and plant–water partitioning by barley (*Hordeum vulgare* L.). Two objectives were: (i) provide BCFs that are predominantly a function of the compound chemical properties, minimizing bias from growth medium, compound bioavailability and toxic effects, and exposure time; and (ii) estimate the upper-bound of the plant uptake process via plant–water partitioning measurements. The compounds included three MCs: TNT; 2,4-DNT; and 2,4-DNAN; and two MLCs: 4-nitroanisole (4-NAN) and 2-methoxy-5-nitropyridine (2-M-5-NPYNE). Additionally, in order to increase chemical variety, three more compounds were studied for plant–water partitioning. These compounds comprised two MCs: RDX and HMX, and a MLC: 2,5-dimethoxy-4-nitroaniline (2,5-DM-4-NANE). While the MLCs here might not be used in current explosives and/or propellants formulations, their structural resemblance to MCs including the presence of nitro functional groups (-NO₂) and N-substituted rings (Table F-3) makes them likely to be related to future MCs for which MLCs can serve as validation proxies.

5.2 Materials and Methods

5.2.1 Chemical and Reagents

Aqueous solutions of TNT; 2,4-DNT; RDX; and HMX at nominal concentrations of 100, 100, 50, and 5 mg L⁻¹, respectively, were obtained from U.S. Army Edgewood Chemical Biological Center (ECBC, Aberdeen Proving Ground, MD) and were used as stock material for all experiments. The other compounds: 2,4-DNAN; 4-NAN; 2,5-DM-4-NANE; and 2-M-5-NPYNE were obtained from Sigma-Aldrich (Milwaukee, WI), all with purity ≥ 97%. Methanol for high performance liquid chromatography (HPLC) was from Fisher Scientific (Suwanee, GA). All other chemicals were either analytical or certified grade. Deionized water (18.1 MΩ) was obtained using a Neu-Ion (Baltimore, MD) purification system and was used throughout the studies.

Sand (Ottawa ACS grade, CAS: 14808-60-7, quartz, particle size: 20–30 mesh, specific gravity: 2.65) was obtained from VWR International (Radnor, PA). Sand was triple rinsed with water prior to use as the solid growth medium.

5.2.2 Plant Growth Conditions

Studies were performed using seeds of hullless barley (*Hordeum vulgare* L.) from Keystone Group AG Seeds (New Columbia, PA). This plant species was selected based on its wide geographical distribution, rapid growth, and ease of cultivation in the laboratory. Barley is an important cereal crop; in 2014 it ranked fourth among cereal crops production in the world ⁴⁴. The monocotyledon *H. vulgare* belongs to the Poaceae family (true grasses) which has several species established for standard plant uptake and translocation tests ^{45,46} and has been listed as one of the species used routinely to study phytotoxicity ⁴⁶. Additionally, barley has been used at military locations as vegetation cover to control wind and water erosion ⁴⁷.

Plant assays were carried out in a dark fabric-surrounded growth chamber with natural light lamp (AGROSUN®, Full Spectrum Grow Light) to maintain an average luminosity of 1281 ± 10 lux (mean \pm standard deviation) for a duration of 16 h per day (see “Plant Growth Conditions” in Appendix F for further details). Temperature and relative humidity in the growth chamber were 25.7 ± 0.4 °C and 38 to 51%, respectively.

Seeds of barley were sterilized following the procedure proposed in Abdul-Baki ⁴⁸, and germinated in darkness for 24 h on wet (water) paper towels in plastic dishes at room temperature (23.3 ± 0.5 °C). Sets of 10 to 20 germinated seeds were sown in individual glass pots (diameter: 6 cm, and height: 14 cm) containing 500 g_{dwt} of sand. Glass pots had a drainage nozzle at the bottom for sampling of displaced solution. A square of stainless steel mesh (40 mesh, 4 cm side) was placed at the bottom to prevent the loss of quartz grains. In order to supply needed nutrients for plant growth in sand, a fixed aliquot (4 mL per day) of modified Hoagland aqueous solution (Table F-4) ^{40,49} was added per pot throughout the uptake assays.

5.2.3 Preliminary Tests

5.2.3.1 Plant Growth in Sand

In order to address possible concerns about limited growth for plants sown in sand relative to those planted in soil, a test comparing plant height of barley (unexposed to MCs or MLCs) among three different growth media was performed. The media were: (i) sand, (ii) 50% (w/w) sand–Matapeake soil, and (iii) Matapeake soil (see “Plant Growth in Sand” in Appendix F for further details).

5.2.3.2 Toxicity Screening

In order to determine a single exposure concentration that was low enough to avoid lethal or inhibitory effects in plant growth during the bioconcentration uptake assays but was high enough to be quantified reliably, a toxicity screening test was performed following the protocol detailed in “Toxicity Screening” in Appendix F.

5.2.4 Bioconcentration Uptake Assays

Plants were grown initially for 2–3 weeks unexposed to MCs, or MLCs, a MC-free period. This period enabled shoots height to reach a steady state thus avoiding growth dilution effects ²⁴ that would otherwise alter the compound concentration measured in the biomass. Immediately after the MC-free growth period, the exposure to a MC, or MLC, aqueous solution at a single non-toxic concentration of 10 mg L^{-1} (determined in the toxicity screening, see Section 5.3.1.2) was initiated as follows. Four consecutive pore volumes (pore volume = 100 mL, determined by fluid displacement method) of the corresponding compound solution were added per pot on the first day of exposure. To ensure that the desired exposure level (10 mg L^{-1} , nominal) had been reached, a set of displaced solution samples were collected from the pot’s bottom drainage nozzle and analyzed by HPLC at the end of each of the 4 pore volumes added. A set of replicate pots per compound not treated with MCs or MLCs were used as negative

controls. Nutrients for plant growth were supplied separately from the solutions added using a fixed aliquot per pot, as described before in Section 5.2.2.

The exposure solution was regarded to be that available for barley root uptake in the interstitial water. The concentration of this exposure solution, i.e., exposure concentration, was considered to be that measured in the displaced solution samples collected from the pot's bottom drainage nozzle. In order to maintain an approximately constant exposure concentration throughout the experiment, a daily replenishment of 2 pore volumes was applied using the corresponding solution added. Displaced solution samples were collected at the end of each of these 2 pore volumes and subsequently analyzed by HPLC for MCs and MLCs concentrations. These samples are hereafter referred to as first- and last-fraction of displaced solution, and also served to quantify the extent of the overnight degradation of the compound in the interstitial water.

Plants were harvested at each of four exposure times: 1, 2, 3, and 4 weeks, and the roots were rinsed with water to remove residual sand. A minimum of two pots were sacrificed per exposure time. The biomass (shoots and roots together) of each pot was cut into small pieces (approx. 0.5 cm) to facilitate extraction, and then placed into a 10 mL centrifuge glass tube for subsequent acetonitrile extraction and HPLC analysis, details are provided in "Procedure for Extraction of MCs and MLCs from Plant Biomass" in Appendix F.

BCFs were calculated using Eq. (5-1) with $C_{i_{plant}}$ determined from the biomass extractions and $C_{i_{iw}}$ measured in the displaced solution samples. In order to verify the reproducibility of the BCFs obtained, bioconcentration uptake assays for one of each MCs and MLCs (2,4-DNAN and 4-NAN, respectively) were performed more than once.

5.2.5 Plant–Water Partitioning

Fresh plant biomass (0.2 - 0.5 g_{dwt}, shoots and roots together) grown for a 2–3 weeks MC-free period was harvested, cut into small pieces (approx. 0.5 cm), and mixed with 5 mL of the corresponding MC, or MLC, aqueous solution and 3 mL of a 0.01 mol L⁻¹ CaCl₂ and NaN₃ solution to repress microbial activity, in a 10 mL glass tube. In order to establish the effect of the compound initial concentration in the resulting plant–water partition coefficients (K_{PW}), most partitioning tests were performed at both a low and high concentration (listed in Table F-14) determined based on the compound aqueous solubility (Table F-3). The ratios of initial concentration to aqueous solubility for the low and high concentration treatments ranged from 0.01 to 0.09 and 0.06 to 0.87, respectively. All treatments were carried out with a minimum of two replicates.

The biomass–MC, or –MLC, suspensions were tumbled end-to-end in darkness at 20 rpm for 24 h. This contact time had been shown to be sufficient for the equilibration of organic compounds during plant sorption experiments in previous work^{41,50}. However, a kinetic sorption experiment using 4-NAN was completed separately to confirm this observation. Following the equilibration period, the aqueous phase from each tube was transferred with disposable glass pipettes into disposable glass culture tubes (10 mL), filtered through Durapore® polyvinylidene difluoride (PVDF) membranes (0.45 µm pore size), and analyzed for MCs and MLCs concentrations by HPLC. The plant phase from each tube was subjected to acetonitrile extractions using the procedure described in "Procedure for Extraction of MCs and MLCs from Plant Biomass" in Appendix F.

The K_{PW} were calculated as the concentration in the plant ($\text{mg kg}_{\text{plant dwt}}^{-1}$) divided by the concentration in the aqueous phase (mg L^{-1}), both measured at the end of the 24 h equilibration period.

5.2.6 Analytical Methods

MCs and MLCs concentrations were analyzed and quantified in an Agilent Technologies (Wilmington, DE) 1200 series HPLC system using modifications of the US EPA Method 8330B⁵¹, details are provided in “High Performance Liquid Chromatography (HPLC) Analytical Method” in Appendix F.

5.2.7 Data Analyses

Two-way analysis of variance (ANOVA) with repeated measures tests were conducted to examine the fluctuation of exposure concentrations over time. One-way ANOVA was used to assess the dependence of the ratios of concentrations in the plant to concentrations in the interstitial water on the exposure duration. In all these statistical tests, a $p\text{-value} \leq 0.05$ was accepted as significant and these analyses were performed using the R software for statistical computing⁵².

5.3 Results and Discussion

5.3.1 Preliminary Tests

5.3.1.1 Plant Growth in Sand

There was no statistically significant difference ($p\text{-value} = 0.68$) in shoots height among plants growing in sand, sand–Matapeake soil, and Matapeake soil over a period of 21 days (see further details in Appendix F, Figure F-1). This result supported the use of sand as the solid growth medium. Additionally, the use of sand made it possible to maintain nearly constant exposure concentrations in both the toxicity screening and bioconcentration uptake assays (“Toxicity Screening” in Appendix F and Section 5.3.2, respectively).

5.3.1.2 Toxicity Screening

Results of the toxicity screening tests for barley exposed to single MCs, or MLCs, are shown in Figure F-2. The No–Observed–Adverse–Effect–Concentration (NOAEC), Lowest–Observed–Adverse–Effect–Concentration (LOAEC), and effective concentrations (EC_{50}) for endpoint shoot height and root elongation are listed in Table F-6. Both the shoot length LOAEC and EC_{50} were $> 10 \text{ mg L}^{-1}$ for all the compounds. This was also the case for root length LOAEC for all compounds except 2,4-DNAN. Since the shoot lengths were not affected and only the root elongation for 2,4-DNAN showed an effect, 10 mg L^{-1} (nominal) was chosen to perform the bioconcentration uptake assays. This also ensured that the concentration of MCs, or MLCs, in the plant biomass after extraction would be high enough to be quantified reliably.

5.3.2 Bioconcentration Uptake Assays

Measured exposure concentrations are shown in Figure 5-2. Fluctuations over time were not different from the mean exposure concentration at the 5% level of statistical significance for any of the compounds except TNT (Table F-8), which reached a steady concentration at the third week of exposure. These significant TNT fluctuations were not the result of a failure of the daily replenishment protocol. They were already observed in the solution added to the pots as seen in Figure 5-2, where the concentrations in the solution added follow the same trend as those of the displaced solutions. Nevertheless, the TNT exposure concentrations eventually stabilized in week 3 when the BCF was determined.

With the use of sand as the solid growth medium and daily replenishment of the exposure solution, overnight degradation of the MCs and MLCs in the growth medium never exceeded 11% during these assays. Also, there was no significant sorption of the compounds by sand (Table F-9). Therefore, it was possible to maintain approximately constant exposure concentrations. The assurance of a nearly constant exposure is one of the advantages and improvements of this experimental protocol as it reduces the uncertainty in BCFs caused by the transformation/degradation of the parent compound in the growth medium. These processes lead to non-constant exposures in uptake experiments where endpoint soil concentrations of TNT and 2,4-DNT have been shown to be below detection limits or only 20 to 50% of the initial concentration^{19,25,28}, and even in carrier controls (i.e., without plants added) or during preliminary incubation periods TNT and 2,4-DNT soil concentrations have been observed to decrease by 20 to 80% in less than a month^{19,25,28}.

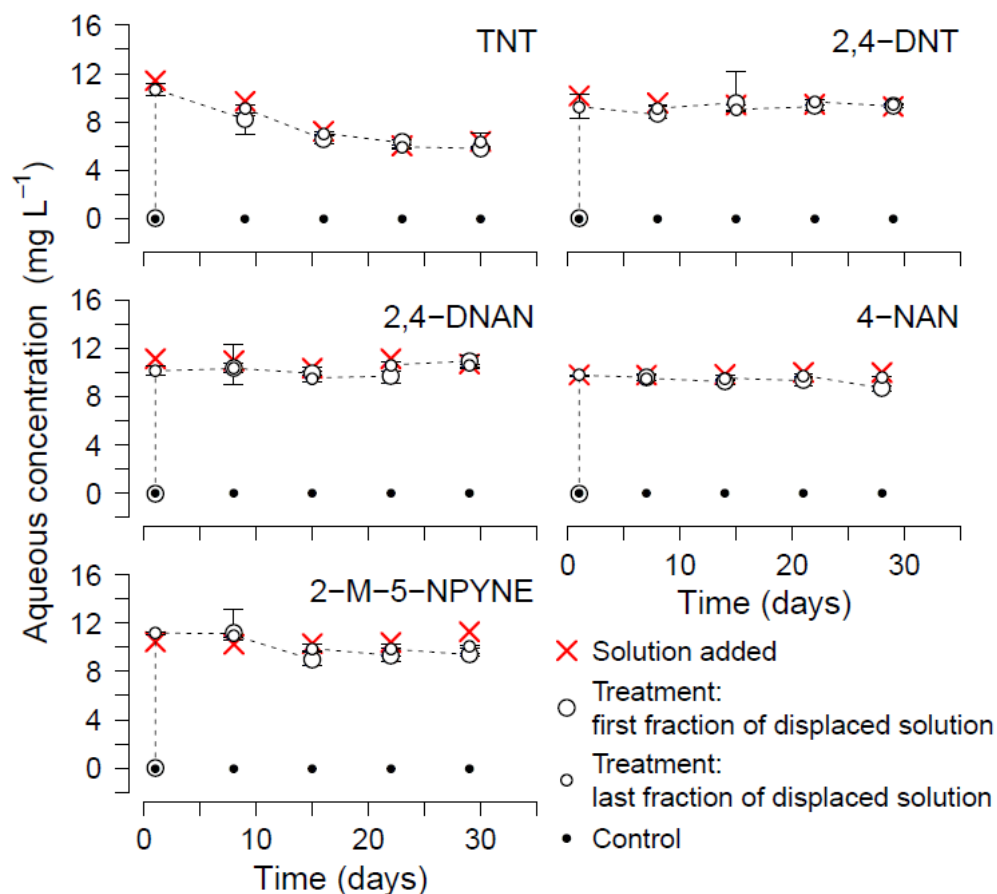


Figure 5-2 Exposure concentrations over time for MCs and MLCs in bioconcentration uptake assays with barley. Legend: Solution added is the aqueous solution sampled just before being loaded into plant pots; Treatment are samples from displaced solutions of pots exposed to MCs or MLCs; first and last fraction of displaced solution refer to the first and last pore volume replenished daily; Control are samples from displaced solutions of untreated plant pots (not exposed to MCs or MLCs). Displaying 2nd trial for 2,4-DNAN and 1st trial for 4-NAN. Data presented as means and error bars represent the range. Sample size ≥ 2 pots (Table F-11). If not visible, error bars are smaller than the symbol.

The ratios of concentration in the plant to concentration in the interstitial water, $\frac{C_{iplant}}{C_{iIW}}$, versus time of exposure are shown in Figure 5-3. These values did not vary significantly with time of exposure for any of the compounds except 4-NAN (Table F-10). However, steady state values were reached after three weeks of constant exposure for all compounds including 4-NAN (1st trial, Table F-10). Therefore, steady state BCFs were calculated with the values from week 3 and 4 (Figure 5-3 and Table F-11), using Eq. (5-1): $\log(\text{BCF}) \pm \text{standard error of the mean (SEM)} = 0.618 \pm 0.017, 0.698 \pm 0.032, 1.300 \pm 0.057, 0.515 \pm 0.027, \text{ and } 0.403 \pm 0.052 \text{ L kg}_{\text{dwt}}^{-1}$ for

TNT; 2,4-DNT; 2,4-DNAN; 4-NAN; and 2-M-5-NPYNE, respectively. The log BCFs for TNT and 2,4-DNT are larger or on the higher end relative to the log BCF_{Solids} reported by Best et al.¹⁶ and Sunahara¹⁹ for perennial ryegrass (*Lolium perenne*), a plant species closely related to barley, which range from 0.04 to 0.23 and from -0.15 to 0.88 for TNT metabolites (TNT reported as not detected in plant material) and 2,4-DNT, respectively. This is perhaps due to both the uncertainty of whether the BCF_{Solids} were steady state values and the reduced availability of the compounds for root uptake in the soil exposures relative to that in the sand medium. No plant BCF or BCF_{Solids} values were found in the literature for 2,4-DNAN; 4-NAN; or 2-M-5-NPYNE.

Reproducible BCFs were obtained for both of the compounds tested for more than one trial (Figure 5-3 and Table F-11). Differences in log BCF values among trials for 2,4-DNAN and 4-NAN were not statistically significant (p-value = 0.13 and 0.08, respectively). No trend was observed in log BCF as a function of the compound being a MC or a MLC. Biomass profiles showed a stable behavior for all compounds (Figure F-6).

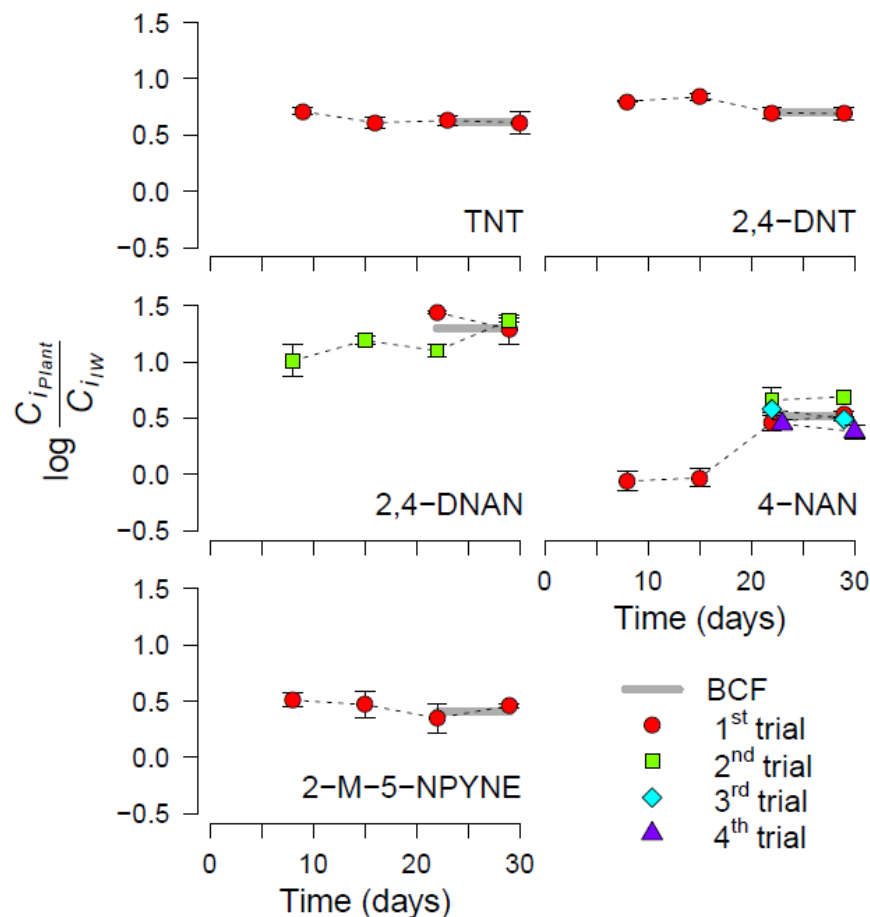


Figure 5-3 Logarithmic ratios of concentration in the plant to concentration in the interstitial water $\left(\log \frac{C_{i_{plant}}}{C_{i_{IW}}}\right)$ versus time of exposure for MCs and MLCs in bioconcentration uptake assays with barley. $C_{i_{plant}}$: concentration of compound i in barley ($\text{mg kg}_{\text{dwt}}^{-1}$), $C_{i_{IW}}$: concentration of compound i in the interstitial water – displaced solution (mg L^{-1}). BCF: steady state bioconcentration factor ($\text{L kg}_{\text{dwt}}^{-1}$). Trials refer to repetitions of a particular uptake assay. Data presented as means \pm standard error of the mean (SEM). Sample size ≥ 2 pots (Table F-11). If not visible, error bars smaller than the symbol.

5.3.3 Plant–Water Partitioning vs. Uptake

Plant–water partitioning experiments were performed to obtain the K_{PW} for MCs and MLCs. The kinetic sorption experiment conducted using 4-NAN confirmed that 24 h was sufficient time to achieve steady state concentrations, as demonstrated in previous work^{41,50}. The result showed no statistically significant difference in the $\log K_{PW}$ between 24, 48, and 144 h contact times (p -value = 0.18; Table F-12). Therefore, 24 h contact time was used in the plant–water partitioning experiments. Differences in $\log K_{PW}$ between experiments performed at a low

and high initial MC, or MLC, concentration were not statistically significant at the 5% level for any of the compounds (Table F-13).

The K_{PW} values are shown in Figure 5-4; experimental octanol–water partition coefficients (K_{OW}) are displayed as a reference. All MCs, except HMX, and 4-NAN had a median $\log K_{PW}$ between 1.180 and 1.520 $L\ kg_{dwt}^{-1}$ showing similar partition affinity for barley biomass to that of undissociated polar aromatic/cyclic compounds including o-chlorophenol and 2,4-dichlorophenol for rice shoots biomass ($1.08 < \log K_{PW} < 1.68\ L\ kg_{dwt}^{-1}$)²¹, while being low relative to that of nonpolar aromatic/cyclic compounds such as 1,2-dichlorobenzene and lindane for plant biomass of grasses in the same family as barley ($2.32 < \log K_{PW} < 4.58\ L\ kg_{dwt}^{-1}$)^{41,42}. Median $\log K_{PW}$ for 2,5-DM-4-NANE, HMX, and 2-M-5-NPYNE were even lower: 0.795, 0.830, 0.960 $L\ kg_{dwt}^{-1}$, respectively. No bias in $\log K_{PW}$ was observed due to the compound being either a MC or MLC.

Overall, the range of K_{PW} for the eight compounds evaluated spans only approximately one order of magnitude (Figure 5-4) despite the differences expected at least for the nitramine MCs (HMX and RDX) given their low affinity for organic phases relative to the aqueous phase ($\log K_{OW} = 0.16$ and 0.87 for HMX and RDX, respectively – Table F-3). In fact, there is no apparent relationship between $\log K_{PW}$ and $\log K_{OW}$. This suggests barley biomass components have solvation properties that differ with those commonly accounted for using lipid surrogates like octanol, something that has also been pointed out in published sorption experiments of aromatic contaminants by grasses^{41,43}.

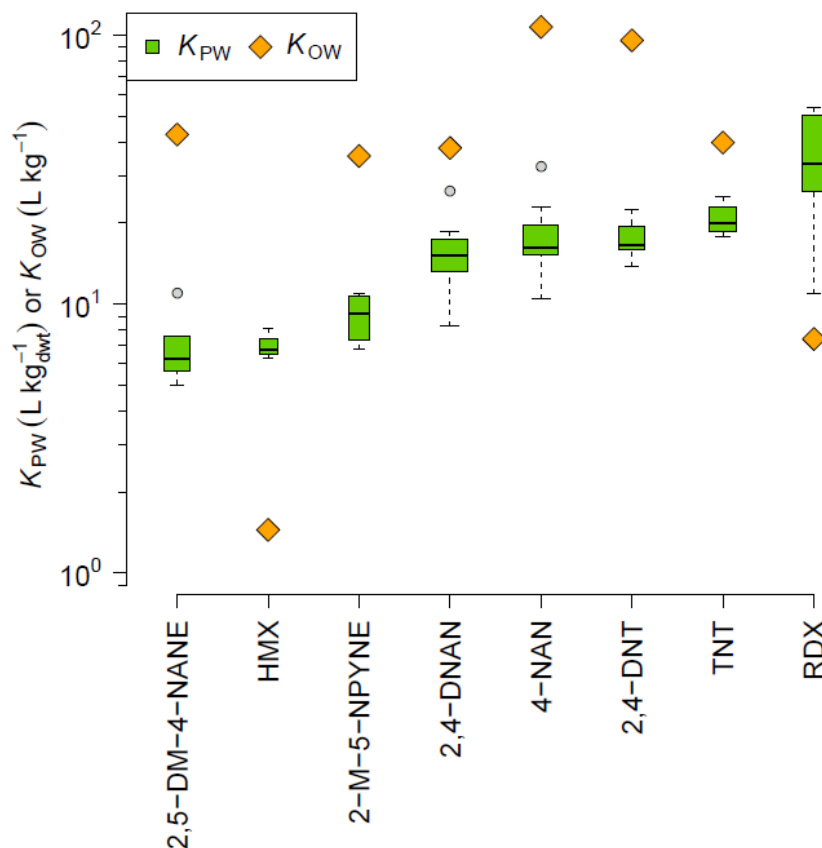


Figure 5-4 Plant–water partition coefficients (K_{PW}) for MCs and MLCs with barley and their respective octanol–water partition coefficients (K_{OW}). Data ordered by K_{PW} . K_{OW} values are experimental data obtained from EPI Suite database⁵³ for all compounds except 2,4-DNAN that is reported by Hawari et al.⁵⁴ and 2,5-DM-4-NANE that is an estimate from EPI Suite⁵³ in absence of an experimental value. Box width proportional to the square–root of the number of observations in the group (Table F-14).

The extent to which the bioconcentration of nitroaromatic MCs and MLCs, as measured by log BCFs, is related to their plant–water partitioning is illustrated in Figure 5-5. Absolute differences between the median values of the log K_{PW} and log BCF were between 0.190 and 0.690, with the BCF in most cases smaller than K_{PW} . These relatively small differences suggest that simple partition between the plant biomass and aqueous phase largely reflects the extent to which these compounds bioconcentrate in barley. Studies have reported similar observations for uptake of compounds including toluene, hexachlorobenzene, and perfluorooctane sulfonate (PFOS) by several plant species, showing the “kinetic uptake limit” or maximum concentration in the plant to be predicted satisfactorily using the equilibrium sorption of the solute by the plant^{42,50,55}.

The differences between K_{PW} and BCF observed in Figure 5-5 are likely due to the compounds being transformed and/or metabolized within the plant. Evidence of the transformation of TNT; 2,4-DNT; and 2,4-DNAN in the interior of grasses and related plants species, for example, has been reported^{19,30,56-59}. Of the three compounds, TNT has been shown to be so readily biotransformed in plants that often only its transformation products have been observed in plant shoots^{16,19,32}. In contrast, 2,4-DNT and 2,4-DNAN and their metabolites have been observed in various plant tissues^{19,30,59}. It is worth noting, however, that 2,4-DNAN has not been studied as extensively as TNT or 2,4-DNT since it has not been as widely utilized due to its novelty as a MC⁶⁰.

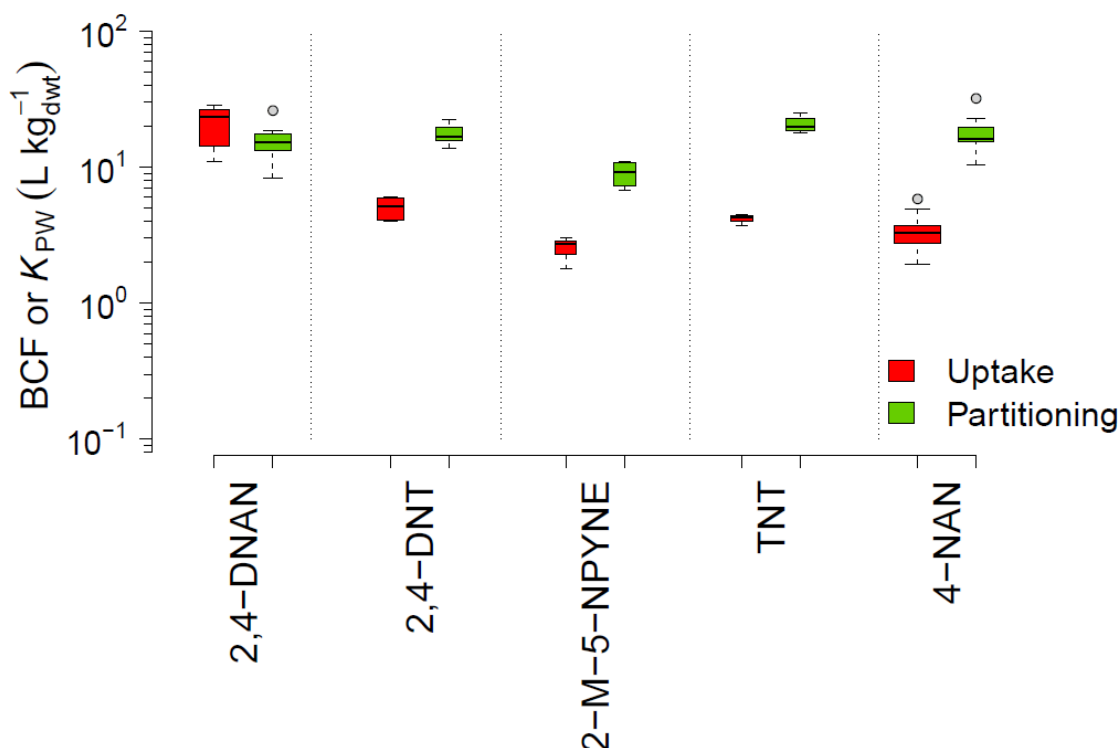


Figure 5-5 Comparison between uptake (as measured by BCF, Figure 5-3) and plant–water partition coefficient (K_{PW} , Figure 5-4) for MCs and MLCs. Compounds ordered from small to larger discrepancy between $\log K_{PW}$ and $\log BCF$. Box width proportional to the square–root of the number of observations in the group.

In order to provide a quantitative analysis for the extent to which the transformation/degradation of the MCs within the plant can explain the differences found between K_{PW} and BCF (Figure 5-5), degradation rates ($k_{\text{degradation}}$) were estimated for TNT; 2,4-DNT; and 2,4-DNAN. An exponential decay model was fitted to a time course dataset of concentrations in perennial ryegrass (*L. perenne*) observed during soil bioconcentration uptake

assays by Sunahara ¹⁹ and Dodard et al. ³⁰ (Table F-15 and Figure F-7). No time course data were found for 2-M-5-NPYNE or 4-NAN. While the estimated $k_{\text{degradation}}$ values are not the result of degradation processes occurring exclusively within the plant tissues, but also account for those taking place in the soil, they do indicate how susceptible to degradation/transformation each compound is relative to the other MCs. The estimated $k_{\text{degradation}}$ values were: 0.066, 0.083, 0.189 d⁻¹ for 2,4-DNAN; 2,4-DNT; and TNT, respectively. This increasing sequence is in agreement with that of the discrepancies found between K_{PW} and BCF as shown in Figure F-8, a comparison of the $k_{\text{degradation}}$ to $\frac{K_{\text{PW}}}{\text{BCF}}$, the ratio of plant–water partitioning to uptake. The increase in $\frac{K_{\text{PW}}}{\text{BCF}}$ is matched by the increase in $k_{\text{degradation}}$ suggesting that degradation is causing the difference between BCF and K_{PW} .

5.4 Conclusions

Reproducible steady state bioconcentration factors for MCs and MLCs in barley can be generated using sand as the solid growth medium with daily replenishment of the exposure solution. Sand provides a solid medium that hydroponic systems with water only lack and that, as mentioned previously, has been shown by other studies to be a key component for normal development of plant roots and hence of plant growth.

Even though plants are complex organisms, simple plant–water partition coefficients were able to estimate the BCFs with a difference between log K_{PW} and log BCF of 0.2 to 0.7 log units. The K_{PW} , therefore, can be used to estimate the upper–bound of the bioconcentration of these compounds in barley. The fact that no particular difference between MCs and MLCs was observed in neither BCFs nor K_{PW} values, suggests that the estimation tool is also applicable to compounds with particular functionalities like those in the MLCs, including methoxy (O-CH₃) and amino (-NH₂) groups.

Although according to the findings in this work, the evaluated compounds have rather low plant uptake upper–bounds, as measured by K_{PW} , relative to other nonpolar aromatic/cyclic contaminants, they can bioconcentrate in barley and thus constitute a risk for ecological receptors and point to the potential for transference to higher trophic levels from plants. The results presented in this work have been included as part of the calibration dataset for a quantitative model that estimates partitioning and BCFs for MCs and other compounds in grasses. The results of the model are presented in Torralba–Sanchez ⁶¹.

REFERENCES

1. Simini M, Wentsel RS, Checkai RT, Phillips CT, Chester NA, Major MA, Amos JC. Evaluation of soil toxicity at Joliet Army Ammunition Plant. *Environ Toxicol Chem*. 1995;14(4):623-630.
2. Jenkins TF, Hewitt AD, Grant CL, Thiboutot S, Ampleman G, Walsh ME, Ranney TA, Ramsey CA, Palazzo AJ, Pennington JC. Identity and distribution of residues of energetic compounds at Army live-fire training ranges. *Chemosphere*. 2006;63(8):1280-1290.
3. Walsh ME, Ramsey CA, Taylor S, Hewitt AD, Bjella K, Collins CM. Subsampling variance for 2,4-DNT in firing point soils. *Soil Sed Contam*. 2007;16(5):459-472.
4. Walsh MR, Walsh ME, Hewitt AD. Energetic residues from field disposal of gun propellants. *J Hazard Mater*. 2010;173(1-3):115-122.
5. Taylor S, Bigl S, Packer B. Condition of *in situ* unexploded ordnance. *Sci Total Environ*. 2015;505:762-769.
6. Spalding RF, Fulton JW. Groundwater munition residues and nitrate near Grand Island, Nebraska, U.S.A. *J Contam Hydrol*. 1988;2(2):139-153.
7. Best EPH, Sprecher SL, Larson SL, Fredrickson HL, Bader DF. Environmental behavior of explosives in groundwater from the Milan Army Ammunition Plant in aquatic and wetland plant treatments. Uptake and fate of TNT and RDX in plants. *Chemosphere*. 1999;39(12):2057-2072.
8. Best EPH, Sprecher SL, Larson SL, Fredrickson HL, Bader DF. Environmental behavior of explosives in groundwater from the Milan Army Ammunition Plant in aquatic and wetland plant treatments. Removal, mass balances and fate in groundwater of TNT and RDX. *Chemosphere*. 1999;38(14):3383-3396.
9. Spiegel K, Headley JV, Peru KM, Haidar N, Gurprasard NP. Residues of explosives in groundwater leached from soils at a military site in Eastern Germany. *Commun Soil Sci Plant Anal*. 2005;36(1-3):133-153.
10. Weeks KR, Veenstra SC, Hill DL. Bioremediation of perchlorate and explosives in groundwater. In: Calabrese EJ, Kostecki PT, Dragun J, eds. *Contaminated Soils, Sediment and Water: Science in the Real World*. New York, NY: Springer US. 2005;9:123-134.
11. Amaral HIF, Fernandes J, Berg M, Schwarzenbach RP, Kipfer R. Assessing TNT and DNT groundwater contamination by compound-specific isotope analysis and ^3H - ^3He groundwater dating: A case study in Portugal. *Chemosphere*. 2009;77(6):805-812.

12. Clausen JL, Korte N. Fate and transport of energetics from surface soils to groundwater. In: Chappell MA, Price CL, George RD, eds. *Environmental Chemistry of Explosives and Propellant Compounds in Soils and Marine Systems: Distributed Source Characterization and Remedial Technologies*. Washington, D.C: American Chemical Society. 2011;1069:273-316.
13. Talmage SS, Opresko DM, Maxwell CJ, Welsh CJE, Cretella FM, Reno PH, Daniel FB. Nitroaromatic munition compounds: Environmental effects and screening values. In: Ware GW, ed. *Reviews of Environmental Contamination and Toxicology*. New York, NY: Springer US. 1999;161: pp.3.
14. Ampleman G, Thiboutot S, Lewis J, Marois A, Gagnon A, Bouchard M, Jenkins T, Ranney TA, Pennington JC. Evaluation of the contamination by explosives and metals in soils, vegetation, surface water and sediment at Cold Lake Air Weapons Range (CLAWR), Alberta, Phase II Final report. Technical Report No. DRDC-Valcartier-TR-2004-204. Valcartier, Québec, Canada: Defence Research and Development Canada - Valcartier, Valcartier QUE (CAN); Cold Regions Research and Engineering Lab, Hanover NH (US). 2004;1-116.
15. Best EPH, Geter KN, Tatem HE, Lane BK. Effects, transfer, and fate of RDX from aged soil in plants and worms. *Chemosphere*. 2006;62(4):616-625.
16. Best EPH, Tatem HE, Geter KN, Wells ML, Lane BK. Effects, uptake, and fate of 2,4,6-trinitrotoluene aged in soil in plants and worms. *Environ Toxicol Chem*. 2008;27(12):2539-2547.
17. Kobayashi T, Navarro RR, Tatsumi K, Iimura Y. Influence of compost amendment on pyrene availability from artificially spiked soil to two subspecies of *Cucurbita pepo*. *Sci Total Environ*. 2008;404(1):1-9.
18. Rocheleau S, Lachance B, Kuperman RG, Hawari J, Thiboutot S, Ampleman G, Sunahara GI. Toxicity and uptake of cyclic nitramine explosives in ryegrass *Lolium perenne*. *Environ Pollut*. 2008;156(1):199-206.
19. Sunahara GI. Development of toxicity benchmarks and bioaccumulation data for N-based organic explosives for terrestrial plants and soil invertebrates. Final Report No. SERDP ER-1416. Québec, Canada: National Research Council of Canada Montreal (Québec) Biotechnology Research Institute. 2012;1-289.
20. Li H, Sheng G, Sheng W, Xu O. Uptake of trifluralin and lindane from water by ryegrass. *Chemosphere*. 2002;48(3):335-341.
21. Su Y, Zhu Y, Liang Y. Interactions of mixed organic contaminants in uptake by rice seedlings. *Chemosphere*. 2009;74(7):890-895.

22. McKone TE, Maddalena RL. Plant uptake of organic pollutants from soil: Bioconcentration estimates based on models and experiments. *Environ Toxicol Chem.* 2007;26(12):2494-2504.
23. Cunningham SD, Anderson TA, Schwab AP, Hsu FC. Phytoremediation of soils contaminated with organic pollutants. In: Sparks DL, ed. *Advances in agronomy*. San Diego, CA: Academic Press. 1996;56:55-114.
24. Collins C, Fryer M, Grosso A. Plant uptake of non-ionic organic chemicals. *Environ Sci Technol.* 2006;40(1):45-52.
25. Pennington JC. Plant uptake of 2,4,6-trinitrotoluene, 4-amino-2,6-dinitrotoluene, and 2-amino-4,6-dinitrotoluene using ¹⁴C-labeled and unlabeled compounds. Technical Report No. EL-88-20. Vicksburg, MS: U.S. Army Waterways Experiment Station, Corps of Engineers. 1988;1-68.
26. Groom CA, Halasz A, Paquet L, Morris N, Olivier L, Dubois C, Hawari J. Accumulation of HMX (octahydro-1,3,5,7-tetranitro-1,3,5,7-tetrazocine) in indigenous and agricultural plants grown in HMX-contaminated anti-tank firing-range soil. *Environ Sci Technol.* 2002;36(1):112-118.
27. Price RA, Pennington JC, Larson SL, Neumann D, Hayes CA. Uptake of RDX and TNT by agronomic plants. *Soil Sediment Contam.* 2002;11(3):307-326.
28. Durringer JM, Craig AM, Smith DJ, Chaney RL. Uptake and transformation of soil [¹⁴C]-trinitrotoluene by cool-season grasses. *Environ Sci Technol.* 2010;44(16):6325-6330.
29. Chen D, Liu ZL, Banwart W. Concentration-dependent RDX uptake and remediation by crop plants. *Environ Sci Pollut Res.* 2011;18(6):908-917.
30. Dodard SG, Sarrazin M, Hawari J, Paquet L, Ampleman G, Thiboutot S, Sunahara GI. Ecotoxicological assessment of a high energetic and insensitive munitions compound: 2,4-dinitroanisole (DNAN). *J Hazard Mater.* 2013;262:143-150.
31. Hannink NK, Rosser SJ, Bruce NC. Phytoremediation of explosives. *Crit Rev Plant Sci.* 2002;21(5):511-538.
32. Panz K, Miksch K. Phytoremediation of explosives (TNT, RDX, HMX) by wild-type and transgenic plants. *J Environ Manage.* 2012;113:85-92.
33. Scheidemann P, Klunk A, Sens C, Werner D. Species dependent uptake and tolerance of nitroaromatic compounds by higher plants. *J Plant Physiol.* 1998;152(2-3):242-247.
34. Pennington JC, Myers TE, Davis WM, Olin TJ, McDonald TA, Hayes CA, Townsend DM. Impacts of sorption on *in situ* bioremediation of explosives-contaminated soils. Technical

Report No. IRRP-95-1. Vicksburg, MS: U.S. Army Waterways Experiment Station, Corps of Engineers. 1995;1-54.

35. Larson SL, Martin WA, Escalon BL, Thompson M. Dissolution, sorption, and kinetics involved in systems containing explosives, water, and soil. *Environ Sci Technol*. 2007;42(3):786-792.
36. Berthelot Y, Valton É, Auroy A, Trottier B, Robidoux PY. Integration of toxicological and chemical tools to assess the bioavailability of metals and energetic compounds in contaminated soils. *Chemosphere*. 2008;74(1):166-177.
37. Savard K, Sarrazin M, Dodard SG, Monteil-Rivera F, Kuperman RG, Hawari J, Sunahara GI. Role of soil interstitial water in the accumulation of hexahydro-1,3,5-trinitro-1,3,5-triazine in the earthworm *Eisenia andrei*. *Environ Toxicol Chem*. 2010;29(4):998-1005.
38. Kalderis D, Juhasz AL, Boopathy R, Comfort S. Soils contaminated with explosives: Environmental fate and evaluation of state-of-the-art remediation processes (IUPAC technical report). *Pure Appl Chem*. 2011;83(7):1407-1484.
39. Crush JR, Care DA, Gourdin A, Woodfield DR. Root growth media effects on root morphology and architecture in white clover. *New Zea J Agric Res*. 2005;48(2):255-263.
40. Lin Y, Allen HE, Di Toro DM. Barley root hair growth and morphology in soil, sand, and water solution media and relationship with nickel toxicity. *Environ Toxicol Chem*. 2016; 35(8): 2125-2133.
41. Barbour JP, Smith JA, Chiou CT. Sorption of aromatic organic pollutants to grasses from water. *Environ Sci Technol*. 2005;39(21):8369-8373.
42. Li H, Sheng G, Chiou CT, Xu O. Relation of organic contaminant equilibrium sorption and kinetic uptake in plants. *Environ Sci Technol*. 2005;39(13):4864-4870.
43. Chiou CT, Sheng G, Manes M. A partition-limited model for the plant uptake of organic contaminants from soil and water. *Environ Sci Technol*. 2001;35(7):1437-1444.
44. Food and Agriculture Organization of the United Nations. FAO Statistical Database (FAOSTAT) Web site. <http://faostat3.fao.org/compare/E>. Accessed October, 2016.
45. US Environmental Protection Agency. OCSPP 850.4800: Plant uptake and translocation test. In: *Ecological effects test guidelines EPA 712-C-002*. Office of chemical safety and pollution prevention. Washington, D.C: US EPA. 2012.
46. American Society for Testing and Materials. E1963 – 09: Standard guide for conducting terrestrial plant toxicity tests. West Conshohocken, PA: ASTM International. 2014.

47. Nielson AB, Reid EH. Use of vegetation in military construction. *J Soil Water Conserv.* 1948;3(3):113-118.
48. Abdul-Baki AA. Hypochlorite and tissue sterilization. *Planta.* 1974;115(4):373-376.
49. Cheng T, Allen HE. Prediction of uptake of copper from solution by lettuce (*Lactuca sativa* Romance). *Environ Toxicol Chem.* 2001;20(11):2544-2551.
50. Chang M, Wang M, Kuo DTF, Shih Y. Sorption of selected aromatic compounds by vegetables. *Ecol Eng.* 2013;61, Part A:74-81.
51. US Environmental Protection Agency. Method 8330B: Nitroaromatics, nitramines, and nitrate esters by high performance liquid chromatography (HPLC). In: *Test methods for evaluating solid waste, physical/chemical methods (SW-846)*. Washington, D.C: Office of solid waste and emergency response. 2006.
52. R Development Core Team. R: A language and environment for statistical computing, v.3.2.0. Vienna, Austria: R Foundation for Statistical Computing. 2015.
53. US Environmental Protection Agency. Estimation Programs Interface (EPI) Suite™ for Microsoft® Windows, v. 4.11. Washington, D.C: US EPA. 2012.
54. Hawari J, Monteil-Rivera F, Perreault NN, Halasz A, Paquet L, Radovic-Hrapovic Z, Deschamps S, Thiboutot S, Ampleman G. Environmental fate of 2,4-dinitroanisole (DNAN) and its reduced products. *Chemosphere.* 2015;119:16-23.
55. Zhao HX, Guan Y, Zhang GL, Zhang Z, Tan F, Quan X, Chen JW. Uptake of perfluorooctane sulfonate (PFOS) by wheat (*Triticum aestivum* L.) plant. *Chemosphere.* 2013;91(2):139-144.
56. Palazzo AJ, Leggett DC. Effect and disposition of TNT in a terrestrial plant. *J Environ Qual.* 1986;15(1):49-52.
57. Gorge E, Brandt S, Werner D. Uptake and metabolism of 2,4,6-trinitrotoluene in higher plants. *Environ Sci Pollut Res.* 1994;1(4):229-233.
58. Nepovim A, Hebner A, Soudek P, Gerth A, Thomas H, Smrcek S, Vanek T. Degradation of 2,4,6-trinitrotoluene by selected helophytes. *Chemosphere.* 2005;60(10):1454-1461.
59. Yoon JM, Oliver DJ, Shanks JV. Phytotransformation of 2,4-dinitrotoluene in *Arabidopsis thaliana*: Toxicity, fate, and gene expression studies in vitro. *Biotechnol Prog.* 2006;22(6):1524-1531.

60. Richard T, Weidhaas J. Dissolution, sorption, and phytoremediation of IMX-101 explosive formulation constituents: 2,4-dinitroanisole (DNAN), 3-nitro-1,2,4-triazol-5-one (NTO), and nitroguanidine. *J Hazard Mater.* 2014;280:561-569.
61. Torralba-Sanchez TL. *Bioconcentration of munitions compounds in plants and worms: Experiments and modeling.* [Doctoral Dissertation]. University of Delaware; 2016.

Appendix F

SUPPLEMENTARY INFORMATION FOR: BIOCONCENTRATION FACTORS AND PLANT–WATER PARTITION COEFFICIENTS OF MUNITIONS COMPOUNDS IN BARLEY

CONTENTS:

Literature data for plant uptake of munitions compounds (MCs)

- | | |
|-----------|---|
| Table F-1 | Literature data for concentrations of MCs in plants grown in soil during uptake assays. |
| Table F-2 | Literature data for MCs bioconcentration factors (BCFs) in plants grown in soil during uptake assays. |

MCs and Munition–Like Compounds (MLCs) studied

- | | |
|-----------|--|
| Table F-3 | Selected characteristics and physicochemical properties of the MCs and MLCs studied. |
|-----------|--|

Plant Growth Conditions

- | | |
|------------|--|
| Table F-4 | Composition of aqueous solution used to supply nutrients for plant growth in sand. |
| Figure F-1 | Growth of barley in three different solid media. |

High Performance Liquid Chromatography (HPLC) Analytical Method

Toxicity Screening

- | | |
|------------|---|
| Table F-5 | Barley shoot height and root elongation for each measured exposure concentration. |
| Figure F-2 | Barley shoot and root lengths versus measured exposure concentrations. |
| Table F-6 | NOAEC, LOAEC, and EC ₅₀ for MCs and MLCs. |
| Figure F-3 | Biomass time profiles (shoot height). |

Figure F-4 Exposure concentrations over time.

Table F-7 Summary statistics for the fluctuation in measured exposure concentrations.

Figure F-5 Concentrations in displaced solutions collected at the end of each consecutive pore volume on the first day of exposure for selected chemicals.

Bioconcentration Uptake Assays

Table F-8 Summary statistics for the fluctuation in measured exposure concentrations.

Table F-9 Summary statistics for the significance of sorption of MCs and MLCs onto the solid growth medium (sand).

Table F-10 Summary statistics for the significance of exposure time in the ratios of $\frac{C_{i\text{plant}}}{C_{i\text{IW}}}$

Table F-11 Ratios of $\frac{C_{i\text{plant}}}{C_{i\text{IW}}}$

Figure F-6 Biomass time profiles (shoot height).

Plant–Water Partitioning vs. BCF

Table F-12 Plant–water partition coefficients (K_{PW}) for 4-NAN with barley and the summary statistics for the significance of contact time (kinetics) on log K_{PW} values

Table F-13 Summary statistics for the significance of the concentration of the initial solution added on log K_{PW} values

Table F-14 Plant–water partition coefficients (K_{PW}).

Table F-15 Time course data obtained from Sunahara ³ and Dodard et al. ⁹, and estimated degradation rates.

Figure F-7 Concentration in the plant ($C_{i\text{plant}}(t)$) over time and estimated degradation rates ($k_{\text{degradation}}$).

Figure F-8 Comparison between the ratios of plant–water partitioning to uptake ($\frac{K_{\text{PW}}}{\text{BCF}}$) and estimated degradation/transformation rates ($k_{\text{degradation}}$).

Literature Data for Plant Uptake of Munitions Compounds (MCs).

Table F-1 Literature data for concentrations of MCs in plants grown in soil during uptake assays.

Compound	Plant ^a	Species ^b	Family	Plant part ^c	Exposure time	Concentration in plant	Concentration in soil ^d	f_{oc}	Source
					days	mg kg _{dwt} ⁻¹	mg kg _{dwt} ⁻¹		
TNT ^e	YN	<i>C. esculentus</i>	Cyperaceae	Shoots	45	27.800	11.300	0.024	1
TNT ^e	YN	<i>C. esculentus</i>	Cyperaceae	Shoots	45	93.400	16.700	0.006	1
TNT	CS	<i>Z. mays</i>	Poaceae	AG	76	2.100	17.050	0.025	2
TNT	CS	<i>Z. mays</i>	Poaceae	AG	76	1.600	213.000	0.025	2
TNT	Corn	<i>Z. mays</i>	Poaceae	Kernels	76	1.700	213.000	0.025	2
2,4-DNT	PR	<i>L. perenne</i>	Poaceae	Shoots	14	2.800	1.000	0.013	3
2,4-DNT	PR	<i>L. perenne</i>	Poaceae	Shoots	14	2.000	3.000	0.013	3
2,4-DNT	PR	<i>L. perenne</i>	Poaceae	Shoots	14	2.800	5.000	0.013	3
2,4-DNT	PR	<i>L. perenne</i>	Poaceae	Shoots	14	1.400	10.000	0.013	3
RDX	PR	<i>L. perenne</i>	Poaceae	Shoots	42	119.000	11.100	0.007	4
RDX	PR	<i>L. perenne</i>	Poaceae	Shoots	42	804.000	104.000	0.007	4
RDX	PR	<i>L. perenne</i>	Poaceae	Shoots	42	764.000	1014.000	0.007	4
RDX	PR	<i>L. perenne</i>	Poaceae	Shoots	42	1690.000	8867.000	0.007	4
RDX	PR	<i>L. perenne</i>	Poaceae	Shoots	55	1083.000	10.000	0.029	5

RDX	PR	<i>L. perenne</i>	Poaceae	Shoots	55	5217.000	59.200	0.026	5
RDX	PR	<i>L. perenne</i>	Poaceae	Shoots	55	2948.000	153.900	0.022	5
RDX	PR	<i>L. perenne</i>	Poaceae	Shoots	55	806.000	13.800	0.037	6
RDX	PR	<i>L. perenne</i>	Poaceae	Shoots	55	2055.000	645.000	0.073	6
RDX	PR	<i>L. perenne</i>	Poaceae	Shoots	55	3886.000	855.500	0.100	6
RDX	PR	<i>L. perenne</i>	Poaceae	Shoots	55	3068.000	1540.500	0.164	6
RDX	PR	<i>L. perenne</i>	Poaceae	Shoots	34	387.567	10.000	0.013	3
RDX	PR	<i>L. perenne</i>	Poaceae	Shoots	34	1965.800	30.000	0.013	3
RDX	PR	<i>L. perenne</i>	Poaceae	Shoots	34	2221.400	100.000	0.013	3
RDX	Alfalfa	<i>M. sativa</i>	Fabaceae	Shoots	55	187.000	13.800	0.037	6
RDX	Alfalfa	<i>M. sativa</i>	Fabaceae	Shoots	55	3997.000	645.000	0.073	6
RDX	Alfalfa	<i>M. sativa</i>	Fabaceae	Shoots	55	4355.000	855.500	0.100	6
RDX	Alfalfa	<i>M. sativa</i>	Fabaceae	Shoots	55	4155.000	1540.500	0.164	6
RDX	YN	<i>C. esculentus</i>	Cyperaceae	Shoots	45	10.385	1.640	0.025	2
RDX	YN	<i>C. esculentus</i>	Cyperaceae	Shoots	45	64.938	50.300	0.025	2
RDX	YN	<i>C. esculentus</i>	Cyperaceae	Shoots	45	8.354	7.680	0.025	2
RDX	YN	<i>C. esculentus</i>	Cyperaceae	Shoots	45	1.037	0.670	0.025	2
RDX	YN	<i>C. esculentus</i>	Cyperaceae	Shoots	45	327.598	1.580	NA	2
RDX	YN	<i>C. esculentus</i>	Cyperaceae	Shoots	45	15.318	2.480	NA	2
RDX	YN	<i>C. esculentus</i>	Cyperaceae	Shoots	45	72.845	3.060	NA	2
RDX	YN	<i>C. esculentus</i>	Cyperaceae	Shoots	45	70.230	5.780	NA	2
RDX	Lettuce	<i>L. sativa</i>	Asteraceae	Leaves	45	9.817	1.640	0.025	2
RDX	Lettuce	<i>L. sativa</i>	Asteraceae	Leaves	45	1197.085	50.300	0.025	2

RDX	Lettuce	<i>L. sativa</i>	Asteraceae	Leaves	45	171.544	7.680	0.025	2
RDX	Lettuce	<i>L. sativa</i>	Asteraceae	Leaves	45	8.977	0.670	0.025	2
RDX	Lettuce	<i>L. sativa</i>	Asteraceae	Leaves	45	409.966	1.580	NA	2
RDX	Lettuce	<i>L. sativa</i>	Asteraceae	Leaves	45	66.453	2.480	NA	2
RDX	Lettuce	<i>L. sativa</i>	Asteraceae	Leaves	45	160.410	4.900	NA	2
RDX	Lettuce	<i>L. sativa</i>	Asteraceae	Leaves	45	120.880	19.000	NA	2
RDX	Lettuce	<i>L. sativa</i>	Asteraceae	Leaves	45	67.131	3.060	NA	2
RDX	Lettuce	<i>L. sativa</i>	Asteraceae	Leaves	45	121.332	5.780	NA	2
RDX	CS	<i>Z. mays</i>	Poaceae	AG	76	1.637	1.640	0.025	2
RDX	CS	<i>Z. mays</i>	Poaceae	AG	76	58.294	50.300	0.025	2
RDX	CS	<i>Z. mays</i>	Poaceae	AG	76	7.774	7.680	0.025	2
RDX	Corn	<i>Z. mays</i>	Poaceae	Kernels	76	6.732	50.300	0.025	2
RDX	Corn	<i>Z. mays</i>	Poaceae	APT	34	120.000	12.500	0.036	7
RDX	Corn	<i>Z. mays</i>	Poaceae	APT	34	300.000	25.000	0.036	7
RDX	Corn	<i>Z. mays</i>	Poaceae	APT	34	802.000	50.000	0.036	7
RDX	Corn	<i>Z. mays</i>	Poaceae	APT	34	1210.000	100.000	0.036	7
RDX	Corn	<i>Z. mays</i>	Poaceae	APT	28	695.000	220.000	0.036	7
RDX	Corn	<i>Z. mays</i>	Poaceae	APT	28	602.000	494.000	0.036	7
RDX	Corn	<i>Z. mays</i>	Poaceae	APT	28	649.000	903.000	0.036	7
RDX	Tomato	<i>L. lycopersicum</i>	Solanaceae	Fruit	50	8.291	50.300	0.025	2
RDX	Tomato	<i>L. lycopersicum</i>	Solanaceae	Fruit	50	5.776	7.680	0.025	2
RDX	Soybean	<i>G. max</i>	Fabaceae	APT	34	104.000	12.500	0.036	7
RDX	Soybean	<i>G. max</i>	Fabaceae	APT	34	181.000	25.000	0.036	7

RDX	Soybean	<i>G. max</i>	Fabaceae	APT	34	314.000	50.000	0.036	7
RDX	Soybean	<i>G. max</i>	Fabaceae	APT	34	492.000	100.000	0.036	7
RDX	Soybean	<i>G. max</i>	Fabaceae	APT	28	322.000	220.000	0.036	7
RDX	Soybean	<i>G. max</i>	Fabaceae	APT	28	358.000	494.000	0.036	7
RDX	Soybean	<i>G. max</i>	Fabaceae	APT	28	274.000	903.000	0.036	7
RDX	Sorghum	<i>S. sudanese</i>	Poaceae	APT	34	94.000	12.500	0.036	7
RDX	Sorghum	<i>S. sudanese</i>	Poaceae	APT	34	314.000	25.000	0.036	7
RDX	Sorghum	<i>S. sudanese</i>	Poaceae	APT	34	1052.000	50.000	0.036	7
RDX	Sorghum	<i>S. sudanese</i>	Poaceae	APT	34	1414.000	100.000	0.036	7
RDX	Sorghum	<i>S. sudanese</i>	Poaceae	APT	28	1133.000	220.000	0.036	7
RDX	Sorghum	<i>S. sudanese</i>	Poaceae	APT	28	975.000	494.000	0.036	7
RDX	Sorghum	<i>S. sudanese</i>	Poaceae	APT	28	1218.000	903.000	0.036	7
RDX	Wheat	<i>T. aestivum</i>	Poaceae	APT	34	290.000	12.500	0.036	7
RDX	Wheat	<i>T. aestivum</i>	Poaceae	APT	34	888.000	25.000	0.036	7
RDX	Wheat	<i>T. aestivum</i>	Poaceae	APT	34	1723.000	50.000	0.036	7
RDX	Wheat	<i>T. aestivum</i>	Poaceae	APT	34	2828.000	100.000	0.036	7
RDX	Wheat	<i>T. aestivum</i>	Poaceae	APT	28	1597.000	220.000	0.036	7
RDX	Wheat	<i>T. aestivum</i>	Poaceae	APT	28	1680.000	494.000	0.036	7
RDX	Wheat	<i>T. aestivum</i>	Poaceae	APT	28	1915.000	903.000	0.036	7
HMX	PR	<i>L. perenne</i>	Poaceae	Shoots	42	39.000	3.900	0.007	4
HMX	PR	<i>L. perenne</i>	Poaceae	Shoots	42	201.000	107.000	0.007	4
HMX	PR	<i>L. perenne</i>	Poaceae	Shoots	42	206.000	1099.000	0.007	4
HMX	PR	<i>L. perenne</i>	Poaceae	Shoots	42	325.000	9282.000	0.007	4

HMX	PR	<i>L. perenne</i>	Poaceae	Shoots	55	29.800	1.600	0.029	5
HMX	PR	<i>L. perenne</i>	Poaceae	Shoots	55	101.700	7.000	0.026	5
HMX	PR	<i>L. perenne</i>	Poaceae	Shoots	55	62.300	17.200	0.022	5
HMX	PR	<i>L. perenne</i>	Poaceae	Shoots	55	NA	0.140	0.037	6
HMX	PR	<i>L. perenne</i>	Poaceae	Shoots	55	26.000	8.600	0.073	6
HMX	PR	<i>L. perenne</i>	Poaceae	Shoots	55	50.000	16.900	0.100	6
HMX	PR	<i>L. perenne</i>	Poaceae	Shoots	55	43.000	41.000	0.164	6
HMX	Alfalfa	<i>M. sativa</i>	Fabaceae	Shoots	55	16.000	0.140	0.037	6
HMX	Alfalfa	<i>M. sativa</i>	Fabaceae	Shoots	55	65.000	8.600	0.073	6
HMX	Alfalfa	<i>M. sativa</i>	Fabaceae	Shoots	55	84.000	16.900	0.100	6
HMX	Alfalfa	<i>M. sativa</i>	Fabaceae	Shoots	55	66.000	41.000	0.164	6
HMX	Alfalfa	<i>M. sativa</i>	Fabaceae	Whole	77	289.300	32.300	0.020	8
HMX	BB	<i>P. vulgaris</i>	Fabaceae	Whole	77	123.300	32.300	0.020	8
HMX	Canola	<i>B. rapa</i>	Brassicaceae	Whole	77	223.500	32.300	0.020	8
HMX	PR	<i>L. perenne</i>	Poaceae	Whole	77	459.700	32.300	0.020	8
HMX	Wheat	<i>T. aestivum</i>	Poaceae	Whole	77	295.100	32.300	0.020	8
2,4-DNAN	PR	<i>L. perenne</i>	Poaceae	Shoots	19	1.059	0.474	0.012	9
2,4-DNAN	PR	<i>L. perenne</i>	Poaceae	Shoots	19	2.085	0.796	0.012	9
2,4-DNAN	PR	<i>L. perenne</i>	Poaceae	Shoots	19	2.893	1.808	0.012	9
2,4-DNAN	PR	<i>L. perenne</i>	Poaceae	Shoots	19	4.723	2.977	0.012	9
2,4-DNAN	PR	<i>L. perenne</i>	Poaceae	Shoots	19	14.908	4.699	0.012	9

^a Plant common name, as reported in the sources; YN: Yellow Nutsedge; CS: Corn Stover; PR: Perennial Ryegrass; BB: Bush Bean

^b Species names, as reported in the sources. *C. esculentus*: *Cyperus esculentus*; *Z. mays*: *Zea mays*; *L. perenne*: *Lolium perenne*; *M. sativa*: *Medicago sativa*; *L. sativa*: *Lactuca sativa*; *L. lycopersicum*: *Lycopersicon lycopersicum*; *G. max*: *Glycine max*; *S. sudanese*: *Sorghum sudanese*; *T. aestivum*: *Triticum aestivum*; *P. vulgaris*: *Phaseolus vulgaris*; *B. rapa*: *Brassica rapa*

^c Plant tissue names, as reported in the sources. AG: Aboveground; APT: Aerial Plant Tissue

^d On the last day of exposure

^e ¹⁴C-TNT

Table F-2 Literature data for MCs bioconcentration factors (BCFs) in plants grown in soil during uptake assays.

Compound	BCF	Exposure time	Concentration in soil ^a	Sources
	kg _{dwt} soil (kg _{dwt} plant) ⁻¹	days	mg kg _{dwt} ⁻¹	
RDX	14.60	42	11.10	4
RDX	8.90	42	104.00	4
RDX	0.70	42	1014.00	4
RDX	0.17	42	8867.00	4
RDX	108.30	55	10.00	5
RDX	88.10	55	59.20	5
RDX	19.20	55	153.90	5
RDX	58.00	55	13.80	6
RDX	3.00	55	645.00	6
RDX	5.00	55	855.50	6
RDX	2.00	55	1540.50	6
RDX	51.60	34	10.00	3
RDX	76.40	34	30.00	3
RDX	23.50	34	100.00	3
HMX	10.70	42	3.90	4
HMX	2.00	42	107.00	4
HMX	0.21	42	1099.00	4
HMX	0.03	42	9282.00	4
HMX	18.60	55	1.60	5
HMX	14.50	55	7.00	5
HMX	3.60	55	17.20	5
HMX	3.00	55	8.60	6
HMX	3.00	55	16.90	6
HMX	1.00	55	41.00	6

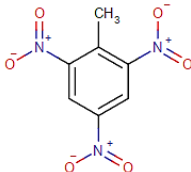
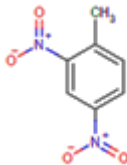
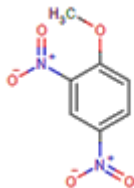
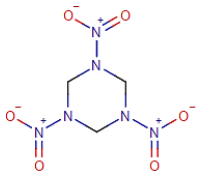
HMX	27.10	35	10.00	3
HMX	14.40	35	30.00	3
HMX	3.90	35	100.00	3
HMX	0.30	35	1000.00	3
TNT ^b	0.00	55	4.90	5
TNT ^b	1.70	55	9.60	5
TNT ^b	1.10	55	18.00	5
2,4-DNT	7.60	21	1.00	3
2,4-DNT	2.50	21	3.00	3
2,4-DNT	1.80	21	5.00	3
2,4-DNT	0.70	21	10.00	3

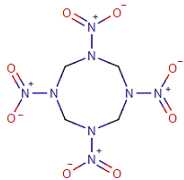
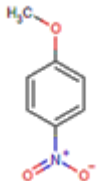
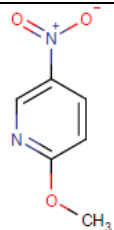
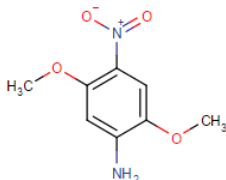
^a At the beginning of the exposure

^b Reported as TNT metabolites

MCs and MLCs Studied

Table F-3 Selected characteristics and physicochemical properties of the MCs and MLCs studied.

Class	Compound ^a	CAS #	Molecular Weight	Structure	Aqueous Solubility ^b mg L ⁻¹	log K _{ow} ^b
MCs: Nitroaromatics	TNT	118-96-7	227.13		115	1.60
	2,4-DNT	121-14-2	182.14		200	1.98
	2,4-DNAN	119-27-7	198.14		155	1.58 ^c
MCs: Nitramines	RDX	121-82-4	222.12		60	0.87

	HMX	2691-41-0	296.16		5	0.16
	4-NAN	100-17-4	153.14		590	2.03
MLCs	2-M-5-NPYNE	5446-92-4	154.13		1406 ^d	1.55
	2,5-DM-4-NANE	6313-37-7	198.18		1801 ^d	1.63 ^d

^a Chemicals: 2,4,6-trinitrotoluene (TNT); 2,4-dinitrotoluene (2,4-DNT); 2,4-dinitroanisole (2,4-DNAN); hexahydro-1,3,5-trinitro-1,3,5-triazine (RDX); octahydro-1,3,5,7-tetranitro-1,3,5,7-tetrazocine (HMX); 4-nitroanisole (4-NAN); 2-methoxy-5-nitropyridine (2-M-5-NPYNE); 2,5-dimethoxy-4-nitroaniline (2,5-DM-4-NANE)

^b Experimental data from EPI Suite database ¹⁰

^c Experimental value from Hawari et al. ¹¹

^d Estimate from EPI Suite ¹⁰ in absence of an experimental value

Plant Growth Conditions

While the 1281 ± 10 lux (mean \pm standard deviation) light level might seem low compared to that used in other plant studies (~ 4000 lux), it allowed barley to reach a steady shoot height (avg. 19 cm), as described in Section 5.3.2 in the main text, that is equal or higher than the shoot height reported in other MCs uptake studies (10 to 15 cm) performed with similar grasses (e.g., big bluestem grass, smooth brome grass) at higher light levels [~ 5000 lux (147 W s^{-2})]^{12,13}.

Table F-4 Composition of aqueous solution used to supply nutrients for plant growth in sand.

Chemical	Concentration
	mol L ⁻¹
MgSO ₄	9.98×10^{-4}
KH ₂ PO ₄	1.25×10^{-4}
KNO ₃	2.50×10^{-3}
H ₃ BO ₃	2.31×10^{-5}
MnCl ₂	4.60×10^{-6}
ZnSO ₄	3.83×10^{-7}
Na ₂ MoO ₄	1.86×10^{-7}
CaCl ₂	2.00×10^{-3}
MES	2.93×10^{-3}

Plant Growth in Sand

Soil characteristics for Matapeake: silt loam texture, 21% sand, 57% silt, 22% clay, 1.5% total organic carbon, 9.9 cmol kg⁻¹ cation–exchange capacity, and pH 5.7. Plant growth in sand was supported using nutrient solution as described in Section 5.2.2 in the main text. Ratios of the average shoot height for plants grown in sand and sand–Matapeake soil relative to that of those growing in only Matapeake soil over a period of 21 days were ≥ 1.0 after the average shoot height started to reach a plateau (approx. 10 days) and until the end of the tested period as shown in Figure F-1 in Appendix F. Two–way analysis of variance (ANOVA) with repeated measures was used to establish the effect of the three different growth media (sand, sand–Matapeake soil, and Matapeake soil) on plant height over time.

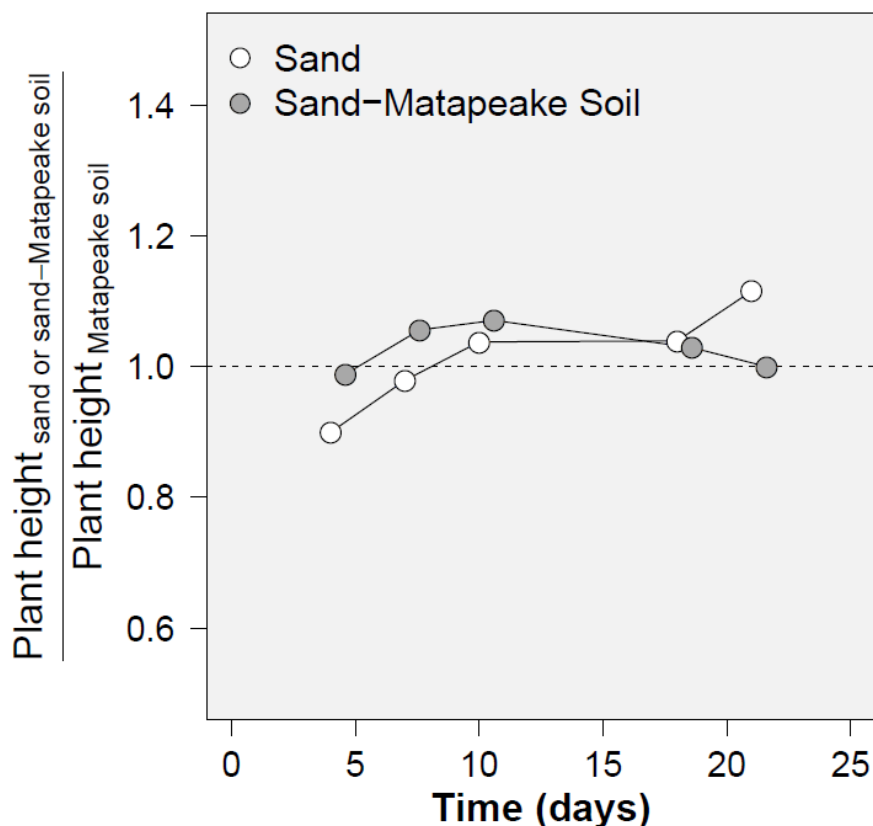


Figure F-1 Growth of barley (unexposed to MCs or MLCs) in three different solid media over a period of 21 days. Data presented as the ratios of the average shoot height of plants grown in either sand or sand-Matapeake soil relative to that of those growing in only Matapeake soil. Horizontal dotted line is a visual reference at ratio = 1.

High Performance Liquid Chromatography (HPLC) Analytical Method

Separation was made on a ZORBAX SB-C18 column (4.6×50 mm; $3.5 \mu\text{m}$ particle size) maintained at 16.5°C (36.5°C for RDX and 2,5-DM-4-NANE to avoid overlap with background signals). The sample injection volume was $100 \mu\text{L}$. A water and methanol gradient was used at a flow rate of 2 mL min^{-1} . The initial solvent system consisted of 70% water and 30% methanol, which was held for 2.80 min. A linear gradient was built from 30% methanol to 65% methanol between 2.80 min and 3.15 min. Subsequently, the solvent ratio was changed to the initial conditions and maintained until the end of the total run time (4.50 min). Chromatograms were generated at a wavelength of 214 nm. Reference HPLC standards for TNT; 2,4-DNT; RDX; HMX; and 4-NAN were from AccuStandard, Inc. (New Haven, CT, USA) or Crescent Chemical Co., Inc. (Islandia, New York, USA). Reference solutions for 2,4-DNAN; 2,5-DM-4-NANE; and 2-M-5-NPYNE were prepared in either methanol or ethanol.

Toxicity Screening

Procedures for the toxicity screening were adapted from the ASTM Standard Guide E1963-09¹⁴ and the OECD Guidelines Test 227¹⁵. Tests were initiated after one day of emergence (2 days after being sown in sand) by adding 4 pore volumes (pore volume = 100 mL, determined by fluid displacement method) of the corresponding compound solution per pot at one of four nominal aqueous concentrations (1, 10, 50, and 100 mg L⁻¹; hereafter referred to as solutions added). These concentrations were selected for the toxicity screening because they could be quantified reliably and were spaced around an average value (~ 18 mg L⁻¹) of the range of dissolved MCs concentrations observed at various military facilities and surrounding locations (4 × 10⁻⁴ to 36 mg L⁻¹)¹⁶⁻¹⁸. Nutrients for plant growth were supplied separately from the solutions added using a fixed aliquot per pot, as described in the main text in Section 5.2.2. To ensure that the desired exposure level had been reached, a set of displaced solution samples were collected from the pot's bottom drainage nozzle and analyzed by HPLC at the end of each of the 4 pore volumes added. All treatments were carried out with a minimum of two replicates. A set of replicate pots per compound not treated with MCs, or MLCs, were used as negative controls.

The exposure solution was regarded to be that available for barley root uptake in the interstitial water. The concentration of this exposure solution, i.e., exposure concentration, was considered to be that measured in the displaced solution samples collected from the pot's bottom drainage nozzle. In order to maintain an approximately constant exposure concentration throughout the experiment, a daily replenishment of 2 pore volumes was applied using the corresponding solution added. Displaced solution samples were collected at the end of each of these 2 pore volumes and subsequently analyzed by HPLC for MCs and MLCs concentrations. These samples are hereafter referred to as first- and last-fraction of displaced solution, and also served to quantify the extent of the overnight degradation of the compound in the interstitial water.

Shoot height was measured periodically to monitor growth over time. Plants were harvested 6 or 8 days after the beginning of the exposure and the shoot and root lengths of every plant were recorded. Shoots were measured to the tallest point and the longest root was measured to the end of the root tip¹⁴. These data are listed in Table F-5 and presented graphically in Figure F-2. Endpoint shoot height and root elongation were used to determine the No-Observed-Adverse-Effect-Concentration (NOAEC) and Lowest-Observed-Adverse-Effect-Concentration (LOAEC) for the tested MCs and MLCs as follows. Two-way ANOVA tests were performed to identify statistically significant differences in the means of plant responses among carrier controls and MCs-, or MLCs-, exposed subjects. Subsequently, Tukey honest significant difference (Tukey HSD) tests were carried out for multiple comparisons to determine statistically significant differences between mean pairs, and to establish values for the No-Observed-Adverse-Effect-Concentration (NOAEC) and the Lowest-Observed-Adverse-Effect-Concentration (LOAEC) for each compound. Effective concentrations producing a 50% decrease (EC₅₀) in the plant responses relative to carrier controls were determined fitting the endpoint shoot height, or root elongation, measurements to either a logistic Gompertz model or a logistic hormetic model. Toxicity screening results that exhibited hormesis (stimulation effects at doses below the toxicity threshold, while causing toxicity at doses above the threshold¹⁹) were fitted to the hormetic model. Models fitted for the determination of the EC₅₀ values in the plant responses relative to carrier controls were

Logistic Gompertz Model:

$$y = a \times e^{\left\{ [\log(1-p)] \times \left(\frac{C}{EC_p} \right)^b \right\}} \quad (F-1)$$

Logistic Hormetic Model:

$$y = \frac{a \times [1 + (h \times C)]}{1 + \left[\frac{p + (h \times C)}{(1 - p)} \times \left(\frac{C}{EC_p} \right)^b \right]} \quad (F-2)$$

where y = measured endpoint shoot height or root elongation (cm), a = control response, i.e., y-axis intercept (cm), p = value for the p effect (0.5 for 50%), C = measured exposure concentration (mg L⁻¹), EC_p = estimate of effect concentration for the specified percent effect (mg L⁻¹), b = scale parameter, and h = hormetic effect parameter^{20,21}. In all these statistical tests, a p-value ≤ 0.05 was accepted as significant and these analyses were performed using the R software for statistical computing²². NOAEC, LOAEC, and EC₅₀ values for the MCs and MLCs studied are listed in Table F-6.

Plant biomass exhibited a typical exponential growth at all concentrations (Figure F-3). ANOVA with repeated measures tests were conducted to examine the fluctuation of exposure concentrations throughout the toxicity screening. Measured exposure concentrations are reported in Figure F-4. For sand as the solid growth medium with daily replenishment of the exposure solution, the fluctuations in the measured exposure concentrations were not different from the mean concentration at the 5% level of statistical significance for any of the compounds in the toxicity screening (Table F-7). Overnight degradation in the growth medium during the toxicity screening was never $> 26\%$ for any of the compounds except TNT, which had a one-time maximum of 34%. This was expected since TNT has been shown to be readily transformed in comparison to other MCs^{23,24}. Addition of four consecutive pore volumes was sufficient to reach the desired concentrations on the day the exposure to MCs, or MLCs, began (Figure F-5).

Table F-5 Barley shoot height and root elongation for each measured exposure concentration in toxicity screening with MCs and MLCs.

Compound	Exposure Concentration ^a	Replicate	Plant	Leaf Height	Root Elongation
	mg L ⁻¹			cm	cm
TNT	0.00E+00	A	1	1.26E+01	6.60E+00
TNT	0.00E+00	A	2	1.86E+01	1.52E+01
TNT	0.00E+00	A	3	7.90E+00	4.40E+00
TNT	0.00E+00	A	4	1.10E+01	4.90E+00
TNT	0.00E+00	A	5	9.90E+00	6.30E+00
TNT	0.00E+00	A	6	1.06E+01	5.50E+00
TNT	0.00E+00	A	7	8.00E+00	5.50E+00
TNT	0.00E+00	A	8	5.60E+00	4.20E+00
TNT	0.00E+00	A	9	1.39E+01	8.50E+00
TNT	0.00E+00	A	10	1.31E+01	3.80E+00
TNT	0.00E+00	B	1	1.16E+01	6.80E+00
TNT	0.00E+00	B	2	1.18E+01	3.20E+00
TNT	0.00E+00	B	3	1.70E+01	1.45E+01
TNT	0.00E+00	B	4	1.31E+01	6.90E+00
TNT	0.00E+00	B	5	1.72E+01	1.08E+01
TNT	0.00E+00	B	6	1.36E+01	5.90E+00
TNT	0.00E+00	B	7	1.07E+01	4.00E+00
TNT	0.00E+00	B	8	8.80E+00	3.60E+00
TNT	0.00E+00	B	9	1.29E+01	5.20E+00
TNT	0.00E+00	B	10	1.02E+01	4.40E+00
TNT	0.00E+00	C	1	1.54E+01	1.20E+01
TNT	0.00E+00	C	2	7.20E+00	4.90E+00
TNT	0.00E+00	C	3	9.80E+00	6.10E+00
TNT	0.00E+00	C	4	1.57E+01	1.26E+01
TNT	0.00E+00	C	5	4.20E+00	1.90E+00
TNT	0.00E+00	C	6	6.10E+00	7.90E+00
TNT	0.00E+00	C	7	4.20E+00	4.00E+00

TNT	0.00E+00	C	8	5.50E+00	3.00E+00
TNT	0.00E+00	C	9	8.30E+00	6.00E+00
TNT	0.00E+00	C	10	1.25E+01	1.35E+01
TNT	6.90E-01	A	1	1.74E+01	1.05E+01
TNT	6.90E-01	A	2	1.01E+01	5.50E+00
TNT	6.90E-01	A	3	1.32E+01	6.30E+00
TNT	6.90E-01	A	4	1.45E+01	7.60E+00
TNT	6.90E-01	A	5	1.46E+01	4.90E+00
TNT	6.90E-01	A	6	1.51E+01	7.40E+00
TNT	6.90E-01	A	7	1.51E+01	7.60E+00
TNT	6.90E-01	A	8	1.61E+01	6.40E+00
TNT	6.90E-01	A	9	1.41E+01	6.30E+00
TNT	6.90E-01	A	10	1.52E+01	5.30E+00
TNT	6.90E-01	B	1	1.22E+01	5.10E+00
TNT	6.90E-01	B	2	1.46E+01	8.70E+00
TNT	6.90E-01	B	3	1.48E+01	1.20E+01
TNT	6.90E-01	B	4	1.61E+01	7.90E+00
TNT	6.90E-01	B	5	7.70E+00	4.30E+00
TNT	6.90E-01	B	6	1.53E+01	9.50E+00
TNT	6.90E-01	B	7	1.40E+01	7.60E+00
TNT	6.90E-01	B	8	1.54E+01	8.00E+00
TNT	6.90E-01	B	9	1.50E+01	7.40E+00
TNT	6.90E-01	B	10	1.54E+01	7.40E+00
TNT	6.90E-01	C	1	7.50E+00	7.00E+00
TNT	6.90E-01	C	2	6.30E+00	4.00E+00
TNT	6.90E-01	C	3	6.20E+00	7.50E+00
TNT	6.90E-01	C	4	6.50E+00	5.30E+00
TNT	6.90E-01	C	5	7.80E+00	6.20E+00
TNT	6.90E-01	C	6	7.90E+00	6.10E+00
TNT	6.90E-01	C	7	8.10E+00	5.20E+00
TNT	6.90E-01	C	8	7.00E+00	2.70E+00
TNT	6.90E-01	C	9	9.90E+00	3.90E+00

TNT	6.90E-01	C	10	1.16E+01	5.30E+00
TNT	7.54E+00	A	1	1.32E+01	1.04E+01
TNT	7.54E+00	A	2	1.72E+01	9.90E+00
TNT	7.54E+00	A	3	1.03E+01	6.60E+00
TNT	7.54E+00	A	4	1.21E+01	7.90E+00
TNT	7.54E+00	A	5	1.36E+01	7.00E+00
TNT	7.54E+00	A	6	1.01E+01	5.50E+00
TNT	7.54E+00	A	7	1.41E+01	8.00E+00
TNT	7.54E+00	A	8	9.60E+00	4.60E+00
TNT	7.54E+00	A	9	1.47E+01	7.70E+00
TNT	7.54E+00	A	10	1.44E+01	7.30E+00
TNT	7.54E+00	B	1	1.36E+01	5.40E+00
TNT	7.54E+00	B	2	1.04E+01	6.50E+00
TNT	7.54E+00	B	3	1.60E+01	4.50E+00
TNT	7.54E+00	B	4	1.02E+01	2.70E+00
TNT	7.54E+00	B	5	1.01E+01	4.40E+00
TNT	7.54E+00	B	6	1.34E+01	7.60E+00
TNT	7.54E+00	B	7	1.02E+01	5.90E+00
TNT	7.54E+00	B	8	1.44E+01	6.00E+00
TNT	7.54E+00	B	9	8.00E+00	4.10E+00
TNT	7.54E+00	B	10	9.60E+00	5.60E+00
TNT	7.54E+00	C	1	8.30E+00	3.50E+00
TNT	7.54E+00	C	2	6.00E+00	1.40E+00
TNT	7.54E+00	C	3	5.50E+00	1.30E+00
TNT	7.54E+00	C	4	4.60E+00	3.00E+00
TNT	7.54E+00	C	5	5.50E+00	4.10E+00
TNT	7.54E+00	C	6	8.50E+00	2.30E+00
TNT	7.54E+00	C	7	5.20E+00	2.80E+00
TNT	7.54E+00	C	8	7.80E+00	2.20E+00
TNT	7.54E+00	C	9	6.80E+00	3.50E+00
TNT	7.54E+00	C	10	9.20E+00	3.40E+00
TNT	3.87E+01	A	1	8.20E+00	7.00E+00

TNT	3.87E+01	A	2	1.54E+01	7.00E+00
TNT	3.87E+01	A	3	9.50E+00	6.10E+00
TNT	3.87E+01	A	4	1.04E+01	4.60E+00
TNT	3.87E+01	A	5	1.09E+01	6.50E+00
TNT	3.87E+01	A	6	9.10E+00	7.60E+00
TNT	3.87E+01	A	7	1.11E+01	6.80E+00
TNT	3.87E+01	A	8	1.12E+01	6.50E+00
TNT	3.87E+01	A	9	1.19E+01	5.80E+00
TNT	3.87E+01	A	10	1.55E+01	6.00E+00
TNT	3.87E+01	B	1	5.50E+00	4.90E+00
TNT	3.87E+01	B	2	5.80E+00	6.10E+00
TNT	3.87E+01	B	3	6.10E+00	3.50E+00
TNT	3.87E+01	B	4	6.50E+00	2.50E+00
TNT	3.87E+01	B	5	1.00E+01	4.40E+00
TNT	3.87E+01	B	6	8.70E+00	5.20E+00
TNT	3.87E+01	B	7	8.70E+00	3.10E+00
TNT	3.87E+01	B	8	1.28E+01	3.30E+00
TNT	3.87E+01	B	9	7.50E+00	4.40E+00
TNT	3.87E+01	B	10	1.16E+01	4.50E+00
TNT	3.87E+01	C	1	7.50E+00	4.50E+00
TNT	3.87E+01	C	2	5.40E+00	5.20E+00
TNT	3.87E+01	C	3	4.40E+00	3.90E+00
TNT	3.87E+01	C	4	5.10E+00	3.00E+00
TNT	3.87E+01	C	5	7.20E+00	4.10E+00
TNT	3.87E+01	C	6	6.30E+00	3.70E+00
TNT	3.87E+01	C	7	8.00E+00	7.00E+00
TNT	3.87E+01	C	8	6.10E+00	5.00E+00
TNT	3.87E+01	C	9	1.23E+01	7.10E+00
TNT	3.87E+01	C	10	6.10E+00	6.90E+00
TNT	7.47E+01	A	1	8.70E+00	5.10E+00
TNT	7.47E+01	A	2	9.50E+00	6.20E+00
TNT	7.47E+01	A	3	1.23E+01	8.00E+00

TNT	7.47E+01	A	4	1.17E+01	7.90E+00
TNT	7.47E+01	A	5	8.80E+00	6.10E+00
TNT	7.47E+01	A	6	1.17E+01	1.00E+01
TNT	7.47E+01	A	7	9.50E+00	4.90E+00
TNT	7.47E+01	A	8	1.18E+01	7.90E+00
TNT	7.47E+01	A	9	1.40E+01	1.01E+01
TNT	7.47E+01	A	10	1.16E+01	5.30E+00
TNT	7.47E+01	B	1	7.10E+00	4.00E+00
TNT	7.47E+01	B	2	4.80E+00	1.50E+00
TNT	7.47E+01	B	3	6.60E+00	3.20E+00
TNT	7.47E+01	B	4	4.30E+00	1.50E+00
TNT	7.47E+01	B	5	4.40E+00	2.10E+00
TNT	7.47E+01	B	6	6.40E+00	2.20E+00
TNT	7.47E+01	B	7	7.90E+00	2.00E+00
TNT	7.47E+01	B	8	6.10E+00	1.40E+00
TNT	7.47E+01	B	9	6.20E+00	2.30E+00
TNT	7.47E+01	B	10	6.70E+00	5.60E+00
TNT	7.47E+01	C	1	4.90E+00	3.40E+00
TNT	7.47E+01	C	2	9.20E+00	5.40E+00
TNT	7.47E+01	C	3	5.70E+00	4.30E+00
TNT	7.47E+01	C	4	8.60E+00	3.50E+00
TNT	7.47E+01	C	5	7.50E+00	5.50E+00
TNT	7.47E+01	C	6	4.70E+00	1.90E+00
TNT	7.47E+01	C	7	6.50E+00	5.00E+00
TNT	7.47E+01	C	8	5.40E+00	2.10E+00
TNT	7.47E+01	C	9	5.20E+00	1.50E+00
TNT	7.47E+01	C	10	6.00E+00	2.00E+00
2,4-DNT	0.00E+00	A	1	1.40E+01	9.10E+00
2,4-DNT	0.00E+00	A	2	9.80E+00	1.12E+01
2,4-DNT	0.00E+00	A	3	1.12E+01	3.70E+00
2,4-DNT	0.00E+00	A	4	1.47E+01	1.16E+01
2,4-DNT	0.00E+00	A	5	9.90E+00	5.50E+00

2,4-DNT	0.00E+00	A	6	1.35E+01	5.70E+00
2,4-DNT	0.00E+00	A	7	7.40E+00	3.70E+00
2,4-DNT	0.00E+00	A	8	1.40E+01	1.17E+01
2,4-DNT	0.00E+00	A	9	1.40E+01	1.40E+01
2,4-DNT	0.00E+00	A	10	1.18E+01	6.50E+00
2,4-DNT	0.00E+00	B	1	1.22E+01	1.22E+01
2,4-DNT	0.00E+00	B	2	1.31E+01	5.50E+00
2,4-DNT	0.00E+00	B	3	1.15E+01	9.00E+00
2,4-DNT	0.00E+00	B	4	1.09E+01	1.19E+01
2,4-DNT	0.00E+00	B	5	9.00E+00	1.05E+01
2,4-DNT	0.00E+00	B	6	8.60E+00	2.90E+00
2,4-DNT	0.00E+00	B	7	8.00E+00	6.00E+00
2,4-DNT	0.00E+00	B	8	1.27E+01	7.20E+00
2,4-DNT	0.00E+00	B	9	1.05E+01	5.60E+00
2,4-DNT	0.00E+00	B	10	1.55E+01	9.00E+00
2,4-DNT	1.06E+00	A	1	1.00E+01	2.50E+00
2,4-DNT	1.06E+00	A	2	6.20E+00	2.50E+00
2,4-DNT	1.06E+00	A	3	1.02E+01	9.00E+00
2,4-DNT	1.06E+00	A	4	9.20E+00	1.50E+00
2,4-DNT	1.06E+00	A	5	3.90E+00	6.10E+00
2,4-DNT	1.06E+00	A	6	1.46E+01	3.40E+00
2,4-DNT	1.06E+00	A	7	1.75E+01	1.40E+01
2,4-DNT	1.06E+00	A	8	1.21E+01	1.13E+01
2,4-DNT	1.06E+00	A	9	1.71E+01	1.40E+01
2,4-DNT	1.06E+00	A	10	5.30E+00	4.40E+00
2,4-DNT	1.06E+00	B	1	1.30E+01	8.50E+00
2,4-DNT	1.06E+00	B	2	6.50E+00	3.20E+00
2,4-DNT	1.06E+00	B	3	4.70E+00	6.60E+00
2,4-DNT	1.06E+00	B	4	3.10E+00	4.00E+00
2,4-DNT	1.06E+00	B	5	1.00E+01	7.20E+00
2,4-DNT	1.06E+00	B	6	1.11E+01	5.00E+00
2,4-DNT	1.06E+00	B	7	7.10E+00	3.10E+00

2,4-DNT	1.06E+00	B	8	1.34E+01	1.00E+01
2,4-DNT	1.06E+00	B	9	5.10E+00	2.50E+00
2,4-DNT	1.06E+00	B	10	7.10E+00	4.50E+00
2,4-DNT	1.13E+01	A	1	1.51E+01	1.21E+01
2,4-DNT	1.13E+01	A	2	1.30E+01	1.00E+01
2,4-DNT	1.13E+01	A	3	9.80E+00	7.60E+00
2,4-DNT	1.13E+01	A	4	9.40E+00	1.03E+01
2,4-DNT	1.13E+01	A	5	1.43E+01	1.30E+01
2,4-DNT	1.13E+01	A	6	1.23E+01	2.20E+00
2,4-DNT	1.13E+01	A	7	1.54E+01	1.23E+01
2,4-DNT	1.13E+01	A	8	8.80E+00	2.10E+00
2,4-DNT	1.13E+01	A	9	8.80E+00	4.70E+00
2,4-DNT	1.13E+01	A	10	7.90E+00	7.00E+00
2,4-DNT	1.13E+01	B	1	1.00E+01	1.02E+01
2,4-DNT	1.13E+01	B	2	6.80E+00	2.10E+00
2,4-DNT	1.13E+01	B	3	1.10E+01	6.40E+00
2,4-DNT	1.13E+01	B	4	6.00E+00	3.10E+00
2,4-DNT	1.13E+01	B	5	8.10E+00	3.80E+00
2,4-DNT	1.13E+01	B	6	8.70E+00	7.50E+00
2,4-DNT	1.13E+01	B	7	1.00E+01	7.60E+00
2,4-DNT	1.13E+01	B	8	1.21E+01	9.50E+00
2,4-DNT	1.13E+01	B	9	1.18E+01	3.40E+00
2,4-DNT	1.13E+01	B	10	8.60E+00	1.13E+01
2,4-DNT	5.83E+01	A	1	8.70E+00	8.00E+00
2,4-DNT	5.83E+01	A	2	1.50E+01	1.45E+01
2,4-DNT	5.83E+01	A	3	8.90E+00	4.50E+00
2,4-DNT	5.83E+01	A	4	1.02E+01	1.02E+01
2,4-DNT	5.83E+01	A	5	8.60E+00	4.90E+00
2,4-DNT	5.83E+01	A	6	6.00E+00	2.00E+00
2,4-DNT	5.83E+01	A	7	1.07E+01	4.10E+00
2,4-DNT	5.83E+01	A	8	1.30E+01	1.20E+01
2,4-DNT	5.83E+01	A	9	6.60E+00	3.80E+00

2,4-DNT	5.83E+01	A	10	1.06E+01	5.60E+00
2,4-DNT	5.83E+01	B	1	5.80E+00	1.90E+00
2,4-DNT	5.83E+01	B	2	7.30E+00	5.20E+00
2,4-DNT	5.83E+01	B	3	7.90E+00	7.20E+00
2,4-DNT	5.83E+01	B	4	1.04E+01	1.03E+01
2,4-DNT	5.83E+01	B	5	8.90E+00	1.00E+01
2,4-DNT	5.83E+01	B	6	6.00E+00	2.00E+00
2,4-DNT	5.83E+01	B	7	6.70E+00	8.50E+00
2,4-DNT	5.83E+01	B	8	1.24E+01	1.07E+01
2,4-DNT	5.83E+01	B	9	7.70E+00	6.00E+00
2,4-DNT	5.83E+01	B	10	8.40E+00	4.50E+00
2,4-DNT	1.09E+02	A	1	6.90E+00	4.00E+00
2,4-DNT	1.09E+02	A	2	1.12E+01	1.20E+01
2,4-DNT	1.09E+02	A	3	7.00E+00	1.02E+01
2,4-DNT	1.09E+02	A	4	1.33E+01	8.30E+00
2,4-DNT	1.09E+02	A	5	1.13E+01	9.60E+00
2,4-DNT	1.09E+02	A	6	1.19E+01	9.30E+00
2,4-DNT	1.09E+02	A	7	8.10E+00	6.00E+00
2,4-DNT	1.09E+02	A	8	1.26E+01	9.40E+00
2,4-DNT	1.09E+02	A	9	7.70E+00	1.01E+01
2,4-DNT	1.09E+02	A	10	1.00E+01	6.20E+00
2,4-DNT	1.09E+02	B	1	7.80E+00	6.20E+00
2,4-DNT	1.09E+02	B	2	1.72E+01	1.32E+01
2,4-DNT	1.09E+02	B	3	1.21E+01	3.10E+00
2,4-DNT	1.09E+02	B	4	1.05E+01	9.00E+00
2,4-DNT	1.09E+02	B	5	9.40E+00	7.00E+00
2,4-DNT	1.09E+02	B	6	5.40E+00	1.90E+00
2,4-DNT	1.09E+02	B	7	5.40E+00	4.10E+00
2,4-DNT	1.09E+02	B	8	7.50E+00	5.30E+00
2,4-DNT	1.09E+02	B	9	6.30E+00	6.10E+00
2,4-DNT	1.09E+02	B	10	8.90E+00	2.70E+00
2,4-DNAN	0.00E+00	A	1	1.70E+01	1.50E+01

2,4-DNAN	0.00E+00	A	2	1.47E+01	1.30E+01
2,4-DNAN	0.00E+00	A	3	1.32E+01	1.25E+01
2,4-DNAN	0.00E+00	A	4	1.90E+01	1.54E+01
2,4-DNAN	0.00E+00	A	5	1.77E+01	1.60E+01
2,4-DNAN	0.00E+00	A	6	1.15E+01	1.79E+01
2,4-DNAN	0.00E+00	A	7	1.43E+01	1.20E+01
2,4-DNAN	0.00E+00	A	8	1.11E+01	1.14E+01
2,4-DNAN	0.00E+00	A	9	1.62E+01	1.45E+01
2,4-DNAN	0.00E+00	A	10	1.43E+01	1.80E+01
2,4-DNAN	0.00E+00	A	11	1.31E+01	1.16E+01
2,4-DNAN	0.00E+00	A	12	1.65E+01	1.58E+01
2,4-DNAN	0.00E+00	A	13	1.65E+01	1.44E+01
2,4-DNAN	0.00E+00	A	14	1.60E+01	1.71E+01
2,4-DNAN	0.00E+00	A ^c	15	1.57E+01	1.00E+01
2,4-DNAN	8.60E-01	A	1	9.50E+00	5.70E+00
2,4-DNAN	8.60E-01	A	2	1.03E+01	1.10E+01
2,4-DNAN	8.60E-01	A	3	1.27E+01	9.70E+00
2,4-DNAN	8.60E-01	A	4	1.54E+01	1.31E+01
2,4-DNAN	8.60E-01	A	5	1.70E+01	8.00E+00
2,4-DNAN	8.60E-01	A	6	2.08E+01	5.30E+00
2,4-DNAN	8.60E-01	A	7	1.70E+01	1.20E+01
2,4-DNAN	8.60E-01	A	8	1.77E+01	1.24E+01
2,4-DNAN	8.60E-01	A	9	1.70E+01	1.31E+01
2,4-DNAN	8.60E-01	A	10	1.30E+01	1.03E+01
2,4-DNAN	8.60E-01	A	11	1.53E+01	1.22E+01
2,4-DNAN	8.60E-01	A	12	1.55E+01	1.45E+01
2,4-DNAN	8.60E-01	A	13	1.40E+01	1.20E+01
2,4-DNAN	8.60E-01	A	14	1.55E+01	1.32E+01
2,4-DNAN	8.60E-01	A	15	1.10E+01	9.65E+00
2,4-DNAN	8.60E-01	B	1	1.01E+01	1.18E+01
2,4-DNAN	8.60E-01	B	2	1.46E+01	1.37E+01
2,4-DNAN	8.60E-01	B	3	1.56E+01	1.43E+01

2,4-DNAN	8.60E-01	B	4	1.86E+01	1.18E+01
2,4-DNAN	8.60E-01	B	5	6.90E+00	1.10E+01
2,4-DNAN	8.60E-01	B	6	1.43E+01	1.45E+01
2,4-DNAN	8.60E-01	B	7	1.06E+01	1.10E+01
2,4-DNAN	8.60E-01	B	8	1.96E+01	1.30E+01
2,4-DNAN	8.60E-01	B	9	1.44E+01	1.60E+01
2,4-DNAN	8.60E-01	B	10	1.10E+01	1.05E+01
2,4-DNAN	8.60E-01	B	11	1.57E+01	1.04E+01
2,4-DNAN	8.60E-01	B	12	1.90E+01	1.15E+01
2,4-DNAN	8.60E-01	B	13	1.46E+01	1.00E+01
2,4-DNAN	8.60E-01	B	14	1.50E+01	1.35E+01
2,4-DNAN	8.60E-01	B	15	1.54E+01	9.00E+00
2,4-DNAN	8.60E-01	C	1	8.00E+00	8.20E+00
2,4-DNAN	8.60E-01	C	2	1.83E+01	8.00E+00
2,4-DNAN	8.60E-01	C	3	1.77E+01	1.02E+01
2,4-DNAN	8.60E-01	C	4	1.73E+01	1.30E+01
2,4-DNAN	8.60E-01	C	5	1.43E+01	1.30E+01
2,4-DNAN	8.60E-01	C	6	1.60E+01	1.10E+01
2,4-DNAN	8.60E-01	C	7	2.08E+01	1.70E+01
2,4-DNAN	8.60E-01	C	8	1.75E+01	7.00E+00
2,4-DNAN	8.60E-01	C	9	1.45E+01	1.05E+01
2,4-DNAN	8.60E-01	C	10	1.66E+01	9.60E+00
2,4-DNAN	8.60E-01	C	11	1.50E+01	6.70E+00
2,4-DNAN	8.60E-01	C	12	1.63E+01	1.00E+01
2,4-DNAN	8.60E-01	C	13	1.96E+01	1.05E+01
2,4-DNAN	8.60E-01	C	14	1.02E+01	1.15E+01
2,4-DNAN	8.60E-01	C	15	1.40E+01	1.11E+01
2,4-DNAN	8.67E+00	A	1	1.22E+01	7.50E+00
2,4-DNAN	8.67E+00	A	2	1.70E+01	5.20E+00
2,4-DNAN	8.67E+00	A	3	1.39E+01	5.10E+00
2,4-DNAN	8.67E+00	A	4	8.50E+00	3.40E+00
2,4-DNAN	8.67E+00	A	5	1.27E+01	4.80E+00

2,4-DNAN	8.67E+00	A	6	1.30E+01	4.00E+00
2,4-DNAN	8.67E+00	A	7	1.42E+01	8.50E+00
2,4-DNAN	8.67E+00	A	8	1.20E+01	3.40E+00
2,4-DNAN	8.67E+00	A	9	1.37E+01	1.00E+01
2,4-DNAN	8.67E+00	A	10	1.80E+01	8.20E+00
2,4-DNAN	8.67E+00	A	11	1.30E+01	2.80E+00
2,4-DNAN	8.67E+00	A	12	1.20E+01	2.80E+00
2,4-DNAN	8.67E+00	A	13	1.63E+01	7.40E+00
2,4-DNAN	8.67E+00	A	14	1.40E+01	2.50E+00
2,4-DNAN	8.67E+00	A	15	1.30E+01	4.40E+00
2,4-DNAN	8.67E+00	B	1	1.40E+01	8.20E+00
2,4-DNAN	8.67E+00	B	2	1.27E+01	1.17E+01
2,4-DNAN	8.67E+00	B	3	1.64E+01	7.30E+00
2,4-DNAN	8.67E+00	B	4	1.50E+01	9.50E+00
2,4-DNAN	8.67E+00	B	5	1.72E+01	1.10E+01
2,4-DNAN	8.67E+00	B	6	1.76E+01	8.60E+00
2,4-DNAN	8.67E+00	B	7	1.42E+01	1.01E+01
2,4-DNAN	8.67E+00	B	8	1.16E+01	7.90E+00
2,4-DNAN	8.67E+00	B	9	1.41E+01	9.30E+00
2,4-DNAN	8.67E+00	B	10	1.24E+01	1.13E+01
2,4-DNAN	8.67E+00	B	11	1.17E+01	7.00E+00
2,4-DNAN	8.67E+00	B	12	1.17E+01	1.17E+01
2,4-DNAN	8.67E+00	B	13	1.70E+01	1.35E+01
2,4-DNAN	8.67E+00	B	14	1.35E+01	3.00E+00
2,4-DNAN	8.67E+00	C	1	1.10E+01	7.50E+00
2,4-DNAN	8.67E+00	C	2	1.73E+01	5.10E+00
2,4-DNAN	8.67E+00	C	3	9.00E+00	8.10E+00
2,4-DNAN	8.67E+00	C	4	1.70E+01	9.00E+00
2,4-DNAN	8.67E+00	C	5	1.23E+01	1.05E+01
2,4-DNAN	8.67E+00	C	6	1.76E+01	1.35E+01
2,4-DNAN	8.67E+00	C	7	1.25E+01	1.06E+01
2,4-DNAN	8.67E+00	C	8	1.34E+01	5.40E+00

2,4-DNAN	8.67E+00	C	9	1.32E+01	9.00E+00
2,4-DNAN	8.67E+00	C	10	1.85E+01	8.40E+00
2,4-DNAN	8.67E+00	C	11	1.40E+01	1.04E+01
2,4-DNAN	8.67E+00	C	12	1.31E+01	3.60E+00
2,4-DNAN	8.67E+00	C	13	1.60E+01	1.15E+01
2,4-DNAN	8.67E+00	C	14	1.55E+01	1.06E+01
2,4-DNAN	8.67E+00	C	15	1.74E+01	8.00E+00
2,4-DNAN	8.67E+00	C	16	1.32E+01	1.50E+01
2,4-DNAN	4.52E+01	A	1	1.01E+01	6.00E+00
2,4-DNAN	4.52E+01	A	2	6.50E+00	7.20E+00
2,4-DNAN	4.52E+01	A	3	1.10E+01	5.00E+00
2,4-DNAN	4.52E+01	A	4	1.16E+01	8.20E+00
2,4-DNAN	4.52E+01	A	5	1.20E+01	7.50E+00
2,4-DNAN	4.52E+01	A	6	9.50E+00	4.30E+00
2,4-DNAN	4.52E+01	A	7	8.50E+00	6.30E+00
2,4-DNAN	4.52E+01	A	8	9.50E+00	2.10E+00
2,4-DNAN	4.52E+01	A	9	1.10E+01	6.50E+00
2,4-DNAN	4.52E+01	A	10	1.14E+01	6.40E+00
2,4-DNAN	4.52E+01	A	11	1.20E+01	4.80E+00
2,4-DNAN	4.52E+01	A	12	8.40E+00	6.80E+00
2,4-DNAN	4.52E+01	A	13	1.07E+01	5.70E+00
2,4-DNAN	4.52E+01	A	14	7.00E+00	2.00E+00
2,4-DNAN	4.52E+01	A	15	1.02E+01	5.00E+00
2,4-DNAN	4.52E+01	B	1	5.70E+00	8.00E-01
2,4-DNAN	4.52E+01	B	2	9.10E+00	5.70E+00
2,4-DNAN	4.52E+01	B	3	6.00E+00	5.60E+00
2,4-DNAN	4.52E+01	B	4	8.50E+00	3.50E+00
2,4-DNAN	4.52E+01	B	5	1.14E+01	6.40E+00
2,4-DNAN	4.52E+01	B	6	1.03E+01	6.60E+00
2,4-DNAN	4.52E+01	B	7	1.05E+01	5.60E+00
2,4-DNAN	4.52E+01	B	8	6.50E+00	9.10E+00
2,4-DNAN	4.52E+01	B	9	9.20E+00	2.00E+00

2,4-DNAN	4.52E+01	B	10	9.60E+00	1.60E+00
2,4-DNAN	4.52E+01	B	11	8.90E+00	3.80E+00
2,4-DNAN	4.52E+01	B	12	1.15E+01	7.00E+00
2,4-DNAN	4.52E+01	B	13	1.05E+01	7.80E+00
2,4-DNAN	4.52E+01	B	14	7.90E+00	2.80E+00
2,4-DNAN	4.52E+01	B	15	9.80E+00	9.00E+00
2,4-DNAN	8.78E+01	A	1	3.20E+00	5.10E+00
2,4-DNAN	8.78E+01	A	2	6.60E+00	5.20E+00
2,4-DNAN	8.78E+01	A	3	7.20E+00	7.60E+00
2,4-DNAN	8.78E+01	A	4	7.00E+00	4.60E+00
2,4-DNAN	8.78E+01	A	5	8.50E+00	1.50E+00
2,4-DNAN	8.78E+01	A	6	4.90E+00	2.40E+00
2,4-DNAN	8.78E+01	A	7	7.50E+00	6.00E+00
2,4-DNAN	8.78E+01	A	8	9.40E+00	3.50E+00
2,4-DNAN	8.78E+01	A	9	7.50E+00	4.50E+00
2,4-DNAN	8.78E+01	A	10	6.60E+00	4.50E+00
2,4-DNAN	8.78E+01	A	11	9.50E+00	5.20E+00
2,4-DNAN	8.78E+01	A	12	8.30E+00	6.00E+00
2,4-DNAN	8.78E+01	A	13	9.60E+00	5.00E+00
2,4-DNAN	8.78E+01	A	14	4.90E+00	3.60E+00
2,4-DNAN	8.78E+01	B	1	4.00E+00	5.20E+00
2,4-DNAN	8.78E+01	B	2	7.50E+00	5.60E+00
2,4-DNAN	8.78E+01	B	3	7.90E+00	3.20E+00
2,4-DNAN	8.78E+01	B	4	7.60E+00	6.00E+00
2,4-DNAN	8.78E+01	B	5	7.50E+00	2.10E+00
2,4-DNAN	8.78E+01	B	6	7.90E+00	6.00E+00
2,4-DNAN	8.78E+01	B	7	5.00E+00	3.50E+00
2,4-DNAN	8.78E+01	B	8	8.20E+00	2.10E+00
2,4-DNAN	8.78E+01	B	9	5.50E+00	5.50E+00
2,4-DNAN	8.78E+01	B	10	5.10E+00	4.20E+00
2,4-DNAN	8.78E+01	B	11	7.20E+00	5.40E+00
2,4-DNAN	8.78E+01	B	12	5.20E+00	8.60E+00

2,4-DNAN	8.78E+01	B	13	7.10E+00	3.00E+00
2,4-DNAN	8.78E+01	B	14	5.30E+00	6.20E+00
2,4-DNAN	8.78E+01	B	15	NR ^b	4.20E+00
2,4-DNAN	8.78E+01	C	1	4.20E+00	2.60E+00
2,4-DNAN	8.78E+01	C	2	6.50E+00	6.00E+00
2,4-DNAN	8.78E+01	C	3	6.50E+00	7.00E+00
2,4-DNAN	8.78E+01	C	4	6.40E+00	2.70E+00
2,4-DNAN	8.78E+01	C	5	4.10E+00	1.30E+00
2,4-DNAN	8.78E+01	C	6	6.20E+00	2.50E+00
2,4-DNAN	8.78E+01	C	7	7.90E+00	3.60E+00
2,4-DNAN	8.78E+01	C	8	7.00E+00	2.90E+00
2,4-DNAN	8.78E+01	C	9	6.20E+00	7.50E+00
2,4-DNAN	8.78E+01	C	10	7.80E+00	6.80E+00
2,4-DNAN	8.78E+01	C	11	7.00E+00	5.30E+00
2,4-DNAN	8.78E+01	C	12	7.30E+00	4.70E+00
2,4-DNAN	8.78E+01	C	13	6.20E+00	5.20E+00
2,4-DNAN	8.78E+01	C	14	9.30E+00	7.10E+00
2,4-DNAN	8.78E+01	C	15	9.40E+00	8.10E+00
<hr/>					
4-NAN	0.00E+00	A	1	1.60E+01	9.40E+00
4-NAN	0.00E+00	A	2	1.65E+01	5.20E+00
4-NAN	0.00E+00	A	3	1.47E+01	1.02E+01
4-NAN	0.00E+00	A	4	1.55E+01	1.30E+01
4-NAN	0.00E+00	A	5	1.40E+01	9.50E+00
4-NAN	0.00E+00	A	6	1.47E+01	8.50E+00
4-NAN	0.00E+00	A	7	1.60E+01	1.65E+01
4-NAN	0.00E+00	A	8	1.30E+01	8.00E+00
4-NAN	0.00E+00	A	9	1.30E+01	1.23E+01
4-NAN	0.00E+00	A	10	1.95E+01	1.33E+01
4-NAN	0.00E+00	A	11	1.60E+01	1.05E+01
4-NAN	0.00E+00	A	12	1.70E+01	1.75E+01
4-NAN	0.00E+00	A	13	1.77E+01	1.05E+01
4-NAN	0.00E+00	A	14	1.60E+01	1.10E+01

4-NAN	0.00E+00	A	15	1.44E+01	1.05E+01
4-NAN	0.00E+00	A	16	1.75E+01	1.20E+01
4-NAN	0.00E+00	A	17	1.75E+01	1.00E+01
4-NAN	0.00E+00	A	18	1.37E+01	8.50E+00
4-NAN	0.00E+00	A	19	1.13E+01	9.30E+00
4-NAN	0.00E+00	A	20	6.70E+00	1.45E+01
4-NAN	0.00E+00	B	1	1.76E+01	8.00E+00
4-NAN	0.00E+00	B	2	1.41E+01	9.50E+00
4-NAN	0.00E+00	B	3	1.90E+01	9.20E+00
4-NAN	0.00E+00	B	4	1.70E+01	1.00E+01
4-NAN	0.00E+00	B	5	1.55E+01	7.00E+00
4-NAN	0.00E+00	B	6	1.95E+01	1.35E+01
4-NAN	0.00E+00	B	7	1.40E+01	8.00E+00
4-NAN	0.00E+00	B	8	1.85E+01	1.00E+01
4-NAN	0.00E+00	B	9	1.20E+01	9.00E+00
4-NAN	0.00E+00	B	10	1.42E+01	9.00E+00
4-NAN	0.00E+00	B	11	1.55E+01	1.00E+01
4-NAN	0.00E+00	B	12	1.60E+01	1.45E+01
4-NAN	0.00E+00	B	13	1.20E+01	1.00E+01
4-NAN	0.00E+00	B	14	1.48E+01	7.50E+00
4-NAN	0.00E+00	B	15	1.60E+01	8.00E+00
4-NAN	0.00E+00	B	16	1.50E+01	1.10E+01
4-NAN	0.00E+00	B	17	3.00E+00	1.50E+00
4-NAN	1.11E+00	A	1	1.70E+01	1.00E+01
4-NAN	1.11E+00	A	2	1.80E+01	1.06E+01
4-NAN	1.11E+00	A	3	1.25E+01	9.00E+00
4-NAN	1.11E+00	A	4	1.55E+01	1.20E+01
4-NAN	1.11E+00	A	5	1.50E+01	1.06E+01
4-NAN	1.11E+00	A	6	1.91E+01	9.00E+00
4-NAN	1.11E+00	A	7	1.57E+01	1.05E+01
4-NAN	1.11E+00	A	8	1.50E+01	1.05E+01
4-NAN	1.11E+00	A	9	1.80E+01	1.04E+01

4-NAN	1.11E+00	A	10	1.55E+01	1.15E+01
4-NAN	1.11E+00	A	11	1.63E+01	1.20E+01
4-NAN	1.11E+00	A	12	1.45E+01	1.06E+01
4-NAN	1.11E+00	A	13	1.61E+01	9.50E+00
4-NAN	1.11E+00	A	14	1.80E+01	1.05E+01
4-NAN	1.11E+00	A	15	1.90E+01	1.00E+01
4-NAN	1.11E+00	A	16	1.95E+01	1.15E+01
4-NAN	1.11E+00	A	17	1.90E+01	1.10E+01
4-NAN	1.11E+00	A	18	1.72E+01	9.50E+00
4-NAN	1.11E+00	A	19	1.67E+01	1.03E+01
4-NAN	1.11E+00	A	20	1.76E+01	1.00E+01
4-NAN	1.11E+00	B	1	1.30E+01	1.08E+01
4-NAN	1.11E+00	B	2	1.73E+01	1.53E+01
4-NAN	1.11E+00	B	3	1.20E+01	1.00E+01
4-NAN	1.11E+00	B	4	8.80E+00	1.00E+00
4-NAN	1.11E+00	B	5	1.85E+01	1.13E+01
4-NAN	1.11E+00	B	6	1.78E+01	8.50E+00
4-NAN	1.11E+00	B	7	1.20E+01	1.10E+01
4-NAN	1.11E+00	B	8	1.52E+01	1.37E+01
4-NAN	1.11E+00	B	9	1.65E+01	1.15E+01
4-NAN	1.11E+00	B	10	1.42E+01	9.00E+00
4-NAN	1.11E+00	B	11	1.45E+01	7.20E+00
4-NAN	1.11E+00	B	12	1.80E+01	1.00E+01
4-NAN	1.11E+00	B	13	1.84E+01	1.00E+01
4-NAN	1.11E+00	B	14	1.55E+01	1.04E+01
4-NAN	1.11E+00	B	15	1.51E+01	1.15E+01
4-NAN	1.11E+00	B	16	1.26E+01	1.14E+01
4-NAN	1.11E+00	B	17	4.50E+00	NR
4-NAN	1.11E+00	B	18	1.41E+01	1.10E+01
4-NAN	1.11E+00	C	1	1.60E+01	8.30E+00
4-NAN	1.11E+00	C	2	2.00E+01	1.35E+01
4-NAN	1.11E+00	C	3	1.35E+01	1.20E+01

4-NAN	1.11E+00	C	4	1.55E+01	1.00E+01
4-NAN	1.11E+00	C	5	1.55E+01	1.30E+01
4-NAN	1.11E+00	C	6	1.72E+01	1.03E+01
4-NAN	1.11E+00	C	7	1.23E+01	9.80E+00
4-NAN	1.11E+00	C	8	1.15E+01	1.01E+01
4-NAN	1.11E+00	C	9	1.53E+01	9.00E+00
4-NAN	1.11E+00	C	10	1.75E+01	1.00E+01
4-NAN	1.11E+00	C	11	1.23E+01	1.20E+01
4-NAN	1.11E+00	C	12	1.45E+01	1.38E+01
4-NAN	1.11E+00	C	13	1.62E+01	1.05E+01
4-NAN	1.11E+00	C	14	1.48E+01	9.30E+00
4-NAN	1.11E+00	C	15	1.30E+01	7.70E+00
4-NAN	1.11E+00	C	16	1.02E+01	1.25E+01
4-NAN	1.11E+00	C	17	1.25E+01	4.00E+00
4-NAN	1.11E+00	C	18	1.13E+01	9.00E+00
4-NAN	1.11E+00	C	19	1.50E+01	9.70E+00
4-NAN	1.11E+00	C	20	1.20E+01	9.00E+00
4-NAN	9.97E+00	A	1	1.90E+01	1.00E+01
4-NAN	9.97E+00	A	2	1.55E+01	1.00E+01
4-NAN	9.97E+00	A	3	1.35E+01	1.00E+01
4-NAN	9.97E+00	A	4	1.37E+01	7.00E+00
4-NAN	9.97E+00	A	5	1.30E+01	5.50E+00
4-NAN	9.97E+00	A	6	1.45E+01	1.00E+01
4-NAN	9.97E+00	A	7	1.58E+01	8.80E+00
4-NAN	9.97E+00	A	8	9.80E+00	1.14E+01
4-NAN	9.97E+00	A	9	1.80E+01	1.15E+01
4-NAN	9.97E+00	A	10	6.60E+00	7.60E+00
4-NAN	9.97E+00	A	11	1.35E+01	8.00E+00
4-NAN	9.97E+00	A	12	7.50E+00	2.50E+00
4-NAN	9.97E+00	A	13	1.67E+01	1.25E+01
4-NAN	9.97E+00	A	14	9.50E+00	8.00E+00
4-NAN	9.97E+00	A	15	1.80E+01	9.00E+00

4-NAN	9.97E+00	A	16	1.80E+01	8.80E+00
4-NAN	9.97E+00	A	17	1.85E+01	8.20E+00
4-NAN	9.97E+00	A	18	1.47E+01	1.05E+01
4-NAN	9.97E+00	A ^c	19	1.60E+01	7.00E+00
4-NAN	4.84E+01	A	1	5.30E+00	2.50E+00
4-NAN	4.84E+01	A	2	8.50E+00	1.70E+00
4-NAN	4.84E+01	A	3	1.60E+01	6.00E+00
4-NAN	4.84E+01	A	4	1.63E+01	7.00E+00
4-NAN	4.84E+01	A	5	6.80E+00	2.00E+00
4-NAN	4.84E+01	A	6	1.57E+01	3.80E+00
4-NAN	4.84E+01	A	7	1.60E+01	9.70E+00
4-NAN	4.84E+01	A	8	1.48E+01	3.00E+00
4-NAN	4.84E+01	A	9	1.20E+01	3.50E+00
4-NAN	4.84E+01	A	10	1.50E+01	7.70E+00
4-NAN	4.84E+01	A	11	9.70E+00	1.80E+00
4-NAN	4.84E+01	A	12	8.50E+00	2.00E+00
4-NAN	4.84E+01	A	13	1.45E+01	7.00E+00
4-NAN	4.84E+01	A	14	9.20E+00	5.50E+00
4-NAN	4.84E+01	A	15	4.00E+00	7.30E+00
4-NAN	4.84E+01	A	16	1.57E+01	4.00E+00
4-NAN	4.84E+01	A	17	2.30E+00	NR
4-NAN	4.84E+01	B	1	1.26E+01	3.00E+00
4-NAN	4.84E+01	B	2	7.00E+00	2.50E+00
4-NAN	4.84E+01	B	3	1.32E+01	5.00E+00
4-NAN	4.84E+01	B	4	9.00E+00	5.00E+00
4-NAN	4.84E+01	B	5	9.00E+00	3.50E+00
4-NAN	4.84E+01	B	6	1.10E+01	5.50E+00
4-NAN	4.84E+01	B	7	1.19E+01	6.00E+00
4-NAN	4.84E+01	B	8	1.20E+01	4.30E+00
4-NAN	4.84E+01	B	9	1.35E+01	7.00E+00
4-NAN	4.84E+01	B	10	8.80E+00	2.00E+00
4-NAN	4.84E+01	B	11	1.45E+01	4.00E+00

4-NAN	4.84E+01	B	12	5.80E+00	NR
4-NAN	4.84E+01	B	13	1.22E+01	6.50E+00
4-NAN	4.84E+01	B	14	1.20E+01	5.00E+00
4-NAN	4.84E+01	B	15	8.40E+00	2.00E+00
4-NAN	4.84E+01	B	16	7.00E+00	3.00E+00
4-NAN	4.84E+01	B	17	4.00E+00	8.00E-01
4-NAN	8.43E+01	A	1	2.70E+00	8.00E-01
4-NAN	8.43E+01	A	2	8.00E+00	2.00E+00
4-NAN	8.43E+01	A	3	6.50E+00	5.00E+00
4-NAN	8.43E+01	A	4	8.00E+00	5.50E+00
4-NAN	8.43E+01	A	5	5.80E+00	2.00E+00
4-NAN	8.43E+01	A	6	4.00E+00	1.00E+00
4-NAN	8.43E+01	A	7	NR	3.20E+00
4-NAN	8.43E+01	A	8	7.00E+00	3.30E+00
4-NAN	8.43E+01	A	9	2.30E+00	7.00E-01
4-NAN	8.43E+01	A	10	7.50E+00	4.50E+00
4-NAN	8.43E+01	A	11	6.00E+00	2.00E+00
4-NAN	8.43E+01	A	12	2.00E+00	NR
4-NAN	8.43E+01	A	13	4.40E+00	NR
4-NAN	8.43E+01	B	1	5.50E+00	4.70E+00
4-NAN	8.43E+01	B	2	5.70E+00	5.20E+00
4-NAN	8.43E+01	B	3	6.80E+00	6.70E+00
4-NAN	8.43E+01	B	4	5.50E+00	2.10E+00
4-NAN	8.43E+01	B	5	7.00E+00	6.70E+00
4-NAN	8.43E+01	B	6	7.50E+00	1.00E+00
4-NAN	8.43E+01	B	7	5.00E+00	3.60E+00
4-NAN	8.43E+01	B	8	7.00E+00	4.30E+00
4-NAN	8.43E+01	B	9	7.00E+00	4.60E+00
4-NAN	8.43E+01	B	10	7.00E+00	4.80E+00
4-NAN	8.43E+01	B	11	5.70E+00	4.10E+00
4-NAN	8.43E+01	B	12	4.80E+00	1.40E+00
4-NAN	8.43E+01	B	13	8.00E+00	6.70E+00

4-NAN	8.43E+01	B	14	3.00E+00	4.00E-01
4-NAN	8.43E+01	B	15	5.80E+00	7.10E+00
4-NAN	8.43E+01	B	16	5.50E+00	5.80E+00
4-NAN	8.43E+01	B	17	3.00E+00	4.90E+00
4-NAN	8.43E+01	B	18	7.00E+00	9.60E+00
4-NAN	8.43E+01	C	1	5.50E+00	2.50E+00
4-NAN	8.43E+01	C	2	8.00E+00	3.50E+00
4-NAN	8.43E+01	C	3	7.00E+00	5.00E+00
4-NAN	8.43E+01	C	4	6.00E+00	6.50E+00
4-NAN	8.43E+01	C	5	5.50E+00	6.00E+00
4-NAN	8.43E+01	C	6	5.50E+00	5.00E+00
4-NAN	8.43E+01	C	7	7.00E+00	6.50E+00
4-NAN	8.43E+01	C	8	4.50E+00	5.50E+00
4-NAN	8.43E+01	C	9	2.50E+00	2.50E+00
4-NAN	8.43E+01	C	10	5.00E+00	5.00E+00
4-NAN	8.43E+01	C	11	6.00E+00	3.20E+00
4-NAN	8.43E+01	C	12	5.50E+00	5.00E+00
4-NAN	8.43E+01	C	13	6.10E+00	4.10E+00
4-NAN	8.43E+01	C	14	6.00E+00	3.80E+00
4-NAN	8.43E+01	C	15	4.00E+00	2.00E+00
4-NAN	8.43E+01	C	16	6.00E+00	2.00E+00
4-NAN	8.43E+01	C	17	4.20E+00	4.00E+00
4-NAN	8.43E+01	C	18	1.00E+00	5.00E-01
4-NAN	8.43E+01	C	19	6.50E+00	4.00E+00
<hr/>					
2-M-5-NPYNE	0.00E+00	A	1	1.35E+01	2.14E+01
2-M-5-NPYNE	0.00E+00	A	2	1.66E+01	1.30E+01
2-M-5-NPYNE	0.00E+00	A	3	1.82E+01	2.10E+01
2-M-5-NPYNE	0.00E+00	A	4	1.32E+01	1.80E+01
2-M-5-NPYNE	0.00E+00	A	5	1.01E+01	1.20E+01
2-M-5-NPYNE	0.00E+00	A	6	1.10E+01	1.60E+01
2-M-5-NPYNE	0.00E+00	A	7	1.33E+01	1.80E+01
2-M-5-NPYNE	0.00E+00	A	8	1.22E+01	1.37E+01

2-M-5-NPYNE	0.00E+00	A	9	1.10E+01	1.55E+01
2-M-5-NPYNE	0.00E+00	A	10	9.40E+00	1.00E+01
2-M-5-NPYNE	0.00E+00	B	1	1.44E+01	1.40E+01
2-M-5-NPYNE	0.00E+00	B	2	1.09E+01	3.00E+00
2-M-5-NPYNE	0.00E+00	B	3	6.70E+00	1.10E+01
2-M-5-NPYNE	0.00E+00	B	4	1.01E+01	5.90E+00
2-M-5-NPYNE	0.00E+00	B	5	1.42E+01	1.80E+01
2-M-5-NPYNE	0.00E+00	B	6	1.15E+01	1.45E+01
2-M-5-NPYNE	0.00E+00	B	7	1.87E+01	1.37E+01
2-M-5-NPYNE	0.00E+00	B	8	1.05E+01	1.50E+01
2-M-5-NPYNE	0.00E+00	B	9	2.00E+01	1.80E+01
2-M-5-NPYNE	0.00E+00	B	10	1.42E+01	1.72E+01
2-M-5-NPYNE	0.00E+00	C	1	7.00E+00	8.00E+00
2-M-5-NPYNE	0.00E+00	C	2	1.26E+01	1.30E+01
2-M-5-NPYNE	0.00E+00	C	3	9.50E+00	1.14E+01
2-M-5-NPYNE	0.00E+00	C	4	8.00E+00	1.12E+01
2-M-5-NPYNE	0.00E+00	C	5	8.00E+00	8.40E+00
2-M-5-NPYNE	0.00E+00	C	6	1.07E+01	1.65E+01
2-M-5-NPYNE	0.00E+00	C	7	7.10E+00	1.10E+01
2-M-5-NPYNE	0.00E+00	C	8	1.32E+01	1.25E+01
2-M-5-NPYNE	0.00E+00	C	9	5.60E+00	1.00E+01
2-M-5-NPYNE	0.00E+00	C	10	4.30E+00	3.50E+00
2-M-5-NPYNE	1.09E+00	A	1	1.42E+01	1.36E+01
2-M-5-NPYNE	1.09E+00	A	2	1.24E+01	1.12E+01
2-M-5-NPYNE	1.09E+00	A	3	1.11E+01	1.20E+01
2-M-5-NPYNE	1.09E+00	A	4	1.50E+01	1.56E+01
2-M-5-NPYNE	1.09E+00	A	5	1.21E+01	7.50E+00
2-M-5-NPYNE	1.09E+00	A	6	1.46E+01	1.45E+01
2-M-5-NPYNE	1.09E+00	A	7	1.75E+01	1.60E+01
2-M-5-NPYNE	1.09E+00	A	8	1.41E+01	1.35E+01
2-M-5-NPYNE	1.09E+00	A	9	1.52E+01	1.09E+01
2-M-5-NPYNE	1.09E+00	A	10	7.00E+00	4.40E+00

2-M-5-NPYNE	1.09E+00	B	1	1.55E+01	1.60E+01
2-M-5-NPYNE	1.09E+00	B	2	1.50E+01	1.45E+01
2-M-5-NPYNE	1.09E+00	B	3	1.76E+01	1.35E+01
2-M-5-NPYNE	1.09E+00	B	4	1.17E+01	1.16E+01
2-M-5-NPYNE	1.09E+00	B	5	1.09E+01	1.25E+01
2-M-5-NPYNE	1.09E+00	B	6	1.80E+01	1.50E+01
2-M-5-NPYNE	1.09E+00	B	7	1.55E+01	1.60E+01
2-M-5-NPYNE	1.09E+00	B	8	1.09E+01	1.10E+01
2-M-5-NPYNE	1.09E+00	B	9	1.83E+01	2.05E+01
2-M-5-NPYNE	1.09E+00	B	10	6.40E+00	1.00E+01
2-M-5-NPYNE	1.09E+00	C	1	1.32E+01	1.55E+01
2-M-5-NPYNE	1.09E+00	C	2	1.35E+01	2.10E+01
2-M-5-NPYNE	1.09E+00	C	3	1.45E+01	1.35E+01
2-M-5-NPYNE	1.09E+00	C	4	1.42E+01	1.45E+01
2-M-5-NPYNE	1.09E+00	C	5	8.50E+00	1.15E+01
2-M-5-NPYNE	1.09E+00	C	6	1.05E+01	1.00E+01
2-M-5-NPYNE	1.09E+00	C	7	1.25E+01	1.27E+01
2-M-5-NPYNE	1.09E+00	C	8	1.06E+01	1.50E+01
2-M-5-NPYNE	1.09E+00	C	9	1.65E+01	1.50E+01
2-M-5-NPYNE	1.09E+00	C	10	1.41E+01	1.56E+01
2-M-5-NPYNE	1.17E+01	A	1	9.10E+00	4.60E+00
2-M-5-NPYNE	1.17E+01	A	2	1.85E+01	1.65E+01
2-M-5-NPYNE	1.17E+01	A	3	1.30E+01	1.40E+01
2-M-5-NPYNE	1.17E+01	A	4	1.71E+01	1.86E+01
2-M-5-NPYNE	1.17E+01	A	5	9.80E+00	1.00E+01
2-M-5-NPYNE	1.17E+01	A	6	7.60E+00	8.50E+00
2-M-5-NPYNE	1.17E+01	A	7	1.66E+01	1.50E+01
2-M-5-NPYNE	1.17E+01	A	8	1.60E+01	1.55E+01
2-M-5-NPYNE	1.17E+01	A	9	1.80E+01	1.70E+01
2-M-5-NPYNE	1.17E+01	A	10	1.20E+01	1.17E+01
2-M-5-NPYNE	1.17E+01	B	1	1.28E+01	1.08E+01
2-M-5-NPYNE	1.17E+01	B	2	1.50E+01	1.34E+01

2-M-5-NPYNE	1.17E+01	B	3	1.50E+01	1.31E+01
2-M-5-NPYNE	1.17E+01	B	4	8.50E+00	7.50E+00
2-M-5-NPYNE	1.17E+01	B	5	2.02E+01	1.65E+01
2-M-5-NPYNE	1.17E+01	B	6	9.80E+00	1.05E+01
2-M-5-NPYNE	1.17E+01	B	7	1.36E+01	1.45E+01
2-M-5-NPYNE	1.17E+01	B	8	1.71E+01	1.45E+01
2-M-5-NPYNE	1.17E+01	B	9	1.72E+01	1.53E+01
2-M-5-NPYNE	1.17E+01	B	10	1.40E+01	1.37E+01
2-M-5-NPYNE	1.17E+01	C	1	1.64E+01	1.28E+01
2-M-5-NPYNE	1.17E+01	C	2	1.50E+01	1.30E+01
2-M-5-NPYNE	1.17E+01	C	3	1.50E+01	1.22E+01
2-M-5-NPYNE	1.17E+01	C	4	1.11E+01	6.40E+00
2-M-5-NPYNE	1.17E+01	C	5	1.33E+01	1.02E+01
2-M-5-NPYNE	1.17E+01	C	6	1.90E+01	1.70E+01
2-M-5-NPYNE	1.17E+01	C	7	6.40E+00	8.20E+00
2-M-5-NPYNE	1.17E+01	C	8	1.97E+01	1.40E+01
2-M-5-NPYNE	1.17E+01	C	9	1.60E+01	1.10E+01
2-M-5-NPYNE	1.17E+01	C	10	1.45E+01	1.65E+01
2-M-5-NPYNE	5.53E+01	A	1	1.33E+01	7.50E+00
2-M-5-NPYNE	5.53E+01	A	2	1.55E+01	1.05E+01
2-M-5-NPYNE	5.53E+01	A	3	1.72E+01	1.05E+01
2-M-5-NPYNE	5.53E+01	A	4	1.37E+01	1.05E+01
2-M-5-NPYNE	5.53E+01	A	5	9.00E+00	7.70E+00
2-M-5-NPYNE	5.53E+01	A	6	8.40E+00	6.20E+00
2-M-5-NPYNE	5.53E+01	A	7	1.32E+01	7.00E+00
2-M-5-NPYNE	5.53E+01	A	8	5.20E+00	6.00E+00
2-M-5-NPYNE	5.53E+01	A	9	1.05E+01	1.00E+01
2-M-5-NPYNE	5.53E+01	A	10	8.50E+00	5.20E+00
2-M-5-NPYNE	5.53E+01	B	1	1.60E+01	8.00E+00
2-M-5-NPYNE	5.53E+01	B	2	1.05E+01	7.50E+00
2-M-5-NPYNE	5.53E+01	B	3	1.00E+01	9.50E+00
2-M-5-NPYNE	5.53E+01	B	4	1.33E+01	9.70E+00

2-M-5-NPYNE	5.53E+01	B	5	1.56E+01	8.20E+00
2-M-5-NPYNE	5.53E+01	B	6	1.58E+01	1.14E+01
2-M-5-NPYNE	5.53E+01	B	7	1.14E+01	1.00E+01
2-M-5-NPYNE	5.53E+01	B	8	1.55E+01	1.17E+01
2-M-5-NPYNE	5.53E+01	B	9	1.31E+01	1.30E+01
2-M-5-NPYNE	5.53E+01	B	10	1.50E+01	1.37E+01
2-M-5-NPYNE	5.53E+01	C	1	1.14E+01	3.50E+00
2-M-5-NPYNE	5.53E+01	C	2	5.60E+00	5.50E+00
2-M-5-NPYNE	5.53E+01	C	3	1.30E+01	1.10E+01
2-M-5-NPYNE	5.53E+01	C	4	1.15E+01	4.70E+00
2-M-5-NPYNE	5.53E+01	C	5	7.70E+00	6.00E+00
2-M-5-NPYNE	5.53E+01	C	6	1.20E+01	1.05E+01
2-M-5-NPYNE	5.53E+01	C	7	6.00E+00	8.70E+00
2-M-5-NPYNE	5.53E+01	C	8	1.57E+01	1.00E+01
2-M-5-NPYNE	5.53E+01	C	9	1.45E+01	1.00E+01
2-M-5-NPYNE	5.53E+01	C	10	1.41E+01	1.00E+01
2-M-5-NPYNE	1.06E+02	A	1	9.70E+00	8.50E+00
2-M-5-NPYNE	1.06E+02	A	2	1.17E+01	1.27E+01
2-M-5-NPYNE	1.06E+02	A	3	8.40E+00	9.50E+00
2-M-5-NPYNE	1.06E+02	A	4	1.20E+01	1.00E+01
2-M-5-NPYNE	1.06E+02	A	5	8.00E+00	8.50E+00
2-M-5-NPYNE	1.06E+02	A	6	1.00E+01	8.50E+00
2-M-5-NPYNE	1.06E+02	A	7	6.50E+00	5.00E+00
2-M-5-NPYNE	1.06E+02	A	8	7.50E+00	7.00E+00
2-M-5-NPYNE	1.06E+02	A	9	1.05E+01	9.00E+00
2-M-5-NPYNE	1.06E+02	A	10	1.00E+01	7.00E+00
2-M-5-NPYNE	1.06E+02	B	1	6.00E+00	3.00E+00
2-M-5-NPYNE	1.06E+02	B	2	7.50E+00	3.00E+00
2-M-5-NPYNE	1.06E+02	B	3	6.00E+00	8.00E+00
2-M-5-NPYNE	1.06E+02	B	4	6.50E+00	7.60E+00
2-M-5-NPYNE	1.06E+02	B	5	1.10E+01	8.60E+00
2-M-5-NPYNE	1.06E+02	B	6	1.20E+01	8.50E+00

2-M-5-NPYNE	1.06E+02	B	7	1.20E+01	9.70E+00
2-M-5-NPYNE	1.06E+02	B	8	1.15E+01	1.10E+01
2-M-5-NPYNE	1.06E+02	B	9	9.20E+00	9.50E+00
2-M-5-NPYNE	1.06E+02	B	10	6.00E+00	3.00E+00
2-M-5-NPYNE	1.06E+02	C	1	6.50E+00	7.50E+00
2-M-5-NPYNE	1.06E+02	C	2	6.20E+00	4.00E+00
2-M-5-NPYNE	1.06E+02	C	3	5.00E+00	9.40E+00
2-M-5-NPYNE	1.06E+02	C	4	6.60E+00	1.28E+01
2-M-5-NPYNE	1.06E+02	C	5	1.32E+01	1.08E+01
2-M-5-NPYNE	1.06E+02	C	6	5.70E+00	2.50E+00
2-M-5-NPYNE	1.06E+02	C	7	1.05E+01	1.35E+01
2-M-5-NPYNE	1.06E+02	C	8	5.70E+00	8.20E+00
2-M-5-NPYNE	1.06E+02	C	9	1.05E+01	1.08E+01
2-M-5-NPYNE	1.06E+02	C	10	9.60E+00	4.40E+00

^a Average of measured exposure concentrations across replicates for the corresponding solution added. The 0 mg L⁻¹ concentration represents controls (pots not exposed to MCs, or MLCs)

^b Not recorded

^c Replicate B was accidentally exposed to the wrong solution added few days after the beginning of the experiment, so it was excluded for further measurements

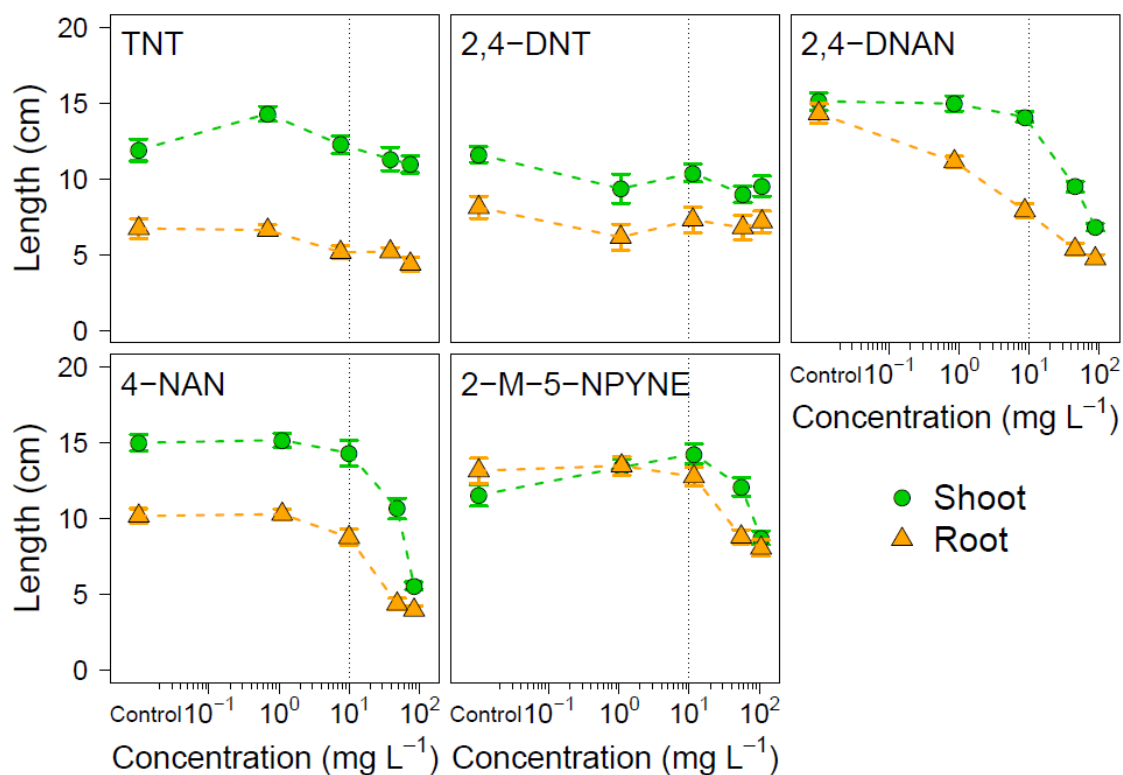


Figure F-2 Barley shoot and root lengths versus measured exposure concentrations of MCs and MLCs. Vertical dotted line shows nominal concentration chosen to perform bioconcentration uptake assays (10 mg L^{-1}). Data presented as means \pm standard error of the mean (SEM). Sample size ≥ 2 pots (Table F-5). Dashed colored lines are visual guides for data trends. If not visible, error bars are smaller than the symbol.

Table F-6 NOAEC, LOAEC, and EC₅₀ for MCs and MLCs in toxicity screening test with barley.

Plant Part	Summary Statistics	MCs and MLCs				
		TNT	2,4-DNT	2,4-DNAN	4-NAN	2-M-5-NYPNE
Shoot	NOAEC ^a	74.675±1.443	109.411±1.036	8.668±0.300	9.972±0.074	55.274±0.872
	p-value ^b	0.87	0.22	0.73	0.93	0.98
	LOAEC ^c	> 74.675±1.443	> 109.411±1.036	45.211±1.774	48.358±0.976	105.984±2.196
	p-value	ND ^d	ND	< 0.001	< 0.001	0.01
	EC ₅₀ ^e	> 74.675±1.443	> 109.411±1.036	26.156±4.200	47.098±3.813	>105.984±2.196
	95% CI ^f	ND	ND	17.874–34.430	39.577–54.619	ND
	Model ^g	Hormetic	Gompertz	Gompertz	Gompertz	Hormetic
Root	NOAEC	74.675±1.443	109.411±1.036	< 0.859±0.055	9.972±0.074	11.703±0.366
	p-value	0.95	0.96	ND	0.19	1.00
	LOAEC	> 74.675±1.443	> 109.411±1.036	0.859±0.055	48.358±0.976	55.274±0.872
	p-value	ND	ND	< 0.001	< 0.001	< 0.001
	EC ₅₀	> 74.675±1.443	> 109.411±1.036	0.916±0.492	15.135±4.768	46.736±13.266
	95% CI	ND	ND	-0.054–1.887	5.730–24.540	20.556–72.916
	Model	Hormetic	Gompertz	Gompertz	Gompertz	Gompertz

^a No–Observed–Adverse–Effect–Concentration in mg L⁻¹ (measured): mean ± standard error of the mean (SEM). Statistical analyses for the determination of the NOAEC values are described above in this section

^b A p-value ≤ 0.05 was accepted as significant

^c Lowest–Observed–Adverse–Effect–Concentration in mg L⁻¹ (measured): mean ± SEM. Statistical analyses for the determination of the LOAEC values are described above in this section

^d Not determinable

^e Effect Concentration (mg L⁻¹) producing a 50% effect relative to carrier control ± SEM. Models fitted for the determination of the EC₅₀ values are described above in this section

^f 95 % Confidence Interval (mg L⁻¹)

^g Defined in equations presented above in this section. Fitted to toxicity screening results (Table F-5) for the determination of EC₅₀

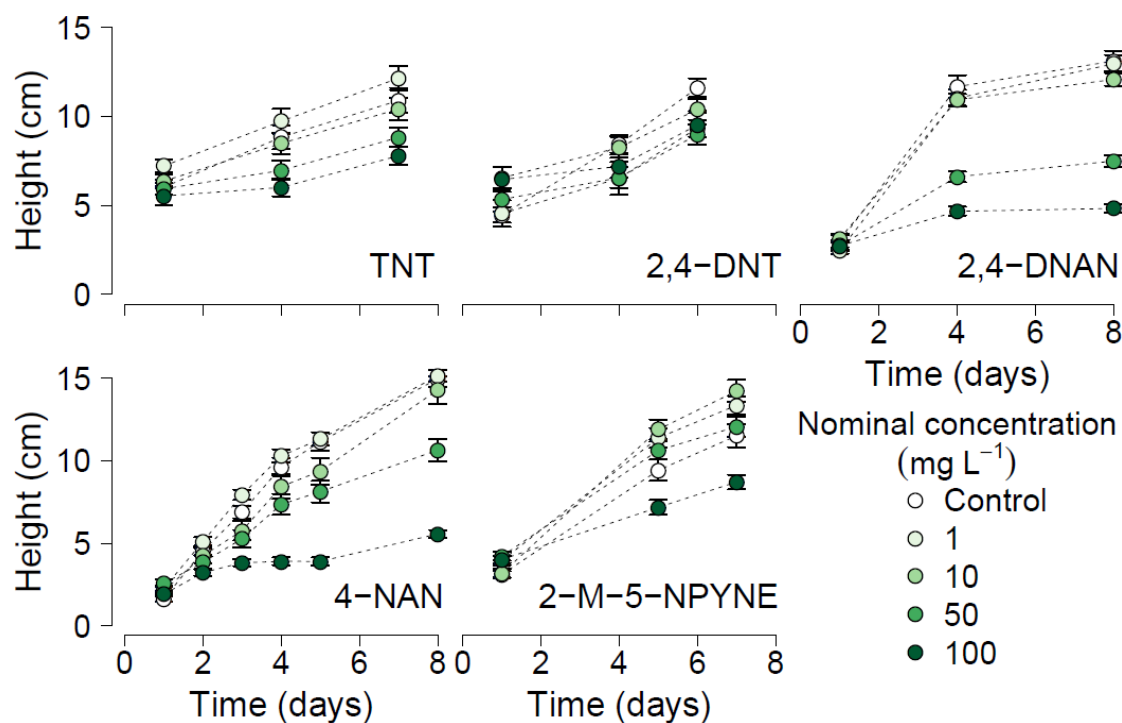


Figure F-3 Biomass profiles (shoot height) for barley exposed to individual munitions compounds (MCs) or munitions-like compounds (MLCs) at increasing concentration of solution added (nominal: Control, 1, 10, 50, and 100 mg L⁻¹) during toxicity screening. Data presented as means \pm standard error of the mean (SEM). If not visible, error bars are smaller than the symbol.

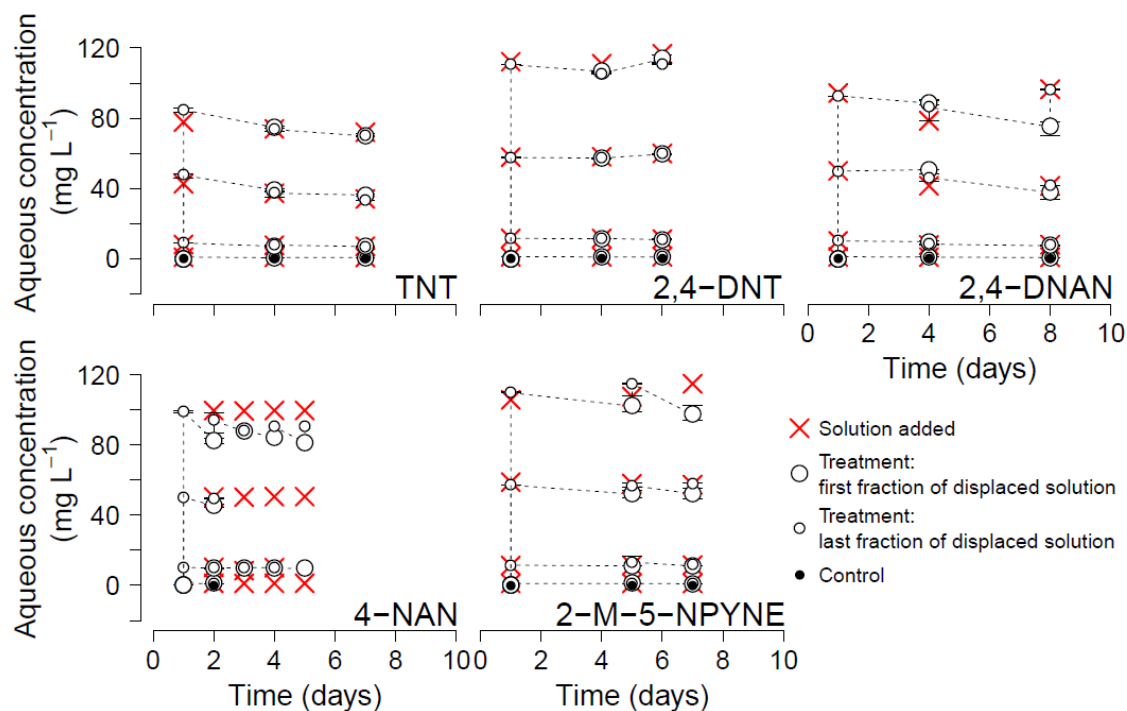


Figure F-4 Exposure concentrations over time for MCs and MLCs in toxicity screening with barley at five concentrations of solution added (nominal: Control, 1, 10, 50, and 100 mg L⁻¹). Legend: Solution added is the solution sampled just before being loaded into plant pots; Treatment are samples from displaced solutions of pots exposed to MCs or MLCs; first and last fraction of displaced solution refer to the first and last pore volume replenished daily; Control are samples from displaced solutions of untreated plant pots (not exposed to MCs or MLCs). Data presented as means and error bars represent the range.

Table F-7 Summary statistics for the fluctuation in measured exposure concentrations for MCs and MLCs during toxicity screening with barley^a.

Compound	NumDF ^b	DenDF ^c	F-value	p-value ^d
TNT	1.00E+00	1.41E+01	1.58E+00	2.29E-01
2,4-DNT	1.00E+00	2.54E+01	3.42E-02	8.55E-01
2,4-DNAN	1.00E+00	5.40E+01	1.04E+00	3.13E-01
4-NAN	1.00E+00	4.70E+01	1.55E-02	9.01E-01
2-M-5-NPYNE	1.00E+00	5.40E+01	2.24E-01	6.38E-01

^a Time effect was analyzed for the four concentration of solutions added (nominal: 1, 10, 50, and 100 mg L⁻¹) altogether per MC or MLC. In cases of unbalanced ANOVA (e.g., missing data), a linear mixed-effect model analysis was conducted using Satterthwaite approximation for degrees of freedom to estimate p-values.

^b Degrees of freedom numerator

^c Degrees of freedom denominator

^d A p-value ≤ 0.05 was accepted as significant

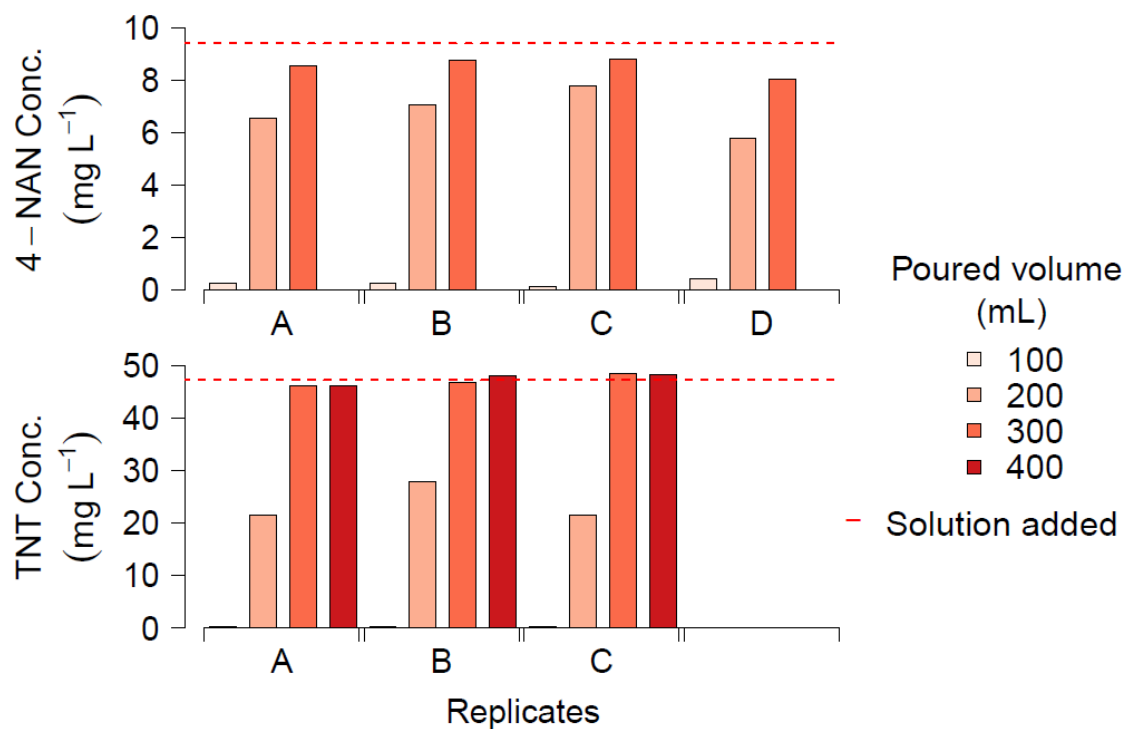


Figure F-5 Concentrations in displaced solutions collected at the end of each consecutive pore volume (pv, 100 mL per pv) on the first day of exposure to MCs and MLCs for selected chemicals during toxicity screening with barley. Solution added: Aqueous solution containing TNT or 4-NAN and being loaded to plant pots. Replicates: Plant pots subjected to the same solution added. Difference in TNT concentration between solution added and displaced solution collected from 4th pore volume were not statistically significant (p-value = 0.80).

Bioconcentration Uptake Assays

Procedure for Extraction of MCs and MLCs from Plant Biomass

The extraction was performed adding 5 mL of acetonitrile and 3 mL of a 0.01 mol L⁻¹ CaCl₂ and NaN₃ solution to repress microbial activity per biomass tube. The biomass-acetonitrile suspensions were tumbled end-to-end in darkness at 20 rpm for 1 h, supernatants were transferred with disposable glass pipettes into disposable glass culture tubes (10 mL), filtered through Durapore[®] polyvinylidene difluoride (PVDF) membranes (0.45 µm pore size, EMD Millipore Corp., Billerica, MA), and analyzed by HPLC. Four consecutive extractions were performed for each biomass tube.

Table F-8 Summary statistics for the fluctuation in measured exposure concentrations for MCs and MLCs during bioconcentration uptake assays with barley^a.

Compound	NumDF ^b	DenDF ^c	F-value	p-value ^d
TNT	1.00E+00	7.20E+01	1.82E+01	5.96E-05 ^e
2,4-DNT	1.00E+00	6.59E+00	4.33E+00	7.86E-02
2,4-DNAN	1.00E+00	7.00E+01	2.78E+00	1.00E-01
4-NAN	1.00E+00	1.74E+01	3.80E-01	5.46E-01
2-M-5-NPYNE	1.00E+00	7.20E+01	2.22E-01	6.39E-01

^a Time effect was analyzed for the four exposure times (1, 2, 3, and 4 weeks) altogether per MC or MLC. Unbalanced ANOVA (unequal number of observations over time due to destructive sampling across exposure weeks) was conducted through a linear mixed-effect model analysis using Satterthwaite approximation for degrees of freedom to estimate p-values

^b Degrees of freedom numerator

^c Degrees of freedom denominator

^d A p-value ≤ 0.05 was accepted as significant

^e Subsequent multiple comparisons test revealed a p-value = 0.90 for the difference between paired means of displaced solution collected on the 3rd and 4th weeks of exposure

Table F-9 Summary statistics for the significance of sorption of MCs and MLCs onto the solid growth medium (sand) during bioconcentration uptake assays with barley^a.

Compound	NumDF ^b	DenDF ^c	F-value	p-value ^d
TNT	1.00E+00	5.70E+01	1.71E-04	9.90E-01
2,4-DNT	1.00E+00	1.39E+01	1.73E+00	2.10E-01
2,4-DNAN	1.00E+00	5.50E+01	1.47E+00	2.30E-01
4-NAN	1.00E+00	3.70E+01	1.92E+00	1.74E-01
2-M-5-NPYNE	1.00E+00	8.05E+00	4.08E+00	7.78E-02

^a Significance of sorption onto sand was analyzed comparing the concentrations of the solutions added and the displaced solutions sampled at the end of the daily replenishment from treated pots for the four exposure times (1, 2, 3, and 4 weeks) altogether per MC or MLC. Unbalanced ANOVA (unequal number of observations over time due to destructive sampling across exposure weeks) was conducted through a linear mixed-effect model analysis using Satterthwaite approximation for degrees of freedom to estimate p-values

^b Degrees of freedom numerator

^c Degrees of freedom denominator

^d A p-value ≤ 0.05 was accepted as significant

Table F-10 Summary statistics for the significance of exposure time in the ratios of $\frac{C_{iPlant}}{C_{iIW}}$ for MCs and MLCs during bioconcentration uptake assays with barley^a.

Compound	Df	Sum Sq	Mean Sq	F-value	p-value ^b
TNT	3	1.83E-02	6.10E-03	2.19E+00	1.90E-01
2,4-DNT	3	3.72E-02	1.24E-02	2.32E+00	1.75E-01
2,4-DNAN	3	1.43E-01	4.76E-02	2.06E+00	2.07E-01
4-NAN	3	5.90E-01	1.97E-01	2.00E+01	7.17E-03 ^c
2-M-5-NPYNE	3	3.32E-02	1.11E-02	6.49E-01	6.12E-01

^a One-way ANOVA was used to assess the significance of exposure time on the ratio of concentration in the plant to concentration in the interstitial water, $\frac{C_{iPlant}}{C_{iIW}}$

^b A p-value ≤ 0.05 was accepted as significant

^c Subsequent multiple comparisons test revealed a p-value = 0.90 for the difference between paired means of $\frac{C_{iPlant}}{C_{iIW}}$ from the 3rd and 4th weeks of exposure

Table F-11 Ratios of $\frac{C_{iPlant}}{C_{iIW}}$ ^b for the compounds evaluated in bioconcentration uptake assays with barley.

Compound	Trial #	Exposure Time	Plant Mass	Concentration in Plant ^c	Concentration in Interstitial Water ^d	$\log\left(\frac{C_{iPlant}}{C_{iIW}}\right)$
		days	g _{dwt} ^a	mg kg _{dwt} ⁻¹	mg L ⁻¹	L kg _{dwt} ⁻¹
TNT	1 st	9	3.82E-01	4.36E+01	8.74E+00	6.97E-01
TNT	1 st	9	4.07E-01	5.32E+01	9.37E+00	7.54E-01
TNT	1 st	9	4.00E-01	4.41E+01	9.35E+00	6.73E-01
TNT	1 st	16	5.68E-01	3.53E+01	7.15E+00	6.93E-01
TNT	1 st	16	5.26E-01	2.72E+01	7.05E+00	5.86E-01
TNT	1 st	16	5.63E-01	2.58E+01	7.11E+00	5.59E-01
TNT	1 st	23	5.23E-01	2.56E+01	6.00E+00	6.30E-01
TNT	1 st	23	4.79E-01	2.46E+01	5.84E+00	6.26E-01
TNT	1 st	30	5.40E-01	3.16E+01	7.09E+00	6.49E-01
TNT	1 st	30	4.41E-01	2.22E+01	6.00E+00	5.69E-01
2,4-DNT	1 st	8	4.19E-01	5.83E+01	9.07E+00	8.08E-01
2,4-DNT	1 st	8	6.28E-01	5.68E+01	9.09E+00	7.96E-01
2,4-DNT	1 st	15	4.26E-01	6.65E+01	9.07E+00	8.65E-01
2,4-DNT	1 st	15	4.96E-01	5.82E+01	8.98E+00	8.11E-01
2,4-DNT	1 st	22	4.30E-01	5.09E+01	9.84E+00	7.14E-01
2,4-DNT	1 st	22	4.36E-01	3.96E+01	9.82E+00	6.05E-01

2,4-DNT	1 st	22	4.50E-01	5.98E+01	9.85E+00	7.83E-01
2,4-DNT	1 st	29	3.76E-01	4.92E+01	9.44E+00	7.17E-01
2,4-DNT	1 st	29	3.77E-01	3.79E+01	9.49E+00	6.01E-01
2,4-DNT	1 st	29	3.19E-01	5.49E+01	9.39E+00	7.67E-01
2,4-DNAN	1 st	22	3.85E-01	2.04E+02	7.56E+00	1.43E+00
2,4-DNAN	1 st	22	3.62E-01	2.20E+02	7.71E+00	1.46E+00
2,4-DNAN	1 st	29	3.92E-01	2.11E+02	7.98E+00	1.42E+00
2,4-DNAN	1 st	29	5.25E-01	1.16E+02	8.10E+00	1.15E+00
2,4-DNAN	2 nd	8	3.70E-01	7.49E+01	9.76E+00	8.85E-01
2,4-DNAN	2 nd	8	3.44E-01	2.41E+02	1.24E+01	1.29E+00
2,4-DNAN	2 nd	8	4.37E-01	7.13E+01	9.75E+00	8.64E-01
2,4-DNAN	2 nd	15	3.78E-01	1.45E+02	1.01E+01	1.16E+00
2,4-DNAN	2 nd	15	3.82E-01	1.76E+02	9.62E+00	1.26E+00
2,4-DNAN	2 nd	15	5.23E-01	1.37E+02	9.64E+00	1.15E+00
2,4-DNAN	2 nd	22	4.73E-01	1.17E+02	1.06E+01	1.04E+00
2,4-DNAN	2 nd	22	4.87E-01	1.59E+02	1.09E+01	1.16E+00
2,4-DNAN	2 nd	29	2.77E-01	2.37E+02	1.07E+01	1.35E+00
2,4-DNAN	2 nd	29	4.28E-01	2.55E+02	1.05E+01	1.39E+00
4-NAN	1 st	8	5.72E-01	1.03E+01	9.73E+00	2.51E-02
4-NAN	1 st	8	4.72E-01	6.91E+00	9.84E+00	-1.53E-01
4-NAN	1 st	15	4.27E-01	1.07E+01	9.66E+00	4.65E-02
4-NAN	1 st	15	3.12E-01	7.28E+00	9.31E+00	-1.07E-01
4-NAN	1 st	22	6.56E-01	2.39E+01	9.71E+00	3.91E-01

4-NAN	1 st	22	5.85E-01	3.31E+01	9.84E+00	5.27E-01
4-NAN	1 st	29	3.40E-01	3.01E+01	9.69E+00	4.93E-01
4-NAN	1 st	29	2.73E-01	3.51E+01	9.62E+00	5.62E-01
4-NAN	2 nd	22	7.22E-01	2.56E+01	7.28E+00	5.46E-01
4-NAN	2 nd	22	7.05E-01	4.08E+01	6.99E+00	7.67E-01
4-NAN	2 nd	29	7.50E-01	3.61E+01	7.48E+00	6.84E-01
4-NAN	2 nd	29	7.94E-01	3.68E+01	7.54E+00	6.88E-01
4-NAN	3 rd	22	5.79E-01	2.76E+01	7.23E+00	5.82E-01
4-NAN	3 rd	22	5.83E-01	2.81E+01	7.27E+00	5.87E-01
4-NAN	3 rd	29	4.64E-01	2.02E+01	7.31E+00	4.42E-01
4-NAN	3 rd	29	5.27E-01	2.32E+01	7.25E+00	5.06E-01
4-NAN	3 rd	29	6.04E-01	2.41E+01	7.26E+00	5.21E-01
4-NAN	4 th	23	4.35E-01	2.05E+01	7.43E+00	4.41E-01
4-NAN	4 th	23	3.87E-01	1.81E+01	7.50E+00	3.84E-01
4-NAN	4 th	23	3.29E-01	2.50E+01	7.53E+00	5.22E-01
4-NAN	4 th	30	4.00E-01	2.41E+01	7.62E+00	5.00E-01
4-NAN	4 th	30	5.53E-01	1.50E+01	7.63E+00	2.92E-01
4-NAN	4 th	30	5.85E-01	1.73E+01	7.65E+00	3.54E-01
<hr/>						
2-M-5-NPYNE	1 st	8	5.77E-01	4.30E+01	1.10E+01	5.94E-01
2-M-5-NPYNE	1 st	8	4.53E-01	3.19E+01	1.09E+01	4.66E-01
2-M-5-NPYNE	1 st	8	4.38E-01	3.26E+01	1.11E+01	4.66E-01
2-M-5-NPYNE	1 st	15	5.35E-01	4.73E+01	9.68E+00	6.89E-01
2-M-5-NPYNE	1 st	15	6.19E-01	2.40E+01	1.03E+01	3.67E-01

2-M-5-NPYNE	1 st	15	7.02E-01	2.20E+01	9.84E+00	3.50E-01
2-M-5-NPYNE	1 st	22	7.18E-01	2.80E+01	1.02E+01	4.39E-01
2-M-5-NPYNE	1 st	22	7.67E-01	1.83E+01	1.02E+01	2.52E-01
2-M-5-NPYNE	1 st	29	7.61E-01	2.79E+01	1.01E+01	4.40E-01
2-M-5-NPYNE	1 st	29	6.35E-01	3.09E+01	1.02E+01	4.82E-01

^a dwt: dry weight

^b $C_{i_{Plant}}$: concentration of compound i in barley ($\text{mg kg}_{\text{dwt}}^{-1}$), $C_{i_{IW}}$: concentration of compound i in the interstitial water, which was measured in the displaced solution (mg L^{-1})

^c Plant = shoots + roots

^d Measured in the displaced solution

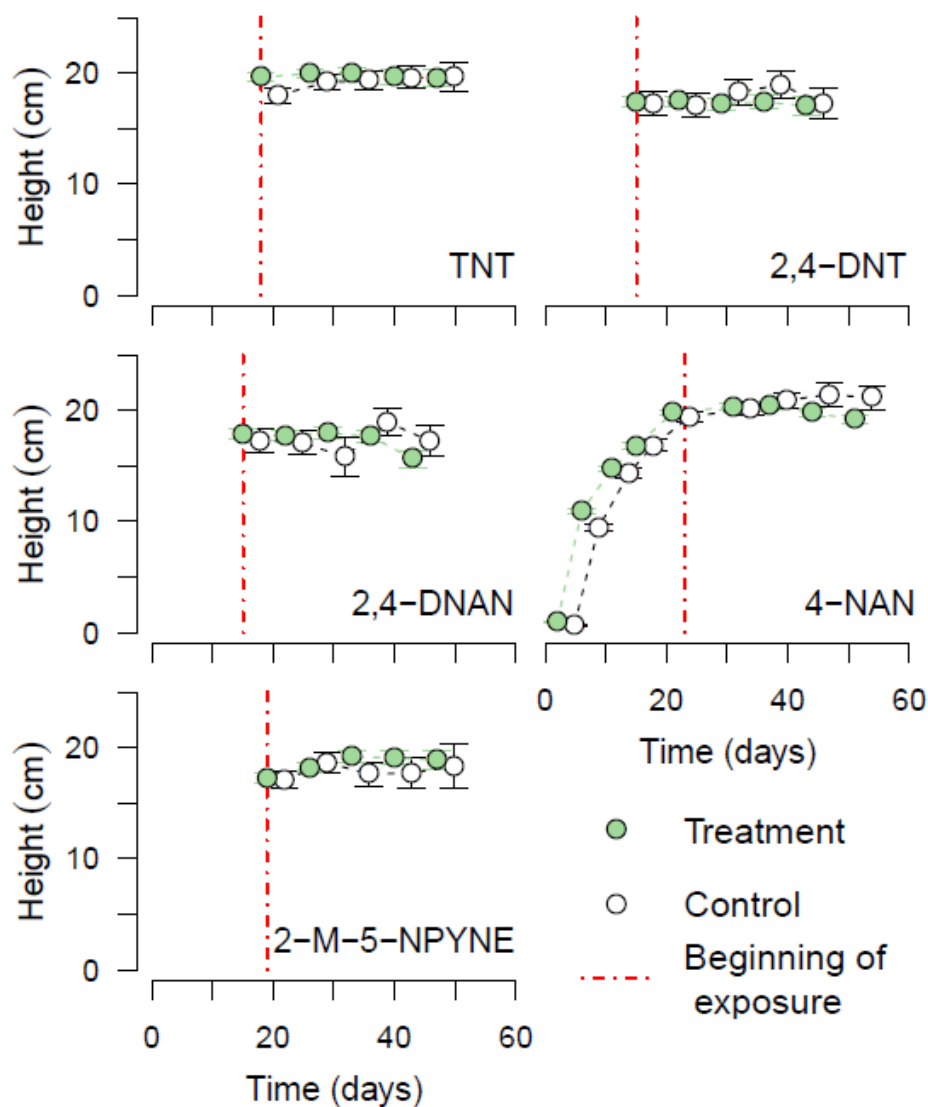


Figure F-6 Biomass profiles (shoot height) for barley exposed to individual MCs, or MLCs, during bioconcentration uptake assays. Legend: Treatment are plant pots exposed to MCs or MLCs at a nominal concentration of 10 mg L^{-1} ; Control are untreated plant pots (not exposed to MCs or MLCs). Displaying 2nd trial for 2,4-DNAN and 1st trial for 4-NAN. Data presented as means \pm standard error of the mean (SEM). Sample size ≥ 2 pots (Table F-11).

Plant–Water Partitioning vs. BCF

Table F-12 Plant–water partition coefficients (K_{PW}) for 4-NAN with barley and the summary statistics for the significance of contact time (kinetics) on $\log K_{PW}$ values^a.

Contact time	Replicate	log K_{PW}			
h		L kg _{dwt} ⁻¹			
24	A	1.16E+00			
24	B	1.13E+00			
24	C	1.19E+00			
48	A	1.07E+00			
48	B	1.13E+00			
48	C	1.19E+00			
144	A	1.09E+00			
144	B	1.12E+00			
144	C	1.03E+00			
Summary statistics					
	Df	Sum Sq	Mean Sq	F	p-value ^b
Contact time	2	9.56E-03	4.78E-03	2.34E+00	1.77E-01
Residuals	6	1.23E-02	2.04E-03		

^a One-way ANOVA was used to assess the significance of contact time on the 4-NAN $\log K_{PW}$ values

^b A p-value ≤ 0.05 was accepted as significant

Table F-13 Summary statistics for the significance of the concentration of the initial solution added on log K_{PW} values^a.

Compound	t-test	Df	p-value ^b
2,5-DM-4-NANE	1.79E+00	2.68E+00	1.83E-01
2-M-5-NPYNE	-4.53E+00	1.16E+00	1.12E-01
2,4-DNAN	1.61E+00	9.79E+00	1.38E-01
4-NAN	1.86E+00	1.39E+00	2.56E-01
2,4-DNT	-2.26E+00	3.23E+00	1.02E-01
TNT	2.27E-01	4.59E+00	8.30E-01
RDX	2.09E+00	1.24E+00	2.44E-01

^a Two-tailed t-tests assuming unequal variances were used to assess the significance of the concentration of the initial solution added on the log K_{PW} values. Values are listed in Table F-14.

^b A p-value ≤ 0.05 was accepted as significant

Table F-14 Plant–water partition coefficients (K_{PW}) for the compounds evaluated.

Compound	Trial #	Nominal Concentration of Initial Solution Added ^a	Plant Mass	Concentration in Plant ^c	Concentration in Water Phase ^c	$\log K_{PW}^e$	Exposure ^f
		mg L ⁻¹	g _{dwt} ^b	mg kg _{dwt} ⁻¹	mg L ⁻¹	L kg _{dwt} ⁻¹	
2,5-DM-4-NANE	1 st	10	4.31E-01	3.06E+01 ^d	5.04E+00	7.83E-01	Low
2,5-DM-4-NANE	1 st	10	5.17E-01	4.28E+01	3.87E+00	1.04E+00	Low
2,5-DM-4-NANE	1 st	10	3.94E-01	3.71E+01	4.85E+00	8.84E-01	Low
2,5-DM-4-NANE	1 st	100	4.34E-01	2.68E+02	4.17E+01	8.07E-01	High
2,5-DM-4-NANE	1 st	100	4.38E-01	2.43E+02	4.31E+01	7.50E-01	High
2,5-DM-4-NANE	1 st	100	4.18E-01	2.24E+02	4.45E+01	7.02E-01	High
HMX	1 st	4	2.75E-01	1.32E+01	1.95E+00	8.32E-01	High
HMX	1 st	4	2.23E-01	1.66E+01	2.03E+00	9.13E-01	High
HMX	1 st	4	2.08E-01	1.39E+01	2.22E+00	7.97E-01	High
2-M-5-NPYNE	1 st	16	6.67E-01	4.29E+01	6.41E+00	8.25E-01	Low
2-M-5-NPYNE	1 st	16	6.68E-01	5.59E+01	6.96E+00	9.05E-01	Low
2-M-5-NPYNE	1 st	160	2.18E-01	1.04E+03	9.95E+01	1.02E+00	High
2-M-5-NPYNE	1 st	160	1.91E-01	1.09E+03	1.00E+02	1.04E+00	High
2,4-DNAN	1 st	10	3.99E-01	6.32E+01	4.24E+00	1.17E+00	Low
2,4-DNAN	1 st	10	4.23E-01	6.94E+01	3.73E+00	1.27E+00	Low

2,4-DNAN	1 st	10	4.76E-01	6.88E+01	3.67E+00	1.27E+00	Low
2,4-DNAN	1 st	10	4.79E-01	3.87E+01	4.63E+00	9.22E-01	Low
2,4-DNAN	1 st	10	3.62E-01	6.33E+01	4.10E+00	1.19E+00	Low
2,4-DNAN	1 st	10	3.10E-01	1.01E+02	3.84E+00	1.42E+00	Low
2,4-DNAN	2 nd	10	3.59E-01	7.63E+01	4.76E+00	1.21E+00	Low
2,4-DNAN	2 nd	10	3.37E-01	7.67E+01	4.99E+00	1.19E+00	Low
2,4-DNAN	3 rd	10	4.25E-01	5.03E+01	4.10E+00	1.09E+00	Low
2,4-DNAN	3 rd	10	4.19E-01	5.53E+01	3.95E+00	1.15E+00	Low
2,4-DNAN	3 rd	100	3.71E-01	5.69E+02	4.26E+01	1.13E+00	High
2,4-DNAN	3 rd	100	4.24E-01	5.29E+02	4.15E+01	1.11E+00	High
2,4-DNT	1 st	6	4.60E-01	3.30E+01	2.37E+00	1.14E+00	Low
2,4-DNT	1 st	6	5.39E-01	3.24E+01	2.03E+00	1.20E+00	Low
2,4-DNT	1 st	60	4.22E-01	3.86E+02	2.00E+01	1.29E+00	High
2,4-DNT	1 st	60	4.30E-01	3.97E+02	2.27E+01	1.24E+00	High
2,4-DNT	2 nd	60	1.40E+00	2.04E+02	1.30E+01	1.20E+00	High
2,4-DNT	2 nd	60	3.40E-01	5.32E+02	2.37E+01	1.35E+00	High
4-NAN	1 st	10	3.79E-01	7.83E+01	4.25E+00	1.27E+00	Low
4-NAN	1 st	10	2.73E-01	6.66E+01	4.41E+00	1.18E+00	Low
4-NAN	1 st	10	4.31E-01	7.67E+01	2.37E+00	1.51E+00	Low
4-NAN	1 st	10	3.85E-01	7.06E+01	3.79E+00	1.27E+00	Low
4-NAN	1 st	10	3.58E-01	8.28E+01	3.99E+00	1.32E+00	Low
4-NAN	1 st	10	2.54E-01	8.87E+01	3.91E+00	1.36E+00	Low
4-NAN	2 nd	10	3.75E-01	7.06E+01	4.35E+00	1.21E+00	Low

4-NAN	2 nd	10	3.10E-01	7.18E+01	4.98E+00	1.16E+00	Low
4-NAN	2 nd	10	3.65E-01	7.05E+01	4.33E+00	1.21E+00	Low
4-NAN	1 st	100	5.24E-01	5.75E+02	5.50E+01	1.02E+00	High
4-NAN	1 st	100	2.83E-01	8.07E+02	5.19E+01	1.19E+00	High
TNT	1 st	10	3.16E-01	5.34E+01	2.97E+00	1.25E+00	Low
TNT	1 st	10	4.19E-01	4.66E+01	2.44E+00	1.28E+00	Low
TNT	2 nd	10	3.63E-01	5.18E+01	2.86E+00	1.26E+00	Low
TNT	2 nd	10	2.37E-01	7.33E+01	2.94E+00	1.40E+00	Low
TNT	2 nd	10	2.41E-01	7.98E+01	3.14E+00	1.40E+00	Low
TNT	2 nd	100	2.41E-01	7.32E+02	3.65E+01	1.30E+00	High
TNT	2 nd	100	1.96E-01	9.09E+02	4.31E+01	1.32E+00	High
RDX	2 nd	4	2.11E-01	5.14E+01 ^d	1.02E+00	1.70E+00	Low
RDX	2 nd	4	2.16E-01	5.22E+01	9.79E-01	1.73E+00	Low
RDX	2 nd	4	2.93E-01	3.59E+01	1.07E+00	1.52E+00	Low
RDX	1 st	40	2.85E-01	3.59E+02	1.36E+01	1.42E+00	High
RDX	1 st	40	3.04E-01	2.03E+02	1.86E+01	1.04E+00	High

^a Difference with respect to measured concentration was never > 20%

^b dwt: dry weight

^c Measured at the end of the 24 h equilibration period

^d Due to failure to completely avoid overlap of 2,5-DM-4-NANE and RDX peaks with background signals in plant extracts samples, all concentrations in plant tissues at the end of the 24 h equilibration period were calculated by mass balance for 2,5-DM-4-NANE and RDX

^e Ratio of concentration in plant to concentration in water phase, both measured at the end of the 24 h equilibration period

^f Calculated as the ratio of the nominal concentration of initial solution added to the aqueous solubility. Ratios ranged from 0.01 to 0.09 and 0.06 to 0.87 for the low and high exposures, respectively.

Table F-15 Time course data obtained from Sunahara ³ and Dodard et al. ⁹, and estimated degradation rates for MCs^a.

Compound	Total time ^b	Time ^c	$C_{i_{plant}}(t)^a$		Fitted Parameters		Median K_{PW}	Median BCF
			Observed	Predicted	$C_{i_{plant}}(0)$ (SEM) ^a	$k_{degradation}$ (SEM) ^a		
			mg kg _{dwt} ⁻¹	mg kg _{dwt} ⁻¹	mg kg _{dwt} ⁻¹	d ⁻¹	L kg _{dwt} ⁻¹	L kg _{dwt} ⁻¹
2,4-DNAN	0	0	5.25E+01 ^d	5.25E+01	5.25E+01	6.63E-02	1.51E+01	2.33E+01
	19	19	1.49E+01	1.49E+01				
2,4-DNT	21	0	3.20E+00 ^e	3.13E+00	3.13E+00 (3.34E-01)	8.32E-02 (2.16E-02)	1.67E+01	5.19E+00
	28	7	1.50E+00	1.75E+00				
	35	14	1.20E+00	9.77E-01				
	14	0	2.04E+01 ^e	2.03E+01				
TNT	21	7	5.00E+00	5.42E+00	2.03E+01 (9.91E-01)	1.89E-01 (2.35E-02)	2.00E+01	4.25E+00
	28	14	1.70E+00	1.44E+00				
	35	21	1.70E+00	3.85E-01				

^a An exponential decay model was fitted to the concentration in the plant ($C_{i_{plant}}(t)$) time course data to obtain the maximum concentration in the plant ($C_{i_{plant}}(0)$) and degradation rate ($k_{degradation}$):

$C_{i_{plant}}(t) = C_{i_{plant}}(0) e^{(-k_{degradation}t)}$. SEM: Standard error of the mean

^b Time starting from beginning of exposure

^c Time starting from when maximum concentration in the plant was observed

^d Assumed to be equal to the sum of the parent compound and transformation product at 19 days in absence of an initial value; data measured in the shoots from a soil exposure at $4.7 \text{ mg kg}_{\text{dwt}}^{-1}$

^e All the time course data for 2,4-DNT and TNT were measurements in the roots from soil exposures at 10 and $100 \text{ mg kg}_{\text{dwt}}^{-1}$, respectively

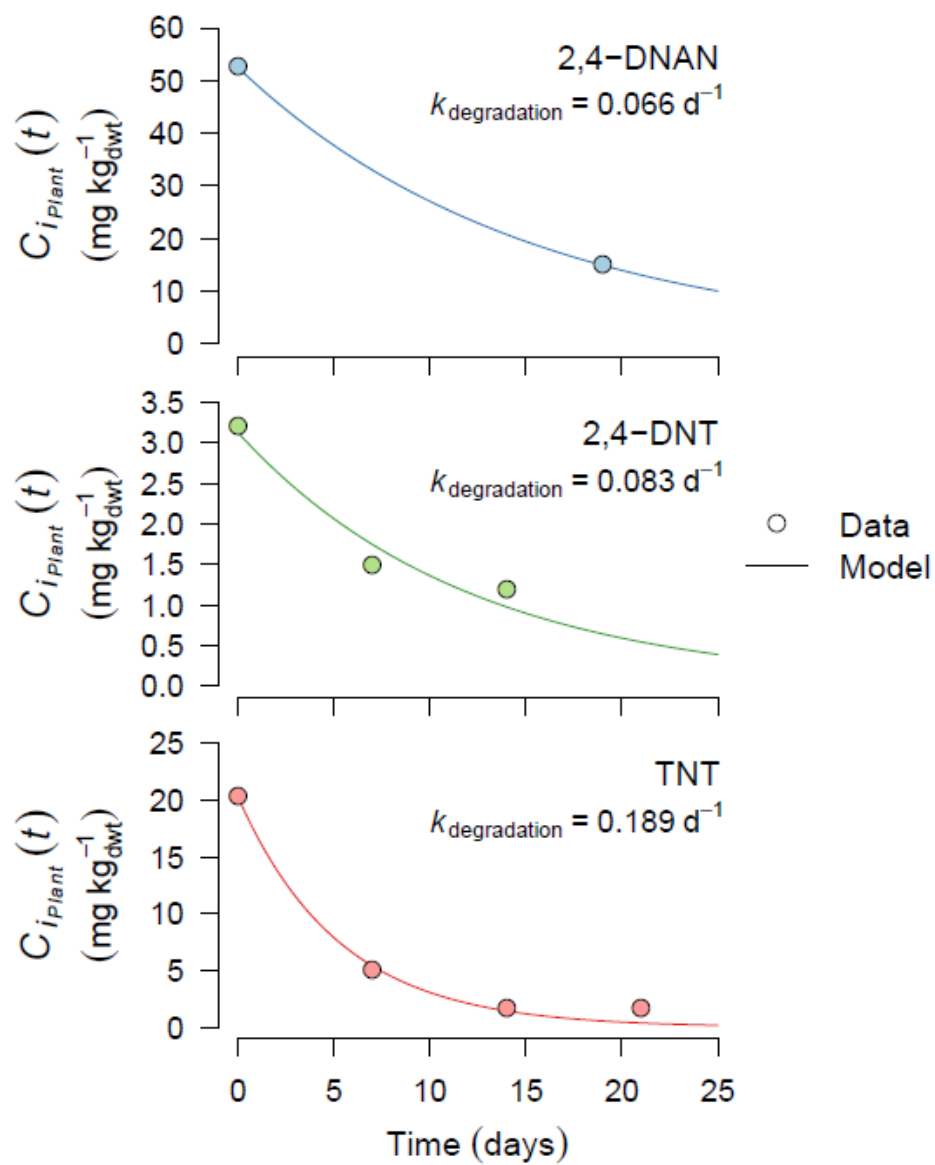


Figure F-7 Concentration in the plant ($C_{i_{plant}}(t)$) over time and estimated degradation rates ($k_{degradation}$) for MCs. An exponential decay model fitted to time course data obtained from Sunahara³ and Dodard et al.⁹ (Table F-15).

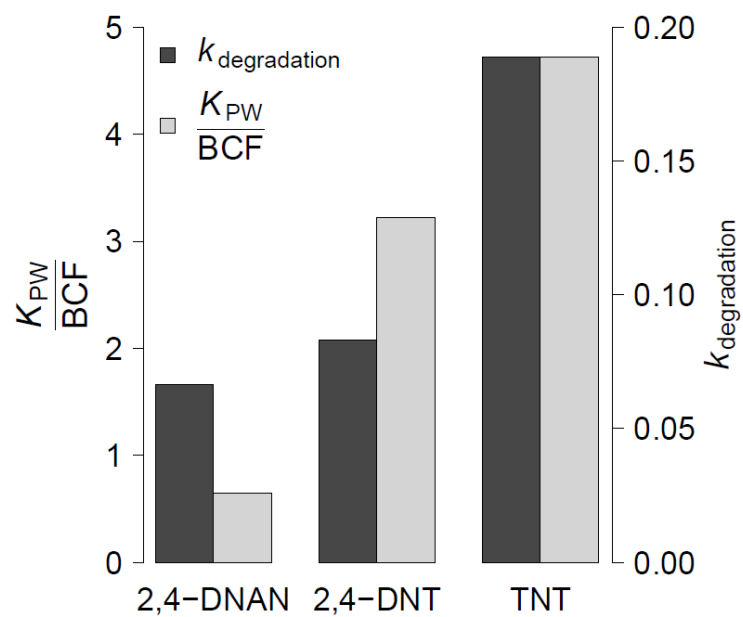


Figure F-8 Comparison between the ratios of plant–water partitioning to uptake $\left(\frac{K_{PW}}{BC}\right)$ and estimated degradation/transformation rates ($k_{degradation}$) for MCs.

REFERENCES

1. Pennington JC. Plant uptake of 2,4,6-trinitrotoluene, 4-amino-2,6-dinitrotoluene, and 2-amino-4,6-dinitrotoluene using ¹⁴C-labeled and unlabeled compounds. Technical Report No. EL-88-20. Vicksburg, MS: U.S. Army Waterways Experiment Station, Corps of Engineers. 1988;1-68.
2. Price RA, Pennington JC, Larson SL, Neumann D, Hayes CA. Uptake of RDX and TNT by agronomic plants. *Soil Sediment Contam.* 2002;11(3):307-326.
3. Sunahara GI. Development of toxicity benchmarks and bioaccumulation data for N-based organic explosives for terrestrial plants and soil invertebrates. Final Report No. SERDP ER-1416. Québec, Canada: National Research Council of Canada Montreal (Québec) Biotechnology Research Institute. 2012;1-289.
4. Rocheleau S, Lachance B, Kuperman RG, Hawari J, Thiboutot S, Ampleman G, Sunahara GI. Toxicity and uptake of cyclic nitramine explosives in ryegrass *Lolium perenne*. *Environ Pollut.* 2008;156(1):199-206.
5. Best EPH, Tatem HE, Geter KN, Wells ML, Lane BK. Effects, uptake, and fate of 2,4,6-trinitrotoluene aged in soil in plants and worms. *Environ Toxicol Chem.* 2008;27(12):2539-2547.
6. Best EPH, Geter KN, Tatem HE, Lane BK. Effects, transfer, and fate of RDX from aged soil in plants and worms. *Chemosphere.* 2006;62(4):616-625.
7. Chen D, Liu ZL, Banwart W. Concentration-dependent RDX uptake and remediation by crop plants. *Environ Sci Pollut Res.* 2011;18(6):908-917.
8. Groom CA, Halasz A, Paquet L, Morris N, Olivier L, Dubois C, Hawari J. Accumulation of HMX (octahydro-1,3,5,7-tetranitro-1,3,5,7-tetrazocine) in indigenous and agricultural plants grown in HMX-contaminated anti-tank firing-range soil. *Environ Sci Technol.* 2002;36(1):112-118.
9. Dodard SG, Sarrazin M, Hawari J, Paquet L, Ampleman G, Thiboutot S, Sunahara GI. Ecotoxicological assessment of a high energetic and insensitive munitions compound: 2,4-dinitroanisole (DNAN). *J Hazard Mater.* 2013;262:143-150.
10. US Environmental Protection Agency. Estimation Programs Interface (EPI) Suite™ for Microsoft® Windows, v. 4.11. Washington, D.C: US EPA. 2012.
11. Hawari J, Monteil-Rivera F, Perreault NN, Halasz A, Paquet L, Radovic-Hrapovic Z, Deschamps S, Thiboutot S, Ampleman G. Environmental fate of 2,4-dinitroanisole (DNAN) and its reduced products. *Chemosphere.* 2015;119:16-23.
12. Krishnan G, Horst GL, Darnell S, Powers WL. Growth and development of smooth brome grass and tall fescue in TNT-contaminated soil. *Environmental Pollution.* 2000;107(1):109-116.
13. Richard T, Weidhaas J. Dissolution, sorption, and phytoremediation of IMX-101 explosive formulation constituents: 2,4-dinitroanisole (DNAN), 3-nitro-1,2,4-triazol-5-one (NTO), and nitroguanidine. *J Hazard Mater.* 2014;280:561-569.

14. American Society for Testing and Materials. E1963 – 09: Standard guide for conducting terrestrial plant toxicity tests. West Conshohocken, PA: ASTM International. 2014.
15. Organisation for Economic Co-operation and Development. Test No. 208: Terrestrial plant test: Seedling emergence and seedling growth test. In: *OECD guidelines for the testing of chemicals, Section 2*. Paris, France: OECD Publishing. 2006.
16. Best EPH, Sprecher SL, Larson SL, Fredrickson HL, Bader DF. Environmental behavior of explosives in groundwater in groundwater from the Milan Army Ammunition Plant in aquatic and wetland plant treatments. Removal, mass balances and fate in groundwater of TNT and RDX. *Chemosphere*. 1999;38(14):3383-3396.
17. Talmage SS, Opreko DM, Maxwell CJ, Welsh CJE, Cretella FM, Reno PH, Daniel FB. Nitroaromatic munition compounds: Environmental effects and screening values. In: Ware GW, ed. *Reviews of Environmental Contamination and Toxicology*. New York, NY: Springer US. 1999;161: pp.3.
18. Amaral HIF, Fernandes J, Berg M, Schwarzenbach RP, Kipfer R. Assessing TNT and DNT groundwater contamination by compound-specific isotope analysis and ^3H – ^3He groundwater dating: A case study in Portugal. *Chemosphere*. 2009;77(6):805-812.
19. Calabrese EJ, Baldwin LA, Holland CD. Hormesis: A highly generalizable and reproducible phenomenon with important implications for risk assessment. *Risk Anal*. 1999;19(2):261-281.
20. Rocheleau S, Kuperman RG, Simini M, Hawari J, Checkai RT, Thiboutot S, Ampleman G, Sunahara GI. Toxicity of 2,4-dinitrotoluene to terrestrial plants in natural soils. *Sci Total Environ*. 2010;408(16):3193-3199.
21. Kuperman RG, Checkai RT, Simini M, Phillips CT, Kolakowski JE, Lanno R. Soil properties affect the toxicities of 2,4,6-trinitrotoluene (TNT) and hexahydro-1,3,5-trinitro-1,3,5-triazine (RDX) to the enchytraeid worm *Enchytraeus crypticus*. *Environ Toxicol Chem*. 2013;32(11):2648-2659.
22. R Development Core Team. R: A language and environment for statistical computing, v.3.2.0. Vienna, Austria: R Foundation for Statistical Computing. 2015.
23. Kalderis D, Juhasz AL, Boopathy R, Comfort S. Soils contaminated with explosives: Environmental fate and evaluation of state-of-the-art remediation processes (IUPAC technical report). *Pure Appl Chem*. 2011;83(7):1407-1484.
24. Esteve-Nunez A, Caballero A, Ramos JL. Biological degradation of 2,4,6-trinitrotoluene. *Microbiol Mol Biol Rev*. 2001;65(3):335-352.

Chapter 6

ESTIMATING GRASS–SOIL BIOCONCENTRATION OF MUNITIONS COMPOUNDS FROM MOLECULAR STRUCTURE

Abstract

A partitioning–based model is presented to estimate the bioconcentration of five munitions compounds and two munition–like compounds in grasses. The model uses polyparameter linear free energy relationships (pp–LFERs) to estimate the partition coefficients between soil organic carbon and interstitial water and between interstitial water and the plant cuticle, a lipid–like plant component. Inputs for the pp–LFERs are a set of numerical descriptors computed from molecular structure only that characterize the molecular properties that determine the interaction with soil organic carbon, interstitial water, and plant cuticle. The model is validated by predicting concentrations measured in the whole plant during independent uptake experiments with a root mean square error (log predicted plant concentration - log observed plant concentration) of 0.429. This highlights the dominant role of partitioning between the exposure medium and the plant cuticle in the bioconcentration of these compounds. The pp–LFERs can be used to assess the environmental risk of munitions compounds and munition–like compounds using only their molecular structure as input.

6.1 Introduction

Munitions compounds (MCs) are widely used in commercial and military activities, and are often released into the environment^{1–3}. Organisms that are exposed may bioconcentrate MCs. This causes concerns regarding the potential for environmental risk due to both direct toxicity and transference of these compounds to higher trophic levels. Hence the need to develop prediction models able to estimate the degree to which MCs are transferred from the ambient environment into plants, i.e., the extent of bioconcentration to be expected.

Studies proposing models to predict bioconcentration of organic compounds in plants from various growth media have been proposed^{4–11}. Some of these models account for transformation and degradation of the parent compound within the plant (e.g., metabolism, photodegradation), volatilization from leaves, and plant physiological processes such as growth and water transpiration^{7, 11}. However, in order to be applied to a specific compound, these models require parameter estimates that quantify each of these mechanisms for that compound. This limits their general applicability.

Models have also been formulated assuming that the uptake of nonionic organic compounds through the plant roots results in a steady state partitioning between the plant components and the soil^{10, 12}. The uptake is driven by concentration gradients between the plant and the external phase(s) where the organic compound is present (e.g., soil), and it occurs along the plant transpiration stream^{4, 5, 13}. In this way, the process can be modeled assuming an equilibrium between the soil solids, soil solution (interstitial water), and the plant.

The concentration of an organic compound available for plant root uptake in soils is that freely dissolved in the interstitial water (IW)^{14, 15}. This concentration is the result of soil solid–soil IW adsorption–desorption and is controlled by both the compound chemical properties and soil properties such as the mass fraction of organic carbon (f_{OC}) and clay size particles (f_{clay})^{16–}

²⁰. It has been shown for a wide variety of nonionic organic compounds that sorption to soil organic carbon (OC) is the dominant mechanism for f_{OC} greater than approximately 0.1 to 0.2 % ²¹⁻²⁶. The soil OC–aqueous phase concentrations ratio is the partition coefficient, K_{OC} , that is commonly estimated using a log–log correlation of K_{OC} with the octanol–water partition coefficient, K_{OW} . This assumes that n–octanol is a good surrogate for soil OC ^{27,28}. While these single–parameter quantitative structure–activity relationships (QSARs) have been shown to work reasonably well for mostly nonpolar hydrophobic organic chemicals ²⁹, they have failed for more polar compounds, compounds that interact by hydrogen–bonding, and for highly hydrophobic compounds ³⁰⁻³². Consequently, a need for comprehensive models of K_{OC} that perform well for a wide range of compound classes has been identified ³³.

Equilibrium sorption of organic contaminants by plant tissue components, such as carbohydrates and lipids, has also been measured and modeled ³⁴⁻³⁶. Similarly to the K_{OC} models, n–octanol is commonly used as a surrogate for plant lipids. While practical, this approach has not been able to fully characterize the interactions between organic compounds and plant tissues ^{12, 34}.

An alternative approach is to use a polyparameter linear free energy relationship (pp–LFER) model ^{37,38}. Unlike single–parameter K_{OW} –based predictions, pp–LFERs predict partitioning by explicitly considering the contributions from different types of chemical interactions (e.g., hydrogen bonding, van der Waals forces) between the solute and the condensed phase (e.g., soil OC, plant lipids). Thus, pp–LFERs are able to more fully characterize the solvation properties of the condensed phase and the strength of its interactions with solutes relative to that of the aqueous phase.

In order to achieve these results the estimation of pp–LFERs parameters require a large and chemically diverse training dataset of partition coefficients. In the case of plants, for example, the pp–LFERs require sufficient data to quantify both the solvation properties of a specific biomass component (e.g., lipids, carbohydrates, proteins) and the molecular properties of the organic contaminant of interest ^{9, 36, 39}.

The purpose of this work is to predict the bioconcentration of MCs and compounds with similar chemical structural functionalities (Table G-1 in Appendix G), which are hereafter referred to as munition–like compounds (MLCs), in plants based on the partitioning between soil solids, IW, and plant. This is achieved using pp–LFERs for predicting the dissolved IW concentration in the soil using K_{OC} , and for predicting the sorption to plant tissue using the partitioning between IW and plant cuticle, a lipid–like component. This procedure is validated by predicting concentrations in plant biomass compiled from published uptake assays in an independent dataset (95 observations). The pp–LFERs employed in this work use only molecular structure to compute the required model parameters. Therefore, they can also be used to evaluate the bioconcentration potential for proposed compounds early in the development stage of new MCs.

6.2 Methodology

6.2.1 Basis for Modeling Approach

The model is designed to predict the bioconcentration of MCs for plants, more specifically, for grasses, in situations where estimates of the parameters required in more detailed

uptake models, e.g., plant water fluxes, growth rates, and contaminant transformation/metabolism rates are not available. The model estimates the upper-bound of the concentration in the plant when exposed to the bioavailable MC in the soil IW using equilibrium partitioning (EqP). The EqP concept has been widely applied to assess the bioconcentration of organic compounds in organisms including fish, worms, and plants^{10, 12, 40-46}.

In the case of grasses, the MCs available in the soil IW are transported in solution through the plant roots and along the plant transpiration stream. Eventually, as shown by Chiou et al.¹⁰, nonionic organic compounds that are relatively water soluble, as is the case for MCs, reach equilibrium between the external and internal aqueous phases (see Appendix G for further details). In the same vein, we have shown⁴⁷ that the bioconcentration factors (BCFs) for MCs in barley reach steady state under constant exposure concentrations in sand culture experiments. The observed BCFs are comparable to plant–water partition coefficients (K_{PW}) measured by equilibrating sectioned barley biomass and the exposure solution used in the sand culture uptake experiments. These results support the use of the EqP model to predict the uptake of MCs by grasses from IW.

Figure 6-1 illustrates MC partitioning between soil and plant components and water. When the root achieves equilibrium with the soil IW and simultaneously with the plant internal water, both the internal and external aqueous phases are at equilibrium. In this case, the root–water partitioning can be bypassed and the MC concentration in the plant internal water is assumed to be equal to that in the soil IW. Therefore, partitioning between soil OC and plant cuticle determines the MCs bioconcentration in grasses.

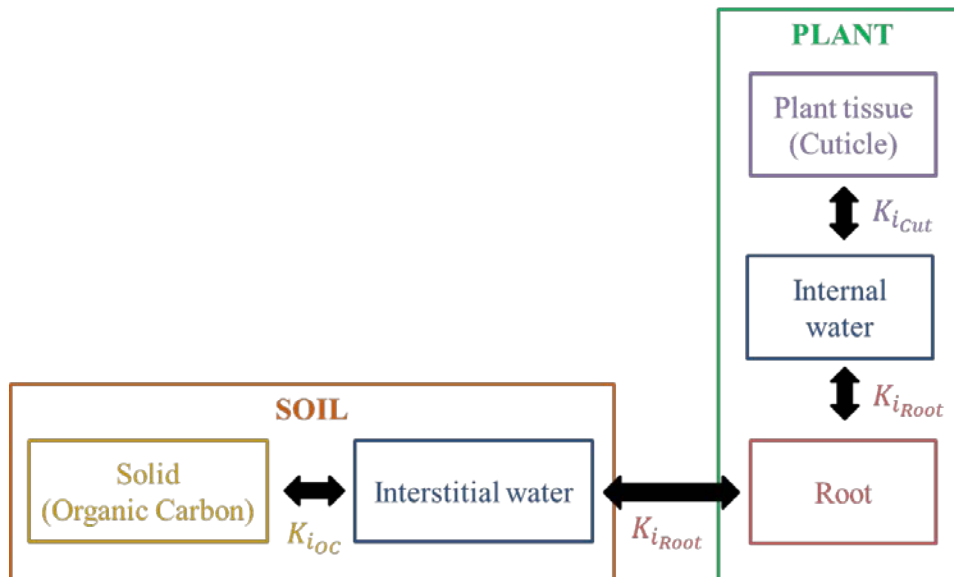


Figure 6-1 Schematic diagram of the basis for the modeling approach: Equilibrium partitioning. Left–right arrows indicate partitioning of MC (or MLC) i between two phases. $K_{i_{OC}}$ = soil organic carbon–water partition coefficient of MC i ($L_{\text{water}} \text{ kg}_{\text{OC}}^{-1}$), $K_{i_{root}}$ = root–water partition coefficient of MC i ($L_{\text{water}} \text{ kg}_{\text{root}}^{-1}$), and $K_{i_{cut}}$ = plant cuticle–water partition coefficient of MC i ($L_{\text{water}} \text{ kg}_{\text{cuticle}}^{-1}$).

Organic carbon is usually assumed to determine the mobility of MCs in soils⁴⁸⁻⁵⁰. It has been shown that OC is the dominant phase for partition of MCs in soils with $f_{oc} > 1 - 2\%$ ^{25, 51, 52}. This is larger than the usual boundary for hydrophobic compounds $f_{oc} = 0.1 - 0.2\%$ as discussed above²¹⁻²⁶.

Plant cuticle is an extracellular hydrophobic membrane composed of interconnected long-chain fatty acids and alkyls^{53, 54} that coats plant organs such as fruits, leaves, and stems⁵⁵, and protects and waterproofs the plant surface. This hydrophobic membrane appears to be the principle site where sorption of MCs occurs. Contributions from plant carbohydrates were also examined before being excluded (see Section 6.3.2).

Uptake through plant leaves from the atmosphere is not included in the model. The model might also be successfully applied to other similar nonionic organic compounds, however, the validation presented in this study is limited to MCs and MLCs only.

6.2.2 Polyparameter Linear Free Energy Relationship (pp-LFER) Models

The pp-LFER models for partitioning between soil OC and water, and between plant cuticle and water used in this work are based on the Abraham polyparameter model³⁷

$$\log K_{SW} = c + eE + sS + aA + bB + vV \quad (6-1)$$

where K_{SW} is the partition coefficient between a solvation phase (e.g., OC, plant cuticle) and water, and the right hand side of Eq. (6-1), are the parameters that account for the free energy contributions from different types of molecular interactions. The uppercase letters in Eq. (6-1) are solute (e.g., MC, MLC) descriptors and the lowercase letters quantify the complementary effect of the solvation phase on the corresponding interaction. The eE term represents the dispersion interactions that are predominant between nonpolar (no permanent multipole moments) molecules and that are not captured by the vV term. The sS term encompasses dipole-dipole or dipole-induced dipole plus some polarizability interactions. The aA and bB terms account for the donation and acceptance of hydrogen bonds, which are bonds between certain types of hydrogen atoms and highly electronegative atoms in polar molecules. aA is solvent acceptor (a)-solute donor (A) and bB is solvent donor (b)-solute acceptor (B). vV accounts for both the energy required for cavity formation and part of the London dispersion interactions, and c is a regression constant^{37, 56}.

6.2.2.1 Plant Cuticle-Water pp-LFER

Platts and Abraham⁹ fitted a pp-LFER model to a dataset of plant cuticle-water partition coefficients, K_{Cut} , for tomato (*Lycopersicum esculentum* Mill) cuticle, for 62 volatile organic compounds ($-0.77 < \log K_{ow} < 6.25$) yielding

$$\log K_{Cut} = -0.415 + 0.596E - 0.413S - 0.508A - 4.096B + 3.908V \quad (6-2)$$

$R^2 = 0.981$; $SD = 0.236$; $F = 566$. K_{Cut} = plant cuticle-water partition coefficient ($L_{water} \text{ kg}_{cuticle}^{-1}$), R^2 = coefficient of determination, SD = regression standard deviation, and F = Fischer's F statistic. The magnitude of the terms in Eq. (6-2) indicate that cuticle is more competitive for solutes than water through π - and n - electron pairs dispersion interactions ($e = 0.596 > 0$), and via cavity formation in the cuticle that requires much less free energy than in water ($v =$

3.908 > 0). This model also indicates that the cuticle is less polar/polarizable ($s = -0.413 < 0$) and accepts hydrogen bonds ($a = -0.508 < 0$) and donates hydrogen bonds ($b = -4.096 < 0$) much less readily than water⁹.

In order to broaden the chemical and plant species diversity and to incorporate MCs and MLCs functionalities, such as aromatic compounds with multiple C-NO₂ groups and non-aromatic cyclic structures with N-NO₂ bonds (Table G-1), into the training set used by Platts and Abraham⁹, additional K_{Cut} data (Table G-5) were collected and included in deriving the plant cuticle–water pp-LFER. Sources for these data are described below.

Since new chemicals and new plant cuticle data were added to the dataset, it was necessary that the solute parameters (uppercase letters in Eq. (6-1)) be obtained from consistent sources. Therefore, three different sources for solute descriptors were compared (Table G-7 to Table G-10): (i) Absolv estimated Abraham Parameters (Absolv-AP) from the Absolv software module of ACD/PhysChem Suite⁵⁷, (ii) Experimentally derived Abraham Parameters (Exp-AP) from Liang et al.⁵⁸ and the UFZ-LSER database⁵⁹, and (iii) Quantum Chemically estimated Abraham Parameters (QCAP) from Liang⁶⁰. These three sources were selected because Absolv-AP have been widely used and are recommended by Platts and Abraham⁹ for any organic structure, and Exp-AP and QCAP have been shown to successfully predict K_{sw} for a wide variety of organic compounds including MCs and MLCs^{58,60}. Three updated plant cuticle–water pp-LFERs were obtained using a multiple linear regression (MLR) with Absolv-AP, Exp-AP, and QCAP as the solute parameters and the full K_{Cut} dataset (Table G-5) as the independent variable. The MLRs were performed using the `lm` function of the R software for statistical computing⁶¹.

6.2.2.2 Soil Organic Carbon–Water pp-LFER

K_{oc} 's were predicted using the pp-LFER developed by Kipka and Di Toro⁶²

$$\begin{aligned} \log K_{\text{oc}} = & 0.670 (\pm 0.088) + 1.075 (\pm 0.061)E - 0.277 (\pm 0.083)S \\ & - 0.363 (\pm 0.100)A - 1.697 (\pm 0.085)B \\ & + 1.468 (\pm 0.077)V \end{aligned} \quad (6-3)$$

for 440 compounds; RMSE = 0.48. K_{oc} = soil organic carbon–water partition coefficient ($\text{L}_{\text{water}} \text{kgoc}^{-1}$), values in parenthesis = \pm the standard error, and RMSE = root mean square error of prediction. This model was built using a large and chemically diverse dataset of nonionic organic compounds with Absolv-AP for the solute parameters. A comparison of the performance of this model relative to other available log K_{oc} pp-LFERs is presented in Appendix G. The solvent parameters in Eq. (6-3) reveal that the soil OC phase has similar solvation capabilities to those shown by plant cuticle in Eq. (6-2). The solute descriptors used to apply this model were the appropriate QCAP reported by Liang⁶⁰ (Table G-14).

6.2.3 Experimental Data

Two types of experimental data were collected from the literature: (i) reported K_{Cut} values, and (ii) measurements of concentrations in plant biomass made during uptake assays where plants were exposed to MCs, or MLCs, in the growth medium. The former dataset was added to the training set used by Platts and Abraham⁹, while the latter served to validate the

partitioning-based bioconcentration model. The MCs, MLCs, and plant species included in the datasets are listed in Table 6-1.

Table 6-1 Munitions Compounds (MCs), Munitions-Like Compounds (MLCs), and plant species included in the datasets.

Abbreviation	Name
MCs and MLCs ^a	
TNT	2,4,6-trinitrotoluene
2,4-DNT	2,4-dinitrotoluene
2,4-DNAN	2,4-dinitroanisoie
RDX	hexahydro-1,3,5-trinitro-1,3,5-triazine
HMX	octahydro-1,3,5,7-tetranitro-1,3,5,7-tetrazocine
4-NAN	4-nitroanisoie
2-M-5-NPYNE	2-methoxy-5-nitropyridine
2,5-DM-4-NANE	2,5-dimethoxy-4-nitroaniline
Plant Species: K_{Cut} dataset ^b	
<i>L. esculentum</i>	Lycopersicum esculentum Mill
<i>F. elastica</i>	Ficus elastica Roxb. var. decora
<i>C. annuum</i>	Capiscum annuum L.
<i>C. aurantium</i>	Citrus aurantium L.
<i>P. laurocerasus</i>	Prunus laurocerasus L.
<i>G. biloba</i>	Ginkgo biloba L.
<i>J. regia</i>	Juglans regia L.
<i>S. lycopersicum</i>	Solanum lycopersicum
<i>M. domestica</i>	Malus domestica
<i>S. tuberosum</i>	Solanum tuberosum
<i>V. heyneana</i>	Vitis heyneana Roem. et Schult
<i>L. multiflorum</i>	Lolium multiflorum Lam.
<i>L. arundinaceum</i>	Lolium arundinaceum
<i>F. rubra</i>	Festuca rubra L.
<i>S. oleracea</i>	Spinacia oleracea

<i>H. vulgare</i> ^c	Hordeum vulgare L.
Plant Species: Uptake dataset ^d	
<i>C. esculentus</i>	Cyperus esculentus
<i>L. perenne</i>	Lolium perenne
<i>M. sativa</i>	Medicago sativa
<i>Z. mays</i>	Zea mays
<i>G. max</i>	Glycine max
<i>S. Sudanese</i>	Sorghum Sudanese
<i>T. aestivum</i>	Triticum aestivum
<i>P. vulgaris</i>	Phaseolus vulgaris
<i>B. rapa</i>	Brassica rapa

^a Further details including chemical properties are listed in Table G-1

^b As reported in corresponding source(s). Data in Table G-5

^c Also in uptake dataset

^d As reported in corresponding source(s). Data in Table G-13

6.2.3.1 Plant Cuticle–Water Partition Coefficients (K_{Cut}) Data

Partition coefficients between plant cuticle and water are commonly determined by individually equilibrating either isolated cuticular membranes (CM) or cuticle matrices (MX, the dewaxed CM) ^{55, 63, 64} with an aqueous solution of an organic compound (i) and calculating the cuticle partition coefficient

$$K_{i_{\text{Cut}}} = \frac{C_{i_{\text{CM or MX}}}}{C_{i_{\text{Water}}}} \quad (6-4)$$

where $C_{i_{\text{CM or MX}}}$ = concentration of compound i in CM or MX ($\text{mg kg}_{\text{dwt}}^{-1}$; dwt: dry weight), and $C_{i_{\text{Water}}}$ = concentration of compound i in the water phase (mg L^{-1}). The K_{Cut} dataset (Table G-5) includes values obtained with CM or MX since the presence of epicuticular wax in the cuticle component proved to have no significant effect on the resulting K_{Cut} (Table G-6) ⁶⁵.

In addition to K_{Cut} from isolated cuticle components, values from experiments performed with whole plant biomass were also included after normalization of the plant–water partition coefficient by the mass fraction of cuticle

$$K_{i_{\text{Cut}}} = \frac{K_{i_{\text{PW}}}}{f_{\text{Cut}}} \quad (6-5)$$

where $K_{i_{\text{PW}}}$ = plant–water partition coefficient of compound i ($\text{L}_{\text{water}} \text{kg}_{\text{dwt plant}}^{-1}$) and f_{Cut} = dry weight fraction of cuticle in the plant ($\text{kg}_{\text{cuticle}} \text{kg}_{\text{dwt plant}}^{-1}$). A total of 143 experimental K_{Cut} for undissociated organic compounds were compiled for the cuticle pp–LFER training set (Table

G-5). The K_{Cut} for compounds containing dissociable groups were either from experiments performed in solutions buffered below the pK_a of the compound or had been corrected for the degree of dissociation using acid dissociation constants as detailed in Kerler and Schonherr⁶⁶. The corrected K_{Cut} were 9 observations for 3 compounds in the training set.

6.2.3.2 Data from Plant Uptake Assays

A dataset was compiled from measurements reported in published uptake assays with grasses and other plants belonging to closely related families exposed to MCs, or MLCs, in the growth medium (Table G-13). In addition to experiments performed in spiked or contaminated field soil (hereafter referred to as "soil"), assays using either coarse quartz sand (99%, 0.85–1.27 mm effective diameter particles, hereafter referred to as "sand") or aqueous solutions as the growth medium were also included in the dataset. The inclusion of these datasets had two purposes: (i) compare the predictions relative to those in soil exposures, and (ii) test only the plant cuticle–water pp–LFER without the need for a soil OC–water pp–LFER. The full dataset includes the concentration in the plant, concentration in the growth medium, exposure time, and dry weight fraction of OC in the soil when applicable (Table G-13).

Concentrations in the plant were for the whole plant or only for the aboveground plant parts when available; measurements in fruits or flowers (e.g., corn kernels or tassels) were not included. Concentrations below reported analytical quantification limits or without clarification on whether they were expressed on a dry or fresh weight basis were excluded. Data from studies not reporting either the soil OC or organic matter content were also excluded (excluded data in Table G-18).

6.2.4 Estimation of Concentrations in Plants Observed in Independent Uptake Assays

Concentrations in grasses and closely related plants reported in published uptake assays were predicted using models of the appropriate partition coefficients. The concentration of MCs and MLCs available for plant root uptake in soil growth medium was estimated using

$$C_{iIW} = \frac{C_{iSoil Solids}}{K_{iSoilW}} = \frac{C_{iSoil Solids}}{K_{iOC} f_{OC}} \quad (6-6)$$

where C_{iIW} = concentration of MC (or MLC) i in the growth medium interstitial water (mg L^{-1}), $C_{iSoil Solids}$ = concentration of MC i in the soil solids (mg kg_{dwt}^{-1}), K_{iSoilW} = soil–water partition coefficient of MC i ($\text{L}_{water} \text{ kg}_{dwt} \text{ soil}^{-1}$), and f_{OC} = dry weight fraction of organic carbon in the soil ($\text{kg}_{OC} \text{ kg}_{dwt} \text{ soil}^{-1}$).

Values for $C_{iSoil Solids}$ were those reported by the sources as the concentrations at the beginning of the exposure or a steady state concentration when available. Values for f_{OC} were also obtained from the sources. A factor of 0.50 was used to convert soil organic matter content (f_{OM}) to f_{OC} (i.e., $f_{OC} = 0.5 f_{OM}$) when needed⁶⁷. K_{iOC} 's were estimated using the pp–LFER in Eq. (6-3) described previously and the appropriate QCAP from Liang⁶⁰ (Table G-14).

The concentration of MCs and MLCs in plant biomass was estimated using

$$C_{iPlant} = K_{iPW} C_{iIW} = K_{iCut} f_{Cut} C_{iIW} \quad (6-7)$$

where $C_{i_{Plant}}$ = concentration of MC i in the plant biomass ($\text{mg kg}_{\text{dwt}}^{-1}$). $C_{i_{IW}}$ directly observed in experiments performed in either sand or aqueous solutions, or predicted using Eq. (6-6) for soil experiments. Due to the scarcity of f_{Cut} values for the species in the uptake assays, a single f_{Cut} from the literature was used for each of the most abundant plant families in the dataset: 0.18 and $0.21 \text{ kg kg}_{\text{dwt}}^{-1}$ for Poaceae and Fabaceae, respectively (Table G-15). An average of these two f_{Cut} values ($0.20 \text{ kg kg}_{\text{dwt}}^{-1}$) was used for the species belonging to the other closely related families. $K_{i_{\text{Cut}}}$'s were estimated using the pp-LFER in Eq. (6-8) described below and the QCAP from Liang⁶⁰ (Table G-14).

6.3 Results and Discussion

6.3.1 Plant Cuticle–Water pp-LFER

The predicted K_{Cut} using Eq. (6-2) versus observed K_{Cut} are shown in Figure 6-2 (Table G-7 to Table G-9). The accuracy of the predictions varied with the source of the Abraham solute descriptors. The predicted K_{Cut} for the nitramine MCs, RDX and HMX, using Absolv-AP were seven orders of magnitude smaller than the observed K_{Cut} (Figure 6-2A). A reason for these large underpredictions might be the absence of the nitramine (N-NO₂) functional group in the Absolv fragment descriptors set⁶⁸. Missing fragments has been identified as a major drawback for the group contribution approach in the estimation of solute descriptors^{60, 69}. N-NO₂ is a highly electronegative group and it increases the potential reactive sites of these MCs⁷⁰. Therefore the fragment descriptor needs to be included.

The predictions for RDX and HMX improved by more than six orders of magnitude when using Exp-AP (Figure 6-2B) and the overall RMSE for all compounds decreased from RMSE = 1.167 (Figure 6-2A) to RMSE = 0.382 (Figure 6-2B). The experimental derivation of molecular properties generally results in high-quality solute descriptors. However, its application to large collections of compounds or proposed MCs early in the development stage, for which no data is available, is limited by time and feasibility constraints. Consequently, an alternative method for the determination of solute descriptors that depends only on molecular structure was also tested.

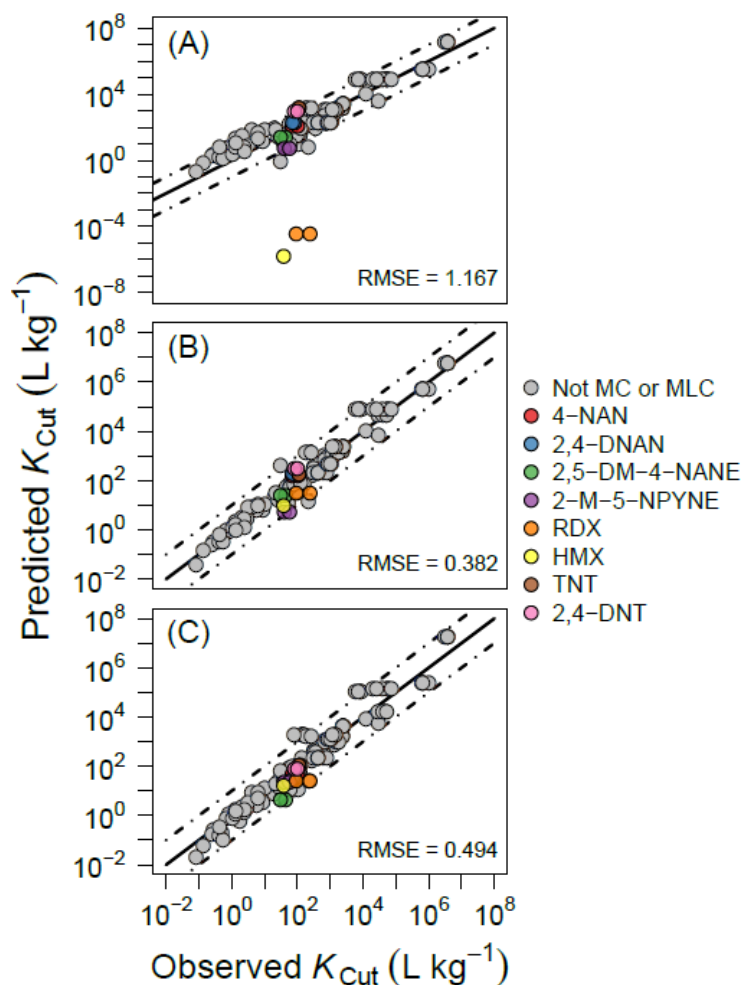


Figure 6-2 pp-LFER-predicted K_{Cut} versus observed K_{Cut} for organic compounds (Table G-5 and Table G-7 to Table G-9). Predictions made using the pp-LFER model from Platts and Abraham⁹, Eq. (6-2), for the full K_{Cut} dataset collected from the literature. Solute descriptors, uppercase letters for Eq. (6-2), are: (A) Absolv-AP⁵⁷; (B) Exp-AP from either Liang et al.⁵⁸ or the UFZ-LSER database⁵⁹, and Absolv-AP when Exp-AP were not available; and (C) Adjusted QCAP⁶⁰. RMSE: root mean square error of prediction (log predicted - log observed) for all compounds included in the full K_{Cut} dataset (Table G-5). The RMSEs for only MCs and MLCs were = (A) 3.154; (B) 0.544; and (C) 0.507. The solid line indicates the best agreement (unity), dashed lines are spaced at 1 log unit from unity.

QCAP's are derived from quantum chemically computed solvent-water partition coefficients and molecular polarizability⁶⁰. The solute descriptors: S , A , and B are simultaneously estimated using 65 quantum chemically computed solvent-water partition coefficients obtained from a continuum solvation model. E and V are independently obtained from quantum mechanical estimated molecular polarizability and molecular volume.^{60, 71} QCAP

are not generated using only experimental solvent–water partitioning data. Therefore, they are incompatible with the solvent parameters in existing pp–LFERs. This inconsistency is corrected by adjusting QCAP using large datasets of Exp–AP (details in Liang ⁶⁰). These adjusted QCAP were used for all the compounds to predict the observed K_{Cut} in Figure 6-2C. The RMSE = 0.494, which is competitive relative to that using Exp–AP.

6.3.1.1 Plant Cuticle–Water pp–LFER Including MCs and MLCs

The dataset employed by Platts and Abraham ⁹ to develop the K_{Cut} pp–LFER in Eq. (6-2), and used to make the predictions in Figure 6-2, did not contain MCs or MLCs. Therefore, pp–LFERs were developed using the expanded K_{Cut} dataset compiled from the literature, which also includes a more heterogeneous group of plant species. The results are shown in Figure 6-3 and the pp–LFERs are listed in Table G-11. The same solute descriptors were used as in Figure 6-2A and B. However, for Figure 6-3C, QCAP were used instead of the adjusted QCAP since QCAP have been found to be superior when a new pp–LFER is being created ⁶⁰.

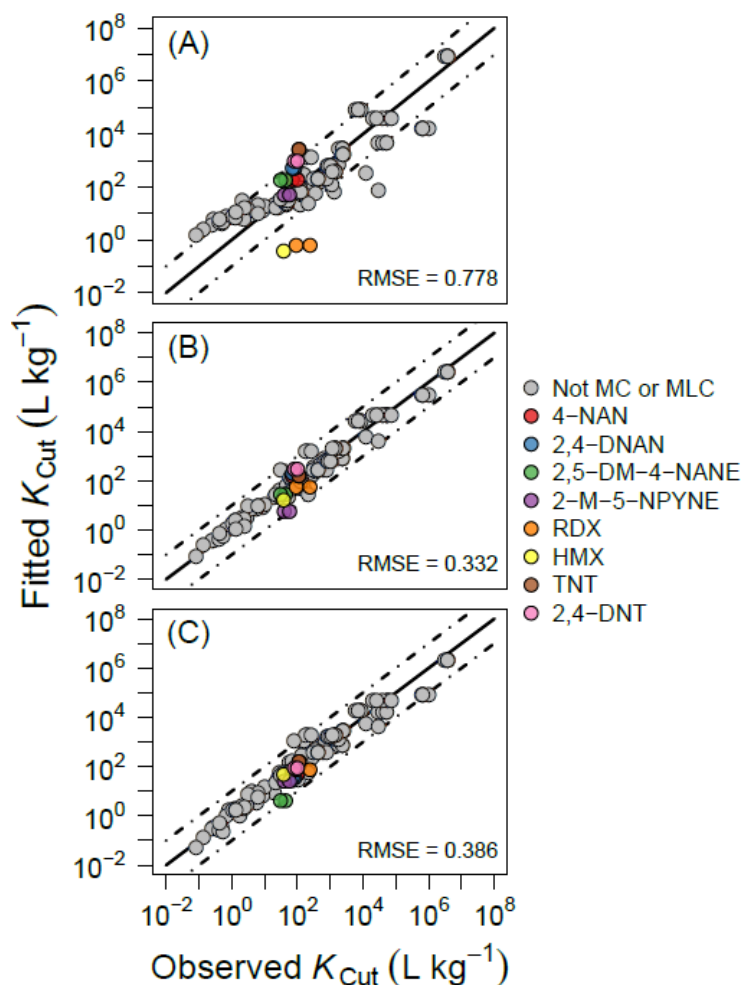


Figure 6-3 pp-LFER-fitted K_{Cut} versus observed K_{Cut} for organic compounds (Table G-5, Table G-7, Table G-8, and Table G-10). Calculations made using the general pp-LFER, Eq. (6-1), fitted to the full K_{Cut} dataset collected from the literature. Solute descriptors, uppercase letters for Eq. (6-1), are: (A) Absolv-AP⁵⁷; (B) Exp-AP from either Liang et al.⁵⁸ or the UFZ-LSER database⁵⁹, and Absolv-AP when Exp-AP were not available; and (C) QCAP⁶⁰. RMSE: root mean square error of prediction (log fitted - log observed) for all compounds included in the full K_{Cut} dataset (Table G-5). The RMSEs for only MCs and MLCs were = (A) 1.261; (B) 0.478; and (C) 0.421. The solid line indicates the best agreement (unity), dashed lines are spaced at 1 log unit from unity.

The K_{Cut} pp-LFER obtained using Absolv-AP improved the overall RMSE (1.167 to 0.778; Figure 6-2A and Figure 6-3A, respectively), but misfits for many of the compounds resulted (Figure 6-3A). The K_{Cut} pp-LFER obtained using Exp-AP slightly changed the already good overall fit (RMSE = 0.382 to 0.332; Figure 6-2B and Figure 6-3B, respectively).

A good fit was also obtained when QCAP were used for all the compounds. The resulting K_{Cut} pp-LFER satisfactorily captured the overall variations in the dataset (Figure 6-3C) yielding a RMSE = 0.386. The resulting plant cuticle–water pp-LFER built using QCAP is

$$\begin{aligned} \log K_{\text{Cut}} = & -0.593 (\pm 0.098) + 0.433 (\pm 0.086)E + 0.900 (\pm 0.164)S \\ & - 0.587 (\pm 0.100)A - 5.409 (\pm 0.253)B \\ & + 3.442 (\pm 0.203)V \end{aligned} \quad (6-8)$$

using 77 compounds; N = 143 data points; RMSE = 0.386; $R_{\text{Adj.}}^2 = 0.939$; SE = 0.394; $F = 437.6$. Values in parenthesis = \pm the standard error, $R_{\text{Adj.}}^2$ = adjusted R^2 and SE = regression residual standard error.

The system parameters in Eq. (6-8), which are the lowercase variables in Eq. (6-1), quantify the extent to which compounds partition to cuticle relative to water. The signs of the system parameters in Eq. (6-8) are consistent with those obtained by Platts and Abraham⁹ (Eq. (6-2)) for all molecular interactions except the dipolarity/polarizability term, s , which is negative $s = -0.413$ in Eq. (6-2) and positive $s = 0.900$ in Eq. (6-8). The $s > 0$ in Eq. (6-8) suggests that cuticle is a stronger solvation phase than water when interacting with polar/polarizable solutes, which is an unexpected result. This is because water is usually stronger than many environmental and biological phases through polarizability interactions⁷², i.e., $s < 0$. However, the ability of a pp-LFER to accurately characterize the properties of a solvation phase such as cuticle, largely relies on the quality and diversity of the solute descriptors used in its calibration dataset⁷².

While the solute descriptors used in Platts and Abraham⁹ (Absolv-AP and/or Exp-AP) produced an excellent agreement to their observed values, the training set used in Eq. (6-8) covers a considerably wider descriptor space in E and S values than that by Eq. (6-2) (range E : 4.29 vs. 3.26; and range S : 2.33 vs. 1.76; respectively. Table G-12). The high end of the S range for Eq. (6-8) comes largely from the MCs and MLCs. These compounds revealed the strength of the cuticle interaction with more polar solutes, which can behave through both specific and nonspecific molecular interactions⁷³. The $s = 0.900$ (Eq. (6-8)) suggests that the cuticle system has a higher ability than water to attract polar solutes through dipolarity/polarizability-type interactions and hence cause the partition coefficient to increase. This might be due in part to the polar characteristics of the fatty acids in the cutin and cutan components of this lipid-like plant component^{53, 54, 74}. It is interesting to note that a positive s is also found in the pp-LFER of the target lipid model (TLM) for the prediction of acute toxicity in aquatic organisms⁷⁵, which uses lipid as the site of action for the sorption of contaminants.

Besides a larger array of plant species in the calibration set, the good quality and wider diversity of solute descriptors supported the choice of Eq. (6-8) over Eq. (6-2) for the prediction of concentrations in plants from published uptake assays.

6.3.2 Estimation of Concentrations in Plants Observed in Independent Uptake Assays

Predictions were made based on the partitioning between soil OC, IW, and plant cuticle, as described previously. The K_{oc} model, Eq. (6-3), was used to estimate the concentration of the MC, or MLC, in the soil IW (i.e., exposure concentration), and the K_{Cut} model, Eq. (6-8), was used to predict the corresponding concentration in the plant biomass. The final equation used to predict the plant concentrations is Eq. (6-9) in Table 6-2, which contains the equations that

comprise the bioconcentration model. An example is presented in Table G-16. Predicted versus observed concentrations in plants for five MCs and two MLCs are shown in Figure 6-4 (Table G-13 and Table G-17).

Table 6-2 Equations for the prediction of concentrations in plants exposed to MCs, or MLCs, in soil and sand or water culture.

A partitioning-based plant bioconcentration model ^a :		
$C_{i_{plant}} = \frac{K_{i_{cut}} f_{cut} C_{i_{soil\ solids}}}{K_{i_{oc}} f_{oc}} \quad (6-9)$		
Var.	Equation	#
$K_{i_{oc}}$:	$\log K_{OC} = 0.670 + 1.075E - 0.277S - 0.363A - 1.697B + 1.468V$	(6-3)
$C_{i_{IW}}$:	$C_{i_{IW}} = \frac{C_{i_{soil\ solids}}}{K_{i_{oc}} f_{oc}}$	(6-6)
$K_{i_{cut}}$:	$\log K_{Cut} = -0.593 + 0.433E + 0.900S - 0.587A - 5.409B + 3.442V$	(6-8)
$C_{i_{plant}}$:	$C_{i_{plant}} = K_{i_{cut}} f_{cut} C_{i_{IW}}$	(6-7)

^a Var.: Variables; *i*: MC, or MLC, of interest; $C_{i_{plant}}$: concentration of compound *i* in the plant biomass (mg kg_{dwt}⁻¹); $K_{i_{cut}}$: plant cuticle–water partition coefficient of *i* (L_{water} kg_{cuticle}⁻¹); f_{cut} : dry weight fraction of cuticle in the plant (kg_{cuticle} kg_{dwt plant}⁻¹); $C_{i_{soil\ solids}}$: concentration of *i* in the soil solids (mg kg_{dwt}⁻¹); $K_{i_{oc}}$: soil organic carbon–water partition coefficient of *i* (L_{water} kg_{oc}⁻¹); f_{oc} : dry weight fraction of organic carbon in the soil (kg_{oc} kg_{dwt soil}⁻¹); *E*, *S*, *A*, *B*, and *V*: solute descriptors for *i* (Table G-14); $C_{i_{IW}}$: concentration of *i* in the growth medium interstitial water (IW) (mg L⁻¹)

The three panels in Figure 6-4 contain the same predicted and observed concentrations in the plant but with different coding by (A) compound, (B) growth medium, and (C) plant species. These are the main factors that affect the performance of the model. Measured concentrations in plants range about four orders of magnitude for seven different compounds including nitroaromatic, nitramines, and nitropyridines. They were predicted within an order of magnitude (Figure 6-4A). No bias in the predictions was observed for either MCs or MLCs.

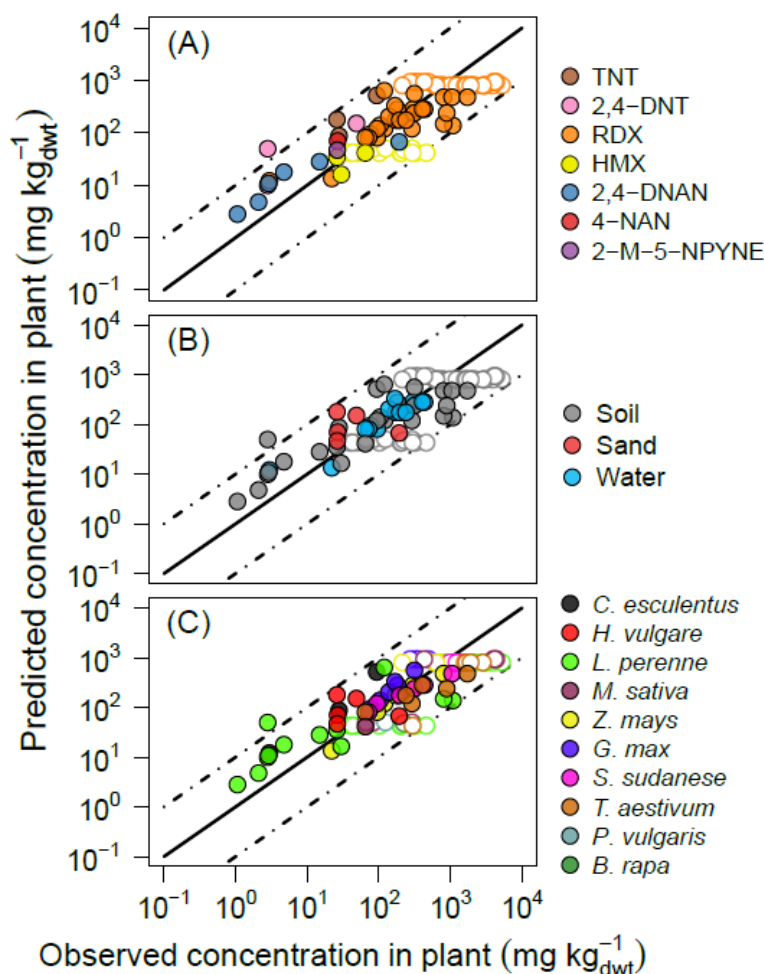


Figure 6-4 Predicted concentrations in the plant versus observed values from published uptake studies (Table 6-2, Table G-13, and Table G-17). Color coding assigned based on: (A) MCs and MLCs (Table 6-1), (B) growth medium, and (C) plant species. Unfilled symbols indicate that the predicted concentration in the interstitial water (using Eq. (6-6)) was replaced by the corresponding MC aqueous solubility as the predicted concentration in the interstitial water exceeded solubility limits. The border color for the unfilled symbols corresponds to the color identification in each panel legend. Root mean square error of prediction ($\log \text{ predicted} - \log \text{ observed}$), excluding predictions bounded at aqueous solubility, $\text{RMSE} = 0.429$. The solid line indicates the best agreement (unity), dashed lines are spaced at 1 log unit from unity.

The data included plant uptake assays carried out in three different growth media: soil, sand, and water (Figure 6-4B). The accuracy of the predictions increased in the order of soil < sand < water as shown by the logarithmic residuals ranging (minimum to maximum) from -0.897 to 1.249, -0.459 to 0.837, and -0.215 to 0.612, respectively (Table G-17). This can be due to both the complexity of the experimental procedure increasing in the order of water < sand < soil and

the inclusion of a K_{oc} model to make the estimations from soil, which contributes to a larger prediction uncertainty relative to that for uptake assays in water or in sand.

Predictions made using only the K_{cut} pp-LFER (Eq. (6-8)), i.e., those for experiments performed with sand and water as the growth medium, produced RMSEs of 0.527 and 0.214, respectively. This indicates that the K_{cut} pp-LFER model alone is capable of estimating within a reasonable uncertainty the bioconcentration of compounds that are available for plant root uptake using only the measured concentration in the water (IW in the case of sand), f_{cut} , and QCAP.

Contribution from plant carbohydrates to the bioconcentration of MCs was also examined before being excluded from the model. A pp-LFER was built using literature data for partition to cellulose and starch from water. Carbohydrate–water partition coefficients, K_{ch} , for MCs and MLCs were small ($-1.016 < (\log K_{ch}) < -0.470$) and accounted for maximum 3.3% of the K_{pw} even assuming carbohydrates were the predominant component of the plant. The overall estimation error of the model changed only by 0.5% when carbohydrates were included as a sorption compartment (see Appendix G for details).

It is difficult to maintain a nearly constant exposure concentration in soils, unlike in water or sand due to both the degradation of the parent compound and the inhomogeneous distribution of the compound in the soil. Unfortunately, for the majority of the data in Figure 6-4 the concentrations in the growth medium were not monitored or prevented from significantly fluctuating. Only the initial concentrations in the growth medium were available (Table G-13). The loss of the parent compound led to the overestimation of some of the resulting plant concentrations (Figure 6-4A and Figure 6-4B), especially for compounds like TNT which have been shown to be readily transformed^{20, 76}.

In order to circumvent the problem of significant compound degradation, large amounts of chemicals are usually applied to soil as the initial exposure treatment during uptake assays (Table G-13). However, for these soil treatments (unfilled symbols in Figure 6-4), the concentration in the IW predicted with the K_{oc} pp-LFER exceeded the aqueous solubility of the compound. Hence, for these cases, the prediction of the concentration in the plant (Eq. (6-7)) was made using the aqueous solubility of the compound as the exposure concentration. This yielded single predictions (the horizontal trends in Figure 6-4), especially for MCs with low aqueous solubilities, such as RDX and HMX (Table G-1).

Figure 6-4C shows the ten plant species in the dataset. No bias in the quality of predictions was observed as a function of plant species. This indicates that using a couple f_{cut} values representing the predominant families in the dataset is not an unreasonable approximation.

Despite the lack of uniformity in the plant concentration data and some uncertainty in the soil concentration over the duration of the exposure, the prediction of concentrations from independent uptake assays for all three growth media using Eq. (6-9) yielded a RMSE = 0.429 (excluding predictions at aqueous solubility). This RMSE is competitive relative to that produced by a detailed dynamic model based on physiological plant uptake by Trapp and Eggen¹¹, RMSE = 0.578 (calculated using data in their Figure 2). Their model predicts concentrations in plants, such as barley and carrot (leaves, stems, and/or roots; excluding fruits for comparison to this work), from greenhouse experiments for nonionic polar organic compounds. Unfortunately, comparison to the other models for bioconcentration of organic compounds in plants cited previously was not possible as a validation to an independent dataset is often not presented or it is performed as a cross-validation⁸.

6.4 Conclusions

Bioconcentration of MCs and MLCs in grasses can be estimated based on the partitioning between the growth medium solids, IW, and plant. Partitioning between soil OC and IW, and between IW and plant cuticle for MCs, MLCs, and other organic compounds can be predicted with pp-LFERs. Smaller estimation errors ($RMSE = 0.386$) for the K_{Cut} pp-LFER are obtained using QCAP as the solute descriptors for all compounds relative to using Absolv-AP or Exp-AP. The superior quality of the QCAP and the diversity of the K_{Cut} solute training dataset, enable the better characterization of the solvation properties of the plant cuticle.

A demonstration of the prediction capabilities of the partitioning-based model to estimate concentrations from independent plant uptake assays provides evidence of the model's usefulness and practicality. More accurate predictions are obtained for the estimation of plant concentrations from assays performed in sand or water than those in complex soils.

The results presented suggest that the partitioning-based plant bioconcentration model proposed (Eq. (6-9)), which utilizes quantum chemically computed Abraham parameters (QCAP) and two pp-LFERs, can be used to predict the MCs concentrations in grasses from molecular structure only.

REFERENCES

1. Ampleman G, Thiboutot S, Lewis J, Marois A, Gagnon A, Bouchard M, Jenkins T, Ranney TA, Pennington JC. Evaluation of the contamination by explosives and metals in soils, vegetation, surface water and sediment at Cold Lake Air Weapons Range (CLAWR), Alberta, Phase II Final report. Technical Report No. DRDC-Valcartier-TR-2004-204. Valcartier, Québec, Canada: Defence Research and Development Canada - Valcartier, Valcartier QUE (CAN); Cold Regions Research and Engineering Lab, Hanover NH (US). **2004**;1-116.
2. Jenkins, T.F.; Hewitt, A.D.; Grant, C.L.; Thiboutot, S.; Ampleman, G.; Walsh, M.E.; Ranney, T.A.; Ramsey, C.A.; Palazzo, A.J.; Pennington, J.C. Identity and distribution of residues of energetic compounds at army live-fire training ranges. *Chemosphere* **2006**, *63* (8), 1280-1290; 10.1016/j.chemosphere.2005.09.066.
3. Clausen, J.L.; Korte, N. Fate and transport of energetics from surface soils to groundwater, In Chappell, M.A.; Price, C.L.; George, R.D., Eds.; American Chemical Society: Washington, DC, **2011**; Vol.1069 pp. 273-316.
4. Briggs, G.G.; Bromilow, R.H.; Evans, A.A. Relationships between lipophilicity and root uptake and translocation of non-ionised chemicals by barley. *Pestic. Sci.* **1982**, *13* (5), 495-504; 10.1002/ps.2780130506.
5. Briggs, G.G.; Bromilow, R.H.; Evans, A.A.; Williams, M. Relationships between lipophilicity and the distribution of non-ionised chemicals in barley shoots following uptake by the roots. *Pestic. Sci.* **1983**, *14* (5), 492-500; 10.1002/ps.2780140506.
6. Travis, C.C.; Arms, A.D. Bioconcentration of organics in beef, milk, and vegetation. *Environ. Sci. Technol.* **1988**, *22* (3), 271-274; 10.1021/es00168a005.
7. Trapp, S.; Matthies, M. Generic one-compartment model for uptake of organic chemicals by foliar vegetation. *Environ. Sci. Technol.* **1995**, *29* (9), 2333-2338; 10.1021/es00009a027.
8. Dowdy, D.L.; McKone, T.E. Predicting plant uptake of organic chemicals from soil or air using octanol/water and octanol/air partition ratios and a molecular connectivity index. *Environ. Sci. Technol.* **1997**, *16* (12), 2448-2456; 10.1002/etc.5620161203.
9. Platts, J.A.; Abraham, M.H. Partition of volatile organic compounds from air and from water into plant cuticular matrix: An LFER analysis. *Environ. Sci. Technol.* **2000**, *34* (2), 318-323; 10.1021/es9906195.
10. Chiou, C.T.; Sheng, G.; Manes, M. A partition-limited model for the plant uptake of organic contaminants from soil and water. *Environ. Sci. Technol.* **2001**, *35* (7), 1437-1444; 10.1021/es0017561.

11. Trapp, S.; Eggen, T. Simulation of the plant uptake of organophosphates and other emerging pollutants for greenhouse experiments and field conditions. *Environ. Sci. Pollut. R.* **2013**, *20* (6), 4018-4029; 10.1007/s11356-012-1337-7.
12. Li, H.; Sheng, G.; Chiou, C.T.; Xu, O. Relation of organic contaminant equilibrium sorption and kinetic uptake in plants. *Environ. Sci. Technol.* **2005**, *39* (13), 4864-4870; 10.1021/es050424z.
13. Bromilow, R.H.; Chamberlain, K. Principles governing uptake and transport of chemicals, In *Plant Contamination: Modeling and Simulation of Organic Chemical Processes*, Trapp, S.; McFarlane, J.C., Eds.; CRC Press, Inc.: Boca Raton, FL, **1995**; pp. 37-68.
14. Cunningham, S.D.; Anderson, T.A.; Schwab, A.P.; Hsu, F.C. Phytoremediation of soils contaminated with organic pollutants, In *Advances in Agronomy*, Sparks, D.L., Ed.; Academic Press, Inc.: San Diego, CA, **1996**; Vol.56 pp. 55-114.
15. Collins, C.; Fryer, M.; Grosso, A. Plant uptake of non-ionic organic chemicals. *Environ. Sci. Technol.* **2006**, *40* (1), 45-52; 10.1021/es0508166.
16. Pennington JC, Myers TE, Davis WM, Olin TJ, McDonald TA, Hayes CA, Townsend DM. Impacts of sorption on in situ bioremediation of explosives-contaminated soils. Technical Report No. IRRP-95-1. Vicksburg, MS: U.S. Army Waterways Experiment Station, Corps of Engineers. **1995**;1-54.
17. Larson, S.L.; Martin, W.A.; Escalon, B.L.; Thompson, M. Dissolution, sorption, and kinetics involved in systems containing explosives, water, and soil. *Environ. Sci. Technol.* **2007**, *42* (3), 786-792; 10.1021/es0717360.
18. Berthelot, Y.; Valton, É; Auroy, A.; Trottier, B.; Robidoux, P.Y. Integration of toxicological and chemical tools to assess the bioavailability of metals and energetic compounds in contaminated soils. *Chemosphere* **2008**, *74* (1), 166-177; 10.1016/j.chemosphere.2008.07.056.
19. Savard, K.; Sarrazin, M.; Dodard, S.G.; Monteil-Rivera, F.; Kuperman, R.G.; Hawari, J.; Sunahara, G.I. Role of soil interstitial water in the accumulation of hexahydro-1,3,5-trinitro-1,3,5-triazine in the earthworm *Eisenia andrei*. *Environ Toxicol Chem.* **2010**, *29* (4), 998-1005; 10.1002/etc.113.
20. Kalderis, D.; Juhasz, A.L.; Boopathy, R.; Comfort, S. Soils contaminated with explosives: Environmental fate and evaluation of state-of-the-art remediation processes (IUPAC Technical Report). *Pure Appl Chem* **2011**, *83* (7), 1407-1484; 10.1351/PAC-REP-10-01-05.
21. Karickhoff, S.W.; Brown, D.S.; Scott, T.A. Sorption of hydrophobic pollutants on natural sediments. *Water Research* **1979**, *13* (3), 241-248; 10.1016/0043-1354(79)90201-X.

22. Karickhoff, S.W. Semi-empirical estimation of sorption of hydrophobic pollutants on natural sediments and soils. *Chemosphere* **1981**, *10* (8), 833-846; 10.1016/0045-6535(81)90083-7.
23. Schwarzenbach, R.P.; Gschwend, P.M.; Imboden, D.M. Sec. 9.3: Sorption of Neutral Organic Compounds from Water to Solid-Phase Organic Matter (POM), In *Environmental Organic Chemistry*, 2nd ed.; Anonymous ; John Wiley & Sons: Hoboken, NJ, 2005; .
24. Liu, Z.; He, Y.; Xu, J.; Huang, P.; Jilani, G. The ratio of clay content to total organic carbon content is a useful parameter to predict adsorption of the herbicide butachlor in soils. *Environmental Pollution* **2008**, *152* (1), 163-171; 10.1016/j.envpol.2007.05.006.
25. Dontsova, K.M.; Hayes C FAU - Pennington, Judith,C.; FAU, P.J.; Porter, B. Sorption of high explosives to water-dispersible clay: influence of organic carbon, aluminosilicate clay, and extractable iron. *Journal of environmental quality JID - 0330666* **2009**, .
26. Milinovic, J.; Lacorte, S.; Rigol, A.; Vidal, M. Sorption behaviour of nonylphenol and nonylphenol monoethoxylate in soils. *Chemosphere* **2015**, *138*, 952-959; 10.1016/j.chemosphere.2014.12.037.
27. Sabljíć, A.; Güsten, H.; Verhaar, H.; Hermens, J. QSAR modelling of soil sorption. Improvements and systematics of log KOC vs. log KOW correlations. *Chemosphere* **1995**, *31* (11–12), 4489-4514; 10.1016/0045-6535(95)00327-5.
28. Gawlik, B.M.; Sotiriou, N.; Feicht, E.A.; Schulte-Hostede, S.; Kettrup, A. Alternatives for the determination of the soil adsorption coefficient, K_{oc} , of non-ionic organic compounds — a review. *Chemosphere* **1997**, *34* (12), 2525-2551; 10.1016/S0045-6535(97)00098-2.
29. Doucette, W.J. Quantitative structure-activity relationships for predicting soil-sediment sorption coefficients for organic chemicals. *Environ. Sci. Technol.* **2003**, *22* (8), 1771-1788; 10.1897/01-362.
30. von Oepen, B.; Kördel, W.; Klein, W.; Schüürmann, G. QSAR in environmental toxicology predictive QSPR models for estimating soil sorption coefficients: potential and limitations based on dominating processes. *Sci. Total Environ.* **1991**, *109*, 343-354; 10.1016/0048-9697(91)90189-L.
31. Wei, D.B.; Wu, C.D.; Wang, L.S.; Hu, H.Y. QSPR-based prediction of adsorption of halogenated aromatics on yellow-brown soil. *SAR QSPR Environ. Res.* **2003**, *14* (3), 191-198; 10.1080/10629360310000101773.
32. Kozerski, G.E.; Xu, S.; Miller, J.; Durham, J. Determination of soil-water sorption coefficients of volatile methylsiloxanes. *Environ. Toxicol. Chem.* **2014**, *33* (9), 1937-1945; 10.1002/etc.2640.

33. Goss, K.; Schwarzenbach, R.P. Linear free energy relationships used to evaluate equilibrium partitioning of organic compounds. *Environ. Sci. Technol.* **2001**, *35* (1), 1-9; 10.1021/es000996d.
34. Barbour, J.P.; Smith, J.A.; Chiou, C.T. Sorption of aromatic organic pollutants to grasses from water. *Environ. Sci. Technol.* **2005**, *39* (21), 8369-8373; 10.1021/es0504946.
35. Zhang, M.; Zhu, L. Sorption of polycyclic aromatic hydrocarbons to carbohydrates and lipids of ryegrass root and implications for a sorption prediction model. *Environ. Sci. Technol.* **2009**, *43* (8), 2740-2745; 10.1021/es802808q.
36. Hung, H.; Lin, T.; Chiou, C.T. Partition coefficients of organic contaminants with carbohydrates. *Environ. Sci. Technol.* **2010**, *44* (14), 5430-5436; 10.1021/es1004413.
37. Abraham, M.H. Scales of solute hydrogen-bonding: their construction and application to physicochemical and biochemical processes. *Chem. Soc. Rev.* **1993**, *22* (2), 73-83; 10.1039/CS9932200073.
38. Goss, K. Predicting the equilibrium partitioning of organic compounds using just one linear solvation energy relationship (LSER). *Fluid Phase Equilibr.* **2005**, *233* (1), 19-22; 10.1016/j.fluid.2005.04.006.
39. Hale, S.E.; Cornelissen, G.; Arp, H.P.H. Comment on 'Partition coefficients of organic contaminants with carbohydrates'. *Environ. Sci. Technol.* **2011**, *45* (3), 1158-1158; 10.1021/es103754p.
40. Meador, J.; Casillas, E.; Sloan, C.; Varanasi, U. Comparative Bioaccumulation of Polycyclic Aromatic-Hydrocarbons from Sediment by 2 Infaunal Invertebrates. *Mar. Ecol. Prog. Ser.* **1995**, *123* (1-3), 107-124; 10.3354/meps123107.
41. Jager, T. Mechanistic approach for estimating bioconcentration of organic chemicals in earthworms (Oligochaeta). *Environmental Toxicology and Chemistry* **1998**, *17* (10), 2080-2090; 10.1897/1551-5028(1998)0172.3.CO;2.
42. Welke, B.; Ettlinger, K.; Riederer, M. Sorption of Volatile Organic Chemicals in Plant Surfaces. *Environ. Sci. Technol.* **1998**, *32* (8), 1099-1104; 10.1021/es970763v.
43. Kraaij, R.; Mayer, P.; Busser, F.; Bolscher, M.; Seinen, W.; Tolls, J. Measured pore-water concentrations make equilibrium partitioning work - A data analysis. *Environ. Sci. Technol.* **2003**, *37* (2), 268-274; 10.1021/es020116q.
44. Arnot, J.A.; Gobas, F.A.P.C. A review of bioconcentration factor (BCF) and bioaccumulation factor (BAF) assessments for organic chemicals in aquatic organisms. *Env. Rev.* **2006**, *14* (4), 257-297; 10.1139/A06-005.

45. Dodard, S.G.; Sarrazin, M.; Hawari, J.; Paquet, L.; Ampleman, G.; Thiboutot, S.; Sunahara, G.I. Ecotoxicological assessment of a high energetic and insensitive munitions compound: 2,4-Dinitroanisole (DNAN). *J. Hazard. Mater.* **2013**, *262* (0), 143-150; 10.1016/j.jhazmat.2013.08.043.
46. Kuo, D.T.F.; Di Toro, D.M. Biotransformation model of neutral and weakly polar organic compounds in fish incorporating internal partitioning. *Environmental Toxicology and Chemistry* **2013**, *32* (8), 1873-1881; 10.1002/etc.2259.
47. Torralba-Sanchez, T.L. Bioconcentration of munitions compounds in plants and worms: experiments and modeling. Doctoral Dissertation, University of Delaware, Newark, DE, USA, **2016**.
48. Singh, N.; Berns, A.E.; Hennecke, D.; Hoerner, J.; Koerdel, W.; Schaeffer, A. Effect of soil organic matter chemistry on sorption of trinitrotoluene and 2,4-dinitrotoluene. *J. Hazard. Mater.* **2010**, *173* (1-3), 343-348; 10.1016/j.jhazmat.2009.08.090.
49. Alavi, G.; Chung, M.; Lichwa, J.; D'Alessio, M.; Ray, C. The fate and transport of RDX, HMX, TNT and DNT in the volcanic soils of Hawaii: A laboratory and modeling study. *J. Hazard. Mater.* **2011**, *185* (2-3), 1600-1604; 10.1016/j.jhazmat.2010.10.039.
50. Clausen, J.L.; Scott, C.; Osgerby, I. Fate of Nitroglycerin and Dinitrotoluene in Soil at Small Arms Training Ranges. *Soil and Sediment Contamination: An International Journal* **2011**, *20* (6), 649-671; 10.1080/15320383.2011.594108.
51. Sharma, P.; Mayes, M.A.; Tang, G. Role of soil organic carbon and colloids in sorption and transport of TNT, RDX and HMX in training range soils. *Chemosphere* **2013**, *92* (8), 993-1000; 10.1016/j.chemosphere.2013.03.028.
52. Miglino, A.N. Modeling the adsorption and desorption of munition constituents on soils using reversible and resistant components. Doctoral Dissertation, University of Delaware, Newark, DE, USA, **2015**.
53. Bargel, H.; Koch, K.; Cerman, Z.; Neinhuis, C. Structure-function relationships of the plant cuticle and cuticular waxes - a smart material? *Funct. Plant Biol.* **2006**, *33* (10), 893-910; 10.1071/FP06139.
54. Dominguez, E.; Cuartero, J.; Heredia, A. An overview on plant cuticle biomechanics. *Plant Sci.* **2011**, *181* (2), 77-84; 10.1016/j.plantsci.2011.04.016.
55. Schreiber, L.; Schonherr, J. *Water and solute permeability of plant cuticles: measurement and data analysis*. Springer-Verlag Berlin Heidelberg: Berlin, Germany, **2009**.
56. Arey, J.; Green, W.; Gschwend, P. The electrostatic origin of Abraham's solute polarity parameter. *J Phys Chem B* **2005**, *109* (15), 7564-7573; 10.1021/jp044525f.

57. Advanced Chemistry Development Inc. ACD/PhysChem Suite. Absolv module. **2013**, v. 5.0.
58. Liang, Y.; Kuo, D.T.F.; Allen, H.E.; Di Toro, D.M. Experimental determination of solvent-water partition coefficients and Abraham parameters for munition constituents. *Chemosphere* **2016**, *161*, 429-437; 10.1016/j.chemosphere.2016.07.028.
59. Ulrich, N., Endo, S., Brown, T.N., Watanabe, N., Bronner, G., Abraham, M.H., Goss, K.-U., UFZ-LSER database v 3.2 [Internet], Leipzig, Germany, Helmholtz Centre for Environmental Research-UFZ. **2016** [accessed on 16.11.2016]. Available from <http://www.ufz.de/lserd>
60. Liang, Y. Determining Abraham solute and system parameters for neutral organic compounds using quantum chemical methods. Doctoral Dissertation, University of Delaware, Newark, DE, USA, **2016**.
61. R Development Core Team R: A language and environment for statistical computing. **2015**, 3.2.0.
62. Kipka, U.; Di Toro, D.M. A linear solvation energy relationship model of organic chemical partitioning to particulate organic carbon in soils and sediments. *Environ. Toxicol. Chem.* **2011**, *30* (9), 2013-2022; 10.1002/etc.611.
63. Holloway, P.J.; Baker, E.A. Isolation of plant cuticles with zinc chloride-hydrochloric acid solution. *Plant Physiol.* **1968**, *43* (11), 1878-1879; 10.1104/pp.43.11.1878.
64. Riederer, M.; Schonherr, J. Accumulation and transport of (2,4-dichlorophenoxy)acetic acid in plant cuticles: I. Sorption in the cuticular membrane and its components. *Ecotoxicol. Environ. Saf.* **1984**, *8* (3), 236-247; 10.1016/0147-6513(84)90027-7.
65. Sabljic, A.; Gusten, H.; Schonherr, J.; Riederer, M. Modeling plant uptake of airborne organic-chemicals .1. Plant cuticle water partitioning and molecular connectivity. *Environ. Sci. Technol.* **1990**, *24* (9), 1321-1326; 10.1021/es00079a004.
66. Kerler, F.; Schonherr, J. Accumulation of Lipophilic Chemicals in Plant Cuticles - Prediction from Octanol Water Partition-Coefficients. *Arch. Environ. Contam. Toxicol.* **1988**, *17* (1), 1-6.
67. Pribyl, D.W. A critical review of the conventional SOC to SOM conversion factor. *Geoderma* **2010**, *156* (3-4), 75-83; 10.1016/j.geoderma.2010.02.003.
68. Platts, J.A.; Butina, D.; Abraham, M.H.; Hersey, A. Estimation of molecular linear free energy relation descriptors using a group contribution approach. *J. Chem. Inf. Comput. Sci.* **1999**, *39* (5), 835-845; 10.1021/ci980339t.
69. Hou, T.J.; Xia, K.; Zhang, W.; Xu, X.J. ADME evaluation in drug discovery. 4. Prediction of aqueous solubility based on atom contribution approach. *J. Chem. Inf. Comput. Sci.* **2004**, *44* (1), 266-275; 10.1021/ci034184n.

70. Kandhakumar, G.; Jothi, M.; Kumaradhas, P. Probing the effect of nitro groups in nitramine based energetic molecules: a DFT and charge density study. *Mol. Simulat.* **2016**, *42* (3), 173-185; 10.1080/08927022.2015.1031130.
71. Lin, S.; Sandler, S.I. A priori phase equilibrium prediction from a segment contribution solvation model. *Ind. Eng. Chem. Res.* **2002**, *41* (5), 899-913; 10.1021/ie001047w.
72. Endo, S.; Goss, K. Applications of polyparameter linear free energy relationships in environmental chemistry. *Environ. Sci. Technol.* **2014**, *48* (21), 12477-12491; 10.1021/es503369t.
73. Schwarzenbach, R.P.; Gschwend, P.M.; Imboden, D.M. Environmental organic chemistry, John Wiley & Sons: Hoboken, NJ, **2005**.
74. Yeats, T.H.; Rose, J.K.C. The Formation and Function of Plant Cuticles. *Plant Physiol.* **2013**, *163* (1), 5-20; 10.1104/pp.113.222737.
75. Kipka, U.; Di Toro, D.M. Technical basis for polar and nonpolar narcotic chemicals and polycyclic aromatic hydrocarbon criteria. III. A polyparameter model for target lipid partitioning. *Environmental Toxicology and Chemistry* **2009**, *28* (7), 1429-1438; 10.1897/08-364.1.
76. Esteve-Nunez, A.; Caballero, A.; Ramos, J.L. Biological degradation of 2,4,6-trinitrotoluene. *Microbiol. Mol. Biol. Rev.* **2001**, *65* (3), 335-352; 10.1128/MMBR.65.3.335-352.2001.

Appendix G

SUPPLEMENTARY INFORMATION FOR: ESTIMATING GRASS–SOIL BIOCONCENTRATION OF MUNITIONS COMPOUNDS FROM MOLECULAR STRUCTURE

CONTENTS: Large tables located in accompanying Microsoft (MS) Excel file.

Munitions Compounds (MCs) and Munitions–Like Compounds (MLCs)

Table G-1 Selected characteristics and physicochemical properties of the MCs and MLCs.

Transport of Munitions Compounds (MCs) between Soil and Plant

Figure G-1 Schematic diagram for the advective and diffusive transport of MCs and MLCs between soil and water.

Table G-2 Literature measured average volumetric flows in xylem and phloem for four plant species

Comparison of pp-LFERs for Soil Organic Carbon–Water Partition Coefficients (K_{oc})

Table G-3 Observed and predicted soil organic carbon–water partition coefficients (K_{oc}). Located in Chapter_6_Appendix G_Tables.xlsx file.

Table G-4 Solute descriptor space coverage for three log K_{oc} polyparameter linear free energy relationships (pp-LFERs).

Figure G-2 Cross–plot of predicted K_{oc} versus observed K_{oc} .

Figure G-3 Cross–plot of predicted K_{oc} versus MC–averaged observed K_{oc} .

Polyparameter Linear Free Energy Relationship (pp-LFER) Models

Table G-5 Plant cuticle–water partition coefficients (K_{cut}) data. Located in Chapter_6_Appendix G_Tables.xlsx file.

Table G-6 Comparison of plant cuticle membrane–water partition coefficients (K_{CM}) and plant cuticle matrix–water partition coefficients (K_{MX}) for undissociated organic compounds.

Table G-7 K_{cut} calculated using pp-LFERs with Absolv estimated Abraham Parameters (Absolv-AP). Located in Chapter_6_Appendix G_Tables.xlsx file.

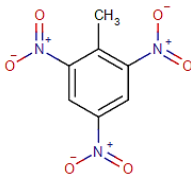
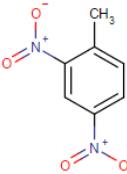
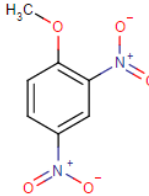
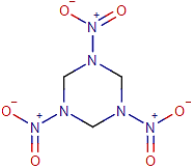
Table G-8	K_{Cut} calculated using pp-LFERs with Experimentally derived Abraham Parameters (Exp-AP). Located in Chapter_6_Appendix G_Tables.xlsx file.
Table G-9	K_{Cut} calculated using pp-LFER with Adjusted Quantum Chemically estimated Abraham Parameters (Adjusted QCAP). Located in Chapter_6_Appendix G_Tables.xlsx file.
Table G-10	K_{Cut} calculated using pp-LFER with Quantum Chemically estimated Abraham Parameters (QCAP). Located in Chapter_6_Appendix G_Tables.xlsx file.
Table G-11	K_{Cut} pp-LFERs obtained using three different sources of solute descriptors.
Table G-12	Range of solute descriptor space for the K_{Cut} pp-LFERs by Platts and Abraham ¹ and this work.

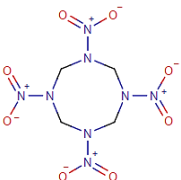
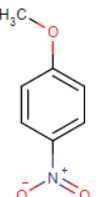
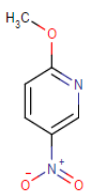
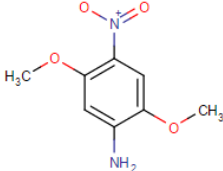
Estimation of Concentrations in Plants Observed in Independent Uptake Assays

Table G-13	Data from published uptake assays with plants exposed to MCs, or MLCs. Located in Chapter_6_Appendix G_Tables.xlsx file.
Table G-14	Solute descriptors used for the prediction of MCs and MLCs concentrations in plant biomass. Located in Chapter_6_Appendix G_Tables.xlsx file.
Table G-15	Fraction of cuticle, f_{Cut} , for plant species in the uptake assays dataset.
Table G-16	Example for prediction of a MC concentration in a grass.
Table G-17	Predictions for published MCs and MLCs uptake assays. Located in Chapter_6_Appendix G_Tables.xlsx file.
Table G-18	Examples of MCs plant uptake data surveyed but excluded from the validation dataset. Located in Chapter_6_Appendix G_Tables.xlsx file.
Table G-19	Observed carbohydrates–water partition coefficients (K_{Ch}) and fitted K_{Ch} with pp-LFER using QCAP. Located in Chapter_6_Appendix G_Tables.xlsx file.
Table G-20	K_{Ch} pp-LFER
Table G-21	Predictions for published MCs and MLCs uptake assays including carbohydrates as a sorption compartment. Located in Chapter_6_Appendix G_Tables.xlsx file.
Figure G-4	Cross-plot of predicted versus observed MCs and MLCs concentrations in plants including carbohydrates as a sorption compartment

MCs and Munitions–Like Compounds (MLCs)

Table G-1 Selected characteristics and physicochemical properties of the MCs and MLCs.

Class	Compound ^a	CAS #	Molecular Weight	Structure	Aqueous Solubility ^b mg L ⁻¹	log K _{ow} ^b
MCs: Nitroaromatics	TNT	118-96-7	227.13		115	1.60
	2,4-DNT	121-14-2	182.14		200	1.98
	2,4-DNAN	119-27-7	198.14		155	1.58 ^c
MCs: Nitramines	RDX	121-82-4	222.12		60	0.87

	HMX	2691-41-0	296.16		5	0.16
	4-NAN	100-17-4	153.14		590	2.03
MLCs	2-M-5-NPYNE	5446-92-4	154.13		1406 ^d	1.55
	2,5-DM-4-NANE	6313-37-7	198.18		1801 ^d	1.63 ^d

^a Abbreviations: 2,4,6-trinitrotoluene (TNT); 2,4-dinitrotoluene (2,4-DNT); 2,4-dinitroanisole (2,4-DNAN); hexahydro-1,3,5-trinitro-1,3,5-triazine (RDX); octahydro-1,3,5,7-tetranitro-1,3,5,7-tetrazocine (HMX); 4-nitroanisole (4-NAN); 2-methoxy-5-nitropyridine (2-M-5-NPYNE); 2,5-dimethoxy-4-nitroaniline (2,5-DM-4-NANE)

^b Experimental data from EPI Suite database ²

^c Experimental value from Hawari et al. ³

^d Estimate from EPI Suite ² in absence of an experimental value

Transport of Munitions Compounds (MCs) between Soil and Plant

MCs can potentially be transported through both advective and diffusive processes between the soil interstitial water and the plant, as seen in Figure G-1. Two water flows in the plant are considered: (i) inward flow (Q_{in}) from the soil interstitial water (IW) to the plant, moving along the plant xylem, and (ii) outward flow (Q_{out}) from the plant to the soil IW, moving along the plant phloem. At steady state, the mass of MC entering the plant should equal the mass of MC leaving the plant. For advective transport only, the mass balance equation is

$$Q_{in}C_{in} = Q_{out}C_{out} \quad (G-1)$$

where C is the concentration of the MC. Rearranging Eq. (G-1) yields

$$\frac{Q_{in}}{Q_{out}} = \frac{C_{out}}{C_{in}} \quad (G-2)$$

At steady state, Eq. (G-2) specifies the ratio of concentrations in the outflow and inflow. Table G-2 contains measured values for average volumetric flows in both xylem and phloem for four different plant species. At night Q_{out} (i.e., Q_{phloem}) can be up to half of Q_{in} (i.e., Q_{xylem}) for herbaceous plants like tobacco; Q_{in} largely dominates on the average daily cycle. As a daily average the concentration ratio is given by Eq.(G-2).

In addition to advective transport, diffusive mass transfer also occurs. Diffusive exchange (ϵ_{diff}) across the root would decrease the ratio of C_{out} to C_{in} . As shown in Figure G-1, both the diffusive exchange in and out occur between the interstitial water and the root. Therefore, if the MC concentration builds up inside the plant, a gradient favoring outward transport of the MC will arise counterbalancing the inward transport. In this way, the diffusive exchange would lower the concentration ratio. If diffusive exchange is much larger than advective exchange, then $C_{out} \cong C_{in}$. In any case the return flow and diffusive exchange prevent the internal plant concentration from increasing indefinitely.

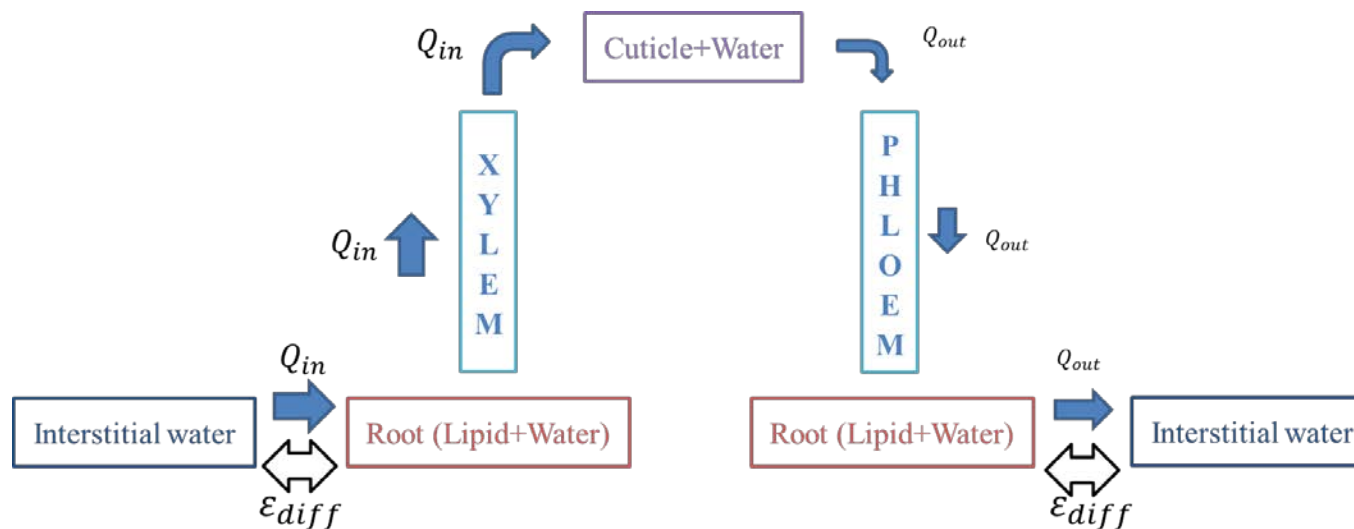


Figure G-1 Schematic diagram for the advective and diffusive transport of MCs and MLCs between soil and water. Q_{in} = inward flow moving along the plant xylem; Q_{out} = outward flow moving along the plant phloem; ϵ_{diff} = diffusive exchange.

Table G-2 Literature measured average volumetric flows in xylem and phloem for four plant species^a.

Plant common name ^b	Q_{xylem}			Q_{phloem}^c	$\frac{Q_{xylem}}{Q_{phloem}}$		
	diurnal mm ³ s ⁻¹	nocturnal mm ³ s ⁻¹	Avg. daily mm ³ s ⁻¹		diurnal mm ³ s ⁻¹	nocturnal mm ³ s ⁻¹	Avg. daily mm ³ s ⁻¹
Grey poplar	16.25	5.00	10.63	0.75	21.67	6.67	14.17
Tomato	7.50	2.50	5.00	0.10	75.00	25.00	50.00
Castor Bean	3.50	0.50	2.00	0.20	17.50	2.50	10.00
Tobacco	1.25	0.20	0.73	0.10	12.50	2.00	7.25

^a Values from Figures 6 and 9 in Windt et al. ⁴

^b Plant species, as reported in source: Grey poplar: *Populus tremula* × *Populus alba*, INRA clone 717 1B4; Tomato: *Lycopersicon esculentum* cv. Counter; Castor bean: *Ricinus communis*; Tobacco: *Nicotiana tabacum* cv. Petit Havana SR1

^c Phloem flow showed small fluctuations throughout the daily cycle, but averaged over a whole day or night period the differences were insignificant (Figure 6 and 7 in Windt et al. ⁴)

Comparison of pp-LFERs for Soil Organic Carbon–Water Partition Coefficients (K_{OC})

There are two pp-LFERs listed in the UFZ–LSER database ⁵ for log K_{OC} predictions: Nguyen et al. ⁶

$$\log K_{OC} = 0.14 + 1.10E - 0.72S + 0.15A - 1.98B + 2.28V \quad (G-3)$$

Poole and Poole ⁷

$$\log K_{OC} = 0.55 + 0.95E - 0.39S - 0.39A - 1.51B + 1.76V \quad (G-4)$$

In their paper, Kipka and Di Toro ⁸ present a comparison of their pp-LFER (Eq. (6-3)) performance to that of other pp-LFERs including those by Nguyen et al. ⁶ (Eq. (G-3)) and Poole and Poole ⁷ (Eq. (G-4)). Kipka and Di Toro ⁸ show that their pp-LFER has a smaller prediction root mean square error for an independent dataset of 740 screened observations (Figure 3 in Kipka and Di Toro ⁸).

In order to compare the performance of these three pp-LFERs to predict log K_{OC} for MCs, an independent dataset ($n = 40$, Table G-3) for five MCs was collected from the literature. The estimated log K_{OC} are presented versus the observed values in Figure G-2. Observed K_{OC} vary up to three orders of magnitude for a single MC (Figure G-2), likely due to the different experimental methodologies and determination methods used to obtain the log K_{OC} (Table G-3). MC-averaged observed log K_{OC} are shown versus the predicted values in Figure G-3. Prediction errors (RMSE: root mean square error) were similar for the pp-LFERs by Kipka and Di Toro ⁸ (RMSE = 0.565; Figure G-3A) and Poole and Poole ⁷ (RMSE = 0.485; Figure G-3C), while the pp-LFER by Nguyen et al. ⁶ yielded a higher uncertainty (RMSE = 0.912; Figure G-3B). The RMSEs obtained with the pp-LFERs by Kipka and Di Toro ⁸ and Poole and Poole ⁷ indicate that approximately 68% of predicted log K_{OC} fall within about half a log unit (a factor of about 3) of the corresponding MC-averaged observed log K_{OC} .

Table G-3 Observed and predicted Soil Organic Carbon–Water Partition Coefficients (K_{OC}) for comparison of log K_{OC} pp-LFERs performance. Located in Chapter_6_Appendix G_Tables.xlsx file.

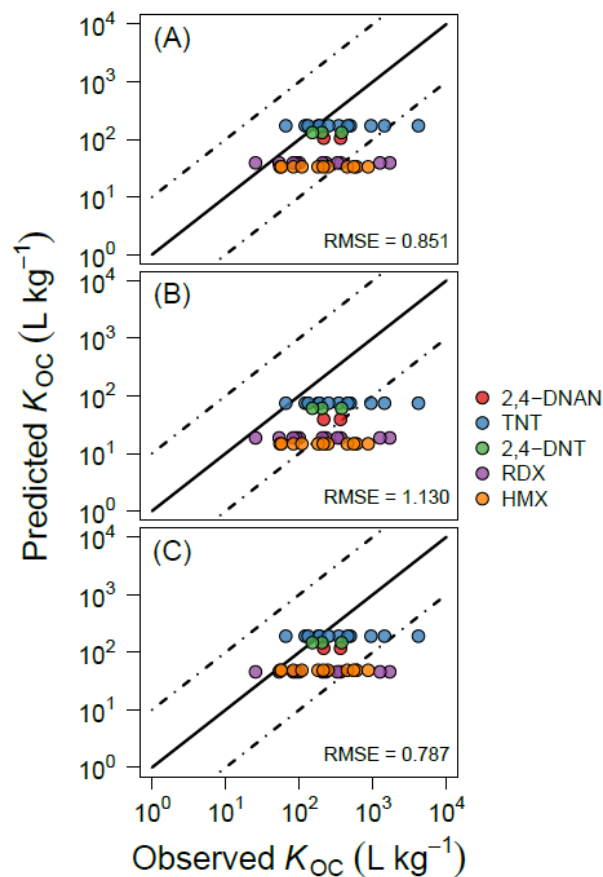


Figure G-2 Predicted soil organic carbon–water partition coefficients (K_{OC}) versus observed K_{OC} from published partitioning studies (Table G-3). Predicted K_{OC} were calculated with pp-LFER from: (A) Kipka and Di Toro ⁸ (Eq. (6-3)), (B) Nguyen et al. ⁶ (Eq. (G-3)), and (C) Poole and Poole ⁷ (Eq. (G-4)). RMSE: Root mean square error of prediction (log predicted - log observed). The solid line indicates the best agreement (unity), dashed lines are spaced at 1 log unit from unity.

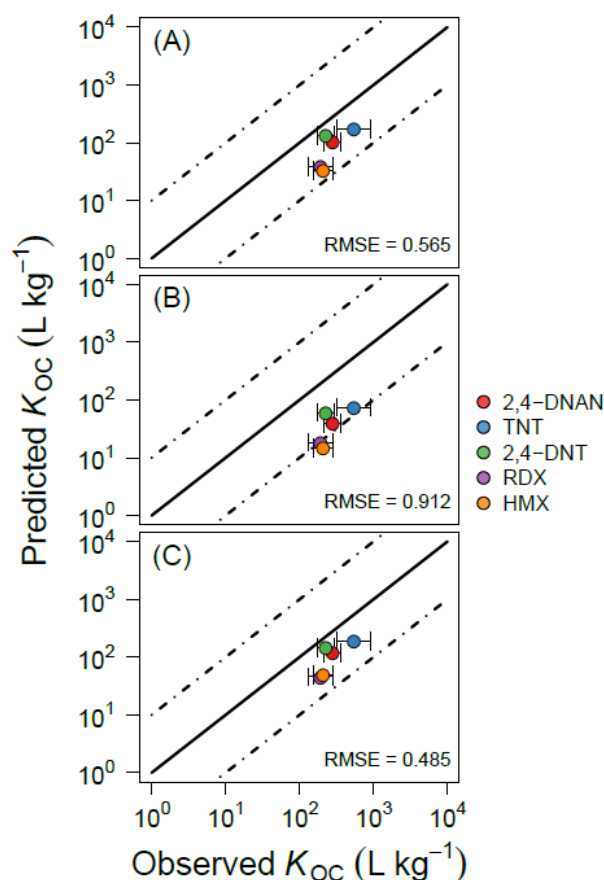


Figure G-3 Predicted soil organic carbon–water partition coefficients (K_{oc}) versus MC–averaged observed K_{oc} from published partitioning studies (Table G-3). Predicted K_{oc} were calculated with pp-LFER from: (A) Kipka and Di Toro ⁸ (Eq. (6-3)), (B) Nguyen et al. ⁶ (Eq. (G-3)), and (C) Poole and Poole ⁷ (Eq. (G-4)). RMSE: Root mean square error of prediction (log predicted - log observed). Error bars represent the standard error of the mean (SEM). The solid line indicates the best agreement (unity), dashed lines are spaced at 1 log unit from unity.

Besides this competitive prediction performance, a wider solute descriptor space coverage dictated the choice of using the pp-LFER by Kipka and Di Toro ⁸ for the estimation of concentrations in plants observed in independent uptake assays described in the main text. The dataset used to build the pp-LFER by Kipka and Di Toro ⁸ is not only larger ($n = 440$) than that used in either Nguyen et al. ⁶ ($n = 75$) or Poole and Poole ⁷ ($n = 138$) but it also covers a wider solute descriptor space for all five solute descriptors (Table G-4) except E for which the pp-LFER by Poole and Poole ⁷ is about 0.5 log units wider. Solute diversity in the calibration dataset expands the range of applicability of a pp-LFER, and that is especially useful for the prediction of MCs with new or uncommon functionalities.

Table G-4 Comparison of solute descriptor space coverage for three log K_{oc} pp-LFERs.

Solute descriptor		Nguyen et al. ⁶	Poole and Poole ⁷	Kipka and Di Toro ⁸
E	Min. =	0.369	0.024	0.060
	Max. =	2.847	4.000	3.430
	Range =	2.478	3.976	3.370
S	Min. =	0.380	0.300	0.370
	Max. =	1.910	2.170	3.250
	Range =	1.530	1.870	2.880
A	Min. =	0.000	0.080	0.000
	Max. =	0.970	1.100	1.490
	Range =	0.970	1.020	1.490
B	Min. =	0.000	0.000	0.000
	Max. =	1.050	0.900	1.920
	Range =	1.050	0.900	1.920
V	Min. =	0.617	0.308	0.308
	Max. =	2.303	1.954	3.401
	Range =	1.687	1.646	3.093

Polyparameter Linear Free Energy Relationship (pp-LFER) Models

Table G-5 Plant cuticle-water partition coefficients (K_{Cut}) data. Located in Chapter_6_Appendix G_Tables.xlsx file.

Table G-6 Plant cuticle membrane–water partition coefficients (K_{CM}) and plant cuticle matrix–water partition coefficients (K_{MX}) for undissociated organic compounds from Sabljic et al. ¹⁵ and the summary statistics for the significance of the cuticular component on the resulting plant cuticle–water partition coefficient (K_{Cut}).

Compound	CAS #	$\log K_{CM \text{ or } MX}^a$					
		<i>C. aurantium</i>		<i>F. elastica</i>		<i>C. annuum</i>	
		CM	MX	CM	MX	CM	MX
phenol	108-95-2	NA	NA	1.51	1.69	1.59	1.67
2-nitrophenol	88-75-5	NA	NA	1.84	1.99	1.92	2.04
4-nitrophenol	100-02-7	1.79	1.76	1.80	1.89	1.97	2.03
atrazine	1912-24-9	2.15	2.17	2.16	2.15	2.19	2.20
pentachlorophenol	87-86-5	4.42	4.46	4.55	4.60	4.66	4.72
hexachlorobenzene	118-74-1	5.70	5.79	5.74	6.01	5.80	5.82
perylene	198-55-0	6.45	6.59	6.20	6.58	6.55	6.58
Summary statistics ^b							
		Df		t stat		p-value ^c	
Cuticle component		36		-0.143		0.887	

^a $L_{water} \text{ kg}_{cuticle}^{-1}$. As reported in the corresponding source(s): *C. aurantium*: *Citrus aurantium* L; *F. elastica*: *Ficus elastica* Roxb. var. decora; and *C. annuum*: *Capiscum annuum* L.

^b t-test: Two-Sample Assuming Unequal Variances

^c A p-value ≤ 0.05 was accepted as significant

Table G-7 Absolv estimated Abraham Parameters (Absolv-AP) ²² and K_{Cut} calculated using pp-LFERs with Absolv-AP. Located in Chapter_6_Appendix G_Tables.xlsx file.

Table G-8 Experimentally derived Abraham Parameters (Exp-AP) ^{5, 23} and K_{Cut} calculated using pp-LFERs with Exp-AP ^a. Located in Chapter_6_Appendix G_Tables.xlsx file.

Table G-9 Adjusted Quantum Chemically estimated Abraham Parameters (Adjusted QCAP) ¹² and K_{Cut} calculated using pp-LFER with QCAP. Located in Chapter_6_Appendix G_Tables.xlsx file.

Table G-10 Quantum Chemically estimated Abraham Parameters (QCAP) ¹² and K_{Cut} calculated using pp-LFER with QCAP. Located in Chapter_6_Appendix G_Tables.xlsx file.

Table G-11 Results of the K_{Cut} pp-LFER multiple linear regression analyses fitting the general Abraham polyparameter model (Eq. (6-1)) to K_{Cut} data using three different sources of solute descriptors^a.

Source of solute descriptors	Plant cuticle phase descriptors		Standard error	<i>t</i> value	p-value ^b
Absolv-AP ^c	<i>c</i>	0.171	0.220	0.776	4.39E-01
	<i>e</i>	1.228	0.221	5.545	1.46E-07
	<i>s</i>	0.013	0.263	0.048	9.62E-01
	<i>a</i>	-0.508	0.267	-1.905	5.89E-02
	<i>b</i>	-1.965	0.245	-8.019	4.22E-13
	<i>v</i>	1.672	0.292	5.730	6.13E-08
	77 compounds; N = 143; RMSE = 0.778; $R_{\text{Adj.}}^2 = 0.751$; SE = 0.795; $F = 86.8$				
Exp-AP ^d	<i>c</i>	-0.175	0.091	-1.926	5.62E-02
	<i>e</i>	0.569	0.098	5.808	4.21E-08
	<i>s</i>	-0.239	0.100	-2.382	1.86E-02
	<i>a</i>	-0.132	0.114	-1.153	2.51E-01
	<i>b</i>	-4.103	0.146	-28.145	< 2.00E-16
	<i>v</i>	3.493	0.147	23.836	< 2.00E-16
	77 compounds; N = 143; RMSE = 0.332; $R_{\text{Adj.}}^2 = 0.955$; SE = 0.400; $F = 600.1$				
QCAP ^e	<i>c</i>	-0.593	0.098	-6.027	1.46E-08
	<i>e</i>	0.433	0.086	5.058	1.33E-06
	<i>s</i>	0.900	0.164	5.501	1.79E-07
	<i>a</i>	-0.587	0.100	-5.895	2.78E-08
	<i>b</i>	-5.409	0.253	-21.353	< 2.00E-16
	<i>v</i>	3.442	0.203	16.921	< 2.00E-16
	77 compounds; N = 143; RMSE = 0.386; $R_{\text{Adj.}}^2 = 0.939$; SE = 0.394; $F = 437.6$				

^a K_{Cut} dataset described in Table G-5. N = number of data points used to estimate the regression equation coefficients, RMSE = root mean square error of prediction, R_{Adj}^2 = adjusted coefficient of determination, SE = regression residual standard error, and F = Fischer's F statistic

^b A p-value ≤ 0.05 was accepted as significant

^c Absolv-AP listed in Table G-7

^d Exp-AP listed in Table G-8

^e QCAP listed in Table G-10

Table G-12 Range of solute descriptor space for the plant cuticle-water pp-LFERs by Platts and Abraham ¹ and this work.

		Platts and Abraham ^a	This work ^b
<i>E</i>	Min. =	0.00	0.47
	Max. =	3.26	4.76
	Range =	3.26	4.29
<i>S</i>	Min. =	0.00	0.12
	Max. =	1.76	2.45
	Range =	1.76	2.33
<i>A</i>	Min. =	0.00	0.00
	Max. =	0.96	1.09
	Range =	0.96	1.09
<i>B</i>	Min. =	0.00	-0.05
	Max. =	1.67	1.31
	Range =	1.67	1.36
<i>V</i>	Min. =	0.308	0.295
	Max. =	2.674	2.498
	Range =	2.366	2.203

^a Eq. (6-2). Range reported in Platts and Abraham ¹

^b Eq. (6-8). QCAP range from Table G-10

Estimation of Concentrations in Plants Observed in Independent Uptake Assays

Table G-13 Data from published uptake assays with plants exposed to MCs, or MLCs, in the growth medium. Located in Chapter_6_Appendix G_Tables.xlsx file.

Table G-14 Solute descriptors used in the partitioning-based bioconcentration model, Eq. (6-9), for the prediction of MCs and MLCs concentrations in plant biomass. Located in Chapter_6_Appendix G_Tables.xlsx file.

Table G-15 Fraction of cuticle, f_{Cut} , for plant species in the uptake assays dataset.

Plant common name	Species ^a	Plant family	Specific Leaf Area	Source	Cuticle per area	Source	f_{Cut}
			$\text{cm}^2 \text{mg}_{\text{dwt}}^{-1}$		$\text{mg}_{\text{dwt}} \text{cm}^{-2}$		$\frac{\text{kg}_{\text{cuticle}}}{\text{kg}_{\text{dwt plant}}^{-1}}$
Barley	<i>H. vulgare</i>	Poaceae	0.30	33	0.62	34	0.18
Weeping acacia	<i>A. floribunda</i>	Fabaceae	0.01	SI in 35	19.65	35	0.21
Avg. =							0.20

^a As reported in source: *H. vulgare*: *Hordeum vulgare* L. cv. Dongboree; *A. floribunda*: *Acacia floribunda*

Table G-16 Example for prediction of a MC (HMX) concentration in grass (*Perennial ryegrass*).

Input data			
<i>i</i> : HMX			
Plant species: <i>Perennial ryegrass</i>			
HMX Adjusted QCAP for prediction of K_{iOC} :			
Variable	Value	Units	Source
E	= 0.881	-	Table G-14
S	= 2.383	-	Table G-14
A	= 0.315	-	Table G-14
B	= 1.020	-	Table G-14
V	= 1.643	-	Table G-14
$C_{iSoil Solids}$	= 41	mg kg _{dwt soil} ⁻¹	28
f_{OC}	= 0.141	kg _{OC} kg _{dwt soil} ⁻¹	Table G-13
HMX QCAP for prediction of K_{iCut} :			
Variable	Value	Units	Source
E	= 1.165	-	Table G-14
S	= 2.451	-	Table G-14
A	= 0.635	-	Table G-14
B	= 1.050	-	Table G-14
V	= 1.631	-	Table G-14
$f_{Cuticle}$	= 0.18	kg _{cuticle} kg _{dwt plant} ⁻¹	Table G-15

Prediction		
Variable		Based on
$K_{i_{OC}}$	$= 10^{(0.670+1.075E-0.277S-0.363A-1.697B+1.468V)}$ $= 10^{(0.670+1.075*0.881-0.277*2.383-0.363*0.315-1.697*1.020+1.468*1.643)}$ $= 33.385 \text{ L}_{\text{water}} \text{ kg}_{OC}^{-1}$	Eq. (6-3)
$C_{i_{IW}}$	$= \frac{C_{i_{Soil Solids}}}{K_{i_{OC}} f_{OC}}$ $= \frac{41 \text{ mg kg}_{dwt}^{-1}}{33.385 \text{ L}_{\text{water}} \text{ kg}_{OC}^{-1} * 0.141 \text{ kg}_{OC} \text{ kg}_{dwt}^{-1}}$ $= 8.710 \text{ mg L}^{-1}$ $> 5 \text{ mg L}^{-1} \text{ HMX aqueous solubility}$ Predicted $C_{i_{IW}}$ is $>$ aqueous solubility; use aqueous solubility as $C_{i_{IW}}$ for onward calculations	Eq. (6-6) Table G-1
$K_{i_{Cut}}$	$= 10^{(-0.593+0.433E+0.900S-0.587A-5.409B+3.442V)}$ $= 10^{(-0.593+0.433*1.165+0.900*2.451-0.587*0.635-5.409*1.050+3.442*1.631)}$ $= 47.705 \text{ L}_{\text{water}} \text{ kg}_{cuticle}^{-1}$	Eq. (6-8)
$C_{i_{Plant}}$	$= K_{i_{Cut}} f_{Cut} C_{i_{IW}}$ $= 47.705 \text{ L}_{\text{water}} \text{ kg}_{cuticle}^{-1} * 0.18 \text{ kg}_{cuticle} \text{ kg}_{dwt plant}^{-1} * 5 \text{ mg L}^{-1}$ $= 42.935 \text{ mg kg}_{dwt}^{-1}$ vs. $43 \text{ mg kg}_{dwt}^{-1}$ observed $C_{i_{Plant}}$	Eq. (6-7) Table G-13

Table G-17 Predicted values for MCs and MLCs concentrations in interstitial water and plant biomass using the partitioning–based bioconcentration model (Eq. (6-9))^a. Located in Chapter_6_Appendix G_Tables.xlsx file.

Table G-18 Examples of MCs plant uptake data surveyed but excluded from the validation dataset. Located in Chapter_6_Appendix G_Tables.xlsx file.

Estimation of Concentrations in Plants Observed in Independent Uptake Assays Including the Contribution from Carbohydrates

Contribution from plant carbohydrates to the bioconcentration of MCs was also examined before being excluded from the model. A pp-LFER for the prediction of carbohydrate–water partition coefficients, K_{Ch} , was built using: (i) QCAP as the solute descriptors, and (ii) a dataset for partition to cellulose and starch from water by Hung et al.⁴⁰ (Table G-19). The K_{Ch} dataset includes alkyl benzenes, halogenated benzenes, aniline derivatives, short–chain chlorinated hydrocarbons, esters, polychlorinated biphenyls, organochlorine pesticides, and polycyclic aromatic hydrocarbons (Table G-19). The resulting K_{Ch} pp-LFER is

$$\log K_{Ch} = -1.801 + 0.472E - 0.297S - 2.662B + 2.305V \quad (G-5)$$

where K_{Ch} = carbohydrate–water partition coefficient ($L_{water} \text{ kg}_{carbohydrate}^{-1}$) and statistics are listed in Table G-20.

Table G-19 Observed K_{Ch} and fitted K_{Ch} with pp-LFER using QCAP. Located in Chapter_6_Appendix G_Tables.xlsx file.

Table G-20 K_{Ch} pp-LFER from the multiple linear regression analysis fitting the general Abraham polyparameter model (Eq. (6-1)) to K_{Ch} data using QCAP solute descriptors^a.

Source of solute descriptors	Carbohydrate phase descriptors		Standard error	<i>t</i> value	p-value ^b
QCAP ^c	<i>c</i>	-1.801	0.087	-20.643	< 2.00E-16
	<i>e</i>	0.472	0.058	8.082	8.26E-11
	<i>s</i>	-0.297	0.134	-2.208	0.031591
	<i>a</i>	0.103	0.219	0.470	0.640282
	<i>b</i>	-2.662	0.209	-12.743	< 2.00E-16
	<i>v</i>	2.305	0.124	18.599	< 2.00E-16
59 compounds; N = 59; RMSE = 0.165; $R_{Adj.}^2$ = 0.965; SE = 0.175; F = 318.4					

^a K_{Ch} dataset described in Table G-19. N = number of data points used to estimate the regression equation coefficients, RMSE = root mean square error of prediction, $R_{Adj.}^2$ = adjusted coefficient of determination, SE = regression residual standard error, and F = Fischer's F statistic

^b A p-value ≤ 0.05 was accepted as significant, hence the *aA* term was excluded from the final pp-LFER (Eq. (G-5))

^c QCAP listed in Table G-19

Predicted K_{Ch} for MCs and MLCs were small ($-1.016 < (\log K_{Ch}) < -0.470$; Table G-21). The partitioning-based plant bioconcentration model (Eq. (6-9)) was modified to include the contribution from carbohydrates

$$C_{iPlant} = \frac{(K_{iCut} f_{Cut} + K_{iCh} f_{Ch}) C_{iSoil Solids}}{K_{iOC} f_{OC}} \quad (G-6)$$

The contribution from carbohydrates ($K_{iCh} f_{Ch}$) accounted for maximum 3.3% of the K_{PW} ($= K_{iCut} f_{Cut} + K_{iCh} f_{Ch}$) (Table G-21) even assuming carbohydrates were the predominant component of the plant (i.e., $f_{Ch} = 1 - f_{Cut}$). The overall estimation error of the bioconcentration model changed only by 0.5% when carbohydrates were included as a sorption compartment ($RMSE_{Cut+Ch} = 0.431$; $RMSE_{Cut} = 0.429$). Results are shown in Table G-21 and Figure G-4.

Table G-21 Predicted values for MCs and MLCs concentrations in plant biomass using the partitioning-based bioconcentration model that includes contributions from carbohydrates (Eq. (G-6))^a. Located in Chapter_6_Appendix G_Tables.xlsx file.

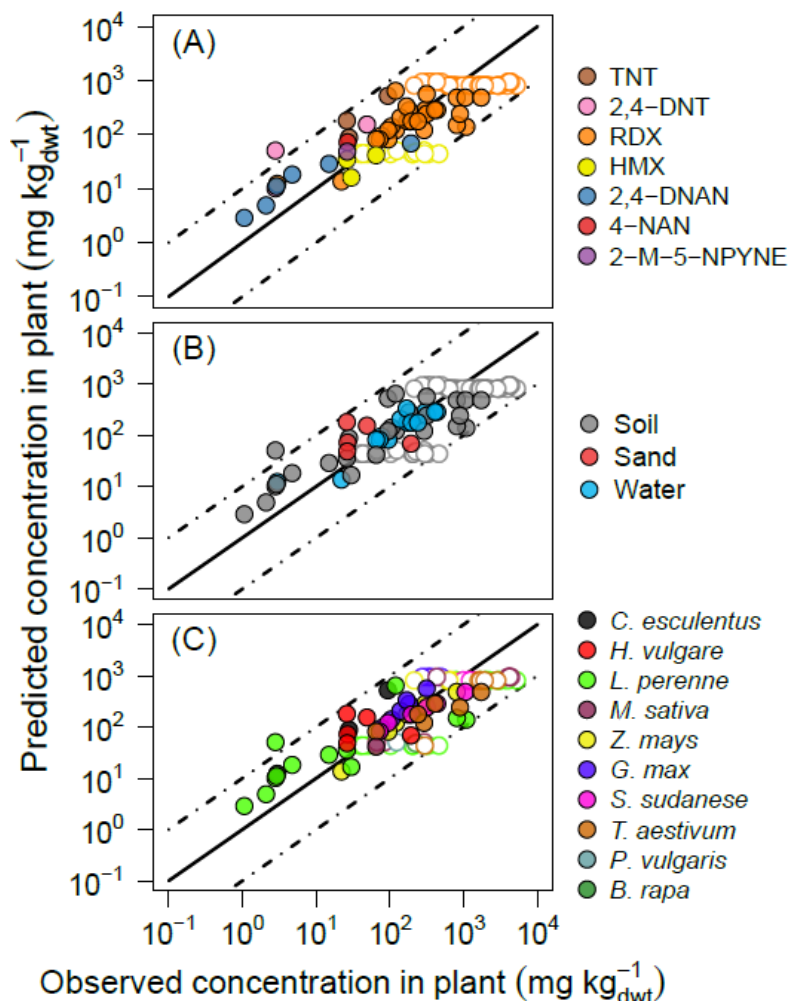


Figure G-4 Predicted concentrations in the plant versus observed values from published uptake studies including the contribution from carbohydrates and cuticle (Eq. (G-6)) (Table G-21). Color coding assigned based on: (A) MCs and MLCs (Table G-1), (B) growth medium, and (C) plant species. Unfilled symbols indicate that the predicted concentration in the interstitial water (using Eq. (6-6)) is substituted for the corresponding MC aqueous solubility since the predicted concentration in the interstitial water exceeds solubility. See main text for further details. The border color for the unfilled symbols corresponds to the color identification in each panel legend. Root mean square error of prediction (log predicted - log observed), excluding predictions bounded at aqueous solubility, RMSE = 0.431. The solid line indicates the best agreement (unity), dashed lines are spaced at 1 log unit from unity.

REFERENCES

1. Platts, J.A.; Abraham, M.H. Partition of volatile organic compounds from air and from water into plant cuticular matrix: An LFER analysis. *Environ. Sci. Technol.* **2000**, *34* (2), 318-323; 10.1021/es9906195.
2. US Environmental Protection Agency Estimation Programs Interface (EPI) Suite™ for Microsoft® Windows, v. 4.11. US EPA: Washington, D.C., 2012.
3. Hawari, J.; Monteil-Rivera, F.; Perreault, N.N.; Halasz, A.; Paquet, L.; Radovic-Hrapovic, Z.; Deschamps, S.; Thiboutot, S.; Ampleman, G. Environmental fate of 2,4-dinitroanisole (DNAN) and its reduced products. *Chemosphere* **2015**, *119* (0), 16-23; 10.1016/j.chemosphere.2014.05.047.
4. Windt, C.W.; Vergeldt, F.J.; De Jager, P.A.; Van As, H. MRI of long-distance water transport: a comparison of the phloem and xylem flow characteristics and dynamics in poplar, castor bean, tomato and tobacco. *Plant Cell and Environment* **2006**, *29* (9), 1715-1729; 10.1111/j.1365-3040.2006.01544.x.
5. Ulrich, N., Endo, S., Brown, T.N., Watanabe, N., Bronner, G., Abraham, M.H., Goss, K.-U., UFZ-LSER database v 3.2 [Internet], Leipzig, Germany, Helmholtz Centre for Environmental Research-UFZ. 2016 [accessed on 16.11.2016]. Available from <http://www.ufz.de/lserd>
6. Nguyen, T.; Goss, K.; Ball, W. Polyparameter linear free energy relationships for estimating the equilibrium partition of organic compounds between water and the natural organic matter in soils and sediments. *Environ. Sci. Technol.* **2005**, *39* (4), 913-924; 10.1021/es048839s.
7. Poole, S.K.; Poole, C.F. Chromatographic models for the sorption of neutral organic compounds by soil from water and air. *Journal of Chromatography A* **1999**, *845* (1-2), 381-400; 10.1016/S0021-9673(98)01085-1.
8. Kipka, U.; Di Toro, D.M. A linear solvation energy relationship model of organic chemical partitioning to particulate organic carbon in soils and sediments. *Environ. Toxicol. Chem.* **2011**, *30* (9), 2013-2022; 10.1002/etc.611.
9. Sharma, P.; Mayes, M.A.; Tang, G. Role of soil organic carbon and colloids in sorption and transport of TNT, RDX and HMX in training range soils. *Chemosphere* **2013**, *92* (8), 993-1000; 10.1016/j.chemosphere.2013.03.028.
10. Sunahara, G.I.; Lotufo, G.; Kuperman, R.G.; Hawari, J. *Ecotoxicology of explosives*. CRC Press, Inc.: 2009.
11. Clausen, J.L.; Korte, N. Fate and transport of energetics from surface soils to groundwater, In Chappell, M.A.; Price, C.L.; George, R.D., Eds.; American Chemical Society: Washington, DC, **2011**; Vol.1069 pp. 273-316.

12. Liang, Y. Determining Abraham solute and system parameters for neutral organic compounds using quantum chemical methods. Doctoral Dissertation, University of Delaware, Newark, DE, USA, 2016.
13. Torralba-Sanchez, T.L. Bioconcentration of munitions compounds in plants and worms: experiments and modeling. Doctoral Dissertation, University of Delaware, Newark, DE, USA, **2016**.
14. Shafer, W.; Schonherr, J. Accumulation and Transport of Phenol, 2-Nitrophenol, and 4-Nitrophenol in Plant Cuticles. *Ecotoxicol. Environ. Saf.* **1985**, *10* (2), 239-252; 10.1016/0147-6513(85)90071-5.
15. Sabljic, A.; Gusten, H.; Schonherr, J.; Riederer, M. Modeling plant uptake of airborne organic-chemicals .1. Plant cuticle water partitioning and molecular connectivity. *Environ. Sci. Technol.* **1990**, *24* (9), 1321-1326; 10.1021/es00079a004.
16. Chen, B.; Johnson, E.J.; Chefetz, B.; Zhu, L.; Xing, B. Sorption of polar and nonpolar aromatic organic contaminants by plant cuticular materials: Role of polarity and accessibility. *Environ. Sci. Technol.* **2005**, *39* (16), 6138-6146; 10.1021/es050622q.
17. Kirsch, T.; Kaffarnik, F.; Riederer, M.; Schreiber, L. Cuticular permeability of the three tree species *Prunus laurocerasus* L., *Ginkgo biloba* L. and *Juglans regia* L.: Comparative investigation of the transport properties of intact leaves, isolated cuticles and reconstituted cuticular waxes. *J. Exp. Bot.* **1997**, *48* (5), 1035-1045; 10.1093/jxb/48.5.1035.
18. Kerler, F.; Schonherr, J. Accumulation of Lipophilic Chemicals in Plant Cuticles - Prediction from Octanol Water Partition-Coefficients. *Arch. Environ. Contam. Toxicol.* **1988**, *17* (1), 1-6.
19. Barbour, J.P.; Smith, J.A.; Chiou, C.T. Sorption of aromatic organic pollutants to grasses from water. *Environ. Sci. Technol.* **2005**, *39* (21), 8369-8373; 10.1021/es0504946.
20. Chen, B.; Li, Y.; Guo, Y.; Zhu, L.; Schnoor, J.L. Role of the extractable lipids and polymeric lipids in sorption of organic contaminants onto plant cuticles. *Environ. Sci. Technol.* **2008**, *42* (5), 1517-1523; 10.1021/es7023725.
21. Li, Y.; Chen, B. Phenanthrene sorption by fruit cuticles and potato periderm with different compositional characteristics. *J. Agric. Food Chem.* **2009**, *57* (2), 637-644; 10.1021/jf802719h.
22. Advanced Chemistry Development Inc. ACD/PhysChem Suite. Absolv module. **2013**, v. 5.0.
23. Liang, Y.; Kuo, D.T.F.; Allen, H.E.; Di Toro, D.M. Experimental determination of solvent-water partition coefficients and Abraham parameters for munition constituents. *Chemosphere* **2016**, *161*, 429-437; 10.1016/j.chemosphere.2016.07.028.

24. Pennington, J.C. Plant uptake of 2,4,6-trinitrotoluene, 4-amino-2,6-dinitrotoluene, and 2-amino-4,6-dinitrotoluene using ^{14}C -labeled and unlabeled compounds. Technical Report No. EL-88-20. Vicksburg, MS: U.S. Army Waterways Experiment Station, Corps of Engineers. **1988**;1-68.
25. Sunahara, G.I. Development of toxicity benchmarks and bioaccumulation data for N-based organic explosives for terrestrial plants and soil invertebrates. Final Report No. SERDP ER-1416. Québec, Canada: National Research Council of Canada Montreal (Québec) Biotechnology Research Institute. **2012**;1-289.
26. Rocheleau, S.; Lachance, B.; Kuperman, R.G.; Hawari, J.; Thiboutot, S.; Ampleman, G.; Sunahara, G.I. Toxicity and uptake of cyclic nitramine explosives in ryegrass *Lolium perenne*. *Environ. Pollut.* **2008**, *156* (1), 199-206; DOI: 10.1016/j.envpol.2007.12.012.
27. Best, E.P.H.; Tatem, H.E.; Geter, K.N.; Wells, M.L.; Lane, B.K. Effects, uptake, and fate of 2,4,6-trinitrotoluene aged in soil in plants and worms. *Environ. Toxicol. Chem.* **2008**, *27* (12), 2539-2547; 10.1897/08-017.1.
28. Best, E.P.H.; Geter, K.N.; Tatem, H.E.; Lane, B.K. Effects, transfer, and fate of RDX from aged soil in plants and worms. *Chemosphere* **2006**, *62* (4), 616-625; 10.1016/j.chemosphere.2005.05.039.
29. Chen, D.; Liu, Z.L.; Banwart, W. Concentration-dependent RDX uptake and remediation by crop plants. *Environ. Sci. Pollut. Res* **2011**, *18* (6), 908-917; 10.1007/s11356-011-0449-9.
30. McKone, T.E.; Maddalena, R.L. Plant uptake of organic pollutants from soil: Bioconcentration estimates based on models and experiments. *Environ Toxicol Chem* **2007**, *26* (12), 2494-2504; 10.1897/06-269.1.
31. Groom, C.A.; Halasz, A.; Paquet, L.; Morris, N.; Olivier, L.; Dubois, C.; Hawari, J. Accumulation of HMX (octahydro-1,3,5,7-tetranitro-1,3,5,7-tetrazocine) in indigenous and agricultural plants grown in HMX-contaminated anti-tank firing-range soil. *Environ. Sci. Technol.* **2002**, *36* (1), 112-118; 10.1021/es0110729.
32. Dodard, S.G.; Sarrazin, M.; Hawari, J.; Paquet, L.; Ampleman, G.; Thiboutot, S.; Sunahara, G.I. Ecotoxicological assessment of a high energetic and insensitive munitions compound: 2,4-Dinitroanisole (DNAN). *J. Hazard. Mater.* **2013**, *262* (0), 143-150; 10.1016/j.jhazmat.2013.08.043.
33. Gunn, S.; Farrar, J.F.; Collis, B.E.; Nason, M. Specific leaf area in barley: individual leaves versus whole plants. *New Phytol.* **1999**, *143* (1), 45-51; 10.1046/j.1469-8137.1999.00434.x.
34. Chun, J.C.; Lee, H.J.; Lim, S.J.; Kim, S.E.; Guh, J.O. Comparative absorption, translocation, and metabolism of foliar-applied oxyfluorfen in wheat and barley. *Pestic. Biochem. Physiol.* **2001**, *70* (2), 118-125; 10.1006/pest.2001.2546.

35. Onoda, Y.; Richards, L.; Westoby, M. The importance of leaf cuticle for carbon economy and mechanical strength. *New Phytol.* **2012**, *196* (2), 441-447; 10.1111/j.1469-8137.2012.04263.x.
36. Durringer, J.M.; Craig, A.M.; Smith, D.J.; Chaney, R.L. Uptake and Transformation of Soil [¹⁴C]-Trinitrotoluene by Cool-Season Grasses. *Environ. Sci. Technol.* **2010**, *44* (16), 6325-6330; 10.1021/es903671n.
37. Price, R.A.; Pennington, J.C.; Larson, S.L.; Neumann, D.; Hayes, C.A. Uptake of RDX and TNT by Agronomic Plants. *Soil Sediment Contam* **2002**, *11* (3), 307-326; 10.1080/20025891106763.
38. Cataldo, D., Harvey, S., Fellows, R. An evaluation of the environmental fate and behavior of munitions material (TNT, RDX) in soil and plant systems: Environmental fate and behavior of RDX. Final Report No. PNL-7529/UC-402, **1990**, Richland, WA, USA: Pacific Northwest Laboratories.
39. Harvey, S.D.; Fellows, R.J.; Cataldo, D.A.; Bean, R.M. Fate of the explosive hexahydro-1,3,5-trinitro-1,3,5-triazine (rdx) in soil and bioaccumulation in bush bean hydroponic plants. *Environmental Toxicology and Chemistry* **1991**, *10* (7), 845-855; 10.1002/etc.5620100701.
40. Hung, H.; Lin, T.; Chiou, C.T. Partition coefficients of organic contaminants with carbohydrates. *Environ. Sci. Technol.* **2010**, *44* (14), 5430-5436; 10.1021/es1004413.

Chapter 7

PREDICTING OLIGOCHAETE WORMS–SOIL BIOCONCENTRATION OF MUNITIONS COMPOUNDS FROM MOLECULAR STRUCTURE

Abstract

Soil uptake studies have shown that munitions compounds (MCs) accumulate in oligochaete worms. This work presents a model for the prediction of MCs bioconcentration in oligochaetes considering chemical partitioning between soil, interstitial water, and worm lipid and protein. All the partition coefficients (K) were calculated using polyparameter linear free energy relationships (pp-LFERs) with Abraham solute descriptors computed from only molecular structure through quantum chemical methods. Two pp-LFERs were compared for the estimation of K_{Lipid} . The first one (i.) was fitted exclusively to oligochaetes data, and the second (ii.) was an existing pp-LFER calibrated to data from various organisms. The oligochaete BCFs calibration data were estimated with a similar root mean square error, RMSE (log estimated - log observed) = (i.) 0.499 and (ii.) 0.677. A validation of the partition-based model's capabilities against independent data yielded RMSEs = 0.396 and 0.523 using (i.) or (ii.), respectively. This bioconcentration model is especially useful when data are unavailable due to scarcity of BCFs experimental values or the MC being at the development stages since the inputs for these pp-LFERs, the Abraham solute descriptors, are estimated from the compound molecular structure.

7.1 Introduction

Residues of munitions compounds (MCs) deposited on soils at military ranges and areas exposed to off-site migration of contaminants come in direct contact with biota inhabiting the soils. As a result, soil dwelling organisms such as oligochaetes are exposed to, and are likely to, accumulate MCs posing risks not only of direct toxicity but also of transference to higher trophic levels. Modeling tools are required to estimate the degree of bioconcentration to be expected.

Worms are crucial for the structure and fertility of soils, and for the recycling of nutrients¹. Terrestrial and aquatic worms are routinely used as test organisms to assess the environmental risk of contaminants^{2,3}. Their abundance, behavior, and contaminant body burden are bioindicators of soil and sediment quality⁴. The bioconcentration of organic compounds in worms is defined as the steady state ratio of the compound concentration in the worm to that in the soil or sediment interstitial/pore water⁵, and it is expressed as

$$BCF_i = \left(\frac{C_{iOrganism}}{C_{iAvailable\ in\ growth\ medium.}} \right)_{SS} = \left(\frac{C_{iWorm}}{C_{iIW}} \right)_{SS} \quad (7-1)$$

where i refers to a compound of interest (e.g., a MC), BCF_i = bioconcentration factor of i ($L_{water} kg_{worm\ dwt}^{-1}$; dwt = dry weight), SS denotes steady state, C_{iWorm} = concentration of i in the worm ($mg\ kg_{dwt}^{-1}$), and C_{iIW} = dissolved concentration of i in the interstitial water (IW) ($mg\ L^{-1}$).

Models that are able to estimate the concentration of organic compounds in worms using the soil concentration rather than the measured interstitial water concentration are preferred because of the analytical challenges associated with separating the interstitial water from soil or

sediment solids. Dynamic models based on first-order kinetics have been proposed⁶⁻¹² to estimate the steady state concentration in the worm using

$$C_{iWorm} = \frac{k_{i_u}}{k_{i_e}} C_{iSolid\ growth\ medium} \quad (7-2)$$

where $C_{iSolid\ growth\ medium}$ = concentration of i in the solid growth medium ($\text{mg kg}_{\text{dwt}}^{-1}$), k_{i_u} = uptake rate constant (d^{-1}), and k_{i_e} = elimination rate constant (d^{-1}). The rate constants k_{i_u} and k_{i_e} represent the summed contributions from various uptake and elimination processes. Worms can take up contaminants through two main routes: (i) dermal via diffusion of the contaminant dissolved in the interstitial water through the skin, and (ii) intestinal via ingestion of contaminated particles^{9,13}. Dynamic models may include both of these uptake routes¹⁰. However, with the exception of very hydrophobic chemicals (octanol–water partition coefficient, $\log K_{ow} > 6$) for which the second route is of major importance, the first route has been shown to be dominant for a variety of organic compounds^{9,14}. These dynamic models incorporate a detailed representation of the mechanisms involved in the uptake process, but they often require a large number of fitting parameters for each chemical¹⁰. Therefore, a large dataset is needed to estimate the parameters for each of the specific uptake and elimination processes. This limits the use of these models for proposed compounds for which only the molecular structure is known.

Models that include only the passive partitioning between soil (or sediment) solids and soil interstitial water, and between soil interstitial water and worm components have been published¹⁵⁻¹⁸. These models consider only the organic phases present in soil and worms to estimate the distribution of contaminants. Soil organic carbon, worm lipid, and worm protein have been suggested as phases that play a major role^{5,19-21}. To estimate the partition coefficients between organic carbon and water (K_{OC}), lipid and water (K_{Lipid}), and protein and water ($K_{Protein}$), these models often use single-parameter quantitative structure-activity relationships (QSARs) that are developed using a log-log correlation of each K_{OC} , K_{Lipid} , and $K_{Protein}$ with the K_{ow} . This assumes that octanol has similar solvation properties to those of soil OC and worm components. However, this is not the case for more polar compounds, compounds that interact by hydrogen-bonding²²⁻²⁴, and certain worm species¹⁷. The reliance on the K_{ow} as the sole chemical property used to estimate the BCF provides little insight into the chemical properties that make a compound more likely to bioconcentrate in worms. This is important information that can be used to aid in selecting among proposed MCs early in the development stage.

Recent models for estimating K_{OC} , K_{Lipid} , and $K_{Protein}$ employ polyparameter linear free energy relationships (pp-LFERs)^{25,26} that estimate partitioning by considering the contributions from different types of interactions between the solute and the condensed phase (e.g., soil organic carbon, worm lipid). Thus, pp-LFERs are able to more fully characterize the solvation properties of the condensed phase and the strength of its interactions with solutes relative to that of water. In order to achieve these results, however, pp-LFERs demand a significantly larger and more chemically diverse training dataset of partition coefficients than that for single-parameter K_{ow} -based models.

Unfortunately, the database available for partitioning of organic compounds between worm and water is rather limited. However, if the uptake of these compounds from soil is mainly driven by passive partitioning between interstitial water and worm components such as lipid and protein, and less dependent on active physiological processes inherent to a particular organism,

then the sources of data for the calibration of K_{Lipid} and $K_{Protein}$ pp-LFERs can be expanded to other organisms such as fish for which numerous measurements exist in the literature. Moreover, experimental fish BCFs have been found to be in the same order of magnitude as worm BCFs for organic compounds including MCs²⁷⁻²⁹. This suggests that the fish data could be used to build models that produce a baseline estimate of the MCs bioconcentration in worms.

The objective of this work is to predict the bioconcentration of MCs (Table H-1 in Appendix H) in oligochaete worms based on the partitioning between soil solids, interstitial water, and worm components. This is achieved using pp-LFERs for the prediction of K_{oc} to calculate the concentration in soil available for dermal uptake, and K_{Lipid} and $K_{Protein}$ to estimate the sorption to worm tissue. Two K_{Lipid} pp-LFERs are compared for the estimation of the bioconcentration in oligochaetes. The first is fitted exclusively to oligochaete data, while the second is an existing model that was calibrated to lipid partitioning data from various organisms. The same $K_{Protein}$ pp-LFER is used for both models.

The procedure for the estimation of concentrations in oligochaetes from soil is validated by predicting concentrations in an independent dataset (23 observations) compiled from published uptake assays. The pp-LFERs use only molecular structure to compute the required model parameters. Therefore, they can also be used to assess the bioconcentration potential for proposed MCs early in the development stage.

7.2 Methodology

Two types of estimations are made: (i) estimation of observed oligochaete BCFs, as defined in Eq. (7-1), for those experiments that report measured concentrations in the interstitial water, and (ii) prediction of concentrations in oligochaetes observed during uptake experiments for which the concentration in the interstitial water was unknown or not reported and, therefore, needs to be predicted. The first set of estimations tests the partitioning-based BCFs models using measured exposure concentrations, while the second set of estimations examine whether the K_{oc} , K_{Lipid} , and $K_{Protein}$ pp-LFERs can be used to predict MCs concentrations in oligochaetes within a reasonable uncertainty for situations where only soil concentration measurements are available.

7.2.1 Estimation of Oligochaete Worms Bioconcentration Factors (BCFs)

The bioconcentration model employed for oligochaetes is similar to that employed for fish³⁰. Three phases are assumed to represent the components in the worm for which partitioning determines the BCF: lipid, protein, and internal water. A three phase partitioning model, based on the BCF definition in Eq. (7-1), is

$$BCF_i = \left(f_{Lipid} K_{iLipid} + f_{Protein} K_{iProtein} + \frac{f_{Water}}{\rho_{Water}} \right) \frac{1}{f_{dwt}} \quad (7-3)$$

where i is an organic compound of interest (e.g., a MC); K_{iLipid} and $K_{iProtein}$ are the lipid–water and protein–water partition coefficients of compound i , respectively ($L_{water} \text{ kg}_{lipid}^{-1}$ and $L_{water} \text{ kg}_{protein}^{-1}$); f_{Lipid} and $f_{Protein}$ are the worm wet weight fraction of lipid and protein, respectively ($\text{kg}_{lipid} \text{ kg}_{wwt}^{-1}$ and $\text{kg}_{protein} \text{ kg}_{wwt}^{-1}$, wwt = wet weight); f_{Water} and f_{dwt} are the worm mass fraction of water and dry weight, respectively ($\text{kg}_{water} \text{ kg}_{wwt}^{-1}$ and $\text{kg}_{dwt} \text{ kg}_{wwt}^{-1}$);

and ρ_{water} is the density of water ($\text{kg}_{water} \text{L}_{water}^{-1}$). The $\frac{1}{f_{dwt}}$ term is included since most of the literature BCFs data are reported on a dry weight basis and the worm fractions of lipid and protein are most commonly presented on a wet weight basis. Eq. (7-3) represents a worm as a three component system: lipid, protein, and internal water, and the BCF is the sum of the individual contributions of compound i in each of the three compartments. The sources for the BCFs data (Table H-2) are described below in Section 7.2.3.1 together with the sources for the fractions of lipid, protein, water, and dry weight (Table H-3 and Table H-4). K_{iLipid} and $K_{iProtein}$ were calculated using the pp-LFERs described below in Section 7.2.2.1.

7.2.2 Polyparameter Linear Free Energy Relationship (pp-LFER) Models

The pp-LFER models for partitioning between water and soil organic carbon, lipid, and protein used in this work are based on the Abraham polyparameter model ²⁵

$$\log K_{sw} = c + eE + sS + aA + bB + vV \quad (7-4)$$

where K_{sw} , the dependent variable, is the partition coefficient between a solvation phase (e.g., organic carbon, worm lipid) and water, and the independent variables, the right hand side of Eq. (7-4), account for the free energy contributions from different types of molecular interactions. The uppercase letters in Eq. (7-4) are solute descriptors for the compound being modeled (e.g., a MC) and the lowercase letters refer to the complementary effect of the solvation phase on the corresponding interaction. The eE term represents the dispersion interactions that occur between non-polar (no permanent multipole moments) molecules. The sS term is the dipolarity/polarizability that arises from dipole-dipole and dipole-induced dipole interactions. The aA and bB terms account for the donation and acceptance of hydrogen bonds, which are bonds between certain types of hydrogen atoms and highly electronegative atoms in polar molecules. The aA term refers to solvent acceptor (a)–solute donor (A) and bB to solvent donor (b)–solute acceptor (B). Finally, vV accounts for the energy required for cavity formation, and c is a regression constant ²⁵.

7.2.2.1 Lipid–Water and Protein–Water pp-LFERs

Two K_{Lipid} pp-LFERs were tested for the estimation of oligochaete BCFs and the validation for the prediction of concentrations in oligochaetes from independent uptake experiments. The same $K_{Protein}$ pp-LFER was used for both tests. The first K_{Lipid} pp-LFER was obtained using Eq. (7-4) substituted into Eq. (7-3) and fit exclusively to BCF oligochaete data collected from the literature, sources described below in Section 7.2.3.1. The solute descriptors, uppercase letters in Eq. (7-4), were Quantum Chemically estimated Abraham Parameters (QCAP) from Liang ³¹ (Table H-5). Briefly, the QCAP E and V are obtained from the compound's computed molecular polarizability and molecular volume, respectively. The QCAP S , A , and B are simultaneously estimated with a multiple linear regression analysis (MLRA) applied to Eq. (7-4) using quantum chemically computed solvent–water partition coefficients for 60 solvents with known lowercase parameters ^{31,32}. The primary reason for using QCAP for the development of the worm lipid–water pp-LFER is the failure of other available Abraham parameter estimation methods for certain MCs, whereas QCAP have been shown to successfully predict K_{sw} values for a wide variety of organic compounds including MCs and compounds with

similar chemical structural functionalities, which are referred to as munition-like compounds (MLCs; Table H-1) ³¹.

The second K_{Lipid} and the $K_{Protein}$ pp-LFERs were obtained from recent publications by Kuo and Di Toro ^{30,33}

$$\begin{aligned} \log K_{Lipid} = & 0.84 (\pm 0.14) + 0.77 (\pm 0.10)E - 1.10 (\pm 0.19)S \\ & - 0.47 (\pm 0.22)A - 3.52 (\pm 0.20)B + 3.37 (\pm 0.13)V \end{aligned} \quad (7-5)$$

248 compounds; N = 248; R² = 0.88; RMSE = 0.57

$$\begin{aligned} \log K_{Protein} = & -0.88 (\pm 0.17) + 0.74 (\pm 0.13)E - 0.37 (\pm 0.15)S \\ & - 0.13 (\pm 0.15)A - 1.37 (\pm 0.16)B + 1.06 (\pm 0.14)V \end{aligned} \quad (7-6)$$

69 compounds; N = 69; R² = 0.76; RMSE = 0.38

where K_{Lipid} and $K_{Protein}$ are expressed as $L_{water} \text{ kg}_{lipid}^{-1}$ and $L_{water} \text{ kg}_{protein}^{-1}$, respectively, values in parenthesis are \pm the standard error, N = number of data points used to estimate the regression equation coefficients, R² = coefficient of determination, and RMSE is the root mean square error of estimation. Kuo and Di Toro ^{30,33} calibrated Eq. (7-5) using data from multiple sources including partitioning experiments with fish fat/oil for a diverse set of organic compounds ($1.0 < \log K_{ow} < 8.5$). Eq. (7-6) was trained with data from partitioning to human serum albumin as a protein surrogate for compounds with low log K_{ow} ($0.0 < \log K_{ow} < 4.5$) for which partitioning to protein is more dominant than partitioning to lipids.

The solvent parameters for lipid–water partitioning in Eq. (7-5) can be used to determine which phase, lipid or water, is more competitive for solutes. A positive solvent coefficient causes an increase in the partition coefficient indicating that lipid is preferred relative to water. For example, dispersion interactions ($e = 0.77 > 0$) favor lipid, and cavity formation in the lipid requires less free energy than in water ($v = 3.37 > 0$), so again lipid is favored. Eq. (7-5), however, shows that the lipid is less polar/polarizable ($s = -1.10 < 0$) and accepts hydrogen bonds ($a = -0.47 < 0$) and donates hydrogen bonds ($b = -3.52 < 0$) less readily than water, indicating that for these type of interactions water is favored over lipid.

The protein solvent parameters in Eq. (7-6) depict protein as a phase with solvation tendencies similar to those of the lipid phase relative to water as the signs for all the solvent parameters are the same in Eq. (7-6) and Eq. (7-5). The competitiveness for solutes between protein and lipid, however, varies with the type of molecular interaction as listed in Table 7-1, which contains the differences in solvent parameters between the two phases. Negative differences in Table 7-1 indicate the molecular interaction type represented by that solvent parameter favors protein over lipid. In this way, protein is stronger than lipid for polarizability (s), acceptance of hydrogen bonds (a), and donation of hydrogen bonds (b). Lipid is favored for dispersion (e) and cavity formation (v).

The solute descriptors, uppercase letters in Eq. (7-4), for the partition coefficient pp-LFERs used here, Eq. (7-5) and Eq. (7-6), were the appropriate QCAP reported by Liang ³¹ (Table H-5).

Table 7-1 Comparison of the competitiveness for solutes between lipid and protein, calculated as the difference between the solvent parameters in the K_{Lipid} and K_{Protein} pp-LFERs obtained by Kuo and Di Toro^{30,33}, Eq. (7-5) and Eq. (7-6), respectively.

Solvent parameter	Phase		Difference
	Lipid	Protein	
<i>e</i>	0.77	0.74	0.03
<i>s</i>	-1.10	-0.37	-0.73
<i>a</i>	-0.47	-0.13	-0.34
<i>b</i>	-3.52	-1.37	-2.15
<i>v</i>	3.37	1.06	2.31

7.2.2.2 Soil Organic Carbon-Water pp-LFER

The K_{OC} values were estimated using the pp-LFER model developed by Kipka and Di Toro³⁴

$$\log K_{\text{OC}} = 0.670 (\pm 0.088) + 1.075 (\pm 0.061)E - 0.277 (\pm 0.083)S - 0.363 (\pm 0.100)A - 1.697 (\pm 0.085)B + 1.468 (\pm 0.077)V \quad (7-7)$$

440 compounds; N = 440; RMSE = 0.48

where K_{OC} is expressed as $L_{\text{water}} \text{ kgOC}^{-1}$. This model was built with a wide and chemically varied dataset for nonionic organic compounds. The solvent parameters in Eq. (7-7) indicate that the soil organic carbon phase has similar solvation tendencies than those of the lipid and protein phases shown in Eq. (7-5) and Eq. (7-6), respectively, as the signs for all the molecular interactions are the same among these three pp-LFERs. A comparison of the difference in solvent parameters between lipid and organic carbon is presented in Table 7-2. Negative differences in Table 7-2 indicate the molecular interaction type represented by that solvent parameter favors organic carbon over lipid. In this way, the organic carbon phase is stronger than lipid for all molecular interactions with the exception of cavity formation (*v*). The solute descriptors used to apply this model here were the appropriate QCAP reported by Liang³¹ (Table H-5).

Table 7-2 Comparison of the competitiveness for solutes between lipid and organic carbon, calculated as the difference between the solvent parameters in the K_{Lipid} pp-LFER by Kuo and Di Toro ^{30,33}, Eq. (7-5), and K_{OC} pp-LFER by Kipka and Di Toro ³⁴, Eq. (7-7).

Solvent parameter	Phase		Difference
	Lipid	OC	
<i>e</i>	0.77	1.08	-0.31
<i>s</i>	-1.1	-0.28	-0.82
<i>a</i>	-0.47	-0.36	-0.11
<i>b</i>	-3.52	-1.70	-1.82
<i>v</i>	3.37	1.47	1.90

7.2.3 Experimental Data

Two datasets were compiled from published uptake assays: oligochaete BCFs from studies with measured concentrations in the interstitial water, and concentrations in oligochaetes from studies performed in soil for which measured concentrations in the interstitial water were unavailable. Data exclusion criteria were: (1) compounds with experimental $\log K_{\text{ow}} > 6.0$ (values from the EPI Suite database ³⁵) given that the worm intestinal uptake route becomes predominant for these highly hydrophobic chemicals, (2) compounds for which QCAP were not available (Liang ³¹), (3) measurements obtained at exposures concentrations causing lethal or inhibitory effects to worms, (4) concentrations below reported analytical quantification limits or without clarification on whether they were expressed on a dry or fresh weight basis, and (5) studies not reporting either the soil organic carbon or organic matter content. The data are listed in Tables H-2 and H-8.

7.2.3.1 Oligochaete Worms Bioconcentration Factors

A BCF dataset was assembled that is both chemically diverse and has oligochaete species variety as well. The compounds include MCs, MLCs, polycyclic aromatic hydrocarbons (PAHs), and organochlorines for studies with seven different terrestrial and aquatic oligochaete species (Table H-2). The exposure media include coarse quartz sand (0.5–1.0 mm effective diameter particles, hereafter referred to as "sand"), spiked or contaminated soil more complex than simple sand (hereafter referred to as "soil"), spiked or contaminated sediment, and water. A total of 60 observed oligochaete BCFs values for undissociated organic compounds were compiled (Table H-2). The oligochaete species in the BCFs dataset are: *Eisenia andrei* (*E. andrei*); *Lumbriculus variegatus* (*L. variegatus*); *Lumbricus terrestris* (*L. terrestris*); *Eisenia fetida* (*E. fetida*); *Lumbricus rubellus* (*L. rubellus*); *Tubifex tubifex* (*T. tubifex*); *Monopylephorus rubroniveus* (*M. rubroniveus*).

Values for f_{Lipid} , f_{Protein} , f_{Water} , and f_{dwt} were found in the literature for five of the seven oligochaete species in the dataset (Table H-3). Values for the missing species were

calculated as the average among oligochaetes of the same type, i.e., terrestrial or aquatic (Table H-4).

7.2.3.2 Concentrations in Oligochaete Worms

A dataset was compiled from measurements reported in published uptake assays with oligochaetes exposed to MCs in soil (Table H-8). The dataset includes the concentration in the worm, concentration in the soil, exposure time, and mass fraction of organic carbon in the soil (f_{OC}). A total of 23 observations were compiled. Further details of the experiments are described in Table H-8. The oligochaete species included in this dataset are *E. andrei* and *E. fetida*.

7.2.4 Prediction of Concentrations in Oligochaete Worms Observed in Independent Uptake Assays

Concentrations of MCs in oligochaetes reported in published soil uptake assays (Table H-8) were predicted using the K_{OC} , K_{Lipid} , and $K_{Protein}$ pp-LFERs. The concentration of MCs available for worm passive uptake in soil exposure medium was estimated using

$$C_{iIW} = \frac{C_{iSoilSolids}}{K_{iSoilIW}} = \frac{C_{iSoilSolids}}{K_{iOC}f_{OC}} \quad (7-8)$$

where C_{iIW} = concentration of compound i in the growth medium interstitial water (IW) (mg L^{-1}), $C_{iSoilSolids}$ = concentration of compound i in the soil solids (mg kg_{dwt}^{-1}), $K_{iSoilIW}$ = soil-water partition coefficient of compound i ($\text{L}_{water} \text{ kg}_{dwt} \text{ soil}^{-1}$), and f_{OC} = dry weight fraction of organic carbon in the soil ($\text{kg}_{OC} \text{ kg}_{dwt} \text{ soil}^{-1}$). Values for $C_{iSoilSolids}$ were those reported by the sources as the concentration at the beginning of the exposure or a steady state exposure concentration when available. Values for f_{OC} were also obtained from the sources when available. However, soil organic matter content (as f_{OM} or %, w/w) is reported in most of the sources. A factor of 0.50 was used to convert f_{OM} to f_{OC} when needed³⁶. K_{iOC} were estimated using Eq. (7-7), described previously in Section 7.2.2.2.

Using the predicted C_{iIW} , the concentration of MCs in worm biomass was estimated as

$$C_{iWorm} = K_{iWW}C_{iIW} = \left(f_{Lipid} K_{iLipid} + f_{Protein} K_{iProtein} + \frac{f_{Water}}{\rho_{Water}} \right) \frac{C_{iIW}}{f_{dwt}} \quad (7-9)$$

where K_{iWW} = worm–water partition coefficient of compound i ($\text{L}_{water} \text{ kg}_{dwt} \text{ worm}^{-1}$). K_{iLipid} were estimated using both of the pp-LFERs described previously in Section 7.2.2.1. $K_{iProtein}$ were estimated using Eq. (7-6). Values for f_{Lipid} , $f_{Protein}$, f_{Water} , and f_{dwt} were obtained from the literature (Table H-3).

7.3 Results and Discussion

7.3.1 Lipid–Water and Protein–Water pp–LFERs and Estimation of Oligochaete Worms BCFs

The estimation of oligochaete BCFs was performed substituting Eq. (7-4) into Eq. (7-3) for the K_{Lipid} , which yields

$$BCF_i = \left[f_{Lipid} 10^{(c+eE+sS+aA+bB+vV)} + f_{Protein} K_{iProtein} + \frac{f_{Water}}{\rho_{Water}} \right] \frac{1}{f_{dwt}} \quad (7-10)$$

where values for f_{Lipid} , $f_{Protein}$, f_{Water} , and f_{dwt} were obtained from the literature (Table H-4), $K_{iProtein}$ were estimated using Eq. (7-6), and the solute descriptors, uppercase letters in Eq. (7-4), were QCAP reported by Liang³¹ (Table H-5), and the solvent parameters, lowercase letters in Eq. (7-4), were the result of the MLRA to the oligochaete BCFs.

The fitted BCFs using Eq. (7-10) are shown in Figure 7-1. The regression yielded a RMSE = 0.499, indicating that approximately 68% of the estimated BCFs fall within ± 0.499 log units (a factor of ± 3.16) of the corresponding observed BCF. The color coding in Figure 7-1 allows to identify each data point by compound (Figure 7-1A), exposure medium (Figure 7-1B), and oligochaete species (Figure 7-1C). The BCFs covered a range of approximately five orders of magnitude ($0.664 < \log BCF < 5.389$) for which MCs and MLCs constitute the lower end of the range (Figure 7-1A). No bias was observed for the estimation of any compound.

On the other hand, the RMSE of the estimates depended on the exposure media (Figure 7-1B) with RMSEs for each group increasing in the order of sand < water < soil < sediment (0.177, 0.365, 0.467, and 0.768, respectively). This was expected as the concentrations measured in worms and exposure phase in experiments with sediments or soils are less reliable than those in assays with sand or water. This is due to the analytical challenges to collect worms or interstitial water (i.e., exposure phase) from sediment or soil without also disturbing the sample and changing it in some way, for example by oxidation.

No trend was observed in the estimation as a function of the oligochaete being terrestrial or aquatic (Figure 7-1C), suggesting that the model could be applied to a variety of oligochaete species.

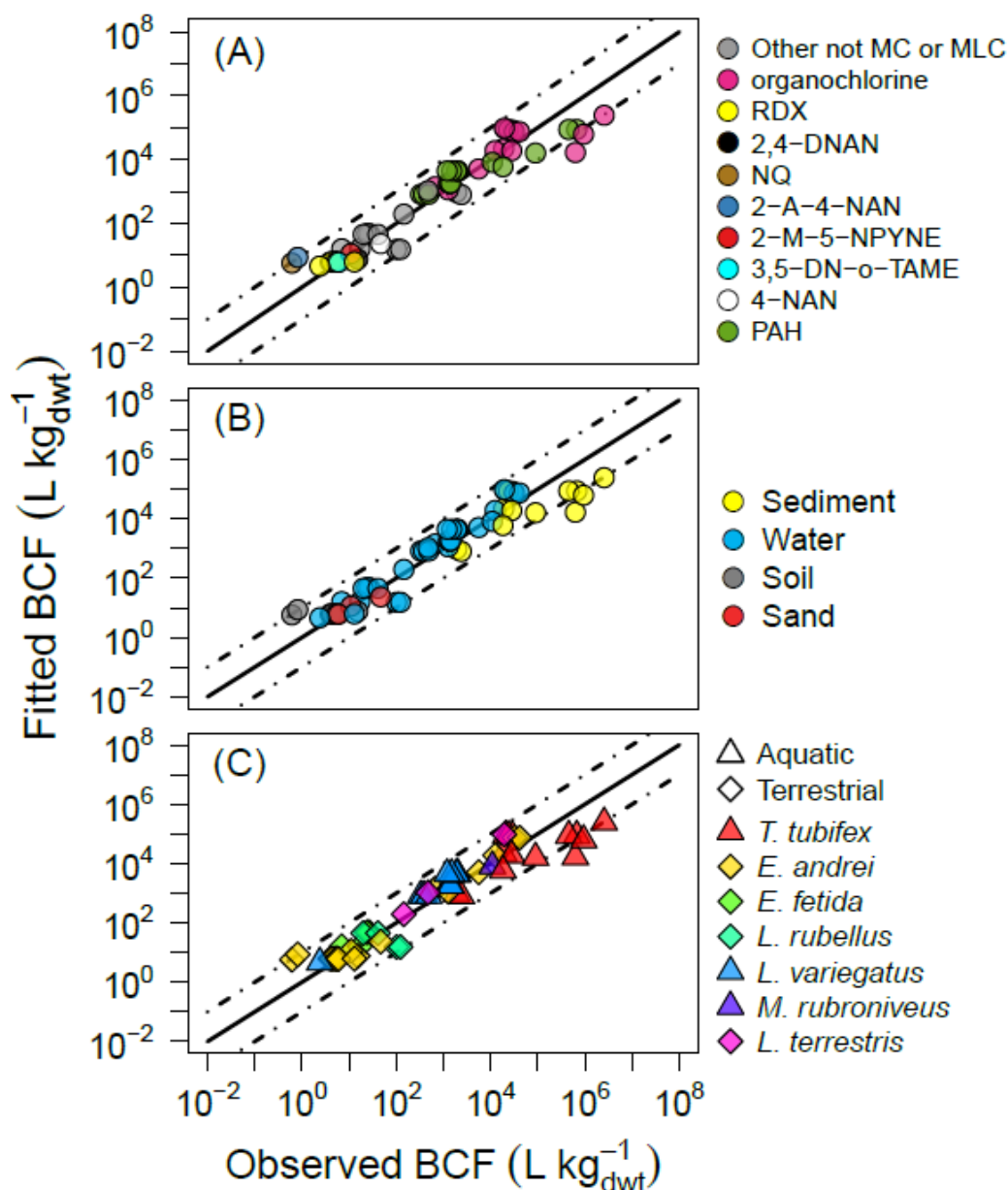


Figure 7-1 Fitted versus observed BCFs for organic compounds (Table H-6). Regression made using a BCF model (Eq. (7-10)) with partitioning to three worm components, lipid (Eq. (7-11)), protein (Eq. (7-6)), and internal water. Color coding assigned based on: (A) organic compound, (B) exposure medium, and (C) oligochaete species. Root mean square error of estimation (log estimated - log observed BCF), RMSE = 0.499. Abbreviations defined in Table H-2. The solid line indicates the best agreement (unity), dashed lines are spaced at 1 log unit from unity.

The K_{Lipid} pp-LFER obtained in this work with the MLRA described for Eq. (7-10) using exclusively BCF oligochaete data was

$$\begin{aligned}\log K_{Lipid} = & 0.751 (\pm 0.780) + 0.431 (\pm 0.189)E - 2.409 (\pm 0.387)S \\ & - 0.787 (\pm 0.393)A - 2.106 (\pm 0.793)B \\ & + 4.553 (\pm 0.673)V \\ & 27 \text{ compounds; } N = 60\end{aligned}\tag{7-11}$$

where the solvent parameters, lowercase variables in Eq. (7-4), resulted to be very similar to those in the K_{Lipid} pp-LFER obtained by Kuo and Di Toro^{30,33} with lipid–water partitioning data from multiple sources including fish fat/oil (Eq. (7-5)). Both Eq. (7-5) and Eq. (7-11) exhibit the same competitiveness of the lipid phase relative to water as the signs of the solvent parameters are the same for all types of molecular interactions and, with the exception of *s*, the values are not different at the 5% level of statistical significance (Table H-7).

Given the similarities between these two K_{Lipid} pp-LFERs, a comparison of estimations for the BCF oligochaete data was performed using either the K_{Lipid} pp-LFER by Kuo and Di Toro^{30,33} (Eq. (7-5)) or that obtained in this work (Eq. (7-11)) and shown in Figure 7-2. The BCF model (Eq. (7-3)) was able to capture the linear variation in the observed oligochaete BCFs in spite of using a K_{Lipid} pp-LFER not trained specifically with oligochaete data (Figure 7-2B). The underestimation of three organochlorines in the higher end of the dataset (Figure 7-2) appears to be an artifact of the experimental measurements as all three observations are from the same study and are approximately two orders of magnitude higher than values corresponding to the same compounds (1,2,3,4-tetrachlorobenzene; pentachlorobenzene; and hexachlorobenzene) and oligochaete species (*Tubifex tubifex*) reported by other studies also included in the set (Table H-2). No bias was observed in the estimates of any of the eight chemical classes in particular.

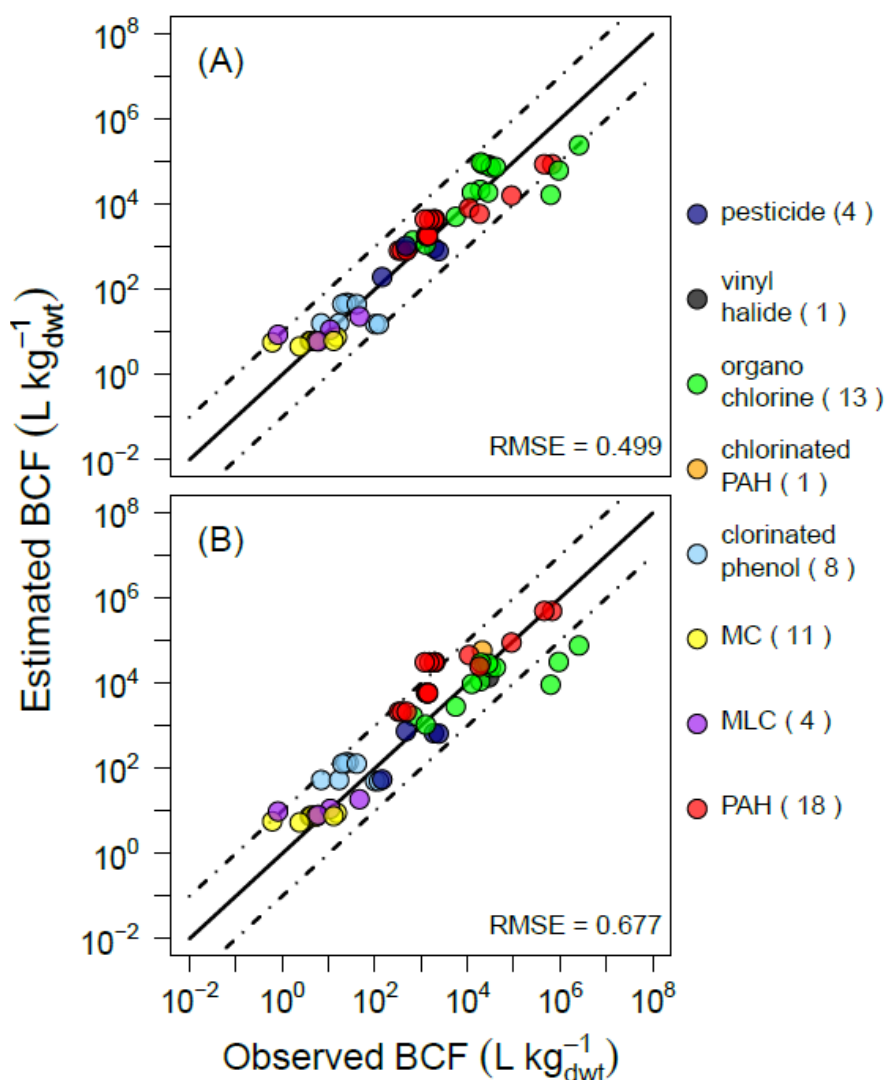


Figure 7-2 Estimated versus observed BCFs for organic compounds (Table H-6). Estimations made using a partitioning-based BCF model (Eq. (7-3)) with the K_{Lipid} pp-LFER from: (A) this work (Eq. (7-11)), and (B) Kuo and Di Toro ^{30,33} (Eq. (7-5)). Legend: Chemical class with corresponding count; PAH: polycyclic aromatic hydrocarbon. RMSE: Root mean square error of estimation (log estimated - log observed BCF). The solid line indicates the best agreement (unity), dashed lines are spaced at 1 log unit from unity.

Obtaining a RMSE for the prediction with Eq. (7-5) (RMSE = 0.677) that is larger than that using Eq. (7-11) (RMSE = 0.499) is expected since unlike the K_{Lipid} pp-LFER built in this work, the K_{Lipid} pp-LFER by Kuo and Di Toro ^{30,33} is not fitted to the data. Figure 7-2B is an independent prediction of the observed oligochaete BCFs. The fact that a reasonable uncertainty in the estimation of oligochaete BCFs is obtained using a K_{Lipid} pp-LFER not specific to worms suggests that the solvation properties of worm lipid and lipid from other organisms such as fish

are indeed similar. Therefore, it appears that the resulting concentration in the oligochaete is mostly chemical-specific, rather than species-specific.

The contribution of the three worm components (lipid, protein, and water) to the estimated BCFs varied among chemical classes, as shown in Figure 7-3, a comparison of the fraction contributed to the BCFs by each worm component. Considerable differences were also found within the MCs (NQ; RDX; 2,4-DNAN) and MLCs (3,5-DN-o-TAME; 2-A-4-NAN; 2-M-5-NPYNE; 4-NAN) and thus they are not grouped together in Figure 7-3. The contributions were more uniform within the other chemical classes; therefore, the values in Figure 7-3 are the average for each of these classes.

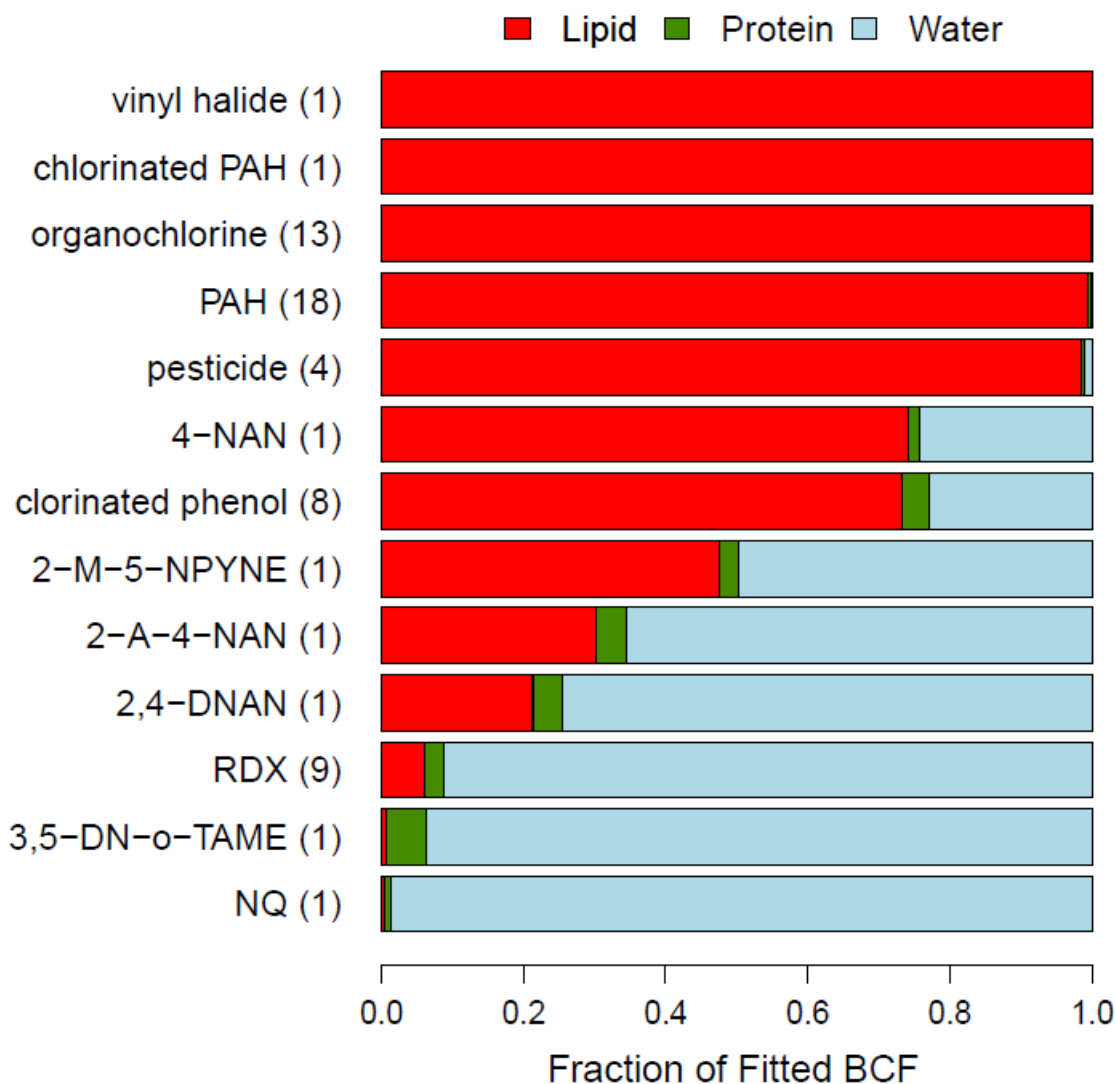


Figure 7-3 Contribution of worm components (lipid, protein and internal water) to the fitted BCF (Eq. (7-3)) for MCs, MLCs, and other chemical classes in the oligochaete dataset presented in Figure 7-1. Estimation of partitioning to lipid component made using K_{Lipid} pp-LFER from this work (Eq. (7-11)), and to protein component using K_{Protein} pp-LFER from Kuo and Di Toro^{30,33} (Eq. (7-6)). Numbers in parenthesis are the corresponding count. Abbreviations are defined in Table H-2.

Lipid rose to be the dominant phase for chlorinated phenols, pesticides, PAHs, organochlorines, chlorinated PAHs, and vinyl halides (Figure 7-3), while water contributed the most to the oligochaete BCFs for all MCs and MLCs with the exception of 4-NAN. Protein resulted to be the phase with no dominant contributions to the BCFs for all chemicals classes including MCs and MLCs (Figure 7-3). A reason is that despite the high content of this phase in oligochaetes (approximately 10%_{wwt}, Table H-4), the energy required for cavity formation in protein is considerably larger in comparison to that needed in lipid. This is indicated by the wide

positive difference for v in Table 7-3 (3.49), a comparison of the solvent parameters between lipid (K_{Lipid} pp-LFER from this work) and protein. In addition to v , a large difference was also found for the dipolarity/polarizability solvent descriptor, s , (Table 7-3), but in this case the discrepancy favors the protein phase (-2.04).

Table 7-3 Comparison of the competitiveness for solutes between lipid and protein, calculated as the difference between the solvent parameters in the K_{Lipid} obtained in this work and K_{Protein} pp-LFER obtained by Kuo and Di Toro^{30,33}, Eq. (7-11) and Eq. (7-6), respectively.

Solvent parameter	Phase		Difference
	Lipid	Protein	
e	0.43	0.74	-0.31
s	-2.41	-0.37	-2.04
a	-0.79	-0.13	-0.66
b	-2.11	-1.37	-0.74
v	4.55	1.06	3.49

The effect of these contrasting solvation capabilities on the resulting K_{Lipid} and K_{Protein} , and ultimately on the estimated oligochaete BCF, for this set of organic compounds is examined more in depth in Figure 7-4. Figure 7-4 pairs the effect of the solvation capabilities with the complementary response from the compounds studied, i.e., a solvent-solute product (xX), which when added together result in the lipid-water and protein-water partition coefficients (Eq. (7-4)). Most of the xX values for the protein phase are near 0 and none are above 3 (Figure 7-4). This illustrates the very low effectiveness of protein to solvate these organic compounds, especially relative to lipid for which some xX values reach approximately 8. The dipolarity/polarizability interactions that show favorability for partition to protein based only on the solvent parameter s (Table 7-3), contrast with the results for the sS product. The sS values for protein are all < 0 (Figure 7-4), and while they are not as negative as those for lipid they contribute to the low competitiveness of protein for solutes relative water. The effect from the dispersion interactions (eE) and the donation and acceptance of hydrogen bonds (aA and bB) to either the K_{Lipid} or the K_{Protein} are small with values between -1.80 and 2.61 (Figure 7-4), which is a very narrow range relative to that covered by the sS and vV terms (-6.3 to 8.3).

Overall, the dominant contribution to the oligochaete BCFs for these compounds is that from the lipid phase. The major role in the partitioning between lipid and water is played by the cavity formation (vV) and dipolarity/polarizability (sS) interactions which are $-6.3 < sS < -1.2$ and $3.0 < vV < 8.3$, respectively (Figure 7-4). These sS and vV terms counteract each other and hence the appropriate term to examine differences across chemical classes is $sS + vV$ (Figure 7-4). Chemical classes of a less polar nature and requiring more energy for cavity formation due to their larger molecular volumes, such as PAHs and organochlorines, have in larger values $sS +$

vV (Figure 7-4), and thus show the most substantial contributions from the lipid phase to the estimated oligochaete BCF (Figure 7-4).

In contrast, compounds that have smaller molecular volumes and are of a more polar nature, such as most of the MCs and MLCs, have in smaller $sS + vV$ values (Figure 7-4), and thus show the most substantial contributions from the water phase to the estimated oligochaete BCF (Figure 7-3). These results add to the importance of chemical-specificity and molecular interactions on the bioconcentration of nonionic organic compounds in oligochaetes.

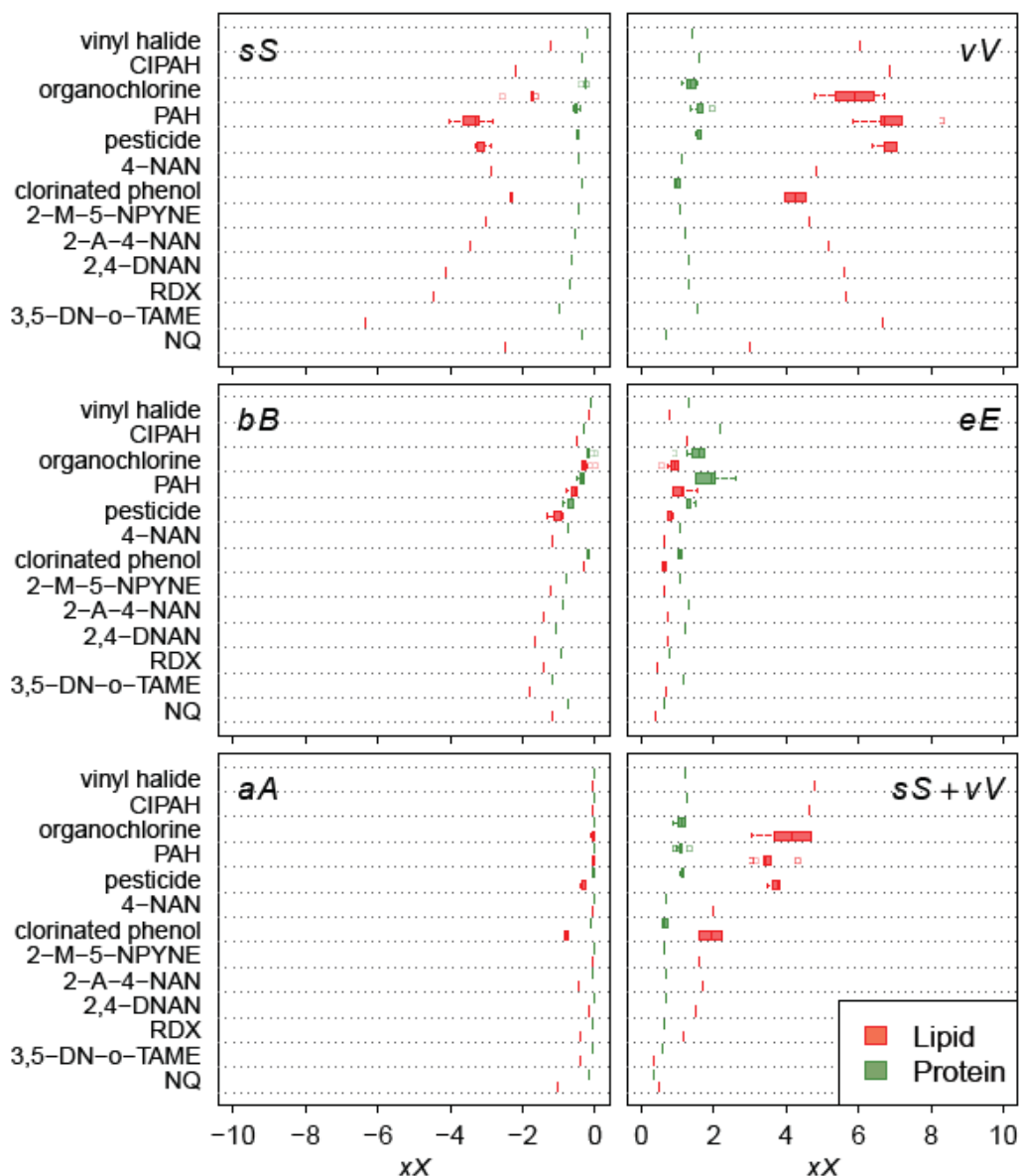


Figure 7-4 Contribution from solute-solvent products (xX , Eq. (7-4)) to the estimated $\log K_{\text{Lipid}}$ (Eq. (7-11)) and $\log K_{\text{Protein}}$ (Eq. (7-6)) for MCs, MLCs, and other chemical classes in the oligochaete BCF dataset presented in Figure 7-1.

7.3.2 Prediction of Concentrations in Oligochaete Worms Observed in Independent Uptake Assays

Predictions of concentrations in oligochaete worms for MCs using the BCF model are shown in Figure 7-5 (Tables H-11 and H-12). The final equation used to predict the worm concentration is Eq. (7-12) in Table 7-4, which contains the equations used ordered in the sequence to generate a prediction. In Eq. (7-12), the $C_{i\text{soil}}$ and f_{OC} were obtained directly from the source of the uptake assay (Table H-8), worm values for f_{Lipid} , f_{Protein} , f_{Water} , and f_{dwt}

were from the literature (Table H-9), and K_{iLipid} , $K_{iProtein}$, and K_{OC} were estimated using the pp-LFERs in Eq. (7-5) (or Eq. (7-11)), Eq. (7-6), and Eq. (7-7), respectively. A worked example on how to proceed with the calculations to make a prediction is shown in Table H-10.

Table 7-4 Sequence of equations for the prediction of concentrations in oligochaetes exposed to MCs, or MLCs, in soil.

A partitioning-based oligochaete worms bioconcentration model^a:

$$C_{iWorm} = \left(f_{Lipid} K_{iLipid} + f_{Protein} K_{iProtein} + \frac{f_{Water}}{\rho_{Water}} \right) \frac{C_{iSoilSolids}}{f_{dwt} f_{OC} K_{iOC}} \quad (7-12)$$

Var.	Equation	#
K_{iOC}	$\log K_{OC} = 0.670 + 1.075E - 0.277S - 0.363A - 1.697B + 1.468V$	(7-7)
C_{iIW}	$C_{iIW} = \frac{C_{iSoilSolids}}{K_{iOC} f_{OC}}$	(7-8)
K_{iLipid}	$\log K_{Lipid} = 0.84 + 0.77E - 1.10S - 0.47A - 3.52B + 3.37V$	(7-5)
K_{iLipid}	$\log K_{Lipid} = 0.751 + 0.431E - 2.409S - 0.787A - 2.106B + 4.553V$	(7-11)
$K_{iProtein}$	$\log K_{Protein} = -0.88 + 0.74E - 0.37S - 0.13A - 1.37B + 1.06V$	(7-6)
C_{iWorm}	$C_{iWorm} = \left(f_{Lipid} K_{iLipid} + f_{Protein} K_{iProtein} + \frac{f_{Water}}{\rho_{Water}} \right) \frac{C_{iIW}}{f_{dwt}}$	(7-9)

^a Var.: Variables; i : MC, or MLC, of interest; C_{iWorm} : concentration of i in the worm (mg kg_{dwt}⁻¹); f_{Lipid} and $f_{Protein}$: wet weight worm fraction of lipid and protein, respectively (kg_{lipid} kg_{wwt worm}⁻¹ and kg_{protein} kg_{wwt worm}⁻¹, wwt: wet weight); K_{iLipid} and $K_{iProtein}$: lipid-water and protein-water partition coefficients of i , respectively (L_{water} kg_{lipid}⁻¹ and L_{water} kg_{protein}⁻¹); f_{Water} and f_{dwt} : worm mass fraction of water and dry weight, respectively (kg_{water} kg_{wwt worm}⁻¹ and kg_{dwt} kg_{wwt worm}⁻¹); ρ_{Water} : density of water (kg_{water} L_{water}⁻¹); $C_{iSoilSolids}$: concentration of compound i in the soil solids (mg kg_{dwt soil}⁻¹); f_{OC} : dry weight fraction of organic carbon in the soil (kg_{OC} kg_{dwt soil}⁻¹); K_{iOC} : organic carbon-water partition coefficient of i (L_{water} kg_{OC}⁻¹); E , S , A , B , and V : QCAP for i (Table H-9); C_{iIW} : dissolved concentration of i in the interstitial water (IW) (mg L⁻¹)

Concentrations exceeding the aqueous solubility in the soil interstitial water were obtained when predicting the dissolved concentration from the reported soil concentrations for RDX and HMX (Table H-1), as shown in Figure 7-5. Often very large concentrations, up to

10000 mg kg_{dwt}⁻¹, of a compound of interest are applied to the soil at the beginning of uptake assays in order to compensate for the losses of the parent compound due to transformation/degradation processes and/or to overcome analytical limitations in the detection of compounds with low aqueous solubilities³⁷⁻³⁹. However, these large concentrations result in both sorbed and pure compound in the soil. In order to predict the concentration in the worm for these cases, it was assumed that the dissolved concentration was at the solubility of the compound and not at the predicted concentration based on a measured soil concentration. This is the reason that the predicted worm concentration is constant for RDX and HMX in Figure 7-5. Also, because the prediction was based on an assumed concentration (solubility of the compound) these data were not included in the calculation of the RMSE for the models.

The RMSEs for the model using either $K_{\text{Lipid pp-LFER}}$ (Eq. (7-11) or Eq. (7-5)) were RMSE = 0.396 (Figure 7-5A) and RMSE = 0.523 (Figure 7-5B), which parallels the result obtained for the estimations of BCFs from experiments with measured concentrations in the interstitial water (RMSE = 0.499 and RMSE = 0.677 in Figure 7-2). The reason for the difference is that the model in panel (A) uses the $K_{\text{Lipid pp-LFER}}$ fitted to the BCF oligochaete data, whereas the model in panel (B) uses the $K_{\text{Lipid pp-LFER}}$ by Kuo and Di Toro^{30,33}, which was calibrated to a set of partitioning data from various lipid sources.

The BCF model (Eq. (7-12)) was able to predict oligochaete concentrations for a small but chemically heterogeneous MCs dataset including nitramines (e.g., RDX, abbreviations for MCs are defined in Table H-1) and nitroaromatics (e.g., TNT) as well as new insensitive MCs (e.g., 2,4-DNAN)⁴⁰. These MCs have diverse molecular structures and functional groups that interact to a different degree with the lipid and protein phases making the prediction of the concentration in the worm components challenging. While the differences among MCs are considerably smaller than those relative to other chemical classes, the BCF model employs pp-LFERs that are sensitive to these variations via the solute Abraham parameters. For example, RDX, TNT, and 2,4-DNAN are described by different values for their ability to undergo hydrogen bonding donation (A : 0.528, 0.302, 0.187, respectively; Table H-9), and RDX and TNT have distinctive values for the extent of their interactions through dispersion forces (E : 1.020 and 1.660, respectively; Table H-9).

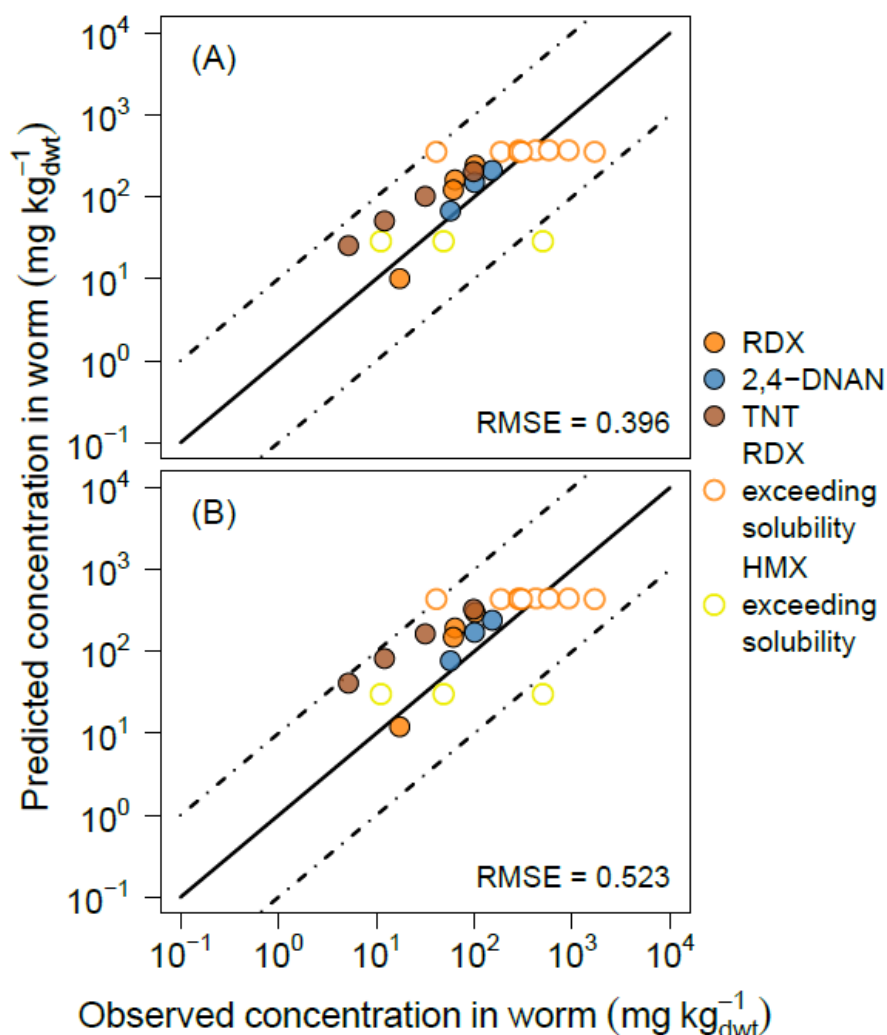


Figure 7-5 Predicted versus observed concentrations of MCs in oligochaetes from independent studies. Predictions made using a partitioning-based model (Eq. (7-12)) with the $K_{\text{Lipid pp-LFER}}$ from (A) this work (Eq. (7-11)) or (B) Kuo and Di Toro^{30,33} (Eq. (7-5)). Unfilled symbols represent predictions made with concentrations in the interstitial water at aqueous solubility. RMSE: Root mean square error (\log predicted - \log observed concentration in worm), excluding predictions at aqueous solubility. The solid line indicates the best agreement (unity), dashed lines are spaced at 1 log unit from unity.

The results shown in Figure 7-5 are for the prediction of data that were not part of the calibration of either BCF model. In this way, Figure 7-5 serves as a validation for the underlying assumptions of the BCF model (Eq. (7-12)), those are, (1) the uptake from soil is mainly from passive diffusion, and (2) the worm components playing a major role in the bioconcentration of MCs are lipid, protein, and water.

7.4 Conclusions

Oligochaete worms bioconcentration factors can be estimated based on the partitioning to three main worm components: lipid, protein, and internal water. The individual contribution of the components to the bioconcentration was dependent on the chemical compound. Compounds that interact mostly through dispersive forces embedded in the cavity formation (vV) and dispersion (eE) terms, such as PAHs and organochlorines, showed a large preference for worm lipid. Compounds that are of a more polar nature interacting predominantly through polarizability (sS) and hydrogen bonding (aA and bB), such as RDX and NQ, concentrated mostly in the worm internal water. The uncertainties for the estimation of the oligochaete BCFs were low using either a lipid–water pp–LFER trained exclusively with oligochaete data (RMSE = 0.499; Eq. (7-11)) or one trained with data from various sources of lipids including fish fat/oil (RMSE = 0.677; Eq. (7-5)). No bias was observed in the model estimates as a function of the oligochaete being a terrestrial or aquatic species, suggesting partitioning to the lipid phase has little dependence on the organism species, something which would be expected for a chemical–dominated process. In this way, the abundant amount of lipid–water partitioning data available for organisms like fish can be used to make a baseline estimation of the BCFs for oligochaetes for which limited data exists.

Concentrations in oligochaete worms exposed to MCs in soil during independent uptake assays were estimated based only on the partitioning between soil organic carbon and interstitial water, and between water and worm components. Using this modeling frame, observed values were predicted within ± 0.396 log units (or ± 0.523 , depending on the K_{Lipid} pp–LFER used for the lipid contribution). This indicates that the concentration available for worm uptake can be predicted from partitioning between soil interstitial water organic carbon, and that partitioning to worm components can estimate the extent of the bioconcentration to be expected.

These results demonstrate the ability of the BCF model to make reasonable estimates without relying on experimental measurements and using only molecular structure to compute the required model parameters. This is particularly useful when data for a specific organism are scarce, predictions need to be made for large libraries of compounds, and/or environmental risk needs to be assessed for compounds in the development stage.

REFERENCES

1. Grdisa M, Grsic K, Grdisa MD. Earthworms - role in soil fertility to the use in medicine and as a food. *Isj-Invertebrate Survival Journal*. 2013;10(1):38-45.
2. Organisation for Economic Co-operation and Development. Test no. 315: Bioaccumulation in sediment-dwelling benthic oligochaetes. In: *OECD guidelines for the testing of chemicals, section 3*. Organisation for Economic Co-operation and Development; 2008. 10.1787/9789264067516-en.
3. Organisation for Economic Co-operation and Development. Test no. 317: Bioaccumulation in terrestrial oligochaetes. In: *OECD guidelines for the testing of chemicals, section 3*. Organisation for Economic Co-operation and Development; 2010. 10.1787/9789264090934-en.
4. Frund H, Graefe U, Tischler S. Earthworms as bioindicators of soil quality. In: Karaca A, ed. *Soil biology*. Vol 24. Berlin, Heidelberg, Germany: Springer-Verlag Berlin Heidelberg; 2011:261-278. 10.1007/978-3-642-14636-7_16.
5. Jager T. Mechanistic approach for estimating bioconcentration of organic chemicals in earthworms (oligochaeta). *Environmental Toxicology and Chemistry*. 1998;17(10):2080-2090.
6. Frank AP, Landrum PF, Eadie BJ. Polycyclic aromatic hydrocarbon rates of uptake, depuration, and biotransformation by lake michigan stylodrilus heringianus. *Chemosphere*. 1986;15(3):317-330. doi: [http://dx.doi.org/10.1016/0045-6535\(86\)90025-1](http://dx.doi.org/10.1016/0045-6535(86)90025-1).
7. Gabric AJ, Connell DW, Bell PRF. A kinetic model for bioconcentration of lipophilic compounds by oligochaetes. *Water Res*. 1990;24(10):1225-1231. doi: [http://dx.doi.org/10.1016/0043-1354\(90\)90045-8](http://dx.doi.org/10.1016/0043-1354(90)90045-8).
8. Belfroid A, Seinen W, VanGestel K, Hermens J, VanLeeuwen K. Modelling the accumulation of hydrophobic organic chemicals in earthworms - application of the equilibrium partitioning theory. *Environmental Science and Pollution Research*. 1995;2(1):5-15.
9. Belfroid AC, Sijm DTHM, Van Gestel CAM. Bioavailability and toxicokinetics of hydrophobic aromatic compounds in benthic and terrestrial invertebrates. *Env Rev*. 1996;4(4):276-299.
10. Jager T. Modeling ingestion as an exposure route for organic chemicals in earthworms (oligochaeta). *Ecotoxicol Environ Saf*. 2004;57(1):30-38.

11. Hu XY, Wen B, Shan XQ, Zhang SZ. Bioavailability of pentachlorophenol to earthworms (*Eisenia fetida*) in artificially contaminated soils. *Journal of Environmental Science and Health Part A-Toxic/hazardous Substances & Environmental Engineering*. 2005;40(10):1905-1916.
12. Henson-Ramsey H, Levine J, Kennedy-Stoskopf S, Taylor SK, Shea D, Stoskopf MK. Development of a dynamic pharmacokinetic model to estimate bioconcentration of xenobiotics in earthworms. *Environmental Modeling & Assessment*. 2009;14(3):411-418.
13. Peijnenburg W, Capri E, Kula C, et al. Evaluation of exposure metrics for effect assessment of soil invertebrates. *Crit Rev Environ Sci Technol*. 2012;42(17):1862-1893.
14. Jager T, Fleuren R, Hogendoorn E, De Korte G. Elucidating the routes of exposure for organic chemicals in the earthworm, *Eisenia andrei* (Oligochaeta). *Environ Sci Technol*. 2003;37(15):3399-3404.
15. Lord KA, Briggs GG, Neale MC, Manlove R. Uptake of pesticides from water and soil by earthworms. *Pestic Sci*. 1980;11(4):401-408.
16. Van Gestel CAM, Ma W. Toxicity and bioaccumulation of chlorophenols in earthworms, in relation to bioavailability in soil. *Ecotoxicol Environ Saf*. 1988;15(3):289-297.
17. Connell DW, Markwell RD. Bioaccumulation in the soil to earthworm system. *Chemosphere*. 1990;20(1):91-100. doi: [http://dx.doi.org/udel.idm.oclc.org/10.1016/0045-6535\(90\)90089-C](http://dx.doi.org/udel.idm.oclc.org/10.1016/0045-6535(90)90089-C).
18. Belfroid A, Vanwezel A, Sikkenk M, Vangestel K, Seinen W, Hermens J. The toxicokinetic behavior of chlorobenzenes in earthworms (*Eisenia andrei*): Experiments in water. *Ecotoxicol Environ Saf*. 1993;25(2):154-165.
19. Bruns E, Egeler P, Roembke J, Scheffczyk A, Spoerlein P. Bioaccumulation of lindane and hexachlorobenzene by the oligochaetes *Enchytraeus luxuriosus* and *Enchytraeus albidus* (Enchytraeidae, Oligochaeta, Annelida). *Hydrobiologia*. 2001;463:185-196.
20. Larson SL, Martin WA, Escalon BL, Thompson M. Dissolution, sorption, and kinetics involved in systems containing explosives, water, and soil. *Environ Sci Technol*. 2007;42(3):786-792.
21. Sharma P, Mayes MA, Tang G. Role of soil organic carbon and colloids in sorption and transport of TNT, RDX and HMX in training range soils. *Chemosphere*. 2013;92(8):993-1000.
22. von Oepen B, Kördel W, Klein W, Schüürmann G. QSAR in environmental toxicology predictive QSPR models for estimating soil sorption coefficients: Potential and limitations based on dominating processes. *Sci Total Environ*. 1991;109:343-354. doi: 10.1016/0048-9697(91)90189-L.

23. Wei DB, Wu CD, Wang LS, Hu HY. QSPR-based prediction of adsorption of halogenated aromatics on yellow-brown soil. *SAR QSAR Environ Res.* 2003;14(3):191-198.
24. Kozerski GE, Xu S, Miller J, Durham J. Determination of soil-water sorption coefficients of volatile methylsiloxanes. *Environ Toxicol Chem.* 2014;33(9):1937-1945.
25. Abraham MH. Scales of solute hydrogen-bonding: Their construction and application to physicochemical and biochemical processes. *Chem Soc Rev.* 1993;22(2):73-83.
26. Goss K. Predicting the equilibrium partitioning of organic compounds using just one linear solvation energy relationship (LSER). *Fluid Phase Equilibr.* 2005;233(1):19-22.
27. Oliver BG. Biouptake of chlorinated hydrocarbons from laboratory-spiked and field sediments by oligochaete worms. *Environ Sci Technol.* 1987;21(8):785-790.
28. Belden JB, Lotufo GR, Lydy MJ. Accumulation of hexahydro-1,3,5-trinitro-1,3,5-triazine in channel catfish (*ictalurus punctatus*) and aquatic oligochaetes (*lumbriculus variegatus*). *Environmental Toxicology and Chemistry.* 2005;24(8):1962-1967.
29. Savard K, Sarrazin M, Dodard SG, et al. Role of soil interstitial water in the accumulation of hexahydro-1,3,5-trinitro-1,3,5-triazine in the earthworm *eisenia andrei*. *Environ Toxicol Chem.* 2010;29(4):998-1005.
30. Kuo DTF, Di Toro DM. A reductionist mechanistic model for bioconcentration of neutral and weakly polar organic compounds in fish. *Environmental Toxicology and Chemistry.* 2013;32(9):2089-2099.
31. Liang Y. *Determining abraham solute and system parameters for neutral organic compounds using quantum chemical methods.* [Doctoral Dissertation]. University of Delaware; 2016.
32. Lin S, Sandler SI. A priori phase equilibrium prediction from a segment contribution solvation model
. *Ind Eng Chem Res.* 2002;41(5):899-913.
33. Kuo DTF, Di Toro DM. Biotransformation model of neutral and weakly polar organic compounds in fish incorporating internal partitioning. *Environmental Toxicology and Chemistry.* 2013;32(8):1873-1881.
34. Kipka U, Di Toro DM. A linear solvation energy relationship model of organic chemical partitioning to particulate organic carbon in soils and sediments. *Environ Toxicol Chem.* 2011;30(9):2013-2022.
35. US Environmental Protection Agency. Estimation programs interface (EPI) suite™ for microsoft® windows, v. 4.11. . 2012;4.11.

36. Pribyl DW. A critical review of the conventional SOC to SOM conversion factor. *Geoderma*. 2010;156(3–4):75-83.
37. Best EPH, Geter KN, Tatem HE, Lane BK. Effects, transfer, and fate of RDX from aged soil in plants and worms. *Chemosphere*. 2006;62(4):616-625.
38. Sarrazin M, Dodard SG, Savard K, et al. Accumulation of hexahydro-1,3,5-trinitro-1,3,5-triazine by the earthworm *Eisenia andrei* in a sandy loam soil. *Environmental Toxicology and Chemistry*. 2009;28(10):2125-2133.
39. Sunahara GI. Development of toxicity benchmarks and bioaccumulation data for N-based organic explosives for terrestrial plants and soil invertebrates. . 2012;Project ER-1416.
40. Hawari J, Monteil-Rivera F, Perreault NN, et al. Environmental fate of 2,4-dinitroanisole (DNAN) and its reduced products. *Chemosphere*. 2015;119(0):16-23.
41. Kuperman RG, Simini M, Checkai RT, et al. Developing earthworm bioconcentration factors of nitrogen-based compounds for predicting environmentally significant parameters for new munition compounds in soil. *Applied Soil Ecology*. 2016;104:25-30.
42. Branquart E, Deleu R, Copin A, Gaspar C. Bioaccumulation and metabolism of isoproturon, linuron and lindane by *Lumbricus terrestris* L. *Mededelingen Faculteit Landbouwkundige en Toegepaste Biologische Wetenschappen Universiteit Gent*. 1995;609(2b):511-519.
43. Ankley GT, Erickson RJ, Sheedy BR, Kosian PA, Mattson VR, Cox JS. Evaluation of models for predicting the phototoxic potency of polycyclic aromatic hydrocarbons. *Aquatic Toxicology*. 1997;37(1):37-50.
44. Kraaij RH, Tolls J, Sijm D, Cornelissen G, Heikens A, Belfroid A. Effects of contact time on the sequestration and bioavailability of different classes of hydrophobic organic chemicals to benthic oligochaetes (tubificidae). *Environmental Toxicology and Chemistry*. 2002;21(4):752-759.
45. Kraaij R, Mayer P, Busser F, Bolscher M, Seinen W, Tolls J. Measured pore-water concentrations make equilibrium partitioning work - A data analysis. *Environ Sci Technol*. 2003;37(2):268-274.
46. Van der Wal L, Jager T, Fleuren RHLJ, et al. Solid-phase microextraction to predict bioavailability and accumulation of organic micropollutants in terrestrial organisms after exposure to a field-contaminated soil. *Environ Sci Technol*. 2004;38(18):4842-4848.
47. Zhenjun S, Xianchun L, Lihui S, Chunyang S. Earthworm as a potential protein resource. *Ecol Food Nutr*. 1997;36(2-4):221-236.

48. Albro PW, Schroeder JL, Corbett JT. Lipids of the earthworm *lumbricus-terrestris*. *Lipids*. 1992;27(2):136-143.
49. Finke MD. Complete nutrient composition of commercially raised invertebrates used as food for insectivores. *Zoo Biol*. 2002;21(3):269-285.
50. Liebig M, Egeler P, Oehlmann J, Knacker T. Bioaccumulation of 14C-17 α -ethinylestradiol by the aquatic oligochaete *lumbriculus variegatus* in spiked artificial sediment. *Chemosphere*. 2005;59(2):271-280.
51. Croce V, De Angelis S, Patrolecco L, Polesello S, Valsecchi S. Uptake and accumulation of sediment-associated 4-nonylphenol in a benthic invertebrate (*lumbriculus variegatus*, freshwater oligochaete). *Environmental Toxicology and Chemistry*. 2005;24(5):1165-1171.
52. Ankley G, Cook P, Carlson A, et al. Bioaccumulation of pcbs from sediments by oligochaetes and fishes - comparison of laboratory and field studies. *Can J Fish Aquat Sci*. 1992;49(10):2080-2085.
53. Egeler P, Meller M, Roembke J, Spoerlein P, Streit B, Nagel R. Tubifex tubifex as a link in food chain transfer of hexachlorobenzene from contaminated sediment to fish. *Hydrobiologia*. 2001;463:171-184.
54. Gong P, Loh P, Barker ND, et al. Building quantitative prediction models for tissue residue of two explosives compounds in earthworms from microarray gene expression data. *Environ Sci Technol*. 2012;46(1):19-26.
55. Dodard SG, Sarrazin M, Hawari J, et al. Ecotoxicological assessment of a high energetic and insensitive munitions compound: 2,4-dinitroanisole (DNAN). *J Hazard Mater*. 2013;262(0):143-150.

Appendix H

SUPPLEMENTARY INFORMATION FOR: PREDICTING OLIGOCHAETE WORMS– SOIL BIOCONCENTRATION OF MUNITIONS COMPOUNDS FROM MOLECULAR STRUCTURE

CONTENTS:

Munitions Compounds (MCs) and Munitions–Like Compounds (MLCs)

Table H-1	Selected characteristics and physicochemical properties of the MCs and MLCs.
-----------	--

Oligochaete Worms bioconcentration factors (BCFs)

Table H-2	Oligochaete worms bioconcentration factors (BCFs) dataset.
Table H-3	Worm mass fraction of dry weight (f_{dwt}), fraction of lipid (f_{Lipid}), and fraction of protein ($f_{Protein}$) obtained from the literature.
Table H-4	Worm f_{Lipid} , $f_{Protein}$, f_{dwt} , and f_{Water} used for the calculation of oligochaete BCFs.
Table H-5	Quantum Chemically estimated Abraham Parameters (QCAP) and adjusted QCAP from Liang ³¹ used for the calculation of oligochaete BCFs.
Table H-6	Calculated oligochaete BCFs.
Table H-7	Statistics for the comparison of the lipid phase descriptors between the two K_{Lipid} pp–LFERs evaluated.

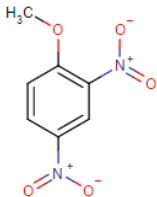
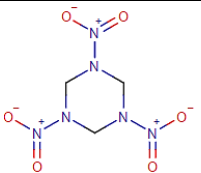
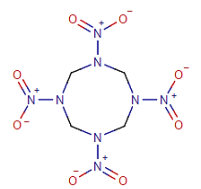

Estimation of Concentrations in Oligochaete Worms Observed in Independent Uptake Assays

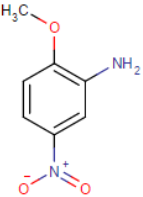
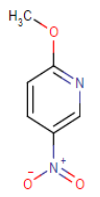
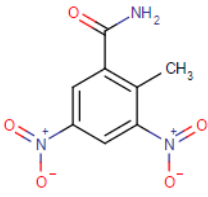
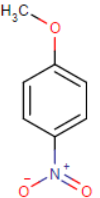
Table H-8	Data from independent uptake assays with oligochaetes exposed to MCs in soil.
Table H-9	Values for f_{Lipid} , $f_{Protein}$, f_{dwt} , and f_{Water} , QCAP, and adjusted QCAP ³¹ used for the prediction of the concentrations in oligochaetes.
Table H-10	Worked example for prediction of a MC concentration in an oligochaete.
Table H-11	Predicted values for soil organic carbon-water partition coefficient (K_{OC}), concentration in interstitial water, and concentration in oligochaetes using the K_{Lipid} pp–LFER from this work.

Table H-12 Predicted values for K_{OC} , concentration in interstitial water, and concentration in oligochaetes using the K_{Lipid} pp-LFER obtained by Kuo and Di Toro ^{30,33}.

Munitions Compounds (MCs) and Munitions-Like Compounds (MLCs)

Table H-1 Selected characteristics and physicochemical properties of the MCs and MLCs included in the oligochaete worms lipid-water pp-LFER and the model validation.

Class	Compound ^a	CAS #	Molecular Weight	Structure	Aqueous Solubility ^b mg L ⁻¹	log K _{ow} ^b
MCs: Nitroaromatics	2,4-DNAN	119-27-7	198.14		155	1.58 ^c
	RDX	121-82-4	222.12		60	0.87
MCs: Nitramines	HMX	2691-41-0	296.16		5	0.16
	NQ	556-88-7	104.07		4400	-0.89

MLCs	2-A-4-NAN	99-59-2	168.15		115	1.47
	2-M-5-NPYNE	5446-92-4	154.13		1406 ^d	1.55
	3,5-DN-o-TAME	148-01-6	225.16		1000	0.19 ^d
	4-NAN	100-17-4	153.14		590	2.03

^a 2,4-DNAN: 2,4-dinitroanisole; RDX: hexahydro-1,3,5-trinitro-1,3,5-triazine; HMX: octahydro-1,3,5,7-tetranitro-1,3,5,7-tetrazocine; NQ: nitroguanidine; 2-A-4-NAN: 2-amino-4-nitroanisole; 2-M-5-NPYNE: 2-methoxy-5-nitropyridine; 3,5-DN-o-TAME: 3,5-dinitro-o-toluidide; 4-NAN: 4-nitroanisole.

^b Experimental data from EPI Suite database ³⁵

^c Experimental value from Hawari et al. ⁴⁰

^d Estimate from EPI Suite ³⁵ in absence of an experimental value

Oligochaete Worms Bioconcentration Factors (BCFs)

Table H-2 Oligochaete worms bioconcentration factors (BCFs) dataset.

Compound ^a	CAS #	Chemical class ^b	log K _{ow} ^c	Exposure medium	Worm species ^f	Aquatic or terrestrial	Obs. log BCF ^h	Source
NQ	556-88-7	MC	-0.89	Soil	<i>E. andrei</i>	terra	-0.211	0
3,5-DN-o-TAME	148-01-6	MLC	0.19 ^d	Sand	<i>E. andrei</i>	terra	0.778	41
RDX	121-82-4	MC	0.87	Soil	<i>E. andrei</i>	terra	0.740	29
RDX	121-82-4	MC	0.87	Soil	<i>E. andrei</i>	terra	0.602	29
RDX	121-82-4	MC	0.87	Soil	<i>E. andrei</i>	terra	0.663	29
RDX	121-82-4	MC	0.87	Soil	<i>E. andrei</i>	terra	0.699	29
RDX	121-82-4	MC	0.87	Soil	<i>E. andrei</i>	terra	0.633	29
RDX	121-82-4	MC	0.87	Soil	<i>E. andrei</i>	terra	0.748	29
RDX	121-82-4	MC	0.87	Soil	<i>E. andrei</i>	terra	0.740	29
RDX	121-82-4	MC	0.87	Water	<i>E. andrei</i>	terra	1.114	29
RDX	121-82-4	MC	0.87	Water	<i>L. variegatus</i>	aqua	0.380	28
2-A-4-NAN	99-59-2	MLC	1.47	Soil	<i>E. andrei</i>	terra	-0.087	0
2-M-5-NPYNE	5446-92-4	MLC	1.55	Sand	<i>E. andrei</i>	terra	1.041	41
2,4-DNAN	119-27-7	MC	1.58 ^e	Soil	<i>E. andrei</i>	terra	1.185	0
4-NAN	100-17-4	MLC	2.03	Sand	<i>E. andrei</i>	terra	1.672	41
simazine	122-34-9	pesticide	2.18	Water	<i>L. terrestris</i>	terra	2.161	15
3-chlorophenol	108-43-0	cL-phenol	2.5	Water	<i>E. fetida</i>	terra	0.845	16

3-chlorophenol	108-43-0	cL-phenol	2.5	Water	<i>E. fetida</i>	terra	1.230	16
3-chlorophenol	108-43-0	cL-phenol	2.5	Water	<i>L. rubellus</i>	terra	2.009	16
3-chlorophenol	108-43-0	cL-phenol	2.5	Water	<i>L. rubellus</i>	terra	2.090	16
3,4-dichlorophenol	95-77-2	cL-phenol	3.33	Water	<i>E. fetida</i>	terra	1.431	16
3,4-dichlorophenol	95-77-2	cL-phenol	3.33	Water	<i>E. fetida</i>	terra	1.380	16
3,4-dichlorophenol	95-77-2	cL-phenol	3.33	Water	<i>L. rubellus</i>	terra	1.301	16
3,4-dichlorophenol	95-77-2	cL-phenol	3.33	Water	<i>L. rubellus</i>	terra	1.613	16
1,2,3-TCB	87-61-6	org-chlorine	4.05	Water	<i>E. andrei</i>	terra	3.103	18
γ-HCH	58-89-9	pesticide	4.14	Sediment	<i>T. tubifex</i>	aqua	3.279	27
γ-HCH	58-89-9	pesticide	4.14	Water	<i>L. terrestris</i>	terra	3.380	42
α-HCH	319-84-6	pesticide	4.14	Sediment	<i>T. tubifex</i>	aqua	2.674	27
fluorene	86-73-7	PAH	4.18	Water	<i>L. variegatus</i>	aqua	2.519	43
fluorene	86-73-7	PAH	4.18	Water	<i>L. variegatus</i>	aqua	2.580	43
fluorene	86-73-7	PAH	4.18	Water	<i>L. variegatus</i>	aqua	2.690	43
1,3,5-TCB	108-70-3	org-chlorine	4.19	Water	<i>E. andrei</i>	terra	2.824	18
anthracene	120-12-7	PAH	4.45	Water	<i>L. variegatus</i>	aqua	3.134	43
anthracene	120-12-7	PAH	4.45	Water	<i>L. variegatus</i>	aqua	3.107	43
anthracene	120-12-7	PAH	4.45	Water	<i>L. variegatus</i>	aqua	3.146	43
anthracene	120-12-7	PAH	4.45	Water	<i>L. variegatus</i>	aqua	3.143	43
anthracene	120-12-7	PAH	4.45	Water	<i>L. variegatus</i>	aqua	3.152	43
phenanthrene	85-01-8	PAH	4.46	Sediment	<i>T. tubifex</i> ^g	aqua	4.263	44,45
1,2,3,4-TCB	634-66-2	org-chlorine	4.6	Water	<i>E. andrei</i>	terra	3.748	18
1,2,3,4-TCB	634-66-2	org-chlorine	4.6	Sediment	<i>T. tubifex</i>	aqua	5.797	44,45
HCBT	87-68-3	vinyl halide	4.78	Sediment	<i>T. tubifex</i>	aqua	4.462	27

pyrene	129-00-0	PAH	4.88	Water	<i>L. variegatus</i>	aqua	3.299	43
pyrene	129-00-0	PAH	4.88	Water	<i>L. variegatus</i>	aqua	3.303	43
pyrene	129-00-0	PAH	4.88	Water	<i>L. variegatus</i>	aqua	3.279	43
pyrene	129-00-0	PAH	4.88	Water	<i>L. variegatus</i>	aqua	3.176	43
pyrene	129-00-0	PAH	4.88	Water	<i>L. variegatus</i>	aqua	3.079	43
fluoranthene	206-44-0	PAH	5.16	Water	<i>M. rubroniveus</i>	aqua	4.037	43
fluoranthene	206-44-0	PAH	5.16	Sediment	<i>T. tubifex</i>	aqua	4.953	44,45
PChB	608-93-5	org-chlorine	5.17	Sediment	<i>T. tubifex</i>	aqua	4.279	27
PChB	608-93-5	org-chlorine	5.17	Water	<i>E. andrei</i>	terra	4.096	18
PChB	608-93-5	org-chlorine	5.17	Sediment	<i>T. tubifex</i>	aqua	5.972	44,45
2,3,4,5,6-PCT	877-11-2	org-chlorine	5.62	Sediment	<i>T. tubifex</i>	aqua	4.447	27
HCB	118-74-1	org-chlorine	5.73	Sediment	<i>T. tubifex</i>	aqua	4.380	27
HCB	118-74-1	org-chlorine	5.73	Water	<i>E. andrei</i>	terra	4.506	18
HCB	118-74-1	org-chlorine	5.73	Water	<i>E. andrei</i>	terra	4.614	18
HCB	118-74-1	org-chlorine	5.73	Water	<i>L. terrestris</i>	terra	4.290	15
HCB	118-74-1	org-chlorine	5.73	Sediment	<i>T. tubifex</i>	aqua	6.408	44,45
1,2,3,4-TCN	20020-02-4	cL-PAH	5.75	Sediment	<i>T. tubifex</i>	aqua	4.322	27
B[a]A	56-55-3	PAH	5.76	Sediment	<i>T. tubifex</i>	aqua	5.828	44,45
chrysene	218-01-9	PAH	5.81	Sediment	<i>T. tubifex</i>	aqua	5.658	44,45

^a 1,2,3-TCB: 1,2,3-trichlorobenzene; γ -HCH: γ -hexachlorocyclohexane; α -HCH: α -hexachlorocyclohexane; 1,3,5-TCB: 1,3,5-trichlorobenzene; 1,2,3,4-TCB: 1,2,3,4-tetrachlorobenzene; HCBT: hexachlorobutadiene; PChB: pentachlorobenzene; 2,3,4,5,6-PCT: 2,3,4,5,6-pentachlorotoluene; HCB: hexachlorobenzene; 1,2,3,4-TCN: 1,2,3,4-tetrachloronaphthalene; B[a]A: benzo[a]anthracene. For all other abbreviations see Table H-1 in Appendix H

^b cL-phenol: chlorinated phenol; org-chlorine: organochlorine; PAH: polycyclic aromatic hydrocarbon; cL-PAH: chlorinated PAH

^c Experimental data from EPI Suite database ³⁵

^d Estimate from EPI Suite ³⁵ in absence of an experimental value

^e Experimental value from Hawari et al. ⁴⁰

^f *E. andrei*: *Eisenia andrei*; *L. variegatus*: *Lumbriculus variegatus*; *L. terrestris*: *Lumbricus terrestris*; *E. fetida*: *Eisenia fetida*; *L. rubellus*: *Lumbricus rubellus*; *T. tubifex*: *Tubifex tubifex*; *M. rubroniveus*: *Monopylephorus rubroniveus*

^g More than 90% of the culture used in the studies reported in Kraaij et al. ⁴⁴ and Kraaij et al. ⁴⁵ consisted of the species *Limnodrilus hoffmeisteri* and *Tubifex tubifex* (both family Tubificidae)

^h Observed log BCF ($L\ kg_{dwt}^{-1}$). Values from Lord et al. ¹⁵ are K_{Lipid} , and were transformed using the corresponding mass fraction of lipid from Table H-4 in Appendix H. Values from Kraaij et al. ⁴⁴ and Kraaij et al. ⁴⁵ were calculated using the concentration in the worm lipid in Kraaij et al. ⁴⁴ and the concentration in the pore water (untreated sediment) reported in Kraaij et al. ⁴⁵; biota-to-sediment accumulation factor (BSAF) and the concentration in the sediment for the 2 days aging time (“contact time” in source) treatment reported in Kraaij et al. ⁴⁴ were used to obtain the concentration in the worm lipid

Table H-3 Worm mass fraction of dry weight (f_{dwt}), fraction of lipid (f_{Lipid}), and fraction of protein ($f_{Protein}$) obtained from the literature.

Species ^a	Aquatic or terrestrial	f_{dwt} ^b kg kg _{wwt} ⁻¹	Qty. ^d	f_{Lipid} kg kg _{wwt} ⁻¹	Qty.	f_{Lipid} kg kg _{dwt} ⁻¹	Qty.	$f_{Protein}$ kg kg _{wwt} ⁻¹	Qty.	$f_{Protein}$ kg kg _{dwt} ⁻¹	Qty.	Source
<i>E. andrei</i>	terra	NA ^c	NA	0.010	Msrd.	0.067	Calc.					18
<i>E. andrei</i>	terra	0.15	Calc.	NA	NA	NA	NA					29
<i>E. andrei</i>	terra	NA	NA	0.023	Msrd.	0.153	Calc.					46
<i>E. andrei</i>	terra	NA	NA	NA	NA	0.142	Msrd.					41
<i>E. andrei</i>	terra	NA	NA	NA	NA	0.105	Msrd.					41
<i>E. andrei</i>	terra	NA	NA	NA	NA	0.121	Msrd.					41
<i>E. fetida</i>	terra	0.157	Msrd.	0.019	Msrd.	0.120	Msrd.	0.110	Msrd.	0.702	Msrd.	47
<i>L. terrestris</i>	terra	NA	NA	0.012	Msrd.	0.075	Calc.					48
<i>L. terrestris</i>	terra	0.164	Msrd.	0.016	Msrd.	0.098	Msrd.	0.105	Msrd.	0.640	Msrd.	49
<i>L. variegatus</i>	aqua	0.19	Msrd.	0.015	Calc.	0.080	Msrd.					50
<i>L. variegatus</i>	aqua	NA	NA	0.010	Msrd.	0.053	Calc.					51
<i>L. variegatus</i>	aqua	NA	NA	0.011	Msrd.	0.055	Calc.					52
<i>T. tubifex</i>	aqua	0.14	Msrd.	0.027	Msrd.	0.197	Msrd.					53
<i>T. tubifex</i>	aqua	0.13	Msrd.	0.010	Msrd.	0.080	Msrd.					27
<i>T. tubifex</i>	aqua	NA	NA	0.030	Msrd.	0.219	Calc.					44

^a Abbreviations defined in Table H-1 in Appendix H

^b dwt: dry weight; wwt: wet or fresh weight

^c Not available

^d Quality of the values in the column immediately to the left. Calc.: values calculated with information either provided in the source (e.g., ratio of BCF to BCF_{Lipid} for f_{Lipid}) or listed in this table. When f_{dwt} was unavailable from the source, calc. f_{Lipid} dwt values were obtained with the average f_{dwt} values listed in this table for the corresponding species. Msrd.: values measured and reported explicitly in the source or elsewhere referred to by the source

Table H-4 Worm mass fractions of lipid (f_{Lipid}), protein ($f_{Protein}$), dry weight (f_{dwt}), and water (f_{Water}) used for the estimation of oligochaete BCFs^a.

Compound ^b	Obs. log BCF ^b	Worm species ^b	f_{Lipid} (kg kg _{wwt} ⁻¹)	$f_{Protein}$ (kg kg _{wwt} ⁻¹)	f_{dwt} (kg kg _{wwt} ⁻¹)	f_{Water} (kg kg _{wwt} ⁻¹) ^c
NQ	-0.211	<i>E. andrei</i>	0.017	0.108	0.150	0.850
3,5-DN-o-TAME	0.778	<i>E. andrei</i>	0.016	0.108	0.150	0.850
RDX	0.740	<i>E. andrei</i>	0.017	0.108	0.150	0.850
RDX	0.602	<i>E. andrei</i>	0.017	0.108	0.150	0.850
RDX	0.663	<i>E. andrei</i>	0.017	0.108	0.150	0.850
RDX	0.699	<i>E. andrei</i>	0.017	0.108	0.150	0.850
RDX	0.633	<i>E. andrei</i>	0.017	0.108	0.150	0.850
RDX	0.748	<i>E. andrei</i>	0.017	0.108	0.150	0.850
RDX	0.740	<i>E. andrei</i>	0.017	0.108	0.150	0.850
RDX	1.114	<i>E. andrei</i>	0.017	0.108	0.150	0.850
RDX	0.380	<i>L. variegatus</i>	0.012	0.108	0.190	0.810
2-A-4-NAN	-0.087	<i>E. andrei</i>	0.017	0.108	0.150	0.850
2-M-5-NPYNE	1.041	<i>E. andrei</i>	0.018	0.108	0.150	0.850
2,4-DNAN	1.185	<i>E. andrei</i>	0.017	0.108	0.150	0.850
4-NAN	1.672	<i>E. andrei</i>	0.021	0.108	0.150	0.850
simazine	2.161	<i>L. terrestris</i>	0.014	0.105	0.164	0.836
3-chlorophenol	0.845	<i>E. fetida</i>	0.019	0.110	0.157	0.843
3-chlorophenol	1.230	<i>E. fetida</i>	0.019	0.110	0.157	0.843
3-chlorophenol	2.009	<i>L. rubellus</i>	0.018	0.108	0.157	0.843

3-chlorophenol	2.090	<i>L. rubellus</i>	0.018	0.108	0.157	0.843
3,4-dichlorophenol	1.431	<i>E. fetida</i>	0.019	0.110	0.157	0.843
3,4-dichlorophenol	1.380	<i>E. fetida</i>	0.019	0.110	0.157	0.843
3,4-dichlorophenol	1.301	<i>L. rubellus</i>	0.018	0.108	0.157	0.843
3,4-dichlorophenol	1.613	<i>L. rubellus</i>	0.018	0.108	0.157	0.843
1,2,3-TCB	3.103	<i>E. andrei</i>	0.010	0.108	0.150	0.850
γ -HCH	3.279	<i>T. tubifex</i>	0.010	0.108	0.130	0.870
γ -HCH	3.380	<i>L. terrestris</i>	0.010	0.108	0.130	0.870
α -HCH	2.674	<i>T. tubifex</i>	0.014	0.105	0.164	0.836
fluorene	2.519	<i>L. variegatus</i>	0.011	0.108	0.190	0.810
fluorene	2.580	<i>L. variegatus</i>	0.011	0.108	0.190	0.810
fluorene	2.690	<i>L. variegatus</i>	0.011	0.108	0.190	0.810
1,3,5-TCB	2.824	<i>E. andrei</i>	0.010	0.108	0.150	0.850
anthracene	3.134	<i>L. variegatus</i>	0.011	0.108	0.190	0.810
anthracene	3.107	<i>L. variegatus</i>	0.011	0.108	0.190	0.810
anthracene	3.146	<i>L. variegatus</i>	0.011	0.108	0.190	0.810
anthracene	3.143	<i>L. variegatus</i>	0.011	0.108	0.190	0.810
anthracene	3.152	<i>L. variegatus</i>	0.011	0.108	0.190	0.810
phenanthrene	4.263	<i>T. tubifex</i> ^g	0.030	0.108	0.135	0.865
1,2,3,4-TCB	3.748	<i>E. andrei</i>	0.010	0.108	0.150	0.850
1,2,3,4-TCB	5.797	<i>T. tubifex</i>	0.030	0.108	0.135	0.865
HCBT	4.462	<i>T. tubifex</i>	0.010	0.108	0.130	0.870
pyrene	3.299	<i>L. variegatus</i>	0.011	0.108	0.190	0.810
pyrene	3.303	<i>L. variegatus</i>	0.011	0.108	0.190	0.810

pyrene	3.279	<i>L. variegatus</i>	0.011	0.108	0.190	0.810
pyrene	3.176	<i>L. variegatus</i>	0.011	0.108	0.190	0.810
pyrene	3.079	<i>L. variegatus</i>	0.011	0.108	0.190	0.810
fluoranthene	4.037	<i>M. rubroniveus</i>	0.017	0.108	0.153	0.847
fluoranthene	4.953	<i>T. tubifex</i>	0.030	0.108	0.135	0.865
PChB	4.279	<i>T. tubifex</i>	0.010	0.108	0.130	0.870
PChB	4.096	<i>E. andrei</i>	0.010	0.108	0.150	0.850
PChB	5.972	<i>T. tubifex</i>	0.030	0.108	0.135	0.865
2,3,4,5,6-PCT	4.447	<i>T. tubifex</i>	0.010	0.108	0.130	0.870
HCB	4.380	<i>T. tubifex</i>	0.010	0.108	0.130	0.870
HCB	4.506	<i>E. andrei</i>	0.010	0.108	0.150	0.850
HCB	4.614	<i>E. andrei</i>	0.010	0.108	0.150	0.850
HCB	4.290	<i>L. terrestris</i>	0.014	0.105	0.164	0.836
HCB	6.408	<i>T. tubifex</i>	0.030	0.108	0.135	0.865
1,2,3,4-TCN	4.322	<i>T. tubifex</i>	0.010	0.108	0.130	0.870
B[a]A	5.828	<i>T. tubifex</i>	0.030	0.108	0.135	0.865
chrysene	5.658	<i>T. tubifex</i>	0.030	0.108	0.135	0.865

^a Values obtained from the literature, sources in Table H-2 in Appendix H. Average of values for the corresponding species were taken when not available in or elsewhere referred to by the source of the oligochaete BCF (Table H-3). If the species was not listed in Table H-3, the average among the values for the corresponding oligochaete type (i.e., terrestrial or aquatic) was taken

^b Values and abbreviations described in Table H-1

^c Calculated as: $1-f_{dwt}$

Table H-5 Quantum Chemically estimated Abraham Parameters (QCAP) and Adjusted QCAP^a from Liang³¹ used for the prediction of the oligochaete BCFs dataset^b.

Compound ^c	Chemical class ^c	QCAP					Adjusted QCAP				
		<i>E</i>	<i>S</i>	<i>A</i>	<i>B</i>	<i>V</i>	<i>E</i>	<i>S</i>	<i>A</i>	<i>B</i>	<i>V</i>
NQ	MC	0.840	1.025	1.310	0.558	0.652	0.679	1.001	0.851	0.777	0.683
3,5-DN-o-TAME	MLC	1.560	2.629	0.487	0.855	1.462	1.314	2.590	0.227	0.704	1.448
RDX	MC	1.020	1.859	0.528	0.667	1.241	0.668	1.746	0.285	0.638	1.236
RDX	MC	1.020	1.859	0.528	0.667	1.241	0.668	1.746	0.285	0.638	1.236
RDX	MC	1.020	1.859	0.528	0.667	1.241	0.668	1.746	0.285	0.638	1.236
RDX	MC	1.020	1.859	0.528	0.667	1.241	0.668	1.746	0.285	0.638	1.236
RDX	MC	1.020	1.859	0.528	0.667	1.241	0.668	1.746	0.285	0.638	1.236
RDX	MC	1.020	1.859	0.528	0.667	1.241	0.668	1.746	0.285	0.638	1.236
RDX	MC	1.020	1.859	0.528	0.667	1.241	0.668	1.746	0.285	0.638	1.236
RDX	MC	1.020	1.859	0.528	0.667	1.241	0.668	1.746	0.285	0.638	1.236
2-A-4-NAN	MLC	1.730	1.430	0.548	0.666	1.133	1.223	1.514	0.306	0.694	1.187
2-M-5-NPYNE	MLC	1.430	1.258	0.105	0.591	1.019	0.870	1.278	0.018	0.579	1.065
2,4-DNAN	MC	1.660	1.704	0.187	0.785	1.231	1.144	1.757	0.056	0.745	1.276
4-NAN	MLC	1.430	1.188	0.101	0.552	1.059	0.819	1.200	0.016	0.543	1.105
simazine	pesticide	1.990	1.199	0.541	0.635	1.402	1.213	1.313	0.297	0.689	1.481
3-chlorophenol	cL-phenol	1.370	0.972	0.937	0.139	0.866	0.923	0.945	0.581	0.177	0.885
3-chlorophenol	cL-phenol	1.370	0.972	0.937	0.139	0.866	0.923	0.945	0.581	0.177	0.885
3-chlorophenol	cL-phenol	1.370	0.972	0.937	0.139	0.866	0.923	0.945	0.581	0.177	0.885

3-chlorophenol	cL-phenol	1.370	0.972	0.937	0.139	0.866	0.923	0.945	0.581	0.177	0.885
3,4-dichlorophenol	cL-phenol	1.530	0.945	1.041	0.138	0.992	1.003	0.941	0.647	0.190	1.020
3,4-dichlorophenol	cL-phenol	1.530	0.945	1.041	0.138	0.992	1.003	0.941	0.647	0.190	1.020
3,4-dichlorophenol	cL-phenol	1.530	0.945	1.041	0.138	0.992	1.003	0.941	0.647	0.190	1.020
3,4-dichlorophenol	cL-phenol	1.530	0.945	1.041	0.138	0.992	1.003	0.941	0.647	0.190	1.020
1,2,3-TCB	org-chlorine	1.690	0.718	0.101	0.108	1.051	0.861	0.729	0.017	0.055	1.098
γ-HCH	pesticide	1.700	1.347	0.341	0.438	1.545	0.873	1.325	0.153	0.392	1.583
γ-HCH	pesticide	1.700	1.370	0.361	0.434	1.543	0.886	1.347	0.166	0.385	1.579
α-HCH	pesticide	1.700	1.347	0.341	0.438	1.545	0.873	1.325	0.153	0.392	1.583
fluorene	PAH	2.590	1.164	0.082	0.311	1.279	1.715	1.350	-0.020	0.191	1.357
fluorene	PAH	2.590	1.164	0.082	0.311	1.279	1.715	1.350	-0.020	0.191	1.357
fluorene	PAH	2.590	1.164	0.082	0.311	1.279	1.715	1.350	-0.020	0.191	1.357
1,3,5-TCB	org-chlorine	1.750	0.731	0.133	0.075	1.063	0.916	0.746	0.036	0.012	1.110
anthracene	PAH	1.993	1.340	0.000	0.232	1.454	1.116	1.345	-0.081	0.068	1.487
anthracene	PAH	1.993	1.340	0.000	0.232	1.454	1.116	1.345	-0.081	0.068	1.487
anthracene	PAH	1.993	1.340	0.000	0.232	1.454	1.116	1.345	-0.081	0.068	1.487
anthracene	PAH	1.993	1.340	0.000	0.232	1.454	1.116	1.345	-0.081	0.068	1.487
anthracene	PAH	1.993	1.340	0.000	0.232	1.454	1.116	1.345	-0.081	0.068	1.487
phenanthrene	PAH	3.020	1.258	0.111	0.321	1.357	2.100	1.524	-0.009	0.174	1.449
1,2,3,4-TCB	org-chlorine	1.900	0.689	0.110	0.133	1.173	0.973	0.737	0.019	0.086	1.234
1,2,3,4-TCB	org-chlorine	1.90	0.69	0.11	0.13	1.17	0.973	0.737	0.019	0.086	1.234
HCBT	vinyl halide	1.770	0.517	0.072	0.087	1.320	0.696	0.519	-0.005	0.061	1.383
pyrene	PAH	2.600	1.517	0.000	0.251	1.585	1.656	1.628	-0.095	0.036	1.635
pyrene	PAH	2.600	1.517	0.000	0.251	1.585	1.656	1.628	-0.095	0.036	1.635

pyrene	PAH	2.600	1.517	0.000	0.251	1.585	1.656	1.628	-0.095	0.036	1.635
pyrene	PAH	2.600	1.517	0.000	0.251	1.585	1.656	1.628	-0.095	0.036	1.635
pyrene	PAH	2.600	1.517	0.000	0.251	1.585	1.656	1.628	-0.095	0.036	1.635
fluoranthene	PAH	3.530	1.390	0.112	0.370	1.495	2.532	1.748	-0.020	0.191	1.607
fluoranthene	PAH	3.530	1.390	0.112	0.370	1.495	2.532	1.748	-0.020	0.191	1.607
PChB	org-chlorine	2.130	0.725	0.088	0.136	1.294	1.120	0.805	-0.003	0.071	1.364
PChB	org-chlorine	2.130	0.725	0.088	0.136	1.294	1.120	0.805	-0.003	0.071	1.364
PChB	org-chlorine	2.130	0.725	0.088	0.136	1.294	1.120	0.805	-0.003	0.071	1.364
2,3,4,5,6-PCT	org-chlorine	1.223	1.069	0.000	0.000	1.469	0.296	0.877	-0.071	-0.146	1.463
HCB	org-chlorine	2.340	0.715	0.053	0.171	1.409	1.235	0.832	-0.030	0.106	1.492
HCB	org-chlorine	2.340	0.715	0.053	0.171	1.409	1.235	0.832	-0.030	0.106	1.492
HCB	org-chlorine	2.340	0.715	0.053	0.171	1.409	1.235	0.832	-0.030	0.106	1.492
HCB	org-chlorine	2.340	0.715	0.053	0.171	1.409	1.235	0.832	-0.030	0.106	1.492
HCB	org-chlorine	2.340	0.715	0.053	0.171	1.409	1.235	0.832	-0.030	0.106	1.492
1,2,3,4-TCN	cL-PAH	2.920	0.915	0.092	0.240	1.501	1.791	1.146	-0.017	0.138	1.604
B[a]A	PAH	2.712	1.664	0.000	0.290	1.823	1.673	1.766	-0.107	0.053	1.873
chrysene	PAH	2.712	1.664	0.000	0.290	1.823	1.673	1.766	-0.107	0.053	1.873

^a The solute descriptors used to apply the K_{Lipid} and K_{Protein} pp-LFERs by Kuo and Di Toro ^{30,33} were obtained with the regression equations for the adjusted QCAP provided in Liang ³¹. Adjusted QCAP are recommended over QCAP to apply existing pp-LFERs that were built using solute descriptors either derived from calibration to experimental measurements or estimated with functional group fragments contributions ³¹

^b Dataset described in Table H-2 in Appendix H

^c Values and abbreviations described in Table H-1

Table H-6 Estimated oligochaete BCFs using the partition-based model (Eq. (7-3)) with K_{Lipid} pp-LFER either from Kuo and Di Toro ^{30,33} (Eq. (7-5)) or from this work (Eq. (7-11)), and K_{Protein} pp-LFER from Kuo and Di Toro ^{30,33} (Eq. (7-6))^a.

Compound ^b	Obs. log BCF ^b	K_{Lipid} pp-LFER from Kuo and Di Toro ^{30,33}			K_{Lipid} pp-LFER from this work		
		Predicted log BCF ^c	Square error ^d	Residuals ^e	Fitted log BCF ^c	Square error ^d	Residuals ^e
NQ	-0.211	0.759	9.41E-01	0.970	0.759	9.41E-01	0.970
3,5-DN-o-TAME	0.778	0.909	1.70E-02	0.130	0.781	1.06E-05	0.003
RDX	0.740	0.884	2.05E-02	0.143	0.794	2.84E-03	0.053
RDX	0.602	0.884	7.92E-02	0.281	0.794	3.67E-02	0.192
RDX	0.663	0.884	4.87E-02	0.221	0.794	1.71E-02	0.131
RDX	0.699	0.884	3.41E-02	0.185	0.794	8.97E-03	0.095
RDX	0.633	0.884	6.25E-02	0.250	0.794	2.57E-02	0.160
RDX	0.748	0.884	1.83E-02	0.135	0.794	2.07E-03	0.045
RDX	0.740	0.884	2.05E-02	0.143	0.794	2.84E-03	0.053
RDX	1.114	0.884	5.31E-02	-0.230	0.794	1.03E-01	-0.320
RDX	0.380	0.735	1.26E-01	0.354	0.664	8.06E-02	0.284
2-A-4-NAN	-0.087	0.991	1.16E+00	1.078	0.938	1.05E+00	1.025
2-M-5-NPYNE	1.041	1.054	1.58E-04	0.013	1.057	2.33E-04	0.015
2,4-DNAN	1.185	0.954	5.30E-02	-0.230	0.881	9.23E-02	-0.304
4-NAN	1.672	1.277	1.56E-01	-0.395	1.366	9.35E-02	-0.306
simazine	2.161	1.741	1.76E-01	-0.420	2.293	1.74E-02	0.132
3-chlorophenol	0.845	1.731	7.84E-01	0.886	1.206	1.30E-01	0.361
3-chlorophenol	1.230	1.731	2.50E-01	0.500	1.206	5.83E-04	-0.024

3-chlorophenol	2.009	1.703	9.32E-02	-0.305	1.187	6.75E-01	-0.822
3-chlorophenol	2.090	1.703	1.49E-01	-0.387	1.187	8.15E-01	-0.903
3,4-dichlorophenol	1.431	2.141	5.04E-01	0.710	1.683	6.34E-02	0.252
3,4-dichlorophenol	1.380	2.141	5.79E-01	0.761	1.683	9.18E-02	0.303
3,4-dichlorophenol	1.301	2.112	6.58E-01	0.811	1.656	1.26E-01	0.355
3,4-dichlorophenol	1.613	2.112	2.49E-01	0.499	1.656	1.90E-03	0.044
1,2,3-TCB	3.103	3.030	5.34E-03	-0.073	3.055	2.32E-03	-0.048
γ -HCH	3.279	2.829	2.02E-01	-0.449	2.975	9.20E-02	-0.303
γ -HCH	3.380	2.820	3.14E-01	-0.561	2.903	2.28E-01	-0.478
α -HCH	2.674	2.877	4.14E-02	0.204	3.024	1.23E-01	0.350
fluorene	2.519	3.332	6.61E-01	0.813	2.916	1.58E-01	0.398
fluorene	2.580	3.332	5.65E-01	0.752	2.916	1.13E-01	0.336
fluorene	2.690	3.332	4.12E-01	0.642	2.916	5.10E-02	0.226
1,3,5-TCB	2.824	3.233	1.68E-01	0.410	3.152	1.08E-01	0.328
anthracene	3.134	3.772	4.08E-01	0.639	3.262	1.65E-02	0.128
anthracene	3.107	3.772	4.43E-01	0.665	3.262	2.39E-02	0.155
anthracene	3.146	3.772	3.92E-01	0.626	3.262	1.34E-02	0.116
anthracene	3.143	3.772	3.96E-01	0.629	3.262	1.41E-02	0.119
anthracene	3.152	3.772	3.85E-01	0.620	3.262	1.20E-02	0.110
phenanthrene	4.263	4.398	1.83E-02	0.135	3.776	2.37E-01	-0.487
1,2,3,4-TCB	3.748	3.453	8.69E-02	-0.295	3.709	1.57E-03	-0.040
1,2,3,4-TCB	5.797	3.968	3.35E+00	-1.829	4.224	2.48E+00	-1.574
HCBT	4.462	4.139	1.05E-01	-0.324	4.925	2.14E-01	0.462
pyrene	3.299	4.495	1.43E+00	1.197	3.647	1.21E-01	0.349

pyrene	3.303	4.495	1.42E+00	1.192	3.647	1.18E-01	0.344
pyrene	3.279	4.495	1.48E+00	1.217	3.647	1.36E-01	0.369
pyrene	3.176	4.495	1.74E+00	1.319	3.647	2.22E-01	0.471
pyrene	3.079	4.495	2.01E+00	1.416	3.647	3.23E-01	0.568
fluoranthene	4.037	4.664	3.93E-01	0.627	3.914	1.52E-02	-0.123
fluoranthene	4.953	4.958	2.73E-05	0.005	4.207	5.56E-01	-0.746
PChB	4.279	4.049	5.30E-02	-0.230	4.342	4.05E-03	0.064
PChB	4.096	3.986	1.19E-02	-0.109	4.280	3.41E-02	0.185
PChB	5.972	4.502	2.16E+00	-1.470	4.796	1.38E+00	-1.176
2,3,4,5,6-PCT	4.447	4.466	3.40E-04	0.018	4.280	2.80E-02	-0.167
HCB	4.380	4.434	2.87E-03	0.054	4.936	3.09E-01	0.556
HCB	4.506	4.372	1.81E-02	-0.134	4.874	1.35E-01	0.368
HCB	4.614	4.372	5.88E-02	-0.243	4.874	6.73E-02	0.259
HCB	4.290	4.484	3.74E-02	0.193	4.986	4.84E-01	0.696
HCB	6.408	4.887	2.31E+00	-1.521	5.389	1.04E+00	-1.019
1,2,3,4-TCN	4.322	4.771	2.02E-01	0.449	4.949	3.93E-01	0.627
B[a]A	5.828	5.699	1.66E-02	-0.129	4.944	7.81E-01	-0.884
chrysene	5.658	5.699	1.71E-03	0.041	4.944	5.09E-01	-0.714

^a Solute descriptors used for the K_{Lipid} pp-LFER obtained in this work (Eq. (7-11)) were QCAP, while those used for the K_{Lipid} and K_{Protein} pp-LFERs by Kuo and Di Toro^{30,33}, (Eq. (7-5)) and (Eq. (7-6)), respectively, were adjusted QCAP. Both QCAP and adjusted QCAP were obtained from Liang³¹ and are listed in Table H-5 in Appendix H. Mass fractions used for each worm component are listed in Table H-4

^b Values and abbreviations described in Table H-2

^c Estimated log BCF ($\text{L kg}_{\text{dwt}}^{-1}$)

^d Calculated as: $[(\text{Estimated log BCF}) - (\text{Observed log BCF})]^2$

^e Calculated as: $(\text{Estimated log BCF}) - (\text{Observed log BCF})$

Table H-7 Statistics for the comparison of the lipid phase descriptors between the K_{Lipid} pp-LFERs from Kuo and Di Toro ^{30,33} (Eq. (7-5)) and the K_{Lipid} pp-LFERs from this work (Eq. (7-11))^a.

Lipid phase descriptor	This work	Standard error ^b	Kuo and Di Toro ^{30,33}	Standard error ^b	z-score	p-value ^c
<i>c</i>	0.751	0.780	0.84	0.14	-0.113	0.912
<i>e</i>	0.431	0.189	0.77	0.10	-1.581	0.114
<i>s</i>	-2.409	0.387	-1.1	0.19	-3.038	0.003
<i>a</i>	-0.787	0.393	-0.47	0.22	-0.703	0.484
<i>b</i>	-2.106	0.793	-3.52	0.20	1.730	0.084
<i>v</i>	4.553	0.673	3.37	0.13	1.726	0.084

^a Results from a z-test with inhomogeneity of the error variances between the groups

^b For the column to the left

^c A p-value ≤ 0.05 was accepted as significant

Prediction of Concentrations in Oligochaete Worms Observed in Independent Uptake Assays

Table H-8 Data from independent uptake assays with oligochaetes exposed to MCs in soil.

Compound ^a	Worm species ^a	Soil	Exposure time	Concentration in worm ^d	Concentration in soil	f_{oc}^e	Source
			days	mg kg _{dwt} ⁻¹	mg kg _{dwt} ⁻¹	kg OC kg _{dwt soil} ⁻¹	
RDX	<i>E. andrei</i>	soil SSL ^c	7	17.341	0.660	0.012	38
RDX	<i>E. andrei</i>	soil SSL	7	63.584	10.600	0.012	38
RDX	<i>E. andrei</i>	soil SSL	7	287.090	102.000	0.012	38
RDX	<i>E. andrei</i>	soil SSL	7	426.590	967.000	0.012	38
RDX	<i>E. andrei</i>	soil SSL	7	579.961	2850.000	0.012	38
RDX	<i>E. andrei</i>	soil SSL	7	920.520	9427.000	0.012	38
RDX	<i>E. fetida</i>	aged soil	28	41.000	645.000	0.063	37
RDX	<i>E. fetida</i>	aged soil	28	1698.000	855.500	0.086	37
RDX	<i>E. fetida</i>	sandy loam	14	61.173	8.000	0.012	54
RDX	<i>E. fetida</i>	sandy loam	14	102.213	16.000	0.012	54
RDX	<i>E. fetida</i>	sandy loam	14	186.615	32.000	0.012	54
RDX	<i>E. fetida</i>	sandy loam	14	284.956	64.000	0.012	54
RDX	<i>E. fetida</i>	sandy loam	14	306.637	128.000	0.012	54
2,4-DNAN	<i>E. andrei</i>	spiked soil	14	57.143	8.909	0.010	55
2,4-DNAN	<i>E. andrei</i>	spiked soil	14	100.840	19.822	0.010	55
2,4-DNAN	<i>E. andrei</i>	spiked soil	14	152.941	27.840	0.010	55

HMX	<i>E. andrei</i>	ammended soil	28	11.046	100.000	0.012	39
HMX	<i>E. andrei</i>	ammended soil	28	48.818	1000.000	0.012	39
HMX	<i>E. andrei</i>	ammended soil	28	501.106	10000.000	0.012	39
TNT ^b	<i>E. fetida</i>	sandy loam	14	5.190	6.000	0.012	54
TNT	<i>E. fetida</i>	sandy loam	14	12.111	12.000	0.012	54
TNT	<i>E. fetida</i>	sandy loam	14	31.575	24.000	0.012	54
TNT	<i>E. fetida</i>	sandy loam	14	98.616	48.000	0.012	54

^a Abbreviations in Tables H-1 and H-3 in Appendix H.

^b [U-¹⁴C]-TNT

^c Sassafras sandy loam

^d Values from Sarrazin et al. ³⁸ taken as the average value per treatment. Values from Gong et al. ⁵⁴ taken as the average of day 4 (“repeat”) and day 14. Values from Sunahara ³⁹ taken as the average of concentrations measured after day 5

^e Mass fraction of organic carbon in the soil. If only mass fraction of organic matter (f_{OM}) in the soil was reported, a factor of 0.50 was used to convert f_{OM} to f_{OC} ³⁶

Table H-9 Values for f_{Lipid} , $f_{Protein}$, f_{dwt} , and f_{Water} , QCAP, and adjusted QCAP³¹ used for the prediction of the concentrations in oligochaetes from the independent uptake assays dataset^a.

Compound	Species	f_{Lipid}	$f_{Protein}$	f_{dwt}	f_{Water}	QCAP					Adjusted QCAP				
						E	S	A	B	V	E	S	A	B	V
RDX	<i>E. andrei</i>	0.017	0.108	0.150	0.850	1.020	1.859	0.528	0.668	1.241	0.668	1.747	0.285	0.639	1.236
RDX	<i>E. andrei</i>	0.017	0.108	0.150	0.850	1.020	1.859	0.528	0.668	1.241	0.668	1.747	0.285	0.639	1.236
RDX	<i>E. andrei</i>	0.017	0.108	0.150	0.850	1.020	1.859	0.528	0.668	1.241	0.668	1.747	0.285	0.639	1.236
RDX	<i>E. andrei</i>	0.017	0.108	0.150	0.850	1.020	1.859	0.528	0.668	1.241	0.668	1.747	0.285	0.639	1.236
RDX	<i>E. andrei</i>	0.017	0.108	0.150	0.850	1.020	1.859	0.528	0.668	1.241	0.668	1.747	0.285	0.639	1.236
RDX	<i>E. andrei</i>	0.017	0.108	0.150	0.850	1.020	1.859	0.528	0.668	1.241	0.668	1.747	0.285	0.639	1.236
RDX	<i>E. fetida</i>	0.019	0.110	0.157	0.843	1.020	1.859	0.528	0.668	1.241	0.668	1.747	0.285	0.639	1.236
RDX	<i>E. fetida</i>	0.019	0.110	0.157	0.843	1.020	1.859	0.528	0.668	1.241	0.668	1.747	0.285	0.639	1.236
RDX	<i>E. fetida</i>	0.019	0.110	0.157	0.843	1.020	1.859	0.528	0.668	1.241	0.668	1.747	0.285	0.639	1.236
RDX	<i>E. fetida</i>	0.019	0.110	0.157	0.843	1.020	1.859	0.528	0.668	1.241	0.668	1.747	0.285	0.639	1.236
RDX	<i>E. fetida</i>	0.019	0.110	0.157	0.843	1.020	1.859	0.528	0.668	1.241	0.668	1.747	0.285	0.639	1.236
RDX	<i>E. fetida</i>	0.019	0.110	0.157	0.843	1.020	1.859	0.528	0.668	1.241	0.668	1.747	0.285	0.639	1.236
RDX	<i>E. fetida</i>	0.019	0.110	0.157	0.843	1.020	1.859	0.528	0.668	1.241	0.668	1.747	0.285	0.639	1.236
2,4-DNAN	<i>E. andrei</i>	0.017	0.108	0.150	0.850	1.660	1.704	0.187	0.785	1.231	1.144	1.757	0.056	0.745	1.276
2,4-DNAN	<i>E. andrei</i>	0.017	0.108	0.150	0.850	1.660	1.704	0.187	0.785	1.231	1.144	1.757	0.056	0.745	1.276
2,4-DNAN	<i>E. andrei</i>	0.017	0.108	0.150	0.850	1.660	1.704	0.187	0.785	1.231	1.144	1.757	0.056	0.745	1.276
HMX	<i>E. andrei</i>	0.017	0.108	0.150	0.850	1.160	2.450	0.635	1.050	1.631	0.825	2.357	0.335	1.026	1.629
HMX	<i>E. andrei</i>	0.017	0.108	0.150	0.850	1.160	2.450	0.635	1.050	1.631	0.825	2.357	0.335	1.026	1.629
HMX	<i>E. andrei</i>	0.017	0.108	0.150	0.850	1.160	2.450	0.635	1.050	1.631	0.825	2.357	0.335	1.026	1.629

TNT	<i>E. fetida</i>	0.019	0.110	0.157	0.843	1.660	1.887	0.302	0.752	1.344	1.164	1.910	0.124	0.684	1.373
TNT	<i>E. fetida</i>	0.019	0.110	0.157	0.843	1.660	1.887	0.302	0.752	1.344	1.164	1.910	0.124	0.684	1.373
TNT	<i>E. fetida</i>	0.019	0.110	0.157	0.843	1.660	1.887	0.302	0.752	1.344	1.164	1.910	0.124	0.684	1.373
TNT	<i>E. fetida</i>	0.019	0.110	0.157	0.843	1.660	1.887	0.302	0.752	1.344	1.164	1.910	0.124	0.684	1.373

^a Data presented in Table H-8 in Appendix H, including abbreviations. Values for f_{Lipid} , $f_{Protein}$, f_{Water} , and f_{dwt} are expressed as kg kg_{wwt}⁻¹ and their sources are in Table H-3; average of values for the corresponding species were taken when not available in or elsewhere referred to by the source of the worm concentration. The solute descriptors used to apply the K_{Lipid} and $K_{Protein}$ pp-LFERs by Kuo and Di Toro^{30,33} were obtained with the regression equations for the adjusted QCAP provided in Liang³¹. Adjusted QCAP are recommended over QCAP to apply existing pp-LFERs that were built using solute descriptors either derived from calibration to experimental measurements or estimated with functional group fragments contributions³¹.

Table H-10 Worked example for the prediction of a MC (2,4-DNAN) concentration in an oligochaete worm (*Eisenia andrei*).

Input data			
<i>i</i> : 2,4-DNAN			
Oligochaete species: <i>Eisenia andrei</i>			
2,4-DNAN Adjusted QCAP for prediction of K_{iOC} and $K_{iProtein}$:			
Variable	Value	Units	Source
$E = 1.144$		-	31
$S = 1.757$		-	31
$A = 0.056$		-	31
$B = 0.745$		-	31
$V = 1.276$		-	31
$C_{iSoil Solids} = 8.909$		mg kg _{dwt soil} ⁻¹	55
$f_{OC} = 0.010$		kg _{OC} kg _{dwt soil} ⁻¹	Table H-8
2,4-DNAN QCAP for prediction of K_{iLipid} :			
Variable	Value	Units	Source
$E = 1.660$		-	31
$S = 1.704$		-	31
$A = 0.187$		-	31
$B = 0.785$		-	31
$V = 1.231$		-	31
$f_{Lipid} = 0.017$		kg _{lipid} kg _{wwt worm} ⁻¹	Table H-9
$f_{Protein} = 0.108$		kg _{protein} kg _{wwt worm} ⁻¹	Table H-9
$f_{dwt} = 0.150$		kg _{dwt} kg _{wwt worm} ⁻¹	Table H-9

f_{Water}	$= 1 - f_{dwt}$		
	$= 0.850$	$\text{kg}_{\text{water}} \text{kg}_{\text{wwt worm}}^{-1}$	Table H-9
ρ_{Water}	$= 1.000$	$\text{kg}_{\text{water}} \text{L}_{\text{water}}^{-1}$	Assumed
Prediction			
Variable			Based on Eq. #
K_{iOC}	$= 10^{(0.670+1.075E-0.277S-0.363A-1.697B+1.468V)}$		(7-7)
	$= 10^{(0.670+1.075*1.144-0.277*1.757-0.363*0.056-1.697*0.745+1.468*1.276)}$		
	$= 100.508 \text{ L}_{\text{water}} \text{kg}_{OC}^{-1}$		
C_{iIW}	$= \frac{C_{iSoil Solids}}{K_{iOC} f_{OC}}$		(7-8)
	$= \frac{8.909 \text{ mg kg}_{dwt}^{-1}}{100.508 \text{ L}_{\text{water}} \text{kg}_{OC}^{-1} * 0.010 \text{ kg}_{OC} \text{kg}_{dwt}^{-1}}$		
	$= 8.864 \text{ mg L}^{-1}$		
	$< 155 \text{ mg L}^{-1}$ 2,4-DNAN aqueous solubility		Table H-1
	Predicted C_{iIW} is $<$ aqueous solubility; ✓ use C_{iIW} for onward calculations		
K_{iLipid}	$= 10^{(0.751+0.431E-2.409S-0.787A-2.106B+4.553V)}$		(7-11)
	$= 10^{(0.751+0.431*1.660-2.409*1.704-0.787*0.187-2.106*0.785+4.553*1.231)}$		
	$= 14.746 \text{ L}_{\text{water}} \text{kg}_{lipid}^{-1}$		
$K_{iProtein}$	$= 10^{(-0.88+0.74E-0.37S-0.13A-1.37B+1.06V)}$		(7-6)
	$= 10^{(-0.88+0.74*1.144-0.37*1.757-0.13*0.056-1.37*0.745+1.06*1.276)}$		
	$= 0.438 \text{ L}_{\text{water}} \text{kg}_{protein}^{-1}$		
C_{iWorm}	$= \left(f_{Lipid} K_{iLipid} + f_{Protein} K_{iProtein} + \frac{f_{Water}}{\rho_{Water}} \right) \frac{C_{iSoil Solids}}{f_{dwt} f_{OC} K_{iOC}}$		(7-12)

$$\begin{aligned}
&= \left(0.017 \text{ kg}_{lipid} \text{ kg}_{wwt worm}^{-1} * 14.746 \text{ L}_{water} \text{ kg}_{lipid}^{-1} + \right. \\
&0.108 \text{ kg}_{protein} \text{ kg}_{wwt worm}^{-1} * 0.438 \text{ L}_{water} \text{ kg}_{protein}^{-1} + \\
&\left. \frac{0.850 \text{ kg}_{water} \text{ kg}_{wwt worm}^{-1}}{1 \text{ kg}_{water} \text{ L}_{water}^{-1}} \right) * \\
&\quad 8.909 \text{ mg kg}_{dwt soil}^{-1} \\
&\quad \left(0.150 \text{ kg}_{dwt} \text{ kg}_{wwt worm}^{-1} * 0.010 \text{ kg}_{OC} \text{ kg}_{dwt soil}^{-1} * 100.508 \text{ L}_{water} \text{ kg}_{OC}^{-1} \right) \\
&= 67.390 \text{ mg kg}_{dwt}^{-1} \\
&\text{vs. } 51.143 \text{ mg kg}_{dwt}^{-1} \text{ observed } C_{iWorm}
\end{aligned}$$

Table H-8

Table H-11 Predicted values for soil organic carbon-water partition coefficient (K_{oc}), concentration in interstitial water, and concentration in worm for MCs data from independent uptake studies using the partition-based model (Eq. (7-12)) with K_{Lipid} pp-LFER from this work (Eq. (7-11)).

Compound ^a	Obs. concentration in worm ^a	Pred. log K_{oc} ^b	Pred. concentration in interstitial water	Pred. concentration in interstitial water_corrected ^c	Pred. concentration in worm ^d
	mg kg _{dwt} ⁻¹	L kg ⁻¹	mg L ⁻¹	mg L ⁻¹	mg kg _{dwt} ⁻¹
RDX	17.341	1.532	1.617	1.617	10.055
RDX	63.584	1.532	25.976	25.976	161.493
RDX	287.090	1.532	249.962	59.700	371.149
RDX	426.590	1.532	2369.739	59.700	371.149
RDX	579.961	1.532	6984.237	59.700	371.149
RDX	920.520	1.532	23101.897	59.700	371.149
RDX	41.000	1.532	303.241	59.700	355.351
RDX	1698.000	1.532	291.180	59.700	355.351
RDX	61.173	1.532	20.457	20.457	121.767
RDX	102.213	1.532	40.915	40.915	243.535
RDX	186.615	1.532	81.829	59.700	355.351
RDX	284.956	1.532	163.658	59.700	355.351
RDX	306.637	1.532	327.316	59.700	355.351
2,4-DNAN	57.143	2.002	8.864	8.864	67.390
2,4-DNAN	100.840	2.002	19.722	19.722	149.942
2,4-DNAN	152.941	2.002	27.699	27.699	210.593
HMX	11.046	1.433	320.874	5.000	29.466

HMX	48.818	1.433	3208.740	5.000	29.466
HMX	501.106	1.433	32087.399	5.000	29.466
TNT	5.190	2.203	3.272	3.272	25.457
TNT	12.111	2.203	6.544	6.544	50.913
TNT	31.575	2.203	13.089	13.089	101.826
TNT	98.616	2.203	26.178	26.178	203.652

^a Dataset described in Table H-8 in Appendix H

^b Prediction made using K_{oc} pp-LFER model developed by Kipka and Di Toro ³⁴ Eq. (7-7) and adjusted QCAP described in Table H-9

^c Predicted concentrations in interstitial water that exceeded solubility limits were corrected to be at the solubility of the compound listed in Table H-1

^d The K_{Lipid} pp-LFER from this work (Eq. (7-11)) was used with the QCAP from Liang ³¹ in Table H-9

Table H-12 Predicted values for soil organic carbon-water partition coefficient (K_{oc}), concentration in interstitial water, and concentration in worm for MCs data from independent uptake studies using the partition-based model (Eq. (7-9)) with K_{Lipid} pp-LFER obtained by Kuo and Di Toro^{30,33} (Eq. (7-5)).

Compound ^a	Obs. concentration in worm ^a	Pred. log K_{oc} ^b	Pred. concentration in interstitial water	Pred. concentration in interstitial water_corrected ^c	Pred. concentration in worm
	mg kg _{dwt} ⁻¹	L kg ⁻¹	mg L ⁻¹	mg L ⁻¹	mg kg _{dwt} ⁻¹
RDX	17.341	1.532	1.617	1.617	12.041
RDX	63.584	1.532	25.976	25.976	193.393
RDX	287.090	1.532	249.962	59.700	444.463
RDX	426.590	1.532	2369.739	59.700	444.463
RDX	579.961	1.532	6984.237	59.700	444.463
RDX	920.520	1.532	23101.897	59.700	444.463
RDX	41.000	1.532	303.241	59.700	435.585
RDX	1698.000	1.532	291.180	59.700	435.585
RDX	61.173	1.532	20.457	20.457	149.261
RDX	102.213	1.532	40.915	40.915	298.522
RDX	186.615	1.532	81.829	59.700	435.585
RDX	284.956	1.532	163.658	59.700	435.585
RDX	306.637	1.532	327.316	59.700	435.585
2,4-DNAN	57.143	2.002	8.864	8.864	76.970
2,4-DNAN	100.840	2.002	19.722	19.722	171.258
2,4-DNAN	152.941	2.002	27.699	27.699	240.531
HMX	11.046	1.433	320.874	5.000	30.796

HMX	48.818	1.433	3208.740	5.000	30.796
HMX	501.106	1.433	32087.399	5.000	30.796
TNT	5.190	2.203	3.272	3.272	41.012
TNT	12.111	2.203	6.544	6.544	82.024
TNT	31.575	2.203	13.089	13.089	164.048
TNT	98.616	2.203	26.178	26.178	328.096

^a Dataset described in Table H-8 in Appendix H

^b Prediction made using K_{OC} pp-LFER model developed by Kipka and Di Toro ³⁴ Eq. (7-7) and adjusted QCAP described in Table H-9

^c Predicted concentrations in interstitial water that exceeded solubility limits were corrected to be at the solubility of the compound, listed in Table H-1

^d The K_{Lipid} pp-LFER by Kuo and Di Toro ^{30,33} (Eq. (7-5)) was used with the adjusted QCAP from Liang ³¹ in Table H-9

Chapter 8

CONCLUSIONS AND IMPLICATIONS FOR FUTURE RESEARCH/IMPLEMENTATION

A methodology has been developed using quantum chemical computations to estimate Abraham solute parameters for two types of applications: for use with presently existing Abraham models, or for use in building new Abraham models. In both cases the solute parameters have a smaller error than all other available estimation methods. This is the case for non-munitions component and for munition components for which parameters were experimentally determined for the comparisons in this project.

Bioaccumulation models for plants (grasses) and soil invertebrates (oligochaetes) that are exposed from compounds in soils have been developed as well as a bioconcentration model for fish exposed from compounds in water. The three models require partition coefficients for which models have also been developed: partitioning between water and organism lipid, organism protein, and plant cuticle, and a previously developed model for water-soil organic carbon. The number of observations in the data sets are: oligochaetes (57), protein (69) grasses (191), lipids (248), soil organic carbon (444) and fish (601).

The performance of the models is gauged using the root mean square error of the residuals: the difference between \log_{10} modeled and \log_{10} observed of either partition coefficients or concentration, which is equal to \log_{10} of the ratio: model/observed. It is approximately equal to 0.40 for all the models, corresponding to approximately 80% of the residuals between 1/3 and 3 and approximately 90% of the residuals between 1/5 and 5.

The models can be used in a number of ways, in particular for the stated objective of the SON: to assess the environmental impact of new munitions compounds. All that is required to make estimates of the extent of bioaccumulation for grasses, oligochaetes and fish is the molecular structure of the compound. In addition the physical chemical parameters: octanol-water and air-water (Henry's Law constant) partition coefficients and aqueous solubility can also be estimated. Both the physical chemical and environmental partition coefficients are not as accurate as experimental determinations. However they are sufficiently quantitative for a number of tasks, for example to rank a sequence of proposed new munitions compounds to bioaccumulate in organisms, or to establish that the risk is either low enough so that no further experimental information is necessary, or, conversely that the risk is estimated to be high enough so that further investigation is required if the compound is to move forward. This ability to determine the potential extent of environmental risk for new munitions compounds is the most immediate benefit from using the models developed in this project.

Future Research

A methodology for estimating Abraham Parameters for neutral munitions compounds has been developed and successfully applied using previously developed pp-LFER models for solvent-water distribution coefficients, particularly K_{OW} , and K_{OC} . New models for soil-grasses and soil-oligochaetes have also been developed using sets of available data and new

MC data developed in this project. This methodology can be extended so that charged compounds can be modeled. A preliminary application to carboxylic cations and certain ionic liquids has been made using a similar procedure to that developed in this project ¹. This procedure could be applied to develop the necessary solvent parameters can be applied to insensitive munitions that are charged, for example NTO as well as proposed charged insensitive munitions that are currently being investigated. The development would require sets of experimental data for solvent-water partition coefficients for charged MC and MC like compounds that can be used to develop the solvent parameters. Data for these compounds for partitioning to between water and soil organic carbon, soil grasses and soil oligochaetes would also be required to develop the models. This would extend the range of applicability to a large set of currently important classes of compounds being developed for new insensitive munitions.

REFERENCES

1. Davis, Craig Warren and Di Toro, Dominic M. (2016) Predicting solvent-water partitioning of charged organic species using quantum-chemically estimated Abraham pp-LFER solute parameters Chemosphere 164 (2016) 634-642

Appendix I

PRESENTATIONS AT CONFERENCES AND PUBLICATIONS GENERATED FROM THIS PROJECT

I.1 Presentations at Conferences

2017

Sunahara G.I. Use of soil organisms for ecotoxicological assessment of contaminated sites. Invited Lecture. Presented at McGill University-Macdonald campus, Ecological Soil Management SOIL 535 (Host: Prof. Joann Whalen), on 26-JAN-2017.

2016

Di Toro D.M., Liang Y., Torralba-Sanchez T. Predicting environmental partitioning via quantum chemistry, Abraham parameters and pp-LFERs. Oral Presentation. ACS Semiannual National Meeting, Philadelphia, PA, 21 – 25 August 2016.

2015

Di Toro D.M., Liang Y., Torralba-Sanchez T. Predicting Abraham Parameters From Molecular Structure Using a Quantum Chemical Method. Oral Presentation. Society of Environmental Toxicology and Chemistry (SETAC) North America 36th Annual Meeting. Salt Lake City, UT, 1 - 5 November 2015.

Liang, Y. Determining Abraham Solvation Parameters using a Quantum Chemical Model. Poster. DENIN Graduate Student Research Symposium, Newark, DE, 08 October 2015.

Torralba-Sanchez, T.L. Predicting Bioconcentration of Munitions Compounds in Grasses From Molecular Structure. Awarded Best Research Poster. DENIN Graduate Student Research Symposium, Newark, DE, 08 October 2015.

2014

Kuo D.T.F. and Di Toro, D.M. Importance of internal partitioning in predicting biotransformation behavior of organic chemicals. Society of Environmental Toxicology and Chemistry 35th Annual Meeting, Vancouver, British Columbia, Canada. 8-14 November 2014.

Kuperman, R.G., Simini, M., Checkai, R.T., Dodard, S.G., Sarrazin, M., Hawari, J., Paquet, L., Sunahara, G.I., and Di Toro, D.M. Bioconcentration of energetic compounds in earthworms using aqueous exposure media. Society of Environmental Toxicology and Chemistry 35th Annual Meeting, Vancouver, British Columbia, Canada. 8-14 November 2014 (Published Abstract #RP118).

Kuperman, R.G., Simini, M., Checkai, R.T., Dodard, S.G., Sarrazin, M., Hawari, J., Paquet, L., Sunahara, G.I., and Di Toro, D.M. Developing earthworm bioconcentration factors of nitrogen-based compounds for predicting environmentally significant parameters for new munition compounds in soil. 10th International Symposium on Earthworm Ecology, 22-28 June 2014, Athens, GA (published abstract).

Liang, Y. Determining Partition Coefficients for Munitions by Experiment and Model Predictions. Poster. Gordon Research Conference, Plymouth, NH, 22 – 28 June 2014.

Torralba–Sanchez, T.L. Bioconcentration Factors (BCFs) of Energetic Compounds in Plants: Modeling BCF by Partitioning Only. Poster. Gordon Research Conference, Plymouth, NH, 22 – 28 June 2014.

Di Toro D.M. Predicting the Partitioning of Contaminants and Munitions Components to Soil, Organisms and Plants from Molecular Structure for use in Risk Assessment. Invited Lecture. Joint Army-Navy-NASA-Air Force (JANNAF) Meeting. Charleston, SC, 19-23 May, 2014.

2013

Di Toro, D. M., Miglino, A., Torralba- Sanchez, T.L. Predicting the Partitioning of Contaminants and Munitions Components to Soil, Organisms and Plants from Molecular Structure. Oral Presentation. SETAC Annual Meeting, Nashville, TN, 17 - 21 November 2013.

Torralba–Sanchez, T.L. Bioconcentration of Energetic Compounds - Munitions Constituents - in Plants. Oral Presentation. SETAC Annual Meeting, Nashville, TN, 17 - 21 November 2013.

Torralba–Sanchez, T.L. Bioconcentration of Energetic Compounds - Munitions Constituents - in Grasses. Oral Presentation. ACS Semiannual National Meeting, Indianapolis, IN, 08 – 12 September 2013.

2012

Torralba–Sanchez, T.L. Bioaccumulation of Energetic Compounds in Grasses. Poster. ACS Semiannual National Meeting, Philadelphia, PA, 21 - 25 August 2012.

2011

Dodard, S.G., Sarrazin, M., Kuperman, R.G., Minyard, M., Checkai, R..T, Hawari, J., Paquet, L., Di Toro, D.M., and Sunahara, G.I. Development of a model bioconcentration assessment system for energetic materials on the basis of earthworm exposure in aqueous media. The 2011 SERDP Partners in Environmental Technology Technical Symposium & Workshop, Washington, DC, 29 November -1 December, 2011 (Published Abstract #G-239).

2010

Di Toro, D.M., Sandler, I.S., Allen, H.E., Kuperman, R.G., and Sunahara, G.I. Developing quantum chemical and polyparameter models for predicting environmentally significant parameters for new munition compounds. The 2010 SERDP Partners in Environmental Technology Technical Symposium & Workshop, Washington, DC, 30 November -2 December, 2010 (Published Abstract #P496).

I.2 Peer-reviewed Publications

2017

Liang, Y., Xiong, R., Sandler S. I., Di Toro, D. M. (2017). Quantum chemically estimated Abraham solute parameters using multiple solvent-water partition coefficients and molecular polarizability. *Environmental Science & Technology*. Accepted for Publication as Research Article.

Torralba-Sanchez, T.L., Kuo, D. T. F., Allen, H.E., Di Toro, D.M. (2017). Bioconcentration Factors and Plant-Water Partition Coefficients of Munitions Compounds in Barley. *Chemosphere*. Accepted for Publication as Research Article.

Torralba-Sanchez, T.L., Liang, Y., Di Toro, D.M. (2017). Estimating grass-soil bioconcentration of munitions compounds from molecular structure. *Environmental Science & Technology*. Accepted for Publication as Research Article.

2016

Liang, Y., Kuo, D. T. F., Allen, H. E., Di Toro, D. M. (2016). Experimental determination of solvent-water partition coefficients and Abraham parameters for munition constituents. *Chemosphere*, 161, 429-437.

Kuperman, R. G., Simini, M., Checkai, R. T., Dodard, S. G., Sarrazin, M., Hawari, J., Paquet, L., Sunahara, G. I., Di Toro, D. M., Allen, H. E., Kuo, D. T. F., Torralba-Sanchez, T. L. (2016). Developing earthworm bioconcentration factors of nitrogen-based compounds for predicting environmentally significant parameters for new munition compounds in soil. *Applied Soil Ecology*, 104, 25-30.

2013

Kuo, D. T. F., & Di Toro, D. M. (2013). Biotransformation model of neutral and weakly polar organic compounds in fish incorporating internal partitioning. *Environmental Toxicology and Chemistry*, 32(8), 1873-1881.

Kuo, D. T. F., & Di Toro, D. M. (2013). A reductionist mechanistic model for bioconcentration of neutral and weakly polar organic compounds in fish. *Environmental Toxicology and Chemistry*, 32(9), 2089-2099.